Dendritic and Self-Assembling Linear RGD Peptides - From Integrin Binding to Responsive Hydrogels

Daniel J. Welsh

A thesis submitted for the degree of Doctor of Philosophy

University of York
Department of Chemistry

September 2011

Abstract

Several studies exist in the literature which utilise either dendritic (covalent) or self-assembling (non-covalent) strategies to achieve multivalent binding to a biological target, but rarely are the two explored together. Herein, we compare and contrast dendritic and self-assembling approaches to organise a multivalent array of ligands to bind the protein, integrin $\alpha_v\beta_3$. In the first instance, linear RGD (Arg-Gly-Asp) peptides were covalently attached to first and second generation dendritic frameworks, and a positive (monovalent) and negative control were synthesised. A fluorescence polarisation (FP) competition assay was used to quantify the binding. The first generation dendron (**2.16**) was the most effective binder, with an EC_{50} of 125 μM (375 μM per peptide unit); significantly better than the monovalent ligand (**2.19**), the binding of which could not be quantified in our assay, even at 1 mM concentration; whilst the second generation dendron (**2.17**) was somewhat less effective, indicating that there is an optimum number of ligands that can be displayed before the multiple ligand array becomes disadvantageous to the binding.

To explore the non-covalent approach, the linear RGD peptide was conjugated to either a single hydrophobic C12 aliphatic chain (**3.2**), an aromatic pyrene (**3.4**), a C22 aliphatic chain (**3.6**), or two C12 aliphatic chains (**3.18**), which gave rise to amphiphilic peptides which were able to self-assemble to differing degrees and into markedly different morphologies, as shown by a Nile Red encapsulation study and TEM imaging. Spherical micelles were formed by amphiphiles **3.2** and **3.4**, whereas **3.6** and **3.18** produced cylindrical, rod-like micelles. Compounds **3.2** and **3.4** were the most effective integrin binders at concentrations of 200 μM and 110 μM, respectively, whilst **3.6** and **3.18** failed to produce a quantifiable binding concentration. The results therefore show that not only does the micellar self-assembly approach yield multivalent ligand displays with improved efficiency of binding compared with the dendritic method, but the morphology of the self-assembled system can also be detrimental to the recognition of the protein, at least in our FP assay and using purified integrin in solution.

Finally, we report on a family of linear RGD peptide conjugate hydrogelators. Of particular interest was the novel bolaamphiphile **C12-[urea-RGD]$_2$** (**4.4**), comprised of linear RGD peptide head groups connected to either end of a hydrophobic C12 aliphatic chain via urea linkages. The molecule undergoes thermoreversible chiral self-assembly in water and generates a sample-spanning nanofibrous gel network, as determined by circular dichroism spectroscopy and TEM/SEM imaging, respectively. Gels were formed at a minimum gel concentration (MGC) of 0.06 wt % (0.6 mg/ml, 0.5 mM), one of the lowest MGCs reported and represents a "super" hydrogel. We report on its responsiveness (breakdown) towards charge dense basic anions such as phosphate and acetate, but its stability in the presence of more charge diffuse halide and nitrate anions. Furthermore, we demonstrate the passive diffusion of encapsulated low MW additives out of the gel phase, whereas high MW, protein-sized molecules remain trapped within the fibrous network.

Table of Contents

List of Figures, Schemes, Tables and Spectra

Acknowledgements

First and foremost, I would like to thank Natalie for being there for me throughout my PhD, especially when times were tough, for the sacrifices you have made for me and for having patience and understanding during the time I have been writing my thesis. Without you to keep me motivated I would not have achieved this feat and I will always be grateful for that.

A big thank you goes to my family, particularly my mum and dad for their help and support over the years, both financial and mental, and their commitment to seeing me succeed during my eight years at university. Words cannot describe how grateful I am.

I will always be appreciative of the guidance and support given to me by my supervisor Professor Dave Smith, and of the knowledge and experience gained while working in his group. I would also like to thank my IPM Professor Gideon Davies for his time and input at TAP meetings, and the EPSRC and the University of York for funding this research through the DTA scheme.

People within the department of Chemistry who have contributed technically to this research include: Heather Fish and Amanda Dixon (NMR), and Dr Trevor Dransfield and Karl Heaton (mass spectrometry); and in Biology: Meg Stark and Karen Hodgkinson (TEM/SEM), Dr Andrew Leech and Berni Strongitharm (advice on fluorescence and circular dichroism spectroscopy), and Dr James Edwards for letting me use his benchspace and consumables and for his help and advice on fluorescence polarisation spectroscopy. I should also mention our collaborators at Boston University, Professor Mark Grinstaff and graduate student Jonah Kaplan for carrying out the preliminary cell growth studies on our hydrogels. A big thank you to all of them.

Finally, I would also like to give thanks to members of the DKS group, including old favourites (but in no particular order mind), Dr Simon Jones (grassing-aside – you know what I'm talking about), Dr Ian 'Golden Nanoballs' Coates (for his dazzling football skills), Dr Bart Nelissen (for being the go-to guy in the lab for advice and for those enjoyable evenings in the Deramore spent watching the footy), and Dr Ting-Chou Hu (lunch and coffee breaks will never be the same again). Current members include Dr Michelle Smith, Amanda Dixon, Anna Barnard, Will Edwards and Stephen Bromfield, and I thank all of them for making my time in the group an enjoyable one – I will miss the summer trips and group meals out.

This thesis is dedicated to my family and friends.

Declaration

I declare that this work is entirely my own except where acknowledged.

Daniel J. Welsh

Chapter 1

Introduction

1 Introduction

1.1 Multivalency in Supramolecular Chemistry – Lessons From Biology

Multivalent ligands, in which multiple copies of a recognition element (RE) are projected from a central scaffold, can be a powerful approach for enhancing the binding of REs to biological targets with multiple recognition sites.[3-6] A RE can be a carbohydrate, peptide, protein, or small molecule – the ligand chosen is dependent on the receptor of interest. Multivalent ligands exhibit enhanced binding through any combination of: (i) a primarily entropic effect, which after binding of the first ligand promotes the binding of a second ligand to a second binding site on the biological target – the translational entropic cost is already paid for by the first ligand-receptor contact, with subsequent binding contacts proceeding without additional penalties in entropy[7] (Fig. 1.1A); (ii) binding to remote secondary (sub)sites which may be present on the receptor by either an RE or another component on the scaffold (Fig. 1.1B); (iii) binding of multiple REs to multiple receptors, facilitated by receptor clustering (Fig. 1.1C); and/or (iv) a local concentration effect, in which once a ligand dissociates from its binding site, there is a high local concentration to favour statistical rebinding (Fig. 1.1D). The structure of the multivalent ligand and the nature of the biological target determine which binding mode is favoured. As such, multivalent scaffolds are widely employed for enhancing the binding of REs to biomolecules with multiple binding sites, such as glycoproteins[8, 9] and DNA.[10-13]

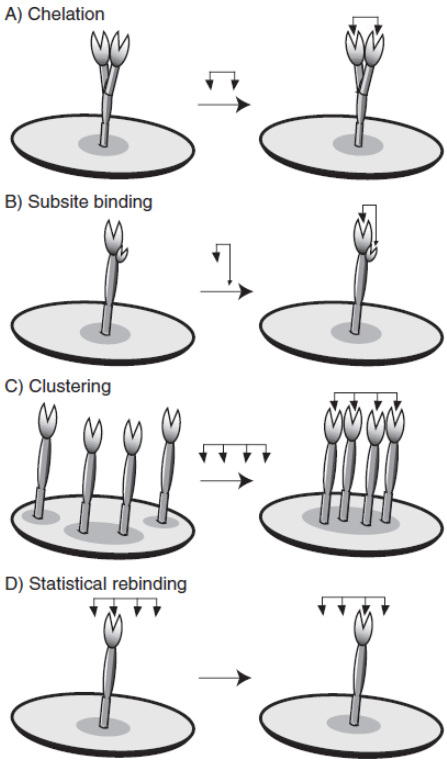

Fig. 1.1 – The different mechanisms of receptor binding exhibited by multivalent ligands. Image reproduced from reference 4.

It has long been understood that multivalent interactions play essential roles in biological processes.[3] Carbohydrates are important in biological systems and most commonly they form host:guest complexes with a range of receptor proteins, such as lectins, on cell surfaces. A problem with this binding process is that carbohydrates interact very weakly with proteins. To overcome this problem, nature uses carbohydrate 'clusters' to improve the binding strength. An example of a multivalent interaction relevant to human biology is the attachment of an influenza virus to the surface of a cell – a prerequisite for viral infection of cells (Fig. 1.2). The attachment occurs via interaction of multiple trimers of hemagglutinin (HA, a sugar-binding protein, or lectin, on the viral surface) and multiple sialic acid units (SA, the terminal sugar on many glycoproteins found on cell surfaces). By mimicking this process, not only has fundamental insight been gained into how nature uses weakly binding ligands and makes them stronger by presenting them in a multivalent fashion, but this has also allowed for the development of new rationally designed potent drugs to inhibit, for example, the attachment of influenza virus to a cell surface therefore preventing infection.

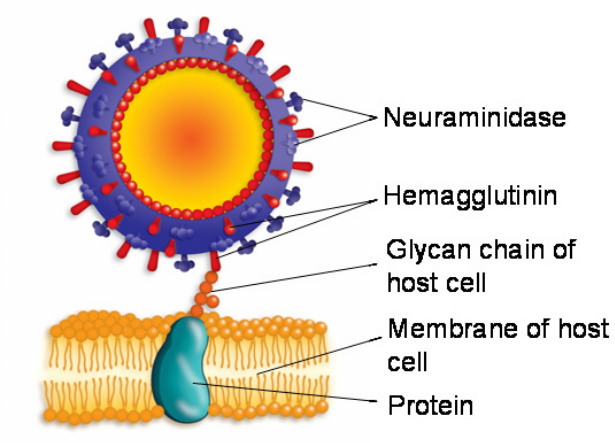

Fig. 1.2 – An influenza virus binding to a host cell. Hemagglutinin binds to sialic acid on the glycan chain of a membrane-bound glycoprotein on the host cell. Image reproduced from reference 14. Original in colour.

1.1.1 Dendritic Multivalency

Figure 1.3 illustrates the anatomy of a dendron/dendrimer.[15] Known as 'cascade' or 'branched' polymers, they can be synthesised convergently (starting from the outside working inwards) or divergently (starting from the inside and working outwards). The surfaces of dendritic molecules constitute an example of *covalent* multivalency.[16] These highly branched, tree-like molecules with multivalent peripheral displays have in the last 20 years or so become fashionable for use as supramolecular multivalent scaffolds.[17-21] Increasing the binding strength of otherwise weak recognition events via the multivalency principle is just one of the advantages that these superstructures offer, particularly in a biological setting.[22] Also, their well-defined 'perfect' molecular

structure means that FDA (Food and Drug Administration) approval for therapeutic use of dendrimer-based drugs, for example, is more likely to be granted than for polymer-based drugs. For these reasons biocompatible dendrimers have been highly sought after as new, low dosage, drug therapies for application in nanomedicine.[23] An example in this context is the binding of dendritic saccharides to proteins on cell or virus surfaces which have implications in anti-bacterial and anti-viral therapies, as well as working towards solving the problem of drug-resistant bacteria and other pathogens.[24-26]

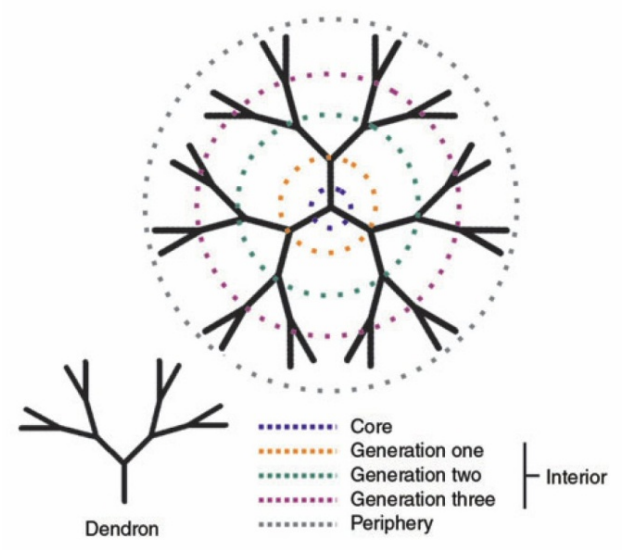

Fig. 1.3 – The general structures of a dendrimer and dendron are represented with solid lines. The coloured, broken lines identify the various key regions of the dendrimer. Image reproduced from reference 15. Original in colour.

Tomalia and co-workers evaluated a series of SA-bearing dendrimers for their ability to inhibit influenza virus HA and block infection of mammalian cells *in vitro*.[27] They found that the most effective were the comb-branched/dendrigraft scaffolds (Fig. 1.4) as they demonstrated up to 50000-fold increase in inhibitory activity over that of monomeric SA due to the multivalency effect. The study was the first demonstration of dose-dependent reduction in infection of influenza in mammalian cells for multivalent SA-based inhibitors. Since this work, more studies have followed into promising anti-adhesive drugs comprised of dendritic carbohydrate-based inhibitors, with potential to interfere with virus-specific-glycoprotein recognition events.[28-31]

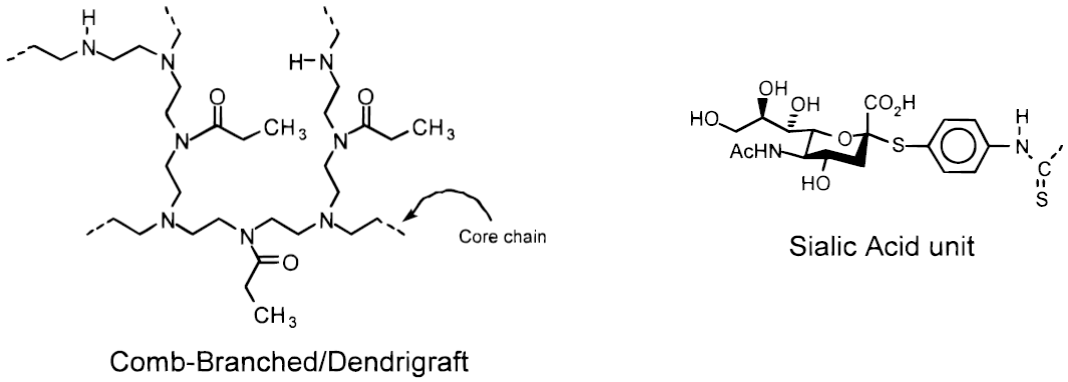

Fig. 1.4 – Chemical structure of a comb-branched/dendrigraft polymer and sialic acid unit. Image reproduced from reference 27.

1.1.2 Self-Assembling Multivalency

Amphiphilic ligands can be synthesised which self-assemble and present multiple REs on the surface of the colloidal structures (aggregates) that form – in much the same way that the influenza virus presents its lectin proteins on its viral membrane – this can be considered as a *non-covalent* method of multivalent organisation. The hydrophobic part of an amphiphile provides the driving force for its self-assembly in water, while the hydrophilic head group provides water solubility. It is widely known that the size and shape of the hydrophobic part in comparison to the hydrophilic part determines the shape of the resulting aggregates.[32] Classic work by Israelachvili has demonstrated the effect of hydrophobic chain length on the self-assembly mode of amphiphiles, including other physical principles related to membrane organisation.[33] Efficient space-filling is important to minimise the energy of the self-assembled system which is dependent on the critical packing shape of the amphiphile. Single-chained lipids with large head group areas have an inverted cone shape, leading to the formation of spherical micelles (Fig. 1.5A); smaller head group areas have a truncated cone or wedge, leading to globular or cylindrical micelles (Fig. 1.5B). Double-chained lipids with large head group areas constitute a truncated cone, leading to flexible bi-layers and usually this results in the formation of liposomes/vesicles (Fig. 1.5C); small head group areas have a cylinder shape which yields rigid, planar bilayers (Fig. 1.5D); and head group areas which are much smaller than the hydrophobic part constitute an inverted truncated cone which assembles into inverted micelles (Fig. 1.5E).

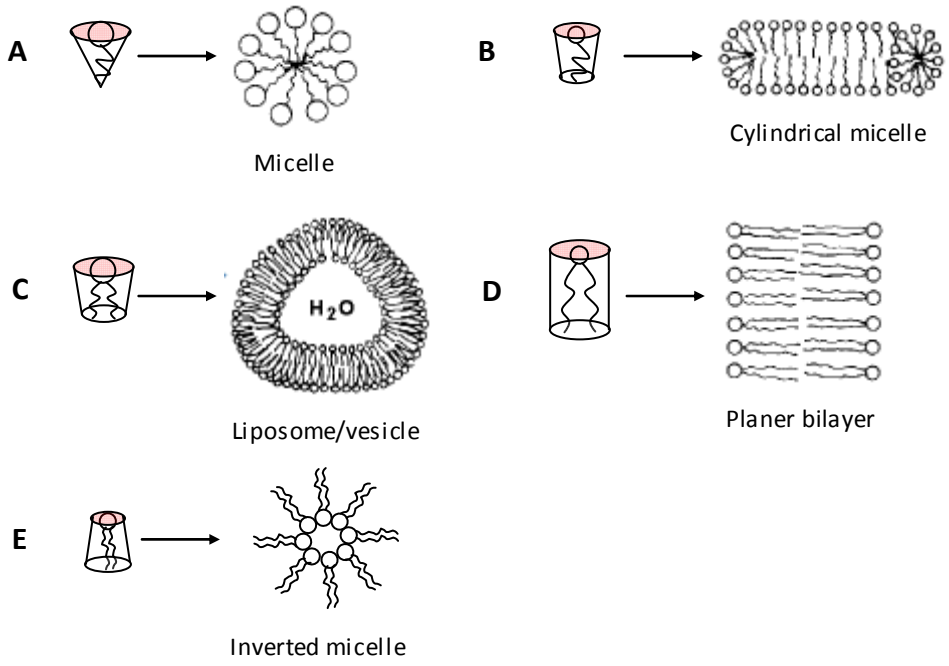

Fig. 1.5 – Critical packing shape of various lipids and the aggregated structures they form.

Wong and co-workers have synthesised a SA-bearing amphiphilic polymer which self-assembles into liposomes – a consequence of its double-chained nature and large head group – and displays multiple SA surface groups as a result (Fig. 1.6).[34] The liposomes bind hemagglutinin (HA) and neuraminidase (NA) proteins which are present on the surface of a flu virus, inhibiting viral attachment to host cells. The potency of the multivalent inhibitor was about 1000 times greater when compared with that of monomeric sialic acid, an enhancement caused by the multivalent clustering effect.

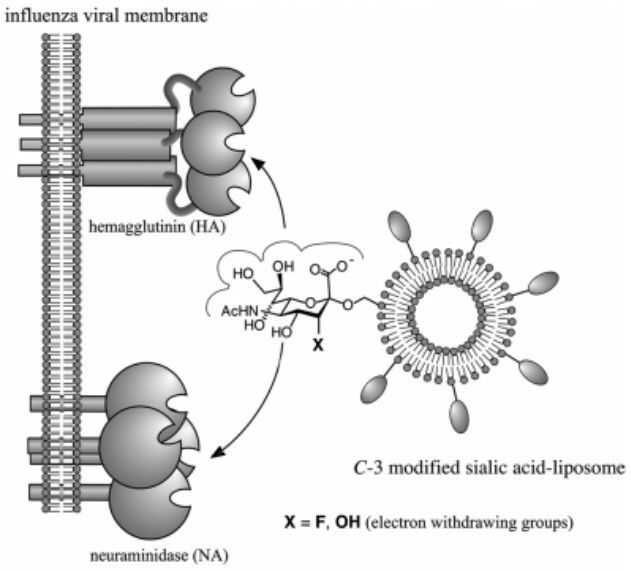

Fig. 1.6 – Wong's 3-deoxy-3-fluorosialic acid-derivatised liposome as a bifunctional multivalent inhibitor of HA and NA. Image reproduced from reference 34.

Clearly, dendritic and self-assembling approaches to multivalency are promising methods of enhancing weak recognition events between a ligand and its receptor. The following section details the cell-adhesive protein integrin – an interesting target for multivalent binding.

1.2 Integrins

Integrins are heterodimeric, transmembrane proteins composed of two non-covalently linked subunits, denoted α and β (Fig. 1.7), and these receptors play pivotal roles in cell-cell and cell-extracellular matrix (ECM) interactions.[35-41] These glue-like adhesive proteins also act as bidirectional signal transducers between the extracellular environment and the cytoskeleton, and modulate complex signalling pathways which are important in the functions of most cells (Fig. 1.8). These processes include cell migration, adhesion, differentiation and survival during embryogenesis, angiogenesis, human development, wound healing and in the immune system for example, detailed events which are beyond the scope of this thesis – the reader is directed to several good reviews by Hynes and other authors.[35, 37-39] Integrins have been of interest in developing biomaterials for use in tissue engineering applications,[42, 43] among other applications, and given that many integrins are now widely recognised as playing vital roles in pathological disorders, they are considered to be important therapeutic targets.[44] Of the 24 known integrin heterodimers (Fig. 1.9), $\alpha_v\beta_3$, $\alpha_v\beta_5$ and $\alpha_5\beta_1$ are the most widely studied for their over-expression on specific cancer cells and angiogenic blood vessels during tumour metastasis and angiogenesis,[45-49] making them attractive candidates for developing site-directed drugs and integrin antagonists as anti-cancer treatments.[50-55] Integrin $\alpha_{IIb}\beta_3$, another key receptor, is found on blood platelet membranes and mediates the adhesion and aggregation of platelets in thrombus formation,[56] antagonists of which are important as potential anti-thrombotic drugs.[57]

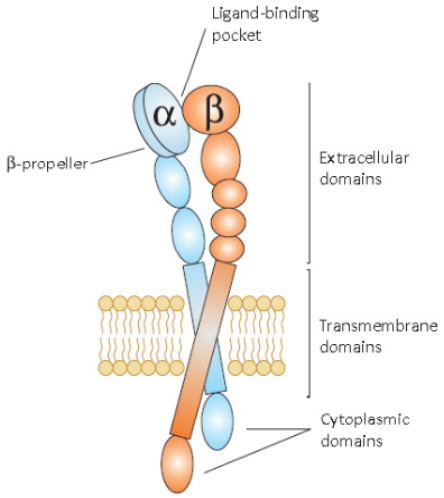

Fig. 1.7 – Schematic representation of an integrin in the unligated state. Image reproduced from reference 2. Original in colour.

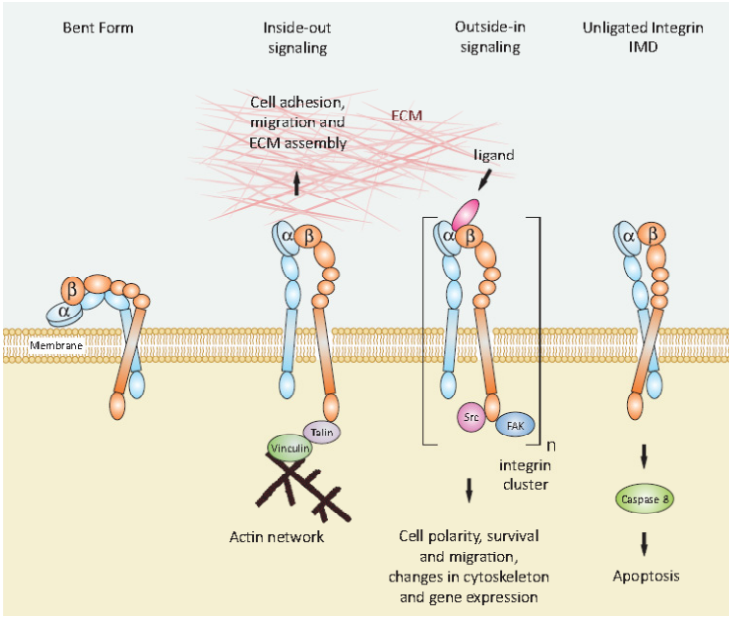

Fig. 1.8 – Schematic representation of integrin activation states and signalling mechanisms. In the bent form the integrin head group points inwards towards the cell surface and has low affinity for ligands.[58] During "inside-out signaling" an intracellular activator binds to the β-subunit, inducing a conformational change leading to increased affinity for extracellular ligands.[59] This process is known to regulate cell adhesion, migration and invasion. During "outside-in signaling" a ligand binds to the integrin and can induce, because of multivalency, integrin clustering. Activation of a signal cascade leads to intracellular signals, which regulate cell polarity, survival and migration, changes in cytoskeleton and gene expression. The presence of unligated integrins can activate caspase-8, and as a consequence, induce apoptosis in a process known as "integrin-mediated death" (IMD).[60, 61] Image reproduced from reference 2. Original in colour.

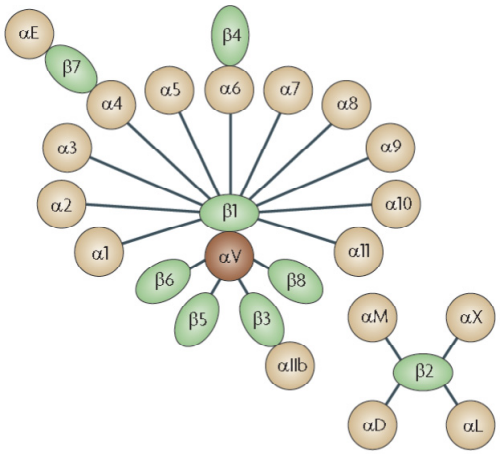

Fig. 1.9 – Integrin families: integrins are heterodimers comprising an α-subunit and a β-subunit, and at least 24 such heterodimers have been identified, which are shown here. Image reproduced from reference 44. Original in colour.

1.2.1 The RGD-Binding Motif

In the early 1980s, pioneering work published by Pierschbacher and Ruoslahti demonstrated that the cell attachment activity of fibronectin, a natural ECM protein for several integrins, could be duplicated by the tri-peptide RGD* (arginine, glycine, aspartic acid), a small synthetic fragment of the protein (Fig. 1.10).[62-66] Initially, RGDS was believed to be the minimum requirement for binding of fibronectin to its receptor,[64] however, further studies revealed that the serine (S) residue can be substituted for other amino acids without significantly affecting binding affinity, whereas RGD is essential for retaining activity.[65] RGD has subsequently been discovered in many other ECM proteins and represents the most common recognition sequence involved in cell adhesion as several different integrin subtypes bind to it (the term *integrin* was introduced by Hynes and co-workers in 1986[67]).[68-75] A good review by Ruoslahti discusses RGD-containing proteins and peptides, as well as other recognition sequences for integrins.[76] Integrin $\alpha_v\beta_3$, for example, promotes tumour-induced angiogenesis and binds to various RGD-containing ECM proteins, such as fibronectin, fibrinogen, vitronectin and collagen.[36] Much attention has therefore been focused on selectively inhibiting this integrin by designing and synthesising RGD-containing peptides and peptidomimetics for use in cancer therapy.[77, 78]

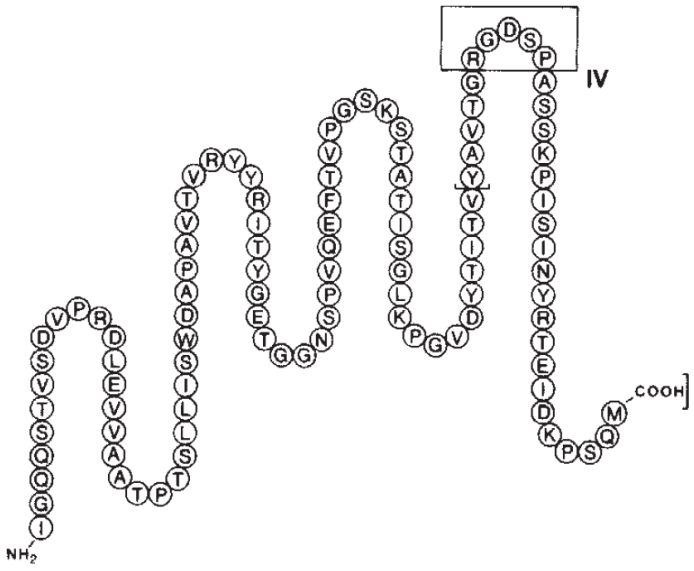

Fig. 1.10 – Early prediction of the secondary conformation of the cell attachment domain of fibronectin based solely on the primary structure, as determined in 1982. The peptide contains a series of potential β-turns, the most hydrophilic of which (boxed) was shown here to contain the cell attachment motif.[64] Image reproduced from reference 63.

* Amino acids are referred to using either three or one letter abbreviations and are used interchangeably throughout this thesis.

1.2.2 "Cilengitide" – The Benchmark Integrin Antagonist

In addition to their findings, Pierschbacher and Ruoslahti also discovered that not only do many integrins bind the RGD motif, but they can also distinguish between the different natural (ECM protein) ligands that possess this same recognition sequence (Table 1.1).[79] Amino acids surrounding the RGD probably contribute to integrin selectivity to an extent, however, a stronger argument was that the RGD sequence is maintained in a conformation unique to each ECM protein's (secondary and tertiary) structure which in turn is recognised by the integrin specific for that conformation of RGD. 'Conformation-dependent recognition' was supported as a concept in early work by Wilson *et al*, who studied identical short peptide sequences which, when inserted into different proteins, displayed different conformations, and as such were bound by different antibodies.[80] Around this time, Horst Kessler was pioneering the small molecule equivalent of this conformation-activity study by inserting hormone recognition motifs into cyclic peptides, restricting the conformational flexibility of the amino acid sequences, and hence improving receptor binding affinities and selectivities.[81]

Prior to the publication of the first crystal structure of an integrin extracellular head group in 2001 for $\alpha_v\beta_3$ (Fig. 1.11),[82] followed by $\alpha_{IIb}\beta_3$ in 2004,[83] initial efforts in drug design were based on a 'ligand-oriented design' which involved optimising RGD peptides using different chemical approaches to establish structure-activity relationships (SARs). Elucidation of the structure of the integrin receptor-binding pocket then led to a more informed 'rational structure-based design' approach being applied in the field of synthetic integrin ligands.

Recognition sequence	Ligand	Integrin
RGD	Adenovirus penton base protein, bone sialoprotein, collagen, decorsin, disintegrins, fibrinogen, fibronectin, prothrombin, tenascin, thrombospondin, vitronectin, von Willebrand factor	$\alpha_3\beta_1$, $\alpha_5\beta_1$, $\alpha_8\beta_1$, $\alpha_v\beta_1$, $\alpha_v\beta_3$, $\alpha_v\beta_5$, $\alpha_v\beta_6$, $\alpha_{IIb}\beta_3$
HHLGGAKQAGDV	γ-Chain of fibrinogen	$\alpha_{IIb}\beta_3$
GPR	α-Chain of fibrinogen	$\alpha_x\beta_2$
P1 peptide	γ-Chain of fibrinogen	$\alpha_M\beta_2$
P2 peptide	γ-Chain of fibrinogen	$\alpha_M\beta_2$
AEIDGIEL	Tenascin	$\alpha_9\beta_1$
QIDS	VCAM-1	$\alpha_4\beta_1$
LDT	MAdCAM-1	$\alpha_4\beta_7$
CS-1 peptide	Fibronectin	$\alpha_4\beta_1$, $\alpha_4\beta_7$
CS-5 peptide	Fibronectin	$\alpha_4\beta_1$
IDAPS	Fibronectin	$\alpha_4\beta_1$
ICAM peptides	ICAM-1, -2, -3	$\alpha_L\beta_2$, $\alpha_M\beta_2$
DLXXL	Tenascin	$\alpha_v\beta_6$
GFOGER[a]	Collagen	$\alpha_1\beta_1$, $\alpha_2\beta_1$

[a] O, hydroxyproline.

Table 1.1 – Integrins, their ECM proteins and respective recognition sequences. Table reproduced from reference 36.

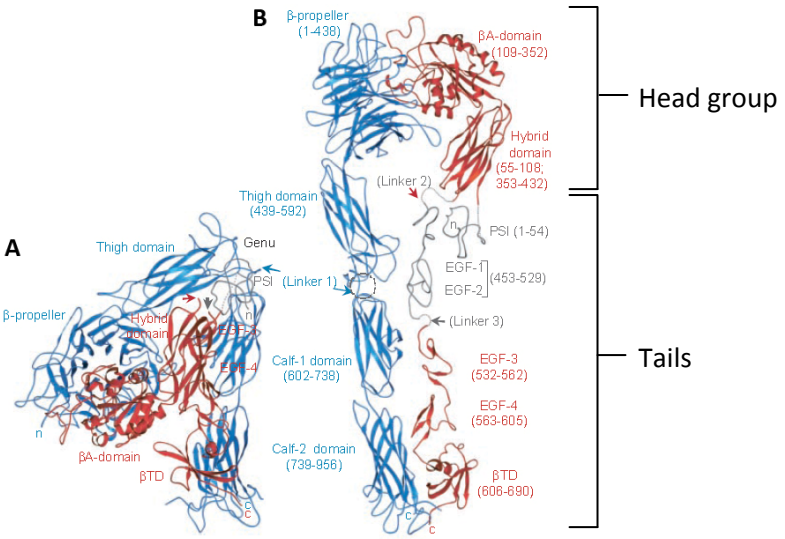

Fig. 1.11 – Structure of the extracellular domains of integrin $\alpha_v\beta_3$. A) Ribbon drawing of crystallised $\alpha_v\beta_3$ [shown in blue (α_v) and red (β_3)]. B) Model of the straightened extracellular domains of $\alpha_v\beta_3$. The two tails would extend into the plasma membrane in the native integrin. A more detailed description of the structure is given by Arnaout *et al.*[82] Image reproduced from reference 82. Original in colour.

Pre-crystal structure, Kessler and co-workers were interested in developing ligands for integrin $\alpha_v\beta_3$ and based their approach on three chemical strategies pioneered by them: (i) restriction of the conformational space by cyclisation;[81] (ii) "spatial screening" of cyclic peptides;[84, 85] and (iii) "*N*-methyl scan".[86] Using strategies (i) and (ii) they produced the cyclic pentapeptide *c*[RGDfV] (Fig. 1.12), the first small, selective, anti-angiogenic molecule described, and up to 100-fold more active (and selective) than the flexible, linear variant GRGDS.[87, 88] A bent conformation of the cyclic RGD sequence was found to fit the binding pocket of $\alpha_v\beta_3$ better than that of the platelet receptor $\alpha_{IIb}\beta_3$ thereby increasing the selectivity of the peptide.[89] SAR investigations showed that the amino acid in position 4 (i.e. f or D-phenylalanine) and the proton of the amide bond between residues 3 and 4 are essential for high affinity toward $\alpha_v\beta_3$.[89] In contrast, the amino acid in position 5 (i.e. V or L-valine) does not have any effect on the activity. This being the case, several studies have looked at exchanging the valine residue for an amino acid such as lysine (i.e. *c*[RGDfK]) and then used the lysine side-chain as a handle for conjugating the cyclic peptide to other functional molecules, such as sugars for improved biokinetics;[90] photosensitisers for photodynamic therapy of tumours;[91, 92] and radioactive metal-chelating agents or fluorescent markers for *in vivo* tumour imaging[93-96] – development of solid-phase synthetic protocols for this useful analogue of *c*[RGDfV] has understandably attracted interest.[97, 98]

N-methylation of *c*[RGDfV], employing chemical strategy (iii) of their ligand-oriented design, yielded the much more potent *c*[RGDf(*N*Me)V] (Fig. 1.12). Discovered in 1995, it possesses sub-nanomolar affinity for integrin $\alpha_v\beta_3$, nanomolar affinities for related integrins $\alpha_v\beta_5$ and $\alpha_5\beta_1$, and high preferential

binding towards $\alpha_v\beta_3$ over $\alpha_{IIb}\beta_3$. Patented with Merck in 1997,[99] the design, synthesis and biological activity and selectivity of this molecule was finally published in 1999.[100] A crystal structure of the extracellular head group of integrin $\alpha_v\beta_3$ in complex with *c*[RGDf(*N*Me)V], now known as "Cilengitide",[2] was published in 2002 (Fig. 1.13).[1] Cilengitide is currently being developed by Merck-Serono (Darmstadt, Germany) and, according to literature published in January 2011,[2] recently entered phase III clinical trials as an anti-angiogenic agent for treating malignant glioblastoma (brain tumour), and phase II for other types of cancers.[101]

Fig. 1.12 – Chemical structure of *c*[RGDfV] (where R = H), and *c*[RGDf(*N*Me)V] (where R = CH_3, "Cilengitide"), first developed by Kessler and co-workers.[2] D-configuration is indicated by a lower case letter for the amino acid. Original in colour.

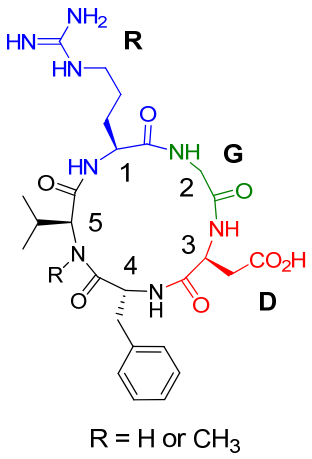

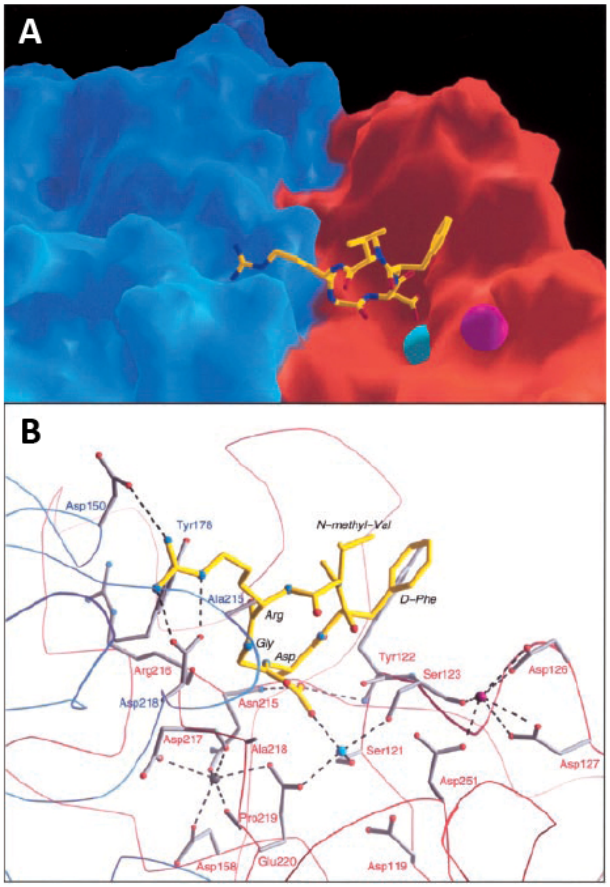

Fig. 1.13 – Structure of the extracellular head group of integrin $\alpha_v\beta_3$ complexed with *c*[RGDf(*N*Me)V].
A) Surface representation of the ligand-binding site, with the ligand shown as ball-and-stick model.
B) Interactions between ligand and integrin. A more detailed description of the integrin-*c*[RGDf(*N*Me)V] complex is given by Arnaout *et al.*[1] Image reproduced from reference 1. Original in colour.

1.2.3 Multivalent RGD Ligands

A plethora of studies have since ensued into the design, synthesis and biological activity of low molecular weight peptide and peptidomimetic integrin antagonists. These small molecule peptide and non-peptide mimics of *c*[RGDfV] have been reviewed extensively elsewhere.[78, 102, 103] Considering these efforts, understanding the binding of synthetic ligands to integrin hosts in detail is therefore important in studies of molecular recognition, particularly multivalent recognition for improving the activity of low affinity ligands. First impressions of an integrin as a target for multivalent binding are poor, as it contains only one ligand binding site. However, integrins are dynamic transmembrane proteins and are often regulated to cluster together at the leading edge of a migrating cell's membrane in the presence of natural ECM ligands, some of which are inherently multivalent, in a process known as 'focal adhesion'.[104-110] As such, multivalent binding of multiple integrins is a genuine possibility. Work in recent years toward the design and application of multivalent RGD-based peptide and semi-peptide arrays, that enhance the binding to integrin $\alpha_v\beta_3$, has recently been reviewed by Casiraghi and co-workers.[111]

The following examples outline some of the recent dendritic and self-assembly approaches for organising multivalent RGD-based arrays. Multivalent RGD-modified polymers,[112-116] surfaces,[117] proteins,[118] and nanoparticles[119, 120] have also been extensively investigated but will not be covered here as they are unrelated to the systems covered in this thesis.

1.2.3.1 Dendritic RGD

RGD-containing peptides have been conjugated to the surfaces of dendrimers (and dendrons) and their biological activities appear to be enhanced compared to those of the monovalent and lower generation analogues, a proposed consequence of the multivalency effect.[121-125] Many of these studies, however, rarely discuss the fundamental aspect of the multivalent RGD-integrin interaction – choosing instead to focus more on favourable biological outcomes. Liskamp and co-workers have synthesised mono-, di- and tetravalent *c*[RGDfK] peptide dendrimers using "click chemistry" (Fig. 1.14, showing tetravalent dendrimer **1** only) and evaluated their integrin $\alpha_v\beta_3$ antagonistic activity.[126, 127] The core of the dendrimers was functionalised with a 1,4,7,10-tetraazadodecane-*N*,*N*',*N*'',*N*'''-tetraacetic acid (DOTA) chelating group and either left unlabeled to monitor receptor binding in an *in vitro* competition assay, or radiolabeled with ^{111}In to monitor tumour targeting properties *in vivo*. IC_{50} binding concentrations from the competition assay were 212 nM for the monovalent system, 356 nM for the divalent, and 50 nM for tetravalent dendrimer **1**. A decrease of the IC_{50} showed tetramerisation of the *c*[RGDfK] moiety resulted in enhanced affinity for integrin $\alpha_v\beta_3$ compared to the mono- and divalent dendrimers. Radiolabeled RGD-dendrimers demonstrated enhanced uptake in integrin $\alpha_v\beta_3$-expressing tumours, with the tetrameric form outperforming the monomeric and dimeric analogues.

Clearly the use of cyclic RGDs, however, led to all compounds having strong integrin binding, and little evidence of a multivalency effect – especially once it is noted that a 50 nM concentration of tetravalent dendrimer actually corresponds to a 200 nM concentration of ligand.

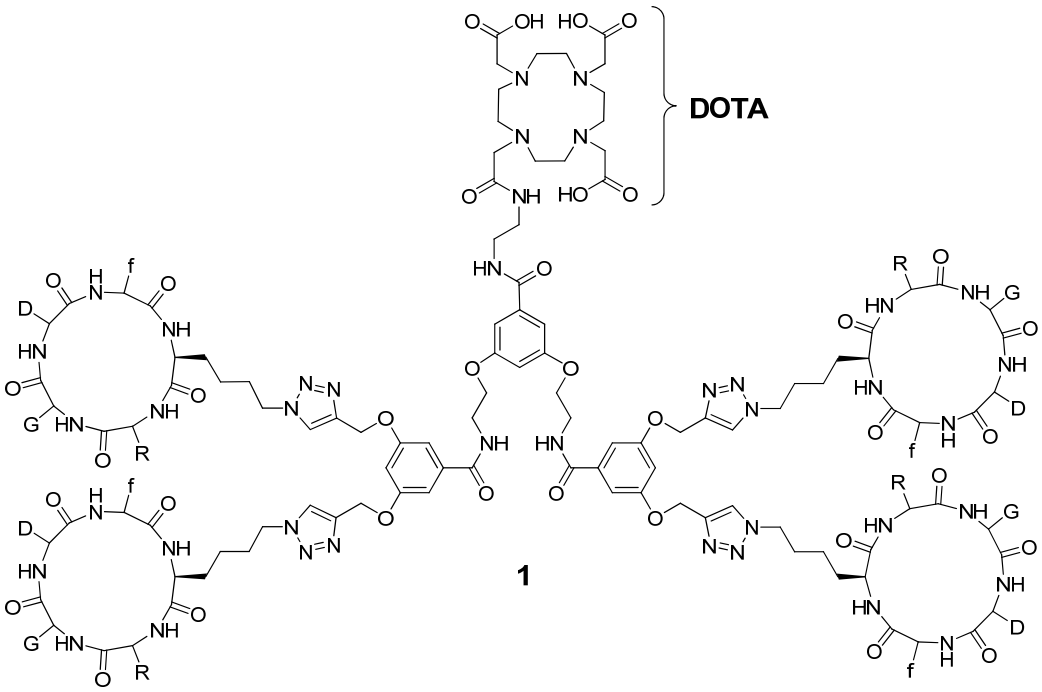

Fig. 1.14 – DOTA-conjugated, tetravalent *c*[RGDfK] peptide dendrimer **1**.

Dumy and co-workers have previously developed a tetravalent cyclic RGD-based structure termed RAFT(*c*[RGDfK])$_4$ (**2**) (Fig. 1.15).[128] This compound contains four copies of the *c*[RGDfK] ligand conjugated onto a cyclic decapeptide scaffold called a 'RAFT' (Regioselectively Addressable Functionalised Template[129, 130]). The advantage of the RAFT is that it presents two chemically addressable domains: i) an upper face for derivatising with targeting ligands; and ii) a lower face for labelling with an effector molecule. Spatial separation of the two domains in this bifunctional vector also helps prevent the effector from interfering with the targeting ligands. The labelling agent is a biomolecule (e.g. a fluorescent dye and/or cytotoxic agent) and the choice is dependent on the desired vectorisation strategy (i.e. imaging,[131-134] therapeutic effect[135] or a combination of the two[136]). Tumour neo-vasculature and integrin $\alpha_v\beta_3$-expressing metastases were specifically and efficiently targeted by compound **2** *in vivo*.[137]

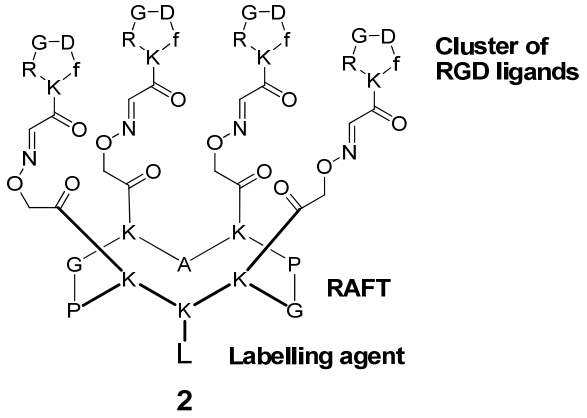

2

Fig. 1.15 – Tetravalent RAFT(*c*[RGDfK])$_4$ (**2**) conjugated to a label.

Dumy and co-workers then examined the multivalency effect and contribution of each *c*[RGDfK] motif in **2**, by synthesising an array of RAFT(*c*[RGDfK])$_n$ derivatives bearing one to four units of *c*[RGDfK] (compounds **3**-**6**) (Fig. 1.16), with inactive *c*[RβADfK] motifs substituting for *c*[RGDfK] when the number of *c*[RGDfK] motifs on the template was less than four (compounds **4**-**7**).[138] As such, each compound had comparable shape, steric hindrance and molecular weight, which was considered to be essential for comparing their activities *in vitro*. Competitive cell adhesion assays on $\alpha_v\beta_3$-expressing cells showed over a 250-fold enhancement in the relative potency of each *c*[RGDfK] peptide from monovalent **6** to tetravalent **3** (IC_{50} of >20000 nM and 19 nM respectively), demonstrating that a significant multivalency effect can be achieved when the target integrin proteins are supported in cell membranes.

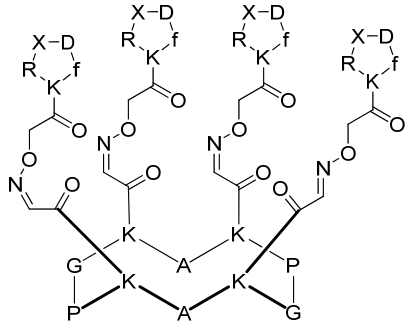

X = G or βA

3: RAFT(*c*[RGDfK])$_4$
4: RAFT(*c*[RGDfK])$_3$, RAFT(*c*[RβADfK])
5: RAFT(*c*[RGDfK])$_2$, RAFT(*c*[RβADfK])$_2$
6: RAFT(*c*[RGDfK]), RAFT(*c*[RβADfK])$_3$
7: RAFT(*c*[RβADfK])$_4$

Fig. 1.16 – Chemical structure of the RAFT(*c*[RGDfK])$_n$ ligands.

1.2.3.2 Self-Assembling RGD

An alternative and less synthetically laborious approach to multimerising an RGD-based peptide is to design lipopeptides, composed of a polar RGD head group and a non-polar lipophilic tail. These then spontaneously aggregate in water to form (or insert into) colloidal structures displaying multiple copies of integrin recognition sites. Bärmann and co-workers have shown that their lipopeptide **8** (Fig 1.17), bearing an RGD-containing cyclic hexapeptide, was able to insert into artificial membranes which subsequently gained enhanced affinity for integrin $\alpha_{IIb}\beta_3$.[139] Fluorescence microscopy and cryogenic transmission electron microscopy (cryo-TEM) were used to image the inter-vesicle cross-linking that resulted from the bridging of giant phospholipid vesicles decorated with **8** by smaller phospholipid vesicles decorated with integrin. The authors described the self-organising system as a new model of cell adhesion processes, allowing the systematic study of integrin clustering in focal adhesion complexes.

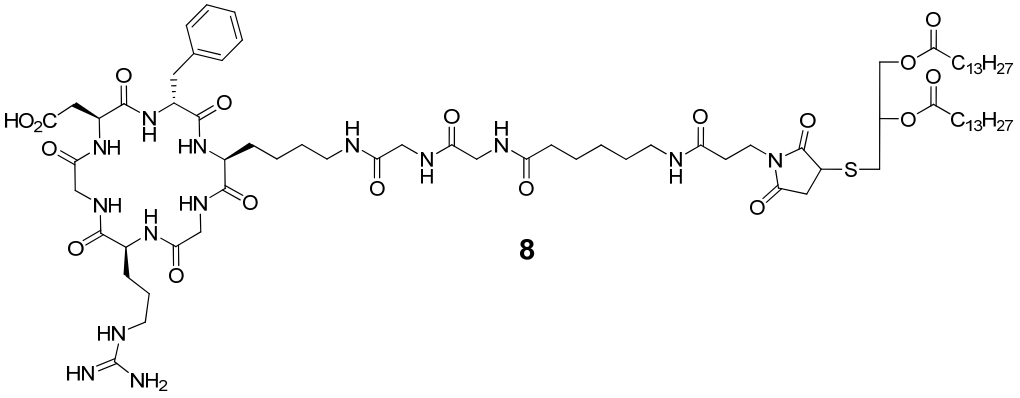

8

Fig 1.17 – Bärmann's RGD-lipopeptide **8** for the formation of membrane-anchored integrin ligands.

Marchi-Artzner and co-workers have also incorporated a similar lipopeptide (**9**) (Fig. 1.18) into artificial membranes of giant phospholipid vesicles, and demonstrated strong and selective tethering of these functional vesicles to substrate-bound endothelial cells, expressing $\alpha_v\beta_3$ and $\alpha_v\beta_5$ receptors, by imaging the behaviour of the system under a hydrodynamic shear flow.[140] Localised pinning contacts were observed, which the authors suggest are a result of integrin clustering induced by the RGD ligands. This was later confirmed by using fluorescence microscopy and fluorescent analogue **10** to visualise the segregation of the RGD ligands into these adhesion 'plaques'.[141] Furthermore, the vesicle-cell interaction can be abolished by saturating the integrin receptors of the cells with the water soluble pentapeptide *c*[RGDfK] prior to the addition of the RGD vesicles, further confirming that the observed adhesion arises from the specific recognition of lipid-coupled RGD by the integrin receptors.[140] Site-directed liposomal vectors for drug delivery to cells was suggested as a future application of this RGD-functionalised system.

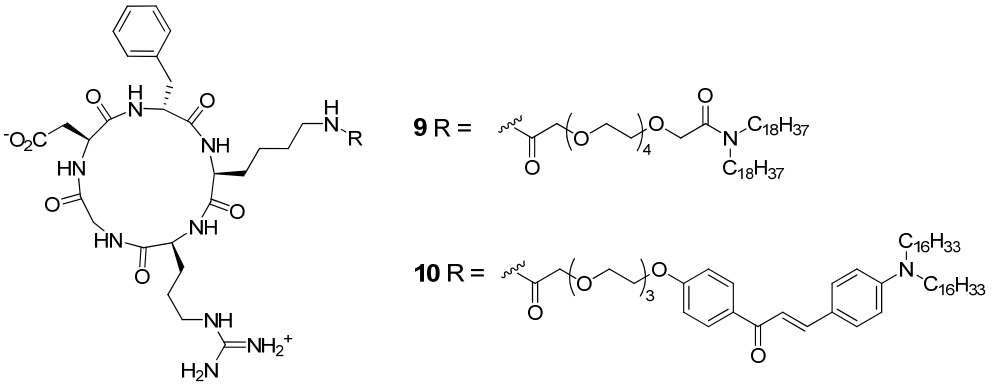

Fig. 1.18 – Marchi-Artzner's RGD-lipopeptides **9** and **10**.

Cell internalisation is also an important factor in the potential therapeutic success of RGD-directed liposomal drug delivery vehicles. Cressman and co-workers have addressed this with the synthesis of their elaborate looking RGD-lipopeptide **11** (Fig. 1.19), comprised of the targeting ligand *c*[RGDfK] conjugated via a linker to the lipid distearoyl phosphatidylethanolamine (DSPE), and incorporated this into phospholipid vesicles.[142] The construction of, what the authors term, well-defined liposomal nanoparticles (LNs) is also important in obtaining approval for clinical application. To this end, a fluorescent label, methoxycoumarin (MCA), was used to accurately quantify the amount of RGD-lipid incorporated into well-defined RGD-LNs. They then showed that increasing the amount of RGD-lipid in the RGD-LNs increased the affinity for $\alpha_v\beta_3$-expressing cells. Furthermore, the anti-cancer drug doxorubicin was loaded into the RGD-LNs and was efficiently delivered inside the cells. No internalisation was observed for non-RGD-displaying LNs demonstrating that the RGD motif plays an active role to enable trafficking into cells.

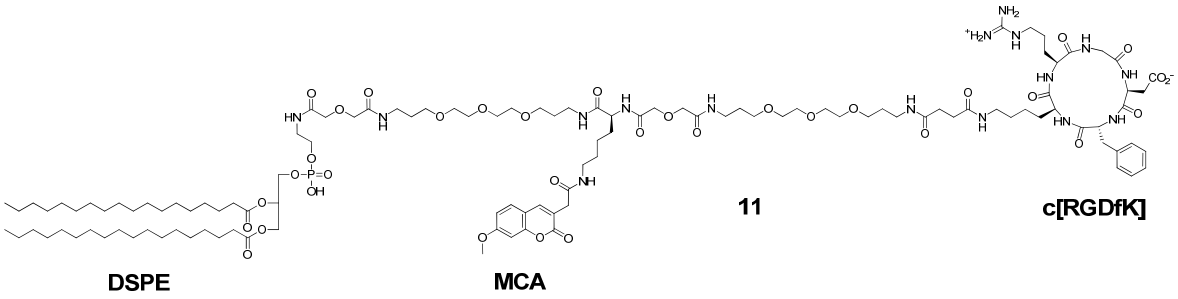

Fig. 1.19 – Cressman's RGD-lipopeptide **11**, comprised of *c*[RGDfK] conjugated to the lipid DSPE.

Self-assembling RGD-functionalised lipids have also been studied in their own right, without the presence of additional phospholipids to direct the assembly process. The synthesis and self-assembly of amphiphiles, such as **12** (Fig 1.20), comprised of linear RGD conjugated to varying extents to poly(ethylene oxide)-b-poly(butadiene) (RGD-PEO-PB or RGD-OB) block copolymer amphiphiles was studied using cryo-TEM by Bates and co-workers.[143] Aqueous dispersions of RGD-OB

copolymers, with different mole fractions of RGD and differing degrees of polymerisation of the O and B blocks, yielded a variety of structures such as spherical and cylindrical micelles, and multilamellar vesicles (Fig 1.20). Implications of this research for the design of site-directed micelles/vesicles for drug delivery was suggested in summary of the work.

Another example of an RGD-functionalised lipid self-assembling in its own right is provided in the work of Lee and co-workers who have reported a cyclic RGD-coated peptide nanoribbon as a selective intracellular nanocarrier (**13**) (Fig. 1.21).[144] A cyclic RGD pseudopeptide was amide-coupled to a β-sheet-forming peptide segment (FKFE), and this was shown to self-assemble into β-sheet-type nanoribbons using TEM (Fig. 1.21) among other studies. Intracellular delivery of hydrophobic guests, such as the fluorescent dye Nile Red, was achieved with cell lines expressing integrin receptors, whereas the negative-control *c*RDD-FKFE β-ribbon showed low uptake levels in comparison, successfully demonstrating the functionality and specificity of the *c*RGD-FKFE system and its potential use as a cancer-cell-specific, multivalent RGD-displaying drug carrier.

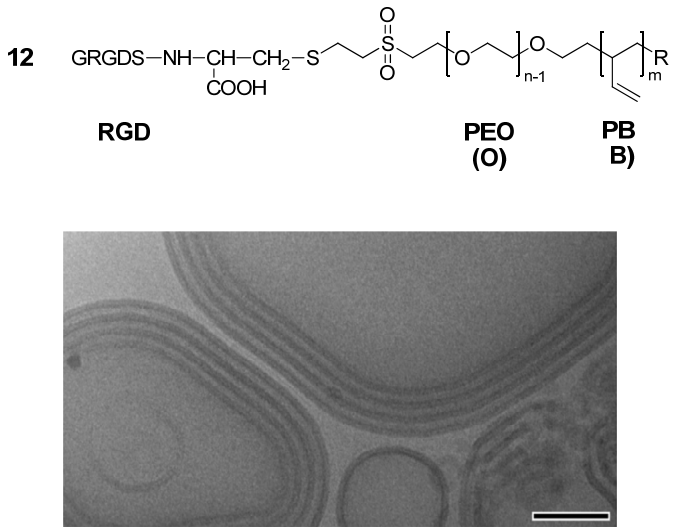

Fig. 1.20 – General structure of RGD-PEO-PB **12** and a cryo-TEM image of multilamellar vesicles formed from a 1 wt% aqueous dispersion of $RGD_{0.6}$-O_{28}-B_{46}. Scale bar = 100 nm. Image reproduced from reference 143.

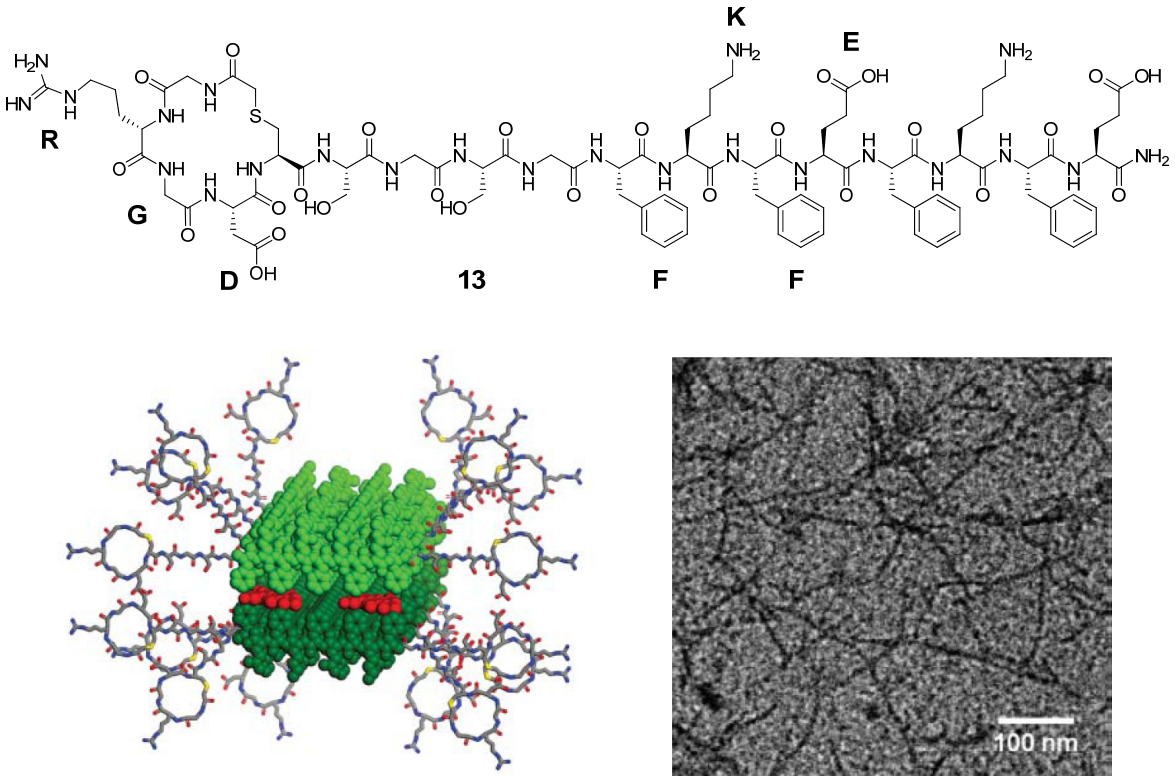

Fig. 1.21 – Structure of *c*RGD-FKFE, **13**, a model of β-ribbon formation by self-assembly of **13**, and a TEM image of the β-ribbons. Images reproduced from reference 144. Original in colour.

Much interest has surrounded understanding, fundamentally, how self-assembly can enhance multivalent interactions with biomolecules, such as glycoproteins,[145-147] collagen[148] and DNA,[149-153] however, it is fair to say that as the limited examples described above indicate, relatively little is known about this phenomenon in fundamental terms for multivalent RGD-integrin interactions.

1.3 Hydrogels

In recent years, a growing area of nanotechnology-themed research has focussed on developing sophisticated soft matter systems, comprised of self-assembled molecular building blocks which respond to some external stimulus and/or impart some functionality onto the materials rendering them useful for a diverse range of advanced and specialised applications.[154, 155] For example, the groups of Stupp and Ulijn, among others, have developed self-assembling soft materials (hydrogels) and they have shown that incorporating RGD peptides into the structure, encouraging cell adhesion, can enhance the tissue engineering properties of the material.[156-158] Soft, gel-like materials have therefore featured heavily in the development of novel biomaterials for wound healing and other applications in regenerative/therapeutic medicine.

A "gel" is generally defined as being comprised of at least two components: a liquid (solvent) dispersed and retained in a sample-spanning, fibrous solid network (the gelating agent) which provides

structure to the liquid phase. The material does not flow under gravity due to physical effects, such as surface tension and capillary forces; it retains its shape upon applying small stress forces; and it is this solid-like rheological behaviour that defines a gel. *Hydro*gels are comprised of water as the immobilised phase, whereas *organo*gels are made up of organic solvent/s. We will focus predominantly on the more biologically-relevant hydrogels, as organogels are beyond the scope of this introduction and have been extensively reviewed elsewhere.[159-162]

Traditionally, hydrogel scaffolds often comprise a natural or synthetic covalent polymer, such as a polysaccharide (e.g. alginate[163]) or cross-linked PEO,[164] respectively. Inter-chain cross-linking, by either covalent or non-covalent interactions, induces the formation of an insoluble (or partially soluble) fibrous matrix, resulting in a polymeric gel (Scheme 1.1A). Alternatively, supramolecular gels (also known as molecular or physical gels) can be formed from the non-covalent self-assembly of small well-defined molecules, so-called low molecular weight gelators (LMWGs).[165-168] The self-assembly process induces the formation of individual fibrils (thought of as supramolecular polymers) which aggregate into fibres, with subsequent entanglement leading to the 3D gel network and immobilisation of the solvent (Scheme 1.1B). Scheme 1.2 depicts this self-organising ('bottom-up') fabrication of a gel with respect to peptide conjugate hydrogelators.[169] Remarkably, even a small amount of hydrogelator (e.g. 1% by weight) can effectively immobilise the solvent. The high versatility of peptide-based molecular hydrogels, in part due to the ability to synthetically tune gel functionality by simple variation of the amino acids used,[170] and the biocompatibility of such materials renders them useful for a number of applications, ranging from controlled drug delivery (the scaffold or immobilised water can be used as a reservoir for drug molecules),[171-173] to regenerative medicine and tissue engineering (the artificial 3D scaffold can be used to support the adhesion and growth of cells, playing a similar role to the natural 3D scaffold of the ECM).[174-177]

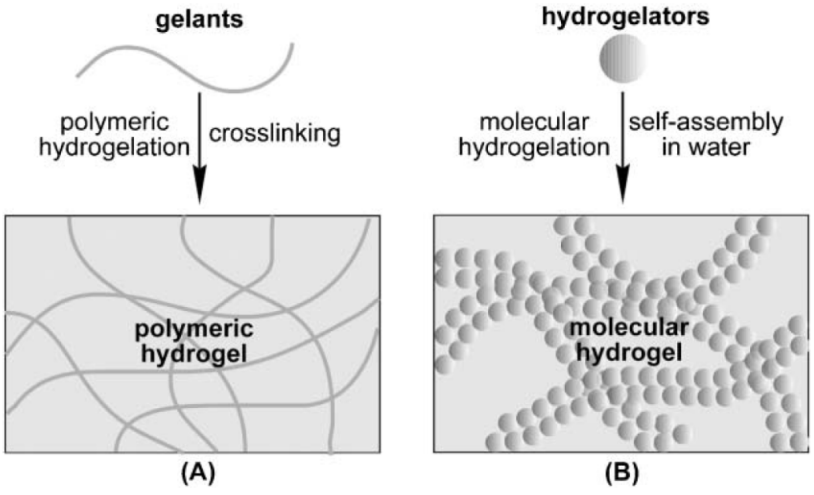

Scheme 1.1 – Schematic of A) a polymeric hydrogel, and B) a molecular hydrogel. Image reproduced from reference 178.

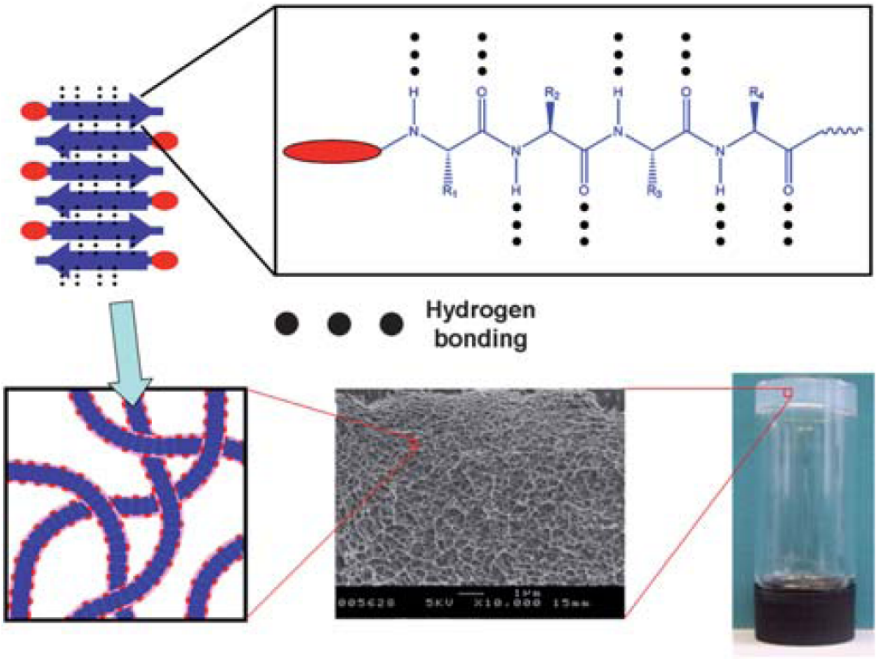

Scheme 1.2 – 'Bottom-up' fabrication of a hydrogel from the self-assembly of peptide-conjugates in water, via non-covalent forces, leads to the formation of fibrous structures, in this case anti-parallel β-sheets. Entanglement leads to the 3D hydrogel network, as seen under the scanning electron microscope (SEM), and the sample survives the 'inversion test'. Image reproduced from reference 169. Original in colour.

There are a number of advantages that LMWGs have over polymeric gels, especially when considering the biological applications of hydrogels:

i. Polymeric gels often require a cross-linking step in the presence of a bifunctional monomer initiated by UV radiation or radical/redox chemistry – harmful to encapsulated cells, and difficult to incorporate a drug which could potentially react with the cross-linker, hence addition post-cross-linking is required which can have drawbacks such as low loading levels. LMWGs can be designed to induce gel formation under comparatively much milder conditions, hence encapsulation *in situ* is tolerated.

ii. Sol-gel reversibility (a "sol" is a dispersion of discrete particles within a liquid) is possible by disrupting the non-covalent interactions, such as hydrogen-bonding, electrostatics, π-stacking and hydrophobicity, which underpin gel formation. Temperature, pH, light, ultrasound, ionic strength, oxidation/reduction state, presence of small molecules or enzymes are examples of physical or chemical stimuli which can affect the transition of a gel to a sol (or vice versa), depending on the nature of the LMWG, by altering its macromolecular structure.[179] This is particularly advantageous when controlled breakdown of the gel is necessary to isolate encapsulated cells or deliver a drug, for example.

iii. Changes to the structural design of LMWGs allows for systematic studies into the effect of this 'molecular tunability' on gel fibre morphology and functionality.[180] This also allows, at least in principle, the incorporation of biologically active units readily into the gelator network.

Materials that are able to respond to changes in their biological environment, when mixed with, or conjugated to, therapeutic drugs or bioactive molecules, have the potential to read-out or instigate biochemical signalling.[181] Hydrogels as controlled drug delivery vehicles,[182] either by passive diffusion or triggered release, can obviously be used in this manner.[183] The molecular gels investigated in this thesis are based on stimuli-responsive LMWGs containing the biologically-relevant RGD motif, which are able to release an encapsulated agent. It is for this reason that the following sections review the properties and applications of some exemplary RGD peptide conjugate hydrogelators, as well as other stimuli-responsive gelators.

1.3.1 RGD Peptide Conjugate Hydrogelators

Pre-requisites in the design of new biomimetic scaffolds for the 3D culture of cells, such as mimics of complex ECMs, are that the systems be simple, cheap, robust and reproducible, while still providing the essential function of a natural ECM in its ability to anchor and control cell behaviour. Natural ECMs serve multiple biological roles and are comprised of a 3D network of interwoven protein-based nanofibres which contain many different bioactive groups to interact with cells.[184] As such they prove to be challenging targets for materials synthesis. Hydrogels comprised of self-assembling peptides (and related structures) can be used to mimic natural ECMs as the nanofibrous networks are similar in both architectures.[174, 179, 185-191] Biofunctionality may be installed by conjugating bioactive ligands to the hydrogelator molecule, and upon self-assembly these are usually presented as flexible surface groups on the nanofibres.[156, 175, 192, 193] One such ligand is the RGD peptide, desirable because of its cell adhesive properties. It has been demonstrated that the incorporation of the RGD ligand into polymeric or supramolecular substrates enhances cell adhesion, spreading and proliferation.[42, 156, 193-196] Density and lateral spacing of the RGD ligand have been shown to be two important parameters for the enhancement of cell adhesion.[197, 198] Cell adhesion and motility are also influenced by nanoscale RGD clustering and configuration where RGD clusters and cyclic RGDs have been used.[108, 193]

Here, we will review the two main classes of low molecular weight RGD peptide conjugates that have been shown to be efficient hydrogelators. Specifically, RGD conjugated to an aromatic group such as Fmoc, and RGD peptide amphiphiles (PAs, where a hydrophobic chain is conjugated to a hydrophilic RGD head group). Polymer-peptide conjugate hydrogelators containing multiple copies of a short and well-defined RGD peptide block are also well known in the literature, but the reader is directed elsewhere as these are not classed as LMWGs.[199-206]

1.3.1.1 RGD Conjugated to an Aromatic Group

A number of reports demonstrate that some dipeptides conjugated to a hydrophobic, π-stacking group can act as efficient hydrogelators. Suitable functional groups include naphthalene,[178] Fmoc[207] and pyrene[208] (Fig 1.22). The most widely studied of these is Fmoc-diphenylalanine (Fmoc-PhePhe, **17**, Fig. 1.22), first reported in 2006 by the groups of Gazit[209] and Ulijn,[190] in part due to its hydrogelation at physiological pH making it suitable for biological applications. However, one drawback of this design, is the incorporation of polyaromatic groups, which are known to be carcinogenic.

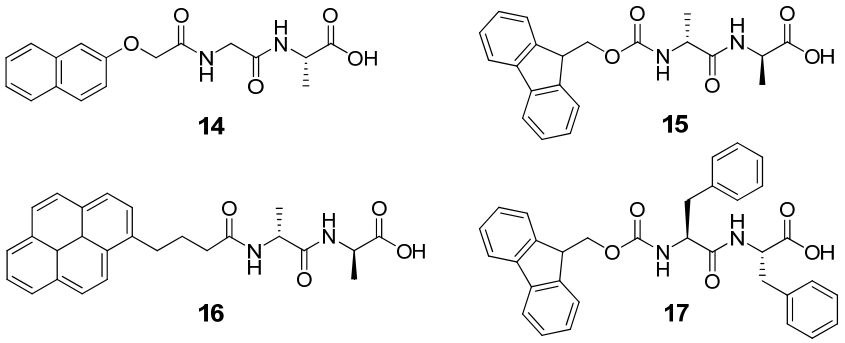

Fig. 1.22 – Example structures of *N*-functionalised dipeptide gelators: naphthalene-dipeptide (**14**),[178] Fmoc-D-Ala-D-Ala (**15**),[207] pyrene-D-Ala-D-Ala (**16**),[208] and Fmoc-PhePhe (**17**).[190, 209]

Ulijn and co-workers have expanded upon their previous work on Fmoc-FF (**17**), which dissolves in alkali solutions and forms gels (10-20 mM) at 37°C when the pH is lowered to 7.0, by co-formulating it with their corresponding hydrogelator Fmoc-RGD (**18**) (Fig 1.23), which on its own dissolves in acidic solutions and forms gels (10-20 mM) when incubated at pH 3.0 between 4-25°C, but is unstable at higher pH and temperatures.[158] In this way, they developed two-component molecular hydrogels that were both bioactive and stable under physiological conditions: mixing 20 mM Fmoc-FF (pH 10) and 20 mM Fmoc-RGD (pH 3) in different volume ratios gave rise to translucent hydrogels at 37°C/pH 7.0 (Fig. 1.24), Fmoc-FF acting as a supporting/host gel at this temperature and pH. The Fmoc-FF/RGD building blocks act as structural components – the FF and RGD peptides self-assemble into β-sheets interlocked by π-π stacking of the Fmoc groups – while the RGD sequence plays a second role as a bioactive ligand on the nanofibre surface, enhancing its accessibility and bioavailability and therefore mimicking essential features of the ECM. Addition of cell culture medium increased gelation kinetics, presumably due to charge screening by the metal ions within the medium reducing molecular repulsion between charged residues, and in 1 min, self-supporting gels were formed. This material was found to promote adhesion of encapsulated anchorage-dependent cells via specific RGD-integrin interactions, followed by cell spreading and proliferation. The density of RGD surface groups was tuned by adjusting the ratio of Fmoc-RGD co-formulated with Fmoc-FF: in the

hydrogels with ≥30% RGD, adequate cell spreading was found to occur with over 90% spread cells; dropping to less than 50% with ≤20% RGD; and cells maintained a round morphology with 0-10% RGD. Gels containing the control peptide Fmoc-RGE did not induce cell spreading.

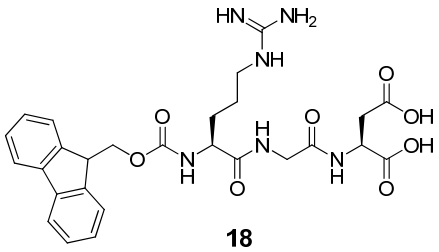

18

Fig. 1.23 – The structure of Fmoc-RGD (**18**).

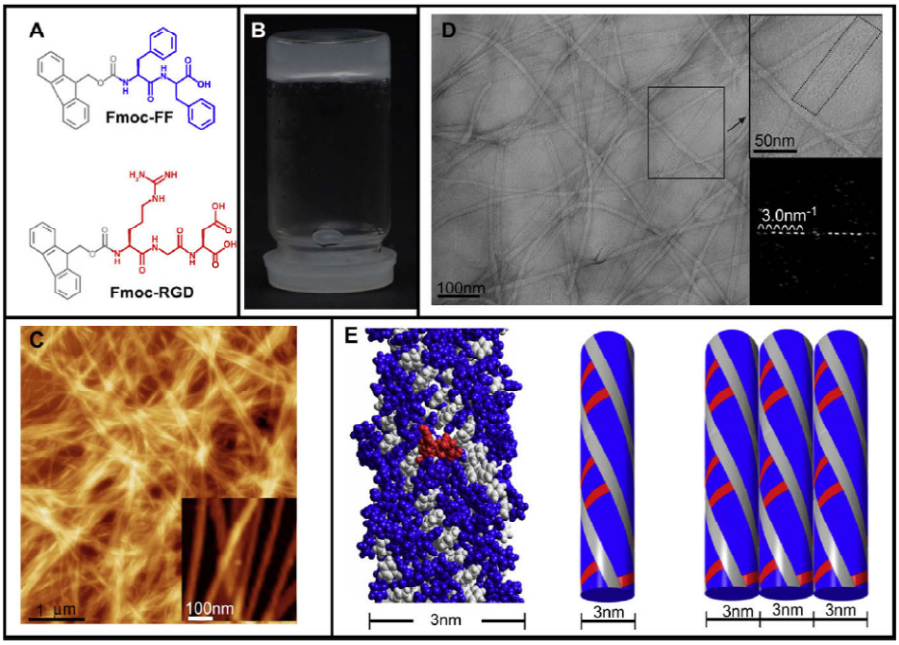

Fig. 1.24 – A) The structures of Fmoc-FF and Fmoc-RGD. B) The self assembled translucent hydrogel of Fmoc-FF/RGD at pH 7.0 and 37°C. C) The atomic force microscopy (AFM) height image of the entangled nanofibrous structure. D) The TEM image showing the nanofibres as 'flat ribbons', made up of 3 nm wide fine fibrils. E) The proposed supramolecular model of the 3 nm fibrils, with RGD ligands (red) presented on the surface. Image reproduced from reference 158. Original in colour.

It should be noted that Gazit and co-workers also tried to prepare hydrogels from Fmoc-RGD.[210] Their method of hydrogel preparation was to make a concentrated sample of the Fmoc-peptide in DMSO and then dilute with water to a final concentration. Upon doing so a hydrogel would form for some of their Fmoc-peptides but not for Fmoc-RGD which remained a clear solution. However, as

the authors noted, Ulijn and co-workers showed that Fmoc-RGD forms transparent hydrogels at pH 3,[158] further confirming that hydrogel formation for this compound is pH dependent.

1.3.1.2 RGD Peptide Amphiphiles

A "peptide-amphiphile" (PA) is generally regarded as being a molecule with a hydrophilic peptide head group covalently attached to a hydrophobic aliphatic chain (Fig 1.25). Conventional PAs have the alkyl chain attached to the *N*-terminus of the peptide leaving the *C*-terminus free.[211] Conversely, reverse PAs have the alkyl chain attached to the *C*-terminus and the *N*-terminus is free.[212] Two other types of PA include amphiphilic oligopeptides (where the constituent amino acids provide the hydrophilic and hydrophobic character),[213-215] and block copolypeptides, although the latter is beyond the scope of this introduction and the reader is directed to the work of Deming.[216, 217] Protein-based hydrogels,[218-220] including ones which are RGD-functionalised,[221] are also known but will not be discussed. Lowik and van Hest have published an excellent tutorial review on the different types of peptide-based amphiphile.[222]

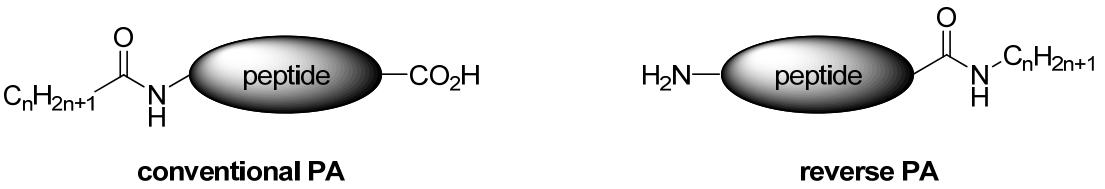

Fig. 1.25 – Conventional and reverse peptide amphiphiles.

PAs behave in a similar way to conventional amphiphilic molecules (the hydrophobic domains are buried within the core of the colloidal structures that form as a consequence of reducing unfavourable interactions with the surrounding water molecules[32, 33]). Depending on the nature of the hydrophobic and hydrophilic portions and the balance of the two in the structure, cylindrical micelles can form which propagate into nanofibres. If the concentration of the PA is high enough, then entanglement of the nanofibres occurs and a hydrogel is formed. The advantage that PAs have over conventional block copolymer amphiphiles is that the peptide sequence (in addition to the alkyl chain length) plays an important role in controlling the self-assembly, physical, chemical and biological properties of the hydrogel. Modifying the peptide (sequence, length, branching, charge etc), and/or the alkyl chain length,[212] can fine-tune or dramatically alter any of these properties.

Pioneering work by Stupp and co-workers involved the synthesis of their RGD-bearing PA hydrogelator **19** (Fig. 1.26).[211] This PA at a concentration >2.5 mg/ml dissolved in water at pH 8 and formed self-supporting gels when the solution was acidified with HCl to below pH 4, but redissolved on addition of KOH to neutral pH. Oxidation of the cysteine thiol groups to form disulfide links allowed for enhancement of the hydrogel structural integrity via interfibre cross-linking, resulting in

stable gels even at pH 8. Cross-linking was reversible under reductive conditions and the gel disassembled. This pH-induced self-assembly and covalent capture was used to generate a nanofibrous scaffold reminiscent of collagen in ECM. Post cross-linking, the fibres were able to direct mineralisation of calcium hydroxyapatite (HA) (the inorganic component of assemblies in bone and teeth). Saturation of the fibre surface with calcium ions, arising from the calcium binding ability of the pendant phosphorylated serine residue, nucleated HA crystallisation and growth of the crystal axes along the long axes of the fibrils was observed – much like the growth of HA within the collagen fibrils of bone tissue during natural biomineralisation. Clearly, the authors had already thought about using the 3D scaffold for cell adhesion and growth, therefore the RGD sequence of the collagen-associated protein, fibronectin, was included in their PA design to demonstrate the ability to functionalise the fibre surface with additional bioactive ligands. However, no cell culture studies were undertaken in this instance.

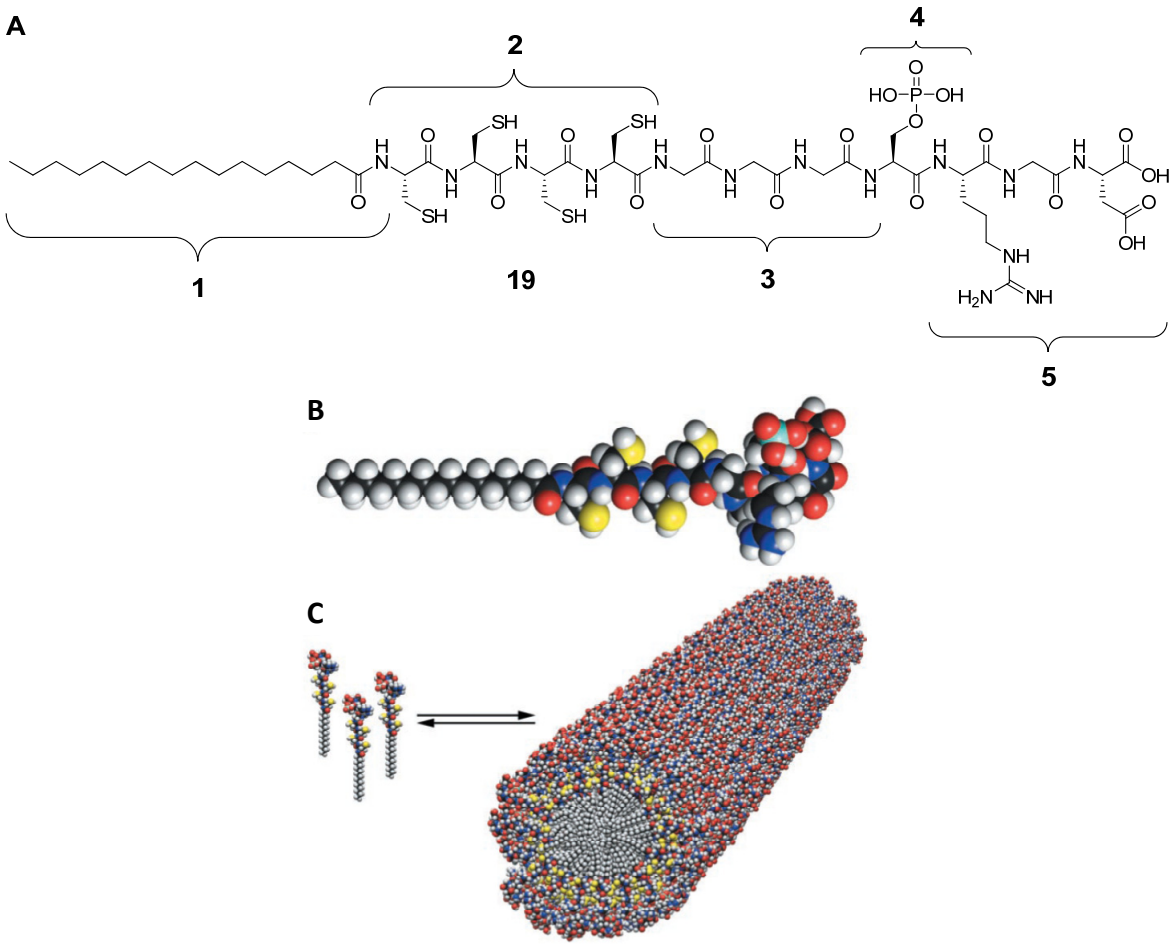

Fig. 1.26 – A) Chemical structure of Stupp's PA (**19**), highlighting five key structural features. Region 1 is a hydrophobic alkyl tail. Regions 2-5 are different peptidic domains important for cross-linking, flexibility, calcium binding, and cell adhesion, respectively. B) Molecular model of the PA. C) Self-

assembly of the PAs into a cylindrical micelle. Image reproduced from reference 211. Original in colour.

Hartgerink and co-workers then simplified the structure of **19** and systematically generated 26 PA variants in order to deduce the design rules that are necessary for effective self-assembly of PAs into hydrogels.[223] One of these, **20**, is shown in Fig 1.27. Hydrogels were prepared at 2 wt% concentration, either at acidic pHs (below 4.5) or in the presence of Ca^{2+} ions at pH 7.4 which quenched the negative charges on the PA, eliminating repulsive forces between molecules and allowing self-assembly to occur. Three distinct regions in the structure were required: i) a C16 hydrophobic tail (although the length depends on the peptide head group[187]), ii) a glycine linker region in which the first four residues are critical for β-sheet hydrogen-bonded formation of the nanofibres (deduced by sequential *N*-methylation of the glycine amide bonds), and iii) a conformationally flexible peripheral ligand for bioactivity. Inhibition of β-sheet formation by disrupting the intermolecular hydrogen bonding of residues 1-4 yielded spherical micelles rather than nanofibres and loss of gel behaviour. Residues 5 and above were found to have little effect on the aggregate morphology; this region could therefore be used to 'dial-in' bioactivity into the hydrogel by conjugating the appropriate ligand depending on the desired application, in this case an adhesion sequence (RGDS). This work helped clarify the mechanism of PA self-assembly (the role of hydrogen bonding and amphiphilic packing) into cylindrical nanofibres, and laid the foundations for future PA hydrogelator design.

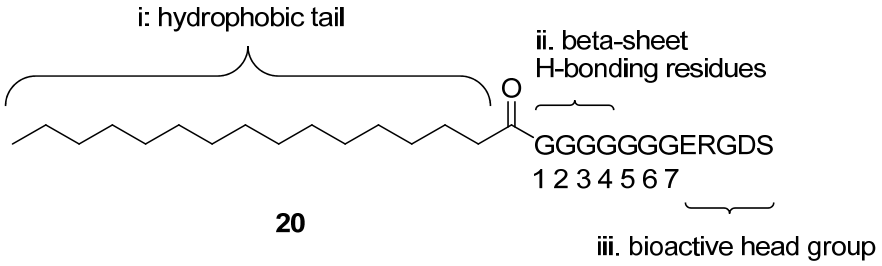

20

Fig. 1.27 – Schematic representation of PA **20**. The molecule has three distinct regions: i) a hydrophobic alkyl tail, ii) a glycine linker region (residues 1-7), and iii) a charged, bioactive head group.

Additionally, Stupp and co-workers have also presented RGDS epitopes on self-assembled nanofibres of elaborate-looking *branched* PAs, such as compound **21** (Fig. 1.28).[156] Gels were prepared at 1 wt% concentration (pH 7.4) and aggregation into cylindrical nanofibres was demonstrated by TEM (Fig. 1.29, left). Fluorescence anisotropy experiments on a derivative of **21**, in which the RGDS head group contained an additional tryptophan residue, showed that the head group was more mobile in the supramolecular aggregates formed from these branched-type structures compared with a linear analogue due to differences in packing; thereby enhancing its accessibility for protein binding. Self-supporting gels were also formed in physiological fluids such as synovial fluid (Fig. 1.29, right); robustness to environmental media which is necessary for applications in biomedicine. In a separate

study, self-assembled PA **21** was coated onto a traditional covalent PGA (poly(glycolic acid)) scaffold in a bid to make it more bioactive.[157] Human bladder smooth muscle cells demonstrated enhanced adhesion in the first few days of the culture period to scaffold coated with **21** than to bare scaffold or to scaffold coated with a linear PA analogue, presumably due to lower availability of the RGDS peptide in the linear version.

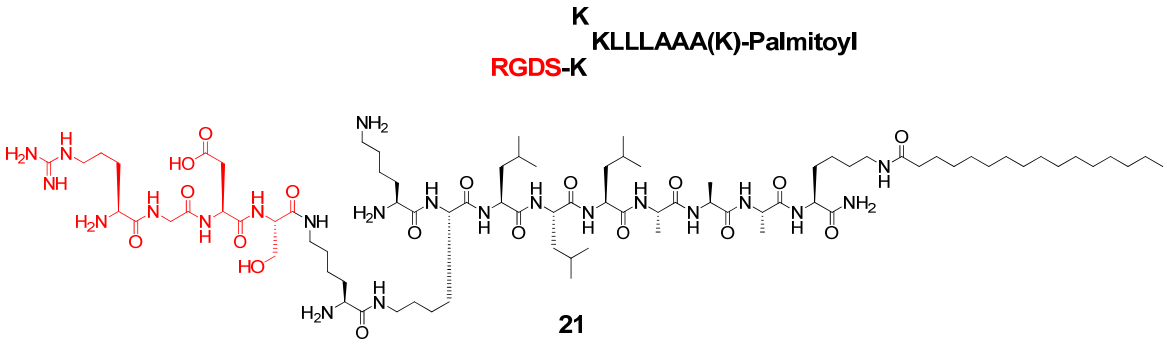

Fig. 1.28 – RGDS presented on branched PA **21**. Original in colour.

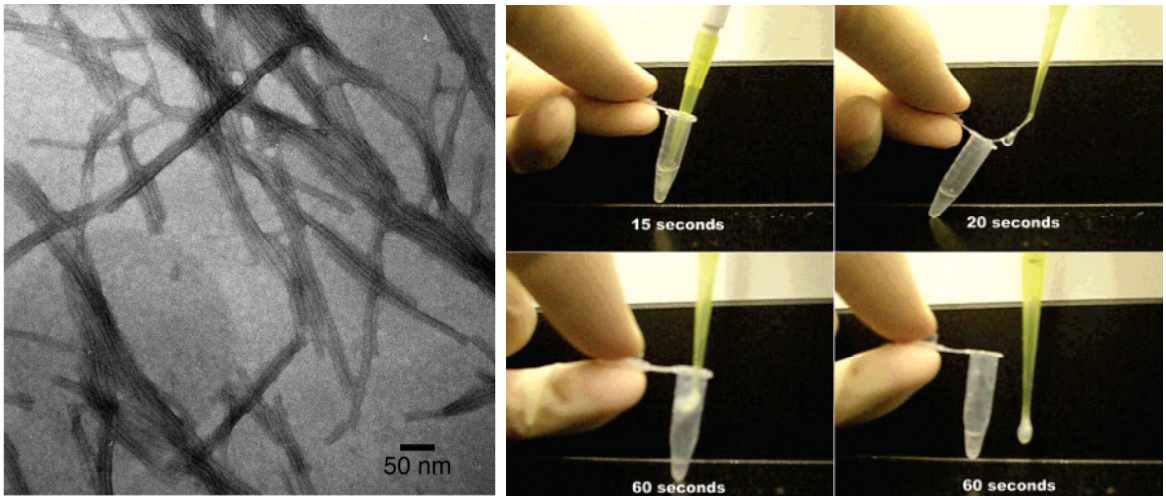

Fig. 1.29 – Left: TEM image of a 1 wt% gel of **21** at pH 7.4. Right: Images of a gel formed upon mixing 1:1 volumes of bovine synovial fluid and a 1 wt% solution of **21**. Image reproduced from reference 156. Original in colour.

Amphiphilic oligopeptides (where the constituent amino acids provide the hydrophilic and hydrophobic character) have also been used to study hydrogel formation. Ellis-Behnke *et al* have developed a hydrogelating peptide called RADA16-I (**22**), comprised of four blocks of repeating Arg-Ala-Asp-Ala (RADA) residues (Scheme 1.3), in which the *N*-terminus is acylated (Ac-) and the *C*-terminus is a primary amide (-NH_2).[224] The sequence is similar to RGD and was found by the authors in previous work to not only support the growth of certain cell lines, but also supports neuronal

growth. The positive and negative charge-bearing arginine and aspartic acid residues, respectively, project from one side of the molecule – the hydrophilic face; and the alanine residues from the other side – the hydrophobic face. This self-complementary peptide (dissolved at 1 wt% in water) self-assembles into hydrogels in physiological fluids, owing to charge screening by ions in the fluid. Impressively, when a solution was injected into the severed optic nerve part of the brain of hamsters (causing *in situ* gel formation), the blinded animals regained ~70% of their response time to a stimulus (as compared with control animals) just 6 weeks after implantation. This material exemplifies the successful use of peptide hydrogels *in vivo* for, in this case, nerve regeneration.

Ac-RADARADARADARADA-NH_2 **RADA16-I** (**22**)

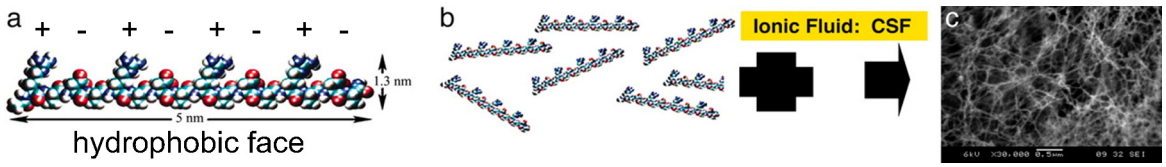

Scheme 1.3 – a) Molecular model of the RADA16-I building block (**22**), b) molecular model of RADA16-I molecules undergoing self-assembly into nanofibres in ionic fluids, c) SEM image of the nanofibres. Image reproduced from reference 224. Original in colour.

1.3.2 Other Stimuli-Responsive LMWGs

As shown with the previous examples, most molecular hydrogelators undergo a gel-sol phase transition on increasing temperature and, in cases where ionisable groups are present in the structure, to changes in pH. Expanding the reversible gel-sol/sol-gel responsive nature of these "smart" nanostructured materials to other external stimuli has allowed researchers to access an array of other sophisticated materials for potential applications, in addition to those already mentioned, such as pollutant capture and removal,[225] semi-wet sensor chips,[226] logic gates,[227] microfluidic valves,[228] nanoreactors,[229] and so on. Indeed, supramolecular gels are ideal for applications where responsivity is required because they are held together by multiple weak non-covalent interactions which can be overcome by putting energy or a competing molecular species into the system. By incorporating the appropriate building block into the gelator structure, triggered response to external stimuli such as UV/visible light, enzymes, complimentary host-gelator interactions, and anions/cations can be achieved.

1.3.2.1 Enzyme-Sensitive Gelators

Enzymes can be used to trigger hydrogelation, whereby a precursor molecule (a masked gelator molecule or "pro-gelator") when mixed with an appropriate enzyme undergoes catalytic enzymatic modification of its structure to form an unmasked gelator which can then self-assemble in water.[230-233]

Xu and co-workers have developed a simple visual assay based on small molecule hydrogels for detecting inhibitors of enzymes.[234] They used an acid phosphatase enzyme to convert an aqueous solution (at pH 6.0) of **23** (the substrate) into product **24** (Scheme 1.4) – when the phosphate group was hydrolysed the molecule became more hydrophobic and self-assembly into a hydrogel proceeded. However, blocking the active site of the enzyme by introducing an inhibitor resulted in loss of gel formation as the hydrophilic phosphate head group remained intact. The same principle could also be applied in the detection of the presence of other enzymes by incorporating the appropriate ligand into the precursor substrate, as long as a gel-sol transition took place upon structural modification by the enzyme.

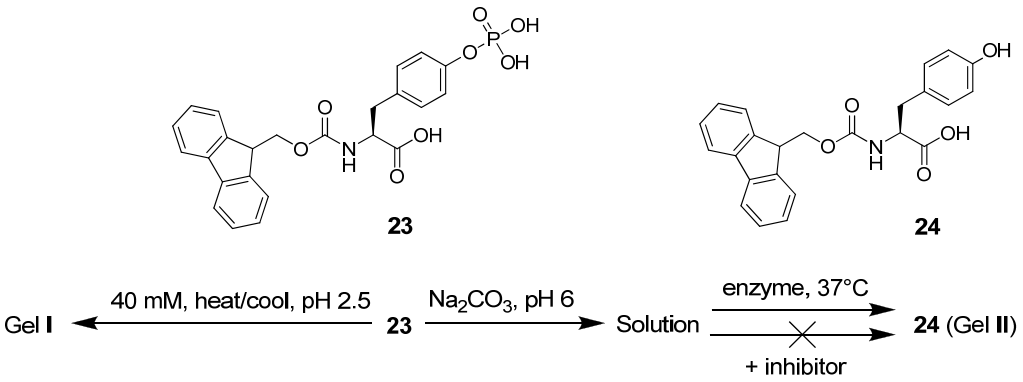

Scheme 1.4 – The chemical structures of the molecules for hydrogelation and a schematic of the gelation process.

The same group have used this approach using gelators with a β-lactam ring in the structure and a β-lactamase enzyme to detect penicillin-resistant strains of bacteria.[235] **25** is the precursor substrate and β-lactamase triggers hydrogelation upon opening the β-lactam ring (Scheme 1.5). Product **26** is more hydrophobic after the hydrophilic β-lactam portion of the molecule has been cleaved and self-assembly in water subsequently occurs to afford the hydrogel. β-lactamases in bacteria hydrolyse the β-lactam ring of penicillin, rendering it inactive, and therefore gelation in the presence of a particular microbe is a simple visual indication of its penicillin resistance.

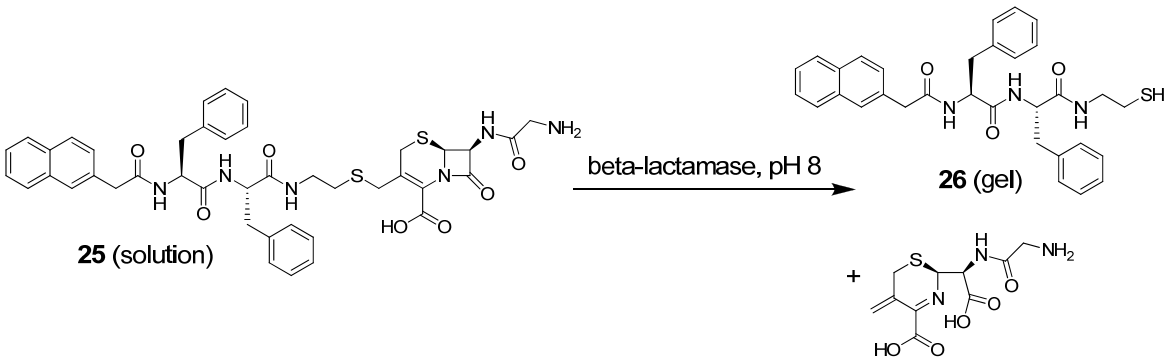

Scheme 1.5 – The chemical structure of **25** and its conversion to hydrogelator **26** in the presence of β-lactamase.

1.3.2.2 Host-Guest Gelators

Xu and co-workers have also reported that molecular recognition of dipeptide hydrogelator Fmoc-D-Ala-D-Ala (**15**, shown previously in Fig 1.22) by vancomycin (known to have a strong ligand-receptor interaction with D-Ala-D-Ala) modified the self-assembly properties of the hydrogelator. By making it more polar upon binding and, more importantly, competing with the intermolecular hydrogen bonding between gelator molecules, gelation was inhibited as a result (Scheme 1.6).[207] Conversely, there was no effect on the gel formed by Fmoc-L-Ala-L-Ala after vancomycin was added, demonstrating that the amino acid configuration is important in host recognition of a hydrogelator and modulation of its stability.

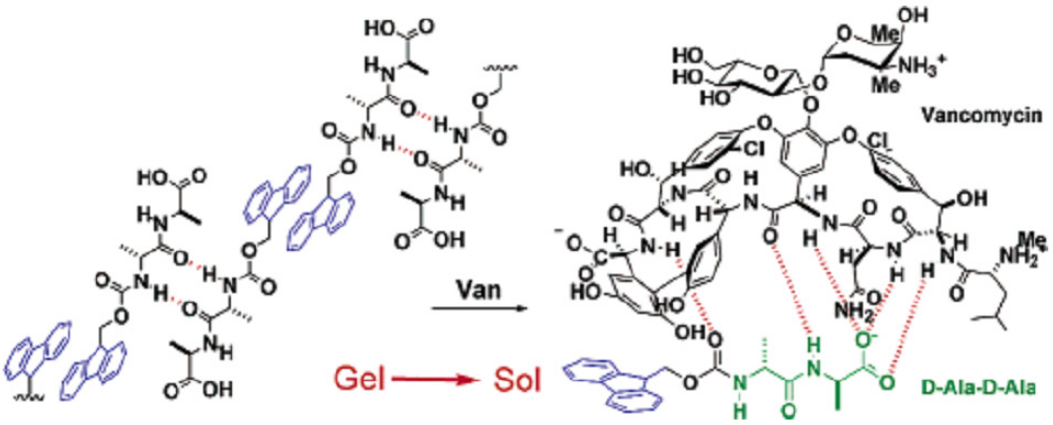

Scheme 1.6 – Possible ligand-receptor interactions between Fmoc-D-Ala-D-Ala (**15**) and vancomycin that induce the gel-sol phase transition, as proposed by Xu and co-workers. Image reproduced from reference 207. Original in colour.

In a separate study, swapping the Fmoc group in Fmoc-D-Ala-D-Ala for pyrene (**16**, shown previously in Fig 1.22) resulted in a 10^6-fold enhancement in hydrogel stiffness from pyrene-D-Ala-D-Ala gelator alone (G' = 0.12 Pa, where G' is known as the elastic (or storage) modulus and is a measure of the elastic behaviour of a gel) to that of the pyrene-D-Ala-D-Ala/vancomycin gelator complex (G' = 160000 Pa).[208] The rationale: intermolecular hydrogen bonding of the dipeptide and π-π stacking of the pyrene group results in supramolecular polymer chains which are non-covalently cross-linked upon binding of the dipeptide by vancomycin due to self-association of the host, resulting in increased rigidity of the supramolecular framework. Furthermore, pyrene-L-Ala-L-Ala gave only a 10-fold increase in G' when vancomycin was added in comparison to the gelator alone.

1.3.2.3 Ion-Responsive Gelators

Owing to the plethora of biologically- and environmentally-relevant cations and anions, much interest has surrounded metal- and anion binding supramolecular gels that induce either breakdown or

formation of the gel structure.[236] It is known that gelator molecules containing crown ethers respond to cations, such as organogelator **27** (Fig 1.30). Shinkai and co-workers have shown that **27** is able to gel a range of organic solvents, and with progressive addition of K^+ up to 1 equivalent the gel phase maintained its stability – one or fewer crown ethers complexes K^+ in the same molecule and electrostatic repulsion is less of an issue as, statistically, bound K^+ does not exist in crown units which are in close proximity to one another. However, addition of more than 1 equivalent of K^+ resulted in a gel-sol transition due to complexation of K^+ by one or both crown ethers in the same molecule, and electrostatic repulsion between neighbouring gelator molecules resulted in destabilisation of the self-assembled network.[237] This result is in accordance with the gel breakdown in the presence of K^+ ions observed by Smith and co-workers with their crown ether-functionalised dendritic organogelator **28** (Fig 1.30).[238]

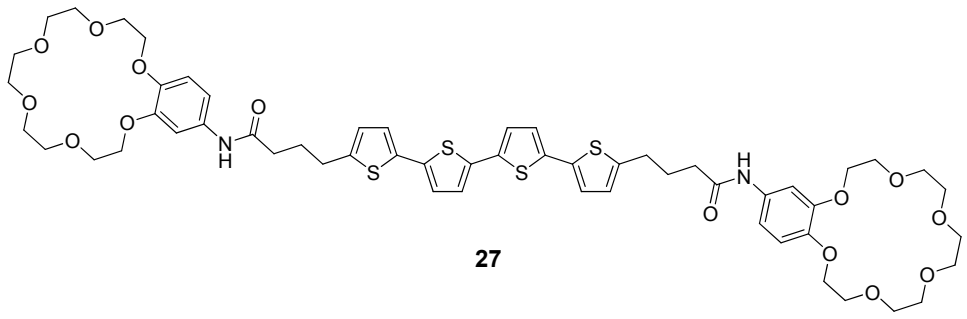

27

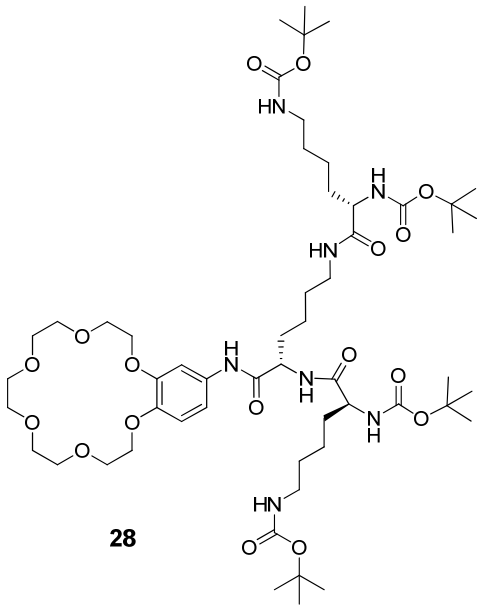

28

Fig 1.30 – Shinkai's oligothiophene organogelator **27**, and Smith's crown ether functionalised dendritic organogelator **28**.

Alternative to the above example, some researchers have used metal ions to improve gel stability and/or rate of formation. In recent work, Huang and co-workers have studied hydrogel formation by

the naturally occurring bile salt sodium cholate (SC, **29**) (Fig, 1.31) in the presence of La^{3+} metal ions.[239] Unique temperature-dependent supramolecular self-assembly was found to occur in that hierarchical 1D nanostructures were formed depending on the temperature: nanotubes (4°C), coiled-coil rope-like structure (15°C), nanohelices (25°C), and nanoribbons (50°C) were formed via La^{3+}-cholate supramolecular self-assembly. This system constitutes a "super" hydrogel as water gelation occurred at concentrations as low as 0.04 wt% SC (0.6 mM/0.6 mM, SC/La^{3+}), although this did take 10 days to form. Normally, increasing temperature compromises the stability of self-assembled hydrogels. Unusually however, heating-enhanced stiffness and heating-promoted gelation kinetics were observed. For instance, the SC/La^{3+} hydrogel at a concentration of 1.0 mM/1.0 mM was formed in ≈3 days at 25°C, but within 2-3 min at 50°C. Coordination of three cholate molecules around one La^{3+} centre, and intermolecular interactions of the polar and non-polar faces in adjacent cholate molecules (intermolecular hydrogen bonding and hydrophobicity, respectively), were found to be the driving forces for self-assembly of the nanostructures. Higher temperatures weaken the hydrogen bonding between the hydroxyl groups of the polar face and surrounding water molecules, the cholate-lanthanum complex becomes more hydrophobic as a result, promoting the aggregating ability of the complex, and so the gel stiffness and kinetics of formation increase to overcome this thermodynamically unfavourable event.

The same group have also studied hydrogelation using sodium cholate with a series of doubly charged metal ions, such as Ca^{2+}, Ni^{2+}, Zn^{2+}, Co^{2+}, and Cu^{2+}.[240] However, hydrogelation at extremely low concentrations was only observed with La^{3+} which stems from the strong lanthanum-cholate interaction and coordination of three cholates around the triply charged metal centre being detrimental to the molecular aggregation at such low concentrations. Studying supramolecular self-assembly of systems comprised of simple, biologically-relevant building blocks like **29** leads to a better understanding of self-assembly in biological systems. Furthermore, it allows straightforward access into applications which require enhanced stability of soft materials at higher temperatures.

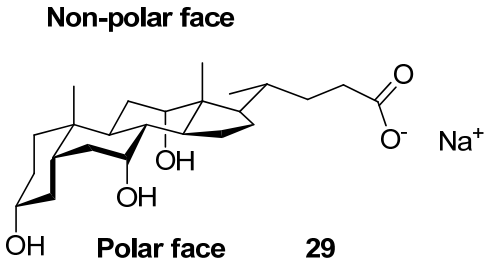

Fig. 1.31 – The chemical structure of sodium cholate.

Anionic guests have been used by Steed and others to control the breakdown of gels formed in organic solvents which were self-assembled by urea-urea hydrogen bond interactions.[241-246] A series of chiral bis-urea molecules (**30**) (Fig. 1.32), which contained odd and even numbered chain lengths (n =

2-8), were synthesised.[247] Only when n was even did the molecules gel an array of organic solvents, demonstrating that the orientation of the functional groups is important for gel behaviour. For **30** (n = 6), the rheological properties of the gels were severely compromised by addition of anions such as chloride, bromide and acetate as the urea groups became involved in binding to the anions, competing with the stabilising intermolecular urea-urea interactions between gelator molecules. In some cases, gelation was completely inhibited, for example, when acetate (0.1 equivalents) was added to **30** (n = 2).

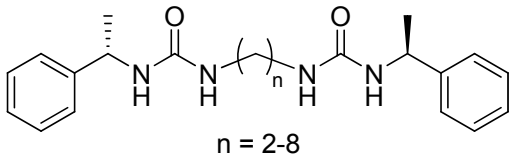

30

Fig. 1.32 – Steed's organogelator **30**. Gelation is dependent on the value of n and also on anion binding.

However, in spite of the elegant work on anion binding by gels in organic solvents, anion binding by gels *in water* has been reported to a much lesser extent.[248, 249] In one such case, Jiang and co-workers demonstrated that a supramolecular hydrogel formed from glutathione (GSH, **31**) (Fig. 1.33) and Ag(I) coordination polymers could be broken down by addition of I^-, and subsequently reformed by adding in more Ag(I) (Scheme 1.7).[250] This behaviour was found to be selective for I^- only, whereas other anions such as F^-, Cl^-, Br^-, and $H_2PO_4^-$ hardly led to any observable changes in the gel state. They concluded that I^- acted as a depolymerising agent, promoted by formation of AgI which sequesters Ag(I) from the self-assembled polymer, resulting in gel breakdown. It was proposed that a highly selective system such as this offers facile recognition of I^- by the naked eye without commonly encountered and problematic spectral interferences in situations where a coloured and/or fluorescent background is present, for example in environmental or biological samples, during traditional spectrophotometric detection of anions.

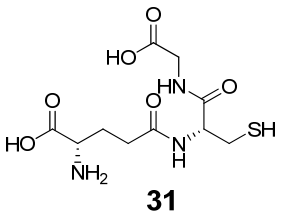

31

Fig. 1.33 – The structure of GSH (**31**).

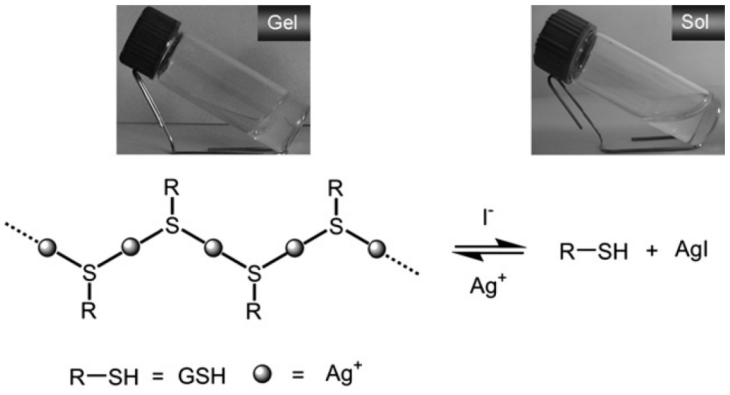

Scheme 1.7 – Reversible gel-sol transition of Ag(I)-GSH hydrogel by adding I^- into the gel or Ag(I) into the resulting sol solution. Image reproduced from reference 250.

1.4 Project Aims

This project was initially inspired by previous work such as that of Liskamp and co-workers. As described earlier, they used cyclic RGD peptides conjugated to a dendritic framework, but found a negligible multivalency effect as all of their compounds (Fig. 1.14, showing tetravalent dendrimer **1** only) possessed strong integrin binding affinity owing to the cyclic RGD unit binding strongly in its own right.[127] The aim of this project was *not* to develop high affinity or highly selective multivalent ligands for integrin $\alpha_v\beta_3$ binding – several research groups have demonstrated this already – but rather, to compare dendritic (covalent) and self-assembling (non-covalent) strategies, exemplified by target structures **Z-G1-[RGD]$_3$** and **C12-RGD** (Fig. 1.34), as two different ways of arranging multivalent displays of RGD ligands as, to the best of our knowledge, these have not been compared in a single study in the literature. The linear form of the RGD peptide was chosen because it was envisaged that this could be synthesised on a multi-gram scale using simple solution-phase chemistry, and because its structure is not conformationally restricted its affinity for integrin is low (mM), and therefore we reasoned that multivalency effects may be more easily observed. Using this approach, it was hoped that an enhanced understanding of the way in which ligands can be organised to achieve multivalent binding to integrin would be accomplished. In the first instance, the hydrophilic RGD peptide will be conjugated to a dendritic framework, as in target structure **Z-G1-[RGD]$_3$** (Fig. 1.34), and its binding affinity for integrin $\alpha_v\beta_3$ will then be compared to that of RGD conjugated to a hydrophobic group such as a C12 aliphatic chain, as in target structure **C12-RGD** (Fig. 1.34).

In the second part of the project, the intention was to develop the water-soluble, self-assembling ligands into low MW supramolecular hydrogels, due to the importance of these soft materials in applications such as tissue engineering and the known ability of RGD peptides to bind to integrins, encouraging cell adhesion. Amphiphilic compounds bearing hydrophilic linear RGD peptides coupled to hydrophobic chains, such as target structure **C12-[urea-RGD]$_2$** (Fig. 1.34), will be synthesised for their potential ability to form self-assembled nanofibrous networks in water. Ureas will be the linkage of choice (between the peptide and hydrophobe) for their ease of synthesis and for their proven importance in underpinning gelation in LMWGs due to their ability to establish intermolecular urea-urea hydrogen bonding molecular recognition pathways, even in competitive solvents such as water.[251, 252] It was suggested that responsivity towards external stimuli such as anions may be observed due to the disruption of the urea-urea hydrogen bonding interactions, constituting one of the few cases where anion binding occurs in water.

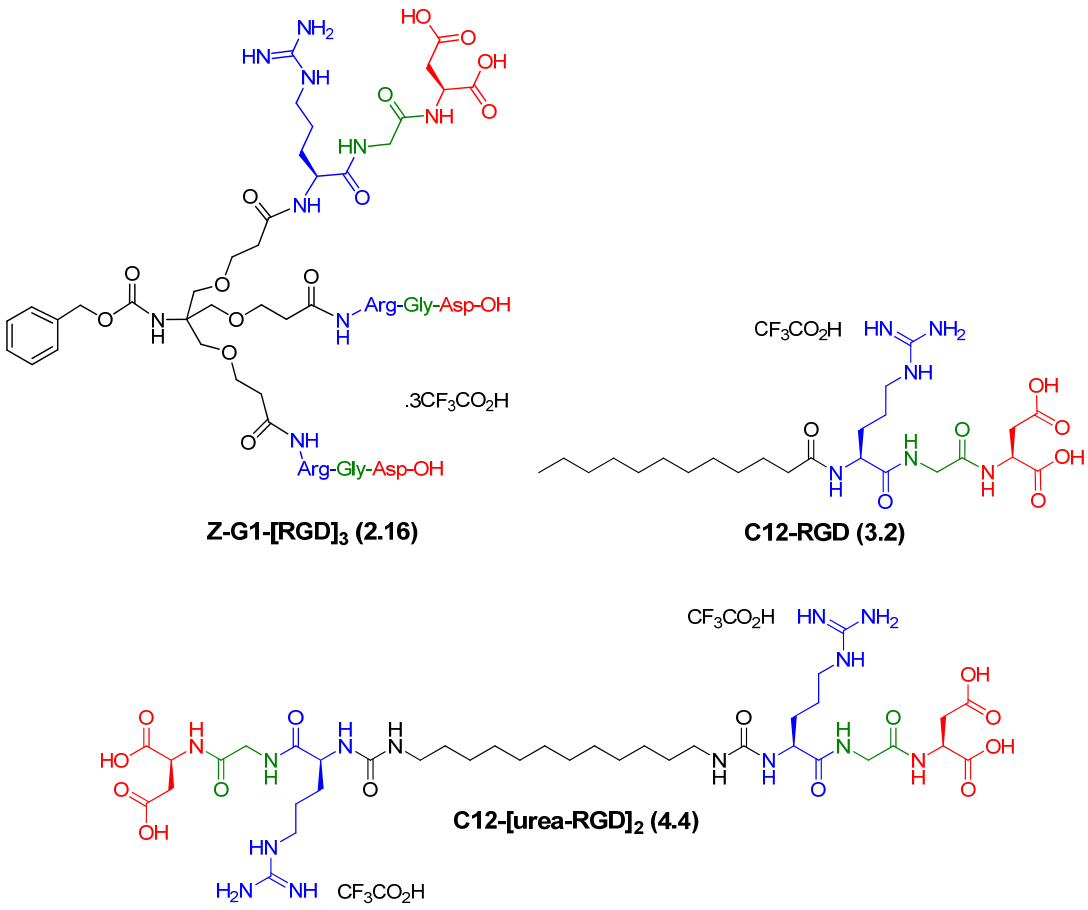

Fig. 1.34 – Some of the project target structures. Original in colour.

Chapter 2

Dendritic

Linear RGD Peptides

2 Dendritic Linear RGD Peptides

2.1 Introduction

The research in this chapter will consider what effect multimerising a linear RGD peptide, using a dendritic approach, has on the ability of the constructs to bind integrin. We opted to use the simpler, linear version of the peptide ligand for two reasons: (i) we have developed a methodology to synthesise the peptide on a cost-effective, large multi-gram scale using straightforward solution-phase peptide chemistry, making it commercially viable, and (ii) linear RGD binds integrin with a much lower affinity (mM) than cyclic RGD (nM), therefore, multivalency effects to enhance binding may be more easily observed. We chose to employ a 'Newkome-type' ether-amide dendritic scaffold as it is composed solely of functional groups that are stable to hydrolysis and should not breakdown under aqueous conditions over the time course of the binding experiments. The synthesis of Newkome-type ether-amide first generation (G1) and second generation (G2) dendrons, protected at the focal point with a benzyl carbamate (Z) group, with the peripheral carboxylic acids peptide-coupled to the N-terminus of the protected RGD peptide, and finally deprotected to yield: **Z-G1-[RGD]$_3$** (**2.16**) with three RGD peptides and **Z-G2-[RGD]$_9$** (**2.17**) with nine RGD peptides attached, will be outlined along with the synthesis of control compounds: **PEG-RGD** (**2.19**) and **PEG-GGG** (**2.20**) (Fig. 2.1).

Following this, a biophysical study employing a fluorescence polarisation (FP) competition assay will investigate the effect of these dendritic scaffolds and whether multivalency plays a role in enhancing the binding strength of linear RGD with integrin $\alpha_v\beta_3$. FP was originally established as a method to probe the integrin binding ability of monovalent, cyclic RGD ligands by Li *et al* in 2005.[75] Their binding results from this non-cell-based study showed a remarkable similarity to those obtained from a cell-based ELISA (enzyme-linked immunosorbent assay). For chemists interested in integrin binding research, FP offers the advantage of a 'chemical' approach to the screening of synthetic ligands, without the need for cell culture equipment. For the FP assay, a fluorescent probe: **5(6)-FL-c[RGDfK]** (**2.24**) (Fig. 2.2), is required and the synthesis of this compound will also be discussed in full.

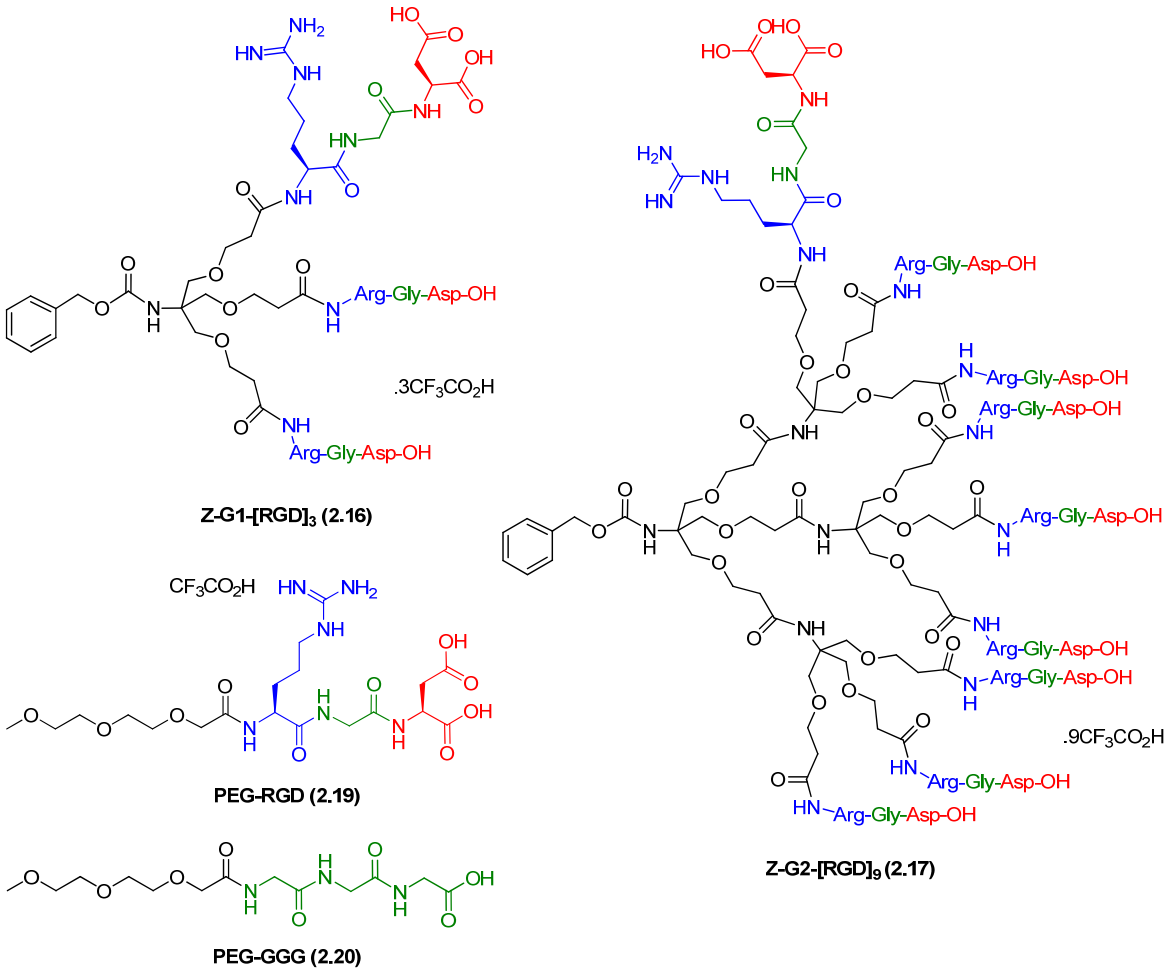

Fig. 2.1 – Structures of the target dendritic linear RGD compounds: **Z-G1-[RGD]$_3$** and **Z-G2-[RGD]$_9$**, and control compounds: **PEG-RGD** and **PEG-GGG**. Original in colour.

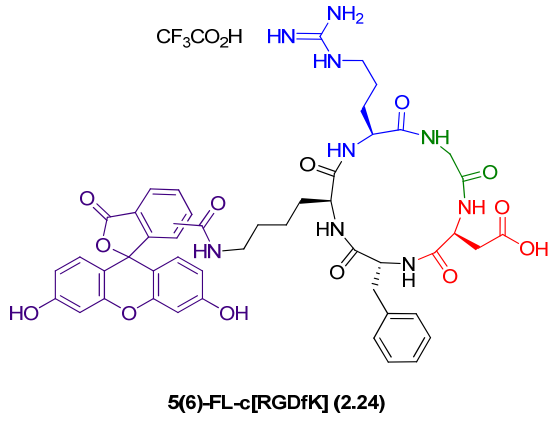

Fig. 2.2 – Structure of the cyclic RGD peptide fluorescent probe: **5(6)-FL-c[RGDfK]**. Original in colour.

2.2 Synthesis

2.2.1 Synthesis of the Protected Linear RGD Peptide: Comparing Fmoc- and Z-Protecting Group Strategies

The solution-phase synthesis of the orthogonally protected linear RGD peptide initially employed 9*H*-fluoren-9-ylmethoxycarbonyl (Fmoc) protection of the alpha amine, a protecting group methodology which is summarised in Scheme 2.1. In the first step, Fmoc-protected glycine (Fmoc-Gly-OH) was amide coupled to L-aspartic acid di-*tert*-butyl ester hydrochloride (H_2N-Asp(O^tBu)-O^tBu.HCl) in the presence of base (DIPEA) and coupling reagent, propylphosphonic anhydride (T3P).[253, 254] T3P was chosen because it usually provides high yields and low racemisation; the fact that it does not require a catalyst such as HOBt; its mild reaction conditions and fast reaction times; and easy aqueous removal of the ring-opened by-product at the end of the reaction. The reaction was cooled in an ice-water bath to avoid racemisation of the amino acid chiral centre, which is possible at higher temperatures. Following an aqueous workup, this afforded the product Fmoc-Gly-Asp(O^tBu)-O^tBu, **2.1**, in 93% yield and no further purification was required. This was confirmed by ^{1}H NMR which showed a doublet peak at 6.86 ppm corresponding to the newly formed amide N*H* proton, and a downfield shift in the aspartic acid α-*H* from below 4.00 ppm to 4.70 ppm due to the formation of the adjacent electron-withdrawing amide functional group. ESI-MS analysis also confirmed the formation of product with a m/z value of 547.2411 (100%, $[M+Na]^+$).

The next step involved the deprotection of the Fmoc group using a solution of 20% piperidine in DCM. This product required laborious silica column chromatographic purification to remove the Fmoc/Fmoc-piperidine by-products and excess piperidine, which could not be extracted using a simple aqueous acid workup. After silica column chromatography this reaction afforded H_2N-Gly-Asp(O^tBu)-O^tBu, **2.2**, in 82% yield. Removal of the Fmoc group resulted in the loss of the electron-withdrawing carbamate group adjacent to the glycine CH_2. This was reflected in the ^{1}H NMR by an upfield shift of each of the doublet-doublet peaks for the two protons of the glycine CH_2 at 3.98 and 3.92 ppm to doublet peaks at 3.39 and 3.34 ppm, respectively, as well as the absence of peaks corresponding to the Fmoc aromatic C*H*'s at 7.76, 7.60, 7.40 and 7.31 ppm; carbamate N*H* at 5.45 ppm; Fmoc CH_2 at 4.39 ppm; and Fmoc C*H* at 4.24 ppm. A reduction in mass to a m/z value of 303.1953 (100%, $[M+H]^+$) was confirmed by ESI-MS.

Compound **2.2** was then amide coupled to the orthogonally protected L-arginine: N_α-Fmoc-N_ω-Pbf-L-arginine (Fmoc-Arg(Pbf)-OH), to yield Fmoc-Arg(Pbf)-Gly-Asp(O^tBu)-O^tBu, **2.3**, in 79% yield. Two amide N*H* peaks at 7.70 and 7.11 ppm, along with downfield shifts in the glycine CH_2 peaks to 4.06 and 3.91 ppm due to the formation of the adjacent electron-withdrawing amide functional group, were indicative of the amide-coupled product. ESI-MS confirmed the mass of the product with a m/z value of 933.4426 (100%, $[M+H]^+$).

Fmoc deprotection of **2.3** again required the need for silica column chromatographic purification to afford the final product H_2N-Arg(Pbf)-Gly-Asp(O^{t}Bu)-O^{t}Bu, **2.4**, in 80% yield. Removal of the Fmoc group resulted in the loss of the electron-withdrawing carbamate group adjacent to the arginine α-*H*. This was reflected in the ^{1}H NMR by an upfield shift of the arginine α-*H* multiplet at 4.44-4.37 ppm to 3.49-3.46 ppm, as well as the absence of peaks corresponding to the Fmoc aromatic C*H*'s at 7.73, 7.58, 7.36 and 7.26 ppm; carbamate N*H* at 6.04 ppm; Fmoc CH_2 at 4.34 ppm; and Fmoc C*H* at 4.16 ppm (see appendix – spectrum 2.1). A reduction in mass to a m/z value of 733.3608 (100%, $[M+Na]^+$) was confirmed by ESI-MS. The synthesis of **2.4** was therefore achieved in 4 steps with an overall yield of 48% using the Fmoc strategy. However, the need for silica column chromatographic purification at each deprotection step was a problem with this approach.

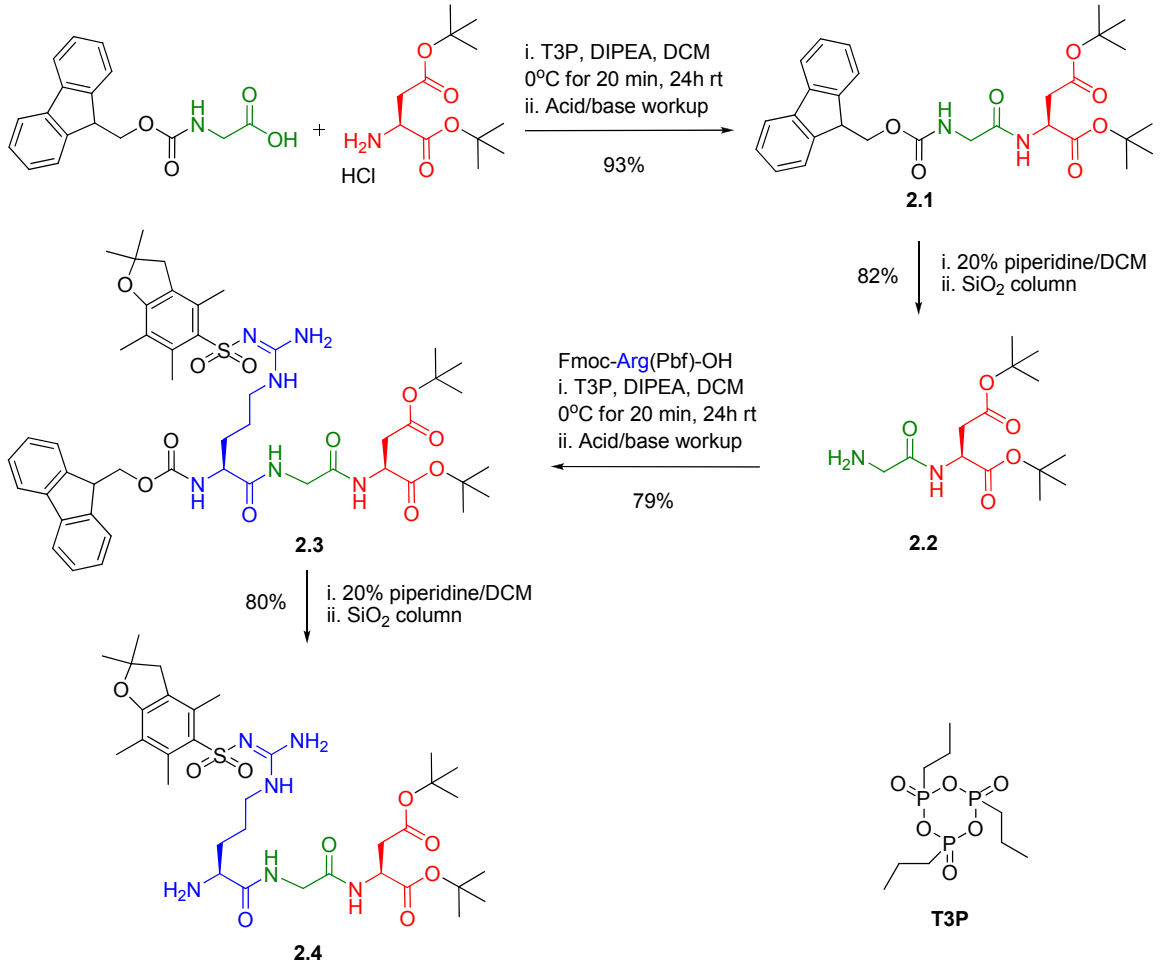

Scheme 2.1 – Reaction scheme for the solution-phase synthesis of protected linear RGD using an Fmoc-protecting group strategy. Original in colour.

As an alternative strategy towards the synthesis of protected RGD **2.4**, benzyl carbamate (Z) protection of the alpha amine was used. Unlike the Fmoc version, it was envisaged that this method would require fewer, synthetically laborious, silica column chromatography steps. This is because the

deprotection of a benzyl carbamate protecting group under catalytic hydrogenolysis conditions usually proceeds to completion in a quantitative fashion.

The solution-phase synthesis of the protected linear RGD peptide using a Z-protecting group strategy is summarised in Scheme 2.2. Firstly, Z-protected glycine (Z-Gly-OH) was amide coupled to H_2N-Asp(O^tBu)-O^tBu.HCl in the presence of DIPEA and coupling reagent, *O*-(Benzotriazol-1-yl)-*N,N,N′,N*'-tetramethyluronium tetrafluoroborate (TBTU).[255, 256] For the same reasons as T3P, TBTU was chosen because it usually provides high yields and low racemisation; the fact that it does not require additional catalyst such as HOBt as, unlike T3P, TBTU produces HOBt *in situ*; its mild reaction conditions and fast reaction times; and easy aqueous removal of the urea by-product at the end of the reaction. Following an aqueous workup, this reaction afforded pure product Z-Gly-Asp(O^tBu)-O^tBu, **2.5**, in 94% yield and no further purification was required. This was confirmed by ^{1}H NMR which showed a doublet peak at 6.98 ppm corresponding to the newly formed amide N*H* proton, and a downfield shift in the aspartic acid α-*H* from below 4.00 ppm to 4.68 ppm due to the formation of the adjacent electron-withdrawing amide functional group. ESI-MS analysis also confirmed the formation of product with a m/z value of 459.2107 (100%, $[M+Na]^+$).

Deprotection of the benzyl carbamate by stirring under an atmosphere of H_2 for 22.5 h in the presence of Pd/C catalyst in ethanol provided H_2N-Gly-Asp(O^tBu)-O^tBu, **2.6**, in quantitative yield after removing the catalyst by filtration over Celite. Loss of peaks in the ^{1}H NMR corresponding to the aromatic protons at 7.34-7.27 ppm; carbamate N*H* at 5.59 ppm and benzyl CH_2 at 5.10 ppm in the precursor compound were key evidence for the formation of the deprotected product, along with an upfield shift of the glycine CH_2 from a broad multiplet at 3.91 ppm for the two protons to doublet peaks at 3.33 and 3.28 ppm for each proton. Peaks for the precursor compound were also absent in the ESI-MS and a new peak was assignable to the product at a m/z value of 303.1921 (100%, $[M+H]^+$). Unlike when this compound was synthesised using the Fmoc approach, no further purification was required resulting in a higher yield for this step.

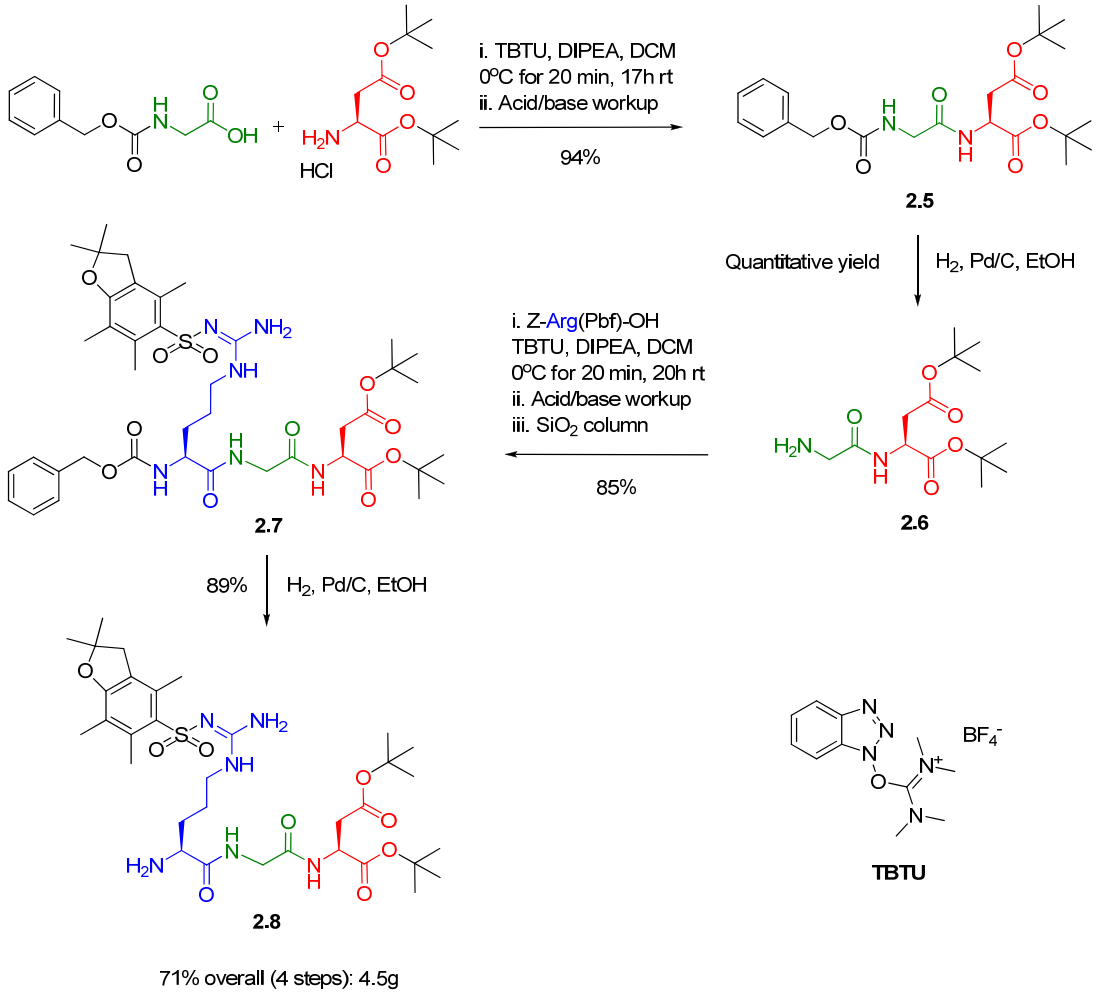

Scheme 2.2 – Reaction scheme for the solution-phase synthesis of protected linear RGD using a Z-protecting group strategy. Original in colour.

The synthesis of Z-Arg(Pbf)-Gly-Asp(O^{t}Bu)-O^{t}Bu, **2.7**, required the use of the orthogonally protected L-arginine: N_α-Z-N_ω-Pbf-L-arginine (Z-Arg(Pbf)-OH). This was purchased as the cyclohexylammonium salt (Z-Arg(Pbf)-OH.CHA), and so before amide coupling could occur we had to convert the protected arginine salt into its free carboxylic acid form (Scheme 2.3). This was generated by dissolving Z-Arg(Pbf)-OH.CHA in ethyl acetate and performing an acid workup with aqueous sodium hydrogen sulfate to yield acidified Z-Arg(Pbf)-OH. A quintet peak at ~3.5 ppm, and multiplet peaks at ~2.3, ~2.0 and ~1.5 ppm corresponding to the C*H* and CH_2 protons, respectively, of the cyclohexylammmonium cation were not detected in the ^{1}H NMR of Z-Arg(Pbf)-OH after workup. Failure to do this would potentially result in a competing side-reaction whereby cyclohexylamine couples with the protected L-arginine in the presence of TBTU, following deprotonation of the cyclohexylammonium cation by DIPEA, to generate the by-product shown (Scheme 2.3). Compound **2.7** was then synthesised by peptide coupling Z-Arg(Pbf)-OH with **2.6** using DIPEA and TBTU (Scheme 2.2). Aqueous workup of the crude reaction mixture, followed by silica column chromatography produced **2.7** in a good 85% yield; 6% higher than that of the

analogous step using the Fmoc strategy. Two amide N*H* peaks at 7.76 and 7.22 ppm, along with downfield shifts in the glycine CH_2 peaks to 3.98 and 3.91 ppm due to the formation of the adjacent electron-withdrawing amide functional group, were indicative of the amide-coupled product. ESI-MS confirmed the mass of the product with a m/z value of 845.4092 (100%, $[M+H]^+$).

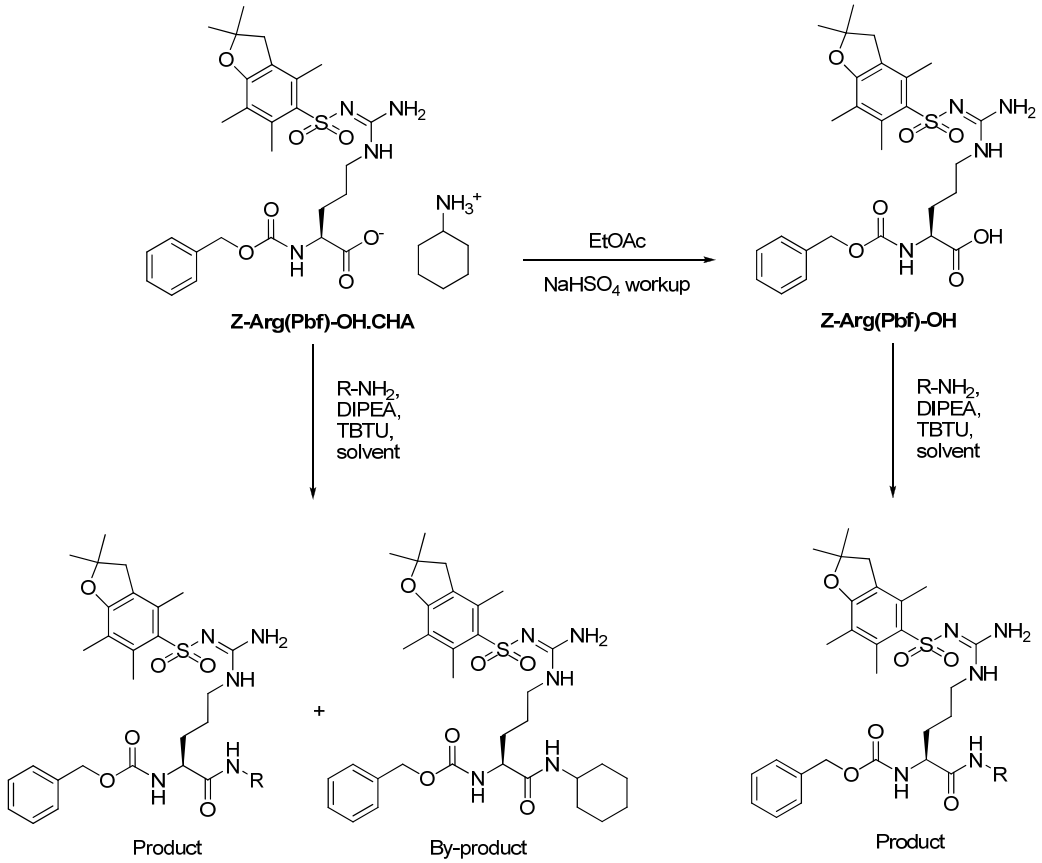

Scheme 2.3 – Reaction scheme showing by-product formation when performing an amide coupling using Z-Arg(Pbf)-OH.CHA directly from the supplier.

Deprotection of the benzyl carbamate yielded the final product H_2N-Arg(Pbf)-Gly-Asp(O^{t}Bu)-O^{t}Bu, **2.8**, in 89% yield without requiring any further purification (Scheme 2.2). Removal of the Z group resulted in the loss of the electron-withdrawing carbamate group adjacent to the arginine α-*H*. This was reflected in the ^{1}H NMR by an upfield shift of the arginine α-*H* multiplet at 4.37-4.32 ppm to 3.44 ppm, as well as the absence of peaks corresponding to the benzyl aromatic C*H*'s at 7.33-7.26 ppm; carbamate N*H* at 6.09 ppm; and benzyl CH_2 at 5.08-5.03 ppm (see appendix – spectrum 2.2). A reduction in mass to a m/z value of 711.3756 (100%, $[M+H]^+$) was confirmed by ESI-MS. The synthesis of **2.8** was achieved in 4 steps with an overall yield of 71% (4.5 g); 23% higher than that of the Fmoc approach. Furthermore, the Z-protecting group strategy required fewer column chromatographic purifications. We considered this to be a successful development of the multi-gram, solution-phase synthesis of the target peptide.

2.2.2 Synthesis of the RGD Dendrons: Z-G1-[RGD]$_3$ and Z-G2-[RGD]$_9$

Dendritic RGD conjugates were synthesised according to the methodology outlined in this section. The synthesis of the dendritic scaffold was first reported by Newkome *et al*,[257, 258] but will be discussed here in full as some modifications were made. A divergent or convergent route to the desired target compounds could be chosen, but it was decided that a divergent synthesis of the dendrons followed by attachment of the linear RGD peptide to the dendron periphery would be used, as this limited the number of synthetic manipulations which had to be done on the peptide. Firstly, the synthesis of the two generations of dendron framework (G1 and G2) is described.

The first synthetic step was a 1,4-Michael addition between tris(hydroxymethyl)aminomethane (TRIS) and *tert*-butyl acrylate in DMSO, using 5 M NaOH as a base (Scheme 2.4). To avoid the retro-Michael reaction, which can occur at elevated temperature, the reaction mixture was cooled in an ice-water bath. Silica column purification afforded the key intermediate dendritic building block, **2.9**, in a somewhat disappointing 26% yield. The absence of peaks in the ^{1}H NMR in the range 4-6 ppm (i.e. no protons corresponding to an alkene), and a triplet peak at 3.63 ppm for O*CH*$_2$CH$_2$ with 6H integration confirmed the conversion of the *tert*-butyl acrylate into **2.9**. In our hands, a yield of 56% reported for this step by Cardona and Gawley could not be replicated,[259] however, by scaling-up the reaction between the two commercially available starting materials we were able to obtain >13 g of pure product, which provided more than enough material for subsequent synthetic steps. The amine at the focal point of **2.9** was then protected as the benzyl carbamate derivative using benzyl chloroformate in DCM and aqueous sodium carbonate (25% w/v) as base; a two-phase reaction which proceeded in 78% yield after purification by silica column chromatography to provide compound **2.10**. A broad singlet in the ^{1}H NMR at 5.31 ppm was assigned to the newly-formed carbamate N*H* proton.

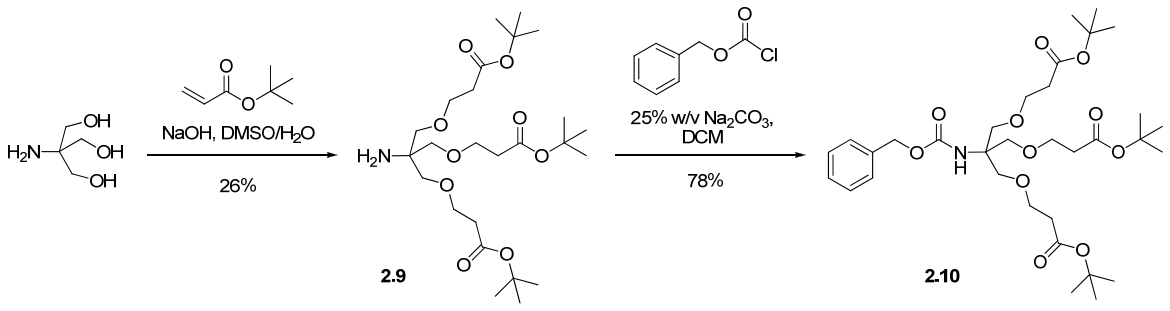

Scheme 2.4 – Reaction scheme showing the synthesis of H_2N-G1-[C(O)O^{t}Bu]$_3$, **2.9**, and Z-G1-[C(O)O^{t}Bu]$_3$, **2.10**.

Hydrolysis of the three *tert*-butyl esters by stirring **2.10** in formic acid for 18 h afforded the G1 triacid, **2.11**, in quantitative yield (Scheme 2.5), as evidenced by the loss of the ^{1}H NMR resonance at 1.43

ppm which corresponded to the *tert*-butyl methyl groups in precursor compound **2.10**. Compound **2.11** is a key intermediate in the synthesis of the two generations of RGD-bearing dendrons.

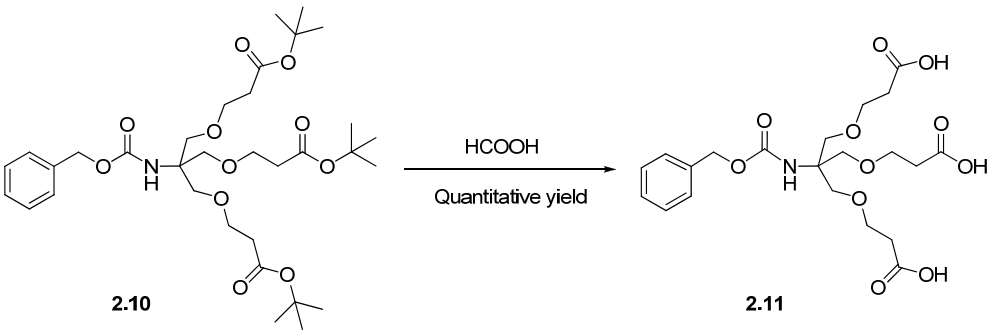

Scheme 2.5 – Reaction scheme showing the synthesis of Z-G1-[C(O)OH]$_3$, **2.11**.

In the next step, we coupled the G1 triacid, **2.11**, with 3.6 eq of amino ester **2.9** to produce Z-protected second generation dendron **2.12** (Scheme 2.6). Two different attempts were made at the synthesis which differ from that reported by Cardona and Gawley who used the more traditional peptide coupling conditions of EDC and HOBt.[259] Due to restrictions on the purchase of activating agent HOBt we were unable to employ the published conditions, therefore reagents which are either a complete substitute for HOBt (T3P) or are self-catalysing and produce HOBt as a consequence of their reactivity (*O*-(Benzotriazol-1-yl)-*N,N,N′,N′*-tetramethyluronium hexafluorophosphate, HBTU) were considered.[260] The first attempt, using T3P with TEA in dry THF, gave an unsatisfactory yield of 12% following silica column purification. This was reasoned to be due to either: (i) the inefficiency of T3P to act as carboxylic acid activating agent in the increasingly sterically bulky surface environment of **2.11** as it reacts at each branching point to generate **2.12**, (ii) the inefficiency of T3P to act as a good leaving group during nucleophilic attack of the sterically hindered amine at the focal point of **2.9** on the T3P-activated acids, or (iii) the purity of the T3P used, which is supplied as a 50 wt % solution in ethyl acetate and can be hydrolysed over time if water is absorbed. The second attempt, using HBTU in the presence of TEA in dry acetonitrile, resulted in a much higher yield of 77% after an aqueous workup and silica column purification. A broad singlet, integrating to three protons at 6.28 ppm in the ^{1}H NMR was one of the main pieces of evidence for the successful formation of **2.12**. ESI-MS analysis also detected the product with a m/z value of 968.0652 (100%, $[M+2H]^{2+}$). Synthesis of the G2 nonaacid, **2.13**, was completed in quantitative yield following hydrolysis of the nine *tert*-butyl esters in **2.12** after stirring in formic acid for 24 h, as evidenced by the loss of the ^{1}H NMR resonance at 1.43 ppm which corresponded to the *tert*-butyl methyl groups in precursor compound **2.12**.

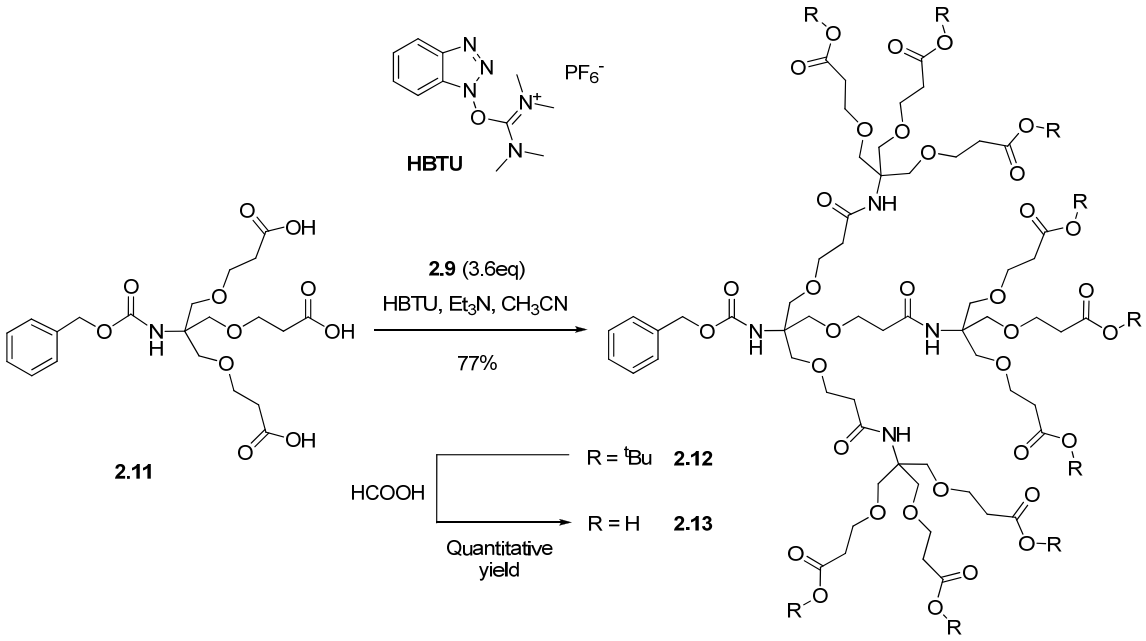

Scheme 2.6 – Reaction scheme showing the synthesis of Z-G2-[C(O)O^{t}Bu]$_9$, **2.12**, and Z-G2-[C(O)OH]$_9$, **2.13**.

Following the synthesis of the Z-protected G1 and G2 dendrons, **2.11** and **2.13** respectively, the penultimate phase of the synthetic design involved amide coupling the protected linear RGD peptide, **2.8** (**2.4**), to the terminal carboxylic acid groups of the dendrons. Due to its significantly cheaper cost compared with HBTU, a newly purchased bottle of T3P was chosen as the coupling agent to couple **2.8** to dendrons **2.11** and **2.13**. This gave products **2.14** and **2.15** in yields of 77% and 76%, respectively, following silica column purification (Scheme 2.7). The synthesis of **2.14** was confirmed in the ^{1}H NMR by a downfield shift in the arginine α-*H* (with 3H integration) from 3.44 ppm to 4.54 ppm on coupling **2.8** to dendron **2.11** to generate the adjacent electron-withdrawing amide functional group (see appendix – spectrum 2.3). ESI-MS analysis also confirmed the formation of **2.14** with a *m*/*z* value of 1297.1096 (100%, $[M+2Na]^{2+}$). Likewise, the successful formation of **2.15** was evidenced by the downfield shift in the arginine α-*H* (with 9H integration) (see appendix – spectrum 2.4), and a *m*/*z* value of 1534.0 (100%, $[M+5H]^{5+}$).

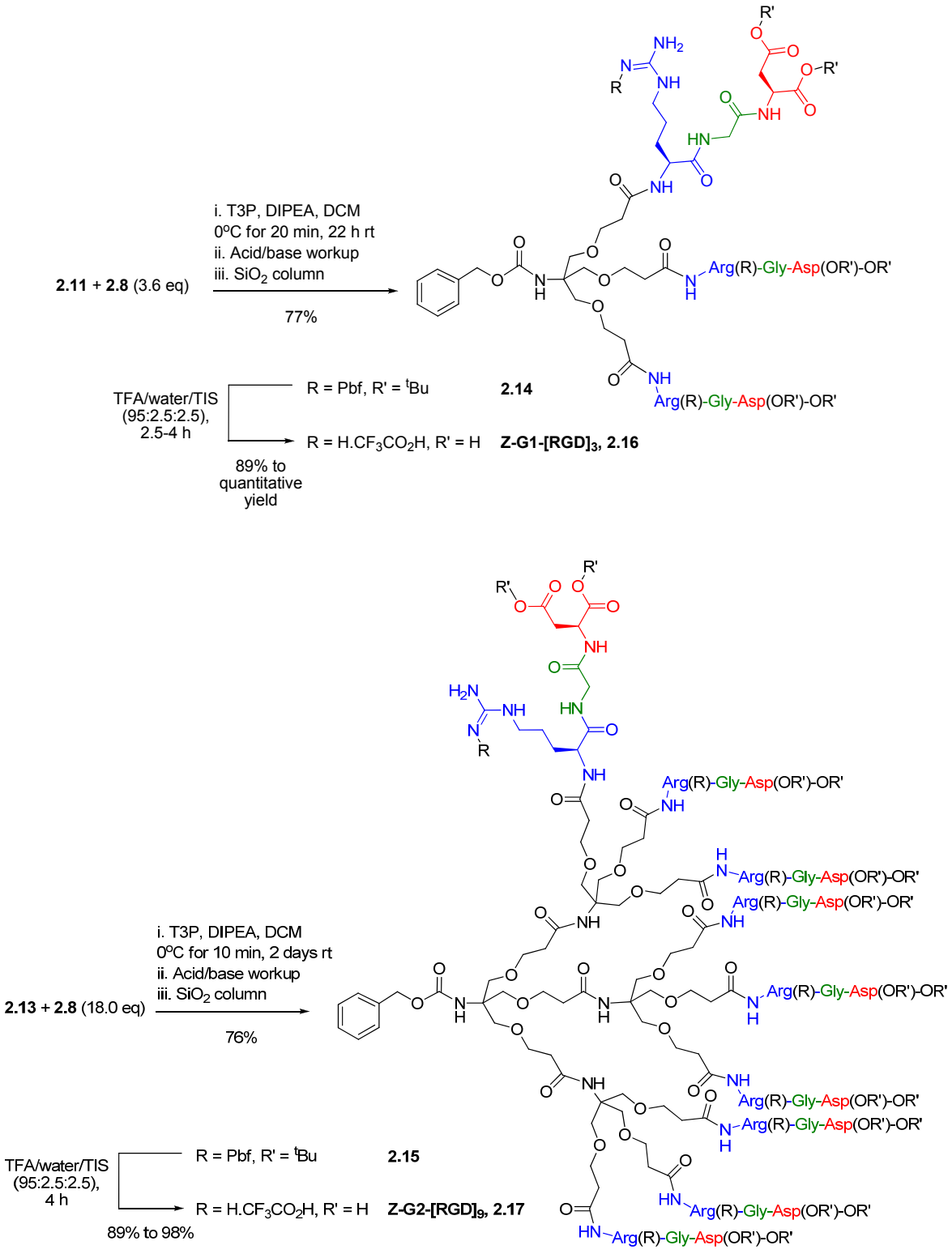

Scheme 2.7 – Reaction schemes showing the synthesis and deprotection of the G1 and G2 dendrons to provide the final target compounds **Z-G1-[RGD]$_3$, 2.16**, and **Z-G2-[RGD]$_9$, 2.17**. Original in colour.

Comparative syntheses of **2.14** and **2.15** using HBTU were not investigated as the yields using T3P were highly satisfactory when considering that the amide coupling of **2.8** with each carboxylic acid

branch progressed with calculated experimental yields of about 92% and 97% in the synthesis of the G1 and G2 dendrons respectively (G1: $\sqrt[3]{0.77} = 0.92$, G2: $\sqrt[9]{0.76} = 0.97$). Interestingly, the marginally higher yield per branch for the G2 dendron can probably be accredited to the use of a greater excess of peptide (2.0 eq) per carboxylic acid, rather than 1.2 eq in the case of the G1 dendron synthesis. Nevertheless, relatively high and similar overall yields for both compounds demonstrates the amide-coupling power of T3P in these reactions – you would normally expect a reduced yield for the G2 dendron compared with that of the G1 for two reasons: i) the G2 requires a greater number of iterative coupling reactions to be performed on the same molecule and ii) there is an increase in steric bulk around the carboxylic acid reactive sites as compound **2.15** forms in solution from its parent dendron **2.13**.

Having obtained the target G1 and G2 dendrons in Pbf/*tert*-butyl ester protected form, the final step in the synthesis of each compound required the hydrolysis of the protecting groups in order to unmask the RGD peptides, allowing them to subsequently bind to the integrin active site. This was achieved by dissolving **2.14** and **2.15** in a mixture of TFA, water and triisopropylsilane (TIS) (Scheme 2.7). TIS is used as a Pbf scavenging agent as it is reported that the hydrolysed Pbf group has a tendency to re-react with the guanidinium group of the arginine side chain.[261] The deprotection reactions were stirred for between 2.5-4 h, after which time TLC indicated that they were complete. The volatiles were removed *in vacuo*, the resulting residue dissolved in 10% aqueous acetic acid and the non-polar by-product (namely the deprotected Pbf group) was extracted with chloroform. The aqueous layer containing the product was then shell-frozen and lyophilised to yield the final target compounds, **2.16** and **2.17**, as their TFA salts in yields ranging from 89% to quantitative. The loss of peaks in the ^{1}H NMRs of **2.16** and **2.17** (see appendix – spectra 2.5 and 2.6, respectively) corresponding to the Pbf methylene (2.93 ppm) and methyl groups at 2.56, 2.49, 2.07 and 1.44 ppm, as well as the *tert*-butyl methyl groups at 1.41 and 1.40 ppm, confirmed successful formation of **2.16** and **2.17**. Further evidence was provided by ESI-MS which revealed the absence of peaks for the precursor compounds and the presence of new peaks with m/z values of 728.8169 (100%, $[M+2H]^{2+}$) and 731.4926 (100%, $[M+6H]^{6+}$) for **2.16** and **2.17**, respectively.

2.2.3 Synthesis of the Control Compounds: PEG-RGD and PEG-GGG

Positive control compound, **PEG-RGD** (**2.19**), was synthesised (Scheme 2.8) to allow us to compare monovalent and multivalent RGD binding to the integrin target. We chose to cap the N-terminus of **2.8** in this fashion, enabling us to compare the same N-terminus 'capped' peptide which is present as a consequence of its attachment to dendrons **2.16** and **2.17**. The short PEG unit was chosen to ensure water solubility and to avoid aggregation of the control peptide. **PEG-RGD** was synthesised by simple conjugation of the N-terminus of protected RGD **2.8** with the carboxylic acid of a short PEG chain, mediated by coupling agent T3P (**2.18**, 73% yield after silica column purification). This was

confirmed in the ^{1}H NMR by a downfield shift in the arginine α-*H* on coupling **2.8** to the short PEG chain to generate the adjacent electron-withdrawing amide functional group. ESI-MS analysis also confirmed the formation of product with a *m*/*z* value of 893.4318 (100%, $[M+Na]^+$).

TFA deprotection of the RGD peptide generated the product **2.19** in 55% yield (Scheme 2.8). The loss of peaks in the ^{1}H NMR (see appendix – spectrum 2.7) corresponding to the Pbf methylene and methyl groups, as well as the *tert*-butyl methyl groups, confirmed the reaction was successful. Further evidence was provided by ESI-MS which revealed the absence of peaks for the precursor compound and the presence of a new peak at a *m*/*z* value of 507.2386 (100%, $[M+H]^+$), corresponding to the product.

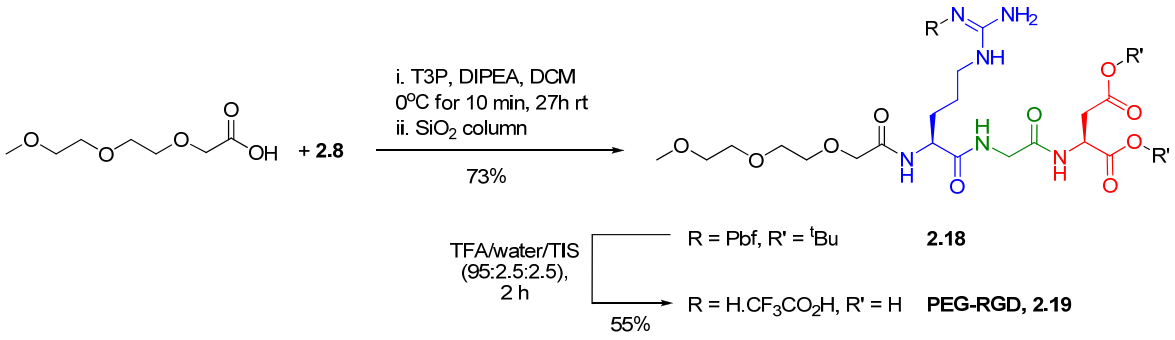

Scheme 2.8 – Reaction scheme showing the formation of **2.18** and subsequent deprotection conditions to form **2.19**. Original in colour.

Negative control compound, **PEG-GGG** (**2.20**), was synthesised to confirm that any binding observed with the aforementioned RGD-bearing compounds was in fact RGD peptide-directed and not just non-specific binding to the integrin target. To save time, and because only a small amount of material was required, compound **2.20** was synthesised on a solid support as shown in Scheme 2.9.

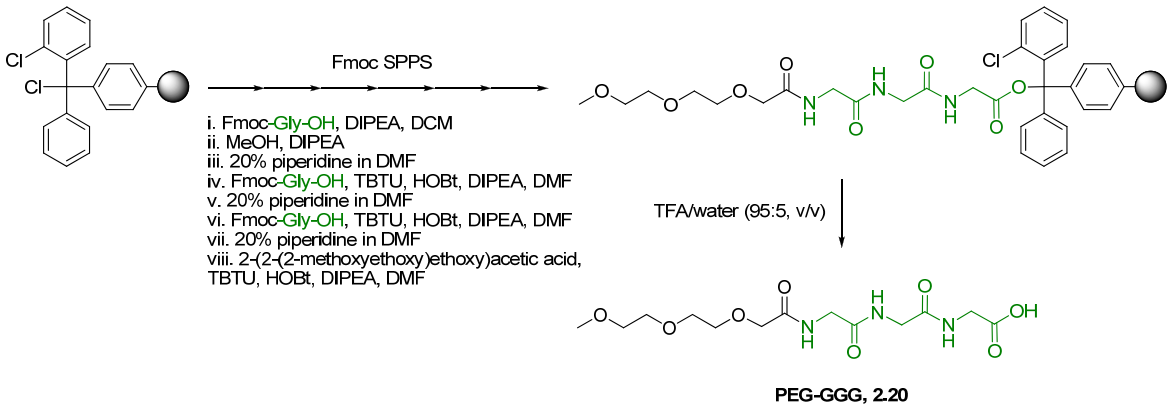

Scheme 2.9 – Reaction scheme showing the solid-phase peptide synthesis of **PEG-GGG**, **2.20**. Original in colour.

The synthesis began with the introduction of Fmoc-protected glycine onto the 2-chlorotrityl chloride Merrifield resin, via nucleophilic substitution, by mixing the resin with a solution of Fmoc-Gly-OH and DIPEA in DCM. The mixture was shaken for 2.25 h, before DIPEA and MeOH were added and then shaken for a further 45 minutes to cap any unreacted sites on the resin. The resin was then filtered and washed with DMF, DCM, MeOH and finally Et_2O before drying *in vacuo*. A loading of 0.91 mmol of Fmoc-Gly was calculated from the difference in mass of the resin used (1.19 g, 1.00-1.50 mmol/g, 1.19-1.79 mmol) and the resultant Resin-O-Gly-Fmoc (1.46 g). The Fmoc-protecting group was removed by twice shaking the resin in a 20% solution of piperidine in DMF for 10 min each time. Filtration of the resin, followed by washing with DMF and DCM, and then drying *in vacuo* yielded Resin-O-Gly-NH_2. The resin had decreased in mass to 1.22 g owing to loss of the Fmoc group. Throughout the solid-phase synthesis, a colorimetric Kaiser Test on a small sample of resin, taken from the reaction at the appropriate time point, was used to monitor the success of each coupling/deprotection step.

A DMF solution comprised of Fmoc-Gly-OH, coupling agents TBTU and HOBt, and DIPEA was then added to the resin and shaken overnight. The resulting resin was then washed with DMF and DCM and dried *in vacuo* to yield Resin-O-Gly-Gly-Fmoc. The dry mass of the resin had increased to 1.59 g, further confirming successful coupling of Fmoc-Gly-OH to the growing peptide. The Fmoc-protecting group was removed as previously described to yield Resin-O-Gly-Gly-NH_2. Subsequently, a third portion of Fmoc-Gly-OH was coupled to the resin in the same manner as that described above to yield 1.58 g of Resin-O-Gly-Gly-Gly-Fmoc. Finally, Fmoc removal yielded Resin-O-Gly-Gly-Gly-NH_2, reflected by a decrease in the mass of the resin to 1.32 g. The final coupling involved 2-[2-(2-methoxyethoxy)-ethoxy)acetic acid, TBTU, HOBt and DIPEA in DMF, which yielded Resin-O-Gly-Gly-Gly-PEG (1.50 g).

The compound was then cleaved from the resin using an acidic mixture of TFA/water, filtered, purified by silica column chromatography, shell-frozen and then lyophilised to yield **PEG-GGG**, **2.20**, in near quantitative yield (320 mg) based on the initial Fmoc-Gly-OH resin loading. Three amide N*H* resonances at around 8.0 ppm in the ^{1}H NMR was one piece of evidence to support the synthesis of **2.20** (see appendix – spectrum 2.8), in addition to ESI-MS analysis which detected the product with a *m*/*z* value of 348.1418 (100%, $[M-H]^-$). The total mass of product obtained was quite low, using 1 g of this expensive resin (>£50/g, Sigma-Aldrich), and that is why the solution-phase approach was preferred for the synthesis of the protected linear RGD peptide **2.8** (**2.4**) so that a multi-gram synthesis of the peptide could be developed, providing plenty of material for use in subsequent reactions.

2.2.4 Synthesis of the Fluorescent Cyclic RGD Probe: 5(6)-FL-c[RGDfK]

A fluorescein-RGD conjugate, **5(6)-FL-c[RGDfK]** (**2.24**), which was to act as a fluorescent probe in our competition binding assay, was synthesised via solid-phase and protecting group methodologies analogous to those of **PEG-GGG**. Conditions for the solid-phase synthesis of the protected linear pentapeptide and subsequent cleavage from the resin were adapted from methods published by Dai *et al*[97] and Bollhagen *et al*,[262] respectively, and will be outlined in full here as some modifications were made. The solution-phase cyclisation of the protected linear pentapeptide was also reported by Dai *et al* (Scheme 2.10).[97]

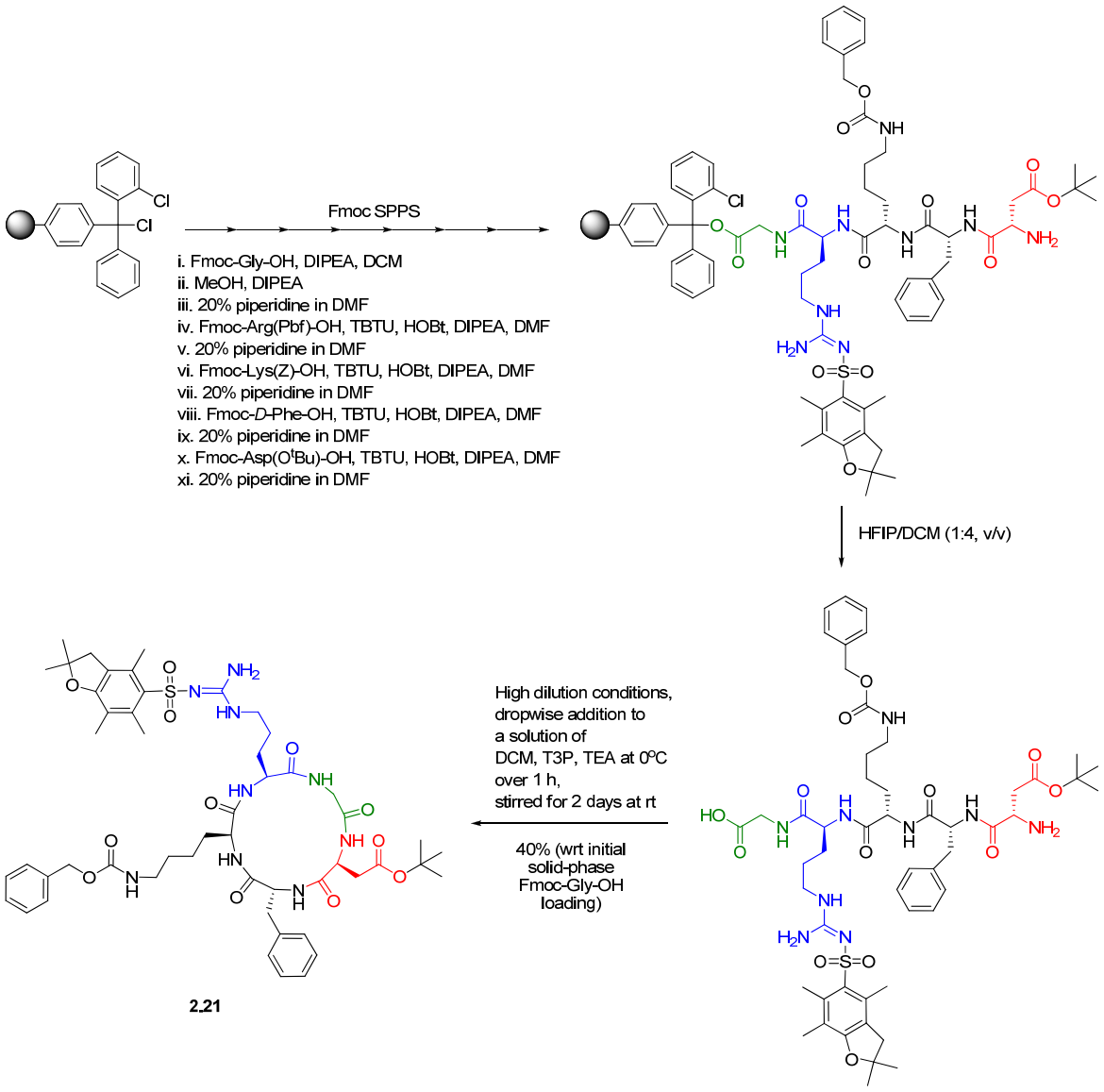

Scheme 2.10 – Reaction scheme showing the synthesis of the protected cyclic RGD **2.21**. Original in colour.

Similar to the literature procedure, synthesis of the protected linear pentapeptide began with the introduction of Fmoc-protected glycine onto the 2-chlorotrityl chloride Merrifield resin, via nucleophilic substitution, by mixing the resin with a solution of Fmoc-Gly-OH and DIPEA in DCM. The mixture was shaken for 2.5 h before DIPEA and MeOH were added and shaken for a further 30 minutes to cap any unreacted sites on the resin. The resin was then filtered and washed with DMF, DCM, MeOH and finally Et_2O before drying *in vacuo*. A loading of 1.75 mmol of Fmoc-Gly was calculated from the difference in mass of the resin used (1.17 g, 1.55 mmol/g, 1.81 mmol) and the resultant Resin-O-Gly-Fmoc (1.69 g). The Fmoc-protecting group was removed by twice shaking the resin in a 20% solution of piperidine in DMF for 20 min each time. Filtration of the resin, followed by washing with DMF and DCM, and then drying *in vacuo* yielded Resin-O-Gly-NH_2 which, as expected, had decreased in mass to 1.48 g. As with the solid-phase synthesis of **PEG-GGG**, a colorimetric Kaiser Test was used to monitor the success of each coupling/deprotection step.

A DMF solution of Fmoc-Arg(Pbf)-OH, coupling agents TBTU and HOBt, and DIPEA was then added to the resin and shaken for 1.5 h. The resulting resin was then washed with DMF and DCM and dried *in vacuo* to yield Resin-O-Gly-Arg(Pbf)-Fmoc (2.19 g). The Fmoc-protecting group was removed as previously described to yield Resin-O-Gly-Arg(Pbf)-NH_2 (2.16 g). At this point our protocol deviates from that given in the literature.[97] Dai *et al* peptide-coupled Fmoc-Lys(Boc)-OH onto the resin-anchored peptide. Boc (*tert*-Butyloxycarbonyl), present here as a protecting group of the amine on the lysine side-chain, requires removal by strong acid. Instead of this, we opted to use Fmoc-Lys(Z)-OH as we wanted to selectively remove the benzyl carbamate (Z) on the lysine side-chain of the cyclic peptide using catalytic hydrogenolysis in the presence of the acid-labile and, crucially, hydrogenolysis-stable protecting groups present on the other amino acids in the structure. This would then allow us to regioselectively couple the fluorescein moiety onto the lysine side-chain without interference from the other (protected) amino acids. Subsequently, Fmoc-Lys(Z)-OH, Fmoc-D-Phe-OH, and Fmoc-Asp(O^tBu)-OH were coupled to the resin in the same manner as that described above for Fmoc-Arg(Pbf)-OH. Finally, Fmoc removal yielded Resin-O-Gly-Arg(Pbf)-Lys(Z)-D-Phe-Asp(O^tBu)-NH_2 (2.65 g, with an estimated peptide loading of 80% (1.4 mmol) based on the initial Fmoc-Gly-OH resin loading).

Dai *et al* report cleavage of the linear peptide from the resin using a mixture of acetic acid, 2,2,2-trifluoroethane (TFE), and DCM.[97] Instead, we decided to cleave using 1,1,1,3,3,3-hexafluoro-2-propanol (HFIP) in DCM[262] to avoid possible acetylation of the terminal amine, which could arise from the presence of trace acetic acid in the T3P-mediated macrolactamisation step employed by Dai *et al*.[97] The resin was treated twice with HFIP/DCM (1:4, v/v), the filtrate and all washings were combined together and the solvent removed *in vacuo* to yield a brown solid (1.61 g, 86% crude yield as calculated from the initial Fmoc-Gly loading). Presumably T3P was used by Dai *et al* for the macrolactamisation step as it has previously been shown to be a useful reagent in the head-to-tail

cyclisation of sterically hindered peptides.[254] Dropwise addition of the crude, protected linear pentapeptide, dissolved in DCM, to a highly diluted solution of T3P and TEA in DCM (in order to favour intramolecular cyclisation), in this way, afforded protected cyclic peptide c[R(Pbf)GD(O^{t}Bu)fK(Z)], **2.21**, in 40% overall yield based on the initial Fmoc-Gly-OH resin loading after purification of the crude peptide mixture by silica column chromatography, followed by size exclusion chromatography using Sephadex beads as the stationary phase. Evidence for success of the macrolactamisation step is provided by the observation of five amide N*H* peaks, among other characteristic peaks, in the ^{1}H NMR. A m/z value of 1046.5018 (100%, $[M+H]^+$) was also detected by ESI-MS, further supporting the successful formation of the product.

The Z group in **2.21** was subsequently removed to yield the free ε-amine on the lysine of c[R(Pbf)GD(O^{t}Bu)fK], **2.22**, in 92% yield (Scheme 2.11). The absence of a multiplet at 7.38-7.28 ppm; a broad singlet at 7.08 ppm and a singlet at 5.02 ppm corresponding to the aromatic protons, benzyl carbamate N*H* and benzyl CH_2 protons, respectively, in the precursor molecule, were clear evidence that the hydrogenolysis reaction had gone to completion. A reduction in mass to a m/z value of 934.4468 (100%, $[M+Na]^+$) also confirmed the formation of the product.

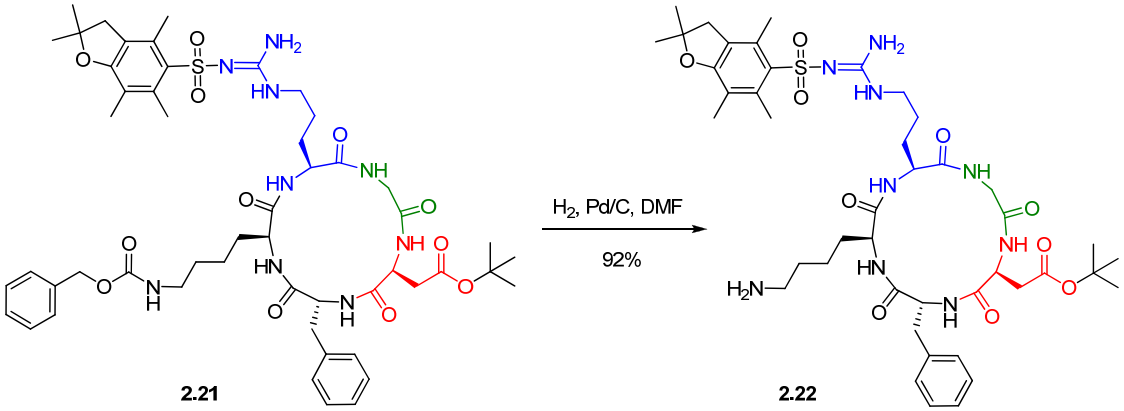

Scheme 2.11 – Benzyl carbamate removal to yield c[R(Pbf)GD(O^{t}Bu)fK], **2.22**. Original in colour.

Finally, the free ε-amine on the lysine of **2.22** was reacted with 5(6)-carboxyfluorescein *N*-hydroxysuccinimide ester and TEA in dry DMF for 18 h (Scheme 2.12). Size exclusion chromatography (Sephadex) on the crude mixture yielded amide coupled 5(6)-FL-c[R(Pbf)GD(O^{t}Bu)fK], **2.23**, as the product in 83% yield. Owing to the complexity of the structure which is present as two positional isomers, the ^{1}H NMR was difficult to interpret (see appendix – spectrum 2.9). However, signature peaks for the protected -Arg(Pbf)-Gly-Asp(OtBu)- portion of the molecule (as observed in the ^{1}H NMR spectra of the compounds previously discussed in this chapter) were discernible. The product was present as one spot by TLC, and there was one major peak in the ESI-MS at a m/z value of 635.7643 (100%, $[M+2H]^{2+}$).

Deprotection of **2.23** using TFA, and isolation by precipitating with Et_2O gave the final target compound **5(6)-FL-c[RGDfK]** (**2.24**) in 83% yield. As expected, the ^1H NMR was very complex (see appendix – spectrum 2.10), but peaks corresponding to the -RGD- portion of the molecule (as observed in the ^1H NMR spectra of the compounds previously discussed in this chapter) were discernible, as well as the aromatic protons of the phenylalanine residue and the fluorescein group. The product was present as one spot by TLC, and there was one major peak in the ESI-MS at a m/z value of 962.3663 (100%, $[M+H]^+$).

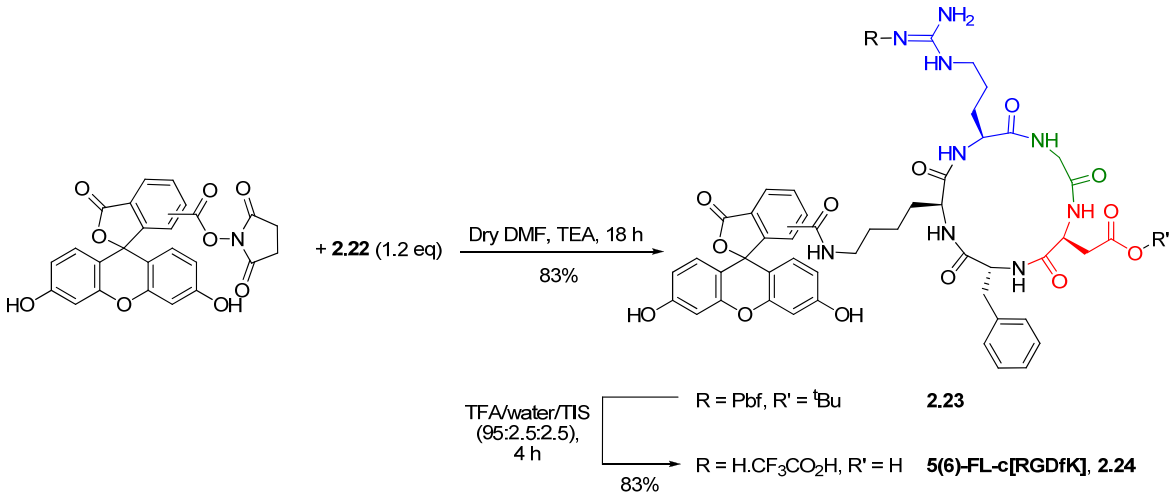

Scheme 2.12 – Reaction scheme showing the formation of **2.23** and subsequent deprotection conditions to form **2.24**. Original in colour.

2.3 Integrin Binding Studies

We then investigated the ability of the dendrons, **Z-G1-[RGD]$_3$** (**2.16**) and **Z-G2-[RGD]$_9$** (**2.17**), and positive and negative monovalent controls, **PEG-RGD** (**2.19**) and **PEG-GGG** (**2.20**), to bind integrin $\alpha_v\beta_3$. To monitor the binding event, we employed a competitive fluorescence polarisation (FP) assay, originally established by Li *et al* with respect to monovalent, cyclic RGD-integrin binding.[75] The principles behind this experiment are illustrated in Scheme 2.13.

In this experiment, the fluorescent probe **5(6)-FL-c[RGDfK]** (**2.24**) is bound to the integrin protein and is excited with polarised light at an appropriate wavelength of excitation. As the resulting probe-integrin complex is large, the complex tumbles/rotates slowly in solution. In other words, the mobility of the bound probe is reduced and the fluorescence emission from the probe retains much of its polarisation yielding a high FP signal. If binding occurs between a synthetic ligand which has been introduced into the system and the integrin; the fluorescent probe is displaced, its tumbling mobility increases, the fluorescence emission from the probe loses some proportion of its polarisation and the FP signal decreases in intensity. An EC_{50} (effective concentration) value can be determined for each

synthetic ligand at the point at which 50% of the probe has been displaced from the integrin. A recent review has discussed many of the advantages and disadvantages of FP as an assay technique.[263] Nevertheless, FP still remains a powerful approach that has allowed us to ascertain the effective comparative binding concentrations of our family of linear RGD peptides for integrin. Ultimately, this has allowed us to compare the relative affinities of a related family of ligands, for the same biological target, under the same experimental conditions.

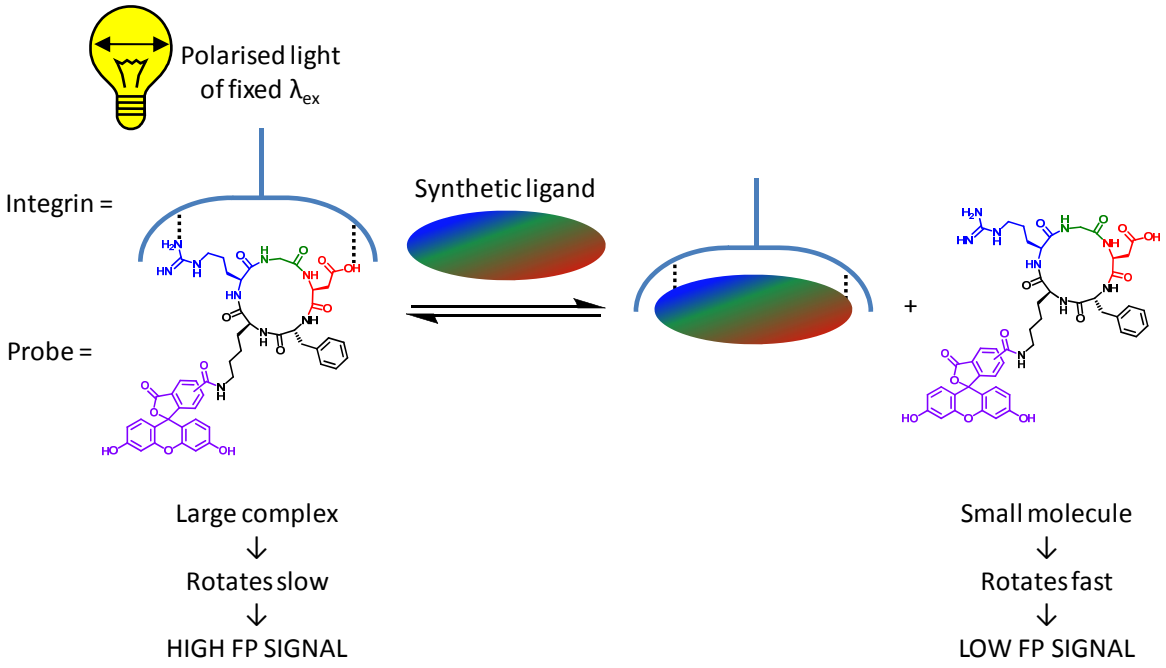

Scheme 2.13 – Schematic of the principles behind the FP competition assay.

It should be noted that this experiment was originally designed to be performed in microwell plates and read on a fluorescence plate reading machine. However, in our hands we could not replicate this and a significant amount of time was spent trying to optimise the conditions for performing the assay. We concluded that the plate reader we were using was not sensitive enough to detect the fluorescent probe binding to the protein. Finally, a successful method was developed using a fluorescence spectrometer and a specially purchased 100 μL volume microcuvette, titrating the synthetic ligand directly into the cuvette. It was important to keep the assay volume as small as possible, hence reducing the amount of integrin consumed per assay, owing to the high cost of the integrin $\alpha_v\beta_3$ protein.

Li and co-workers firstly tested the ability of probe **2.24** to bind integrin $\alpha_v\beta_3$. To the probe (10 nM) was added increasing amounts of protein, and the FP signal was shown to increase from the background value of 40 mP (millipolarisation units) – the intrinsic FP of the probe in the absence of integrin – to over 100 mP when the concentration of integrin was >350 nM (Fig. 2.3). Our results

(Fig. 2.4) were in agreement with this. As observed in the literature, the binding was kinetically fast and incubating the samples for >5 min did not significantly affect the FP signal (data not shown).

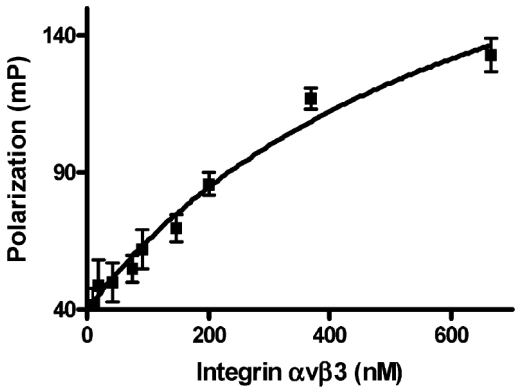

Fig. 2.3 - Titration data for binding of **5(6)-FL-c[RGDfK]** probe to integrin $\alpha_v\beta_3$ as a function of integrin concentration. FP values (mP) were measured after incubation of a **5(6)-FL-c[RGDfK]** probe (10 nM) and integrin $\alpha_v\beta_3$ (0-650 nM) mixture at 29 °C for 30 min. Data are presented as mean values ± standard deviations from 3 independent experiments. Figure reproduced from reference 75.

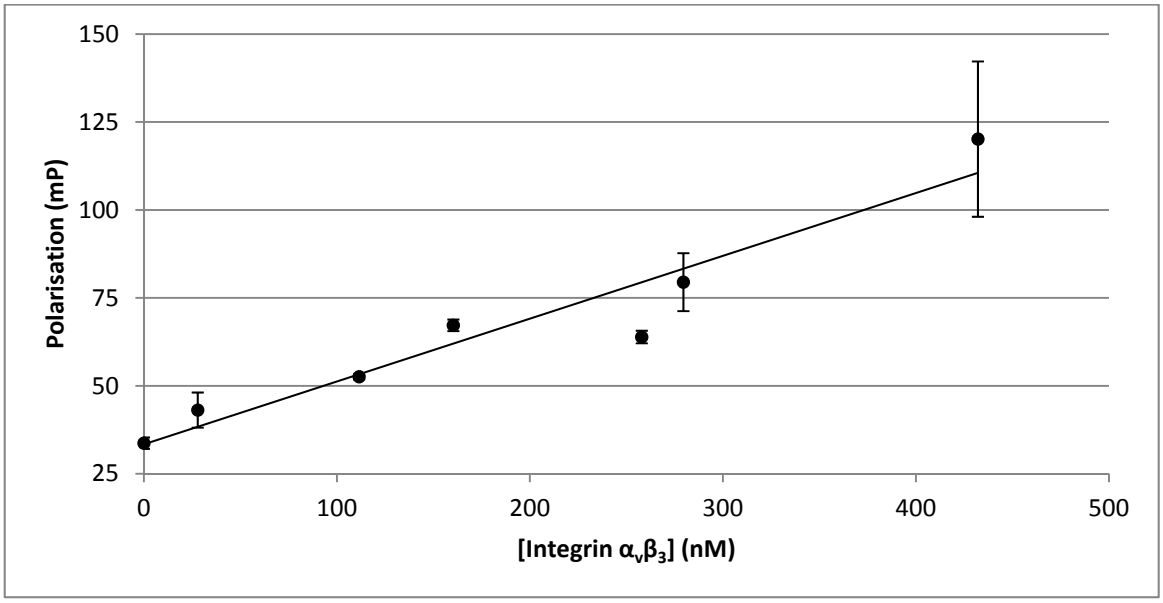

Fig. 2.4 - Titration data for binding of **5(6)-FL-c[RGDfK]** probe to integrin $\alpha_v\beta_3$ as a function of integrin concentration. FP values (mP) were measured after incubation of a **5(6)-FL-c[RGDfK]** probe (10 nM) and integrin $\alpha_v\beta_3$ (0-432 nM) mixture at 29 °C for 5 min. Data are presented as mean values ± standard deviations from at least 5 independent scans.

Competition experiments were then carried out using fixed concentrations of probe (10 nM) and integrin (280 nM), as the signal under these conditions was deemed to provide a suitable starting FP value. We initially compared the binding of **PEG-RGD** with **Z-G1-[RGD]$_3$** in order to determine

whether a trivalent dendritic approach to multivalency enhanced the binding of linear RGD to integrin $\alpha_v\beta_3$. Monovalent positive control, **PEG-RGD**, was unable to reduce the normalised FP signal to below 50% of its initial value in the range of concentrations tested (upto 1 mM), and only achieved a 30% reduction at best (shown in green, Fig. 2.5). As was expected, therefore, monovalent linear RGD has a low affinity for integrin,[119] and cannot displace enough of the strongly binding cyclic RGD fluorescent probe from the protein to reach 50% of the initial FP signal. Encouragingly, negative control, **PEG-GGG**, did not displace **5(6)-FL-c[RGDfK]** from its integrin binding site even at the maximum tested concentration of >3 mM, with the FP signal remaining unchanged (shown in purple, Fig. 2.5). Importantly, this provides evidence that the reduction in the FP signal using **PEG-RGD** is RGD-directed and not due to non-specific binding of the compound with the integrin. To explore this further, it would be desirable to synthesise and test another negative control (e.g. PEG-RGE or PEG-RAD) which is more similarly related to PEG-RGD (in terms of structure and charge distribution) but does not possess the required RGD binding sequence. This would further confirm the specificity of integrin binding to the linear RGD peptide in this assay.

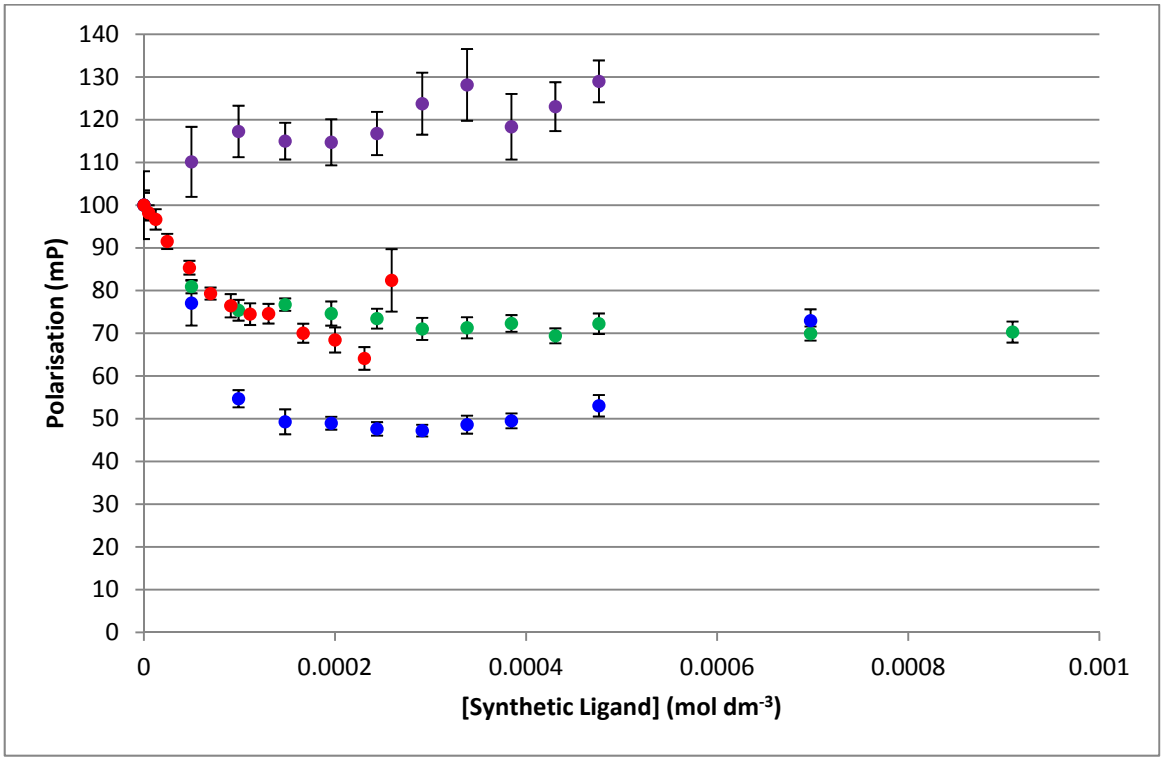

Fig. 2.5 – Normalised titration curves for the displacement of **5(6)-FL-c[RGDfK]** probe (10 nM) from integrin $\alpha_v\beta_3$ (280 nM) on the addition of the synthetic ligands: **Z-G1-[RGD]$_3$** (blue), **Z-G2-[RGD]$_9$** (red), **PEG-RGD** (green) and **PEG-GGG** (purple) after incubating at 29 °C for 5 min.

Unlike **PEG-RGD**, **Z-G1-[RGD]$_3$** was able to reduce the normalised FP signal to below 50% of the initial value at concentrations above 125 μM (shown in blue, Fig. 2.5). Although this is a very modest binding concentration compared with cyclic RGD, possibly a consequence of having to displace the

strongly binding cyclic RGD probe in the competition experiment, we can still conclude that there is a significant enhancement over the binding of the monovalent compound. We can hence conclude that trivalent RGD is a much more effective ligand in its binding to integrin under the conditions of this assay. If we consider the binding to integrin by each compound on a 'per-RGD' basis (Table 2.1), the EC_{50} value per RGD for **Z-G1-[RGD]$_3$** is 375 μM, much less than **PEG-RGD** which did not achieve significant enough binding to allow extrapolation of an EC_{50} value, even at concentrations as high as 1 mM.

Ligand	EC_{50} / μM	K_i / μM	No. of RGD's	EC_{50} 'per RGD' / μM	K_i 'per RGD' / μM
PEG-RGD	-	-	1	-	-
Z-G1-[RGD]$_3$	125	123	3	375	369

Table 2.1 – EC_{50}, K_i, EC_{50} 'per RGD' and K_i 'per RGD' values obtained for **PEG-RGD** and **Z-G1-[RGD]$_3$** using FP.

As we are displacing a tight binding probe from the RGD-binding site, it was suggested that EC_{50} is not closely related to K_i (the equilibrium dissociation constant of inhibitor (i.e. synthetic ligand)) and in our case EC_{50} may substantially underestimate the binding constant of each of our synthetic ligands. K_i is mathematically accessible using the equation of Cheng and Prusoff:[264]

$$K_i = \frac{EC_{50}}{1 + \frac{[probe]}{K_d}} \qquad (Eq.\ 2.1)$$

where EC_{50} is the effective concentration of the synthetic ligand at the point at which 50% of the probe has been displaced from the integrin, [probe] is the concentration of **5(6)-FL-c[RGDfK]**, and K_d is the equilibrium dissociation constant of the **5(6)-FL-c[RGDfK]**-integrin complex.

Li and co-workers calculated that K_d was 0.67 ± 0.15 μM, as determined by analysis of their **5(6)-FL-c[RGDfK]**-integrin binding isotherm (Fig. 2.3) using GraphPad PRISM software and curve fitting with the one-site binding equation:

$$FP = \frac{FP_{max}.C}{K_d + C} \qquad (Eq.\ 2.2)$$

where FP is the change in fluorescene polarisation, FP_{max} is the maximum fluorescence polarisation, and C is the concentration of integrin protein.

Unfortunately our binding isotherm (Fig. 2.4) does not reach saturation in the range of integrin concentrations tested, and therefore we cannot calculate K_d for the **5(6)-FL-c[RGDfK]**-integrin complex under our experimental conditions using the non-linear regression method. However, for the

purpose of this study we have used the K_d value calculated by Li and co-workers as the initial (linear) part of their binding isotherm closely matches that of ours. As such, the K_i for **Z-G1-[RGD]$_3$** was calculated using Eq. 2.1:

$$K_i = \frac{125 \times 10^{-6}\text{M}}{1 + \frac{10 \times 10^{-9}\text{M}}{0.67 \times 10^{-6}\text{M}}} = 123 \times 10^{-6}\text{M}$$

As K_d >> [probe], $K_i \approx EC_{50}$ and we can conclude that EC_{50} is, in actual fact, a good approximation of the K_i of **Z-G1-[RGD]$_3$** (and K_i on a 'per-RGD' basis, Table 2.1) and of the dissociation constants of the other synthetic ligands that were subsequently investigated in this competition assay. Therefore, the reported binding concentrations *are* modest as previously stated and are not significantly improved when the affinity of the probe for integrin is taken into consideration.

Nevertheless, comparing and contrasting the FP data obtained for **PEG-RGD** and **Z-G1-[RGD]$_3$** reveals that a multivalency effect is playing an active role in enhancing the binding of the trivalent linear RGD peptide to the integrin protein. However, the mechanism by which the multivalency effect manifests itself is unclear. Integrin is known to only have one binding site and so the opportunity for more than one RGD peptide to bind to the protein is prohibited, and as such, multivalency cannot operate by multiple binding of several RGD's to one integrin. Two other possible mechanisms of multivalency may be occurring: (i) a high local concentration effect of ligand about the integrin binding site, in which when one ligand dissociates from its partner protein, another ligand is close enough in space to significantly favour ligand rebinding, and/or (ii) a multi-binding effect where, after the first binding of an RGD-integrin partnership has taken place, a second ligand binding to a second protein in solution becomes favoured (Fig. 2.6). For this latter scenario to operate, the integrins must be clustered together in some way, almost like when they are bound in a cell membrane. As integrin is a transmembraneous protein, the isolated protein has to be supplied formulated in a surfactant (non-ionic Triton X-100) (Fig. 2.7), in order to stabilise the protein and solubilise it in water. Interestingly, the concentration of Triton X-100 in the integrin-surfactant formulation (the integrin is presented in a buffered solution containing 0.2 wt % Triton X-100 which represents a 3.2 mM concentration of this surfactant) used in the FP assay is above the critical micelle concentration (CMC = 0.22 to 0.24 mM[*]) of Triton X-100 and so the protein cannot be viewed as being strictly 'free' in solution, but rather held in micellar-like Triton assemblies. The transmission electron microscopy (TEM) image of the 'as supplied' integrin $\alpha_v\beta_3$ solution (Fig. 2.8) shows clusters of spherical micellar assemblies formed from the self-assembly of Triton X-100 which – owing to the hydrophobic domain of integrin, the reported dimensions of the integrin $\alpha_v\beta_3$ extracellular headgroup (~9 nm × 6 nm × 4.5 nm) connected to the extracellular tails (~16 nm long and ~2 nm in diameter),[82] and the size of the micelle clusters (~250 to

[*] Source: Sigma-Aldrich

500 nm across) – are suggested to contain multiple copies of the protein with its hydrophilic headgroup-tail domains protruding from the surface of the micelles. This clustering of integrins within a micelle or vesicle is somewhat similar to the situation on the extracellular region of a cell membrane, and as such, we suggest that this formulation of integrin in a surfactant phase may permit the enhancement in binding of a multivalent, dendritic ligand to multiple integrins. However, the longest distance between two RGD ligands conjugated to the same dendritic construct is estimated to be about 1.5 nm at most, at least when considering our G1 system as a representative example. Considering the dimensions of the integrin headgroup-tail domains and the approximate distance between two adjacent RGD-binding pockets (estimated to be ~4.5-6 nm apart), the multiple binding events scenario seems geometrically unfeasible. We therefore believe the enhanced binding is due to a high local concentration effect. Nevertheless, integrin-surfactant formulations could provide quantitative insight into the binding processes of integrin proteins in (artificial) cell membranes without the need for cell-based assays and cell culture equipment.

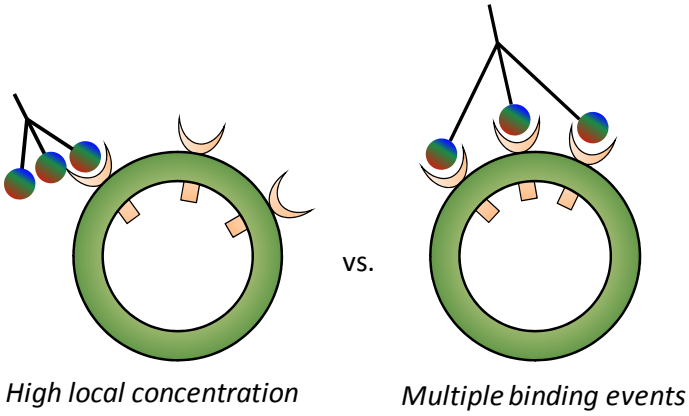

Fig. 2.6 – The possible mechanisms of multivalency in integrin recognition by **Z-G1-[RGD]$_3$**.

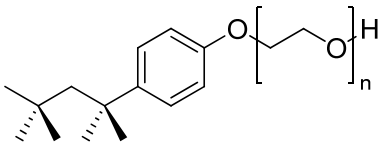

Fig. 2.7 – The structure of Triton X-100.

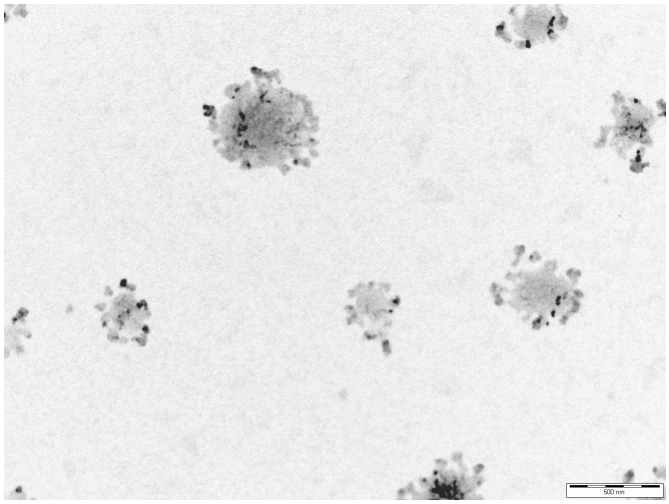

Fig. 2.8 – TEM image of integrin-Triton X-100 assemblies prior to addition of synthetic RGD peptide ligands. Scale bar = 500 nm.

We then went on to study the **Z-G2-[RGD]$_9$** system using the same FP assay, in order to determine whether a nonavalent (second generation) dendritic approach to multivalency further enhanced the binding of linear RGD to integrin $\alpha_v\beta_3$ over that of **Z-G1-[RGD]$_3$**, as would perhaps be expected. The results showed that although there was an initial decrease in the FP signal, this was not as significant as the displacement of fluorescent probe by **Z-G1-[RGD]$_3$**, and furthermore the signal was found to plateau off before reaching the EC_{50} mark (shown in red, Fig. 2.5). This is rather counterintuitive and suggests, surprisingly, that the first generation dendron with 6 fewer RGD ligands is able to bind integrin better. Analogous trends have previously been observed in glycodendrimers binding to glycoproteins,[8] where bulky surface ligands can hinder the binding of a higher generation dendrimer to a biological host due to increased steric hindrance at the interface between the guest and host. In this particular assay, out of the two dendrons tested, the first generation system can therefore be deemed optimum for integrin binding.

In addition to the binding characteristics already discussed, when we look at the binding profiles at even higher concentration we observe a turning point in the FP signal of each compound, with the signal increasing in intensity far above that of the initial FP value before the addition of synthetic ligand (Fig. 2.9). The increases were found to start at approximate values of 250 μM, 800 μM, and 2 mM for **Z-G2-[RGD]$_9$**, **Z-G1-[RGD]$_3$** and **PEG-RGD** respectively. We propose that the rise in FP signal is caused by non-specific binding between the RGD ligands and the target protein, generating probe-integrin-ligand complexes which are larger in size than the initial probe-integrin partnerships. The linear RGD peptide conjugated to each of the molecules is not zwitterionic and each RGD has an overall net negative charge at pH 7 of -1, owing to the fact that there are two carboxylic acids but only one basic guanidinium group. Therefore, each compound can be said to have an overall anionic character: 1- for **PEG-RGD**, 3- for **Z-G1-[RGD]$_3$** and 9- for **Z-G2-[RGD]$_9$**. We suggest that this

negative charge may induce ligand-protein aggregation/precipitation, for example, via integrin surface binding, leading to the apparent increase in FP intensities. This hypothesis is supported by the observation that the turning point of the FP signal occurs at approximately the same effective RGD concentration, and hence approximately the same level of net negative charge, for each of the three synthetic ligands: 250 μM for **Z-G2-[RGD]$_9$**, an effective RGD concentration of 2.25 mM (250 μM × 9); 800 μM for **Z-G1-[RGD]$_3$**, an effective RGD concentration of 2.4 mM (800 μM × 3); and 2 mM for **PEG-RGD**. This does open the question of why **PEG-GGG** (which also has one negative charge) does not show the same effect within the range of concentrations tested (0 to 3.33 mM). Clearly, RGD binding to integrin *and* the excess negative charge must be important for aggregation to occur.

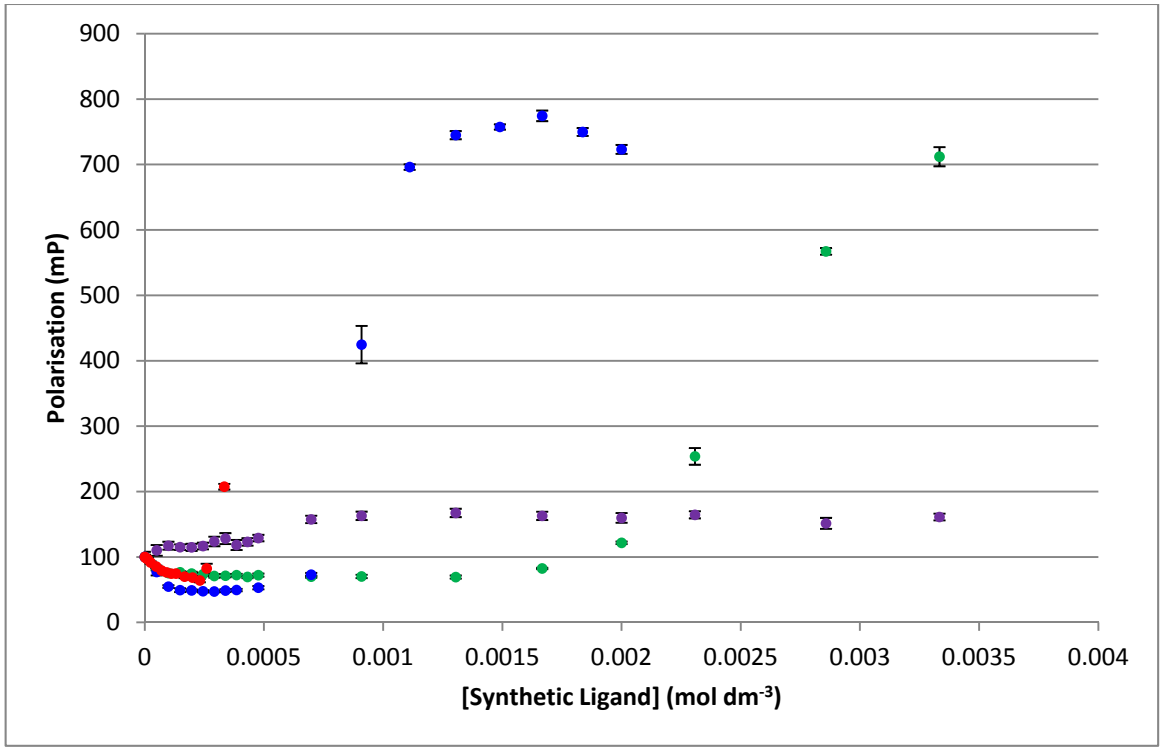

Fig. 2.9 – Normalised titration curves at elevated concentrations for the displacement of **5(6)-FL-c[RGDfK]** probe (10 nM) from integrin $\alpha_v\beta_3$ (280 nM) on the addition of the synthetic ligands: **Z-G1-[RGD]$_3$** (blue), **Z-G2-[RGD]$_9$** (red), **PEG-RGD** (green) and **PEG-GGG** (purple) after incubating at 29 °C for 5 min.

2.4 Attempts at 'Capping' the C-terminus

Based on the information gained from the FP data, we hypothesised that chemically modifying the RGD peptide by 'capping' the C-terminus carboxylic acid, so as to make the peptide zwitterionic, might further enhance the binding of the synthetic ligands by inhibiting the non-specific interactions observed above. This section discusses the steps taken towards further derivatising the RGD peptide and the synthetic problems encountered.

2.4.1 Attempted Synthesis of R-Arg(Pbf)-Gly-Asp(O^{t}Bu)-OMe (where R = Z or Fmoc)

Several attempts were made to 'cap' the C-terminus of the peptide with a methyl ester as we predicted that this small capping group should not hinder the peptide epitope accessing the RGD binding site on the integrin (Fig. 2.10). These attempts were performed using solution-phase peptide chemistry.

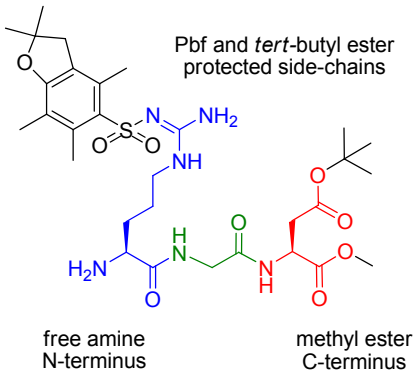

Fig. 2.10 – Target peptide H_2N-Arg(Pbf)-Gly-Asp(O^{t}Bu)-OMe bearing a methyl ester 'capped' C-terminus, ready to couple onto the G1 and G2 dendrons via the free amine N-terminus. Original in colour.

We initially opted to use a benzyl carbamate protecting group on the N-terminus, having optimised the synthesis of the protected RGD with this strategy, as described earlier. Starting at the C-terminus end of the peptide, the coupling of Z-Gly-OH with H_2N-Asp(O^{t}Bu)-OMe.HCl using DIPEA and coupling reagent T3P yielded the desired product, **2.25**, in quantitative yield (Scheme 2.14). A simple acid/base workup procedure was the only purification step needed to produce the product with high purity. This was confirmed by ^{1}H NMR which showed a doublet peak at 7.05 ppm corresponding to the newly formed amide N*H* proton, and a downfield shift in the aspartic acid α-*H* from below 4.00 ppm to 4.84-4.80 ppm due to the formation of the adjacent electron-withdrawing amide functional group.

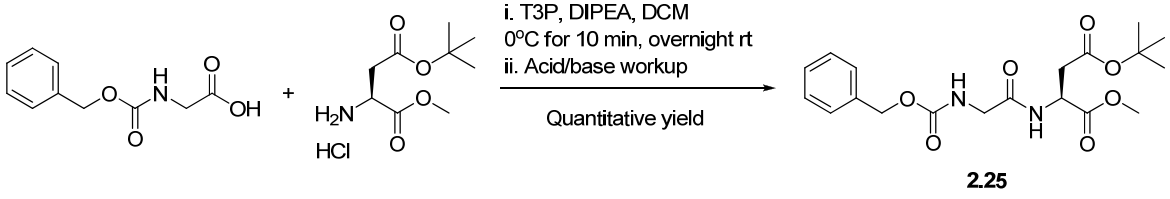

Scheme 2.14 – Reaction scheme showing the synthesis of Z-Gly-Asp(O^{t}Bu)-OMe, **2.25**.

The next step was to remove the benzyl carbamate (Z) group using catalytic hydrogenolysis. Z-Arg(Pbf)-OH, could then be coupled to the deprotected amine. Deprotection of the Z group proved

unsuccessful however, as the desired product, H_2N-Gly-Asp(O^{t}Bu)-OMe, underwent an intramolecular lactamisation to yield the unwanted cyclic by-product, **2.26**, in 93% yield (Scheme 2.15), as determined by the absence of the methyl ester resonance at 3.72 ppm in the ^{1}H NMR. ESI-MS also detected the mass of the cyclised by-product at a m/z value of 251.1 (100%, [cyclised M+Na]$^+$) but no peak for the mass of the product (MW = 260 g mol^{-1}). This may be due to an acidic environment at the catalyst surface promoting acid-catalysed, intramolecular nucleophilic attack of the free amine on the methyl ester to form a stable 6-membered ring, promoted by the entropically favourable loss of MeOH.

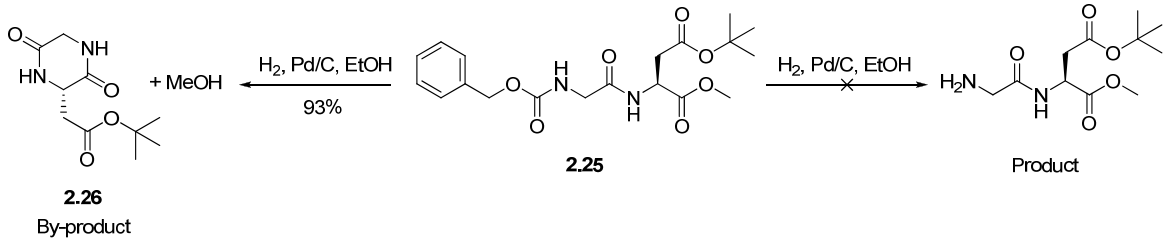

Scheme 2.15 – Reaction scheme showing unwanted by-product formation during the Z deprotection of **2.25**.

Adapting our strategy, we turned to the Fmoc protecting group approach. Fmoc is removed under mildly basic (20% piperidine) conditions as opposed to an acid catalysed reaction, so it was hoped that after Fmoc removal, the product would remain intact and not undergo cyclisation as before. Fmoc-Gly-OH and H_2N-Asp(O^{t}Bu)-OMe.HCl were coupled together using DIPEA and T3P to generate the product, **2.27**, in 85% yield via acid/base workup, without requiring further purification (Scheme 2.16). This was confirmed by ^{1}H NMR which showed a doublet peak at 7.07 ppm corresponding to the newly formed amide N*H* proton, and a downfield shift in the aspartic acid α-*H* from below 4.00 ppm to 4.85 ppm due to the formation of the adjacent electron-withdrawing amide functional group.

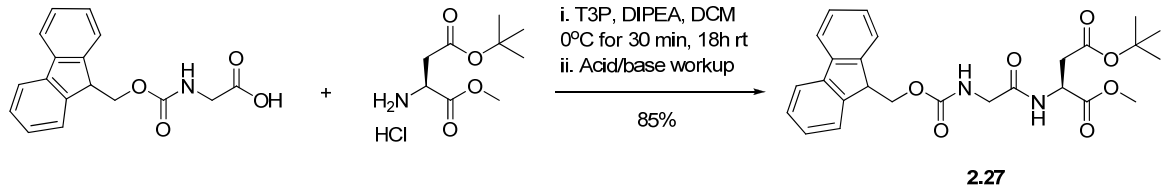

Scheme 2.16 – Reaction scheme showing the synthesis of Fmoc-Gly-Asp(O^{t}Bu)-OMe, **2.27**.

Deprotection of the Fmoc group was carried out using 20% piperidine in DCM (Scheme 2.17). Unfortunately, the unwanted cyclisation reaction still occurred, yielding compound **2.28**. The spectroscopic data to support the formation of **2.28** was in agreement with that of **2.26** (formed from the deprotection of **2.25**). A crude NMR was not obtained before silica column purification of the material, so it is not known whether cyclisation took place during the reaction or when the crude

mixture was loaded onto silica. However, the crude material could not have been used in the amide coupling reaction with Fmoc-Arg(Pbf)-OH that was to follow without silica column purification first to remove excess piperidine and Fmoc/Fmoc-piperidine by-products.

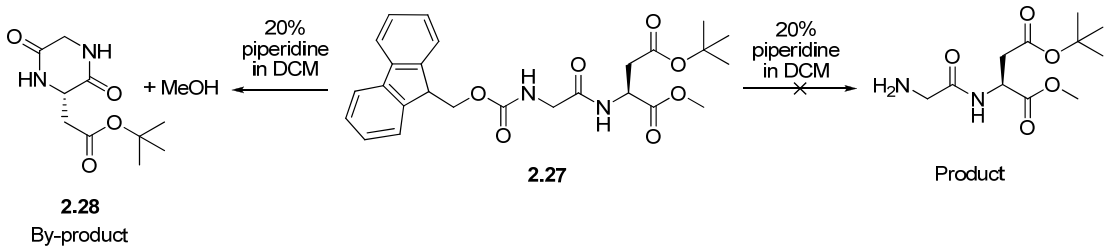

Scheme 2.17 - Reaction scheme showing unwanted by-product formation during the Fmoc deprotection of **2.27**.

An alternative strategy was to carry out the synthesis starting at the N-terminus, deprotecting the C-terminus and growing the peptide out in this manner. The cyclohexylammonium salt of Z-Arg(Pbf)-OH was amide coupled with H_2N-Gly-OMe.HCl using DIPEA and T3P and the product, **2.29**, was formed in anywhere between 86% and quantitative yield following an acid/base workup procedure (Scheme 2.18). The newly formed amide N*H* resonance at 7.69 ppm was enough evidence to support the formation of **2.29**. As Z-Arg(Pbf)-OH.CHA was used without aqueous acid extraction of the cyclohexylammonium group and converting Z-Arg(Pbf)-OH.CHA to the free carboxylic acid, as discussed earlier, a trace amount of the cyclohexylamide coupled impurity was seen in the NMR and mass spec. For example, in addition to the peak corresponding to the product at m/z 632.2763 (100%, $[M+H]^+$), we also observed a peak for the trace impurity at m/z 642.3 (8%, [trace impurity+H]$^+$).

Simple hydrolysis of the methyl ester of **2.29** using 1 M NaOH at 40°C should then have facilitated the coupling of H_2N-Asp(O^tBu)-OMe to the deprotected carboxylic acid. However, it is unclear from the NMR and MS data what had actually happened in the saponification reaction, except that the only species to be isolated was a trace impurity carried through from the synthesis of starting material **2.29** (Scheme 2.19). We hypothesised that base hydrolysis of the benzyl carbamate (it is known that NaOH in aqueous organic solvents can achieve this[261]), and/or acid hydrolysis of the acid-sensitive Pbf protecting group upon acidification of the basic aqueous phase to pH 1 (in order to try and extract the free carboxylic acid product from the reaction) may have resulted in irreversible loss of the peptide to the aqueous phase. The synthesis was abandoned as a result.

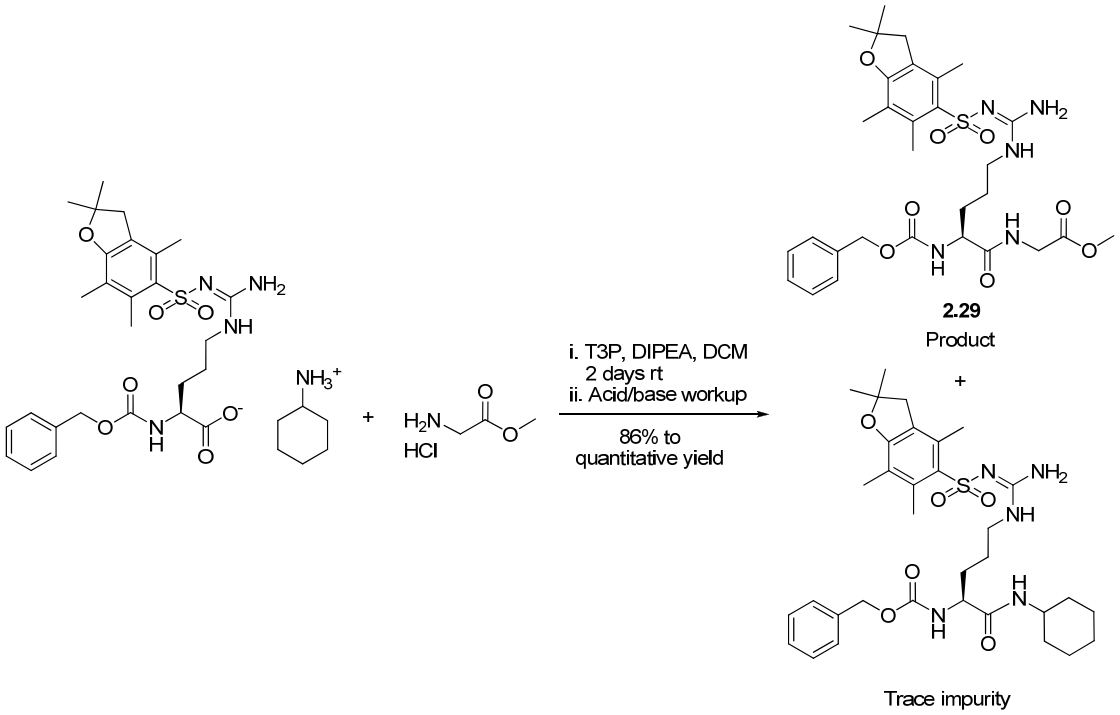

Scheme 2.18 – Reaction scheme showing the synthesis of Z-Arg(Pbf)-Gly-OMe, **2.29**, and the cyclohexylamide coupled trace impurity.

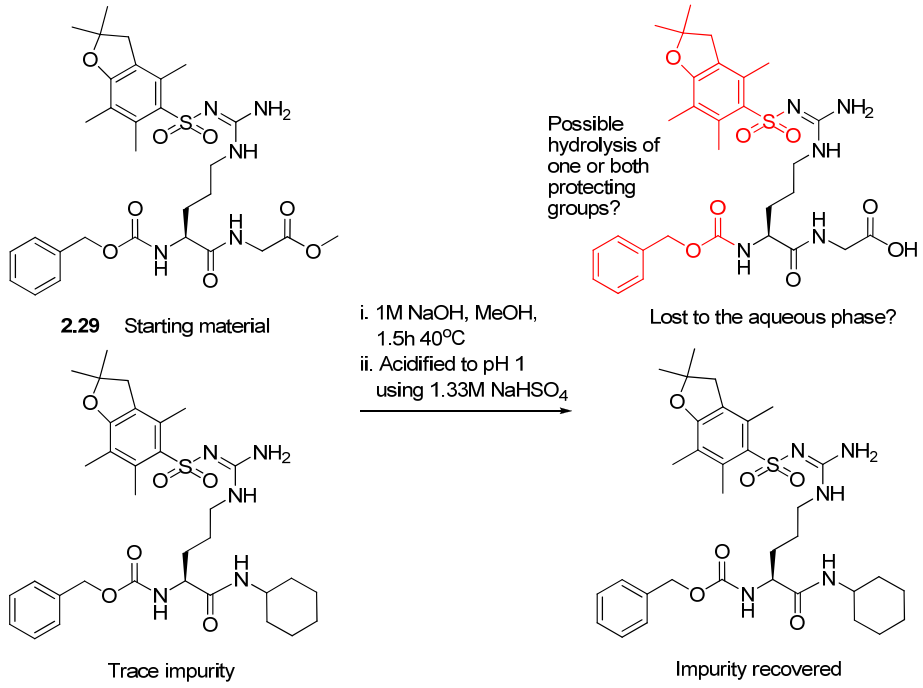

Scheme 2.19 – Reaction scheme showing the outcome of the saponification reaction of **2.29**. Original in colour.

2.4.2 Attempted Synthesis of Fmoc-Arg(Pbf)-Gly-Asp(OBn)-NH_2

Following the problematic synthesis of the peptide bearing a methyl ester protected C-terminus, a protecting group which we reasoned was too labile for the solution-phase deprotection methods we were employing, we decided to change the methyl ester for a more chemically robust primary amide (Fig. 2.11). Once again, such a group would effectively cap the C-terminus of the RGD peptide.

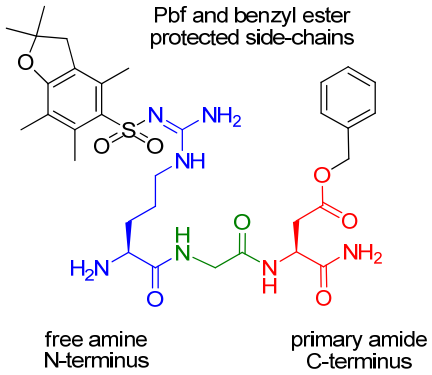

Fig. 2.11 – Target peptide H_2N-Arg(Pbf)-Gly-Asp(OBn)-NH_2 bearing a primary amide 'capped' C-terminus, ready to couple onto the G1 and G2 dendrons via the free amine N-terminus. Original in colour.

The only L-aspartamide amino acid commercially available with a protecting group on the side-chain carboxylic acid was L-aspartamide β-benzyl ester hydrochloride. Our synthetic design of the target peptide was therefore limited to a Boc/Fmoc protecting group methodology on the N-terminus, as catalytic hydrogenolysis of a Z group would also cleave the benzyl ester on the aspartamide side-chain. The attempted solution-phase synthesis is summarised in Scheme 2.20.

In the first step, Boc-protected glycine was amide coupled to L-aspartamide β-benzyl ester hydrochloride in the presence of DIPEA and TBTU. Following an aqueous workup procedure, this afforded the product Boc-Gly-Asp(OBn)-NH_2, **2.30**, in yields between 94% and quantitative. No further purification was required. This was confirmed by ^{1}H NMR which showed a doublet peak at 7.70 ppm corresponding to the newly formed amide N*H* proton, and a downfield shift in the aspartic acid α-*H* from below 4.00 ppm to 4.91-4.86 ppm due to the formation of the adjacent electron-withdrawing amide functional group. Boc-protected glycine was specifically chosen, as the benzyl ester present on the protected aspartic acid is stable to the acid conditions required for the removal of a Boc group. The next step involved the deprotection of the Boc group using TFA. Removal of the volatiles *in vacuo* yielded the TFA salt of H_2N-Gly-Asp(OBn)-NH_2, **2.31**, in yields between 70-89%, as evidenced by the loss of the ^{1}H NMR resonance at 1.42 ppm which corresponded to the *tert*-butyl methyl groups in precursor compound **2.30**. Compound **2.31** was then amide coupled to the orthogonally protected L-arginine, N_α-Fmoc-N_ω-Pbf-L-arginine, to yield Fmoc-Arg(Pbf)-Gly-

Asp(OBn)-NH_2, **2.32**, in yields between 81% and quantitative. The presence of two secondary amide N*H* peaks in the ^{1}H NMR at 8.12 and 7.82 ppm, in addition to the downfield shift of the glycine CH_2 resonance from 3.77-3.65 to 4.00-3.82 ppm due to the newly formed adjacent electron-withdrawing amide group, was evidence enough that the reaction was successful (see appendix – spectrum 2.11). Fmoc-protected arginine was coupled onto the free amine of **2.31** because the Boc-protected version would require acidic conditions to deprotect the Boc group which would also induce unwanted hydrolysis of the Pbf group on the arginine side-chain.

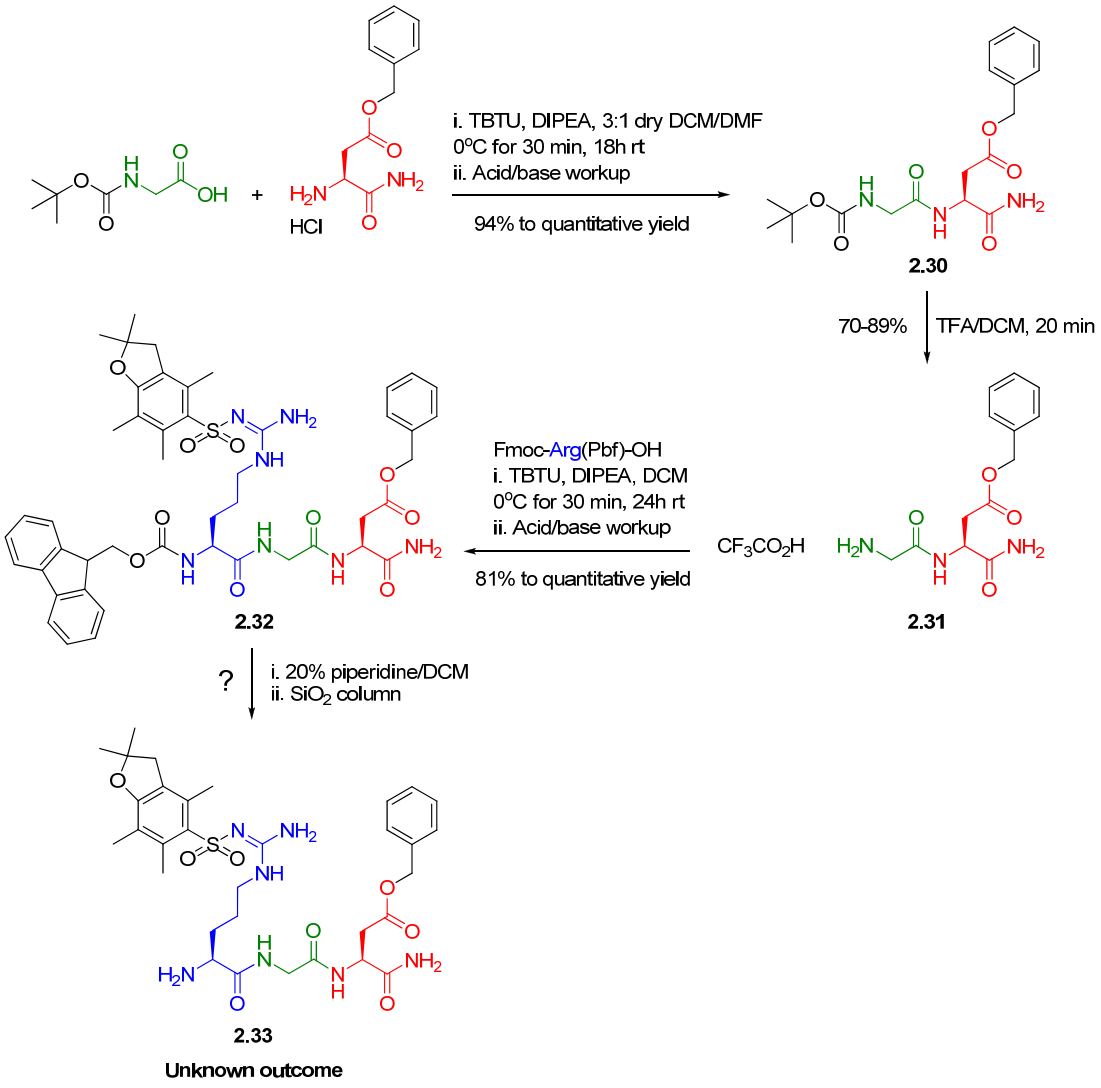

Scheme 2.20 – Reaction scheme showing the attempted synthesis of H_2N-Arg(Pbf)-Gly-Asp(OBn)-NH_2, **2.33**.

The final synthetic step should have been a straightforward one, as it involved simple Fmoc deprotection of **2.32** using 20% piperidine in DCM. Silica column purification of the crude reaction mixture using a gradient elution of DCM, to 98:2 DCM/MeOH, to 95:5 DCM/MeOH, to 9:1 DCM/MeOH, all containing 1% TEA to neutralise the acidic silica and prevent the free amine of the

compound from sticking to the column, afforded a white solid (1.6 g, quantitative yield). ^{1}H NMR of the isolated material showed peaks corresponding to TEA (from the column eluent) and piperidine (carried through from the reaction) (see appendix – spectrum 2.12). The solid was dissolved in DCM and washed with water and brine to try and extract the water soluble TEA and piperidine impurities, but after drying over $MgSO_4$, filtering and evaporating the solvent *in vacuo*, this only yielded a broad and unclear ^{1}H NMR spectrum (see appendix – spectrum 2.13).

In addition, the ESI-MS of the silica columned material (prior to the aqueous workup) does not show the required molecular ion peak for the target compound **2.33** (MW = 687.3 g/mol). A peak at *m/z* 688.3 for the $[M+H]^+$ adduct is absent. Peaks at *m/z* 665.3 (1+), 687.3 (1+) and 333.2 (2+) which have been assigned as $[X+H]^+$, $[X+Na]^+$ and $[X+2H]^{2+}$ respectively, correspond to a major unidentified by-product (X) of the reaction/purification procedure. The mass of the unknown molecule giving rise to these major peaks in the MS is 23 mass units less than the desired target product **2.33** indicating that part of the molecule has been lost in the reaction in some way. The obtained compound could not be identified and as such, the synthesis was abandoned due to time constraints.

2.4.3 Progress Towards the Synthesis of Alloc-Arg(Pbf)-Gly-Asp(O^{t}Bu)-OBn

Revisiting our RSA of the protected RGD, we sought an alternative strategy for the derivatisation of the tripeptide. With the premise of 'capping' the C-terminus still in mind, we devised a design where the C-terminus is protected by a benzyl ester and the N-terminus an Alloc group. This not only enables the C-terminus to be capped but also allows orthogonal protection of the side-chains, N-terminus and C-terminus. Similar to our approach with the methyl ester protected C-terminus of R-Arg(Pbf)-Gly-Asp(O^{t}Bu)-OMe (where R = Z or Fmoc), the advantage of this, unlike the previous method where the C-terminus is permanently blocked with a primary amide, lies in the ability to chemoselectively remove one of the protecting groups on either terminus and derivatise the peptide further (Fig. 2.12). The deprotection conditions of each of the protecting groups in the target peptide are summarised in Table 2.2 which has been adapted from the review by Albericio and co-workers.[261] The authors quote that the Pbf, *tert*-butyl ester and benzyl ester groups are stable to the removal conditions of Alloc, although Alloc is incompatible with the catalytic hydrogenolysis removal of groups such as *p*NZ (*p*-Nitrobenzyloxycarbonyl). However, the benzyl ester can be hydrolysed using NaOH in aqueous organic solvents, making the assumption that the Alloc, Pbf and *tert*-butyl ester groups are stable under these conditions, should the need to cleave this protecting group arise.

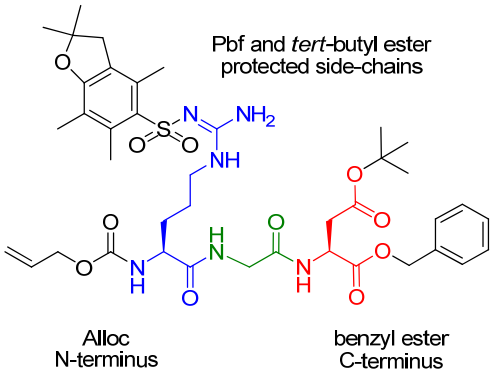

Fig. 2.12 – Target peptide Alloc-Arg(Pbf)-Gly-Asp(O^{t}Bu)-OBn bearing a benzyl ester protected C-terminus and an Alloc protected N-terminus. Original in colour.

Name and Structure	Removal conditions	Stable to the removal of
Allyloxycarbonyl (Alloc) 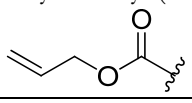	Pd(PPh$_3$)$_4$ cat., scavengers: $H_3N{\cdot}BH_3$, $Me_2NH{\cdot}BH_3$ or $PhSiH_3$ in organic solvents.	Boc, Fmoc, Trt, *p*NZ [a]
Benzyl (Bn) 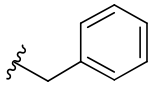	1) HF 2) TFMSA 3) H_2 cat. 4) NaOH in aq. organic solvents	Boc,[b] Fmoc, *p*NZ,[a] Trt, Alloc
2,2,4,6,7-pentamethyldihydrobenzofuran-5-sulfonyl (Pbf) 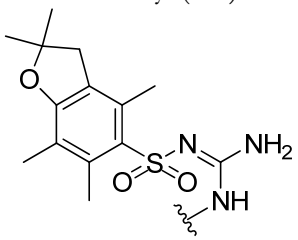	90% TFA + scavengers (H_2O and TIS) 1 h (longer times in multiple arginine containing peptides)	Fmoc, Trt, Alloc
tert-Butyl (^{t}Bu) 	1) 90% TFA in DCM (solid phase and solution) 2) 4 M HCl in dioxane (solution)	Fmoc, Z,[c] Trt, Alloc, *p*NZ

[a] Except catalytic hydrogenolysis removal. [b] Except repetitive removals. [c] Catalytic hydrogenolysis removal.

Table 2.2 – Protecting groups of the target peptide in Fig. 2.12, their removal conditions and stability to the removal of other protecting groups. Adapted from ref. 5.

Progress has been made towards the synthesis of the target peptide (Scheme 2.21) and this will be outlined here. As H_2N-Asp(O^{t}Bu)-OBn is not commercially available, the first step required the synthesis of P-Asp(O^{t}Bu)-OBn from P-Asp(O^{t}Bu)-OH (where P = protecting group: Z or Fmoc). The choice of alpha-amine protecting group was made such that it should be removable under

conditions which do not involve acids or catalytic hydrogenolysis, therefore Fmoc was chosen. Following the procedure of Zajdel *et al*,[265] Fmoc-Asp(O^{t}Bu)-OH, tetra-*n*-butylammonium bromide (TBAB), and potassium carbonate were suspended in a mixture of acetonitrile/DCM, followed by dropwise addition of benzyl bromide, then the reaction was allowed to stir for 18 h at rt. After a basic workup, the crude material was recrystallised from DCM/cyclohexane to provide the product, **2.34**, in 95% yield (Scheme 2.21). The structure of the product was confirmed with ^{1}H NMR by the presence of two doublet resonances corresponding to each proton of the benzyl C*H*$_2$, in which the protons are shifted downfield from ~4.5 ppm (when adjacent to Br) to 5.26-5.19 ppm when adjacent to the electron-withdrawing ester group, and are geminally (^2J) coupled to one another due to the chirality of the molecule (δ 5.26 (d, C*H*^{A} benzylic, J = 12.5 Hz, 1H); 5.19 (d, C*H*^{B} benzylic, J = 12.5 Hz, 1H)).

Fmoc deprotection using 20% piperidine in DCM, followed by silica column purification gave the product, **2.35**, in 61% yield (Scheme 2.21). Removal of the Fmoc group resulted in the loss of the electron-withdrawing carbamate group adjacent to the aspartic acid α-*H*. This was reflected in the ^{1}H NMR by an upfield shift of the aspartic acid α-*H* at 4.67 ppm to 3.52 ppm, as well as the absence of peaks corresponding to the Fmoc aromatic C*H*'s at 7.78, 7.61, 7.41 and 7.37-7.30 ppm; carbamate N*H* at 5.90 ppm; Fmoc C*H*$_2$ at 4.43-4.35 ppm; and Fmoc C*H* at 4.24 ppm. A reduction in mass to a m/z value of 224.0912 (100%, $[M+H–C_4H_8]^+$) was confirmed by ESI-MS.

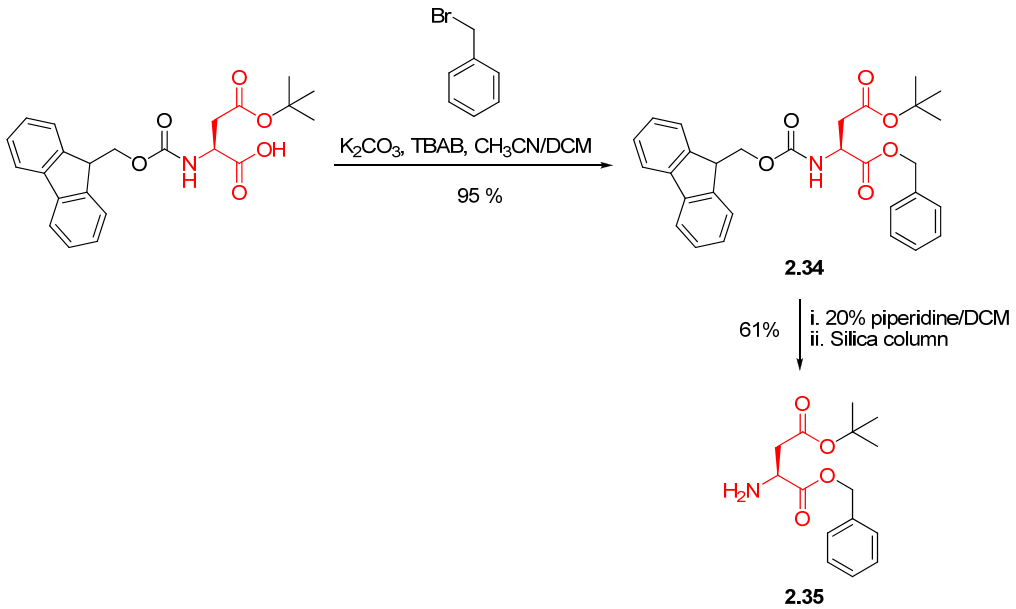

Scheme 2.21 – Reaction scheme showing the synthesis of Fmoc-Asp(O^{t}Bu)-OBn, **2.34**, and subsequent deprotection to H$_2$N-Asp(O^{t}Bu)-OBn, **2.35**. Original in colour.

Alloc-Gly-OH is not commercially available so this was synthesised from glycine according to a typical literature method.[266] Glycine was reacted with allyl chloroformate overnight and then the product, **2.36**, was isolated by a straightforward extraction in 75% yield (Scheme 2.22). This was evidenced by

the appearance of the carbamate N*H* triplet resonance in the ^{1}H NMR at 5.72 ppm, as well as the presence of peaks corresponding to the allyl portion of the molecule (δ 5.29-5.24 (m, *H*-CH=CHCH$_2$, 1H); 5.20-5.16 (m, *H*-CH=CHCH$_2$, 1H); 4.59-4.54 (m, H$_2$C=CHC*H*$_2$, 2H)).

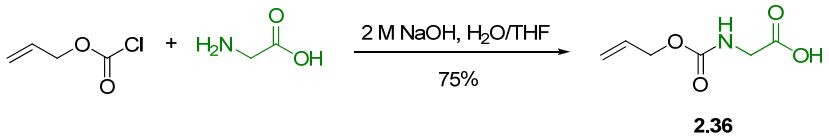

2.36

Scheme 2.22 – Reaction scheme showing the synthesis of Alloc-Gly-OH, **2.36**. Original in colour.

TBTU coupling of **2.35** and **2.36** gave the amide-coupled product, **2.37**, in 95% yield after a simple workup (Scheme 2.23). This was confirmed by ^{1}H NMR which showed a doublet peak at 7.09 ppm corresponding to the newly formed amide N*H* proton, and a downfield shift in the aspartic acid α-*H* from 3.52 ppm to 4.86 ppm due to the formation of the adjacent electron-withdrawing amide functional group.

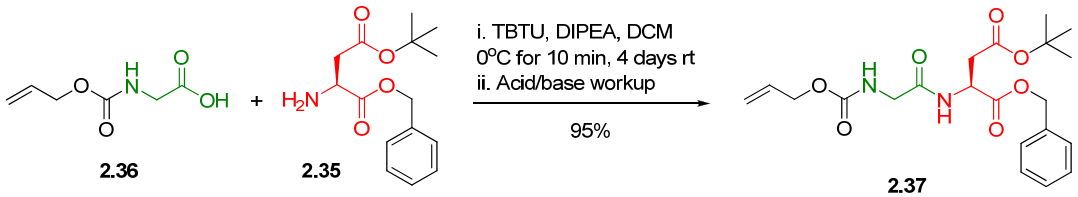

2.36 **2.35** **2.37**

Scheme 2.23 – Reaction scheme showing the synthesis of Alloc-Gly-Asp(O^{t}Bu)-OBn, **2.37**. Original in colour.

It should be noted that an attempt at deprotecting the Fmoc anologue of **2.37**, Fmoc-Gly-Asp(O^{t}Bu)-OBn **2.38** – synthesised in quantitative yield from TBTU coupling Fmoc-Gly-OH with **2.35** (Scheme 2.24), and evidenced by ^{1}H NMR which showed a doublet peak at 7.20 ppm corresponding to the newly formed amide N*H* proton, and a downfield shift in the aspartic acid α-*H* from 3.52 ppm to 4.90 ppm due to the formation of the adjacent electron-withdrawing amide functional group – was unsuccessful as there were problems in isolating the product from the Fmoc/Fmoc-piperidine by-products by silica column chromatography. We speculate that the choice of Alloc group rather than Fmoc will result in a cleaner deprotection reaction (i.e. there would be fewer by-products produced) which would make it easier to identify the product by TLC.

We believe the synthesis of compound **2.37** is progress towards a protected RGD peptide with both a 'capped' C-terminus and also orthogonal protecting groups on the N- or C-terminus to allow the peptide to be selectively derivatised at either end. Future synthetic work (Scheme 2.25) involves optimising the conditions for selective removal of the Alloc group (**2.39**), amide coupling Alloc-Arg(Pbf)-OH (not commercially available so this would require synthesis from an arginine derivative)

(**2.40**), and then removal of the Alloc group to allow coupling of the benzyl ester 'capped' peptide (**2.41**) in further reactions. Coupling **2.41** to the Newkome-type dendrons, deprotection, and a subsequent FP study would then reveal if the derivatised dendritic peptide binds more strongly to the integrin by inhibiting the non-specific interactions discussed earlier in this chapter.

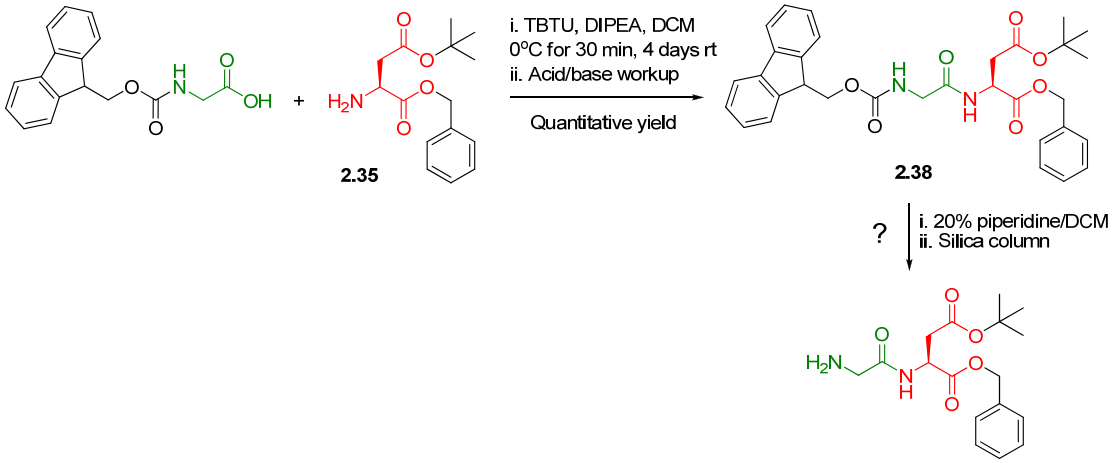

Scheme 2.24 – Reaction scheme showing the synthesis of Fmoc-Gly-Asp(O^{t}Bu)-OBn, **2.38**, and attempted Fmoc deprotection. Original in colour.

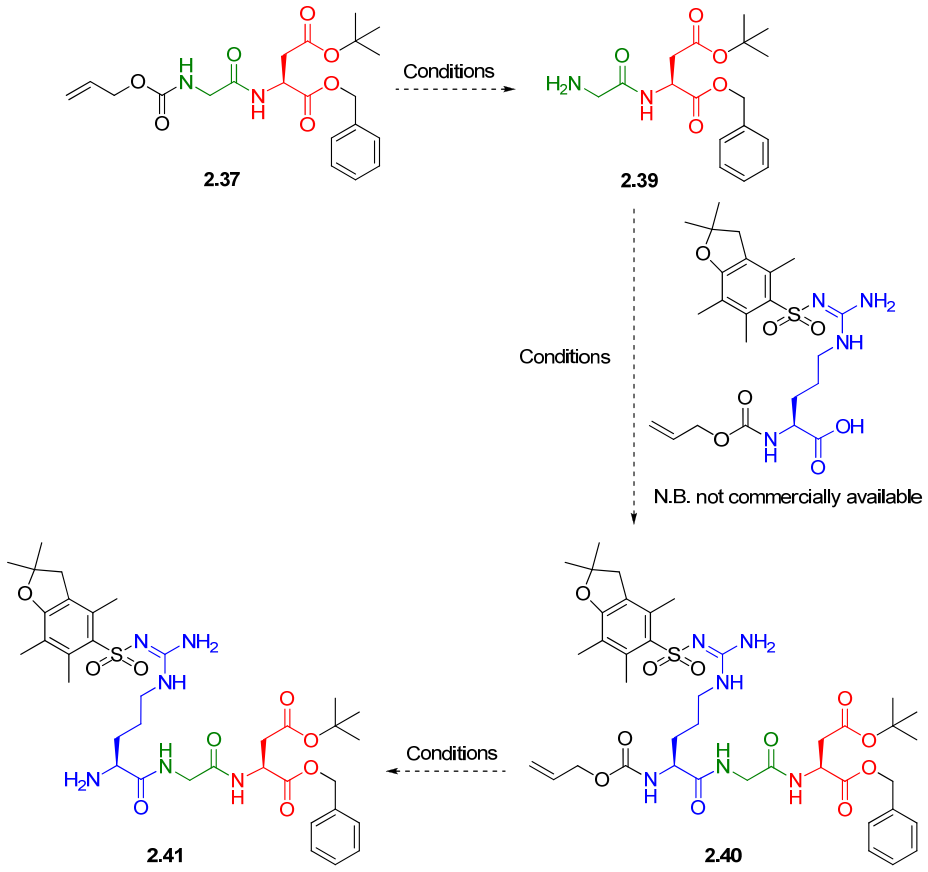

Scheme 2.25 – Proposed synthesis of target peptide H_2N-Arg(Pbf)-Gly-Asp(O^{t}Bu)-OBn, **2.41**. Original in colour.

2.5 Conclusions

In conclusion, we have synthesised, in high purity and yield, first and second generation Newkome-type dendrons with linear RGD peptides attached at the periphery. Prior to this, we developed a large, multi-gram scale, solution-phase synthesis of the linear RGD peptide in its precursor/protected form. Subsequently, we went on to test the integrin $\alpha_v\beta_3$ binding ability of the synthetic ligands in a fluorescence polarisation assay which we adapted from a literature protocol. By being limited to performing the titrations on a spectrometer rather than a plate reader this significantly prolonged the duration of the experiments. Developing the assay to run on a plate reader, as it was originally intended to be run, would result in a more efficient ligand screening process.

A multivalency effect was observed when we compared the monovalent control, **PEG-RGD**, with the first generation dendron, **Z-G1-[RGD]$_3$**. Interestingly, optimal binding was found to occur for the G1 dendron which has three surface RGD groups. The higher generation G2 system displaying nine RGDs, **Z-G2-[RGD]$_9$**, had a lower affinity and more non-specific ligand-protein interactions. This suggests that there is an optimal number of RGD peptides which allows enhanced integrin $\alpha_v\beta_3$ binding, but above this number the RGD ligands become sterically crowded and the specific binding affinity drops off, whilst non-specific ligand-protein aggregation is encouraged.

Synthetic efforts towards modification of the C-terminus of the RGD peptide have been reported. However, these were challenging and further work would be required to complete these syntheses. In the future, capped derivatives of the linear RGD peptide may possess enhanced integrin $\alpha_v\beta_3$ affinity by inhibiting non-specific ligand-protein interactions.

In summary, a covalent, dendritic approach to multimerising the linear RGD ligand has led to improvements in integrin $\alpha_v\beta_3$ binding with the extent of dendritic branching tuning the affinity. This encouraged us to apply the multivalency principle further using a non-covalent, self-assembling strategy, with the hope of observing even greater improvements in integrin $\alpha_v\beta_3$ binding ability, and work towards this goal is described in the next chapter.

Chapter 3

Self-Assembling Linear RGD Peptides

3 Self-Assembling Linear RGD Peptides

3.1 Introduction

The results in Chapter 2 showed that covalent multivalency leads to an increase in affinity of the linear RGD peptide for integrin $\alpha_v\beta_3$. Compound **Z-G1-[RGD]$_3$** (**2.16**) exhibited stronger binding in the FP assay over that of the monovalent control compound **PEG-RGD** (**2.19**). This work highlighted the importance of multivalency in linear RGD-integrin binding. We argued that either a high local concentration of RGD peptide near the integrin binding site, or a series of multiple binding events due to the integrins being held together in artificial cell-like membranes was the reason for the increased ligand-protein affinity. Although we have obtained promising results from our dendritic RGD system, we became interested in what effect an alternative non-covalent approach to multimerising the linear peptide would have on binding strength. Lipidic RGD's should have the ability to self-assemble in aqueous solution due to the hydrophobic effect (Scheme 3.1), whereas **PEG-RGD** should not as its structure is overall hydrophilic. As such, we predicted that it should be possible to determine whether self-assembled aggregates possessing a multivalent display of RGD enhances integrin binding in our FP assay. Furthermore, a self-assembling approach to multivalency is a somewhat easier synthetic strategy than the iterative steps required to make dendrimers. Self-assembled systems are dynamic due to the non-covalent forces that hold then together, and therefore possess a greater flexibility/responsiveness which might be advantageous if the linear RGD aggregates can rearrange to satisfy the requirements of the integrin binding site. A family of hydrophobic, self-assembling peptide amphiphiles was therefore designed (Fig. 3.1).

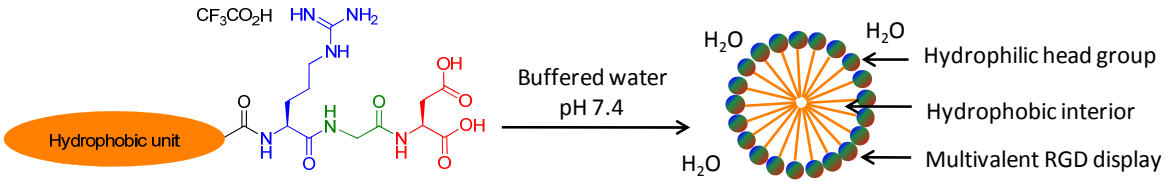

Scheme 3.1 – General target structure of RGD peptide amphiphiles and their self-assembly in water. Original in colour.

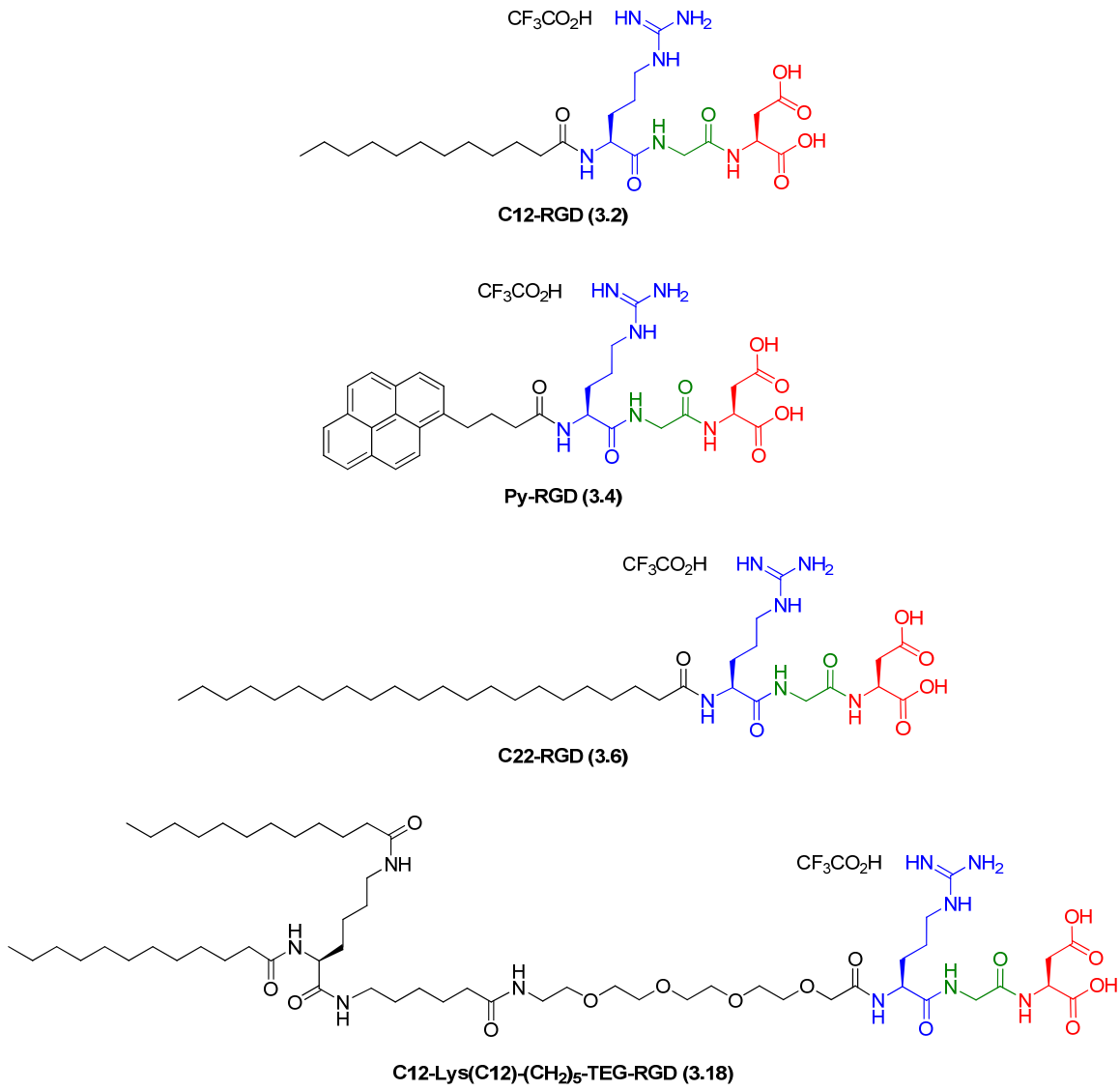

Fig. 3.1 – Structures of our self-assembling linear RGD peptides. Original in colour.

3.2 Synthesis

3.2.1 Synthesis of C12-RGD

Lipopeptide **C12-RGD** (**3.2**) has been synthesised previously, albeit in an alternative manner, by Shen *et al.*[267] We synthesised it in protected form by simple conjugation of the N-terminus of protected RGD **2.8** with the carboxylic acid of lauric acid, mediated by coupling agent TBTU (**3.1**, 94% yield) (Scheme 3.2). The synthesis of **3.1** was confirmed in the ^{1}H NMR by a downfield shift in the arginine α-*H* from 3.44 ppm to 4.50-4.45 ppm on coupling **2.8** to lauric acid to generate the adjacent electron-withdrawing amide functional group.

TFA deprotection of the RGD peptide generated the product **3.2** in 78% yield. The loss of peaks in the ^{1}H NMR (see appendix – spectrum 3.1) corresponding to the Pbf methylene (2.89 ppm) and

methyl groups at 2.51, 2.44, 2.02 and 1.39 ppm, as well as the *tert*-butyl methyl groups at 1.35 ppm, confirmed successful reaction. ESI-MS confirmed the mass of the product with a *m*/*z* value of 529.3331 (100%, $[M+H]^+$). All steps throughout the synthesis of **3.2** are high yielding and as such, it is possible to easily synthesise this compound on a relatively large scale.

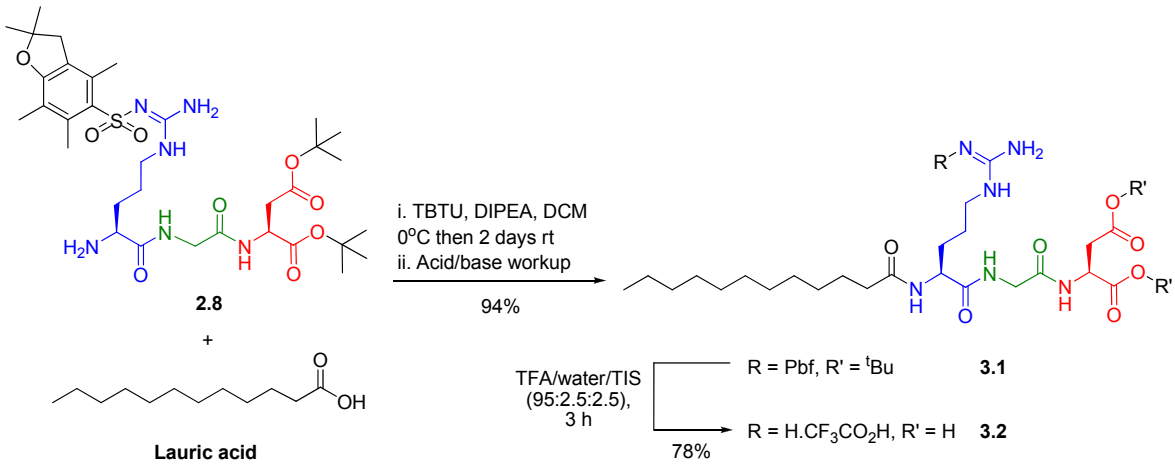

Scheme 3.2 – Reaction scheme showing the formation of **3.1** and subsequent deprotection conditions to form **3.2**. Original in colour.

3.2.2 Synthesis of Py-RGD

The conjugation of an aromatic pyrene (Py) unit onto the RGD peptide would allow us to study the effect of π-π stacking on the self-assembly and integrin binding affinity of the peptide. We chose to use 1-pyrenebutyric acid as the butyric acid chain would hopefully act as a linker to allow the RGD to bind the protein without being inhibited by the bulky pyrene ring system. Protected RGD **2.8** was amide coupled with 1-pyrenebutyric acid using TBTU to give the protected pyrene-RGD conjugate, **3.3**, in quantitative yield (Scheme 3.3). Again, the most conclusive form of evidence was the downfield shift in the ^{1}H NMR of the arginine α-*H* on coupling **2.8** to 1-pyrenebutyric acid to generate the adjacent electron-withdrawing amide functional group.

TFA deprotection provided the final product **3.4** in 77% yield. ^{1}H NMR resonances corresponding to the Pbf CH_2's and CH_3's, as well as the *tert*-butyl methyl groups in **3.3** were absent in product **3.4** (see appendix – spectrum 3.2). ESI-MS detected the product with a *m*/*z* value of 617.2722 (100%, $[M+H]^+$).

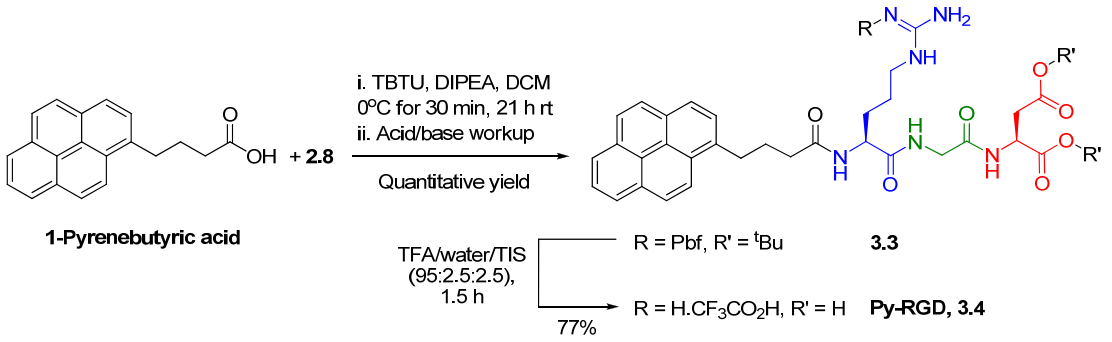

Scheme 3.3 – Reaction scheme showing the formation of **3.3** and subsequent deprotection conditions to form **3.4**. Original in colour.

3.2.3 Synthesis of C22-RGD

We were also interested in what effect the extension of the aliphatic hydrocarbon tail from C12 to C22 would have on the self-assembly and integrin binding affinity of the peptide. In accordance with previous amide coupling procedures, behenic acid was amide coupled with the protected RGD **2.8** using TBTU to provide the protected **C22-RGD** conjugate, **3.5**, in 96% yield (Scheme 3.4). The downfield shift in the ^{1}H NMR of the arginine α-*H* on coupling **2.8** to behenic acid, to generate the adjacent electron-withdrawing amide functional group, was again observed.

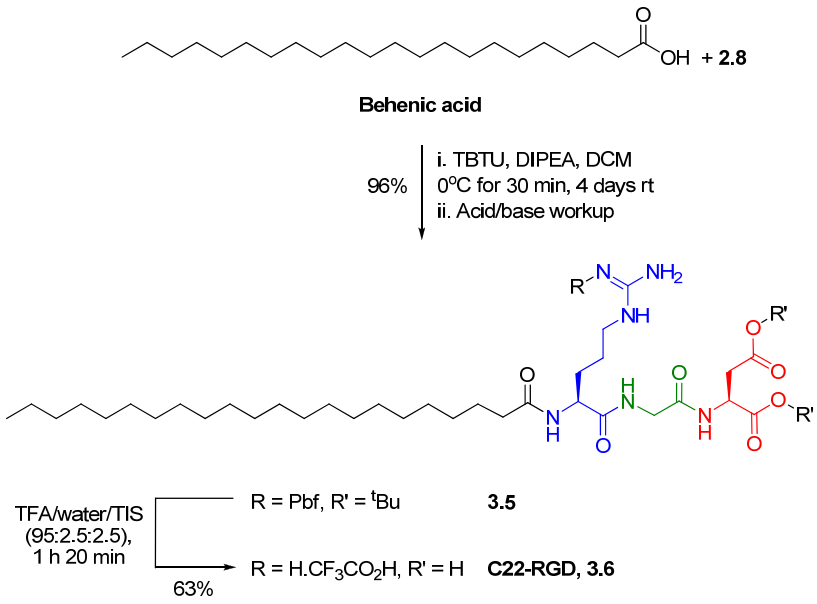

Scheme 3.4 – Reaction scheme showing the formation of **3.5** and subsequent deprotection conditions to form **3.6**. Original in colour.

TFA deprotection generated the final product **3.6** in 63% yield. ^{1}H NMR resonances corresponding to the Pbf CH_2's and CH_3's, as well as the *tert*-butyl methyl groups in **3.5** were absent in product **3.6** (see

appendix – spectrum 3.3). ESI-MS detected the product with a m/z value of 669.4932 (100%, $[M+H]^+$).

3.2.4 Attempted Synthesis of Chol-RGD

The hydrophobic and biologically relevant cholesterol unit was also targeted for inclusion in our family of RGD lipopeptides. Unlike previous syntheses, the synthesis of this compound employed carbamate bond forming chemistry in which the free amine of **2.8** reacted with cholesteryl chloroformate in a nucleophilic substitution reaction to produce the carbamate-linked protected **Chol-RGD** conjugate, **3.7**, in 89% yield following silica column purification (Scheme 3.5). TEA was used to neutralise the HCl that was produced during the reaction, hence driving it to completion and also protecting the *tert*-butyl and Pbf protecting groups from acid hydrolysis. In the ^{1}H NMR, a downfield shift of the arginine α-*H* from 3.44 ppm to 4.34-4.23 ppm due to the adjacent electron-withdrawing carbamate group, whose N*H* resonance appeared at 5.94 ppm, was strong evidence for the formation of the product.

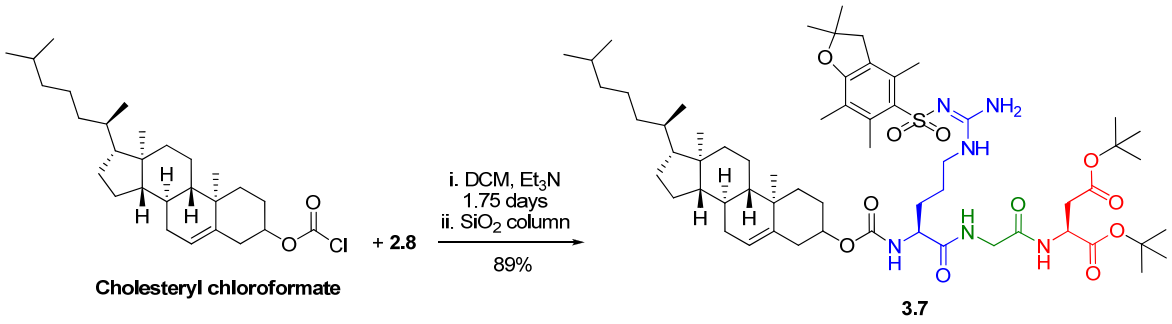

Scheme 3.5 – Reaction scheme showing the formation of protected **Chol-RGD**, **3.7**. Original in colour.

The next step involved acid hydrolysis of the protecting groups. However, upon treating the protected **Chol-RGD**, **3.7**, with TFA and attempting to precipitate out the desired product with Et_2O, ESI-MS revealed that the solid which was recovered contained a mixture of product, **3.8**, and also the hydrolysed by-product (Scheme 3.6). This was evidenced by peaks in the MS at m/z values of 759.5 (20%, $[M+H]^+$) for the product and 347.2 (100%, $[H_2N\text{-Arg-Gly-Asp-OH} + H]^+$) for the by-product. The synthesis of **Chol-RGD** was therefore abandoned due to the acid instability of the carbamate linkage. To circumvent this problem it is envisaged that activating the alcohol of cholesterol with tosyl (or mesyl) chloride, followed by an S_N2 reaction with **2.8** would enable direct conjugation of the protected peptide with cholesterol via direct C-N bond formation. The resultant compound should then be acid stable in the final deprotection step. This is just one of several possibilities for conjugating **2.8** with cholesterol and forms the basis of future work.

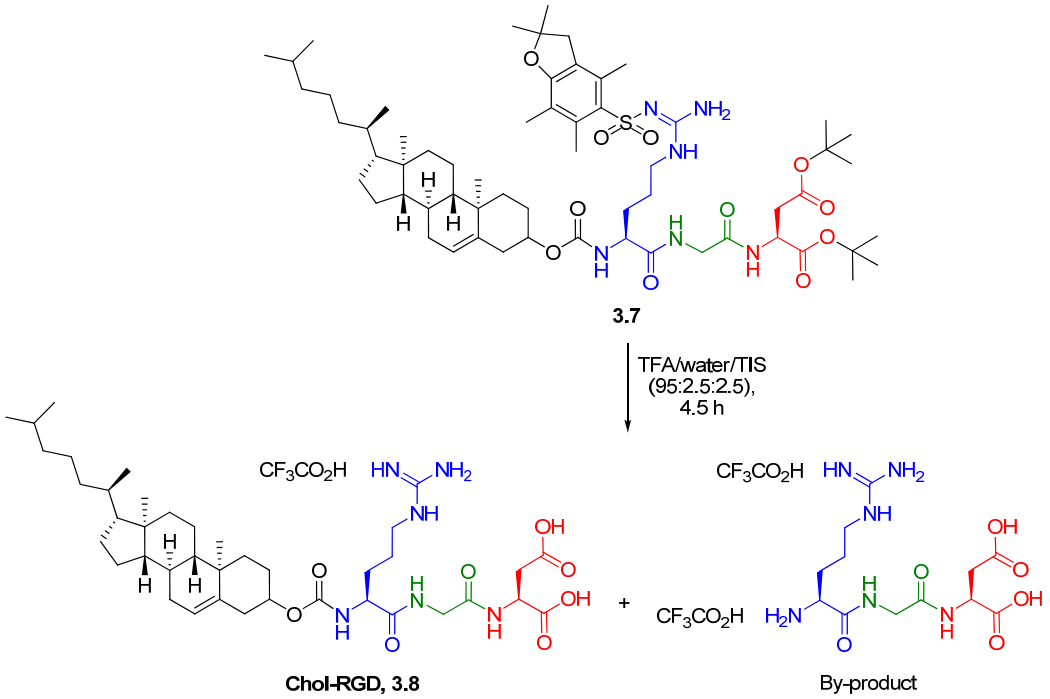

Scheme 3.6 – Reaction scheme showing the deprotection of **3.7** to produce a mixture of product, **3.8**, and hydrolysed by-product. Original in colour.

3.2.5 Synthesis of C12-Lys(C12)-$(CH_2)_5$-TEG-RGD

In addition to the **C12-RGD** amphiphile, **3.2**, we were also interested in investigating the effect of branching the hydrophobic portion of the molecule to generate twin-tailed C12 system **3.18** (Fig. 3.2). The tetraethyleneglycol (TEG) linker was an integral part of the design process to ensure good water solubility of the amphiphilic molecule. As discussed in the introduction, according to Israelachvili's critical packing principles,[33] incorporating a branched/larger hydrophobic group into the structure can impact on the self-assembly mode of the molecule by generating a lipid which, in this case, has more of a truncated cone shape and possibly a preferred tendancy to form cylindrical or liposomal aggregates. On the other hand, it is reasonable to suggest that **C12-RGD** and **Py-RGD** have larger hydrophilic head groups with respect to their hydrophobic units, which may favour an inverted cone shape, leading to the formation of spherical micelles. In this way, we envisaged a comparison of different self-assembled morphologies and how they affect integrin binding as a potentially interesting outcome of this systematic RGD lipopeptide design process.

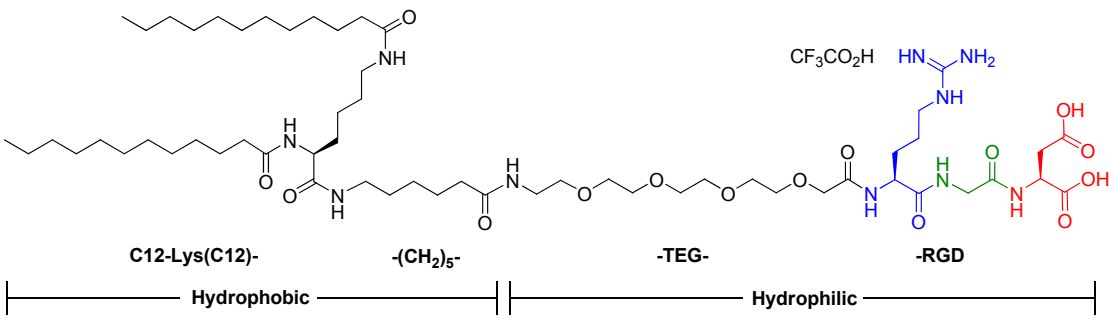

Fig. 3.2 – Structure of **C12-Lys(C12)-$(CH_2)_5$-TEG-RGD** (**3.18**). Original in colour.

The two building blocks for the convergent synthesis of **C12-Lys(C12)-$(CH_2)_5$-TEG-RGD** were made in parallel. For the synthesis of the hydrophobic fragment (Scheme 3.7), two equivalents of lauric acid were TBTU coupled to L-lysine methyl ester dihydrochloride to yield C12-Lys(C12)-OMe, **3.9**, in 89% yield after an aqueous workup.[268] ^{1}H NMR resonances at 6.40 ppm (doublet) and 6.01 ppm (triplet) corresponded to the α-N*H* amide and the ε-N*H* amide, respectively. Following on from the protocol of Marques *et al* concerning the preparation of lysine-based double-chained anionic surfactants, saponification of the methyl ester using 1 M NaOH in methanol was then carried out. Marques and co-workers report that they carried out the saponification reaction at 0°C. However, solubilising **3.9** in methanol proved difficult and required lengthy sonication to get the solid to dissolve. Once dissolved, the reaction flask was cooled in an ice-water bath, but upon doing so the starting material crashed out of solution as a solid again. Continuing with the method, 1 M NaOH was added and the reaction stirred at 0°C for almost 2 h when the ice-water bath was removed and the reaction allowed to warm to rt. The reaction was stirred vigorously overnight but the white solid of the starting material still remained so a decision was made to heat the reaction to 40°C. After ~30 min of heating the solid dissolved and TLC showed that the reaction was complete after a further 30 min of stirring. An aqueous workup procedure yielded the product, **3.10**, in 83% yield. The absence of the methyl ester singlet resonance at 3.68 ppm in the ^{1}H NMR confirmed hydrolysis of the methyl ester group.

The next step was to TBTU couple the hydrochloride salt of the methyl 6-aminohexanoate linker with **3.10** to provide **3.11** in 85% yield following an acid/base workup. A downfield shift in the ^{1}H NMR resonance of C*H*$_2$NH$_2$ of the methyl 6-aminohexanoate linker upon coupling to the carboxylic acid of **3.10,** from ~2.7 ppm to 3.18-3.12 ppm, due to the newly-formed, adjacent electron-withdrawing amide group proved the formation of the product, in addition to the mass spec *m*/*z* value of 638.5465 (78%, $[M+H]^+$). Saponification of the methyl ester using 1 M NaOH in methanol and refluxing at 60°C then yielded the target hydrophobic fragment, **3.12**, in 73% yield. The absence of the methyl ester singlet resonance at 3.64 ppm in the ^{1}H NMR confirmed hydrolysis of the methyl ester group.

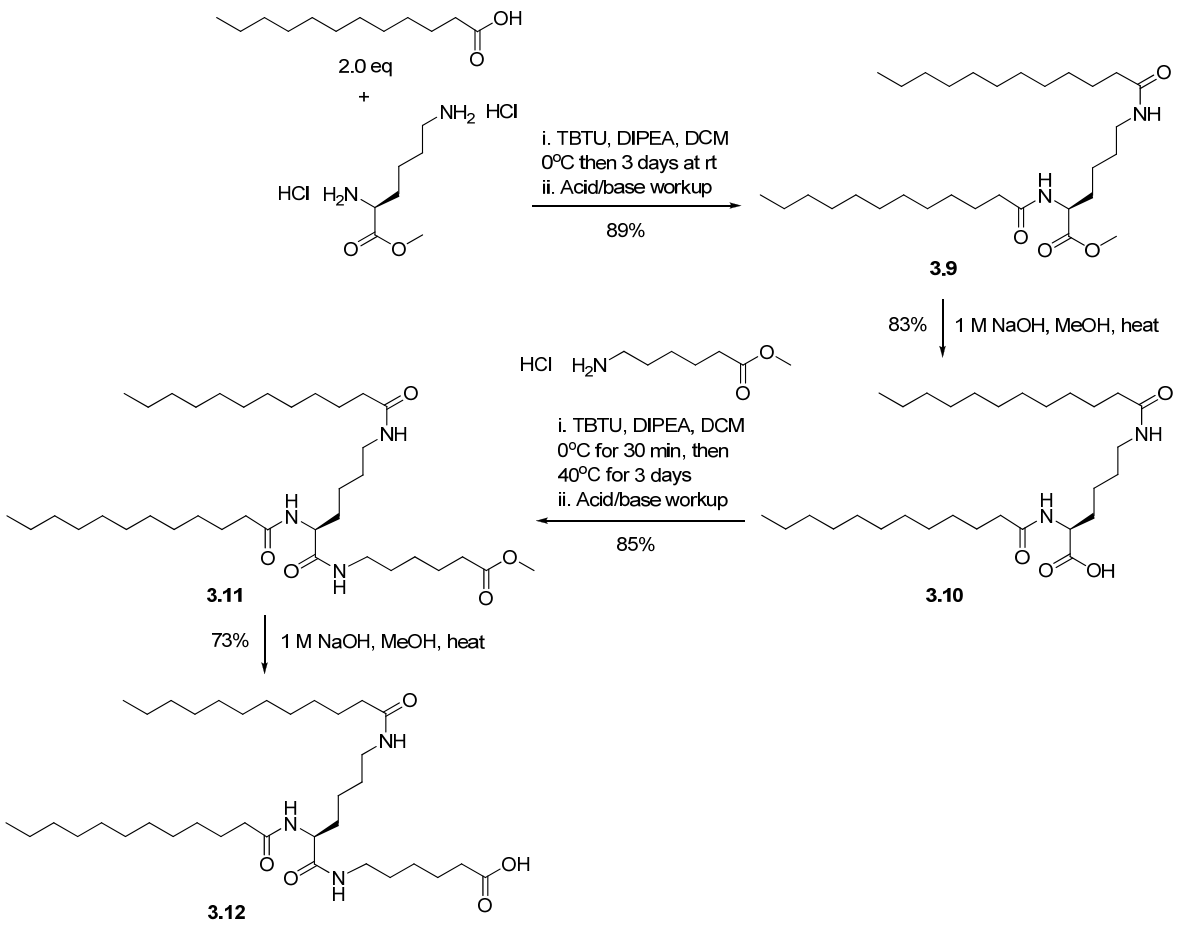

Scheme 3.7 – Reaction scheme showing the overall synthesis of C12-Lys(C12)-$(CH_2)_5$-C(O)OH, **3.12**.

For the synthesis of the TEG linker (Scheme 3.8), tetraethyleneglycol was activated at one end with tosyl chloride to yield the monotosylated intermediate.[269] This was reacted on *in situ* by refluxing with sodium azide in ethanol to yield mono azide **3.13** in 50% yield after silica column purification.[269] An upfield shift in the CH_2CH_2OH ^{1}H NMR resonance from the overlapping multiplets at 3.73-3.59 ppm to an individual 2H triplet at 3.39 ppm upon converting to the electron-shielding, azide-functionalised analogue $CH_2CH_2N_3$, confirmed formation of the product. A Williamson-ether synthesis then afforded **3.14** in 54% yield by reacting **3.13** with 2-bromoacetic acid in the presence of sodium hydride in dry THF. ^{1}H NMR confirmed the structure of the product owing to the appearance of a 2H singlet peak at 4.12 ppm corresponding to the $OCH_2C(O)OH$ portion of the molecule. ESI-MS detected the product with m/z value 300.1165 (100%, $[M+Na]^+$).

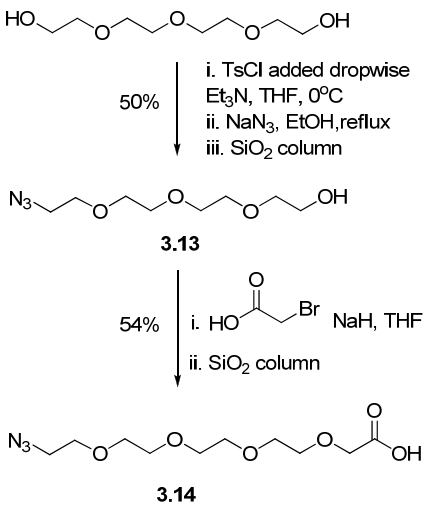

Scheme 3.8 – Reaction scheme showing the synthesis of the tetraethyleneglycol (TEG) linker, **3.14**.

Synthesis of the protected hydrophilic fragment was then completed by TBTU coupling compounds **3.14** and **2.8** to provide conjugate **3.15** in 52% yield after acid/base workup and silica column purification (Scheme 3.9). In the ^{1}H NMR, a downfield shift of the arginine α-*H* from 3.44 ppm to 4.61-4.55 ppm due to the adjacent electron-withdrawing amide group, and the appearance of a third amide N*H* resonance, were strong evidence for the formation of the product. To allow amide coupling of the two halves of the target molecule, the azide functionality was reduced under catalytic hydrogenation to form the amine terminated **3.16** in quantitative yield. The most conclusive form of evidence for the synthesis of the product was the reduction in the *m*/*z* value from 970.4893 (100%, $[M+H]^+$) (for **3.15**) to 944.4978 (100%, $[M+H]^+$) (for **3.16**).

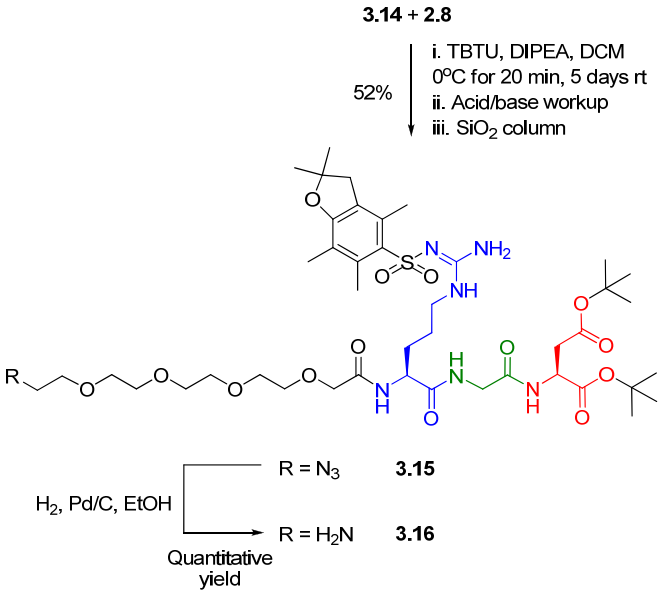

Scheme 3.9 – Reaction scheme showing the synthesis of the protected H_2N-TEG-RGD conjugate, **3.16**. Original in colour.

The penultimate step in the synthesis involved TBTU-coupling of fragments **3.12** and **3.16** to provide the target molecule in protected form, **3.17**, in a fairly low 26% yield (Scheme 3.10). The appearance of a 7th amide N*H* resonance was one of the most conclusive forms of evidence for the successful formation of the product, as well as its detection by ESI-MS at a m/z value of 775.5089 (100%, $[M+2H]^{2+}$). The reason for such a low yield may be due to: (i) inefficient coupling of the two fragments, (ii) loss of material in the aqueous workup due to the presence of the hydrophilic TEG linker, or (iii) loss of material during the silica column purification step. In any case, this still provided enough material to proceed with TFA deprotection to produce the final target molecule, **3.18**, in 41% yield. ^{1}H NMR resonances corresponding to the Pbf CH_2's and CH_3's, as well as the *tert*-butyl methyl groups in **3.17** were absent in product **3.18** (see appendix – spectrum 3.4). ESI-MS detected the product with a m/z value of 593.4052 (100%, $[M+2H]^{2+}$).

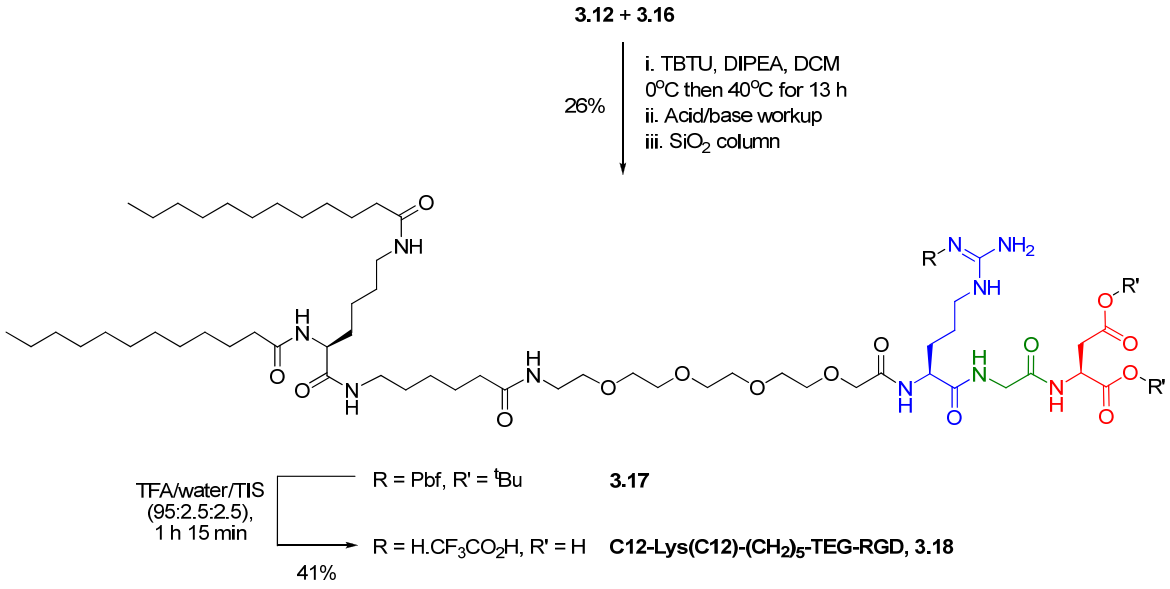

Scheme 3.10 – Reaction scheme showing the formation of **3.17** and subsequent deprotection conditions to form **3.18**. Original in colour.

3.3 Self-Assembly Studies

To determine whether the peptide amphiphiles self-assembled in aqueous solution, we employed a phase-transfer-type encapsulation experiment using the hydrophobic dye Nile Red (Fig. 3.3).[270] In water, Nile Red is insoluble and its fluorescence emission is 'switched off'. In organic solvents, or the hydrophobic interior of self-assembled aggregates, Nile Red is solubilised and its fluorescence emission is 'switched on'. The fluorescence emission intensity is proportional to the amount of solubilised dye, which in turn is proportional to the concentration of self-assembling peptide in solution.

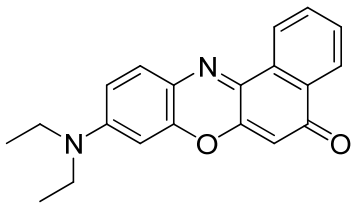

Fig. 3.3 – The structure of Nile Red.

We first studied the ability of **C12-RGD** (**3.2**) to self-assemble and encapsulate Nile Red. Increasing the concentration of **C12-RGD** led to an increase in the fluorescence emission intensity of the dye, which was direct evidence of increased levels of solubilisation in the interior of self-assembled aggregates (Fig. 3.4). Plotting the fluorescence emission intensity at λ_{max} (635 nm) vs. log[peptide] allows for the determination of the critical aggregation concentration (CAC) (Fig. 3.5). The CAC is calculated at the point where the two lines of best fit intersect. For **C12-RGD**, the CAC was calculated as ~300 μM in phosphate buffered saline (PBS) at pH 7.4.

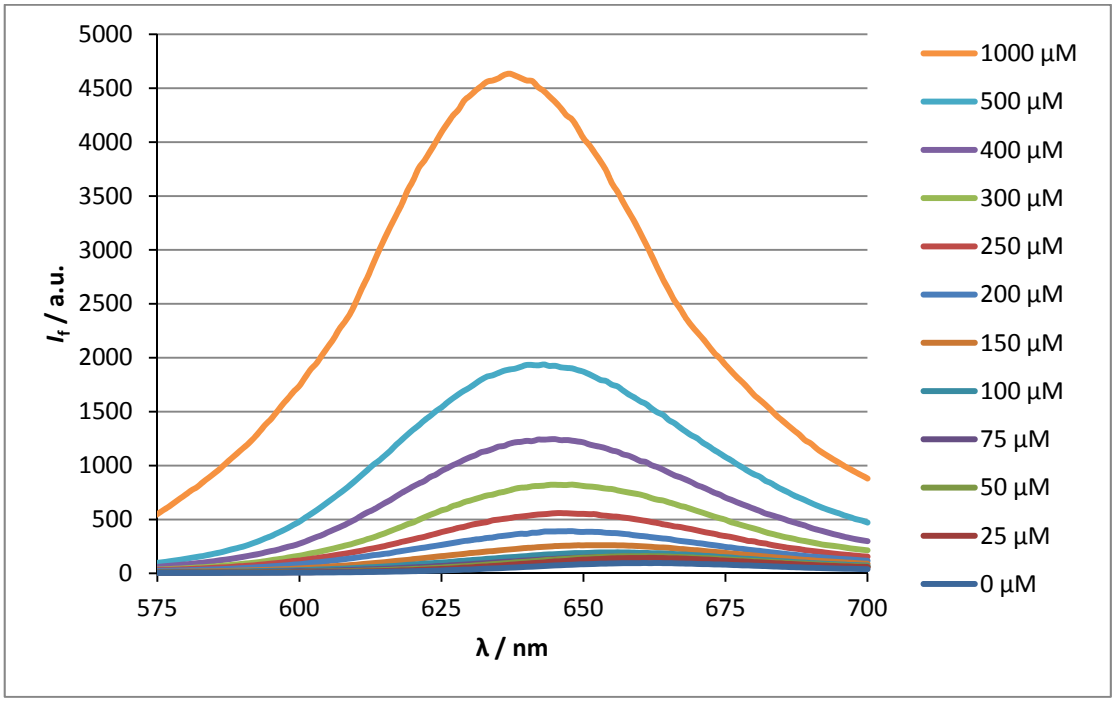

Fig. 3.4 – Averaged Nile Red fluorescence emission spectra in the presence of increasing concentrations of **C12-RGD**. λ_{ex} = 550 nm. Experiments were run in triplicate. Original in colour.

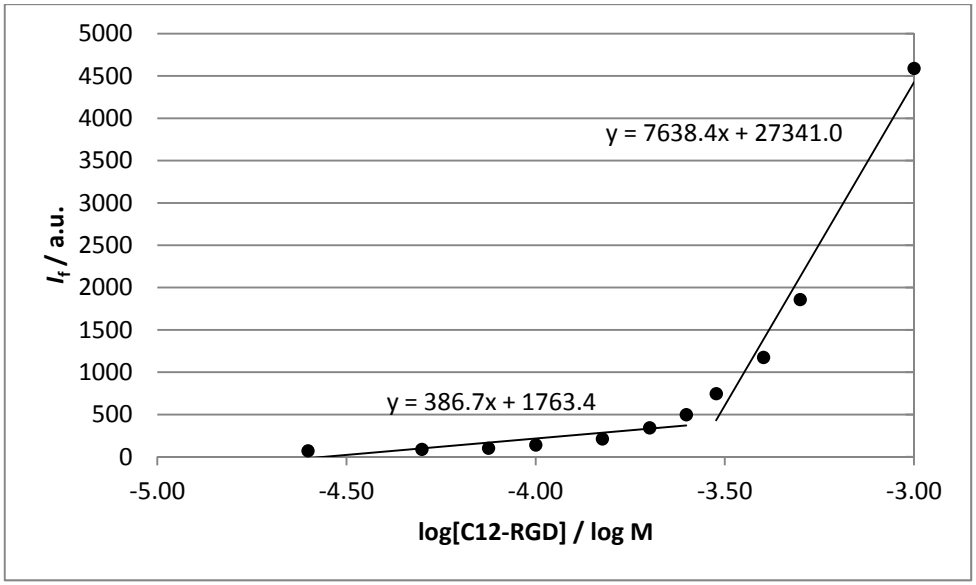

Fig. 3.5 – Averaged Nile Red fluorescence emission intensities at 635 nm plotted against log[**C12-RGD**]. λ_{ex} = 550 nm. Experiments were run in triplicate.

Conversely, the dendritic compounds studied in Chapter 2, **Z-G1-[RGD]$_3$** (Fig. 3.6) and **Z-G2-[RGD]$_9$** (Fig. 3.7), caused no increase in Nile Red fluorescence emission at any concentration up to 1 mM which, as expected, implies that no self-assembly occurs for these compounds in the range of concentrations tested.

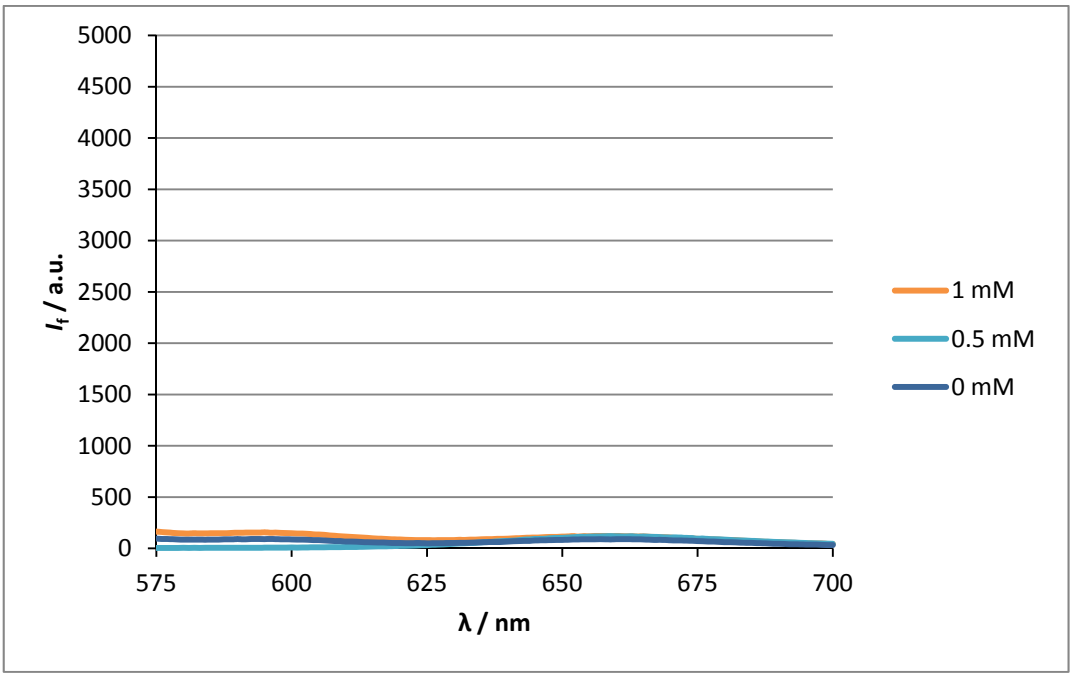

Fig. 3.6 – Nile Red fluorescence emission spectra in the presence of increasing concentrations of **Z-G1-[RGD]$_3$**. λ_{ex} = 550 nm. Original in colour.

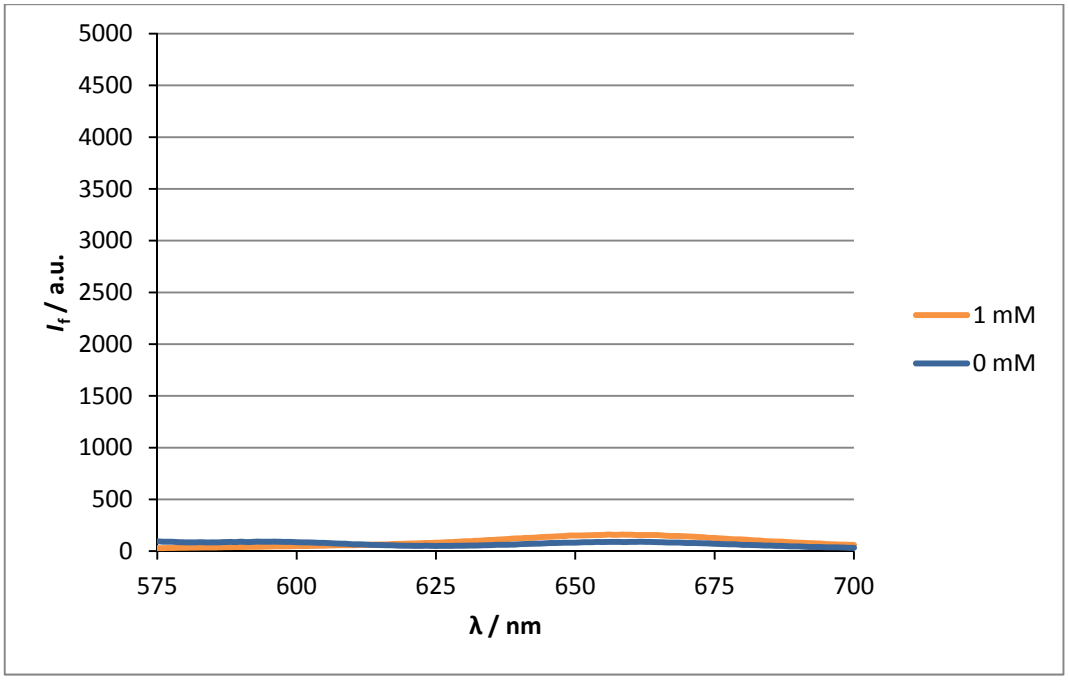

Fig. 3.7 – Nile Red fluorescence emission spectra in the presence of increasing concentrations of **Z-G2-[RGD]$_9$**. λ_{ex} = 550 nm. Original in colour.

Transmission electron microscopy (TEM) was then used to determine the morphology of the aggregates formed from the self-assembly of **C12-RGD**. At high concentration (1 mM), bundled structures comprised of small spherical micelles (~5 nm diameter) were observed in TRIS (tris(hydroxymethyl)aminomethane) (Fig. 3.8A) and PBS buffers (not shown) at pH 7.4. The micellar radius is therefore in accordance with the estimated head-to-tail molecular length of ~3 nm* for the **C12-RGD** amphiphile (Fig. 3.9). However, larger unilamellar structures can be seen on dilution to just above the CAC (400 μM) (Fig. 3.8B). This is clear visual evidence that self-assembly of **C12-RGD** is taking place, although the actual mode of self-assembly is dependent on the concentration.

We would like to take this opportunity to point out that as with all images obtained by TEM, the artefacts observed are subject to drying effects as the material in solution is cast onto a TEM grid and allowed to dry. The images obtained are therefore open to interpretation and do not necessarily represent the structures that would be found in their native 'wet' state.

* Calculated using ChemBioDraw Ultra 11.0

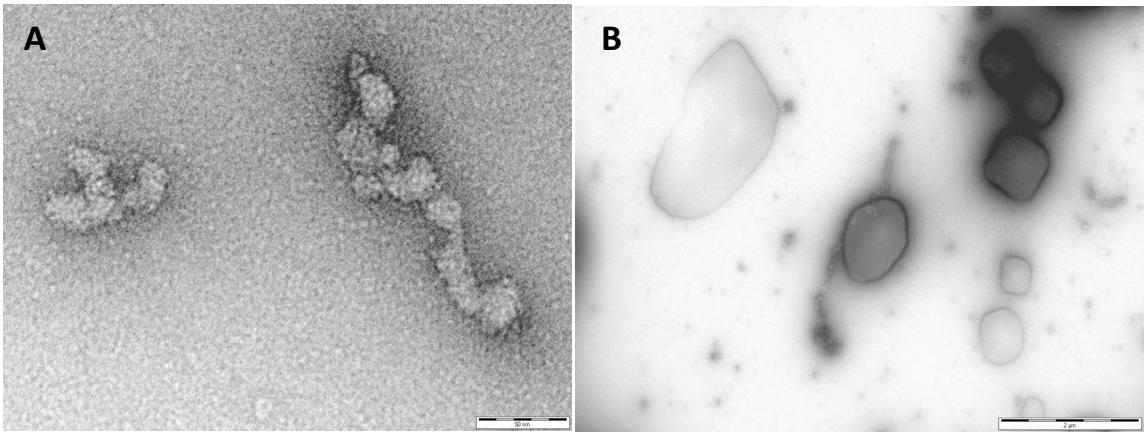

Fig. 3.8 – TEM images of assemblies formed by **C12-RGD** in TRIS buffer (pH 7.4) at: A) 1 mM, scale bar = 50 nm, and B) 400 μM, scale bar = 2 μm. Negatively stained with uranyl acetate.

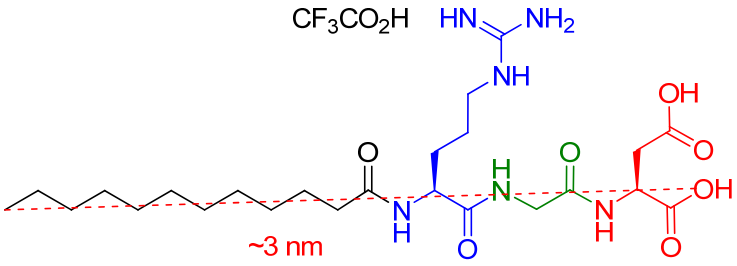

Fig. 3.9 – Structure showing the head-to-tail molecular length of **C12-RGD**. Original in colour.

We then studied the ability of **Py-RGD** (**3.4**) to self-assemble and encapsulate Nile Red. As we expected, increasing the concentration of **Py-RGD** led to an increase in the fluorescence emission intensity of the dye (Fig. 3.10). Plotting the fluorescence emission intensity at λ_{max} (650 nm) vs. log[peptide] (Fig. 3.11), the CAC was calculated to be ~110 μM in PBS at pH 7.4.

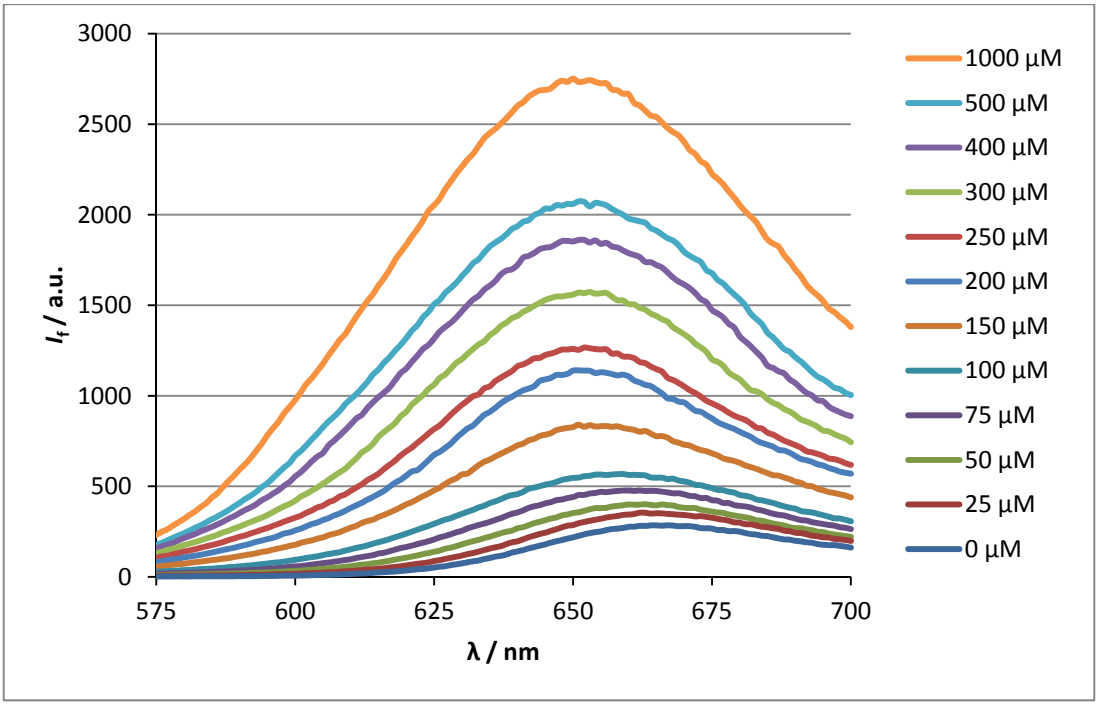

Fig. 3.10 – Averaged Nile Red fluorescence emission spectra in the presence of increasing concentrations of **Py-RGD**. λ_{ex} = 550 nm. Experiments were run in triplicate. Original in colour.

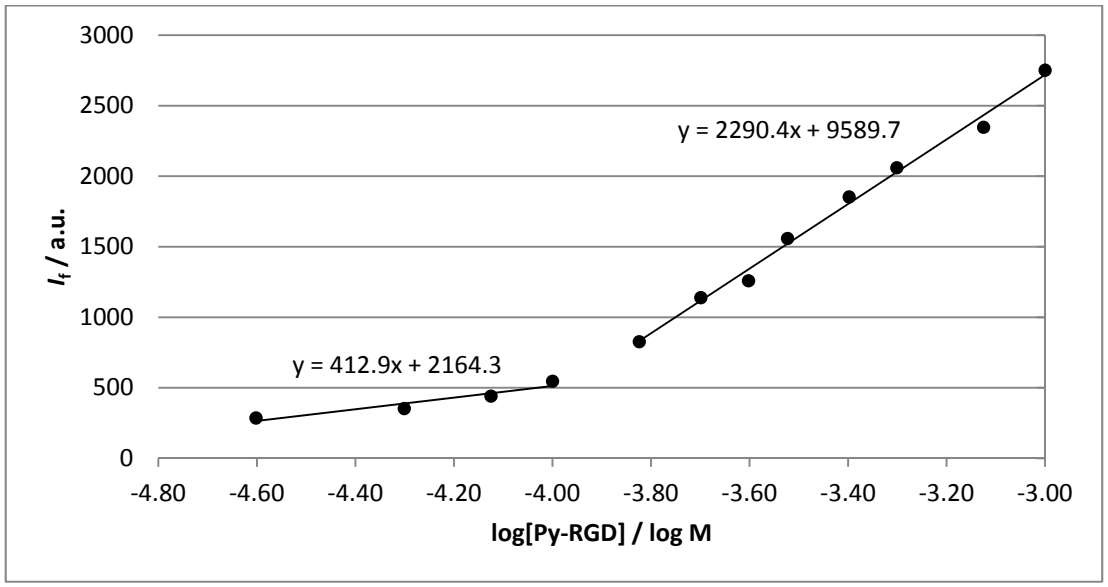

Fig. 3.11 – Averaged Nile Red fluorescence emission intensities at 650 nm plotted against log[**Py-RGD**]. λ_{ex} = 550 nm. Experiments were run in triplicate.

The UV-Vis absorption spectrum of **Py-RGD** is shown in Fig. 3.12. **Py-RGD** does not absorb at 550 nm, therefore, exciting Nile Red at this wavelength does not induce any fluorescence emission contributions from **Py-RGD** (Fig. 3.13). This confirms that the Nile Red encapsulation study is unperturbed by the presence of the pyrene unit.

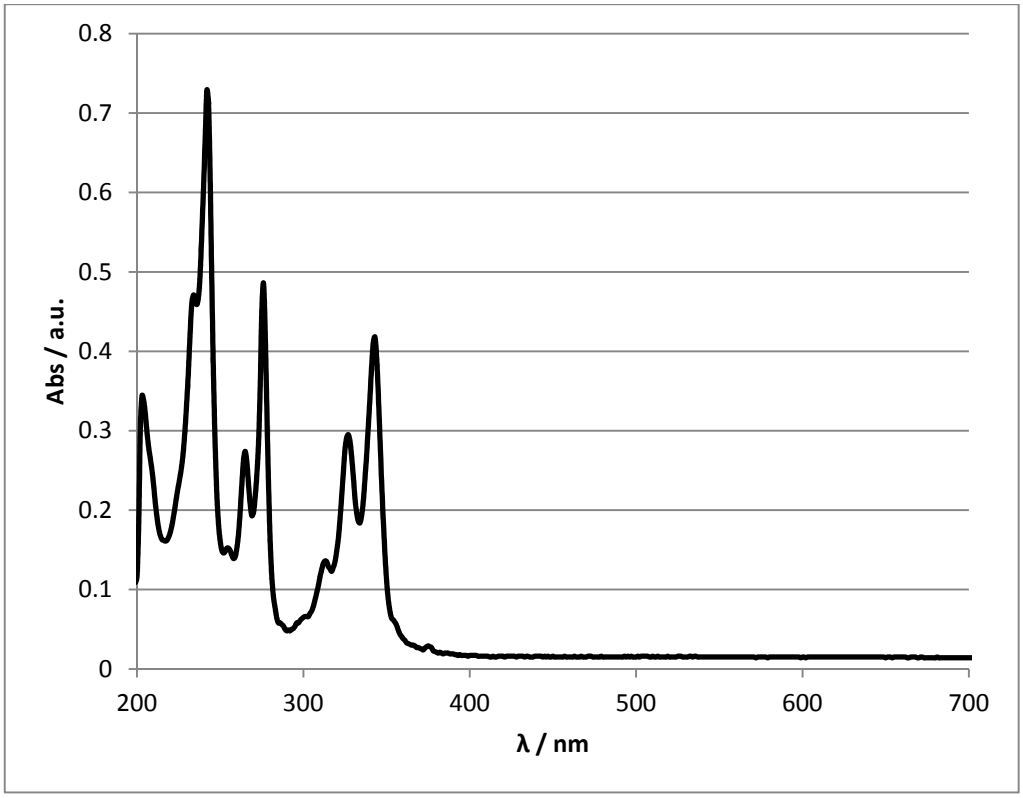

Fig. 3.12 – UV-Vis absorption spectrum of **Py-RGD** (0.01 mg/ml in PBS, pH 7.4).

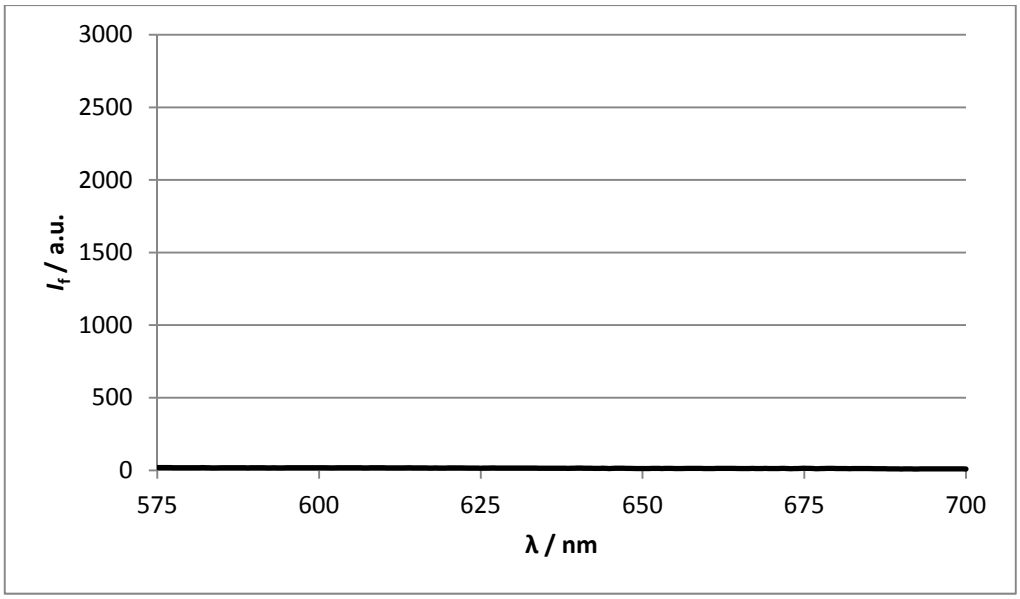

Fig. 3.13 – Fluorescence emission spectrum of **Py-RGD** (1 mM in PBS, pH 7.4). λ_{ex} = 550 nm.

However, the photophysical properties of the pyrene unit itself are useful in investigating the phase separation of pyrene lipids. The fluorescence emission spectra of various **Py-RGD** sample concentrations were recorded using an excitation wavelength of 343 nm (Fig. 3.14). The fluorescence emission of **Py-RGD** decreases in intensity as the concentration of **Py-RGD** increases. However, it

would be expected that the fluorescence emission of free pyrene should increase as the concentration of **Py-RGD** increases. This result therefore indicates that aggregation of the pyrenes (initially as dimers, trimers etc, in the early stages of pyrene stacking below the CAC, and then in the core of the micelles above the CAC) results in quenching of the pyrene fluorescence. We therefore hypothesised that the CAC could also be calculated by plotting the pyrene monomer emission (at 382 nm) against [**Py-RGD**] (Fig. 3.15). A similar method has been employed by other researchers.[271, 272] The CAC (122 μM) was calculated at the point where the two lines of best fit intersect. Using the direct fluorescence quenching of pyrene as a fluorescent probe, intrinsic to the **Py-RGD** molecule, was found to produce a CAC value which matched quite favourably with that obtained from the Nile Red assay, and confirms that using Nile Red as an indirect method appears to be an accurate way of determining the critical micelle/aggregation concentration of our amphiphilic molecules.

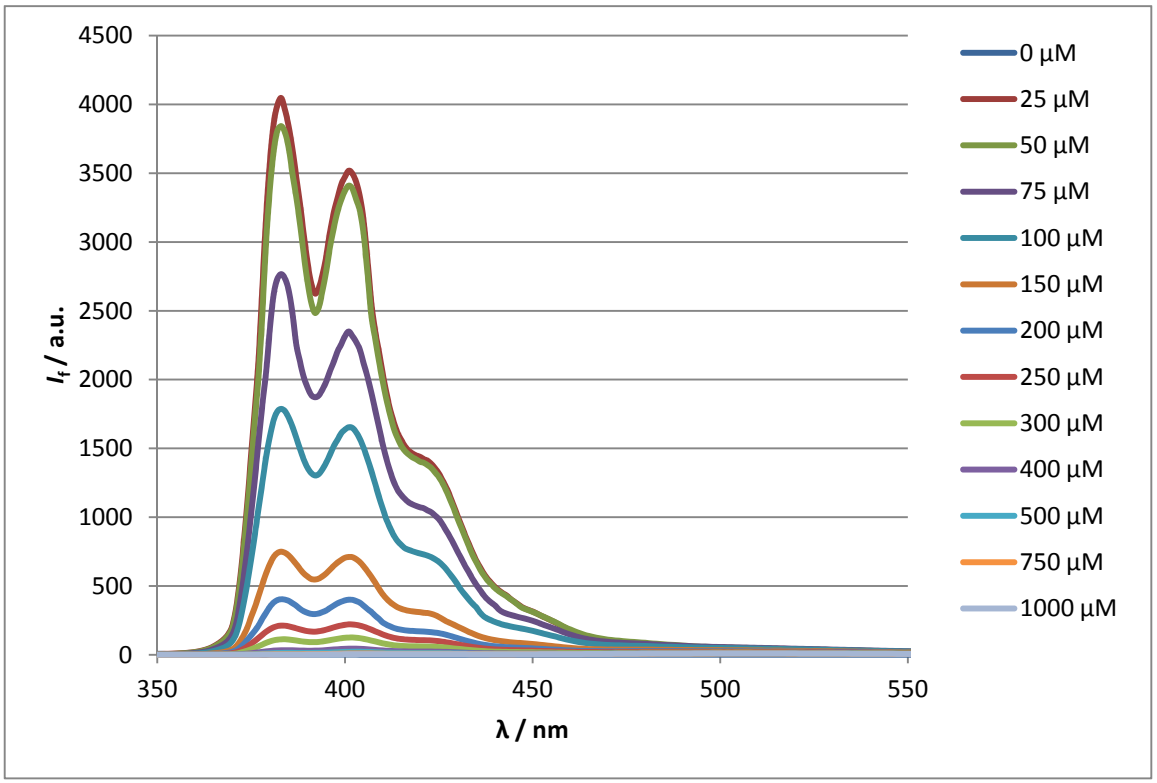

Fig. 3.14 – Averaged **Py-RGD** fluorescence emission spectra at different concentrations of **Py-RGD**. λ_{ex} = 343 nm. Experiments were run in triplicate. Original in colour.

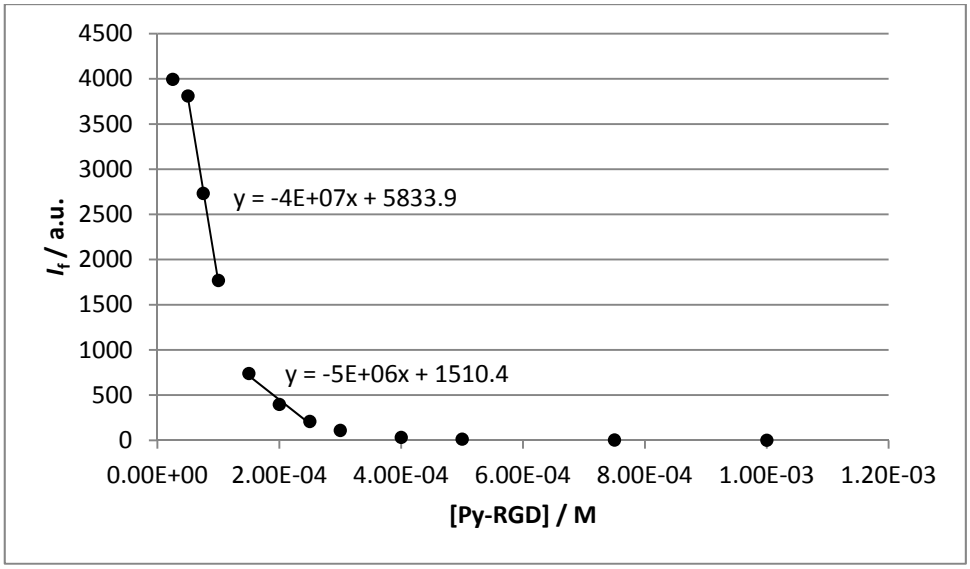

Fig. 3.15 – **Py-RGD** monomer emission (at 382 nm) versus [**Py-RGD**]. λ_{ex} = 343 nm.

TEM images of **Py-RGD** at high concentration (1 mM), show bundled structures comprised of small spherical micelles (<5 nm diameter) in PBS (pH 7.4) (Fig. 3.16A), similar to those observed for **C12-RGD**. The micellar radius is therefore in accordance with the head-to-tail molecular length of ~2.5 nm* for the **Py-RGD** amphiphile (Fig. 3.17). Similar structures are observed on dilution to just above the CAC (200 μM) (Fig. 3.16B). Unlike **C12-RGD**, large unilamellar structures were not observed for **Py-RGD** upon dilution, therefore, the mode of self-assembly is different and seemingly not as concentration dependent. This may be accredited to the different driving forces involved for the self-assembly of **Py-RGD** (π-π stacking and hydrophobicity) compared with those of **C12-RGD** (van der Waals interactions and hydrophobicity).

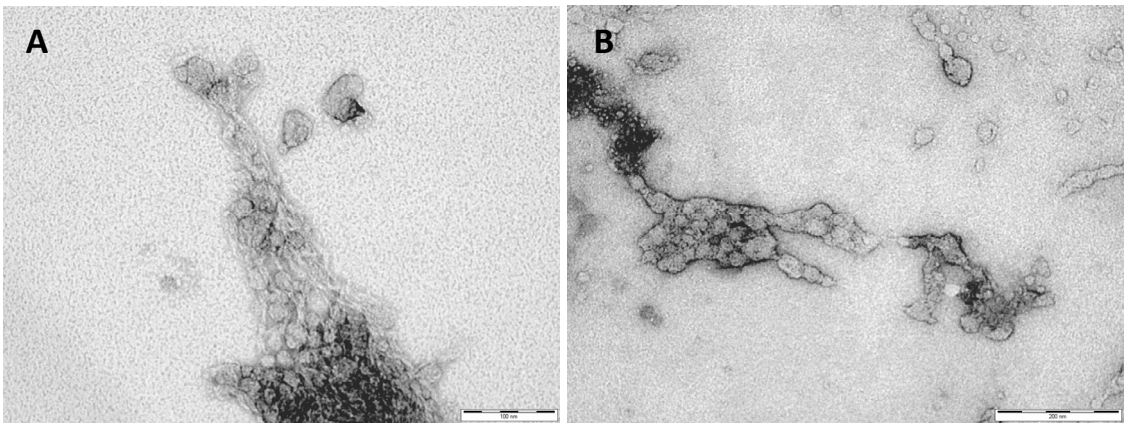

Fig. 3.16 – TEM images of assemblies formed by **Py-RGD** in PBS buffer (pH 7.4) at: A) 1 mM, scale bar = 100 nm, and B) 200 μM, scale bar = 200 nm. Negatively stained with uranyl acetate.

* Calculated using ChemBioDraw Ultra 11.0

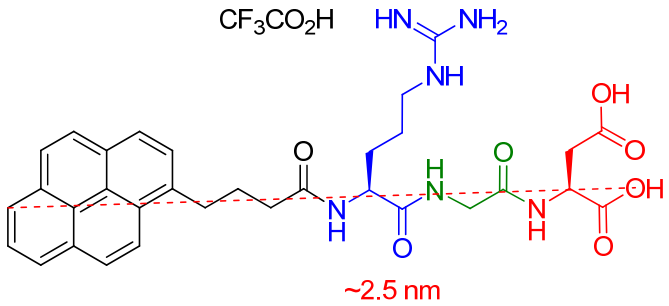

Fig. 3.17 – Structure showing the head-to-tail molecular length of **Py-RGD**. Original in colour.

A Nile Red study was then conducted on **C22-RGD** (**3.6**). As we expected, increasing the concentration of **C22-RGD** led to an increase in the fluorescence emission intensity of the dye (Fig. 3.18). It should be noted at this point that the fluorescence emission intensities are several orders of magnitude higher than those observed when **C12-RGD**, **Py-RGD** and **C12-Lys(C12)-$(CH_2)_5$-TEG-RGD** were studied, as a different spectrofluorimeter was used to acquire the data, therefore making it difficult to reason that the higher intensities are due to the assemblies formed from **C22-RGD** being better at solubilising/incorporating Nile Red. Plotting the fluorescence emission intensity at λ_{max} (640 nm) vs. log[peptide] gave an unusual trend (Fig. 3.19). Nonetheless, the CAC was estimated to be around 30 μM in PBS at pH 7.4. Interestingly, a less than 2-fold extension of the hydrocarbon tail from **C12-RGD** (CAC ≈ 300 μM) to **C22-RGD** appears to induce a 10-fold reduction in the CAC value, presumably owing to an enhancement in the hydrophobic effect for the longer alkyl chain.

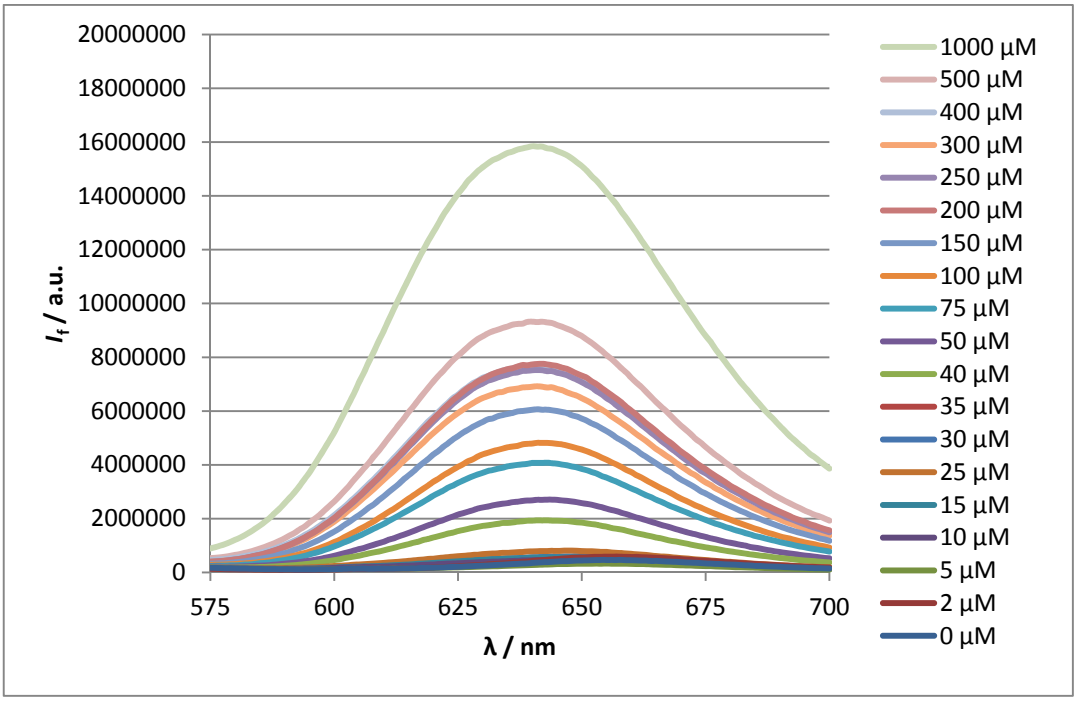

Fig. 3.18 – Nile Red fluorescence emission spectra in the presence of increasing concentrations of **C22-RGD**. λ_{ex} = 550 nm. Original in colour.

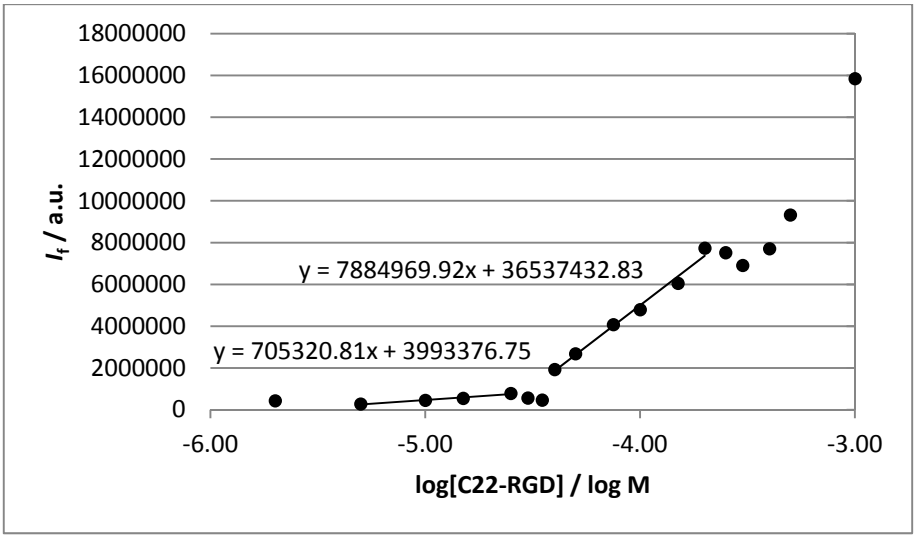

Fig. 3.19 – Nile Red fluorescence emission intensities at 640 nm plotted against log[**C22-RGD**]. λ_{ex} = 550 nm.

Instead of the usual bundled spherical micelle aggregates seen for the previous compounds, TEM imaging of **C22-RGD** (1 mM in PBS, pH 7.4) yielded rod-like micelle assemblies with diameters of ~20 nm (Fig. 3.20). Extension of the hydrocarbon tail from C12- to C22- evidently significantly modifies the mode of self-assembly from spherical to cylindrical morphologies, due to the more efficient packing of the longer C22 tail into the latter shape. This is in accordance with Israelachvili's critical packing principles[33] – the smaller head group area with respect to the longer hydrophobic chain length causes **C22-RGD** to adopt a truncated cone shape which preferentially self-assembles into cylindrical micelles. The head-to-tail molecular length of **C22-RGD** is ~4 nm* (Fig. 3.21), therefore, the rod-like micelles formed by **C22-RGD** are probably composed of bundles of fibres aggregated together.

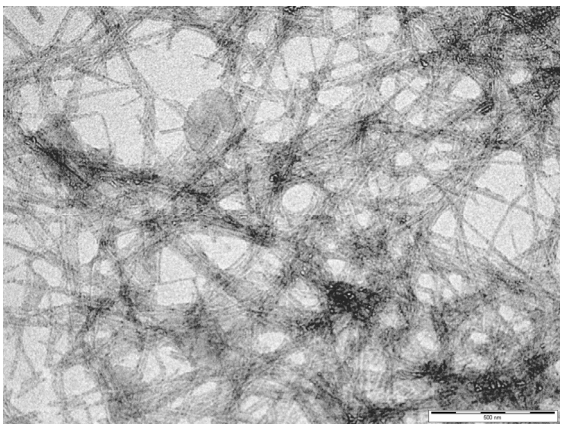

Fig. 3.20 – TEM image of assemblies formed by 1 mM **C22-RGD** in PBS buffer (pH 7.4), scale bar = 500 nm. Imaged without stain.

* Calculated using ChemBioDraw Ultra 11.0

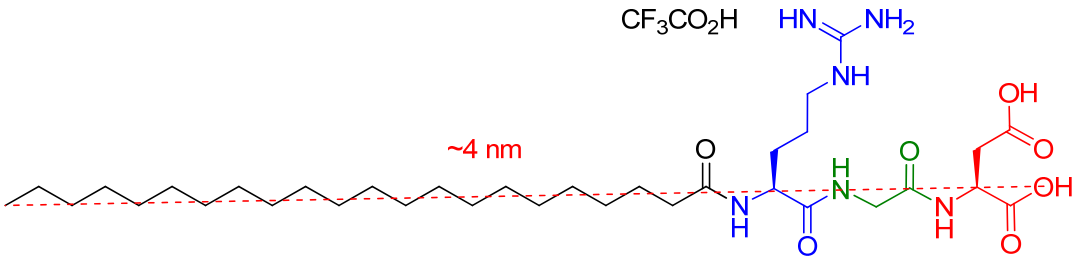

Fig. 3.21 – Structure showing the head-to-tail molecular length of **C22-RGD**. Original in colour.

Interestingly, this bundling of rod-like micelles produced a fibrous network which was able to restrict the flow of solvent molecules and induced gel formation in DMSO-d_6 when we tried to characterise the molecule by NMR (Fig. 3.22).

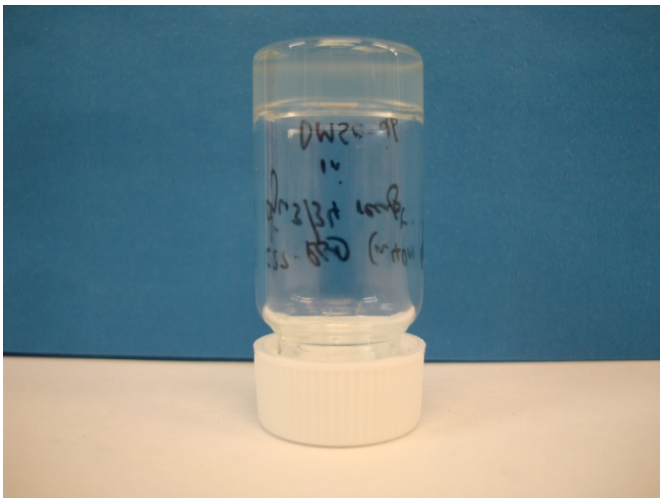

Fig. 3.22 – Inverted vial method to demonstrate gel formation of **C22-RGD** in DMSO-d_6. Original in colour.

Finally, the twin-tailed system, **C12-Lys(C12)-$(CH_2)_5$-TEG-RGD** (**3.18**), was studied for its potential self-assembling properties. As we expected, increasing the concentration of **C12-Lys(C12)-$(CH_2)_5$-TEG-RGD** led to an increase in the fluorescence emission intensity of Nile Red (Fig. 3.23). Plotting the fluorescence emission intensity at λ_{max} (635 nm) vs. log[peptide] (Fig. 3.24), the CAC was calculated to be ~6 μM in PBS at pH 7.4. In this case, doubling the number of hydrocarbon tails from **C12-RGD** (CAC ≈ 300 μM) to **C12-Lys(C12)-$(CH_2)_5$-TEG-RGD** induces a 50-fold reduction in the CAC value.

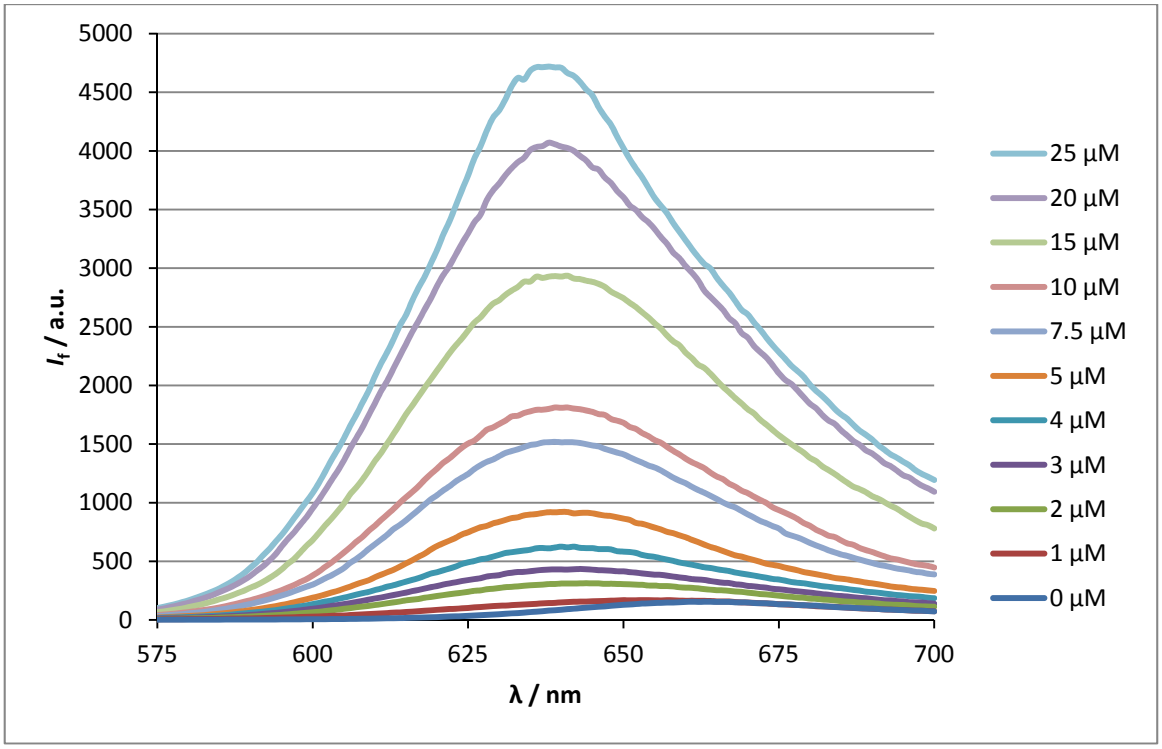

Fig. 3.23 – Averaged Nile Red fluorescence emission spectra in the presence of increasing concentrations of **C12-Lys(C12)-$(CH_2)_5$-TEG-RGD**. λ_{ex} = 550 nm. Experiments were run in triplicate. Original in colour.

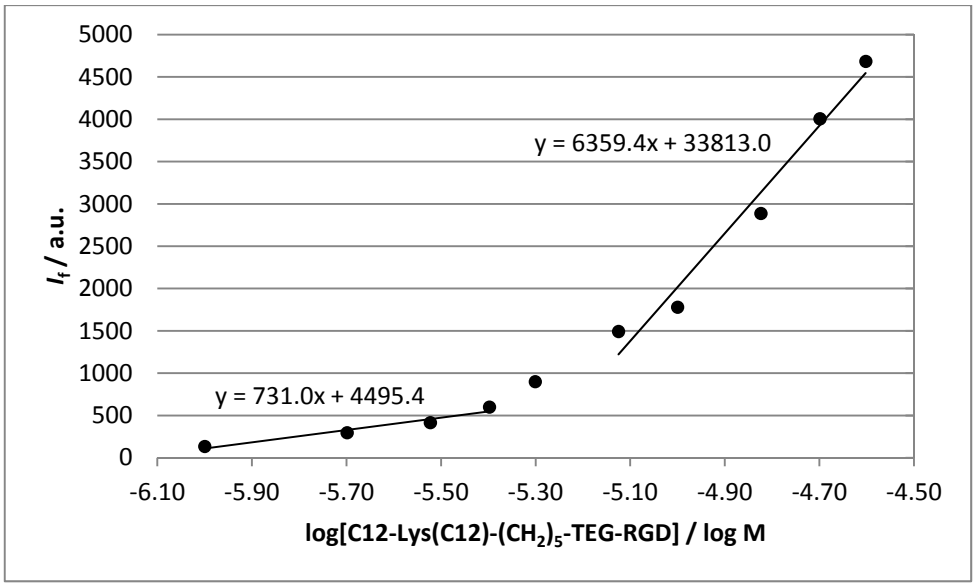

Fig. 3.24 – Averaged Nile Red fluorescence emission intensities at 635 nm plotted against log[**C12-Lys(C12)-$(CH_2)_5$-TEG-RGD**]. λ_{ex} = 550 nm. Experiments were run in triplicate.

TEM images both at 1 mM and 100 μM show similar rod-like micelles to those of **C22-RGD** (Fig. 3.25). Similarly, Marques and co-workers observed extended tubular structures when they investigated

the self-assembly in water of their lysine-based double-chained anionic surfactant, C12-Lys(C12)-O-Na^+, after heating to 40-45°C to induce solubilisation and then cooling to rt.[273]

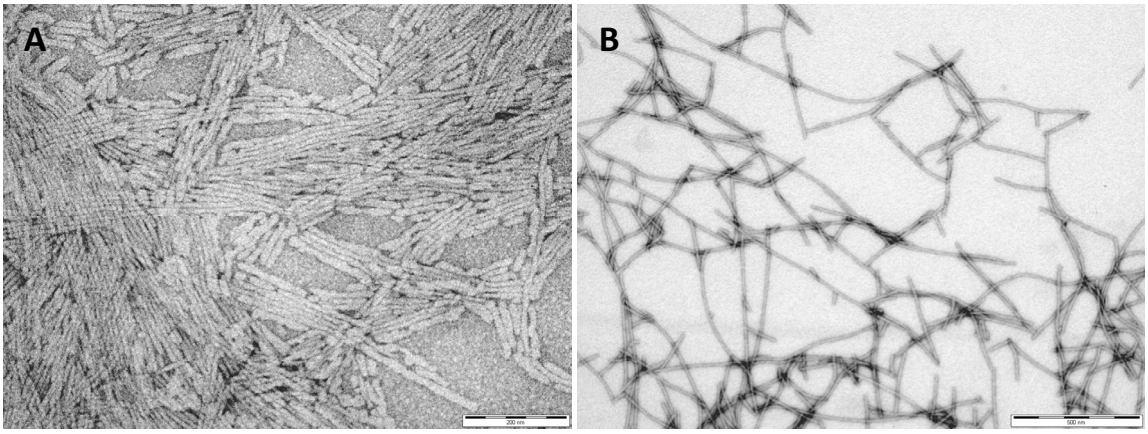

Fig. 3.25 – TEM images of assemblies formed by **C12-Lys(C12)-$(CH_2)_5$-TEG-RGD** in PBS buffer (pH 7.4) at: A) 1 mM, scale bar = 200 nm, and B) 100 μM, scale bar = 500 nm. Negatively stained with uranyl acetate.

Isolated structures are observed and their dimensions can be calculated; here an individual rod is shown with dimensions 11.5 × 152 nm (Fig. 3.26). The micellar radius is roughly in accordance with the head-to-tail molecular length of ~6 nm* (Fig. 3.27). However, as with all the molecules drawn in this chapter, this is a rigid depiction and the molecule will likely adopt a less linear conformation in solution.

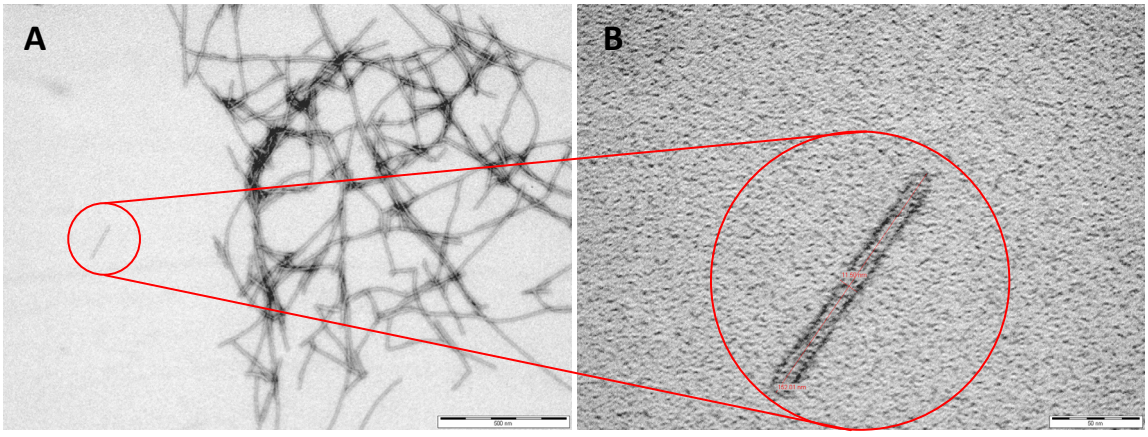

Fig. 3.26 – TEM images of assemblies formed by 100 μM **C12-Lys(C12)-$(CH_2)_5$-TEG-RGD** in PBS buffer (pH 7.4): A) scale bar = 500 nm, and B) scale bar = 50 nm. Negatively stained with uranyl acetate.

* Calculated using ChemBioDraw Ultra 11.0

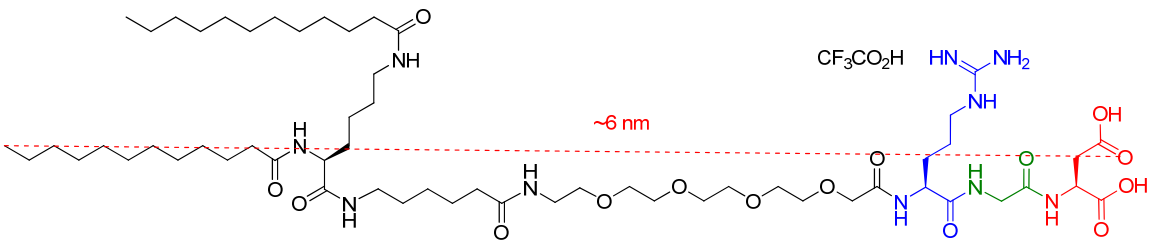

Fig. 3.27 – Structure showing the head-to-tail molecular length of **C12-Lys(C12)-$(CH_2)_5$-TEG-RGD**. Original in colour.

In summary, we found that functionalising the linear RGD peptide with a C12 alkyl chain (**C12-RGD**, CAC ≈ 300 μM) or aromatic pyrene unit (**Py-RGD**, CAC ≈ 110 μM) yielded amphiphilic structures which self-assembled into spherical micelles. Conversely, a larger C22 alkyl chain (**C22-RGD**, CAC ≈ 30 μM) or a branched/twin-tailed C12 system (**C12-Lys(C12)-$(CH_2)_5$-TEG-RGD**, CAC ≈ 6 μM) generated amphiphilic structures which adopted cylindrical/rod-like micelle morphologies.

3.4 Integrin Binding Studies

We then went on to investigate, firstly, whether **C12-RGD** (**3.2**) could bind integrin $\alpha_v\beta_3$, and determine if a non-covalent self-assembling strategy produces multivalent RGD ligand arrays with higher integrin affinities than those found using the more synthetically demanding covalent dendritic approach, such as **Z-G1-[RGD]$_3$** (**2.16**) and **Z-G2-[RGD]$_9$** (**2.17**). Unlike non-self-assembling **PEG-RGD** (**2.19**), lipopeptide **C12-RGD** was able to reduce the normalised FP signal down to below 50% of the initial value at an effective concentration of ~200 μM (shown in orange, Fig. 3.28). Using the Cheng-Prusoff equation (Eq. 2.1) the K_i = 197 μM ≈ EC_{50} (as discussed in Chapter 2). We propose that this binding concentration is evidence of a multivalency effect, as the self-assembly of **C12-RGD** can generate a multivalent ligand display and therefore bind integrin proteins significantly better than the non-self-assembling, monovalent control **PEG-RGD**.

As the integrin is held in the Triton X-100 surfactant assemblies, we had concerns over whether the **C12-RGD** lipopeptide was giving a false positive result in the FP assay by disrupting the stability of the integrin-Triton assemblies rather than directly binding with the integrin itself. We therefore used sodiumdodecylsulfate (SDS) as a model monoanionic surfactant (Fig. 3.29), also comprised of a twelve carbon hydrophobic tail, and tested its ability to affect the FP signal (shown in red, Fig. 3.28). The signal did not decrease, unequivocally demonstrating that the decreasing FP signal for **C12-RGD** can be attributed to interactions between the RGD head group and the protein, rather than the surfactant-like nature of the compound disrupting the integrin stability.

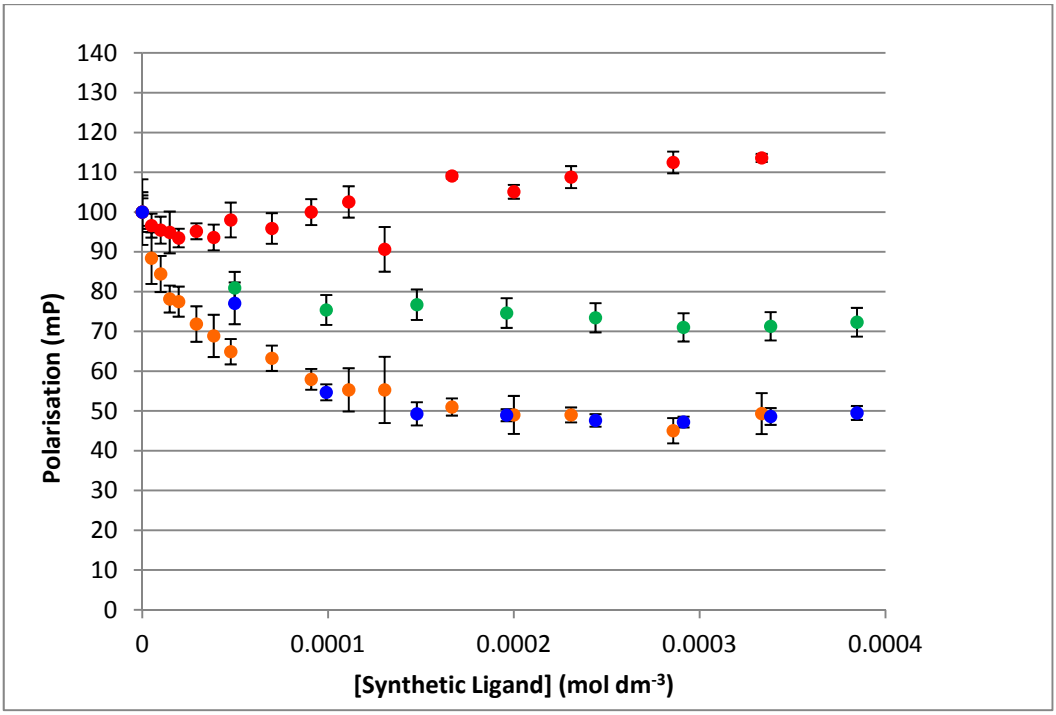

Fig. 3.28 – Normalised titration curves for the displacement of **5(6)-FL-c[RGDfK]** probe (10 nM) from integrin $\alpha_v\beta_3$ (280 nM) on the addition of the synthetic ligands: **Z-G1-[RGD]$_3$** (blue), **C12-RGD** (orange), **PEG-RGD** (green) and SDS (red) after incubating at 29 °C for 5 min.

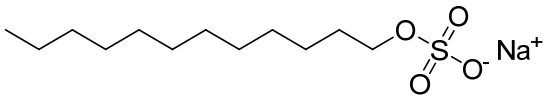

Fig. 3.29 – The structure of sodiumdodecylsulfate (SDS).

Interestingly, on a per RGD basis, **C12-RGD** (200 μM) is a stronger integrin binder than **Z-G1-[RGD]$_3$** (375 μM) (Fig. 3.30). We speculate that the reversible nature of the self-assembly process generates large arrays with a greater degree of flexibility, and potentially a better ability to satisfy the binding requirements of the integrin (Fig. 3.31). The mechanism of binding, rather than a high local concentration of ligand around just one integrin (Fig. 3.31A), is speculated to be a multiple binding event with the bundles of spherical micelles interacting across clusters of integrins in the integrin-Triton assemblies (Fig. 3.31B). Indeed, it is also plausible that the larger unilamellar structures, which also arise from **C12-RGD** self-assembling, interact across integrin clusters (Fig. 3.31C).

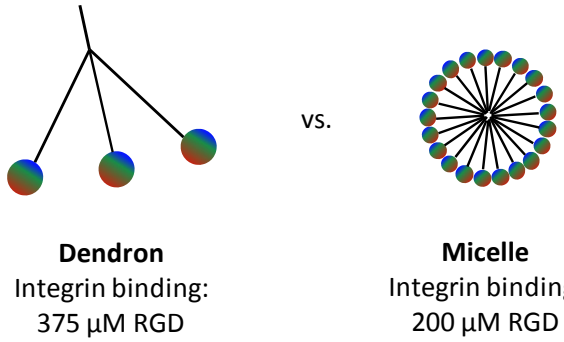

Fig. 3.30 – Comparison of dendritic and self-assembled approaches to multivalency.

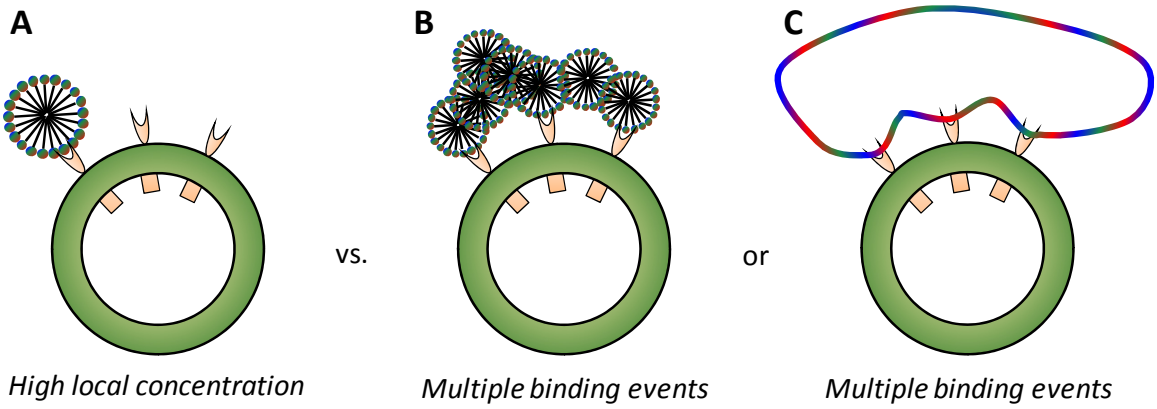

Fig. 3.31 – The possible mechanisms of multivalency in integrin recognition by C12-RGD.

It should be noted that **C12-RGD** (EC_{50} = 200 µM) appears to bind integrin at a concentration lower than its apparent CAC (~300 µM). Two possibilities are suggested for this: (i) the presence of the integrin causes the peptide amphiphile to self-assemble below its apparent CAC, possibly initiated upon binding, or (ii) the lipopeptide inserts itself into the Triton X-100 assemblies and the overall RGD-displaying aggregate is then able to bind to adjacent integrin-Triton assemblies. In support of the latter possibility, TEM images indicate that the integrin-Triton assemblies are somewhat perturbed by the presence of **C12-RGD** (Fig. 3.32). This work comparing dendritic and self-assembling strategies to multivalency, with respect to RGD peptide-integrin interactions, has recently been published.[274]

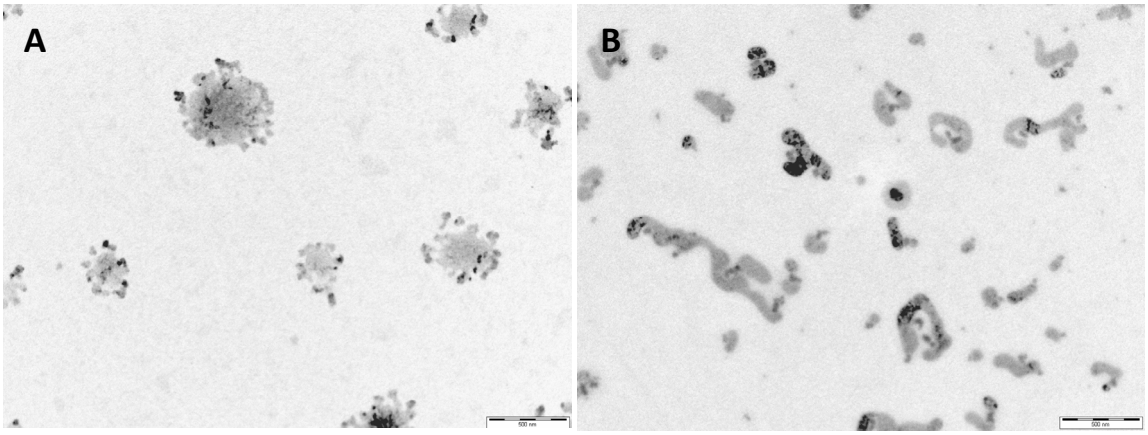

Fig. 3.32 – TEM images of integrin-Triton X-100 assemblies: A) prior to the addition of **C12-RGD** peptide, scale bar = 500 nm, and B) post-FP assay of **C12-RGD**, scale bar = 500 nm. Imaged without stain.

Py-RGD (**3.4**) was then investigated for its ability to bind integrins and found to decrease the FP signal to 50% of its initial intensity at a concentration of ~110 μM (shown in light blue, Fig. 3.33). Using the Cheng-Prusoff equation (Eq. 2.1) the K_i = 108 μM ≈ EC_{50} (as discussed in Chapter 2). Once again, this is evidence of a multivalency effect as **Py-RGD** binds better than the non-self-assembling monovalent control **PEG-RGD**. We can speculate that the reason for the EC_{50} of **Py-RGD** being almost two-fold less than that of **C12-RGD** is a consequence of **Py-RGD** having a lower CAC value i.e. it spontaneously forms aggregates with a multivalent display of RGD surface groups at a much lower concentration. The mechanism of binding, however, is likely to be similar to that of **C12-RGD** (Fig. 3.31B or C) as **Py-RGD** also aggregates to form large clusters of spherical micelles thereby possessing the ability to bind several integrins on one assembly at once. It should be noted that the CAC of **Py-RGD** is the same as its EC_{50} binding value, indicating that **Py-RGD** binds integrin at the point at which it spontaneously self-assembles. This may be coincidental, however, as the binding curve for **Py-RGD**, like **C12-RGD**, decreases much more dramatically than that represented by **PEG-RGD** signifying self-assembly and enhanced integrin binding is taking place below the calculated CAC, and the reasoning for this is the same as that discussed for **C12-RGD**.

Contrary to the promising results we have obtained with **C12/Py-RGD**, when we tested synthetic ligands **C22-RGD** (**3.6**) and **C12-Lys(C12)-$(CH_2)_5$-TEG-RGD** (**3.18**), which form rod-like micelles above their CACs, they were found to drastically underperform in this assay (Fig. 3.33); so much so that the binding profile for **C12-Lys(C12)-$(CH_2)_5$-TEG-RGD** (shown in purple) overlays that of the weakly binding **PEG-RGD**, while **C22-RGD** (shown in red) fluctuates very little below the initial normalised signal of 100 mP units.

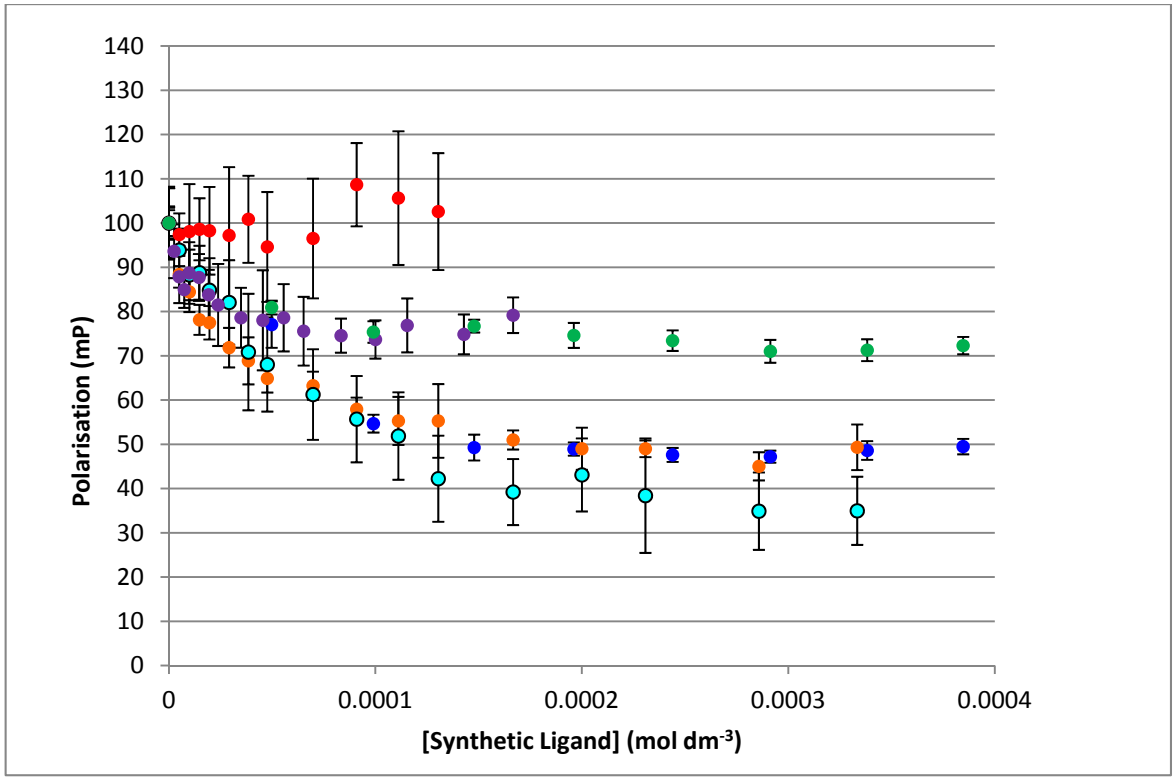

Fig. 3.33 – Normalised titration curves for the displacement of **5(6)-FL-c[RGDfK]** probe (10 nM) from integrin $\alpha_v\beta_3$ (280 nM) on the addition of the synthetic ligands: **Z-G1-[RGD]$_3$** (blue), **C12-RGD** (orange), **Py-RGD** (light blue), **C22-RGD** (red), **C12-Lys(C12)-(CH$_2$)$_5$-TEG-RGD** (purple) and **PEG-RGD** (green) after incubating at 29 °C for 5 min.

We hypothesise that although the cylindrical structures formed by these two amphiphiles will also possess a multivalent surface comprised of RGD ligands, either: (i) the cylindrical morphology is too rigid and does not possess the degree of flexibility required to satisfy the binding requirements of the integrin protein – this would explain why **C12-Lys(C12)-(CH$_2$)$_5$-TEG-RGD** which has a flexible TEG linker appears to be slightly better at interacting with integrin than **C22-RGD**; (ii) in relation to (i), it may be that on a less curved cylindrical surface the RGD ligand is less able to bind to the active site of integrin than it is on a highly curved spherical micelle surface; or (iii) the viscosity of the assay solution increases because of the formation of these rod-like fibres which lowers the rotational mobility of the probe (whether bound as the probe:protein complex or unbound), and hence the FP signal does not decrease as much as it would have if the viscosity of the solution remained unchanged, even if the probe is being displaced from the integrin by the synthetic ligand. It is known that probes used in biophysical studies utilising fluorescence polarisation are sensitive to changes in viscosity.[263] Evidence for the latter hypothesis was the observation of gel-like turbidity during the titration of **C22-RGD** into the assay cuvette. Further experimental evidence to prove this would need to investigate any change in viscosity of the **C22-RGD** and **C12-Lys(C12)-(CH$_2$)$_5$-TEG-RGD** assay solutions with

increasing **C22-RGD** and **C12-Lys(C12)-$(CH_2)_5$-TEG-RGD** concentration, respectively, in more detail.

In support of this, TEM images indicate that the integrin-Triton assemblies (Fig. 3.34A) although not perturbed themselves, unlike the case of **C12-RGD** (Fig. 3.32), are 'tangled up' in the rod-like fibres that **C22-RGD** forms (Fig. 3.34B). Any reduction in the FP signal by displacement of probe from the integrin binding site would most likely be outweighed by the restricted rotation of free probe and probe:integrin complexes in the fibrous mass which formed – a similar effect on the FP signal to that of the non-specific aggregation of the synthetic ligands discussed in Chapter 1. In the case of **C12-Lys(C12)-$(CH_2)_5$-TEG-RGD**, the fibres were so dense that it was difficult to observe any integrin-Triton assemblies (Fig. 3.34C). Or perhaps **C22-RGD** and **C12-Lys(C12)-$(CH_2)_5$-TEG-RGD** are unable to insert into the Triton assemblies, which was one hypothesis for the improved binding of **C12-RGD**, as they are possibly more stable in their own rod-like micelles (as evidenced by the unchanged integrin-Triton assemblies in Fig. 3.34B).

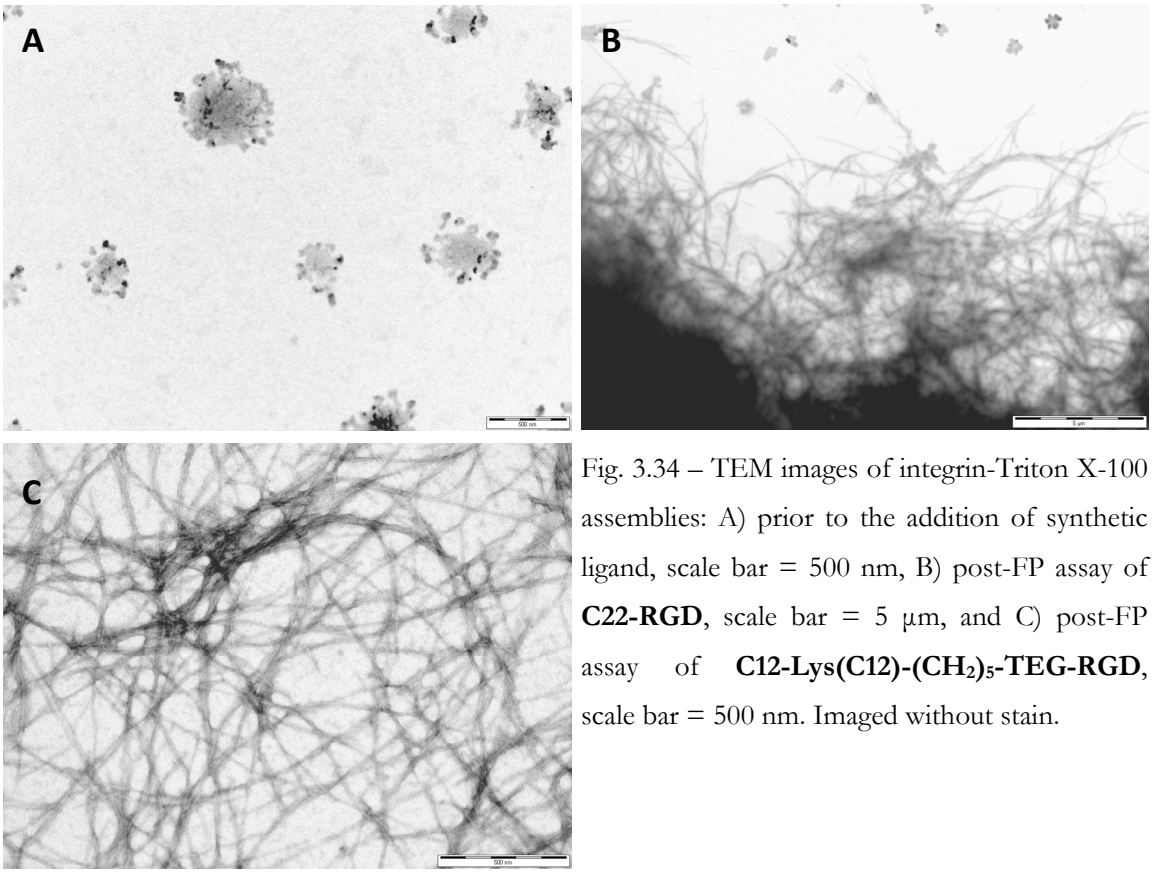

Fig. 3.34 – TEM images of integrin-Triton X-100 assemblies: A) prior to the addition of synthetic ligand, scale bar = 500 nm, B) post-FP assay of **C22-RGD**, scale bar = 5 μm, and C) post-FP assay of **C12-Lys(C12)-$(CH_2)_5$-TEG-RGD**, scale bar = 500 nm. Imaged without stain.

These results suggest that the rod-like micelle forming compounds are poor ligands, but perhaps the choice of spectroscopic study, sensitive to changes in viscosity, limits the types of synthetic ligands that can be employed. A summary of the CAC and EC_{50} for each compound is given in Table 3.1.

Synthetic Ligand	Compound No.	Micelle Morphology	CAC (μM)	EC_{50} 'per RGD' (μM)
Z-G1-[RGD]$_3$	**2.16**	-	-	375
C12-RGD	**3.2**	Spherical	~300	200
Py-RGD	**3.4**	Spherical	~110	110
C22-RGD	**3.6**	Rod-like	~30	-
C12-Lys(C12)-(CH$_2$)$_5$-TEG-RGD	**3.18**	Rod-like	~6	-

Table 3.1 – Summary of synthetic ligands, their aggregate morphologies, CACs and EC_{50}s.

3.5 Conclusions

In conclusion, we have synthesised an array of self-assembling, linear RGD peptide amphiphiles. **C12-RGD** and **Py-RGD** self-assembled to produce spherical micelle-type aggregates, whereas the longer hydrophobic-tailed **C22-RGD** and twin-tailed system, **C12-Lys(C12)-(CH$_2$)$_5$-TEG-RGD**, generated rod-like micelles above their CACs. We then went on to test their ability to bind integrin $\alpha_v\beta_3$ in our established fluorescence polarisation assay.

Multivalency effects were observed when we compared the monovalent control, **PEG-RGD**, with **C12-RGD** and **Py-RGD**. However, **C22-RGD** and **C12-Lys(C12)-(CH$_2$)$_5$-TEG-RGD** surprisingly underperformed and could not reduce the FP signal to 50% of its initial value. This was reasoned to be due to either ineffective binding of the rigid rod-like structures formed, or a possible increase in viscosity as the concentration of the synthetic ligand increases meaning the FP assay is inappropriate for these types of surfactant. Further work is required to monitor these suspected changes in viscosity and an alternative binding assay, possibly cell-based, would provide further comparative evidence as to whether or not **C22-RGD** and **C12-Lys(C12)-(CH$_2$)$_5$-TEG-RGD** are indeed poor ligands for binding of integrin $\alpha_v\beta_3$.

We have successfully shown that a self-assembly (non-covalent) approach to multimerising the linear RGD ligand has led to even further improvements in integrin $\alpha_v\beta_3$ binding ability compared to that of a dendritic (covalent) approach, and suggest that this is a consequence of the greater flexibility and responsiveness of self-assembled micellar systems.

Chapter 4

Linear RGD Peptide Conjugate Hydrogelators

4 Linear RGD Peptide Conjugate Hydrogelators

4.1 Introduction

As discussed in the introduction, low MW peptide-based hydrogels are currently generating interest as promising smart materials for a wide variety of applications, ranging from pollutant capture and removal[225] to nerve regeneration.[224] In this chapter, a small library of linear RGD peptide amphiphiles and bolaamphiphiles was designed (Fig. 4.1), comprising a variety of different aliphatic or aromatic chains conjugated to the peptide through urea linkages, and their hydrogelation properties under thermal and sonochemical stimuli were studied. We decided to use urea linkages, not only for their relative ease of synthesis, but also because of their proven importance in underpinning supramolecular gels as a consequence of their intermolecular urea-urea hydrogen bonding, even in competitive solvents such as water.[252] Related bis-urea bolaamphiphilic hydrogelators possessing different length aliphatic chains have previously been synthesised and studied by Hamilton and co-workers, but these had a much simpler single amino acid (glutamic acid) as the head group.[251, 275]

We report on amphiphile vs. bolaamphiphile, the effects of changing the aliphatic chain length and aliphatic vs. aromatic chain type and how this impacts on gelation ability, providing insight into structure-gelation relationships for low MW linear RGD peptide conjugate hydrogelators. By incorporating lysine (K) into the RGD structure (RGDK) (Fig. 4.1), an understanding of charge and/or packing effects on gelation is reported. We also compare and contrast the gelation ability of the urea-based RGD compounds with an amide-based 'twin-tailed' system (Fig. 4.2) and two urea-based, oligo(phenylene ethynylene), linear RGD peptide conjugates (Fig. 4.3).

We then move on to examine gelator **C12-[urea-RGD]$_2$**, **4.4**, in more detail: controlling hydrogelation by varying temperature, while the role played by the urea functionality and the effect of different anions on gelation will also be explored. These studies provide fundamental insight into how factors external to the gelator can control gel formation and breakdown. Finally, a small molecule encapsulation-release study with the hydrogel of **4.4** demonstrates the feasibility of using such hydrogels in controlled drug delivery as well as tissue engineering applications.

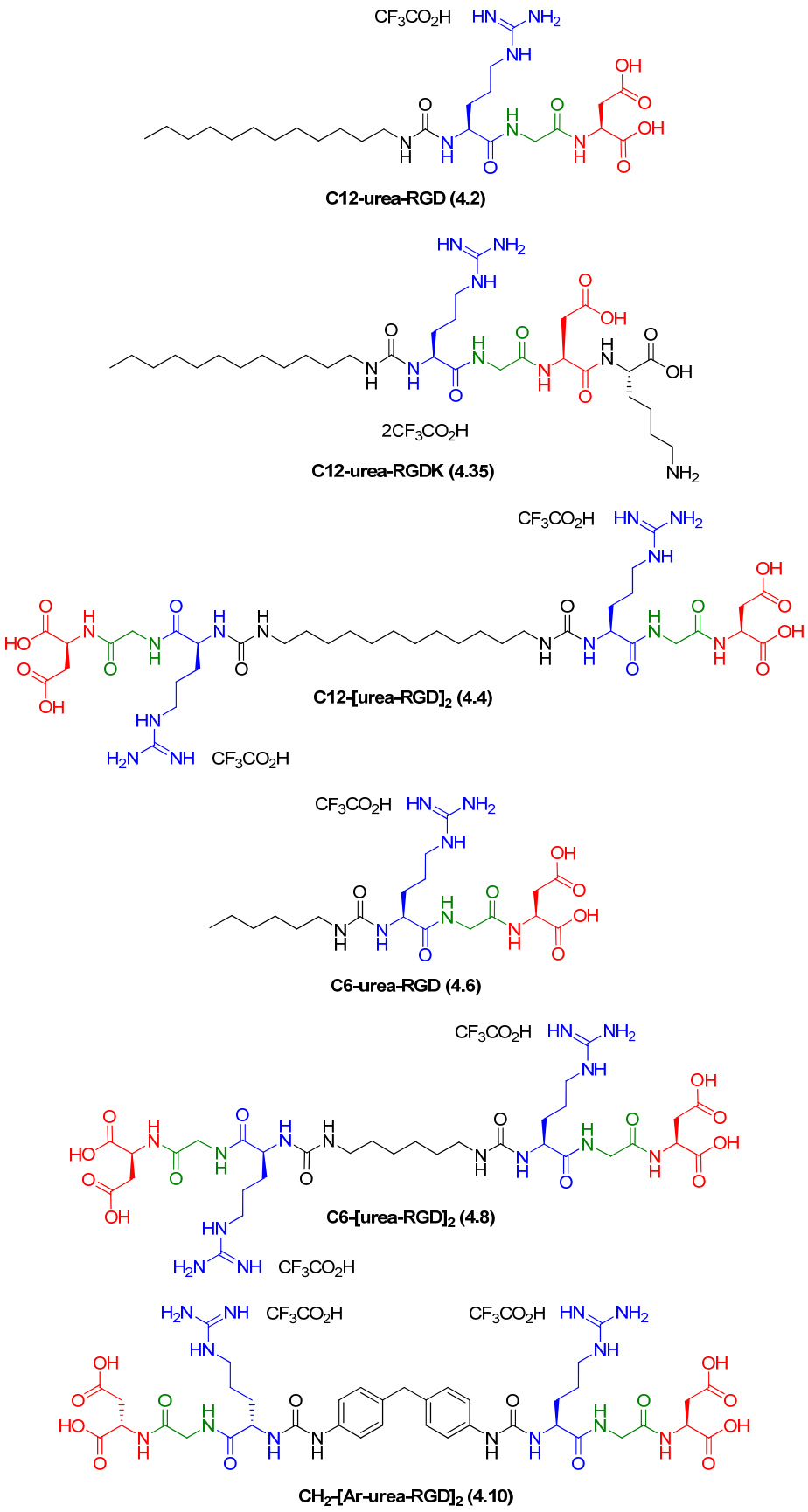

Fig. 4.1 – Our library of urea-based linear RGD(K) peptide amphiphiles and bolaamphiphiles. Original in colour.

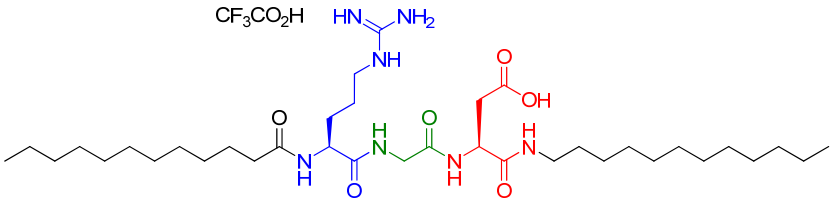

Fig. 4.2 – Our amide-based 'twin-tailed' system: **C12-RGD-C12**. Original in colour.

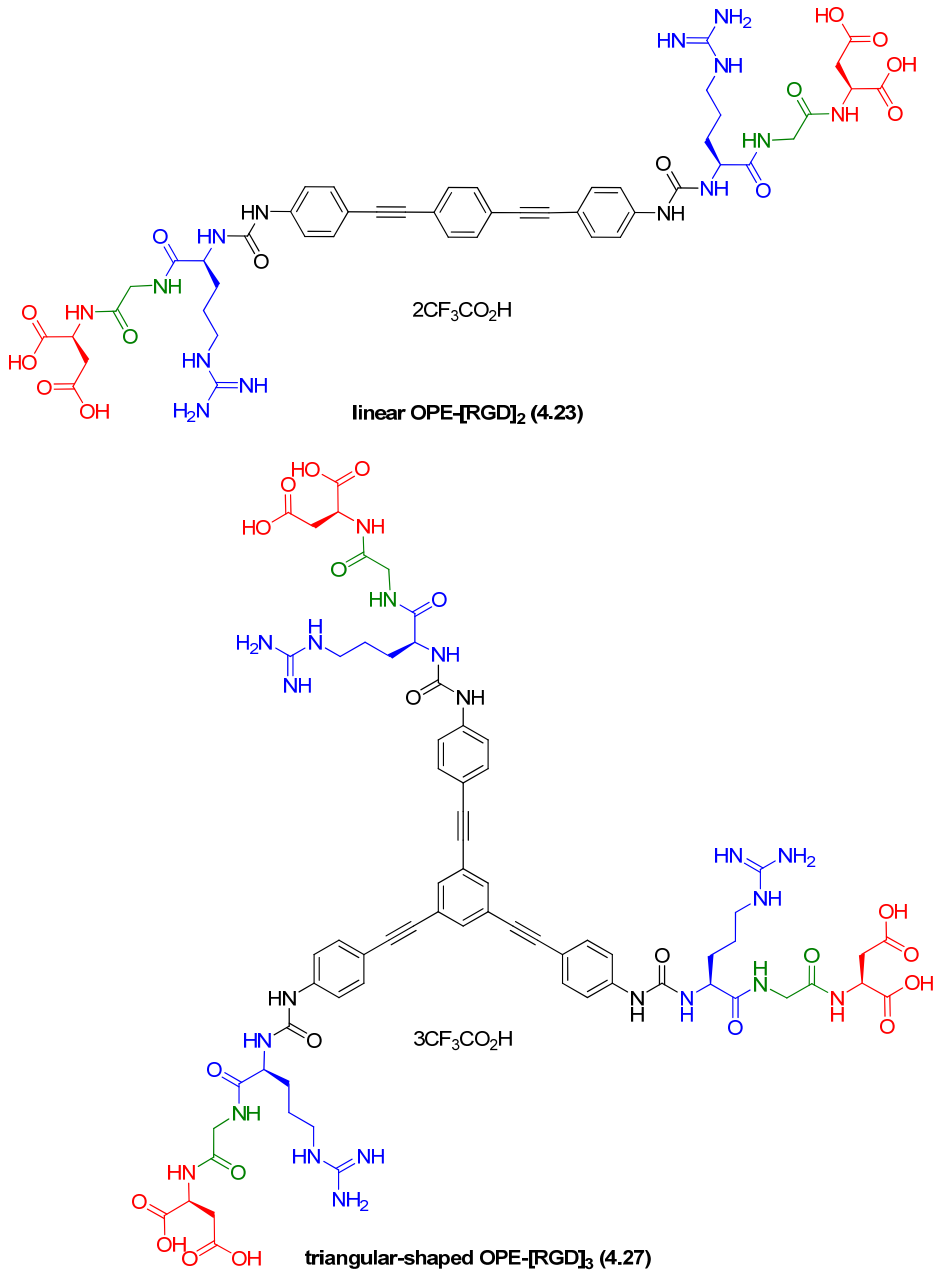

Fig. 4.3 – Our urea-based, linear and triangular-shaped oligo(phenylene ethynylene) (OPE), linear RGD peptide conjugates, **4.23** and **4.27**, respectively. Original in colour.

4.2 Synthesis

4.2.1 Synthesis of C12-urea-RGD

Dodecyl isocyanate (in DCM) and compound **2.8** (in DCM) were combined at a 1:1 molar ratio, then a further portion of dodecyl isocyanate was added (providing a final molar ratio of 2:1) after 1.5 h, because TLC analysis indicated that the reaction was incomplete, and stirred overnight at rt. Silica column purification of the crude reaction mixture afforded **4.1** in 77% yield (Scheme 4.1). This was confirmed in the ^{1}H NMR by a downfield shift in the arginine α-*H* from 3.44 ppm to 4.31-4.22 ppm on coupling **2.8** to the isocyanate to generate the adjacent electron-withdrawing urea functional group. ESI-MS analysis also confirmed the formation of product with a *m*/*z* value of 922.5692 (100%, $[M+H]^+$).

TFA deprotection of the RGD peptide generated final product **C12-urea-RGD**, **4.2**, in 80% yield (Scheme 4.1). The loss of peaks in the ^{1}H NMR (see appendix – spectrum 4.1) corresponding to the Pbf methylene (2.93 ppm) and methyl groups at 2.55, 2.50, 2.06 and 1.44 ppm, as well as the *tert*-butyl methyl groups at 1.44 and 1.39 ppm, confirmed successful reaction. Further evidence was provided by ESI-MS which revealed the absence of peaks for the precursor compound and the presence of a new peak with a *m*/*z* value of 558.3621 (100%, $[M+H]^+$), corresponding to the product.

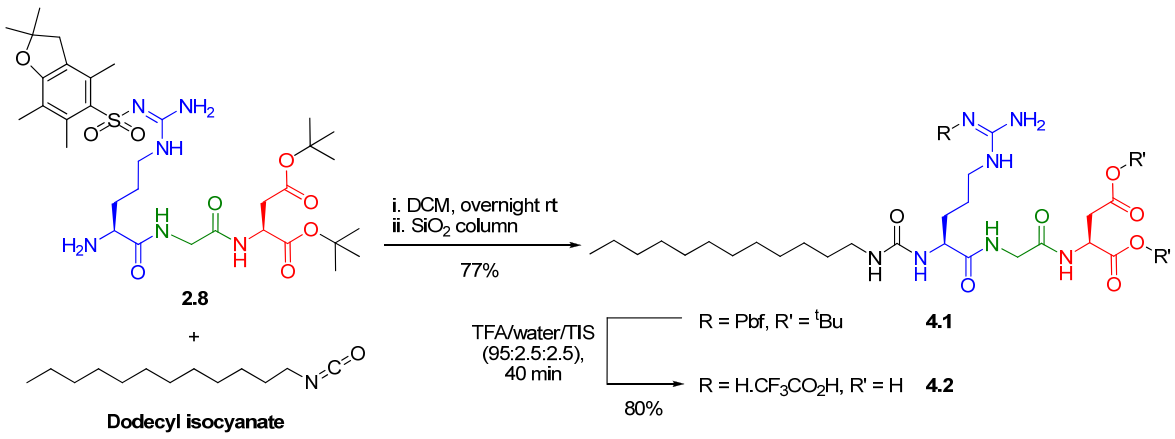

Scheme 4.1 – Reaction scheme showing the formation of **4.1** and subsequent deprotection conditions to form **C12-urea-RGD**, **4.2**. Original in colour.

4.2.2 Synthesis of C12-[urea-RGD]$_2$

1,12-diisocyanatododecane (in DCM) and compound **2.8** (in DCM) were combined at a 1:2 molar ratio, and stirred for 21.5 h at rt. It should be noted that a white gel-like precipitate had formed overnight from an initially colourless and clear solution, indicating that the reaction had progressed. Silica column purification of the crude reaction mixture afforded di-substituted product, **4.3**, in 80%

yield (Scheme 4.2). This was confirmed in the ^{1}H NMR by a downfield shift in the arginine α-*H* on coupling **2.8** to the isocyanate to generate the adjacent electron-withdrawing urea functional group. ESI-MS analysis also confirmed the formation of product with a *m*/*z* value of 837.4638 (100%, $[M+2H]^{2+}$). Repeating the reaction using a 1:2.4 molar ratio of 1,12-diisocyanatododecane:**2.8**, followed by the same purification procedure gave **4.3** in an improved 98% yield, confirming that an excess of the peptide nucleophile helps to drive the nucleophilic addition reaction to completion.

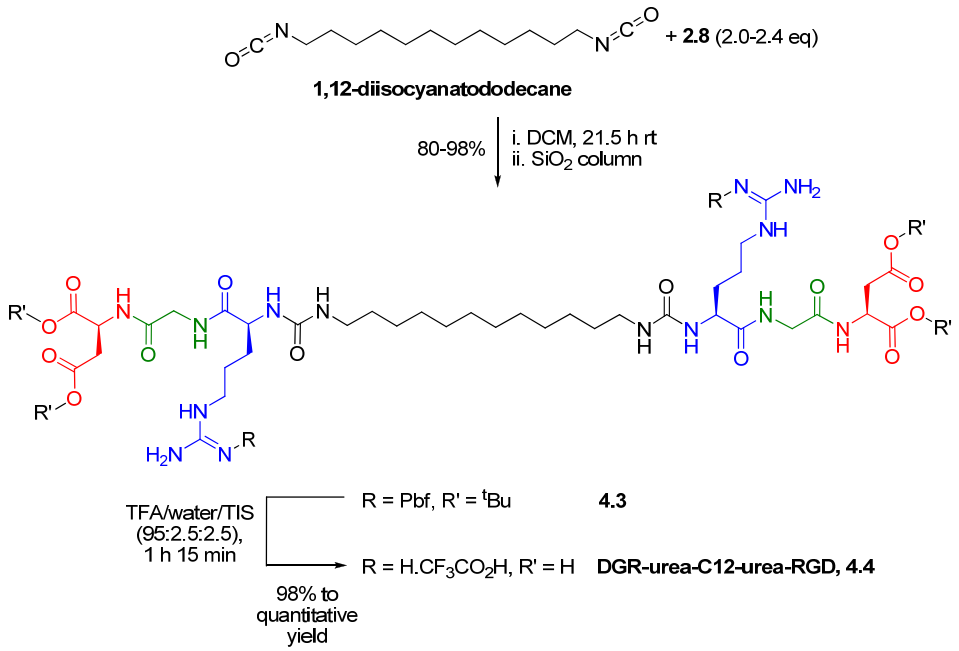

Scheme 4.2 – Reaction scheme showing the formation of **4.3** and subsequent deprotection conditions to form **C12-[urea-RGD]$_2$**, **4.4**. Original in colour.

TFA deprotection of the RGD peptide generated final product **C12-[urea-RGD]$_2$**, **4.4**, in near quantitative yields (Scheme 4.2). The loss of peaks in the ^{1}H NMR (see appendix – spectrum 4.2) corresponding to the Pbf methylene and methyl groups, as well as the *tert*-butyl methyl groups, confirmed the reaction was successful. Further evidence was provided by ESI-MS which revealed the absence of peaks for the precursor compound and the presence of a new peak at a *m*/*z* value of 473.2538 (100%, $[M+2H]^{2+}$), corresponding to the product.

4.2.3 Synthesis of C6-urea-RGD

Hexyl isocyanate (in DCM) and compound **2.8** (in DCM) were combined at a 1:1 molar ratio, and stirred for 3 days at rt. Silica column purification of the crude reaction mixture afforded **4.5** in 89% yield (Scheme 4.3). As seen previously, a downfield shift in the arginine α-*H* on coupling **2.8** to the isocyanate, a consequence of the newly formed adjacent electron-withdrawing urea functional group,

was observed in the ^{1}H NMR. ESI-MS analysis also confirmed the formation of product with a *m/z* value of 838.4734 (100%, $[M+H]^+$).

TFA deprotection of the RGD peptide generated final product **C6-urea-RGD**, **4.6**, in 87% yield (Scheme 4.3). Peaks corresponding to the Pbf methylene and methyl protons in **4.5**, including the *tert*-butyl methyl protons, were absent in the ^{1}H NMR of **4.6** (see appendix – spectrum 4.3) which confirmed the structure and purity of the product. Further evidence was provided by ESI-MS which revealed the absence of peaks for the precursor compound and the presence of the product peak at a *m/z* value of 474.2681 (100%, $[M+H]^+$).

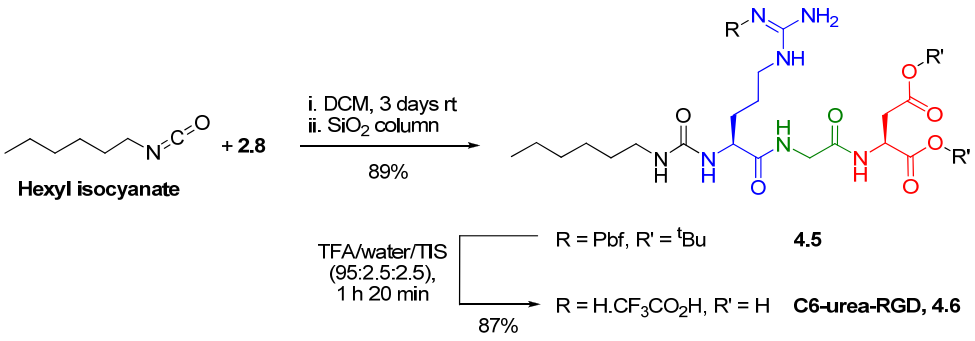

Scheme 4.3 – Reaction scheme showing the formation of **4.5** and subsequent deprotection conditions to form **C6-urea-RGD**, **4.6**. Original in colour.

4.2.4 Synthesis of C6-[urea-RGD]$_2$

1,6-Diisocyanatohexane (in DCM) and compound **2.8** (in DCM) were combined at a 1:2 molar ratio, and stirred for 17 h at rt. It should be noted that although the reaction mixture remained clear, it became very viscous after a few minutes of stirring following the addition of the diisocyanate, indicating that the reaction had progressed. Silica column purification of the crude reaction mixture afforded di-substituted product, **4.7**, in 92% yield (Scheme 4.4). As usual, a downfield shift in the arginine α-*H* on coupling **2.8** to the isocyanate was observed. ESI-MS detected the product with a *m/z* value of 795.4137 (100%, $[M+2H]^{2+}$).

TFA deprotection of the RGD peptide generated final product **C6-[urea-RGD]$_2$**, **4.8**, in near quantitative yield (Scheme 4.4). The loss of peaks in the ^{1}H NMR (see appendix – spectrum 4.4) corresponding to the Pbf methylene and methyl groups, including the *tert*-butyl methyl groups, confirmed the isolation of the product. Peaks in the ESI-MS corresponding to the precursor compound were absent, and a new peak was detected at a *m/z* value of 431.2016 (100%, $[M+2H]^{2+}$) for the product.

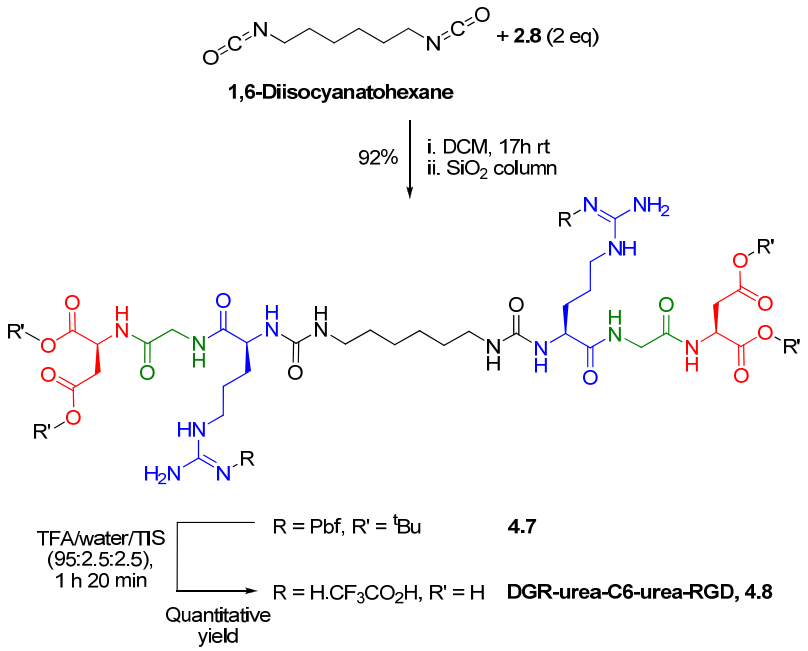

Scheme 4.4 – Reaction scheme showing the formation of **4.7** and subsequent deprotection conditions to form **C6-[urea-RGD]$_2$**, **4.8**. Original in colour.

4.2.5 Synthesis of CH$_2$-[Ar-urea-RGD]$_2$

4,4'-Methylenebis(phenyl isocyanate) (in DCM) and compound **2.8** (in DCM) were combined at a 1:2.4 molar ratio, and stirred for 3 days at rt. It should be noted that the initially colourless and clear solution became viscous and a white gel-like precipitate formed after a few minutes of stirring following the addition of the diisocyanate, indicating that the reaction had progressed. Silica column purification of the crude reaction mixture afforded di-substituted product, **4.9**, in 93% yield (Scheme 4.5). Again, a downfield shift in the arginine α-*H* on coupling **2.8** to the isocyanate was observed in the ^{1}H NMR. ESI-MS analysis also confirmed the formation of product with a *m/z* value of 836.4090 (100%, $[M+2H]^{2+}$).

TFA deprotection of the RGD peptide generated final product **CH$_2$-[Ar-urea-RGD]$_2$**, **4.10**, in 95% yield (Scheme 4.5). The structural integrity and purity of the product was confirmed using ^{1}H NMR (see appendix – spectrum 4.5), as peaks corresponding to the Pbf and *tert*-butyl protecting groups in the precursor compound, **4.9**, were absent in the spectrum of **4.10**. The product was detected with a *m/z* value of 943.3989 (100%, $[M+H]^+$) in the ESI-MS.

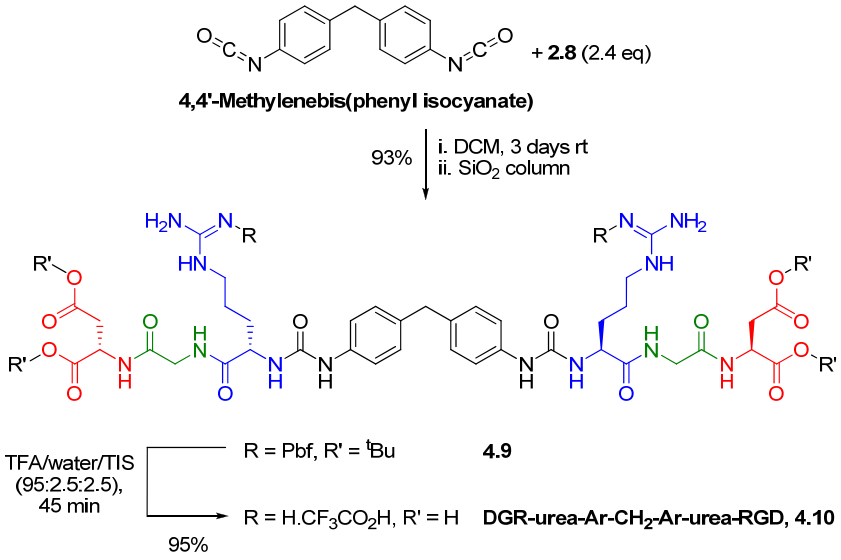

Scheme 4.5 – Reaction scheme showing the formation of **4.9** and subsequent deprotection conditions to form **CH_2-[Ar-urea-RGD]$_2$**, **4.10**. Original in colour.

4.2.6 Synthesis of C12-RGD-C12

The solution-phase synthesis of amide-based twin-tailed system **C12-RGD-C12**, **4.18**, using Z-protecting group methodology is summarised in Scheme 4.6. Firstly, dodecylamine was amide coupled to Z-Asp(O^{t}Bu)-OH using TBTU to provide **4.11** in 68% yield after an aqueous workup and silica column purification to remove residual dodecylamine. ^{1}H NMR identified an apparent broad triplet at 6.54 ppm corresponding to the newly formed amide C(O)N*H* group, along with the ESI-MS product peak at a *m*/*z* value of 491.3462 (100%, $[M+H]^+$).

Catalytic hydrogenolysis to remove the benzyl carbamate afforded **4.12** in 90% yield without the need for further purification. Loss of peaks in the ^{1}H NMR corresponding to the aromatic protons at 7.34-7.27 ppm; carbamate N*H* at 6.05 ppm and benzyl CH_2 at 5.10 ppm in the precursor compound were key evidence for the formation of the deprotected product, along with an upfield shift from 4.50-4.45 to 3.63 ppm of the aspartic acid α-*H*. Peaks for the precursor compound were also absent in the ESI-MS and a new peak was assignable to the product at a *m*/*z* value of 357.3114 (100%, $[M+H]^+$).

Z-Gly-OH was then TBTU coupled to the free amine of **4.12** yielding pure **4.13** in excellent quantitative yield after only an acid/base workup. Doublet and multiplet peaks at 7.55 and 4.79-4.74 ppm in the ^{1}H NMR were assignable to the newly formed amide C(O)N*H* group and the aspartic acid α-*H* (shifted downfield from 3.63 ppm in **4.12**) respectively. ESI-MS showed a new peak at a *m*/*z* value of 570.3511 (100%, $[M+Na]^+$).

Catalytic hydrogenolysis was achieved in 87% yield, to give free amine **4.14**. Again, an absence of peaks at 7.34-7.28, 6.12 and 5.13-5.09 ppm corresponding to the aromatic protons, carbamate N*H* and benzyl CH_2, respectively, in the precursor compound, were evidence for the formation of the deprotected product, along with an upfield shift of the glycine CH_2 peak from 3.93-3.77 to 3.55-3.48 ppm. ESI-MS detected the product with a m/z value of 414.3324 (100%, $[M+H]^+$).

Z-Arg(Pbf)-OH was then reacted with **4.14**, using TBTU as the coupling agent, which resulted in the formation of product **4.15** in a slightly lower than expected, but still acceptable, yield of 57% post-silica column purification. A downfield shift in the glycine CH_2 peak from 3.55-3.48 to 4.16-3.74 ppm, along with the formation of a new apparent broad singlet peak at 8.19 ppm corresponding to the newly formed amide C(O)N*H* group, confirmed the formation of the product. ESI-MS also detected the product at a m/z value of 956.5553 (100%, $[M+H]^+$).

Catalytic hydrogenolysis afforded free amine, **4.16**, in 92% yield. As usual, an absence of peaks at 7.32-7.23, 6.03 and 5.12-4.99 ppm, corresponding to the aromatic protons, carbamate N*H* and benzyl CH_2 in the precursor compound, respectively, were evidence for the formation of the deprotected product, along with an upfield shift of the arginine α-*H* peak from 4.42-4.28 to 3.99-3.75 ppm. ESI-MS detected the product with a m/z value of 822.5171 (100%, $[M+H]^+$).

The penultimate step in the synthesis involved TBTU-mediated coupling of lauric acid to **4.16**. Reaction progress was confirmed, in addition to TLC analysis, by the change in appearance from a clear solution to a thick, gel-like, white precipitate in DCM. Product **4.17** was obtained following silica column purification in 74% yield. The arginine α-*H* peak shifted from 3.99-3.75 ppm in the precursor compound to 4.53-4.41 ppm in the product, and a new apparent broad singlet peak formed at 6.97 ppm corresponding to the newly formed amide C(O)N*H* group. ESI-MS also confirmed successful formation of the product with a peak at m/z 1004.6823 (100%, $[M+H]^+$).

Finally, the protecting groups in **4.17** were removed using TFA, and the compound precipitated using Et_2O and freeze-dried to afford final product **C12-RGD-C12**, **4.18**, in 78% yield. The loss of peaks in the ^{1}H NMR (see appendix – spectrum 4.6) corresponding to the Pbf methylene (2.92 ppm) and methyl groups at 2.56, 2.48, 2.06 and 1.44 ppm, as well as the *tert*-butyl methyl groups at 1.37 ppm, confirmed the isolation of the product. Further evidence was provided by ESI-MS which revealed the absence of peaks for the precursor compound and the presence of a new peak at a m/z value of 696.5389 (100%, $[M+H]^+$), corresponding to the product.

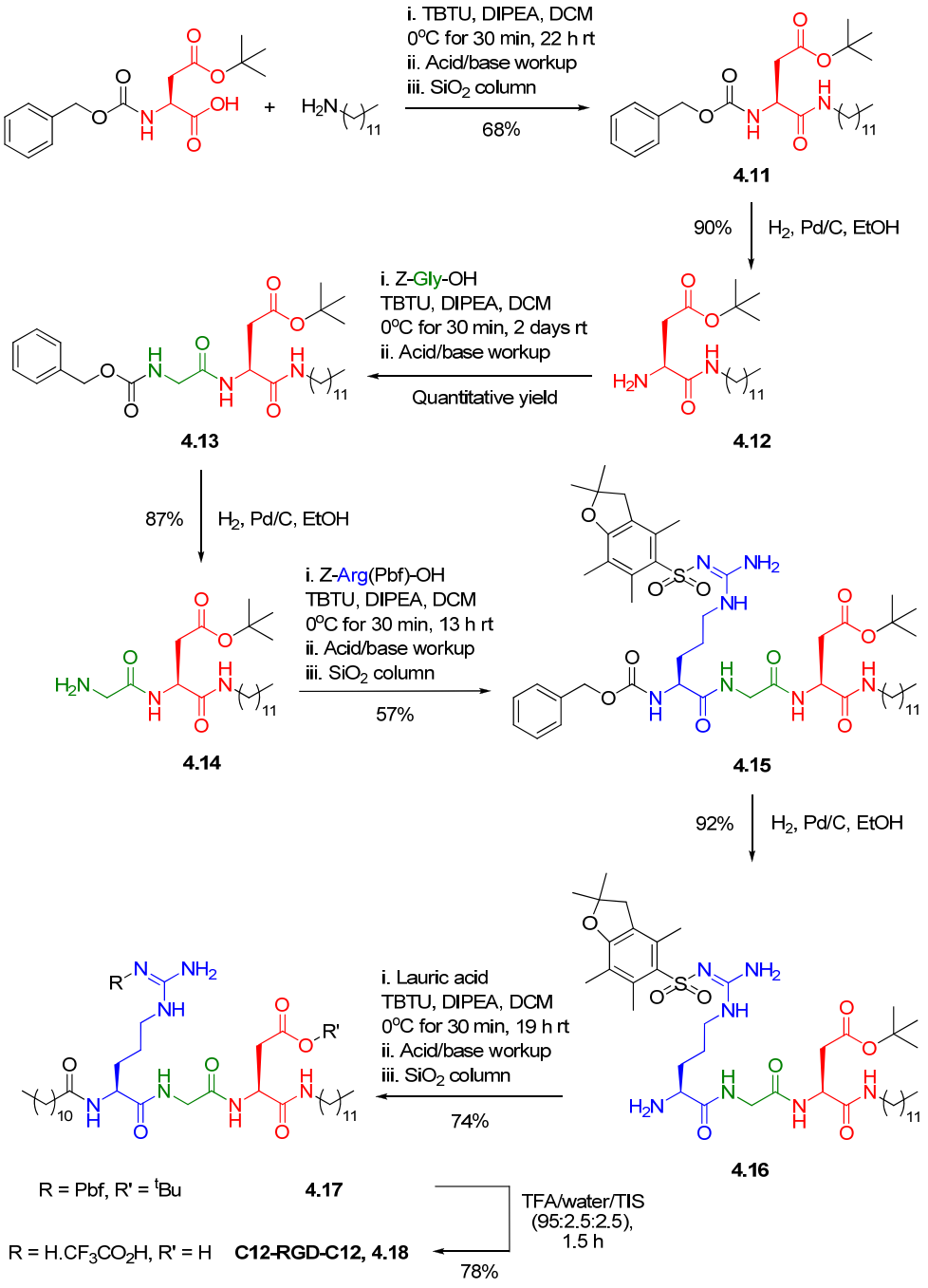

Scheme 4.6 – Reaction scheme showing the synthesis of **4.11**-**4.17** using a Z-protecting group strategy and subsequent deprotection conditions to form **C12-RGD-C12**, **4.18**. Original in colour.

4.2.7 Attempted synthesis of linear oligo(phenylene ethynylene)-[RGD]$_2$

Reacting protected RGD **2.8** with 4-iodophenyl isocyanate (Scheme 4.7), followed by silica column purification yielded 4-I-phenyl-urea-R(Pbf)GD(O^{t}Bu)-O^{t}Bu, **4.19**, in 91% yield. This was confirmed by ^{1}H NMR owing to a downfield shift in the arginine α-*H* from 3.44 ppm in **2.8** to 4.22 ppm in the product due to the adjacent electron-withdrawing urea functional group. Further evidence was

provided by the molecular ion peak in the ESI-MS, assigned to a m/z value of 956.3057 (100%, $[M+H]^+$).

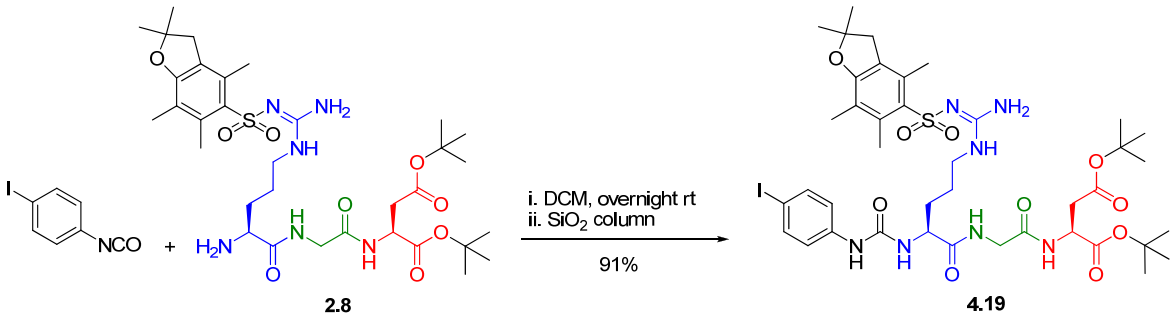

Scheme 4.7 – Reaction scheme showing the synthesis of 4-I-phenyl-urea-R(Pbf)GD(O^{t}Bu)-O^{t}Bu, **4.19**. Original in colour.

The synthesis of 1,4-diethynylbenzene, **4.21**, is outlined in Scheme 4.8 and was adapted from published methodology detailing the synthesis of 1,3,5-triethynylbenzene.[276, 277] Utilising the Sonogashira cross-coupling reaction[278] between mono-protected trimethylsilylethyne and 1,4-dibromobenzene afforded protected compound **4.20**[276] in 83% yield, following purification by silica column chromatography. Although we were unable to detect the product by ESI-MS or EI-MS techniques, a problem we concluded that was intrinsic to the molecule, ^{1}H NMR did not show a peak in the region 1.5-3 ppm which is indicative of an alkyne proton. Instead, singlet peaks at 7.39 and 0.25 ppm, assigned to the aromatic protons and methyl protons, respectively, confirmed the conversion of trimethylsilylethyne into the product.

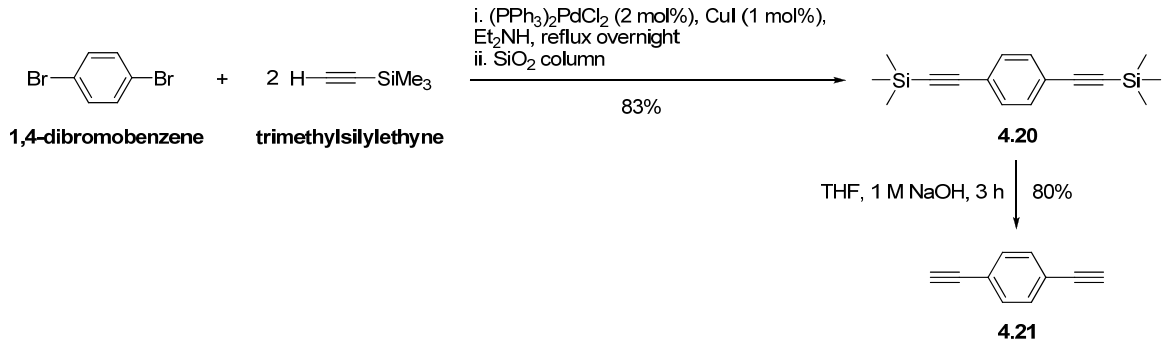

Scheme 4.8 – Reaction scheme showing the synthesis of 1,4-diethynylbenzene, **4.21**.

Deprotection of the trimethylsilyl groups in the presence of 1 M NaOH gave the desired product, **4.21**,[277] in 80% yield after a simple workup procedure. We were unable to obtain a mass spectrum for the compound using either ESI-MS or EI-MS which, again, we concluded was a problem intrinsic to the molecule. ^{1}H NMR showed a singlet peak at 7.42 ppm for the aromatic protons and a new singlet peak at 3.15 ppm for the unmasked alkyne protons, while the singlet peak at 0.25 ppm for the methyl

protons in the precursor molecule was absent, confirming the deprotection reaction had gone to completion.

A 2-fold excess of aromatic iodide **4.19** (4 eq) was then used to couple to 1,4-diethynylbenzene, **4.21**, using Sonogashira chemistry, providing protected **linear oligo(phenylene ethynylene) (OPE)-[R(Pbf)GD(O^{t}Bu)O^{t}Bu]$_2$, 4.22**, in 97% yield (Scheme 4.9). Pleasingly, the Pd-coupling chemistry is compatible with the structure of the peptide; generating the desired product, in protected form and in good yield after silica column purification. ^{1}H NMR (see appendix – spectrum 4.7) did not show a singlet peak at 3.15 ppm, representative of the alkyne protons in precursor compound **4.21**, which confirmed the conversion of **4.21** into the product. In addition, the presence of 3 × aromatic *C* and 3 × aromatic *C*H resonances (δ 140.33 (aromatic *C*); 132.84, 131.86 (aromatic *C*H × 2); 123.74 (aromatic *C*); 119.06 (aromatic *C*H); 117.19 (aromatic *C*)) and two signals diagnostic of the triple bonds (δ 91.96 and 88.72 (alkyne *C* × 2)) of the OPE framework, confirmed the C_2 symmetry of the molecule. ESI-MS verified isolation of the product with a m/z value of 891.9160 (100%, [M{^{13}C}+2H]$^{2+}$).

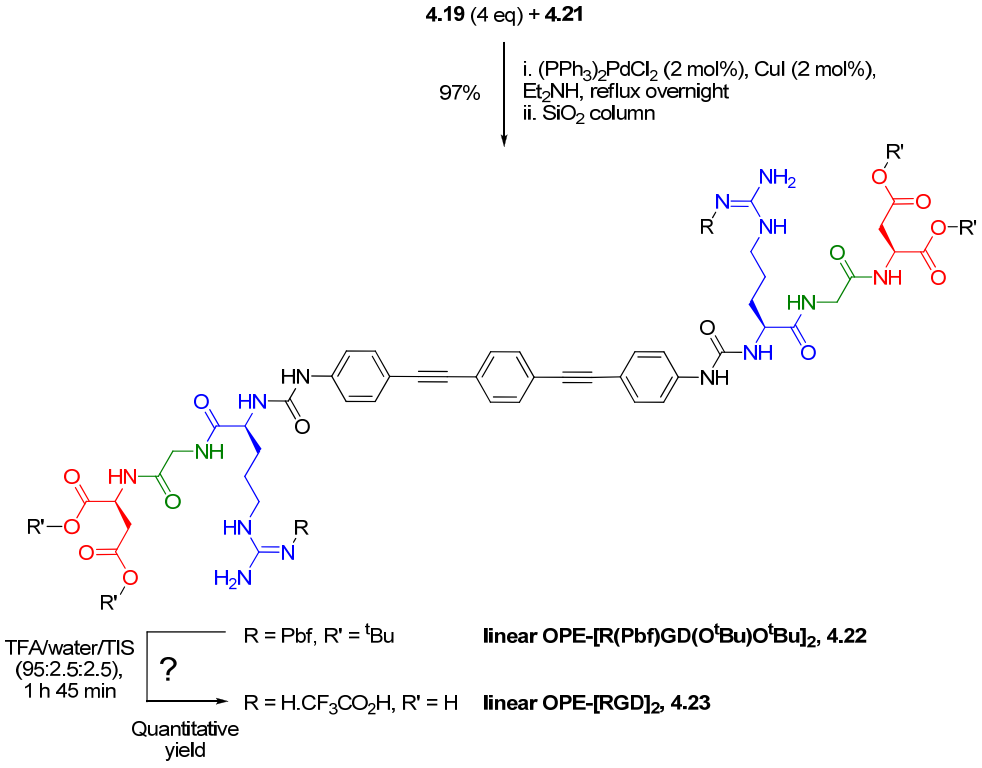

Scheme 4.9 – Reaction scheme showing the synthesis of **linear OPE-[R(Pbf)GD(O^{t}Bu)O^{t}Bu]$_2$, 4.22**, and the deprotection conditions used in an attempt to form **linear OPE-[RGD]$_2$, 4.23**. Original in colour.

It should be noted that the product was obtained with 97% purity due to the presence of residual diethylamine from the Sonogashira coupling conditions – ^{1}H NMR (see appendix – spectrum 4.7) shows quartet and triplet peaks at 3.02 and 1.30 ppm for the methylene and methyl protons, respectively. We believe this may coordinate to one of the urea groups (a ratio of 0.8:1 diethylamine to product was determined by ^{1}H NMR) and is very difficult to fully remove – even after drying the compound under vacuum at 60°C overnight (the b.p. of diethylamine is 55.5°C), or after precipitating the product out of DCM/MeOH (9:1) using Et_2O. An aqueous acid extraction of the organic base was not a plausible option due to the limited solubility of the compound in water immiscible solvents, therefore, a decision was made to deprotect the compound regardless of the residual diethylamine.

Employing exactly the same conditions as those used for previous RGD peptide deprotections, **4.22** was deprotected using TFA, precipitated using Et_2O and lyophilised in an attempt to form **linear OPE-[RGD]$_2$**, **4.23**. A yellow powder was obtained in near quantitative yield. However, the ^{1}H NMR of this material, dissolved in a mixture of TFA-*d*/D_2O (see appendix – spectrum 4.8) and also in DMSO-d_6 (spectrum not shown), is very broad and untidy and therefore difficult to interpret, bringing into question the identity of the product. The spectrum should appear similar to that of the starting material (see appendix – spectrum 4.7), but without peaks corresponding to the Pbf methylene (2.93 ppm) and methyl groups at 2.56, 2.49, 2.05 and 1.43 ppm, as well as the *tert*-butyl methyl groups at 1.42 and 1.40 ppm, following the deprotection. We are unsure of the reason for this unexpected appearance of the spectrum, but we speculate that peak broadening occurs due to aggregation of the molecules in the NMR solvent used for dissolution of the compound. The presence of residual diethylamine before deprotecting with trifluoroacetic acid undoubtedly produces the corresponding diethylammonium-trifluoroacetate salt and this also contributes to the untidiness and erroneous integrations within the spectrum. In any case, due to the synthetic effort involved, we decided to check the solubility and possible self-assembly properties of this material regardless of its questionable identity (see '**4.3 Gelation Studies**' for a discussion).

4.2.8 Attempted synthesis of triangular-shaped oligo(phenylene ethynylene)-[RGD]$_3$

The synthesis of 1,3,5-triethynylbenzene, **4.25**,[276, 277] is outlined in Scheme 4.10. Following a literature procedure, trimethylsilylethyne was Sonogashira cross-coupled to 1,3,5-tribromobenzene, and after refluxing overnight and then purifying the crude material by column chromatography (SiO_2), this afforded protected compound **4.24**[276] in 77% yield. ^{1}H NMR did not show a peak in the region 1.5-3 ppm which is indicative of an alkyne proton. Instead, singlet peaks at 7.49 and 0.23 ppm, assigned to the aromatic protons and methyl protons, respectively, confirmed the conversion of trimethylsilylethyne into the product. Unlike analogous compound **4.20**, we were able to detect the product by EI-MS with a m/z of 366.1668 (18%, $M^{+\bullet}$) for the molecular ion peak. The base peak at m/z 41.0195 was assigned to the fragment ion Si≡C-H$^+$.

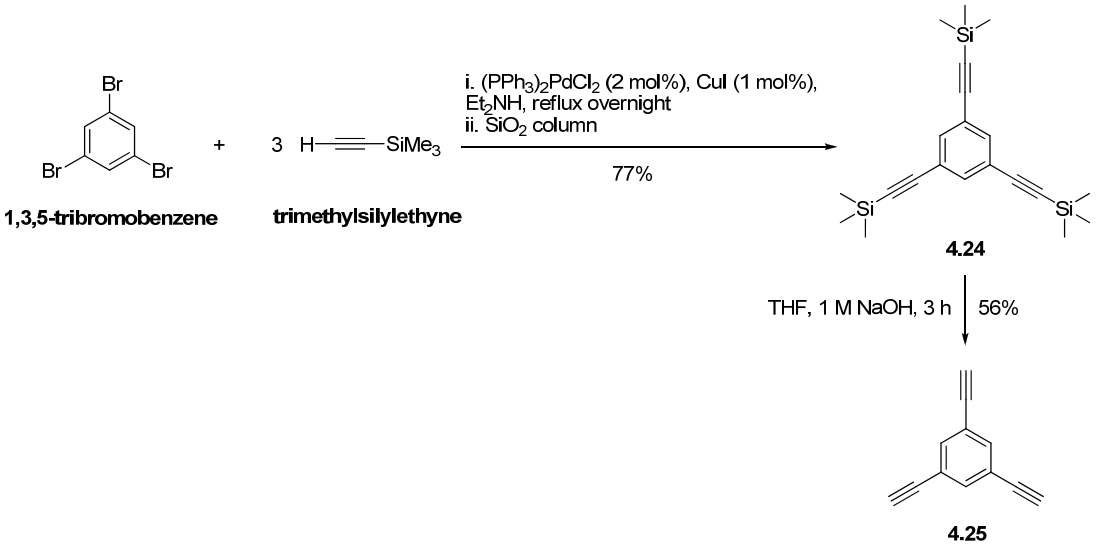

Scheme 4.10 – Reaction scheme showing the synthesis of 1,3,5-triethynylbenzene, **4.25**.

Deprotection of the trimethylsilyl groups in the presence of 1 M NaOH produced 1,3,5-triethynylbenzene, **4.25**,[277] in 56% yield after a simple workup procedure. ^{1}H NMR showed a singlet peak at 7.57 ppm for the aromatic protons and a new singlet peak at 3.11 ppm for the unmasked alkyne protons, while the singlet peak at 0.23 ppm for the methyl protons in the precursor molecule was absent, confirming the deprotection reaction had gone to completion. EI-MS detected a peak at m/z 150.0461 (29%, $M^{+\bullet}$) assigned to the molecular ion of the product. The base peak at m/z 83.9512 was assigned to a fragment of **4.25** or a by-product of the deprotection reaction.

The penultimate step involved Sonogashira cross-coupling three equivalents of aromatic iodide **4.19** (present in a 2-fold excess) onto the trivalent 1,3,5-triethynylbenzene, **4.25**, yielding protected **triangular-shaped OPE-[R(Pbf)GD(O^{t}Bu)O^{t}Bu]$_3$**, **4.26**, in 82% yield after refluxing overnight and then purifying by column chromatography (SiO_2) (Scheme 4.11). Unambiguous confirmation of the proposed structure for conjugate **4.26** was obtained from ^{1}H and ^{13}C NMR spectra. For example, ^{1}H NMR (see appendix – spectrum 4.9) did not show a singlet peak at 3.11 ppm, representative of the alkyne protons in precursor compound **4.25**, which confirmed the conversion of **4.25** into the product. Additionally, in the ^{13}C NMR spectrum, the presence of 3 × aromatic *C* and 3 × aromatic *C*H resonances (δ 140.26 (aromatic *C*); 133.29, 132.98 (aromatic *C*H × 2); 124.85 (aromatic *C*); 119.00 (aromatic *C*H); 117.02 (aromatic *C*)) and two signals diagnostic of the triple bonds (δ 91.24 and 87.62 (alkyne *C* × 2)) of the OPE framework, confirmed the C_3 symmetry of the molecule. ESI-MS verified isolation of the product with m/z values of 878.7668 (100%, $[M\{^{13}C\}+3H]^{3+}$) and 1317.6704 (100%, $[M\{^{13}C\}+2H]^{2+}$).

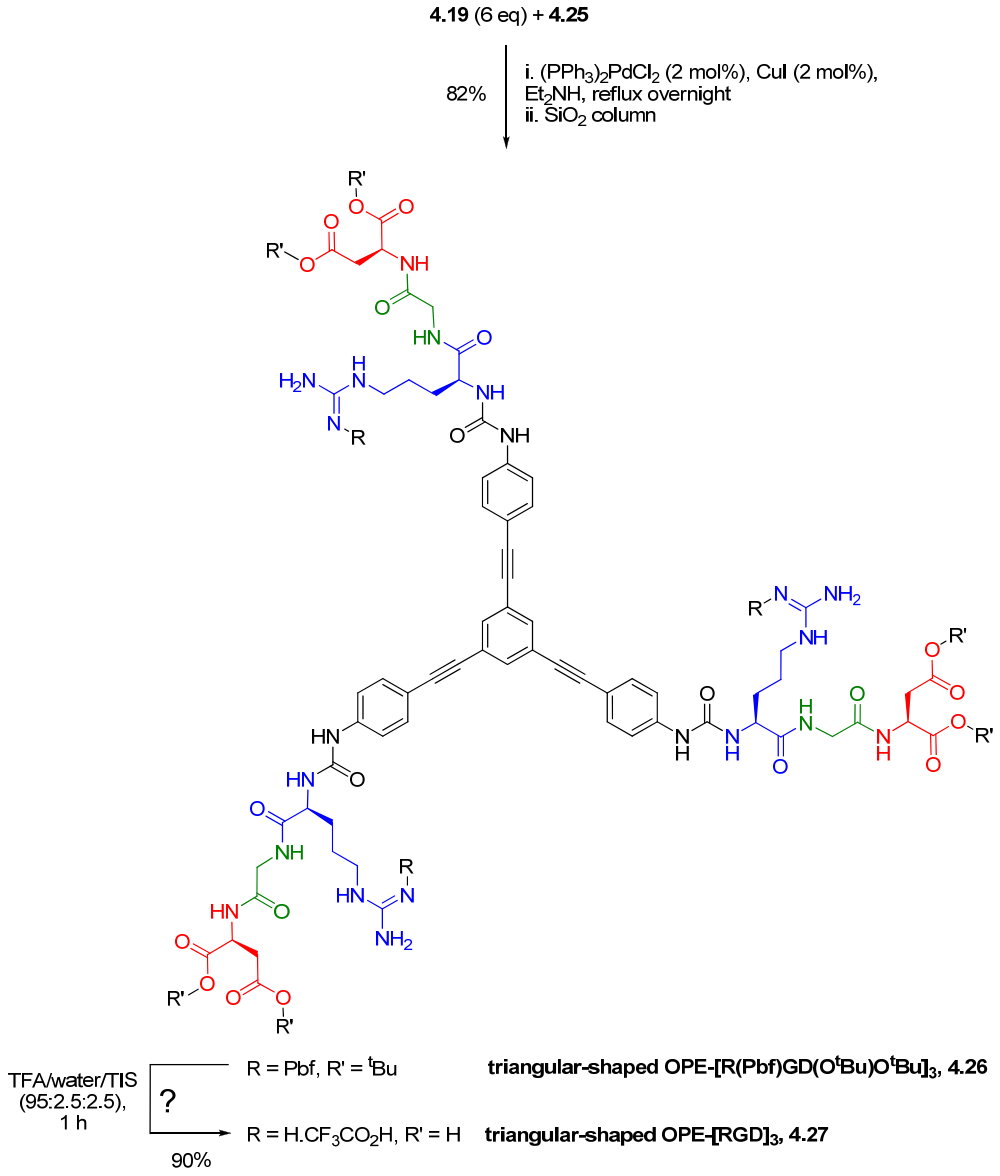

Scheme 4.11 – Reaction scheme showing the synthesis of **triangular-shaped OPE-[R(Pbf)GD(O^{t}Bu)O^{t}Bu]$_3$, 4.26**, and the deprotection conditions used in an attempt to form **triangular-shaped OPE-[RGD]$_3$, 4.27**. Original in colour.

Analogous to the synthesis of **4.22**, the product was obtained with 97% purity due to the presence of residual diethylamine from the coupling procedure – ^{1}H NMR (see appendix – spectrum 4.9) shows quartet and triplet peaks at 3.02 and 1.30 ppm for the methylene and methyl protons, respectively. Once again, this was very difficult to fully remove, therefore a decision was made to deprotect the compound regardless of the residual diethylamine.

We employed exactly the same conditions as those used for previous RGD peptide deprotections. Compound **4.26** was deprotected using TFA, precipitated using Et_2O and lyophilised in an attempt to form **triangular-shaped OPE-[RGD]$_3$, 4.27**. A beige powder was obtained in 90% yield.

Unsurprisingly, the ^{1}H NMR of this material, dissolved in a mixture of TFA-*d*/D_2O (see appendix – spectrum 4.10) and also in DMSO-d_6 (spectrum not shown), is very broad and untidy and therefore difficult to interpret in much the same way as that of **linear OPE-[RGD]$_2$**, **4.23**, yet again bringing into question the identity of the product. The spectrum should appear similar to that of the starting material (see appendix – spectrum 4.9), but without peaks corresponding to the Pbf methylene (2.94 ppm) and methyl groups at 2.56, 2.49, 2.06 and 1.43 ppm, as well as the *tert*-butyl methyl groups at 1.43 and 1.42 ppm, following the deprotection. We speculate that the suspected aggregation in solution of **linear OPE-[RGD]$_2$**, **4.23**, also occurs with **triangular-shaped OPE-[RGD]$_3$**, **4.27**. In any case, due to the synthetic effort involved, we decided to check the solubility and possible self-assembly properties of this material regardless of its questionable identity (see '**4.3 Gelation Studies**' for a discussion).

4.2.9 Synthesis of the Protected Linear RGDK Peptide

The solution-phase synthesis of protected linear RGDK, **4.33**, using Z-protecting group methodology is summarised in Scheme 4.12. Firstly, Z-Asp(O^{t}Bu)-OH was amide coupled to H_2N-Lys(Boc)-O^{t}Bu.HCl in the presence of DIPEA and coupling reagent, TBTU. Following an aqueous workup procedure, this afforded pure product Z-Asp(O^{t}Bu)-Lys(Boc)-O^{t}Bu, **4.28**, in 98% yield. This was confirmed in the ^{1}H NMR by the appearance of a broad doublet at 7.04 ppm corresponding to the amide N*H* peak, and a downfield shift in the aspartic acid α-*H* from below 4.00 ppm to 4.60-4.51 ppm due to the formation of the adjacent electron-withdrawing amide functional group. ESI-MS analysis also confirmed the formation of the product with a *m*/*z* value of 608.3555 (100%, $[M+H]^+$).

Deprotection of the benzyl carbamate by stirring under an atmosphere of H_2 for 17.5 h in the presence of Pd/C catalyst in ethanol yielded H_2N-Asp(O^{t}Bu)-Lys(Boc)-O^{t}Bu, **4.29**, in 98% yield after removing the catalyst by filtration over Celite. The absence of a multiplet at 7.39-7.29 ppm; a broad doublet at 6.05 ppm and a singlet at 5.13 ppm corresponding to the aromatic protons, benzyl carbamate N*H* and benzyl CH_2 protons, respectively, in the precursor molecule, along with an upfield shift in the aspartic acid α-*H* to 3.75-3.66 ppm, were clear evidence that the hydrogenolysis reaction had gone to completion. ESI-MS analysis also confirmed the formation of the product with a *m*/*z* value of 474.3182 (100%, $[M+H]^+$).

Compound **4.30** was then synthesised by amide coupling Z-Gly-OH with **4.29** using DIPEA and TBTU. Aqueous workup of the crude reaction mixture produced **4.30** in a good 88% yield. Two amide N*H* peaks at 7.42 and 7.10 ppm, along with a downfield shift in the aspartic acid α-*H* to 4.80-4.75 ppm were indicative of the amide-coupled product. ESI-MS confirmed the mass of the product with a *m*/*z* value of 687.3569 (100%, $[M+Na]^+$).

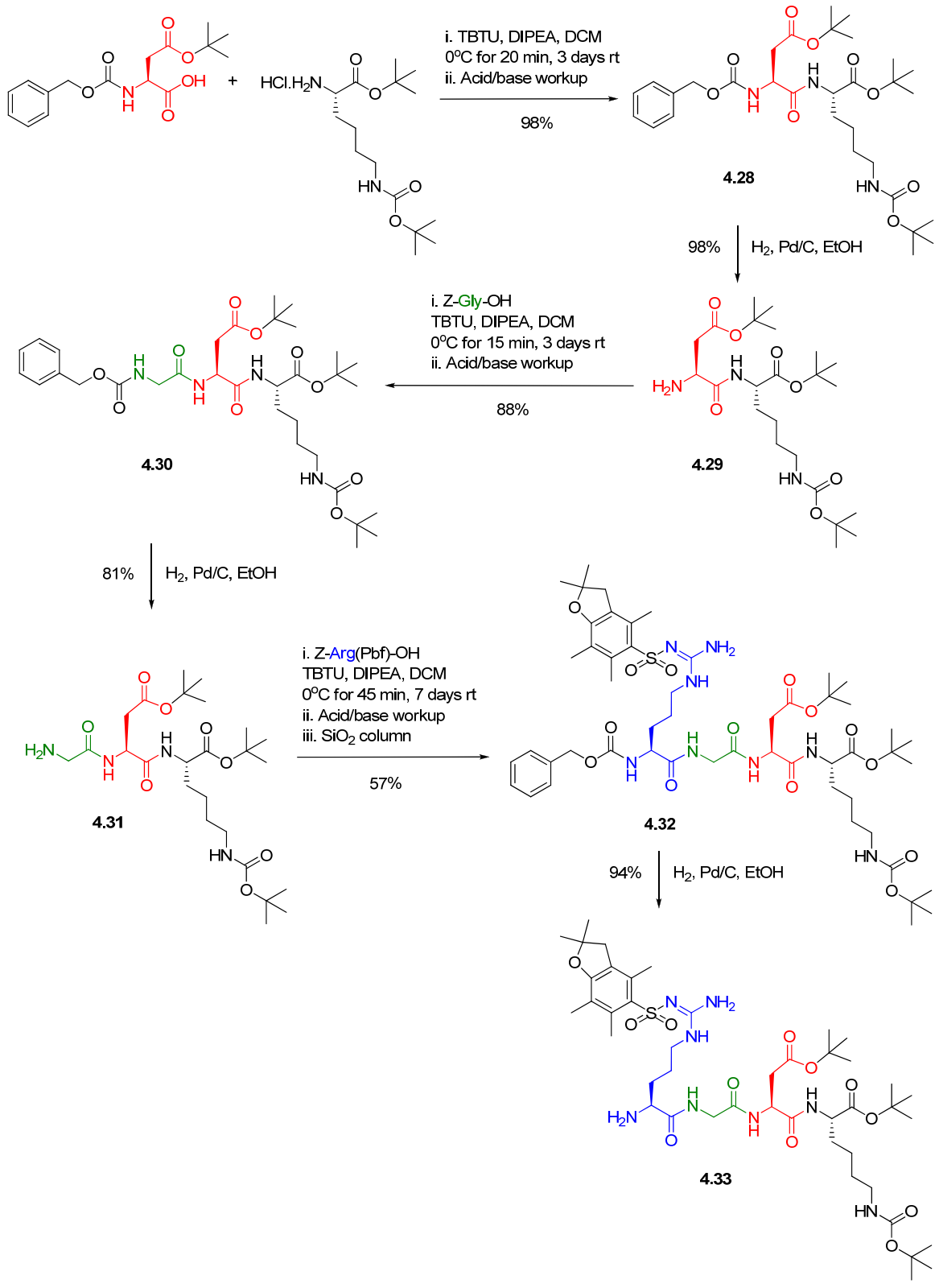

Scheme 4.12 – Reaction scheme for the solution-phase synthesis of protected linear RGDK, **4.33**, using a Z-protecting group strategy. Original in colour.

Deprotection of the benzyl carbamate by stirring under an atmosphere of H_2 for 23 h in the presence of Pd/C catalyst in ethanol yielded H_2N-Gly-Asp(O^{t}Bu)-Lys(Boc)-O^{t}Bu, **4.31**, in a good 81% yield after removing the catalyst by filtration over Celite. The absence of a multiplet at 7.33-7.25 ppm; a broad singlet at 5.96 ppm and a singlet at 5.09 ppm corresponding to the aromatic protons, benzyl carbamate N*H* and benzyl C*H*$_2$ protons, respectively, in the precursor molecule, along with an upfield shift of the glycine CH_2 peak from 3.92-3.84 to 3.39 ppm, were clear evidence that the hydrogenation reaction had gone to completion. ESI-MS detected the product with a m/z value of 531.3402 (100%, $[M+H]^+$).

Amide coupling Z-Arg(Pbf)-OH with **4.31** provided Z-Arg(Pbf)-Gly-Asp(O^{t}Bu)-Lys(Boc)-O^{t}Bu, **4.32**, in a moderate 57% yield following a silica column purification step. Three amide N*H* peaks at 8.00 ppm (Arg-Gly), 7.56 ppm (Gly-Asp) and 7.29-7.23 ppm (Asp-Lys); including a downfield shift of the glycine CH_2 peak to 4.01-3.78 ppm, confirmed the formation of product. ESI-MS detected the product with a m/z value of 1073.5533 (100%, $[M+H]^+$).

Finally, the benzyl carbamate group in **4.32** was removed using catalytic hydrogenolysis over a 2 day period to produce H_2N-Arg(Pbf)-Gly-Asp(O^{t}Bu)-Lys(Boc)-O^{t}Bu, **4.33**, in excellent 94% yield after removing the catalyst by filtration over Celite. As usual, an absence of peaks at 7.29-7.23 and 5.09-5.01 ppm corresponding to the aromatic protons and benzyl C*H*$_2$, respectively, in the precursor compound, were evidence for the formation of the deprotected product, along with an upfield shift of the arginine α-*H* peak from 4.37-4.21 to 4.02-3.94 ppm (see appendix – spectrum 4.11). ESI-MS detected the product with a m/z value of 939.5189 (100%, $[M+H]^+$).

4.2.10 Synthesis of C12-urea-RGDK

Dodecyl isocyanate (in DCM) and protected RGDK, **4.33**, (in DCM) were combined and stirred overnight at rt. Silica column purification of the crude reaction mixture afforded **4.34** in a rather modest 45% yield (Scheme 4.13). This was confirmed in the ^{1}H NMR by a downfield shift in the arginine α-*H* from 4.02-3.94 ppm to 4.22-4.19 ppm on coupling **4.33** to the isocyanate to generate the adjacent electron-withdrawing urea functional group. ESI-MS analysis also confirmed the formation of product with a m/z value of 1150.7165 (100%, $[M+H]^+$).

TFA deprotection of the RGDK peptide generated final product **C12-urea-RGDK**, **4.35**, in 56% yield. The loss of peaks in the ^{1}H NMR (see appendix – spectrum 4.12) corresponding to the Pbf methylene (3.00 ppm) and methyl groups at 2.58, 2.52, 2.08 and 1.45 ppm, as well as the *tert*-butyl methyl groups at 1.43 and 1.42 ppm, confirmed the isolation of the product. Further evidence was provided by ESI-MS which revealed the absence of the peak for the precursor compound and the presence of a new peak at a m/z value of 343.7310 (100%, $[M+2H]^{2+}$), corresponding to the product.

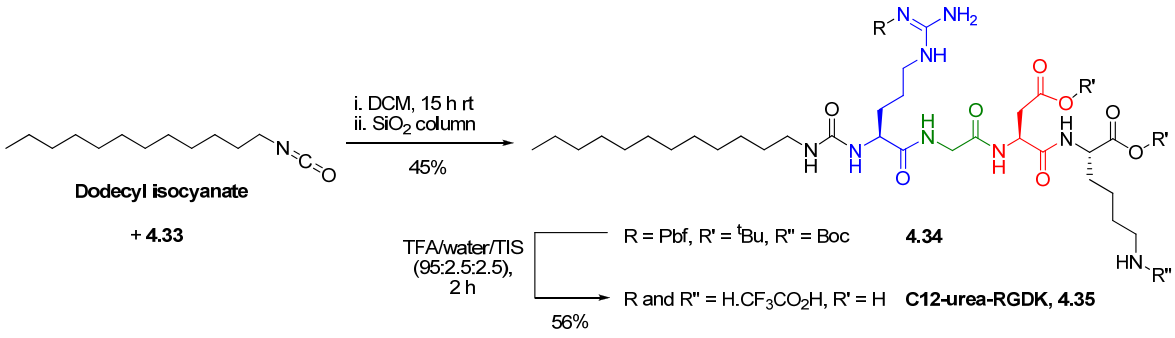

Scheme 4.13 – Reaction scheme showing the formation of **4.34** and subsequent deprotection conditions to form **4.35**. Original in colour.

4.2.11 Synthesis of C12-amide-RGDK

Lauric acid (in DCM) and protected RGDK, **4.33**, (in DCM) were combined and stirred overnight at rt in the presence of DIPEA and TBTU. Silica column purification of the crude reaction mixture afforded **4.36** in good 75% yield (Scheme 4.14). This was confirmed in the ^{1}H NMR by a downfield shift in the arginine α-*H* from 4.02-3.94 ppm to 4.28-4.19 ppm on coupling **4.33** to lauric acid to generate the adjacent electron-withdrawing amide functional group. ESI-MS analysis also confirmed the formation of the product with a *m*/*z* value of 1121.6819 (100%, $[M+H]^+$).

TFA deprotection of the RGDK peptide generated final product **C12-amide-RGDK**, **4.37**, in 65% yield. Peaks corresponding to the Pbf methylene and methyl groups, as well as the *tert*-butyl methyl groups, were absent in the ^{1}H NMR (see appendix – spectrum 4.13) and confirmed the isolation of the product. Further evidence was provided by ESI-MS which revealed the absence of the peak for the precursor compound and the presence of a new peak at a *m*/*z* value of 329.2185 (100%, $[M+2H]^{2+}$), corresponding to the product.

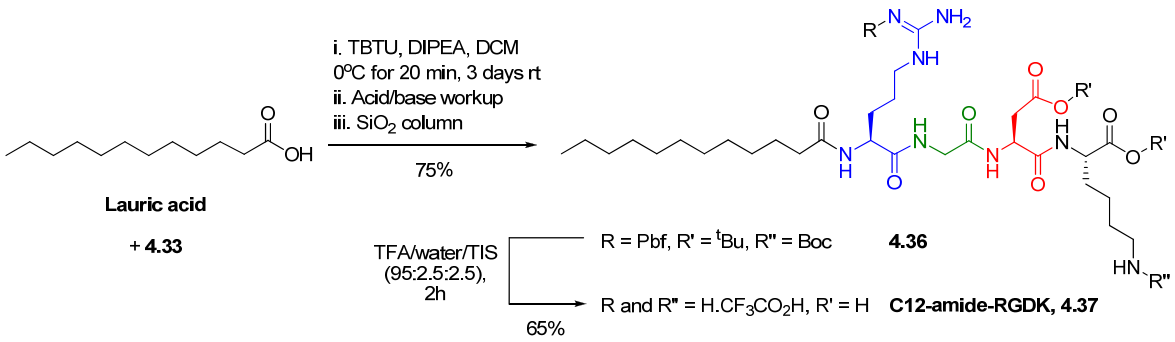

Scheme 4.14 – Reaction scheme showing the formation of **4.36** and subsequent deprotection conditions to form **4.37**. Original in colour.

4.3 Gelation Studies

Having synthesised this family of RGD-derived amphiphiles and bolaamphiphiles, we then went on to investigate their gelation potential.

Preparation of a gel sample involved weighing out a known amount of compound into a 2 ml Eppendorf tube, 1 ml of Millipore ultrapure water at natural (i.e. unbuffered) pH was added using a Gilson pipette and then the tube was sealed. One of two methods for inducing gelation was then employed: (i) an alternating process of sonicating for 15-30 min, vortexing, then sonicating for 15-30 min over the course of a day, then allowing the sample to stand at rt, or (ii) heating the sample with a heat gun to near boiling point to form a homogeneous suspension of the material and then allowing it to cool to rt induced self-assembly of the sample with subsequent gel formation. The sample was deemed to be a gel if it survived for longer than 1 min using the tube inversion method, and identified as loose or strong depending on how long it took to collapse. Analysis was always carried out on freshly prepared gel samples.

As it collapsed shortly after 1 min of inversion, compound **C12-urea-RGD** (**4.2**) formed a loose, translucent gel after subjecting it to sonication in water at a minimum gel concentration (MGC) of 1.0 wt % (10 mg/ml, 15 mM) in the range of concentrations tested (0.1-1.0 wt %, Fig. 4.4). At lower concentrations, a gel-like precipitate formed but did not result in a sample-spanning gel network. The compound did not become fully solubilised using either of the two gel preparation methods and, hence, did not form a gel under thermal conditions.

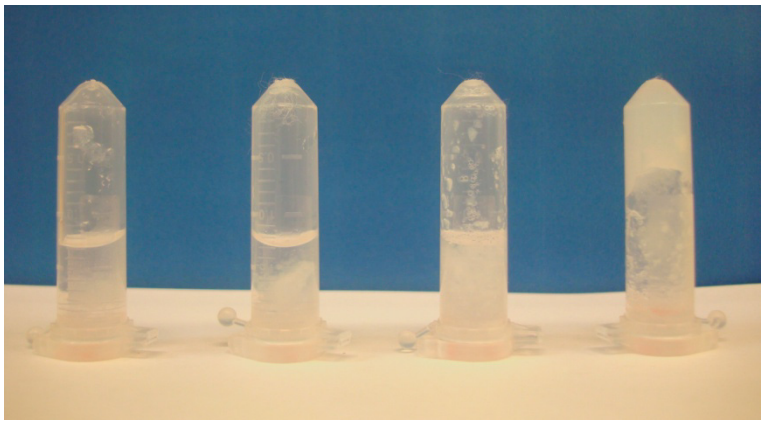

Fig. 4.4 – **C12-urea-RGD** sonicated in water (from left to right: 0.1, 0.2, 0.5 and 1.0 wt %). Original in colour.

The proposed mode of self-assembly is a stacked arrangement of the molecules, primarily directed by hydrogen bonding between the urea groups, and a hydrophobic effect coupled with van der Waals interactions between the aliphatic hydrocarbon chains (Scheme 4.15). By bringing the molecules

together in this fashion, intermolecular hydrogen bonding interactions between the amides of the peptide head groups are also possible.

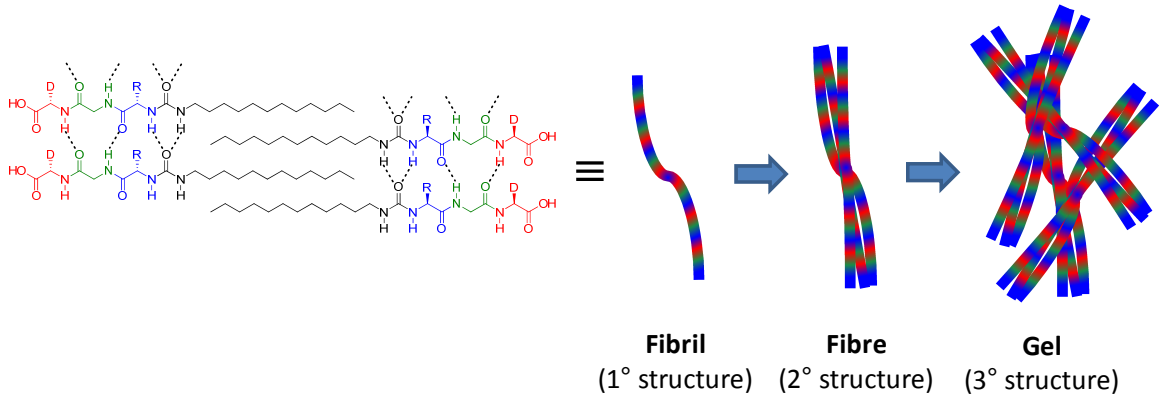

Scheme 4.15 – Proposed mode of self-assembly of **C12-urea-RGD**. Dashed lines signify intermolecular hydrogen bonding interactions. Amino acid side-chains are omitted for clarity. Original in colour.

To test the importance of the urea functionality in **C12-urea-RGD**, compound **C12-RGD** (**3.2**), which uses an amide group to connect the hydrophobic tail to the hydrophilic peptide head group, was used as a control compound. We checked the gelation ability of **C12-RGD** and found that even at concentrations as high as 1.0 wt % (15.6 mM) the material fully solubilised during heating and then precipitated as an amorphous white solid on cooling, indicating that the urea group in **C12-urea-RGD** plays an important role in mediating the supramolecular self-assembly and prevents crystallisation in pure water.

After incorporating lysine (K) into the peptide, we found that compound **C12-urea-RGDK** (**4.35**) did not form hydrogels either; in fact, the compound was completely solubilised in water at rt, forming a clear solution. Inclusion of the bulky lysine into the peptide head group, which bears a 1+ charge and therefore changes the charge state of the peptide, implies that charge and/or packing considerations are also important in controlling the gelation-solubilisation balance. In fact, it is known that lysine is not desirable for the design of self-assembling peptide amphiphiles that form nanofibres with β-sheet characteristics, as it tends to break the β-sheet formation in proteins,[279] as well as peptide amphiphiles.[280] For this reason, we declined to synthesise the bolaamphiphile derivative of this compound as we hypothesised it would also solubilise in water. However, due to the amphiphilic structure we propose that **C12-urea-RGDK**, and its amide-based analogue **C12-amide-RGDK** (**4.37**), would demonstrate some propensity to undergo micellisation in water using the previously employed (Chapter 3) Nile Red encapsulation study and TEM imaging. We therefore propose that the lysine (K) unit changes the mode of self-assembly from cylindrical fibrillar aggregates to spherical micelles – either as a consequence of its larger size changing the Israelachvili critical packing parameter of the

lipid structure,[33] or the change in charge state of the peptide minimising head group repulsions. Nevertheless, compounds **4.35** and **4.37** constitute possible self-assembling integrin-binding peptides and form the basis of future work.

Impressively however, bolaamphiphile structured **C12-[urea-RGD]$_2$** (**4.4**) formed stronger gels than **C12-urea-RGD** at a much lower MGC of 0.06 wt % (0.6 mg/ml, 0.5 mM); to our knowledge one of the lowest MGCs reported in the literature for any sort of gelator and as such constitutes a "super" hydrogel, with water gelation being achieved at extremely low concentrations (for a super gel, the concentration of gelator is usually below 0.1 wt %).[165, 281-283] To put this into perspective, and quite remarkably, at this MGC one molecule of our gelator 'immobilises' approximately 109,000 water molecules. To the best of our knowledge, the MGC of our **C12-[urea-RGD]$_2$** system is comparable to the most efficient super hydrogelators published thus far in the literature.[239, 284-286] Unlike **C12-urea-RGD**, gelation could be induced thermally; solubilising the compound to form a clear suspension after prolonged heating and then allowing it to cool. This process was found to be thermoreversible – heating the gel to a clear suspension and then allowing the sample to cool induced gelation again. When the concentration of gelator was increased, hydrogelation kinetics were promoted to a matter of minutes or less, however, the gels became more opaque in appearance – indicative of either some undissolved material, or the formation of larger microscale aggregates (Fig. 4.5). Although gelation could also be initiated using sonication (Fig. 4.6), the MGC was higher (1.0 wt %, 8.5 mM) and the gel stability was less, and very similar to that of **C12-urea-RGD**. This may be a consequence of sonication limiting the persistence length of fibre formation by encouraging a greater number of nucleation sites.[287] In view of this, the **C12-[urea-RGD]$_2$** gels were all produced thermally for subsequent studies.

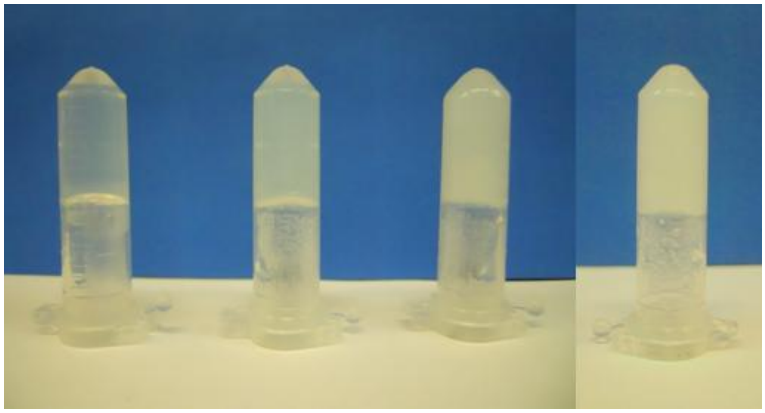

Fig. 4.5 – **C12-[urea-RGD]$_2$** after heating then cooling in water (from left to right: 0.1, 0.2, 0.5 and 1.0 wt %). Original in colour.

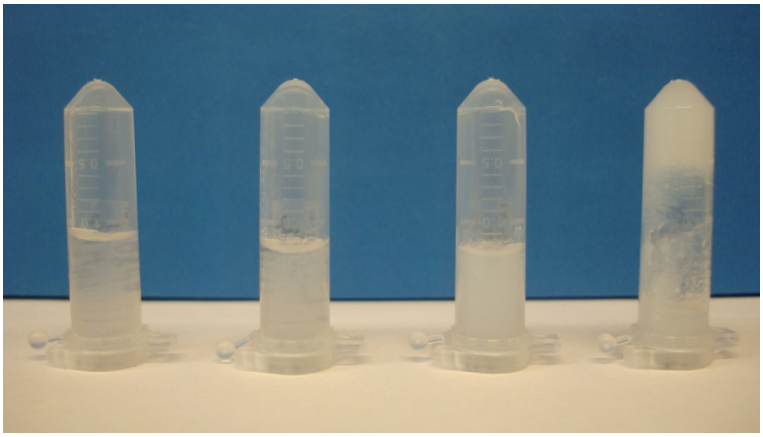

Fig. 4.6 – **C12-[urea-RGD]$_2$** sonicated in water (from left to right: 0.1, 0.2, 0.5 and 1.0 wt %). Original in colour.

In the same respect as **C12-urea-RGD**, the proposed mode of self-assembly is a parallel arrangement of the molecules, primarily directed by hydrogen bonding between the urea groups, and a hydrophobic effect coupled with van der Waals interactions between the aliphatic hydrocarbon chains (Scheme 4.16). Again, additional intermolecular hydrogen bonding interactions between the amides of the peptide head groups are also possible. The bolaamphiphilic structure leads to better preorganisation of the hydrophilic and hydrophobic units for fibrillar self-assembly and should enhance intermolecular contacts, and hence, we reason the MGC is lowered compared to that of **C12-urea-RGD**. We also believe this to be the reason for its enhanced solubility in water under thermal conditions – the double RGD head group providing a 2-fold increase in the number of stabilising contacts with the surrounding water molecules at elevated temperatures.

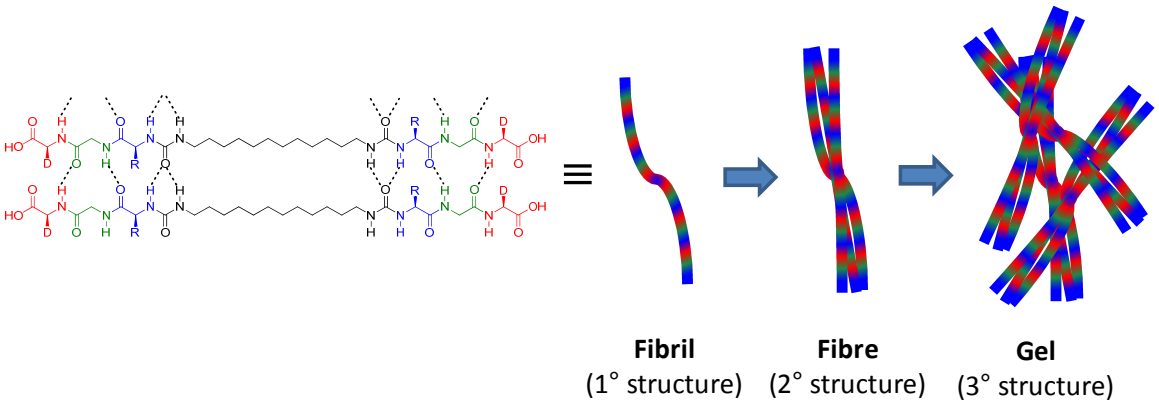

Scheme 4.16 – Proposed mode of self-assembly of **C12-[urea-RGD]$_2$**. Dashed lines signify intermolecular hydrogen bonding interactions. Amino acid side-chains are omitted for clarity. Original in colour.

A phase diagram was plotted showing T_{gel} values as a function of concentration for **C12-[urea-RGD]$_2$** (Fig. 4.7). A T_{gel} is the temperature at which the gel-sol transition occurs and we denote it, in this case, as the point at which the gel collapses, although in some cases the point at which solvent flows from the gel structure can also be used to signify the onset of the gel-sol transition.[288] A freshly prepared gel sample was placed in a high precision thermoregulated oil bath and heated from 20°C at a rate of 1°C min^{-1}. The T_{gel} value increased at concentrations upto 0.09 wt % and then above this concentration plateaued at about 58°C. This means that gel samples with concentrations upwards of 0.09 wt % remain, for the most part, intact until a temperature of 58°C ± 1°C is reached, as network formation is complete, and adding more gelator does not significantly enhance the thermal stability of the network. To check the long-term stability of the gels, samples were prepared ranging from 0.1 to 0.5 wt % in concentration, inverted and left to stand at rt. All samples had good long-term stability and retained their structure for at least 6 months.

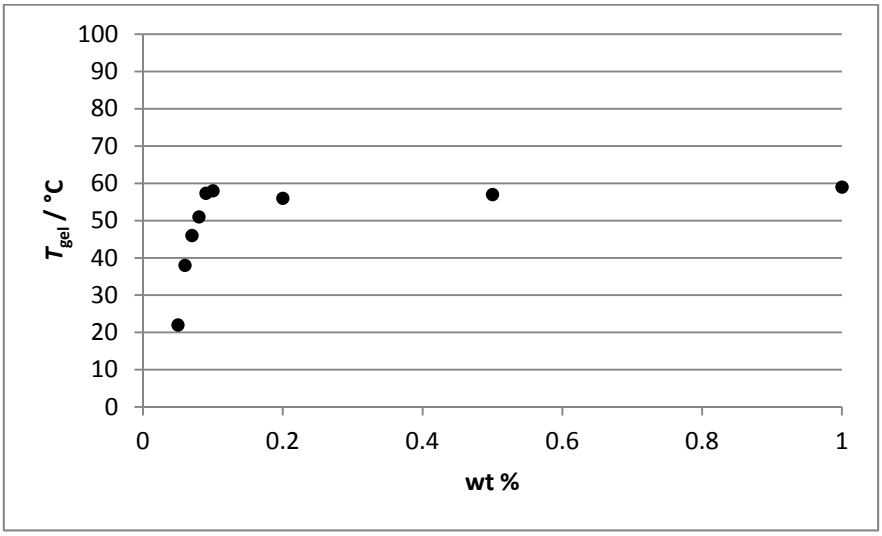

Fig. 4.7 – Phase diagram for **C12-[urea-RGD]$_2$**: T_{gel} values as a function of concentration.

We were also interested in what effect amide coupling a C12 tail to the C-terminus, as well as the N-terminus, had on the self-assembling properties of the RGD peptide. In this way the hydrophilic hydrogen bonding unit is at the centre of the structure flanked by two hydrophobic units. Inverse bolaamphiphile **C12-RGD-C12** (**4.18**) was therefore examined for its self-assembling properties. Initially, we tried to dissolve the compound by heating it in water; however its solubility was limited. Quite commonly in the literature, an alternative method of generating a hydrogel is to prepare a relatively concentrated stock solution of the gelator in a solvent such as dimethyl sulfoxide (DMSO) or hexafluoroisopropanol (HFIP) and add water or buffer to this.[209, 210, 289] Gratifyingly, we were able to form a transparent gel from 0.1 wt % **C12-RGD-C12** (1 mg/ml, 1.2 mM) in a 1:9 mixture of DMSO/water from an initial gelling agent concentration of 10 mg/ml in DMSO (Fig. 4.8). However,

we understand that this is not strictly a pure "hydrogel". In addition to this, sonicating the material in pure water lead to an opaque gel, albeit at a higher MGC of 1.0 wt % (12 mM) (Fig. 4.9).

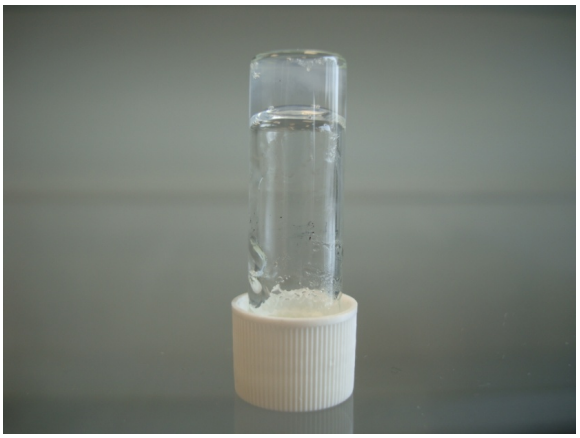

Fig. 4.8 – 0.1 wt % **C12-RGD-C12** in 1:9 DMSO/water. Original in colour.

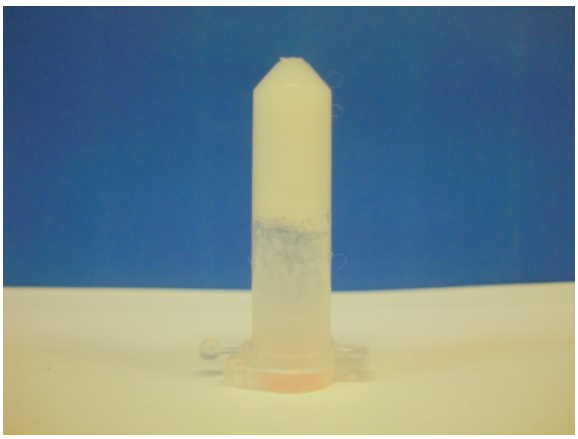

Fig. 4.9 – 1.0 wt % **C12-RGD-C12** sonicated in water. Original in colour.

It is apparent, therefore, that an additional novel hydrogelator can be prepared from the linear tripeptide RGD without the presence of a urea functionality, but this requires attachment of a C12 hydrophobic tail to *both* ends of the peptide sequence in order to satisfy the hydrophilic-lipophilic balance (HLB) of the gelator molecule. Classification using HLB criteria, with respect to surfactant-type molecules at least, was first studied by Griffin and subsequently by Davies.[290, 291] With the presence of urea groups in the structure of our compounds, we see that hydrophobicity is less important for gelation as the non-covalent hydrogen bond-directed self-assembly of the ureas is ultimately one of the main driving forces and this is confirmed by comparing gelator **C12-urea-RGD** with non-gelator **C12-RGD**, and also gelator **C12-[urea-RGD]$_2$** with the more hydrophobic and amide-bearing gelator **C12-RGD-C12**. We hypothesise, however, that the reason for this efficient intermolecular H-bonding between the ureas in **C12-[urea-RGD]$_2$** (as well as **C12-urea-RGD**) is possibly due to them being located directly next to a C12 hydrophobic chain. Hence, it is feasible to

suggest that they are located within, or are adjacent to, a hydrophobic domain when self-assembled and as such water cannot compete with the urea-urea interaction. A similar combination of hydrophobic 'shielding' of hydrogen bonding interactions is known to stabilise the secondary structures of peptide foldamers.[292]

We should note at this point that the 'design paradigms' (i.e. the Israelachvili packing rules) for various amphiphiles and the aggregated structures that they form in solution seem to breakdown in this work. For example, although **C12-RGD** and **C12-urea-RGD** are similar in size (and hence critical packing shape), the former self-assembles into spherical micelles and the latter into nanofibres. We have reasoned this to be due to the non-directionality of the dominant C12 hydrophobic/vdWs interactions between adjacent **C12-RGD** molecules, whereas the directionality of the urea-urea hydrogen bonding (coupled with the non-directional C12 hydrophobic/vdWs interactions) between adjacent **C12-urea-RGD** molecules induces the 1-dimensional β-sheet assembly which underpins the 3-dimensional nanofibre formation. This directional self-assembly also applies to the bolaform derivative, **C12-[urea-RGD]$_2$**, as previously discussed. **C12-RGD-C12** on the other hand is somewhat more difficult to explain why it contravenes the Israelachvili rules, as a simplistic view would suggest it has the double-chained structure that would normally result in soluble liposome/vesicle or planar bilayer-type structures. However, attachment of the C12 chains at opposite ends of the peptide seems to induce either the formation of sample-spanning cylindrical micelle-type nanofibres (if the two C12 chains point into the supramolecular structure) or an extended supramolecular polymer-type network (if the two C12 chains point away from each other) that restricts the flow of water molecules. If the two C12 chains were conjugated at one end of the peptide (as in the idealised Israelachvili critical packing shapes), the amphiphile might behave differently and form the soluble aggregates predicted by the Israelachvili rules accordingly, assuming the HLB was not significantly affected (c.f. **C12-Lys(C12)-(CH$_2$)$_5$-TEG-RGD** in Chapter 3 which forms soluble rod-like micelles).

We then went on to investigate the possible gelation ability of our other urea-based RGD peptide amphiphiles and bolaamphiphiles. Unfortunately, even at a maximum tested concentration of 1.0 wt %, neither **C6-urea-RGD** (**4.6**) (17 mM) nor **C6-[urea-RGD]$_2$** (**4.8**) (9.2 mM) were able to self-assemble and form gels in water. **C6-urea-RGD** formed a clear solution but required heating, whereas **C6-[urea-RGD]$_2$** solubilised immediately upon the addition of water. This provides further evidence that the double RGD head group lends itself to improved solubility of the bolaamphiphilic molecules in water. Reducing the aliphatic chain length from C12 to C6 for both the amphiphile and bolaamphiphile derivatives, however, clearly results in loss of gelation ability by making the compounds too water soluble. To permit gelation, a fine balance between solubilisation and precipitation is required i.e. the HLB of the molecule must be carefully considered, therefore, it is proposed that a critical chain length between C6 ≤ C12 is optimum to provide enough hydrophobicity for the molecules to self-assemble and gel.

CH_2-[Ar-urea-RGD]$_2$ (**4.10**) was then synthesised to investigate the effect of an aromatic hydrocarbon spacer on the gelation ability of the bolaamphiphile. Unfortunately, at 0.1 wt % (0.85 mM) the compound remained soluble after heating, and even at a maximum tested concentration of 1.0 wt % (8.5 mM) the compound solubilised upon heating and then precipitated out upon cooling. This suggests that the intermolecular π-π stacking interactions which can form between the aromatic groups may be too strong for gelation in water and instead bulk precipitation was observed, again clearly illustrating the required balance between solubility and precipitation which is of key importance in gelation.

In a bid to optimise the structure of **CH_2-[Ar-urea-RGD]$_2$** we either needed to make it more hydrophobic or more hydrophilic. To make it more hydrophobic, a flexible aliphatic chain or a rigid linker with increased aromaticity were two plausible options. We opted for a rigid aromatic linker so as to make a direct comparison with the flexible aliphatic chain gelator molecules we had already successfully synthesised. Additional aromatic units were incorporated into the linker by starting from commercially available 1,4-dibromobenzene, as shown in Schemes 4.7 through to 4.9, to yield the linear, rigid-rod-type structure: **linear OPE-[RGD]$_2$** (**4.23**). In an attempt to make it more hydrophilic, and in keeping with a rigid aromatic linker, we needed to incorporate more than two RGD peptides into the structure. By simply changing 1,4-dibromobenzene for 1,3,5-tribromobenzene, and repeating the same chemistry as that used for the synthesis of **4.23**, we were able to dendronise the linear, rigid-rod-type structure to generate trivalent derivative: **triangular-shaped OPE-[RGD]$_3$** (**4.27**) (Schemes 4.10 and 4.11).

Recently, García *et al* demonstrated the synthesis and nanofibrillar self-assembly behaviour in aqueous solution of triangular-shaped oligo(phenylene ethynylene) (OPE) amphiphiles, decorated at the ends with two- and four-branched hydrophilic triethyleneglycol dendron wedges (Scheme 4.17).[293] The sterically bulky glycol branches induced a twisted face-to-face π-π stacking of the aromatic OPE cores. Inspired by this, we were hopeful that our linear and triangular-shaped OPE amphiphiles (see **4.23** and **4.27**, respectively, for predicted structures) would behave in a similar manner, owing to the presence of the bulky hydrophilic RGD peptide branches, and possibly even generate a sample-spanning fibrous gel network – the enhanced self-assembly promoted by the interfacial π-π stacking of the OPEs coupled with the intermolecular urea-urea H-bonding at the OPE-RGD conjugation points.

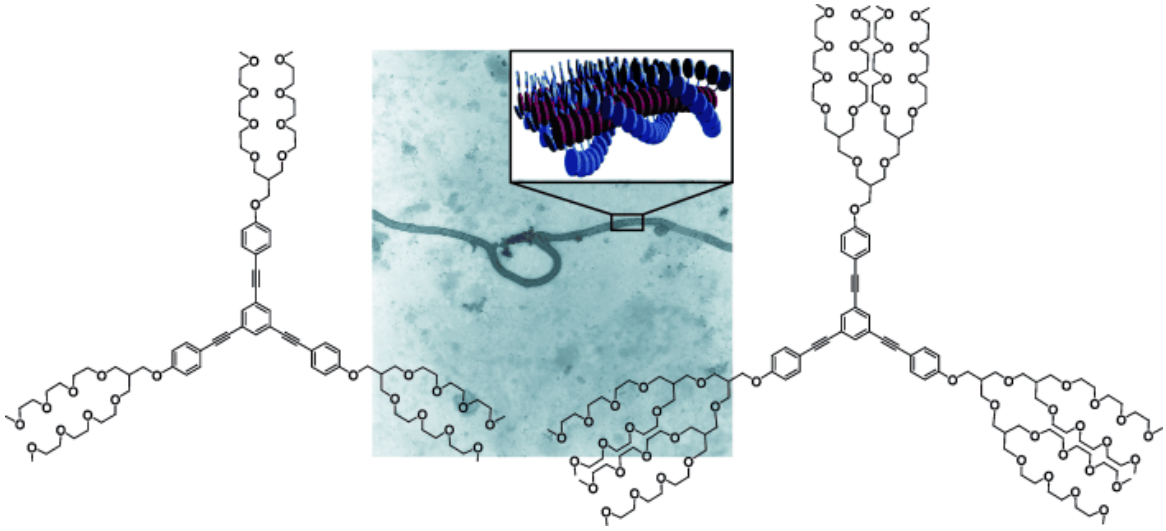

Scheme 4.17 – Schematic representation of the self-assembly of dendronised triangular oligo(phenylene ethynylene) amphiphiles into long fibrillar structures in aqueous solution, investigated by García *et al.* Original in colour. Image reproduced from the graphical abstract of reference 28.

Frustratingly, neither **4.23** nor **4.27** formed gels in pure water. In fact, the solubility of both compounds was limited to TFA, DMSO or PBS buffered water (pH 7.4). Both were found to be insoluble, using either sonication or heating, in pure water and in a variety of polar and non-polar organic solvents; including methanol, acetonitrile, THF, ethyl acetate, hexane, toluene, DCM and chloroform – although **linear OPE-[RGD]$_2$** was more readily soluble than **triangular-shaped OPE-[RGD]$_3$** in a mixture of water/^{t}BuOH when the compounds were being prepared for freeze-drying. It is unsurprising that neither compound dissolves or forms gels in non-polar solvents owing to the polar RGD head groups. It is also unsurprising that **linear OPE-[RGD]$_2$** behaves similarly to **CH$_2$-[Ar-urea-RGD]$_2$**; incorporating the oligo(phenylene ethynylene) linker into the structure does not help overcome the strong intermolecular π-π stacking interactions of the hydrophobic aromatic units in polar solvents, such as water, resulting in insolubility. What is surprising is that the additional polar RGD head group in **triangular-shaped OPE-[RGD]$_3$** is not enough to counteract the insolubility of the four non-polar aromatic units to yield the partial solubility in water that is required to permit gelation. Packing considerations may also be key in these rigid aromatic systems, which cannot easily conceal the exposed hydrophobic interior of the molecules from the surrounding polar water molecules compared to our previous compounds which possess a flexible aliphatic linker. Interestingly, in PBS buffered water the compounds are soluble which might indicate the important, and in this case disruptive, role of the urea-urea interactions – phosphate perhaps competes with the intermolecular H-bonding and allows the molecules to re-assemble in such a way that the aromatic and alkyne groups are no longer exposed, thereby inducing solubilisation.

To summarise, the key RGD hydrogelator design rules based on the series of compounds synthesised in this chapter are:

i. The RGD peptide must bear an aliphatic chain of at least C12 length at the N-terminus (requires further work to determine if the critical length is between C6 and C12) AND be conjugated to the peptide via a urea group to provide the amphiphile with enough hydrophobicity and hydrogen bonding ability to induce self-assembly into fibrous aggregates (the same applies to the **C12-[urea-RGD]$_2$** bolaform derivative). Conjugation via an amide group does not provide enough hydrogen bonding character to induce fibrous self-assembly and merely induces micelle formation (at least for the non-bolaform derivative, **C12-RGD**, investigated in Chapter 3). Further investigation is required to determine if the hypothetical bolaamphiphile **C12-[amide-RGD]$_2$** would have enough hydrogen bonding character to induce hydrogelation compared with **C12-[urea-RGD]$_2$**.

ii. The RGD peptide must bear an aliphatic chain of at least C12 length at both the N- and C-termini, if the aliphatic chains are conjugated via an amide group, to provide the correct HLB (and also possibly the requisite number of hydrogen bonding interactions by having the additional amide group at the C-terminus of the peptide) required for hydrogelation by this compound.

iii. Addition of lysine into the peptide (C12-RGDK) inhibits hydrogelation, whether the C12 chain is conjugated via an amide or a urea group, and hence this modification to the peptide conformation and/or the additional positive charge prevents the compounds from gelating water.

iv. Attempts at introducing aromaticity into the amphiphilic structures (to determine the effects of π-π stacking on gelation) has so far failed to yield RGD hydrogelators – possibly due to perturbation of the sensitive HLB required for hydrogelation and, in conjunction with this, the limited solubility of the compounds in pure water.

Having identified three new gelators: **C12-urea-RGD**, **C12-[urea-RGD]$_2$** and **C12-RGD-C12**, we then went on to investigate these materials in more detail.

4.4 TEM and SEM Imaging

TEM and SEM images were obtained for hydrogelators **C12-urea-RGD**, **C12-[urea-RGD]$_2$** and **C12-RGD-C12**. For TEM: a small portion of the gel was removed with a spatula and 'drop-cast' onto a heat-treated (HT) copper TEM grid, excess material was wicked off using filter paper and left to dry for 15-30 min prior to imaging. Depending on the sample, a uranyl acetate stain was sometimes used for contrast, as denoted in each figure. For SEM: a small portion of the gel was removed with a spatula and placed on a copper support, then freeze-dried by immersing in liquid nitrogen and then lyophilising overnight. Excess solid material was broken off with a spatula and then the sample was

sputter coated with a thin layer (about 12 nm) of gold/palladium to prevent sample charging, before placing the sample on a metal SEM stub and imaging. Both methods yield 'xerogel' images which is another term for the dried-down version of the hydrogel and are subject to drying effects. However, the freeze drying used for preparation of the SEM sample is proposed to cause less network reorganisation as there is significantly less thermal energy available during the removal of solvent from the gel.

The xerogel of 1.0 wt % **C12-urea-RGD** showed fibrils, with diameters ranging from approximately 40-120 nm, which bunch together to form dense areas of interpenetrating nanofibres in the TEM (Fig. 4.10A-B). This was corroborated with SEM (Fig. 4.10C-D).

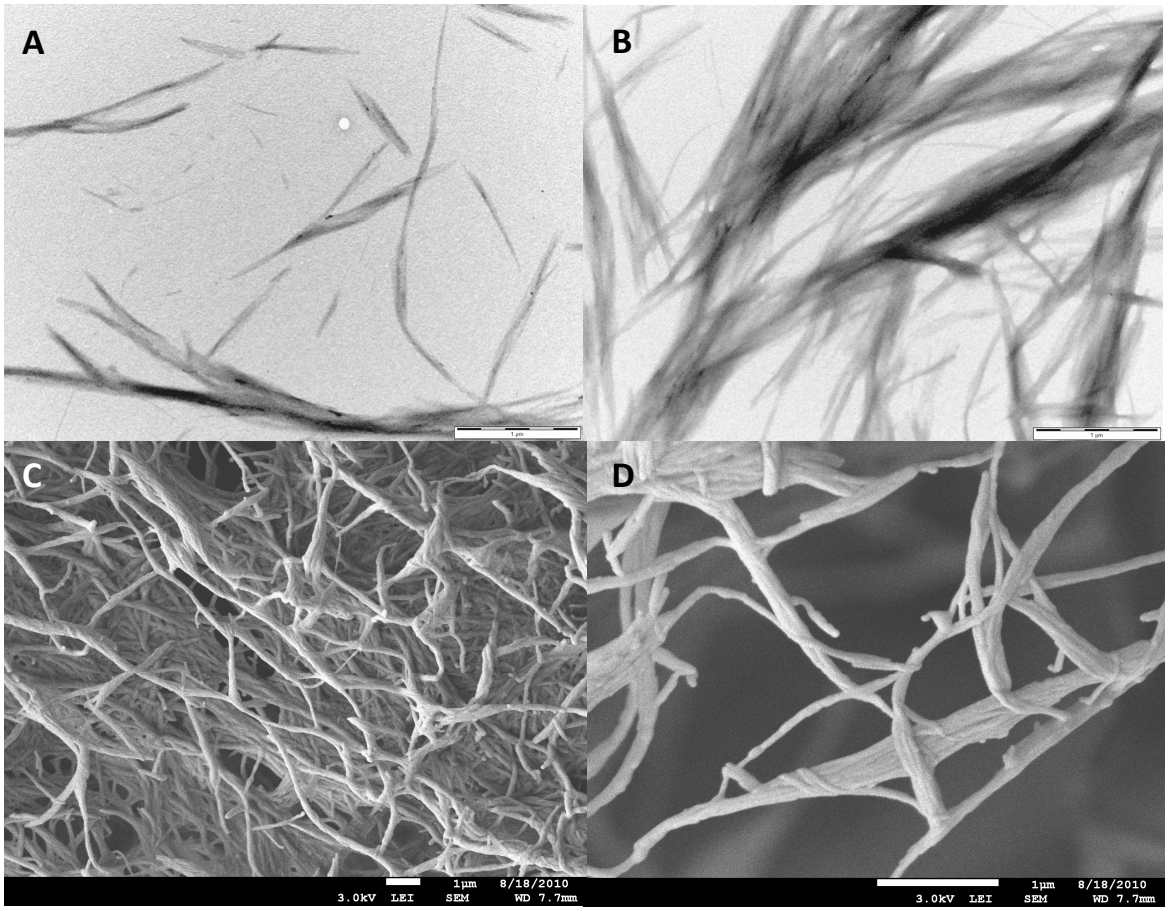

Fig. 4.10 – TEM images of 1.0 wt % **C12-urea-RGD** xerogel: A)-B) scale bar = 1 µm. Imaged without stain. SEM images of 1.0 wt % **C12-urea-RGD** xerogel: C)-D) scale bar = 1 µm.

The xerogel of 0.5 wt % **C12-[urea-RGD]$_2$**, compound **C12-urea-RGD**'s structural analogue, showed thin nanoribbons/tapes in the TEM, with widths ranging from approximately 40-100 nm and thicknesses of about 10-15 nm or less (Fig. 4.11A-B). The same structures were seen using SEM which confirmed the flat morphology of the fibrils (Fig. 4.11C-D). With both imaging techniques, rope-like structures formed from intertwined ribbons could be identified (circled in red), which points

to a chiral arrangement of the fibres, consistent with transfer of chiral information from the molecular level upto the nanoscale. The change from amphiphile (**C12-urea-RGD**) to bolaamphiphile (**C12-[urea-RGD]$_2$**) has caused a significant change in morphology of the self-assembled material, from rounded fibrils to slightly narrower, flatter, sheet-like fibrils which bundle together less. We suggest this is due to the increased H-bonding between molecules of **C12-[urea-RGD]$_2$** and an alternative packing arrangement which helps to shield the hydrophobic interior of one fibril from an adjacent fibril, thereby reducing the amount of bundling of 'sticky' fibrils, although the exact arrangement is unknown and forms the basis of future work. Interestingly, it is **C12-[urea-RGD]$_2$** which forms the more effective transparent gel network, and this is in agreement with the observation of more homogenous, narrower, evenly dispersed fibres by electron microscopy methods.

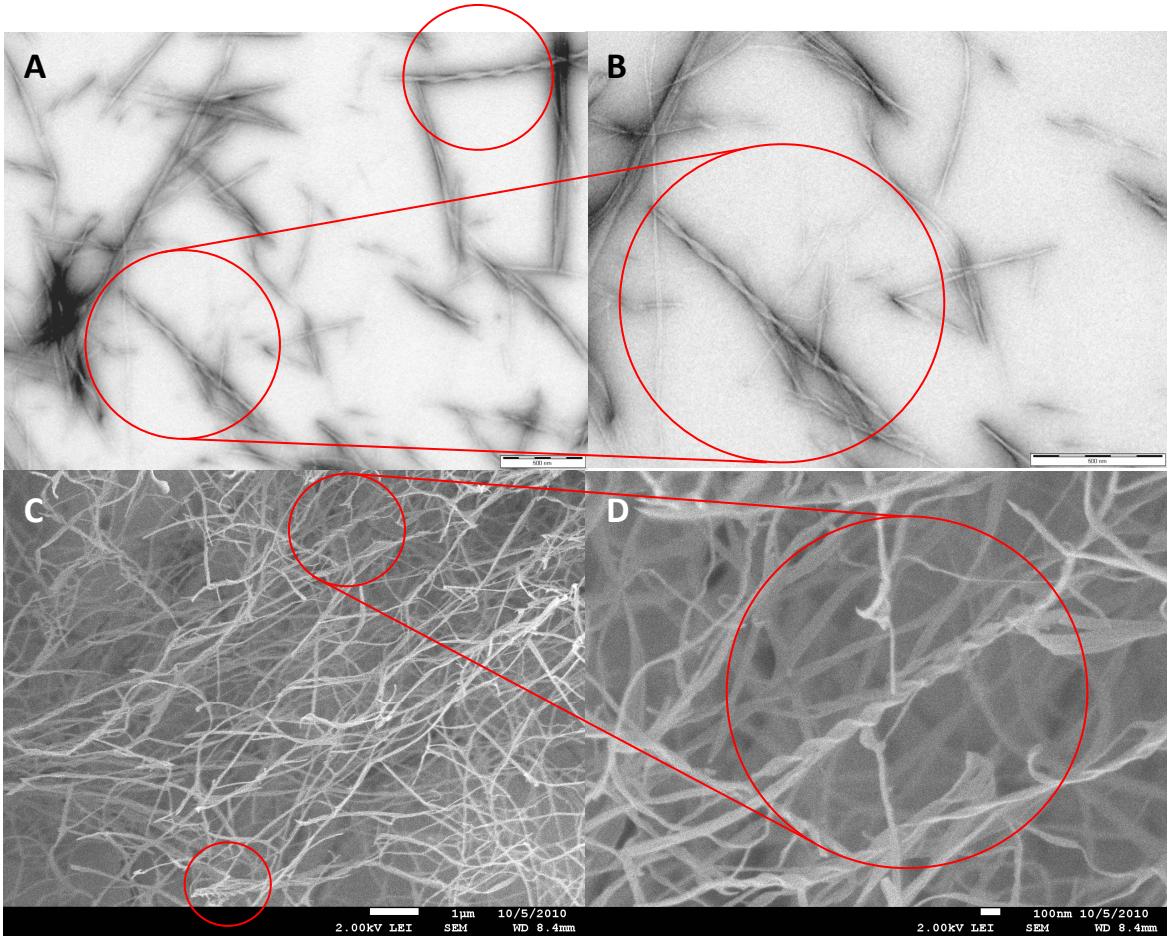

Fig. 4.11 – TEM images of 0.5 wt % **DGR-urea-C12-urea-RGD** xerogel: A)-B) scale bar = 500 nm. Negatively stained with uranyl acetate. SEM images of 0.5 wt % **DGR-urea-C12-urea-RGD** xerogel: C) scale bar = 1 µm, and D) scale bar = 100 nm.

Fibrils of **C12-RGD-C12** were found to have similar morphology to those of **C12-urea-RGD** – rounded, with diameters ranging from approximately 50-100 nm, which then bundle together to form denser areas – with no real difference in morphology, whether the hydrogel was formed from 1:9 DMSO/water (Fig. 4.12A-B) or from sonicating in water (Fig. 4.12C-D). This bundling would

therefore appear to be indicative of a material with a greater degree of hydrophobicity, consistent with more opaque and less effective gels – particularly in the case of the sonicated sample in pure water.

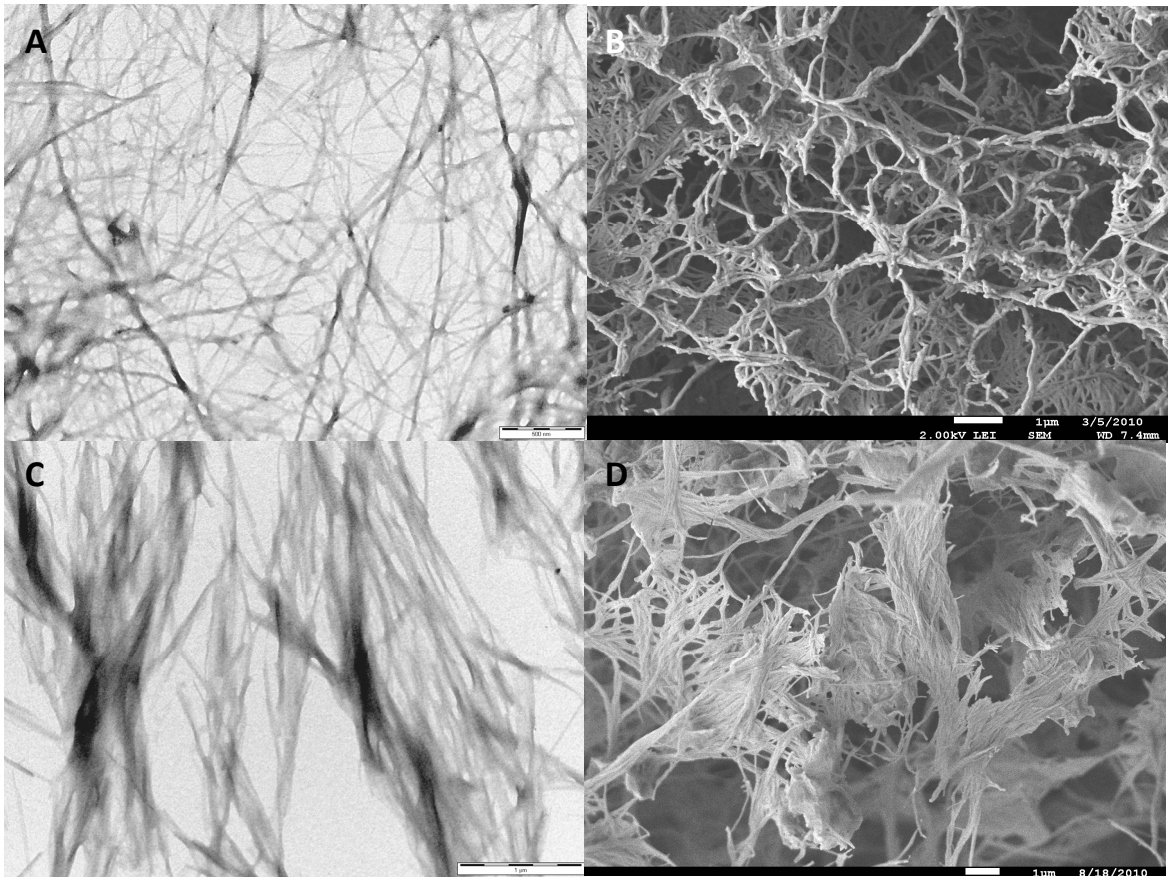

Fig. 4.12 – Xerogel of 0.1 wt % **C12-RGD-C12** in 1:9 DMSO/water: A) TEM image without stain, scale bar = 500 nm, and B) SEM, scale bar = 1 μm. Xerogel of 1.0 wt % **C12-RGD-C12** sonicated in water: C) TEM image without stain, scale bar = 1 μm, and D) SEM, scale bar = 1 μm.

Artefacts in TEM and SEM images are often caused by drying effects because of the way the sample is prepared for these techniques. Atmospheric scanning electron microscopy (ASEM) is a recent innovation in electron microscopy which allows the user to capture images of liquid-based samples under atmospheric pressure without having to dry them. This yields images of materials which are in their native (solvated) state and are more 'true-to-life' representations of the sample. ASEM is a hybrid of TEM and SEM in that the sample requires staining with uranyl acetate for contrast, but the sample is placed on a thin film dish on top of the inverted SEM detector which separates the sample in atmosphere from the vacuum of the detector and electron source, and the imaging is achieved using backscattered electrons through the silicon nitride window of the dish (Scheme 4.18). The same area of view of the sample can also be imaged in real-time through the optical microscope on top.

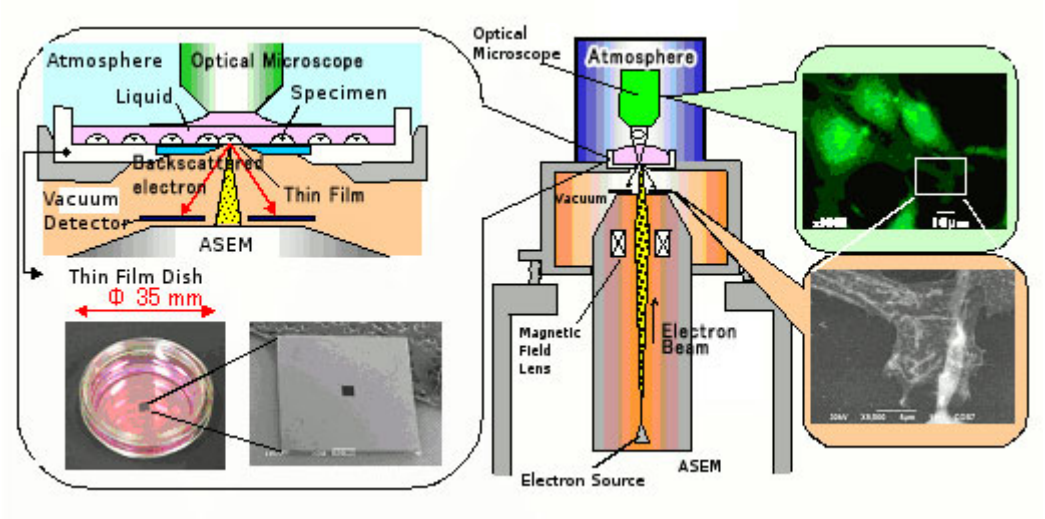

Scheme 4.18 – Schematic representation of the ASEM setup. Image reproduced from www.jeol.com. Original in colour.

Hydrogels of **C12-[urea-RGD]$_2$** at concentrations of 0.1, 0.2 and 0.5 wt % were imaged with ASEM using uranyl acetate as negative stain, with water containing 10 mg/ml glucose deposited onto the sample as a free radical scavenger to try and prevent decomposition under the electron beam (Fig. 4.13). However, the samples still damaged easily in the beam – so much so that the 0.5 wt % hydrogel could not be imaged – and had to be captured quickly before complete degradation occurred. The images of the 0.1 and 0.2 wt % gels are much hazier than those obtained with TEM and SEM as the samples are within fluid and hence the self-assembled structures are more dynamic compared to when they are dried down as the xerogel, although pleasingly nanofibres are still discernible against the black, negatively stained background. To the best of our knowledge, this is one of the first times this technique has been used for the analysis of a self-assembled hydrogel.

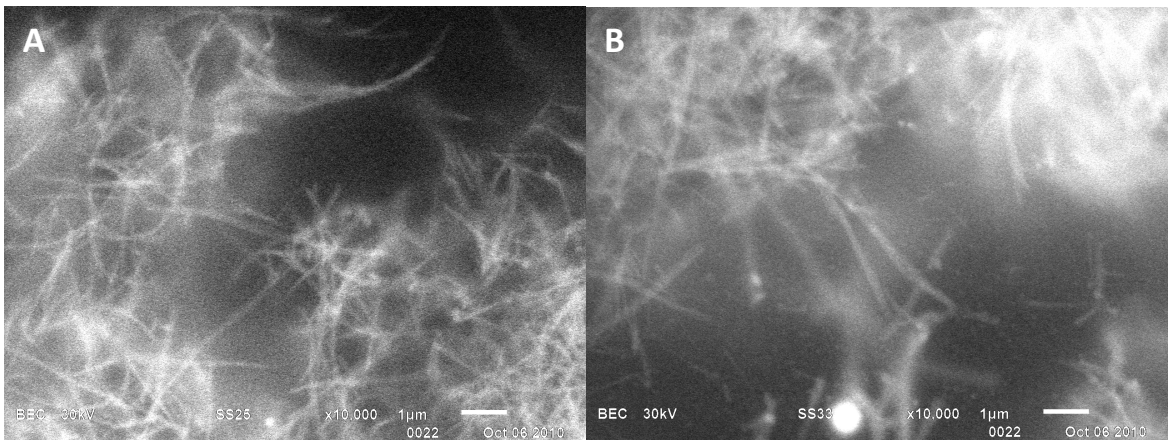

Fig. 4.13 – ASEM images of A) 0.1 wt % **C12-[urea-RGD]$_2$** hydrogel, scale bar = 1 μm, and B) 0.2 wt % **C12-[urea-RGD]$_2$** hydrogel, scale bar = 1 μm. Water containing 10 mg/ml glucose was deposited on top of the samples and then negatively stained with uranyl acetate.

ASEMs were obtained for the hydrogel formed from 1.0 wt % **C12-RGD-C12** sonicated in water (Fig. 4.14). Again, the images are hazier due to the dynamic systems but fibres, with diameters of approximately 100 nm or less, can still be observed on closer inspection.

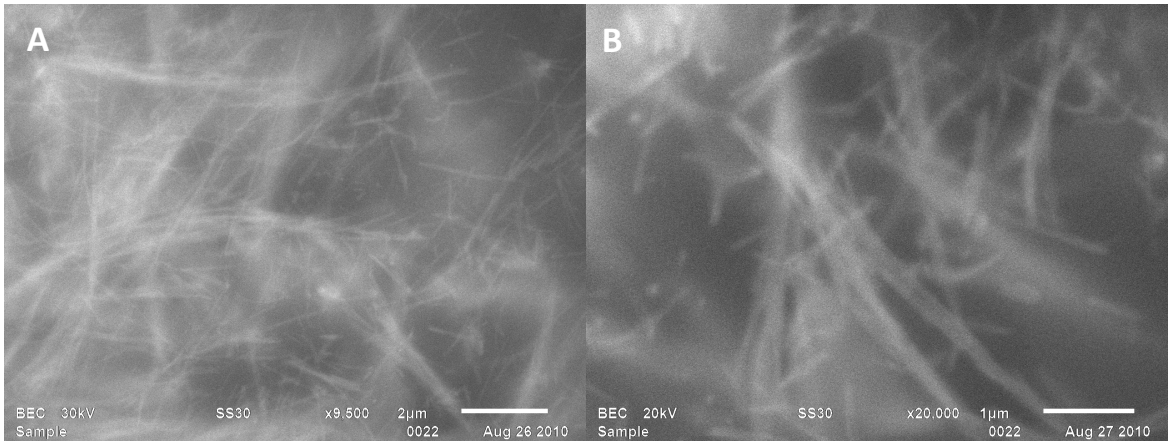

Fig. 4.14 – ASEM images of the hydrogel formed from 1.0 wt % **C12-RGD-C12** sonicated in water A) scale bar = 2 μm, and B) scale bar = 1 μm. Water containing 10 mg/ml glucose was deposited on top of the samples and then negatively stained with uranyl acetate.

4.5 Further Studies with C12-[urea-RGD]$_2$

Bolaamphiphile **C12-[urea-RGD]$_2$** was our most promising hydrogelator owing to its thermally-initiated gelation, thermoreversibility, long-term stability, low MGC, and T_{gel} properties. We therefore decided to investigate the gel structure and properties further.

4.5.1 Circular Dichroism (CD) and Variable Temperature-Circular Dichroism (VT-CD)

CD spectroscopy[294] is a widely used technique for determining the secondary structural motifs of proteins (e.g. α-helix, β-sheet etc).[295] We employed CD to gain further insight into the nanoscale self-assembly process responsible for gelation, as it is a useful method for probing the organisation of gelator building blocks within a chiral nanostructured environment. Amide groups absorb at ca. 220 nm due to the n→π* transition of the amide carbonyl (a contribution at ca. 190 nm due to the higher energy π→π* transition is also sometimes observed), and the intensity is dependent on the ϕ and ψ torsion angles about the amide group.[296] Hence, the shape and magnitude of the CD signal provides characteristic information about the arrangement of the gelator molecules within the chiral environment of a gel network, mediated by exciton coupling between adjacent amide groups. For example, the CD signal for a random coil structure is positive at 212 nm (n→π*) and negative at 195 nm (π→π*); a β-sheet structure is negative at 218 nm (π→π*) and positive at 196 nm (n→π*); and for an α-helix structure, the exciton coupling of the π→π* transition leads to positive (π→π*)

perpendicular at 192 nm, negative (π→π*) parallel at 208 nm, and the negative peak at 222 nm is the red shifted n→π* transition (Fig. 4.15).[296]

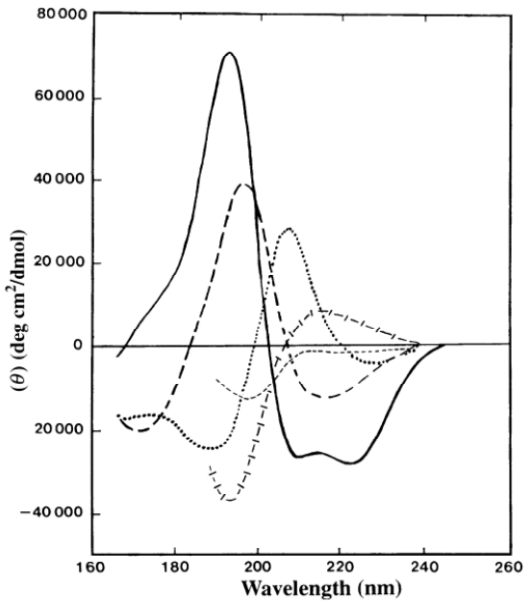

Fig. 4.15 – Examples of far-UV CD spectra corresponding to various types of secondary structure. Solid line, α-helix; long dashed line, antiparallel β-sheet; dotted line, type I β-turn; cross-dashed line, extended 3_1-helix or poly (Pro) II helix; short-dashed line, irregular structure. Image reproduced from reference 31.

CD spectra were collected for 1 and 2 mg/ml **C12-[urea-RGD]$_2$** hydrogel samples from 300 to 190 nm (Fig. 4.16). The signal below 210 nm corresponds to noise, as the CD spectrometer, operated under a nitrogen atmosphere not vacuum, was not sensitive enough to collect data into the far and vacuum UV region. The band at 220 nm in the CD spectrum of **C12-[urea-RGD]$_2$** increases in intensity with increasing concentration which is due to an increased concentration of the chiral molecules. The broad band shape at this wavelength is evidence that the molecules align into a hydrogen-bonded β-sheet arrangement within the fibrils of the gel network,[296] as previously proposed (see Scheme 4.16).

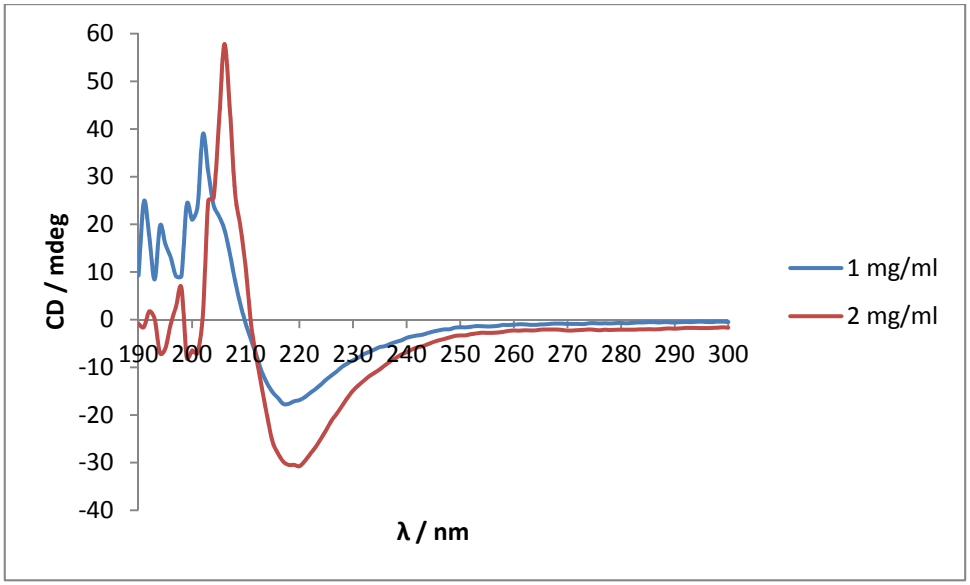

Fig. 4.16 – CD spectra of **C12-[urea-RGD]$_2$** hydrogels at 20°C. Original in colour.

Importantly, VT-CD showed that the CD band decreased in intensity with increasing temperature (Fig. 4.17) and clearly indicates that the CD signal therefore corresponds to a temperature-responsive, self-assembled system and is not just due to the inherent CD spectrum of individual isolated chiral gelator molecules. At higher temperatures (70-90°C) the CD signal does not decrease any further and a bathochromic shift to 226 nm occurs. This residual signal is most likely due to the inherent CD signal of the individual chiral gelator molecules as a consequence of the complete breakdown of the gel network to a sol.

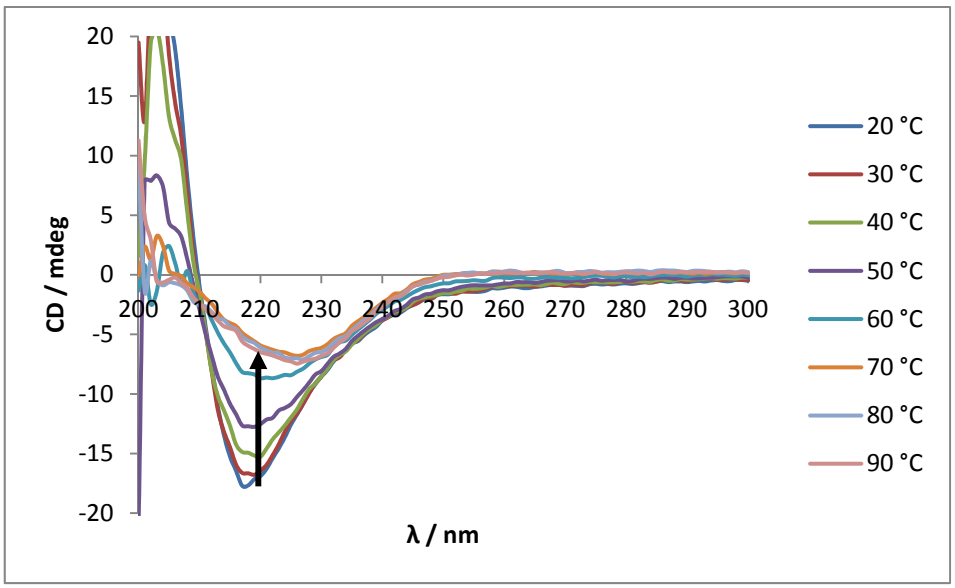

Fig. 4.17 – VT-CD spectra of a 1 mg/ml **C12-[urea-RGD]$_2$** hydrogel. Original in colour.

Plotting the CD signal intensities at λ_{max} against temperature reveals that the biggest decrease in the trend (i.e. the biggest disruption in the self-assembled network) is at the 50-60°C transition, which then plateaus out at higher temperatures (Fig. 4.18). This is in agreement with the T_{gel} phase diagram for this compound where we discovered that a 1 mg/ml gel sample collapsed at 58°C, and demonstrates that the loss of chiral self-assembly corresponds to the loss of material integrity.

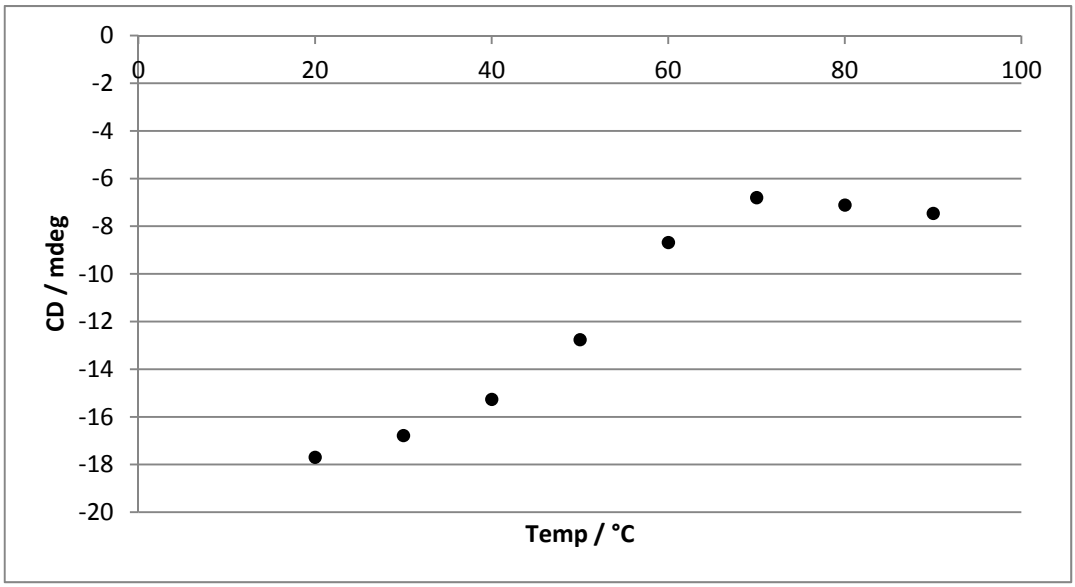

Fig. 4.18 – CD signal at λ_{max} vs. temperature for a 1 mg/ml **C12-[urea-RGD]$_2$** hydrogel.

4.5.2 Variable Temperature-NMR (VT-NMR)

The fully annotated ^{1}H NMR of **C12-[urea-RGD]$_2$**, dissolved in CD_3OD, is shown in the appendix (spectrum 4.2). Fully 'immobilised' gel-phase molecules are NMR silent, therefore this technique can detect only solubilised individual molecules and small oligomers, and systems which are in fast exchange with the gel fibres.[297, 298] Hydrogel samples of **C12-[urea-RGD]$_2$** in D_2O, containing 0.05 wt % TSP-d_4 as reference, were prepared *in situ* in NMR tubes at concentrations ranging from 20 mg/ml down to 2 mg/ml (Fig. 4.19). The 20 mg/ml sample appeared to be quite opaque, presumably as a consequence of undissolved material, while the 2 mg/ml sample appeared to form the most translucent and homogenous gel.

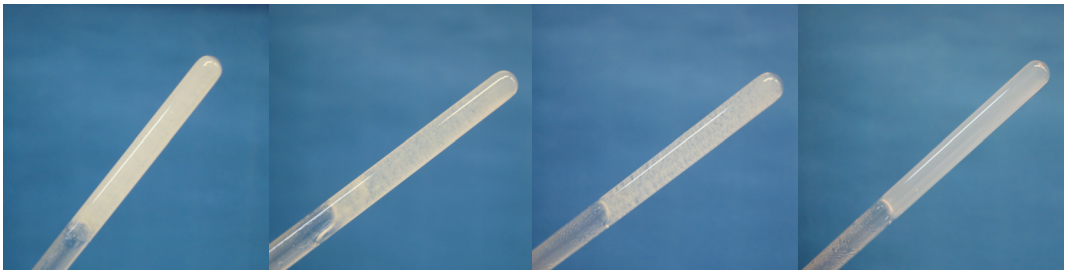

Fig. 4.19 – Inverted **C12-[urea-RGD]$_2$** hydrogel NMR samples, from left to right: 20, 10, 5 and 2 mg/ml. All samples contained 0.5 ml D_2O (+0.05 wt % TSP-d_4 as internal standard). Original in colour.

VT-NMR studies of the **C12-[urea-RGD]$_2$** hydrogels demonstrated to some degree an increase in the broad peak intensities with increasing temperature as the mobility and hence solubility of the **C12-[urea-RGD]$_2$** molecules increased in solution – a consequence of the gel-sol transition. Although the 2 mg/ml sample formed the most homogenous gel, the more concentrated 20 mg/ml sample provided the most discernible spectra (Fig. 4.20). The major peak shifting between 4.8 and 4.2 ppm corresponds to the water peak, the hydrogen bonding of which is temperature sensitive.

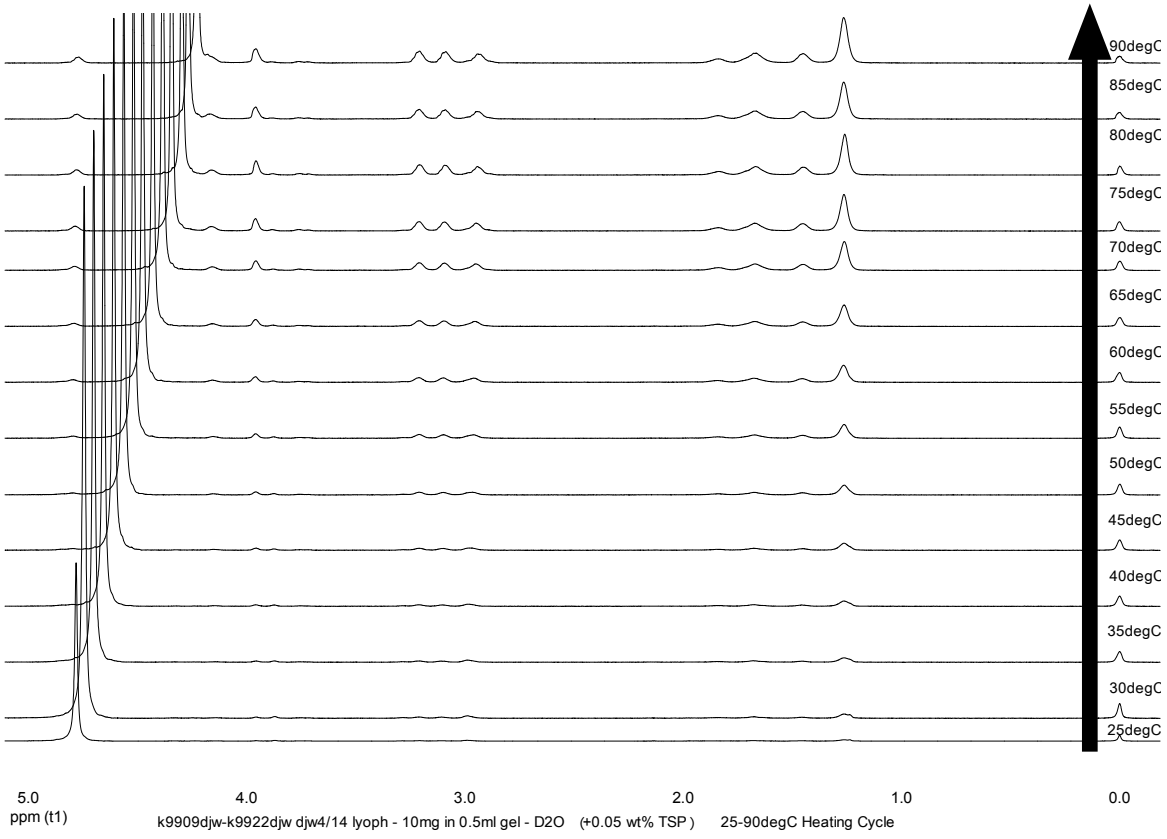

Fig. 4.20 – VT-NMR of the 20 mg/ml **C12-[urea-RGD]$_2$** hydrogel in 0.5 ml D_2O (+0.05 wt % TSP-d_4 as internal standard).

Usually, this is a powerful technique for probing the non-covalent intermolecular interactions responsible for the gel-phase self-assembly. However, as the study was conducted in D_2O, useful information about shifts in the urea and amide N*H* peaks with increasing temperature, as a consequence of the breakdown of the H-bonding interactions, could not be ascertained because of the absence of these peaks in the ^{1}H NMR due to proton exchange between protic solvent and gelator molecule. However, upfield shifts in the aspartic acid C*H*$_2$ (2.99 ppm, shifting to 2.94 ppm) and α-*H* (4.80 ppm, shifting to 4.77 ppm) peaks as the temperature increased were observed (Fig. 4.21). This indicates that the carboxylic acids of the aspartic acid side-chain and C-terminus become increasingly more associated with the surrounding water molecules as the sample heats up. Assuming the carboxylic acids are in their protonated form in the gel state, as the molecules become more mobile and eventually solubilise, deprotonation would occur and upfield (shielded) shifts in the Asp C*H*$_2$ and Asp α-*H* peaks represents formation of the negative charge adjacent to these groups and the increasing degree of deprotonation in the sample. The Arg α-*H* peak shifts downfield (deshielded) slightly (4.14 ppm, shifting to 4.17 ppm) as this is probably a consequence of the disruption in the adjacent urea group's urea-urea H-bonding interaction with increasing temperature. No obvious shifts in any of the other peaks could be detected.

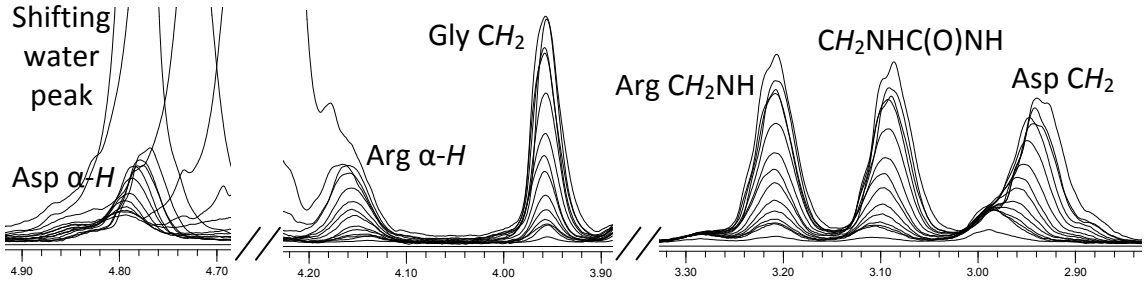

Fig. 4.21 – Superimposed spectra of the Asp α-*H*, Arg α-*H*, Gly C*H*$_2$, Arg C*H*$_2$NH, C*H*$_2$NHC(O)NH and Asp C*H*$_2$ regions in the VT-NMR of the 20 mg/ml **C12-[urea-RGD]$_2$** hydrogel.

It is widely known that the pK$_a$ of an ionisable group can vary depending on whether a molecule is in the gel or sol phase.[214, 299] Previous studies have shown what effect solution pH has on the hydrogelation properties of amphiphilic peptides composed of acidic and basic amino acids, where it was demonstrated that deprotonation and protonation occurred at pH values which were, respectively, a number of units above or below their nominal pK values.[300] Electrostatic ionic screening or repulsion forces were associated with this effect. Earlier, we were unable to confirm the ionisation state of the peptide head group in the gel (see Scheme 4.16). The information obtained from VT-NMR now leads us to believe that within the gel the basic guanidine group of the arginine side-chain is, as would be expected, protonated as the guanidinium form with trifluoroacetate as the counter anion, while the two carboxylic acids of the aspartic acid are protonated, and it is only when the sample is heated to a sol that the acids (pK$_a$ 4-5) become deprotonated in water that is at natural pH

(~7). This scenario seems to satisfy the lower energy requirement for a charge neutral state of the peptide head group, or at least one in which the positive charge on the guanidinium group is screened by the trifluoroacetate counter anion as shown here (Scheme 4.19), decreasing the head group interaction with water, and hence, enabling the individual gelator molecules to come together without charge repulsion effects inhibiting self-assembly. In addition to this work, potentiometry would provide a means of quantifying the pK_a's of the molecule in the gel and sol states, including the effect of pH on gel formation, and this constitutes the basis of future studies.

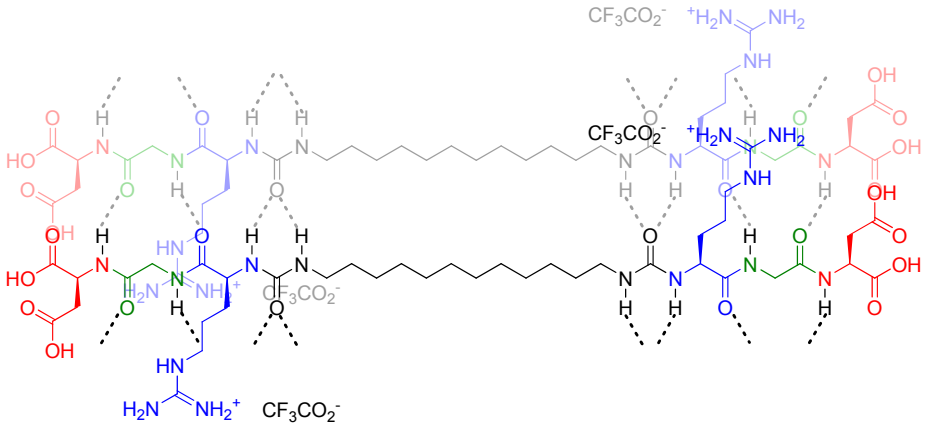

Scheme 4.19 – Proposed mode of self-assembly of **C12-[urea-RGD]$_2$**, including the proposed side-chain and C-termini charge states within the fibrils in water at natural (unbuffered) pH. Original in colour.

4.5.3 Buffer and Anion Sensitivity

Thus far, we have reported the hydrogelation behaviour of **C12-[urea-RGD]$_2$** in ultrapure water as the bulk medium. We then moved on to study its gel formation in buffered water. Samples at 1 mg/ml in concentration were prepared by dissolving the gelator, with heating, in two readily available buffers, allowing them to cool, and then the effect on gelation was noted (Table 4.1).

In phosphate buffered saline (PBS) solution, at pH 7.4, we observed no gel formation, whereas in biological SHE buffer, at pH 7, a loose transparent gel formed which collapsed shortly after inverting the sample. It should be noted at this point that at higher gelator concentrations, gels (or at least stronger ones in the case of the biological SHE buffer) may have been observed, however, the study was limited by the amount of gelator that was available. In any case, both buffers contain similar concentrations of sodium chloride, and hence, the 10 mM phosphate content in the PBS was reasoned to be the cause for the inhibition of gel formation at this concentration of gelator. The mechanism by which gel inhibition occurs is reasoned to be due to the anionic phosphate, a strong hydrogen bond acceptor, coordinating to the hydrogen bond donating urea groups thereby inhibiting the intermolecular urea-urea interactions and preventing the molecules from stacking (Scheme 4.20) – it

would be interesting, in the future, to conduct a Nile Red encapsulation study on **C12-[urea-RGD]$_2$** in PBS to check for any self-assembly into colloidal aggregates and, if so, analysis by TEM to check the morphology. In addition, weakening of the 1 mg/ml gel sample in biological SHE buffer, containing 2 mM HEPES – a sulfonate-based buffer molecule (Fig. 4.22), compared to that of the ultrapure water sample further confirmed the anion sensitivity of gel formation.

Medium	Result
Ultrapure water	Transparent gel
PBS, pH 7.4 (10mM phosphate, 138mM NaCl)	Clear solution
Biol. SHE, pH 7 (2mM HEPES, 0.05mM EDTA, 150mM NaCl)	Loose, transparent gel

Table 4.1 – The choice of medium dictates the hydrogelation ability of **C12-[urea-RGD]$_2$** (1 mg/ml) using the heat-cool method. Yellow shading highlights the conditions which permit gel formation. Original in colour.

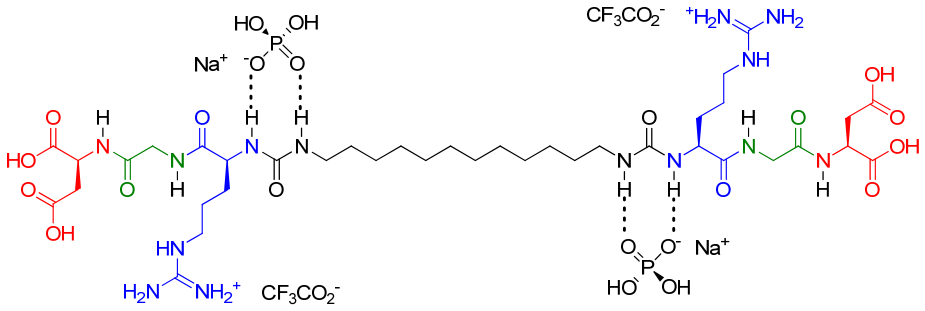

Scheme 4.20 – Proposed structure of the **C12-[urea-RGD]$_2$**-phosphate coordination complex. Note, sodium dihydrogen phosphate is shown as an example, however this is in equilibrium with disodium hydrogen phosphate, at pH 7.4, which could also coordinate. Original in colour.

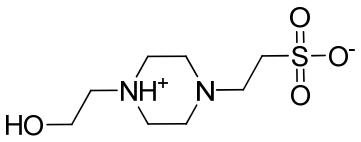

Fig. 4.22 – The structure of HEPES.

In contrast, 1 mg/ml **C12-urea-RGD** did form a loose gel in PBS, surviving for over 1 h before collapsing (Table 4.2). We predict that higher concentrations of gelator would result in more robust gels. This behaviour is surprising because **C12-urea-RGD** is insoluble in pure water alone, even with

heating. However, phosphate seemingly aids dissolution upon heating, with subsequent gelation upon cooling to rt. We are unsure of the reason why phosphate promotes gelation in this case if phosphate binding to the urea groups prevents gelation for its bolaform analogue. We suggest that interdigitation of the hydrophobic chains might still occur if two **C12-urea-RGD** molecules bind to one phosphate, thereby directing self-assembly into fibrillar structures while at the same time providing the partial solubility in water that is required for gel formation to occur (Scheme 4.21). Future work involves imaging the gel in PBS using TEM/SEM and comparing the fibre morphology with the images obtained for hydrogel **C12-urea-RGD** sonicated in pure water.

Medium	Result
Ultrapure water	Insoluble
PBS, pH 7.4 (10mM phosphate, 138mM NaCl)	Loose, transparent gel
Biol. SHE, pH 7 (2mM HEPES, 0.05mM EDTA, 150mM NaCl)	Insoluble

Table 4.2 – The choice of medium dictates the hydrogelation ability of **C12-urea-RGD** (1 mg/ml) using the heat-cool method. Yellow shading highlights the conditions which permit gel formation. Original in colour.

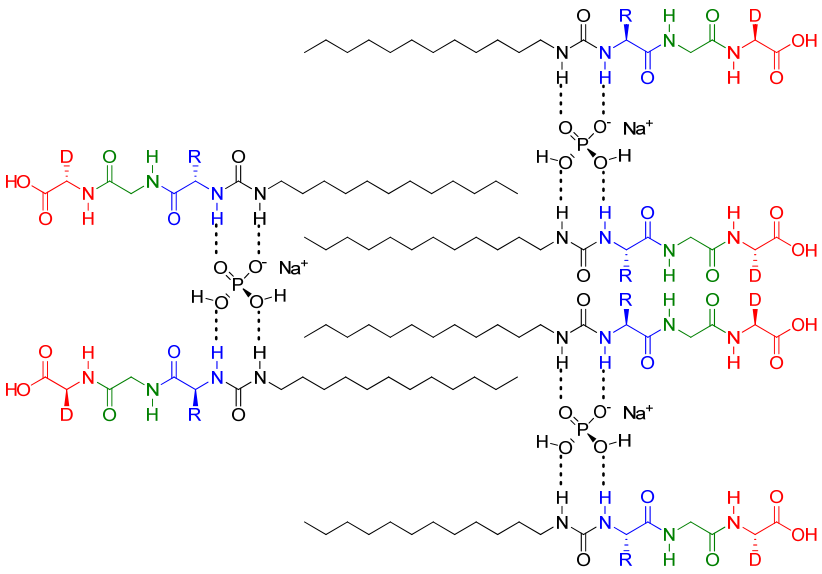

Scheme 4.21 – Proposed mechanism of self-assembly of **C12-urea-RGD** via phosphate coordination complexes. Note, sodium dihydrogen phosphate is shown as an example, however this is in equilibrium with disodium hydrogen phosphate, at pH 7.4, which could also coordinate. Original in colour.

To clearly distinguish the gel disrupting effect of phosphate compared to chloride in the case of bolaform gelator **C12-[urea-RGD]$_2$**, 1 mg/ml gelator samples were prepared in various concentrations of phosphate buffered water (containing 0.48 M sodium dihydrogen phosphate and 0.52 M disodium hydrogen phosphate – pH adjusted from 4 to 7 using aqueous NaOH), with no sodium chloride present, and these were compared with samples prepared in pure water containing different concentrations of sodium chloride (pH unadjusted, pH ~7) (Fig. 4.23).

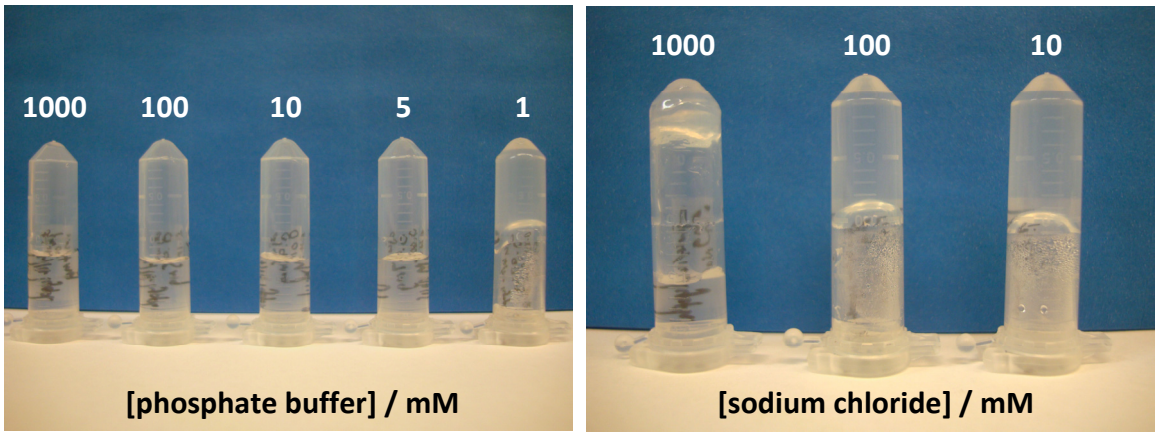

Fig. 4.23 – The effect of [phosphate] vs. [chloride] on the hydrogelation ability of **C12-[urea-RGD]$_2$** (1 mg/ml). pH was adjusted from 4 to 7 in the case of phosphate buffer but unadjusted (pH ~7) in the case of sodium chloride. Original in colour.

It is evident that gel formation is much more sensitive to phosphate levels than chloride – it is not until the concentration of phosphate has decreased to 1 mM that gel formation is observed, whereas even at 1 M sodium chloride a partial gel is formed and more stable gels are observed at concentrations of 100 mM and below. Interestingly, at 1 mg/ml **C12-[urea-RGD]$_2$**, the concentration of this gelator is 0.85 mM and hence there is 1.7 mM of functionalised ureas in solution owing to the gelator bearing two urea groups. Careful analysis of the data seems to indicate a critical phosphate concentration: only when the concentration of phosphate is less than the number of ureas in solution is gelation permitted via the intermolecular hydrogen bonding of the free/uncoordinated ureas. Chloride on the other hand does not seem to disrupt the sample spanning network by interfering with this interaction, at least not in the same concentration range tested as for phosphate, as chloride concentrations as high as 100 mM can be reached before disruption occurs upwards of this concentration.

We were keen to probe this further and understand whether this effect was due to the differentiation of oxy-anions over spherical anions; or perhaps due to anion charge density, as reflected in the anion basicity (pK_a value). **C12-[urea-RGD]$_2$** samples, at concentrations of 1 mg/ml, were screened in the

presence of different salt solutions, containing either oxy- or spherical anions, and the results tabulated (Table 4.3).

		[Anion] / M	
Anion[a]	**pK_a[b]**	**1**	**0.1**
$CH_3C(O)O^-$	4.75	S (8.3[c])	S (7.8[c])
$H_2PO_4^-$	2.15	S (7[d])	S (~7[d])
NO_3^-	-1.4	LG (6.3-6.5[c])	G (6.9[c])
Cl^-	-6.1	LG (~7[c])	G (~7[c])
Br^-	-9	LG (6.5[c])	G (6.1[c])
I^-	-9.5	P (9.4[c])	G (6.8[c])

[a] Counter-ion: Na^+. [b] pK_a of the corresponding acid in water at 25°C, *I*=0; *Pure Appl. Chem.*, **1969**, *20*, 133-236. [c] Unadjusted pH of the salt solution used. [d] Adjusted pH of the salt solution used; adjusted using aqueous NaOH. S = clear solution, LG = loose gel, G = gel, P = precipitate.

Table 4.3 – The effect of anion concentration and basicity on the hydrogelation ability of **C12-[urea-RGD]$_2$** (1 mg/ml) using the heat-cool method. Yellow shading highlights the conditions which permit gel formation. Original in colour.

The results reveal that gel formation is still permitted in the presence of different spherical anions such as bromide and iodide, in agreement with the observation made with chloride and, in line with the results observed with tetrahedral-shaped phosphate, planar-shaped acetate disrupts gel formation in the range of concentrations tested. However, in the presence of nitrate, an oxy-anion with a trigonal planar geometry like that of acetate, gel formation still occurs. We therefore conclude that the shape of the anion is not the determining factor on gelation ability, rather the basicity (or charge density) of the anion and this is apparent when the anions are ranked in order of basicity (Table 4.3). The more basic, charge dense anions such as acetate and phosphate have a greater affinity for the hydrogen bond-donating ureas and hence a greater propensity to disrupt the hydrogen-bonded network, whereas the less basic, charge diffuse anions from nitrate to iodide are less likely to coordinate. A similar trend has been observed with bis(urea)- and bis(thiourea)-based neutral receptors, in DMSO-d_6, for acetate but with particular selectivity for dihydrogen phosphate.[301, 302]

Further spectroscopic analysis of the gels is required to determine conclusively whether or not the breakdown of **C12-[urea-RGD]$_2$** hydrogels is a consequence of the direct binding of anions such as phosphate and acetate in water. If not, then the anion effect on gel stability may be related to their effect on the solubility of the compound, perhaps in a Hofmeister fashion. The Hofmeister series is shown in Figure 4.24, and Zang and Cremer have published a short review on the interactions between macromolecules and ions within the series.[303] The more hydrated anions are to the left of Cl^- and are salting-out (kosmotropes) which were originally found to reduce protein solubility, while the less hydrated anions to the right of Cl^- are salting-in (chaotropes) and increase protein solubility.

Unusually, it is phosphate, a kosmotropic anion, that induces gel breakdown (disaggregation and increased solubility) in our **C12-[urea-RGD]$_2$** system, whereas the chaotropic anions of nitrate, chloride, bromide and iodide all allow aggregation of the gelator to still take place. Hence, the observed efficacy seems to be linked to an *anti*-Hofmeister effect – a trend previously reported on by Ogden and co-workers with their proline-functionalised calix[4]arene: halide and nitrate salts triggered hydrogelation but sulfate afforded the same homogenous solution that the compound formed in the absence of anions.[304] To test our theory, attempting to form the gel in the presence of the other kosmotropic anions (carbonate, sulfate and thiosulfate) to see if gel formation is inhibited would be further evidence for this anti-Hofmeister trend.

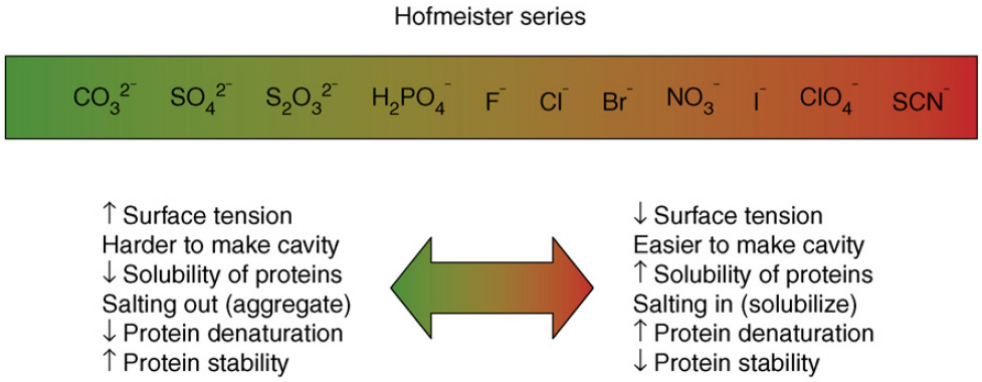

Fig. 4.24 – The Hofmeister series. Image reproduced from reference 303.

These findings are open to interpretation however, as phosphate is both a proton donor and acceptor and is therefore able to buffer its aqueous environment, whereas nitrate and the halide anions are non-buffering ions. This buffering effect on the ionisable groups in the RGD peptide may be the real reason for gel breakdown in the presence of phosphate. That said, the origin of the anion effect on **C12-[urea-RGD]$_2$** gel stability remains an open question and a complex area, due to the number/type of equilibria involved, requiring further investigation.

In any case, these qualitative and preliminary observations on the responsivity of **C12-[urea-RGD]$_2$** offer promising insight in the search for new water-based, anion-tunable soft materials – solution-phase anion recognition in water in its own right is a highly challenging concept in supramolecular chemistry – most anion-responsive gels only work in organic solvents. A current application of anion-reversible gels includes their use as crystal growth media for templating the growth of both inorganic and organic crystals, such as calcite[305] – important in understanding biomineralisation;[211, 306] and comparing gel phase with solution phase crystallisation of pharmaceuticals with different polymorphic forms[307] – an important issue in tuning the activity of pharmaceutical ingredients,[308] albeit these examples employ bis(urea) organogels which break down in response to anions allowing isolation of the crystalline material. Responsive materials such as **C12-[urea-RGD]$_2$** may find their place in

molecular sensor technology to monitor phosphate levels in waste water runoff for example, or as a controlled release device which breaks down and releases an encapsulated guest species in response to increasing levels of phosphate anions in the surrounding environment.

Further work will involve preparing gels in pure water and standing them with a phosphate solution suspended above the gel layer to monitor breakdown of the pure water gels over time; quantifying any differences in the response to phosphate compared with acetate; elucidating the selectivity, if any, and possible modification of the **C12-[urea-RGD]$_2$** structure to try and make it more selective towards one type of anion. However, this may prove quite challenging without compromising the current interesting gelation behaviour of this material of which its physicochemical properties need to be studied in more detail.

4.5.4 Small Molecule Encapsulation-Release

As observed by SEM, the fibrillar network of our bolaform gelator contains microcavities which, in the native state of the hydrogel, would be fluid-filled. Mixing via convection cannot occur between a gel and a surrounding fluid, only by diffusion, hence these microcavities could be utilised for encapsulation and controlled drug release.[216] In order to monitor the ability of our system to encapsulate and gradually release a guest species, the gel was self-assembled in the presence of fluorescent molecules of two different molecular sizes – an experiment which can be described as the "fishing net" experiment – a study adapted from a previously published method.[209] Firstly fluorescein, with a molecular weight of 332 g mol^{-1}, a model 'drug' compound, and secondly FITC-dextran (FITC: fluorescein isothiocyanate), with an average molecular weight of 70,000 g mol^{-1}, were incorporated within the gel to determine whether diffusion was limited by molecular size. **C12-[urea-RGD]$_2$** (5 mg/ml) was self-assembled into a hydrogel in an aqueous solution of the fluorescent molecule, making sure that all of the solution was incorporated into the hydrogel. To do this, a stock of the gelator was made in 200 μL of DMSO, and then 800 μL of a 50 μM stock solution of the fluorescent molecule was gently pipetted into the dissolved gelator. Gel formation was rapid and analysis was performed immediately afterwards (Fig. 4.25A).

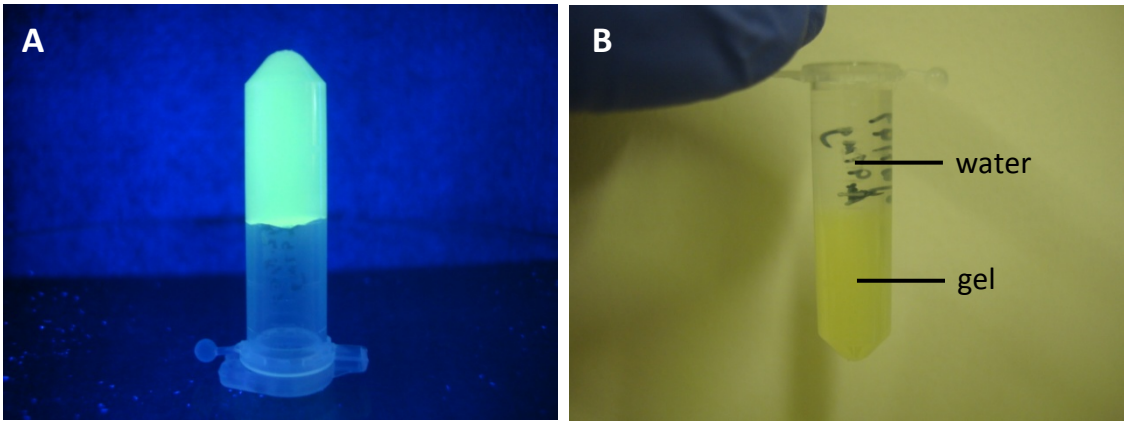

Fig. 4.25 – A) **C12-[urea-RGD]$_2$** (5 mg/ml) hydrogel with fluorescein encapsulated within it. B) The same gel sample covered with water (1 ml). Original in colour.

Next, the fluorescent gel sample was covered with 1 ml of Millipore pure water to determine whether or not diffusion of the fluorescent molecules occurred into the bulk water phase above the gel. (Fig. 4.25B). The water covering the gel was replaced with fresh water every 5 min and the fluorescence was recorded (Fig. 4.26).

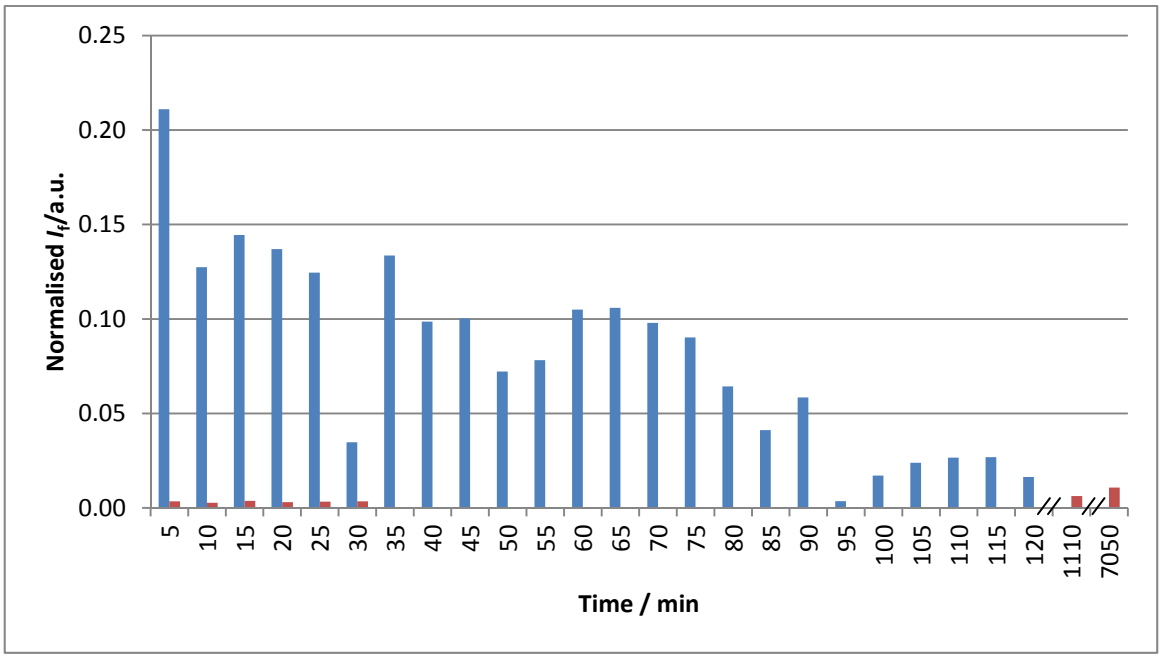

Fig. 4.26 – Normalised fluorescence emission at 512 nm and 521 nm from the water covering the gel, containing either fluorescein (blue) or FITC-dextran (red), respectively, as a function of time. Every 5 min, unless otherwise stated, the water was replaced with fresh water and the fluorescence measured. λ_{ex} = 495 nm. Original in colour.

It should be noted at this point that the total normalised fluorescence emission of fluorescein in the recovered water samples in this 2 h period was calculated to be almost 200%, which suggests that the amount of fluorescein released had doubled over that which we put in, which is obviously erroneous. We believe the reason for this error is a consequence of the DMSO/water preparation of the hydrogel. Pure water is suspended above the gel phase and if erratic leaching of DMSO from the gel into the pure water phase occurs, along with the migration of the fluorescein, then this will affect the fluorescence emission, which is solvent-dependent, resulting in a higher total fluorescence emission than expected. This was further confirmed, as the gel sample at the end of the 2 h period was still strongly fluorescent. An improvement in the experiment would be to prepare a shallower gel as fluorescein molecules at the base of the 1 ml gel sample shown here have further to diffuse than the ones nearer the surface i.e. the total release of guest is sample thickness-dependent. Nevertheless, this data clearly shows that fluorescein, the smaller of the two fluorescent molecules, exhibits typical diffusion behaviour from the gel within the experimental time range (5 to 120 min). For FITC-dextran, which is much larger, we see negligible fluorescence in the suspended water phase – even after suspending water above the gel at time point 30 min and leaving it until 1110 min (18 h) or beyond this until 7050 min (4 days) – as its diffusion is inhibited by the fibres which encapsulate it and is therefore retained in the gel network. We conclude that the hydrogel can retain molecules of size 70,000 g mol^{-1} or higher; whereas small molecules of a few hundred g mol^{-1} can readily diffuse out of the structure and into the surrounding environment over time. A more detailed study of the encapsulation and release of molecules, intermediate of the two size extremes investigated here, forms the basis of future work.

These results suggest that large molecules, such as proteins, should be trapped within the gel network for as long as the gel remains intact.[309] This allows us to propose interesting potential applications for **C12-[urea-RGD]$_2$** hydrogels as soft host materials, capable of size-dependent release or retention of guests. Two-stage controlled release of drug/protein combination therapies is one feasible application – the smaller drug molecules passively diffuse out of the gel over time, whilst the larger therapeutic protein molecules remain trapped until an appropriate anion is introduced to break down the gel and initiate a 'burst-phase' release of the protein.

4.6 Conclusions

A number of amphiphilic and bolaamphiphilic hydrogelators have been synthesised based around the linear RGD peptide motif. These materials, or derivatives thereof, have important potential applications as tissue engineering scaffolds owing to the multivalent display of the cell-adhesive RGD ligand on the gel fibres. The hydrophobic functionality at the N-terminus (and also at the C-terminus in the case of **C12-RGD-C12**), as well as whether the conjugation of the hydrophobe to the peptide is via an amide or urea group dictates whether or not these molecules form gels in water. **C12-RGD**, in

which the conjugating group is an amide, did not form hydrogels whereas **C12-urea-RGD** did after long periods of repeated vortexing and sonication, and was also found to gel PBS after heating and cooling. This compound no longer formed gels after introduction of lysine at the C-terminus (**C12-urea-RGDK**), presumably due to a change in the charge and/or packing constraints required to form gels. Bolaamphiphile **C12-[urea-RGD]$_2$** on the other hand formed the most thermally stable gels in water using the heat-cool method of gel formation – with a T_{gel} of 58°C and an MGC of 0.06 wt % (0.6 mg/ml, 0.5 mM); to the best of our knowledge one of the lowest MGCs reported in the literature and therefore constitutes a "super" hydrogel.

Attempts were made to synthesise linear and triangular-shaped hydrogelators with a more rigid aromatic framework (**linear OPE-[RGD]$_2$** and **triangular-shaped OPE-[RGD]$_3$**), however, characterisation of the final materials proved difficult, possibly due to aggregation of the compounds in solution, and the products were insoluble in a variety of organic solvents and water. Future work involves optimising the structures to provide the partial water solubility required to permit hydrogel formation, thus providing fundamental insight into the materials properties of hydrogelators which have a propensity to π-π stack based on an aromatic framework compared with the analogous compounds possessing aliphatic chains discussed throughout this chapter.

The hydrogelation properties of **C12-[urea-RGD]$_2$** were studied in more detail using CD, VT-CD and VT-NMR spectroscopy. It was demonstrated that **C12-[urea-RGD]$_2$** self-assembles with a β-sheet arrangement of the molecules and that this arrangement is temperature-responsive, as observed by CD and VT-CD. VT-NMR enabled us to propose a charge state for the RGD head group in the gel phase; this being one of a protonated guanidinium group on the arginine side-chain, where the positive charge is screened by the trifluoroacetate counter anion, and protonated carboxylic acids on the aspartic acid side-chain and C-terminus. All peaks in the ^{1}H NMR were found to increase in intensity with increasing temperature, which represents gel break down and increased solubility of individual molecules and soluble oligomers. In particular, the aspartic acid C*H*$_2$ and α-*H* were found to gradually shift further upfield with increasing temperature, which represents a gradual shift in the acid dissociation equilibrium towards deprotonated carboxylic acids adjacent to the aspartic acid C*H*$_2$ and α-*H* resulting in a shielded environment.

A check of the buffer and anion-tunability of **C12-[urea-RGD]$_2$** revealed that it did not form gels in the presence of charge dense, basic anions, such as phosphate and acetate, which strongly compete with the intermolecular urea-urea hydrogen bonding interactions, whereas in the presence of less basic, more charge diffuse anions, such as nitrate and chloride, gel formation was uninhibited. This discovery has important implications in water-based, anion-switchable, low MW supramolecular gels. Finally, an encapsulation-release study demonstrated the size-selective ability of **C12-[urea-RGD]$_2$** to release fluorescein, a small molecule guest encapsulated inside the gel structure, into surrounding

water via diffusion. However, the much larger polymeric FITC-dextran was trapped indefinitely inside the gel. We propose controlled drug delivery applications of this material, with a time profile of release tailored by the size of encapsulated guest; the size of the microcavities within the gel network, tuned by gelator concentration which determines the density of gel fibres; and/or the stimulated breakdown of the host material in response to anions in the surrounding environment.

Chapter 5

Conclusions & Future Work

5 Conclusions & Future Work

5.1 Chapter 2 – Dendritic Linear RGD Peptides

In this study we demonstrated the ability to couple linear RGD peptides to the surface of first and second generation Newkome-type dendrons, as well as the synthesis of positive and negative control peptides, and investigated the effect multivalency had on the integrin $\alpha_v\beta_3$ binding affinities of the dendritic constructs. Interestingly, the first generation dendron, **Z-G1-[RGD]$_3$** (**2.16**), displayed the most significant improvement in integrin $\alpha_v\beta_3$ binding over that of monovalent control **PEG-RGD** (**2.19**) whilst, rather counter-intuitively, the more highly branched second generation system, **Z-G2-[RGD]$_9$** (**2.17**), showed a diminished integrin $\alpha_v\beta_3$ binding profile and a greater degree of non-specific ligand-protein interaction in comparison.[274] The results suggest that there is an optimum number of RGD peptides that can be presented to allow enhanced integrin $\alpha_v\beta_3$ recognition, but that above this number the RGD peptides become sterically crowded and the specific binding affinity drops off whilst non-specific aggregation is promoted – at least with this form of RGD peptide and multivalent scaffold, as well as this choice of assay (FP) being used to monitor the binding event.

A non-exhaustive list of ideas for future work includes a systematic study into the effect on binding affinity of these dendritic linear RGDs by modifying the peptide in some way. These modifications could include flanking the RGD sequence with additional amino acids (e.g. RGDS) (Fig. 5.1A) to more accurately mimic the amino acid sequence found in fibronectin – the natural ECM protein for integrin $\alpha_v\beta_3$; conjugating the peptide via its C-terminus to an amine-terminated dendritic scaffold, effectively 'flipping' the sequence (Fig. 5.1B); or, as attempted at the end of Chapter 2, capping the C-terminus as a non-ionisable group such as a primary amide (Fig. 5.1C) – the synthesis of which requires further development – thereby rendering the peptide overall charge neutral and potentially reducing the amount of non-specific ligand-protein interaction which was thought to be arising from the free C-terminus and overall negative charge on the peptide.

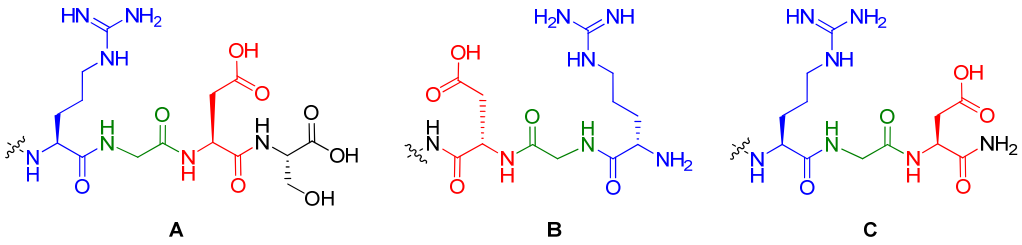

Fig. 5.1 – Ideas for future modification of the RGD peptide: A) RGDS sequence, B) conjugation to an amine-terminated dendritic scaffold via the C-terminus, C) amide-modified C-terminus.

An optimum number of linear RGDs exists between three and nine for the current dendritic system and, therefore, re-evaluating the structure of the dendron so that the number of branches can be

changed systematically – but without significantly changing the basic dendritic structure hence allowing direct comparison of analogues – would provide fundamental insight into the optimum number of RGDs required for highest affinity integrin binding. The dendritic scaffold could also be redesigned to make the branches longer, perhaps addressing flexibility, and thus the nonavalent G2 system might become less sterically challenged and maybe an improvement would be seen in its binding profile.

Ultimately, priority was given to comparing this covalent, dendritic approach to multivalency with a non-covalent, self-assembling strategy, by coupling different hydrophobic moieties to the linear RGD peptide and studying the effect on integrin $\alpha_v\beta_3$ recognition. A discussion of this work was subsequently given in Chapter 3.

5.2 Chapter 3 – Self-Assembling Linear RGD Peptides

A library of RGD lipopeptides was synthesised and evaluated for their self-assembly and integrin $\alpha_v\beta_3$ binding properties. Conjugating a C12 chain or a pyrene group to the RGD unit, **C12-RGD** (**3.2**) and **Py-RGD** (**3.4**) respectively, encouraged self-assembly into aggregates composed of spherical micelles and appeared to significantly enhance integrin $\alpha_v\beta_3$ binding over that of monovalent control **PEG-RGD**. Noteworthy is the fact that, in these two cases, this self-assembled (non-covalent) approach gave rise to slightly higher integrin binding affinities than that achieved using a first generation dendritic (covalent) scaffold to organise a multivalent ligand display.[274] We speculate that the dynamic nature of self-assembled micellar systems endows them with a greater degree of flexibility and responsiveness, and hence ligand arrays are presented with a better ability to recombine and adapt to satisfy the requirements of the integrin binding site. This is most evident when comparing self-assembling **C12-RGD** and **Py-RGD** with second generation dendron **Z-G2-[RGD]$_9$** – the self-assembly approach leading to significantly higher integrin $\alpha_v\beta_3$ affinities. In stark contrast to this, the longer hydrophobic-tailed **C22-RGD** (**3.6**) and twin-tailed system, **C12-Lys(C12)-(CH$_2$)$_5$-TEG-RGD** (**3.18**), generated rod-like micelles but significantly underperformed as ligands for integrin $\alpha_v\beta_3$. We reasoned this to be due to either the rigidity of the colloidal structures formed, leading to hindered systems which cannot adapt as well to the integrin binding site, or a possible increase in viscosity of the solutions as the concentration of rod-like micellar structures increases – FP is an inappropriate technique for systems with variable viscosity.

Future work involves monitoring the solutions comprised of **C22-RGD** and **C12-Lys(C12)-(CH$_2$)$_5$-TEG-RGD** for any change in viscosity with concentration, or if any thixotropic behaviour is exhibited, to verify whether or not the weak binding is due to the rigidity of the rod-like self-assembled structures or whether simply FP is unsuitable for testing these types of colloidal dispersions. A cell-based assay would also clarify the results obtained, not just for these two RGD

amphiphiles but for all of the dendrons and lipopeptides discussed throughout Chapters 2 and 3. This would allow us to compare the binding of our synthetic ligands to integrins held in cell membranes with the binding data obtained in the FP assays using purified integrins in solution.

Another interesting area of future work would involve the synthesis and testing of 'hybrid' molecules, using the information obtained in each of the previous two chapters to guide the structural design, comprised of RGD peptides on the surface of a first generation Newkome-type dendron and either a C12 tail or a pyrene unit coupled at the focal point (Fig. 5.2). These structures would have the propensity to self-assemble into micellar aggregates and, depending on the shape, possibly provide the flexibility and responsiveness required to satisfy the integrin binding site. They also possess a trivalent ligand display which was found to be less sterically crowded than that of the nonavalent second generation dendron. Synergistically, these two design criteria may well yield synthetic ligands with even further improvements in the specific binding affinity of linear RGD for integrin $\alpha_v\beta_3$.

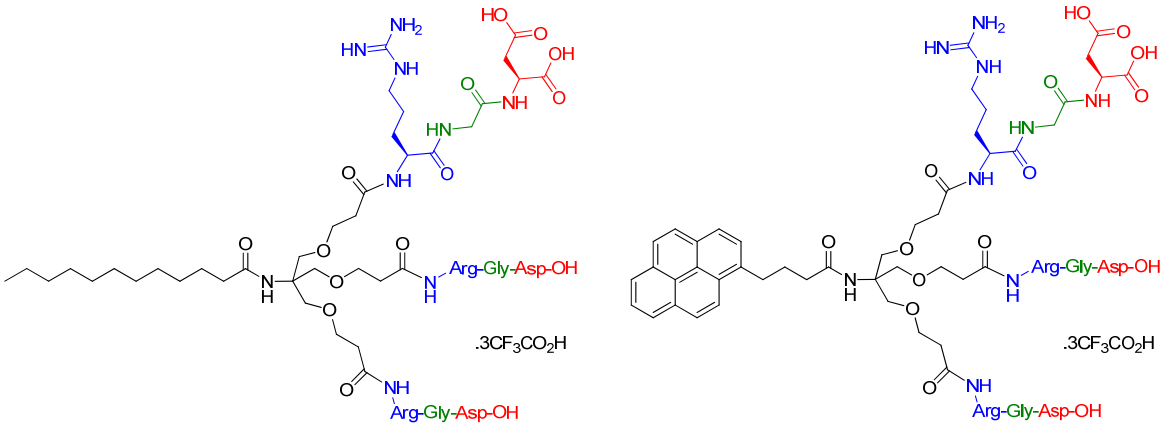

Fig. 5.2 – Self-assembling dendrons bearing linear RGD peptides – ideal future synthetic ligands for integrin $\alpha_v\beta_3$ based on the information obtained. Original in colour.

5.3 Chapter 4 – Linear RGD Peptide Conjugate Hydrogelators

Three new hydrogelators based around the linear RGD peptide motif – non-bolaform **C12-urea-RGD** (**4.2**), bolaform **C12-[urea-RGD]$_2$** (**4.4**) and inverse bolaform **C12-RGD-C12** (**4.18**) – have been designed, synthesised and studied. Gelation of **C12-urea-RGD**, under sonochemical stimulus, was compared to non-gelator **C12-RGD** (**3.2**) (conjugation of the C12 chain via an amide bond). This confirmed the important role played by the urea group in the self-assembly of **C12-urea-RGD** in pure water to form a hydrogen-bonded, sample-spanning, fibrous network, with contributions from the hydrophobic effect and van der Waals interactions of the alkyl chains also presumably playing a stabilising role. Hydrogels of the bolaform analogue, **C12-[urea-RGD]$_2$**, under thermal stimulus, demonstrated significantly improved and quantifiable stability (T_{gel}) and very low MGC values in pure water constituting a "super" hydrogel – consequences we believe to be due to: (i) the double RGD

head groups provide better water solubility at elevated temperatures and hence more material gets into solution to initiate gelation at lower concentrations using the heat-cool method of gel formation, compared with sonication which limits the persistence length of fibre formation, and (ii) the bolaamphiphilic structure leads to better preorganisation of the hydrophilic and hydrophobic units for fibrillar self-assembly and should enhance intermolecular contacts.

Shorter alkyl chains than C12 (**C6-urea-RGD** (**4.6**) and **C6-[urea-RGD]$_2$** (**4.8**)) did not permit gelation and resulted in water soluble materials, whereas attempts at swapping the linear aliphatic spacer for an aromatic one (**CH$_2$-[Ar-urea-RGD]$_2$** (**4.10**), **linear OPE-[RGD]$_2$** (**4.23**), and **triangular-shaped OPE-[RGD]$_3$** (**4.27**)) yielded precipitates and insoluble materials – confirming that not only is the urea group important, but the length of hydrocarbon tail/spacer (and type of spacer) also dictates whether a molecule is a gelator or not. In contrast to these examples, hydrogels arising from bolaform **C12-RGD-C12**, under sonochemical stimulus, proved that urea groups were not always necessary to direct self-assembly. However, it is apparent that the hydrophobicity of the molecule had to be increased, by amide-coupling a C12 chain to the C-terminus as well as the N-terminus of the peptide, in order to promote gelation via the hydrophobic effect and van der Waals interactions.

Further studies with **C12-[urea-RGD]$_2$** using CD, VT-CD and VT-NMR demonstrated the temperature-responsive and thermoreversible nature of the gel, a β-sheet arrangement of the molecules in the gel fibrils, and an indication of the charge state of the RGD head group in pure water gels. Anion-triggered gel breakdown was demonstrated in the presence of phosphate and acetate anions. Another external chemical stimulus which could be considered for breaking down the gels includes enzymes such as ureases. Small molecule encapsulation-release from the gel was also observed, whilst large molecules were trapped within the gel network. Future work is required to investigate the encapsulation and release of molecules that are intermediate of the two size extremes of fluorescein (a small molecule) and FITC-dextran (a large polysaccharide). Collectively, these observations lend this functional material to potential applications ranging from controlled drug delivery implants to anion-tunable soft materials in sensor devices.

Other methods of physical property characterisation, for future reference, include rheology which can be used to measure the viscosity as well as the elastic modulus (G') with respect to the loss modulus (G") of a gel under oscillatory shear at constant or increasing temperature; AFM as an alternative means of imaging the xerogel fibres on a surface providing height profiles of the material as well as other useful sizing information; and small angle X-ray/neutron scattering (SAXS/SANS) which are also useful for obtaining fibre dimensions and elucidating the spatial orientation of the self-assembled molecules within the gel fibres based on computer modelling of the data. pK_a measurements of the RGD head group in our gelators would provide quantitative insight into the charge state of the

peptide when in the gel state compared to the sol state, as well as the effect of pH on gel formation/breakdown.

There are a number of possibilities for developing these materials further. Examples include, but are not limited to, extending the length of the tail/spacer beyond C12 to look at the effect on gelation, and synthesising derivatives of **C6/C12-[urea-RGD]$_2$** with spacer lengths between C6 and C12 to determine what length is limiting to gelation. Covalent cross-linking of the fibres formed from a future derivative of the structure discussed in this work, via a chemically- or photo-initiated reaction for example, may result in more robust materials that possess greater thermal stability and are more stable towards mechanical stress. An example would be the incorporation of a polymerisable diacetylene segment into the backbone of **C12-[urea-RGD]$_2$**. If nanofibres are still able to form after derivatising the molecule in this way (formed by physical interaction only), irradiation with UV light can be used to permanently hold the self-assembled structures together (Fig 5.3) thereby improving the toughness of the material (although it is appreciated that anion-responsivity would perhaps no longer be observed). Stupp and co-workers have carried out similar work on chemically cross-linked RGD peptide amphiphile hydrogelators, albeit with more elaborate versions of the peptide and using non-bolaform amphiphiles.[310]

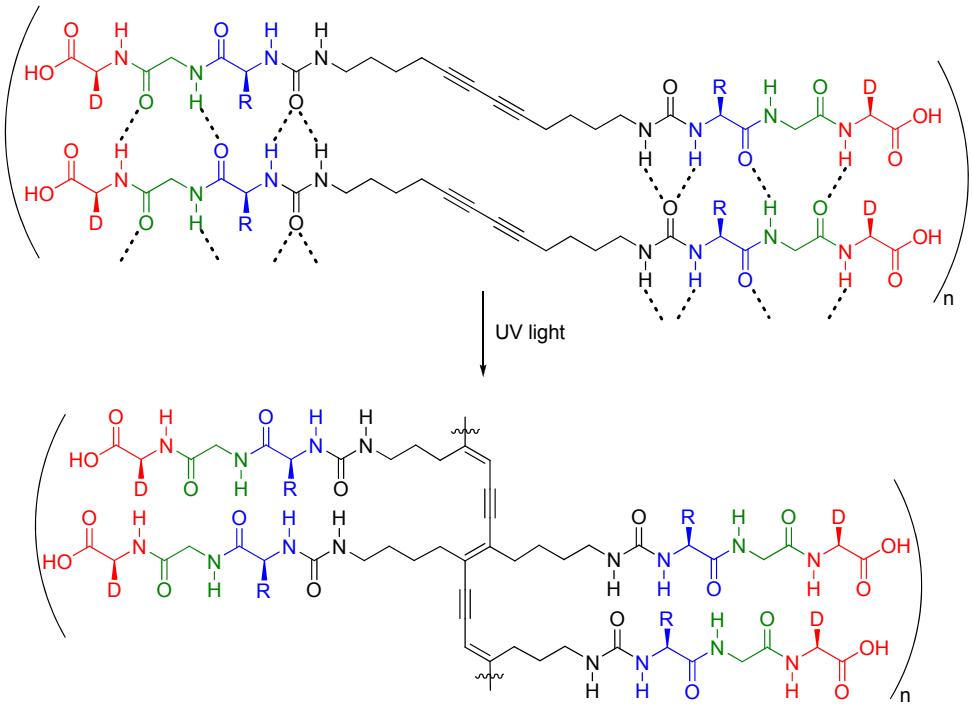

Fig. 5.3 – Photochemical cross-linking of diacetylenes in a hypothetical, self-assembling derivative of **C12-[urea-RGD]$_2$**.

Preliminary attempts to grow cells on the surface of the gels indicated toxicity, which may be associated with the TFA counter anion in **C12-[urea-RGD]$_2$**, as the pH indicator in the cell culture

medium indicated an increasingly acidic solution with increasing gelator concentration which was extremely detrimental to cell viability. To overcome this, an idea would be to exchange the TFA with a more biocompatible anion such as chloride using either an anion exchange column or dialysis. This might not be as trivial as it first seems though due to the compounds having either limited or no water solubility, therefore, the synthesis would have to be readdressed at the protecting group level so that the Pbf protecting group on the arginine is swapped for one that is labile to a reagent other than TFA. It should be noted that work towards this goal was carried out in an attempt to deprotect the peptide using 4 M HCl in 1,4-dioxane, commonly used in the deprotection of Boc-protected amines,[311] which would have resulted in chloride being the counter anion associated with the protonated guanidinium of the arginine side-chain, but unfortunately this was not a strong enough acid to hydrolyse the Pbf group. Nevertheless, anion exchange should be approached with caution – exchanging the TFA, possibly of significant importance to the gel forming process, for an alternative anion might result in the material no longer forming hydrogels (although chloride anions were still compatible with gelation).

Chapter 6

Experimental

6 Experimental

6.1 General Materials and Methods

All solvents and reagents were commercially available and used as supplied without further purification unless otherwise stated. Human integrin $\alpha_v\beta_3$ Triton X-100 formulation purified protein was purchased from Millipore and used without further purification. Column chromatography was performed on silica using silica gel 60 provided by Fluka Ltd. (35-70 μm) while TLC was performed on Merck aluminium-backed plates, coated with 0.25 mm silica gel 60. Spots were visualised either by UV, or by use of an appropriate stain (ninhydrin solution 0.2% (by mass) in ethanol or cerium molybdate stain: 180 ml H_2O, 20 ml conc. H_2SO_4, 5 g ammonium dimolybdate, 2 g cerium sulfate). Preparative gel permeation chromatography was carried out using Bio-Beads SX-1 supplied by Bio-Rad. Preparative gel filtration chromatography was carried out using Sephadex LH-20 purchased from Sigma Aldrich.

Nuclear magnetic resonance chemical shifts (δ) are reported in ppm using residual solvent as internal reference, as noted, and peak assignments were deduced with ^{13}C/DEPT-135 as well as 2D NMR experiments such as COSY and HSQC. All spectra were recorded on either a JEOL ECX400 or a JEOL ECS400 (^1H 400 MHz, ^{13}C 100 MHz) spectrometers or a JEOL EX270 (^1H 270 MHz, ^{13}C 68 MHz) spectrometer, as noted. In some cases a Bruker 500 (^1H 500 MHz, ^{13}C 125 MHz) spectrometer was used. All *J* values are reported to the nearest 0.5 Hz. ESI and HR ESI mass spectra were recorded on Thermo-Finnigan LCQ and Bruker Daltonics MicrOTOF mass spectrometers, respectively. In some cases, a Bruker Daltonics MicrOTOF II mass spectrometer was used to record both ESI and HR ESI mass spectra. EI mass spectra were recorded on a Waters GCT Premier TOF mass spectrometer. In the mass spectra, all compounds presented the expected isotope patterns. Infrared spectra were recorded using a Shimadzu IR Prestige-21 FT-IR spectrometer. Melting points were measured on a Gallenkamp or Stuart melting point apparatus and are uncorrected. Optical rotation was measured as $[\alpha]_D$ on a JASCO DIP-370 digital polarimeter. UV-Vis spectra were recorded on a Shimadzu UV 2401 PC UV-Vis spectrophotometer. Fluorescence data was collected on a Hitachi F-4500 and FluoroMax-4 spectrofluorimeters. Fluorescence polarisation data was collected on FluoroMax-3 and FluoroMax-4 spectrofluorimeters. Circular dichroism spectra were recorded on a Jasco J810 CD spectrophotometer. T_{gel} values were recorded on a high precision thermoregulated oil bath. TEM was carried out on a FEI Tecnai 12 BioTWIN running at 120 kV. SEM was carried out on a JEOL JSM-7500F. ASEM was carried out on a JEOL Clairscope, JASM-6200.

Dendritic compounds **2.9-2.12**[259] and **2.13**[10] have been previously reported but are included with full characterisation for completeness and to assist reproduction of the work as some of the methods have been adapted. The synthesis of **c[R(Pbf)GD(O^{t}Bu)fK(Z)]**, **2.21**, was adapted from previously

published methods.[97, 127, 262] The solid-phase methodology of our solution-phase-synthesised **5(6)-FL-c[RGDfK]**, **2.24**, has been previously reported although no characterisation data was provided by the authors.[75] Compounds **3.2**,[267] **3.9**,[268] **3.10**,[268] **3.13**[269] and **3.14**[269] have been made previously but are included with full characterisation for completeness and to assist reproduction of the work as some of the methods have been adapted. Compounds **4.24**[276] and **4.25**[277] were obtained according to literature procedures, and the synthesis of **4.20** and **4.21** was adapted from these methods.

Note, amino acids are referred to using either three or one letter abbreviations and are used interchangeably throughout this chapter.

6.2 Chapter 2 – Dendritic Linear RGD Peptides

Synthesis of Fmoc-Gly-Asp(O^{t}Bu)-O^{t}Bu (2.1)

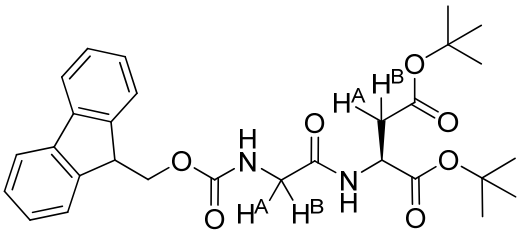

H_2N-Asp(O^{t}Bu)-O^{t}Bu.HCl (2.85 g, 10.1 mmol, 1.0 eq) and Fmoc-Gly-OH (3.01 g, 10.1 mmol, 1.0 eq) were dissolved in DCM (100 ml) upon addition of DIPEA (3.52 ml, 20.2 mmol, 2.0 eq) with stirring. The solution was cooled in an ice-water bath to 0°C and then T3P (50 wt. % in EtOAc, 7.25 ml, 12.3 mmol, 1.2 eq) was added dropwise over 20 min. The ice-water bath was removed and the reaction mixture was stirred at rt for 24 h. The reaction was quenched with water (100 ml), and then the organic layer was washed with saturated $NaHCO_3$ (100 ml), 1.33 M $NaHSO_4$ (100 ml), saturated $NaHCO_3$ (100 ml), neutralising to pH 7 and finally water (100 ml). The organic layer was dried over $MgSO_4$ and filtered before removing the solvent *in vacuo* to produce the product **2.1** as a white foam (4.90 g, 93%). No further purification was required.

R_f 0.64 (9:1 DCM/MeOH, UV and cerium stain). $[\alpha]_D$ = +22.9° (c = 1.0, $CHCl_3$). M.p: 54.4-60.2°C. ^{1}H NMR ($CDCl_3$, 400 MHz) δ 7.76 (d, C*H* aromatic, *J* = 8.0 Hz, 2H); 7.60 (d, C*H* aromatic, *J* = 8.0 Hz, 2H); 7.40 (t, C*H* aromatic, *J* = 8.0 Hz, 2H); 7.31 (t, C*H* aromatic, *J* = 8.0 Hz, 2H); 6.86 (d, N*H* amide, *J* = 8.0 Hz, 1H); 5.45 (br s, N*H* carbamate, 1H); 4.70 (dt, Asp α-*H*, *J* = 8.0 Hz and 4.0 Hz, 1H); 4.39 (d, Fmoc CH_2, *J* = 7.0 Hz, 2H); 4.24 (t, Fmoc C*H*, *J* = 7.0 Hz, 1H); 3.98 (dd, Gly CH^A, *J* = 17.0 Hz and 5.0 Hz, 1H); 3.92 (dd, Gly CH^B, *J* = 17.0 Hz and 5.0 Hz, 1H); 2.91 (dd, Asp CH^A, *J* = 17.0 Hz and 4.5 Hz, 1H); 2.72 (dd, Asp CH^B, *J* = 17.0 Hz and 4.5 Hz, 1H); 1.45 (s, C(CH_3)$_3$, 9H); 1.42 (s, C(CH_3)$_3$, 9H). ^{13}C NMR ($CDCl_3$, 100 MHz) δ 170.30, 169.60, 168.69 (*C*(O)O^{t}Bu × 2, *C*(O)NH amide); 156.53 (*C*(O)NH carbamate); 143.92, 141.35 (*C* aromatic); 127.80, 127.19, 125.24, 120.06 (*C*H

aromatic); 82.66, 81.82 (*C*(CH_3)$_3$ × 2); 67.36 (Fmoc *C*H_2); 49.19 (Asp α-*C*H); 47.16 (Fmoc *C*H); 44.40 (Gly *C*H_2); 37.44 (Asp *C*H_2); 28.11, 27.97 (C(*C*H_3)$_3$ × 2). $\tilde{\nu}_{max}$ (cm^{-1}) (solid): 3314*w* (N-H amide stretch); 3086*w* (C-H arene stretch); 2979*w* (C-H alkyl stretch); 1723*s* (C=O ester stretch); 1665*s* (C=O amide stretch); 1506*s* (N-H amide bend and C=C arene stretch); 1478*w*, 1450*m*, 1394*w*, 1367*m* (C-H alkyl bends); 1244*s*, 1224*s*, 1145*s*, 1045*m*, 1002*w* (C-O ester and C-N amide stretches, C-H arene bends); 948*w*, 845*m*, 759*s*, 739*s* (C-H arene bends). ESI-MS (*m*/*z*): Calc. for $C_{29}H_{36}N_2NaO_7$ 547.2415; found: 547.2411 (100%, $[M+Na]^+$); 491.1782 (15%, $[M+Na–C_4H_8]^+$); 435.1157 (79%, $[M+Na–2C_4H_8]^+$).

Synthesis of H_2N-Gly-Asp(O^{t}Bu)-O^{t}Bu (2.2)

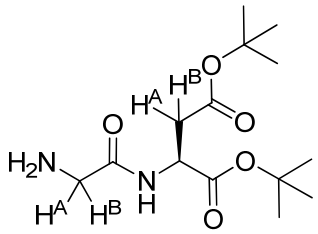

Compound **2.1** (4.58 g, 8.74 mmol) was stirred in a solution of 20% piperidine in DCM (30 ml). The solvent was removed *in vacuo* after stirring for 4 h to produce a pale yellow crude solid (6.62 g). The crude solid was purified by column chromatography (SiO_2, 9:1 DCM/MeOH) to yield **2.2** as a clear colourless oil (2.16 g, 82%).

R_f 0.20 (9:1 DCM/MeOH, ninhydrin stain). $[\alpha]_D$ = +36.5° (c = 1.0, $CHCl_3$). ^{1}H NMR ($CDCl_3$, 400 MHz) δ 7.99 (d, N*H* amide, 8.0 Hz, 1H); 4.71 (dt, Asp α-*H*, *J* = 8.5 Hz and 4.5 Hz, 1H); 3.39 (d, Gly C*H*^{A}, *J* = 17.5 Hz, 1H); 3.34 (d, Gly C*H*^{B}, *J* = 17.5 Hz, 1H); 2.89 (dd, Asp C*H*^{A}, *J* = 17.0 Hz and 4.5 Hz, 1H); 2.70 (dd, Asp C*H*^{B}, *J* = 17.0 Hz and 4.5 Hz, 1H); 1.53 (br s, N*H*$_2$, 2H); 1.45 (s, C(C*H*$_3$)$_3$, 9H); 1.44 (s, C(C*H*$_3$)$_3$, 9H). ^{13}C NMR ($CDCl_3$, 100 MHz) δ 172.61, 169.95, 169.79 (*C*(O)O^{t}Bu × 2, *C*(O)NH amide); 82.10, 81.43 (*C*(CH_3)$_3$ × 2); 48.58 (Asp α-*C*H); 44.68 (Gly *C*H_2); 37.71 (Asp *C*H_2); 27.99, 27.86 (C(*C*H_3)$_3$ × 2). $\tilde{\nu}_{max}$ (cm^{-1}) (oil): 3357*w* (N-H amine and amide stretches); 2978*w*, 2936*w* (C-H alkyl stretches); 1726*s* (C=O ester stretch); 1666*s* (C=O amide stretch); 1509*s* (N-H amide bend); 1480*w*, 1458*w*, 1394*w*, 1367*s*, 1350*m* (C-H alkyl bends); 1288*m*, 1249*m*, 1226*m*, 1145*s* (C-O ester and C-N stretches); 1079*w*; 1051*w*; 1032*w*; 845*m*; 752*w*; 732*w*. ESI-MS (*m*/*z*): Calc. for $C_{14}H_{26}N_2NaO_5$ 325.1734; found: 325.1739 (60%, $[M+Na]^+$); 303.1953 (100%, $[M+H]^+$); 247.129 (17%, $[M+H–C_4H_8]^+$); 191.0659 (10%, $[M+H–2C_4H_8]^+$).

Synthesis of Fmoc-Arg(Pbf)-Gly-Asp(O^{t}Bu)-O^{t}Bu (2.3)

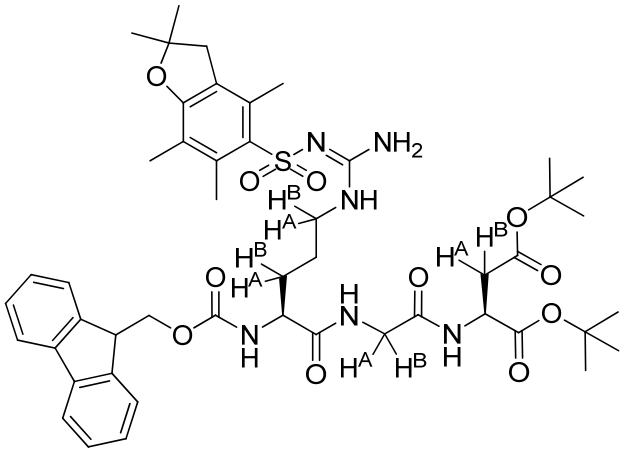

Compound **2.2** (2.02 g, 6.68 mmol, 1.0 eq) and Fmoc-Arg(Pbf)-OH (4.33 g, 6.68 mmol, 1.0 eq) were dissolved in DCM (120 ml) upon addition of DIPEA (2.42 ml, 13.9 mmol, 2.0 eq) with stirring. The solution was cooled in an ice-water bath to 0°C and then T3P (50 wt. % in EtOAc, 5.00 ml, 8.49 mmol, 1.2 eq) was added dropwise over 20 min. The ice-water bath was removed and the reaction mixture was stirred at rt for 24 h. The reaction was quenched with water (100 ml), and then the organic layer was washed with saturated $NaHCO_3$ (100 ml), 1.33 M $NaHSO_4$ (100 ml), saturated $NaHCO_3$ (100 ml), neutralising to pH 7 and finally water (100 ml), upon which the organic phase became milky white. The organic layer was dried over $MgSO_4$ and filtered before removing the solvent *in vacuo* to produce the product **2.3** as a white foam (4.90 g, 79%). No further purification was required.

R_f 0.51 (9:1 DCM/MeOH, UV and cerium stain). $[\alpha]_D$ = +8.6° (c = 1.0, $CHCl_3$). M.p: 114.0-120.0°C. ^{1}H NMR ($CDCl_3$, 400 MHz) δ 7.73 (d, C*H* aromatic, *J* = 7.5 Hz, 2H); 7.70 (m, N*H* amide (Arg-Gly), 1H); 7.58 (m, C*H* aromatic, 2H); 7.36 (t, C*H* aromatic, *J* = 7.0 Hz, 2H); 7.26 (t, C*H* aromatic, *J* = 7.5 Hz, 2H); 7.11 (d, N*H* amide (Gly-Asp), *J* = 7.5 Hz, 1H); 6.33 (br s, NH_2 guanidine, 2H); 6.12 (br s, N*H* guanidine, 1H); 6.04 (d, N*H* carbamate, *J* = 7.5 Hz, 1H); 4.64 (dt, Asp α-*H*, *J* = 8.0 Hz and 5.0 Hz, 1H); 4.44-4.37 (m, Arg α-*H*, 1H); 4.34 (d, Fmoc CH_2, *J* = 7.0 Hz, 2H); 4.16 (t, Fmoc C*H*, *J* = 7.0 Hz, 1H); 4.06 (dd, Gly CH^A, *J* = 16.5 Hz and 5.5 Hz, 1H); 3.91 (dd, Gly CH^B, *J* = 17.0 Hz and 5.0 Hz, 1H); 3.42-3.28 (m, Arg CH^ANH, 1H); 3.24-3.14 (m, Arg CH^BNH, 1H); 2.92 (s, Pbf CH_2, 2H); 2.82 (dd, Asp CH^A, *J* = 17.0 Hz and 5.0 Hz, 1H); 2.66 (dd, Asp CH^B, *J* = 17.0 Hz and 4.5 Hz, 1H); 2.59 (s, Pbf CH_3Ar, 3H); 2.51 (s, Pbf CH_3Ar, 3H); 2.07 (s, Pbf CH_3Ar, 3H); 2.01-1.89 (m, Arg CHCH^A, 1H); 1.76-1.66 (m, Arg CHCH^B, 1H); 1.65-1.50 (m, Arg CH_2CH$_2$NH, 2H); 1.43 (s, Pbf CH_3 × 2, 6H); 1.40 (s, C(CH_3)$_3$ × 2, 18H). ^{13}C NMR ($CDCl_3$, 100 MHz) δ 173.07, 170.17, 169.82, 169.39 (*C*(O)O^{t}Bu × 2, *C*(O)NH amide × 2); 158.79, 156.68, 156.56 (Pbf aromatic *C*-O, *C*=N guanidine, *C*(O)NH carbamate); 143.96, 143.84, 141.30, 141.28 (Fmoc aromatic *C*); 138.46, 132.86, 132.37 (Pbf aromatic

C); 127.73, 127.15, 125.31 (Fmoc aromatic *C*H); 124.67 (Pbf aromatic *C*); 119.97 (Fmoc aromatic *C*H); 117.56 (Pbf aromatic *C*); 86.42 (Pbf $CH_2C(CH_3)_2O$); 82.66, 81.73 ($C(CH_3)_3$ × 2); 67.14 (Fmoc CH_2); 54.33 (Arg α-*C*H); 49.45 (Asp α-*C*H); 47.14 (Fmoc *C*H); 43.28, 42.90, 40.20 (Pbf ArCH_2, Gly CH_2, Arg CH_2NH); 37.37 (Asp CH_2); 29.88 (Arg $CHCH_2$); 28.65 (Pbf $CH_2C(CH_3)_2O$); 28.08, 27.92 ($C(CH_3)_3$ × 2); 25.28 (Arg CH_2CH_2NH); 19.43, 18.08, 12.57 (Pbf ArCH_3 × 3). $\tilde{\nu}_{max}$ (cm^{-1}) (solid): 3422*w*, 3321*w* (N-H amide stretches); 2974*w*, 2932*w* (C-H alkyl and arene stretches); 1724*m* (C=O ester stretch); 1667*m*, 1620*m* (C=O amide stretches); 1543*s* (N-H amide bend and C=C arene stretch); 1450*m*, 1408*w*, 1393*w*, 1366*m* (C-H alkyl bend and S=O stretch); 1281*m*, 1246*s*, 1150*s*, 1103*s*, 1088*s* (C-O ester and C-N amide stretches, C-H arene bends); 1034*m*, 991*m*, 849*m*, 818*w*, 756*w*, 737*m*, 660*m* (C-H arene bends); 640*m*; 617*m*; 598*m*. ESI-MS (*m/z*): Calc. for $C_{48}H_{65}N_6O_{11}S$ 933.4427; found: 933.4426 (100%, $[M+H]^+$).

Synthesis of H_2N-Arg(Pbf)-Gly-Asp(O^{t}Bu)-O^{t}Bu (2.4)

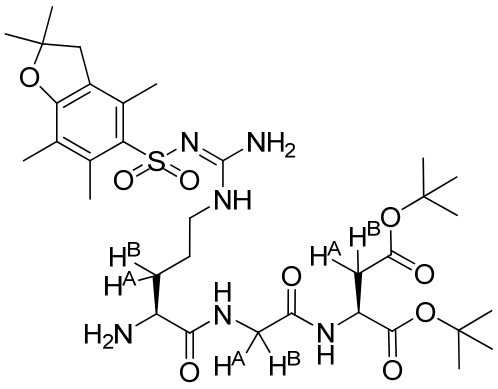

Compound **2.3** (4.51 g, 4.84 mmol) was stirred in a solution of 20% piperidine in DCM (30 ml). The solvent was removed *in vacuo* after stirring for 3 h to produce a pale yellow crude solid (7.5 g). The crude solid was purified by column chromatography (SiO_2, 9:1 DCM/MeOH) to yield **2.4** as a fluffy white solid (2.75 g, 80%).

R_f 0.15 (9:1 DCM/MeOH, UV and ninhydrin stain). $[\alpha]_D$ = +18.2° (c = 1.0, $CHCl_3$). M.p: 83.0-84.0°C. ^{1}H NMR ($CDCl_3$, 400 MHz) δ 7.98 (t, N*H* amide (Arg-Gly), *J* = 6.0 Hz, 1H); 7.10 (d, N*H* amide (Gly-Asp), *J* = 8.0 Hz, 1H); 6.32 (br s, NH_2 guanidine, 2H); 6.14 (br s, N*H* guanidine, 1H); 4.64 (dt, Asp α-*H*, *J* = 8.0 Hz and 4.5 Hz, 1H); 4.02 (dd, Gly CH^A, *J* = 17.0 Hz and 5.5 Hz, 1H); 3.90 (dd, Gly CH^B, *J* = 17.0 Hz and 6.0 Hz, 1H); 3.49-3.46 (m, Arg α-*H*, 1H); 3.27-3.15 (br m, Arg CH_2NH, 2H); 2.95 (s, Pbf CH_2, 2H); 2.86 (dd, Asp CH^A, *J* = 17.0 Hz and 5.0 Hz, 1H); 2.70 (dd, Asp CH^B, *J* = 17.0 Hz and 4.5 Hz, 1H); 2.57 (s, Pbf CH_3Ar, 3H); 2.50 (s, Pbf CH_3Ar, 3H); 2.08 (s, Pbf CH_3Ar, 3H); 1.82-1.74 (m, Arg CHCH^A, 1H); 1.72-1.53 (m, Arg CHCH^B and Arg C$H_2$$CH_2$NH, 3H); 1.45 (s, Pbf C$H_3$ × 2, 6H); 1.424, 1.418 (s × 2, C(CH_3)$_3$ × 2, 18H). ^{13}C NMR ($CDCl_3$, 100 MHz) δ 176.41, 170.32, 169.79, 169.34 (*C*(O)O^{t}Bu × 2, *C*(O)NH amide × 2); 158.69, 156.49 (Pbf aromatic *C*-O, *C*=N

guanidine); 138.30, 133.05, 132.23, 124.62, 117.48 (Pbf aromatic *C*); 86.42 (Pbf $CH_2C(CH_3)_2O$); 82.61, 81.76 ($C(CH_3)_3 \times 2$); 54.54 (Arg α-*C*H); 49.27 (Asp α-*C*H); 43.28, 42.76, 40.61 (Pbf Ar*C*H_2, Gly *C*H_2, Arg *C*H_2NH); 37.38 (Asp *C*H_2); 32.08 (Arg CH*C*H_2); 28.66 (Pbf $CH_2C(CH_3)_2O$); 28.09, 27.93 ($C(CH_3)_3 \times 2$); 25.42 (Arg *C*H_2CH_2NH); 19.36, 18.02, 12.55 (Pbf Ar*C*$H_3 \times 3$). $\tilde{\nu}_{max}$ (cm^{-1}) (solid): 3320*w* (N-H amide stretch); 2972*w* (C-H alkyl stretch); 1735*w* (C=O ester stretch); 1647*w* (C=O amide stretch); 1540*w* (N-H amide bend, C-H alkyl bend, C=C arene stretch and S=O stretch); 1251*w*, 1145*w* (C-O ester and C-N amide stretches). ESI-MS (*m*/*z*): Calc. for $C_{33}H_{55}N_6O_9S$ 711.3746; found: 711.3761 (93%, $[M+H]^+$); 733.3608 (100%, $[M+Na]^+$); 367.1796 (73%, $[M+H+Na]^{2+}$).

Synthesis of Z-Gly-Asp(O^{t}Bu)-O^{t}Bu (2.5)

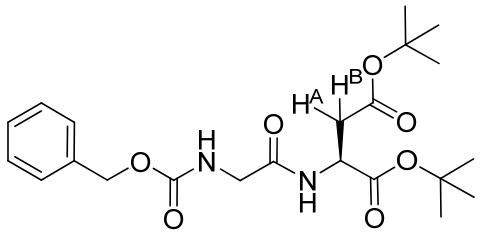

H_2N-Asp(O^{t}Bu)-O^{t}Bu.HCl (5 g, 17.8 mmol, 1.0 eq) was dissolved in DCM (100 ml) and DIPEA (6.2 ml, 35.6 mmol, 2.0 eq) was added. The reaction flask was cooled over an ice-water bath then Z-Gly-OH (3.72 g, 17.8 mmol, 1.0 eq) was added as a solid. TBTU (5.71 g, 17.8 mmol, 1.0 eq) was added as a solid and the reaction was stirred at 0°C for a further 20 min before removing the ice-water bath and stirring the reaction at rt for 17 h. The organic phase was washed successively with 1.33 M $NaHSO_4$ (300 ml), saturated $NaHCO_3$ (300 ml), 1.33 M $NaHSO_4$ (300 ml), saturated $NaHCO_3$ (300 ml), water (300 ml), and finally brine (300 ml). The organic phase was dried over $MgSO_4$ and filtered before removing the solvent *in vacuo* to produce the product as a clear, colourless oil which turned to a white solid overnight (~9 g). ^{1}H NMR indicated that the product still contained some urea by-product from the TBTU reaction and so the residue was re-dissolved in EtOAc (100 ml) and washed with water (3 x 100 ml). The organic phase was dried over $MgSO_4$ and filtered before removing the solvent *in vacuo* to produce the product **2.5** as a white solid (7.26 g, 94%). No further purification was required.

R_f 0.62 (9:1 DCM/MeOH, cerium stain). $[\alpha]_D$ = +29.4° (c = 1.0, $CHCl_3$). M.p not acquired. ^{1}H NMR ($CDCl_3$, 400 MHz) δ 7.34-7.27 (m, C*H* aromatic, 5H); 6.98 (d, N*H* amide, *J* = 8.0 Hz, 1H); 5.59 (br t, N*H* carbamate, *J* = 5.0 Hz, 1H); 5.10 (s, CH_2 benzylic, 2H); 4.68 (dt, Asp α-*H*, *J* = 8.0 Hz and 4.5 Hz, 1H); 3.91 (br m, Gly CH_2, 2H); 2.86 (dd, Asp CH^A, *J* = 17.0 Hz and 4.5 Hz, 1H); 2.70 (dd, Asp CH^B, *J* = 17.0 Hz and 4.0 Hz, 1H); 1.43, 1.41 (s × 2, $C(CH_3)_3 \times 2$, calc 18H, found 17H). ^{13}C NMR ($CDCl_3$, 100 MHz) δ 170.01, 169.39, 168.60. 156.37 (*C*(O)O^{t}Bu × 2, *C*(O)NH amide, *C*(O)NH carbamate); 136.11 (*C* aromatic); 128.38, 128.02, 127.96 (*C*H aromatic); 82.32, 81.51 ($C(CH_3)_3 \times 2$); 66.94 (*C*H_2 benzylic); 48.93 (Asp α-*C*H); 44.24 (Gly *C*H_2); 37.26 (Asp *C*H_2); 27.88, 27.75 ($C(CH_3)_3 \times 2$). $\tilde{\nu}_{max}$ (cm^-

[1]) (solid): 3256*w* (N-H amide stretch); 3055*w* (C-H arene stretch); 2932*w* (C-H alkyl stretch); 1721*s* (C=O ester stretch); 1659*s* (C=O amide stretch); 1535*s* (N-H amide bend and C=C arene stretch); 1450*m*, 1366*w*, 1342*m* (C-H alkyl bends); 1250*s*, 1219*m*, 1126*s*, 1080*m*, 1042*s* (C-O ester and C-N amide stretches, C-H arene bends); 957*s*, 926*s*, 841*s*, 748*s* (C-H arene bends). ESI-MS (*m/z*): Calc. for $C_{22}H_{33}N_2O_7$ 437.2282; found: 437.2282 (78%, $[M+H]^+$). Calc. for $C_{22}H_{32}N_2NaO_7$ 459.2102; found: 459.2107 (100%, $[M+Na]^+$).

Synthesis of H_2N-Gly-Asp(O^{t}Bu)-O^{t}Bu (2.6)

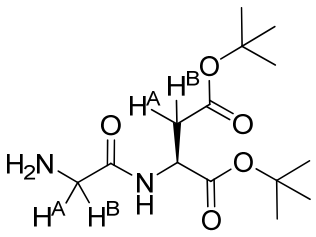

Compound **2.5** (7.19 g, 16.5 mmol) was dissolved in EtOH (80 ml) followed by the addition of Pd/C catalyst (1.44 g, 20%). The flask was subjected to several vacuum/H_2 purges and then stirred for 22.5 h under an atmosphere of H_2. The catalyst was filtered off over Celite, washed with MeOH, and the filtrate evaporated *in vacuo* to yield **2.6** as a clear colourless oil (5 g, quantitative yield). No further purification was required.

R_f 0.28 (9:1 DCM/MeOH, cerium stain). $[\alpha]_D$ = +46.5° (c = 1.0, $CHCl_3$). ^{1}H NMR ($CDCl_3$, 400 MHz) δ 7.94 (d, N*H* amide, *J* = 8.5 Hz, 1H); 4.64 (dt, Asp α-*H*, *J* = 9.0 Hz and 4.5 Hz, 1H); 3.33 (d, Gly C*H*^{A}, *J* = 17.5 Hz, 1H); 3.28 (d, Gly C*H*^{B}, *J* = 17.5 Hz, 1H); 2.82 (dd, Asp C*H*^{A}, *J* = 17.0 Hz and 4.5 Hz, 1H); 2.63 (dd, Asp C*H*^{B}, *J* = 17.0 Hz and 4.5 Hz, 1H); 1.69 (br s, N*H*$_2$, 2H); 1.39, 1.37 (s × 2, C(C*H*$_3$)$_3$ × 2, 18H). ^{13}C NMR ($CDCl_3$, 100 MHz) δ 172.72, 170.01, 169.83 (*C*(O)O^{t}Bu × 2, *C*(O)NH amide); 82.20, 81.52 (*C*(CH$_3$)$_3$ × 2); 48.65 (Asp α-*C*H); 44.73 (Gly *C*H$_2$); 37.75 (Asp *C*H$_2$); 28.04, 27.90 (C(*C*H$_3$)$_3$ × 2). $\tilde{\nu}_{max}$ (cm^{-1}) (oil): 3325*w,* 3256*w* (N-H amine and amide stretches); 2978*m* (C-H alkyl stretches); 1721*s* (C=O ester stretch); 1659*s* (C=O amide stretch); 1528*s* (N-H amide bend); 1366*s* (C-H alkyl bends); 1288*m*, 1250*m*, 1150*s* (C-O ester and C-N stretches). ESI-MS (*m/z*): Calc. for $C_{14}H_{27}N_2O_5$ 303.1914; found: 303.1921 (100%, $[M+H]^+$); 325.1734 (4%, $[M+Na]^+$).

Synthesis of Z-Arg(Pbf)-Gly-Asp(O^{t}Bu)-O^{t}Bu (2.7)

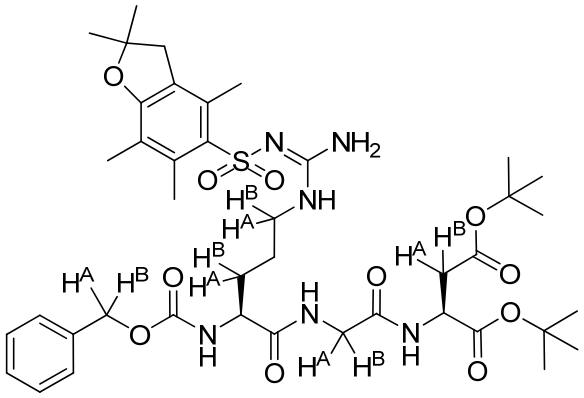

Z-Arg(Pbf)-OH.CHA (5.52 g, 8.37 mmol) was taken up in EtOAc (200 ml) and washed with $NaHSO_4$ (3 × 50 ml). The organic layer was then separated off and evaporated *in vacuo* to yield Z-Arg(Pbf)-OH as a white solid. Z-Arg(Pbf)-OH (4.69 g, 8.37 mmol, 1.0 eq) was dissolved in DCM (50 ml), cooled over an ice-water bath, followed by the addition of DIPEA (2.92 ml, 16.7 mmol, 2.0 eq) and TBTU (2.70 g, 8.37 mmol, 1.0 eq). The reaction mixture was stirred at 0°C for 20 min, then H_2N-Gly-Asp(O^{t}Bu)-O^{t}Bu **(2.6)** (2.55 g, 8.44 mmol, 1.0 eq) was taken up in DCM (25 ml) and added in one portion to the reaction flask, and a further portion of DCM (25 ml) used to rinse any residual H_2N-Gly-Asp(O^{t}Bu)-O^{t}Bu into the reaction flask. The reaction was stirred at 0°C for a further 20 min before removing the ice-water bath and stirring the reaction at rt for 20 h. The organic phase was washed with 1.33 M $NaHSO_4$ (2 × 100 ml), saturated $NaHCO_3$ (2 × 100 ml), water (3 × 100 ml) and finally brine (100 ml). The organic phase was dried over $MgSO_4$ and filtered before removing the solvent *in vacuo* to produce the crude product as a pale yellow solid (6.8 g, 97%). Purification by column chromatography (SiO_2, 100% DCM, to 98:2 DCM/MeOH, to 95:5 DCM/MeOH) yielded **2.7** as a white solid (6.02 g, 85%).

R_f 0.46 (9:1 DCM/MeOH, UV and cerium stain). $[\alpha]_D$ = +7.1° (c = 0.5, $CHCl_3$). M.p not acquired. ^{1}H NMR ($CDCl_3$, 400 MHz) δ 7.76 (app br t, N*H* amide (Arg-Gly), 1H); 7.33-7.26 (m, C*H* aromatic, 5H); 7.22 (d, N*H* amide (Gly-Asp), *J* = 8.0 Hz, 1H); 6.33 (br s, N*H*$_2$ guanidine, 2H); 6.16 (br s, N*H* guanidine, 1H); 6.09 (d, N*H* carbamate, *J* = 7.0 Hz, 1H); 5.08 (d, C*H*^{A} benzylic, *J* = 12.0 Hz, 1H); 5.03 (d, C*H*^{B} benzylic, *J* = 12.5 Hz, 1H); 4.64 (br dt, Asp α-*H*, *J* = 7.5 Hz and 5.0 Hz, 1H); 4.37-4.32 (br m, Arg α-*H*, 1H); 3.98 (dd, Gly C*H*^{A}, *J* = 17.0 Hz and 5.5 Hz, 1H); 3.91 (dd, Gly C*H*^{B}, *J* = 17.0 Hz and 5.5 Hz, 1H); 3.38-3.21 (br m, Arg C*H*^{A}NH, 1H); 3.19-3.07 (br m, Arg C*H*^{B}NH, 1H); 2.92 (s, Pbf C*H*$_2$, 2H); 2.79 (dd, Asp C*H*^{A}, *J* = 17.0 Hz and 5.0 Hz, 1H); 2.66 (dd, Asp C*H*^{B}, *J* = 17.0 Hz and 5.0 Hz, 1H); 2.56 (s, Pbf C*H*$_3$Ar, 3H); 2.48 (s, Pbf C*H*$_3$Ar, 3H); 2.06 (s, Pbf C*H*$_3$Ar, 3H); 1.96-1.79 (m, Arg CHC*H*^{A}, 1H); 1.74-1.62 (m, Arg CHC*H*^{B}, 1H); 1.59-1.50 (m, Arg C*H*$_2$CH$_2$NH, 2H); 1.44 (s, Pbf C*H*$_3$ × 2, 6H); 1.40, 1.39 (s × 2, C(C*H*$_3$)$_3$ × 2, calc 18H, found 17H). ^{13}C NMR ($CDCl_3$, 100 MHz) δ 173.01, 170.17, 169.82, 169.38, 158.79, 156.68, 156.54 (*C*(O)O^{t}Bu × 2, *C*(O)NH amide × 2, *C*(O)NH

carbamate, Pbf aromatic *C*-O, *C*=N guanidine); 138.47 (Pbf aromatic *C*); 136.40 (Z group aromatic *C*); 132.90, 132.38 (Pbf aromatic *C*); 128.56, 128.16, 128.06 (Z group aromatic *C*H); 124.65, 117.55 (Pbf aromatic *C*); 86.43 (Pbf $CH_2C(CH_3)_2O$); 82.64, 81.73 ($C(CH_3)_3 \times 2$); 67.01 (CH_2 benzylic); 54.31 (Arg α-*C*H); 49.47 (Asp α-*C*H); 43.32, 42.88 (Pbf ArCH_2, Gly CH_2); 40.35 (Arg CH_2NH); 37.42 (Asp CH_2); 29.91 (Arg $CHCH_2$); 28.69 (Pbf $CH_2C(CH_3)_2O$); 28.11, 27.94 ($C(CH_3)_3 \times 2$); 25.31 (Arg CH_2CH_2NH); 19.40, 18.06, 12.57 (Pbf Ar$CH_3 \times 3$). $\tilde{\nu}_{max}$ (cm^{-1}) (solid): 3318*w* (N-H amide stretches); 2974*w*, 2932*w* (C-H alkyl and arene stretches); 1724*m* (C=O ester stretch); 1667*m* (C=O amide stretches); 1543*s* (N-H amide bend and C=C arene stretch); 1450*m*, 1404*w*, 1366*m* (C-H alkyl bend and S=O stretch); 1288*m*, 1242*m*, 1150*s*, 1088*w* (C-O ester and C-N amide stretches, C-H arene bends); 1042*m*; 910*m*; 849*m*, 779*m* (C-H arene bends). ESI-MS (*m*/*z*): Calc. for $C_{41}H_{60}N_6O_{11}S$ 845.4114; found: 845.4092 (100%, $[M+H]^+$); 867.3909 (30%, $[M+Na]^+$).

Synthesis of H_2N-Arg(Pbf)-Gly-Asp(O^{t}Bu)-O^{t}Bu (2.8)

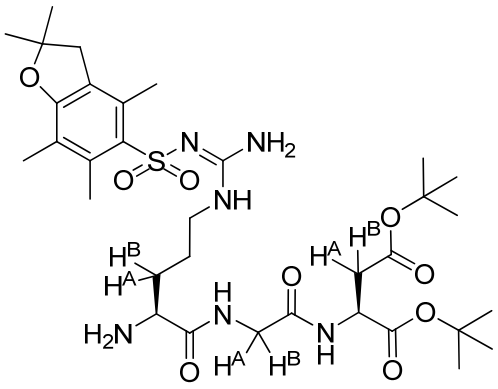

Compound **2.7** (6.02 g, 7.13 mmol) was dissolved in EtOH (75 ml) followed by the addition of Pd/C catalyst (1.20 g, 20%). The flask was subjected to several vacuum/H_2 purges and then stirred for 16 h under an atmosphere of H_2. The catalyst was filtered off over Celite, washed with MeOH, and the filtrate evaporated *in vacuo* to yield **2.8** as a white solid (4.50 g, 89%). No further purification was required.

R_f 0.15 (9:1 DCM/MeOH, UV and cerium stain). $[\alpha]_D$ = +23.0° (c = 0.25, $CHCl_3$). M.p not acquired. ^{1}H NMR ($CDCl_3$, 400 MHz) δ 8.04 (br t, N*H* amide (Arg-Gly), *J* = 5.0 Hz, 1H); 7.19 (d, N*H* amide (Gly-Asp), *J* = 8.0 Hz, 1H); 6.39 (br s, NH_2 guanidine, 2H); 6.29 (br s, N*H* guanidine, 1H); 4.63 (dt, Asp α-*H*, *J* = 8.0 Hz and 5.0 Hz, 1H); 3.98 (dd, Gly CH^A, *J* = 17.0 Hz and 5.5 Hz, 1H); 3.91 (dd, Gly CH^B, *J* = 17.0 Hz and 5.0 Hz, 1H); 3.44 (app br t, Arg α-*H*, *J* = 7.0 Hz, 1H); 3.26-3.12 (br m, Arg CH_2NH, 1H); 2.93 (s, Pbf CH_2, 2H); 2.82 (dd, Asp CH^A, *J* = 17.0 Hz and 5.0 Hz, 1H); 2.68 (dd, Asp CH^B, *J* = 17.0 Hz and 5.0 Hz, 1H); 2.55 (s, Pbf CH_3Ar, 3H); 2.48 (s, Pbf CH_3Ar, 3H); 2.06 (s, Pbf CH_3Ar, 3H); 1.94 (br s, NH_2, 2H); 1.84-1.73 (m, Arg CHCH^A, 1H); 1.68-1.49 (m, Arg CHCH^B, Arg CH_2CH_2NH, overlapping, 3H); 1.43 (s, Pbf $CH_3 \times 2$, 6H); 1.401, 1.395 (s × 2, $C(CH_3)_3 \times 2$, calc 18H,

found 17H). ^{13}C NMR ($CDCl_3$, 100 MHz) δ 176.11, 170.16, 169.62, 169.14, 158.56, 156.34 (*C*(O)O^{t}Bu × 2, *C*(O)NH amide × 2, Pbf aromatic *C*-O, *C*=N guanidine); 138.17, 132.97, 132.11, 124.47, 117.33 (Pbf aromatic *C*); 86.26 (Pbf $CH_2C(CH_3)_2O$); 82.46, 81.60 ($C(CH_3)_3$ × 2); 54.37 (Arg α-*C*H); 49.15 (Asp α-*C*H); 43.16, 42.64 (Pbf ArCH_2, Gly CH_2); 40.48 (Arg CH_2NH); 37.25 (Asp CH_2); 31.91 (Arg $CHCH_2$); 28.52 (Pbf $CH_2C(CH_3)_2O$); 27.95, 27.80 ($C(CH_3)_3$ × 2); 25.28 (Arg CH_2CH_2NH); 19.21, 17.86, 12.39 (Pbf ArCH_3 × 3). $\tilde{\nu}_{max}$ (cm^{-1}) (solid): 3318*w* (N-H amide stretch); 2986*w*, 2974*w*, 2932*w* (C-H alkyl stretch); 1735*m* (C=O ester stretch); 1659*m* (C=O amide stretch); 1543*s*, 1450*w*, 1404*w*, 1366*m* (N-H amide bend, C-H alkyl bend, C=C arene stretch and S=O stretch); 1296*m*, 1242*m*, 1150*s* (C-O ester and C-N amide stretches). ESI-MS (*m*/*z*): Calc. for $C_{33}H_{55}N_6O_9S$ 711.3746; found: 711.3756 (100%, $[M+H]^+$); 733.3572 (47%, $[M+Na]^+$).

Synthesis of Tris{[2-(*tert*-butoxycarbonyl)ethoxy]methyl}methylamine (H_2N-G1-[C(O)O^{t}Bu]$_3$) (2.9)[259]

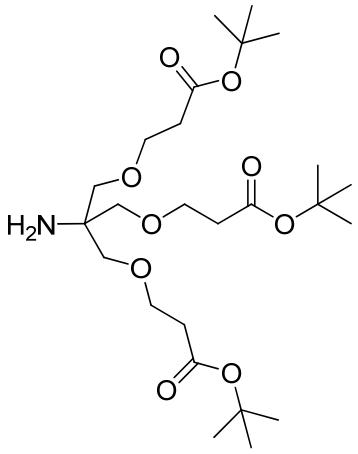

TRIS (12.03 g, 100 mmol) in a solvent mixture of DMSO/H_2O (90:10, 20 ml) was cooled in an ice-water bath. 5 M NaOH (2 ml) was then added with stirring, followed by a dropwise addition of *tert*-butyl acrylate (50 ml, 340 mmol) over 2 h. The ice-water bath was removed and the reaction was then stirred at rt for 24 h. The excess *tert*-butyl acrylate and most of the DMSO were then removed *in vacuo* at high temperature. Subsequently, the crude residue (41.5 g) was purified by column chromatography (SiO_2, 2:1 EtOAc/cyclohexane + 0.05% NH_4OH) to yield **2.9** as a pale yellow oil (13.23 g, 26%).

R_f 0.21 (2:1 EtOAc/cyclohexane, cerium stain). ^{1}H NMR ($CDCl_3$, 400 MHz) δ 3.63 (t, OCH_2CH_2, *J* = 6.5 Hz, 6H); 3.30 (s, CCH_2O, 6H); 2.45 (t, CH_2CH_2C(O), *J* = 6.5 Hz, 6H); 1.67 (br s, NH_2, 2H); 1.44 (s, $(CH_3)_3$C, 27H). ^{13}C NMR ($CDCl_3$, 100 MHz) δ 170.90 (*C*(O)O^{t}Bu); 80.38 ($C(CH_3)_3$); 72.85 (CCH_2O); 67.09 (OCH_2CH_2); 55.91 (*C*CH_2O); 36.29 (CH_2CH_2C(O)); 28.07 ($(CH_3)_3$C). IR not acquired. ESI-MS (*m*/*z*): Calc. for $C_{25}H_{48}NO_9$ 506.3324; found: 506.3327 (11%, $[M+H]^+$); 450.2704 (27%, $[M+H-C_4H_8]^+$); 394.2080 (44%, $[M+H-2C_4H_8]^+$); 338.1466 (100%, $[M+H-3C_4H_8]^+$).

Synthesis of Benzyl *N*-Tris{[2-(*tert*-butoxycarbonyl)ethoxy]methyl}methylcarbamate (Z-G1-[C(O)O^{t}Bu]$_3$) (2.10)[259]

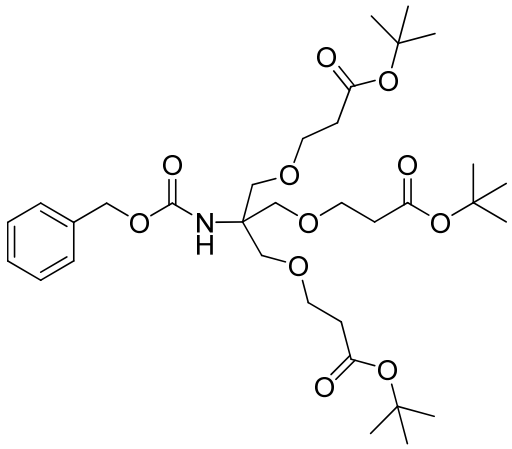

Compound **2.9** (1.39 g, 2.74 mmol) was dissolved in DCM (20 ml) and aqueous Na_2CO_3 (25% w/v, 10 ml) was added with stirring. Benzyl chloroformate (1.2 ml, 8.4 mmol) was added rapidly in one portion and the reaction was stirred at rt for 24 h. The product was extracted with DCM (50 ml), dried over $MgSO_4$, and then the solvent was removed *in vacuo*. The crude product (2.42 g) was purified by column chromatography (SiO_2, 2:1 cyclohexane/EtOAc) to yield **2.10** as a clear colourless oil (1.37 g, 78%).

R_f 0.60 (2:1 cyclohexane/EtOAc, cerium stain). ^{1}H NMR ($CDCl_3$, 400 MHz) δ 7.28-7.34 (m, C*H* aromatic, 5H); 5.31 (br s, N*H* carbamate, 1H); 5.03 (s, CH_2 benzylic, 2H); 3.66 (s, CCH_2O, 6H); 3.63 (t, OCH_2CH$_2$, J = 6.5 Hz, 6H); 2.43 (t, CH$_2$CH_2C(O), J = 6.5 Hz, 6H); 1.43 (s, (CH_3)$_3$C, 27H). ^{13}C NMR ($CDCl_3$, 100 MHz) δ 170.89 (*C*(O)O^{t}Bu); 155.14 (*C*(O)NH); 127.94, 128.02, 128.44, 136.79 (*C*H aromatic); 80.50 (*C*(CH$_3$)$_3$); 69.41 (C*C*H$_2$O); 67.12 (O*C*H$_2$CH$_2$); 66.14 (*C*H$_2$ benzylic); 58.77 (*C*CH$_2$O); 36.26 (CH$_2$*C*H$_2$C(O)); 28.14 ((*C*H$_3$)$_3$C). IR not acquired. ESI-MS (*m*/*z*): Calc. for $C_{33}H_{53}NNaO_{11}$ 662.3511; found: 662.3494 (100%, [M+Na]$^+$); 606.2876 (68%, [M+Na-C_4H_8]$^+$); 550.2261 (37%, [M+Na-2C_4H_8]$^+$); 494.1643 (21%, [M+Na-3C_4H_8]$^+$); 472.1804 (21%, [M+H–3C_4H_8]$^+$).

Synthesis of Benzyl *N*-Tris[(2-carboxyethoxy)methyl]methylcarbamate (Z-G1-[C(O)OH]$_3$) (2.11)[259]

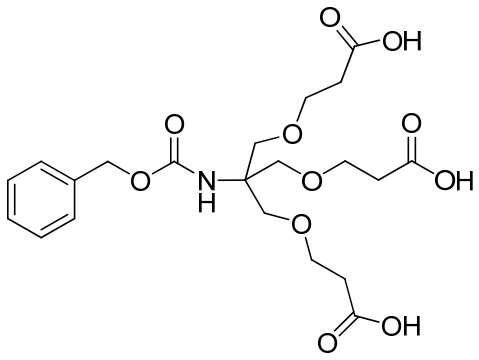

Compound **2.10** (0.85 g, 1.32 mmol) was stirred in formic acid (96%, 15 ml) for 18 h. The formic acid was then removed *in vacuo* at 50°C. The resultant oil was dissolved in methanol which was then removed *in vacuo*. This process of dissolving in methanol and then rotary evaporating was repeated a further two times to yield **2.11** as a viscous, colourless oil (0.62 g, quantitative yield).

R_f 0.23 (9:1 DCM/MeOH, cerium stain). ^{1}H NMR ($CD_3C(O)CD_3$, 400 MHz) δ 7.27-7.36 (m, C*H* aromatic, 5H); 5.78 (br s, N*H* carbamate, 1H); 5.02 (s, CH_2 benzylic, 2H); 3.68 (s, CCH_2O, 6H); 3.68 (t, OCH_2CH$_2$, J = 6.5 Hz, 6H); 2.53 (t, CH$_2$CH_2C(O), J = 6.5 Hz, 6H). ^{13}C NMR ($CD_3C(O)CD_3$, 100 MHz) δ 172.90 (*C*(O)OH); 155.50 (*C*(O)NH); 138.12, 128.90, 128.28, 128.24 (*C*H aromatic); 69.64 (C*C*H$_2$O); 67.40 (O*C*H$_2$CH$_2$); 65.86 (*C*H$_2$ benzylic); 59.54 (*C*CH$_2$O); 34.86 (CH$_2$*C*H$_2$C(O)). IR not acquired. ESI-MS (*m*/*z*): Calc. for $C_{21}H_{29}NNaO_{11}$ 494.1633; found: 494.1643 (100%, $[M+Na]^+$); 472.1817 (50%, $[M+H]^+$).

Synthesis of Benzyl *N*-Tris[(2-{[(tris{[2-(*tert*-butoxycarbonyl)ethoxy]methyl}methyl)amino]carbonyl}ethoxy)methyl]methylcarbamate (Z-G2-[C(O)O^{t}Bu]$_9$) (2.12)[259]

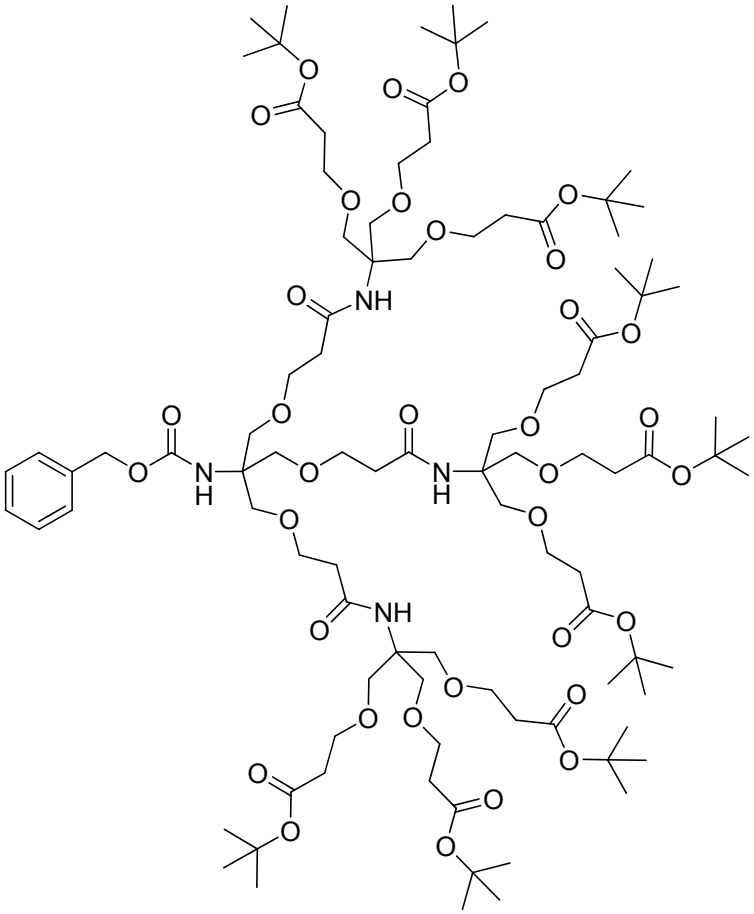

Method A (using T3P as the coupling reagent):

Compounds **2.11** (0.41 g, 0.86 mmol, 1.0 eq) and **2.9** (1.59 g, 3.14 mmol, 3.6 eq) were dissolved in dry THF (10 ml) and TEA (0.43 ml, 3.08 mmol, 3.6 eq) with stirring. The solution was cooled in an ice-water bath to 0°C and then T3P (50 wt. % in EtOAc, 1.85 ml, 3.14 mmol, 3.6 eq) was added dropwise over 20 min. The ice-water bath was removed and the reaction mixture was stirred at rt for 18 h under N_2. TLC analysis revealed no obvious product spot. The reaction was then refluxed at 50°C for 2.5 h. TLC analysis gave a faint spot corresponding to the product by UV and cerium stain. The solvent was removed *in vacuo* and the residue dissolved in DCM, then washed with 0.5 M HCl (3 × 30 ml) and brine (3 × 30 ml). The organic layer was dried over $MgSO_4$ before removing the solvent *in vacuo* and column chromatography (SiO_2, 2:1 EtOAc/cyclohexane) produced **2.12** as a colourless oil (200 mg, 12%).

Method B (using HBTU as the coupling reagent):

HBTU (1.29 g, 3.39 mmol, 3.6 eq) and TEA (0.48 ml, 3.4 mmol, 3.6 eq) were added to compound **2.11** (0.44 g, 0.94 mmol, 1.0 eq) in dry acetonitrile (10 ml). Compound **2.9** (1.72 g, 3.38 mmol, 3.6 eq) dissolved in dry acetonitrile (10 ml) was then added rapidly and the reaction was stirred at rt for 24 h under N_2. Following the removal of the solvent *in vacuo*, the residue was dissolved in Et_2O and subsequently washed with 0.5 M HCl then saturated brine solution. The organic layer was then dried over $MgSO_4$ and the solvent removed *in vacuo* to yield a crude pale yellow oil. Purification by column chromatography (SiO_2, 2:1 EtOAc/cyclohexane) produced **2.12** as a pale yellow oil (1.4 g, 77%).

R_f = 0.27 (2:1 EtOAc/cyclohexane, cerium stain). ^{1}H NMR ($CDCl_3$, 400 MHz) δ 7.28-7.36 (m, C*H* aromatic, 5H); 6.28 (br s, N*H* amides, 3H); 5.58 (br s, N*H* carbamate, 1H); 5.03 (s, CH_2 benzylic, 2H); 3.60-3.66 (m, OCH_2CH_2 gen. 1 & 2, CCH_2O gen. 1 & 2, 48H); 2.43 (t, CH_2CH_2C(O) gen. 2, J = 6.5 Hz, 18H); 2.43 (t, CH_2CH_2C(O) gen. 1, J = 6.5 Hz, 6H); 1.43 (s (CH_3)$_3$C, 81H). ^{13}C NMR ($CDCl_3$, 100 MHz) δ 170.97 (*C*(O)O^{t}Bu); 170.91 (*C*(O)NH amides); 155.16 (*C*(O)NH carbamate); 127.95, 128.09, 128.47, 136.91 (*C*H aromatic); 80.49 (*C*(CH$_3$)$_3$); 69.38 (C*C*H$_2$O, gen. 1); 69.16 (C*C*H$_2$O, gen. 2); 67.62 (O*C*H$_2$CH$_2$, gen. 1); 67.08 (O*C*H$_2$CH$_2$, gen. 2); 66.08 (*C*H$_2$ benzylic); 59.81 (*C*CH$_2$O, gen. 2); 58.90 (*C*CH$_2$O, gen. 1); 37.38 (CH$_2$*C*H$_2$C(O), gen. 1); 36.18 (CH$_2$*C*H$_2$C(O), gen. 2); 28.18 ((*C*H$_3$)$_3$C). IR not acquired. ESI-MS (*m*/*z*): Calc. for $C_{96}H_{165}N_4O_{35}$ 1934.1249; found: 1934.1289 (11%, $[M+H]^+$); 1951.1566 (32%, $[M+NH_4]^+$); 1956.1190 (5%, $[M+Na]^+$); 968.0652 (100%, $[M+2H]^{2+}$).

Synthesis of Benzyl *N*-Tris[(2-{[(tris[(2-carboxyethoxy)methyl]methyl)amino]carbonyl}ethoxy)methyl]methylcarbamate (Z-G2-[C(O)OH]$_9$) (2.13)[10]

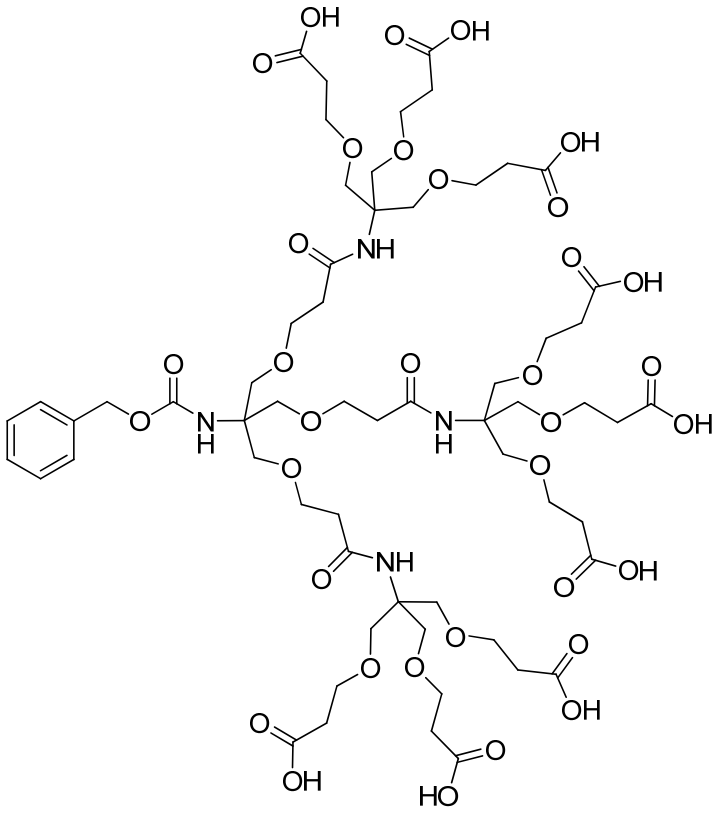

Compound **2.12** (217 mg, 0.11 mmol) was stirred in formic acid (96%, 3.5 ml) for 24 h. The formic acid was then removed *in vacuo* at 50°C. The resultant oil was dissolved in methanol which was then removed *in vacuo*. This process of dissolving in methanol and then rotary evaporating was repeated a further two times to yield **2.13** as a viscous, colourless oil (160 mg, quantitative yield).

R_f = 0.20 (9:1 DCM/MeOH, cerium stain). ^{1}H NMR ($CD_3C(O)CD_3$, 270 MHz) δ 7.28-7.47 (m, C*H* aromatic, 5H); 6.84 (br s, N*H* amides, 3H); 6.01 (br s, N*H* carbamate, 1H); 5.07 (s, CH_2 benzylic, 2H); 3.66-3.73 (m, OCH_2CH$_2$ gen. 1 & 2, CCH_2O gen. 1 & 2, 48H); 2.54 (t, CH$_2$CH_2C(O) gen. 2, J = 6.0 Hz, 18H); 2.43 (t, CH$_2$CH_2C(O) gen. 1, J = 6.0 Hz, 6H). ^{13}C NMR ($CD_3C(O)CD_3$, 68 MHz) δ 173.50 (*C*(O)OH); 172.73 (*C*(O)NH amides); 172.65 (*C*(O)NH carbamate); 128.61, 128.75, 129.24 (*C*H aromatic); 70.00 (C*C*H$_2$O, gen. 1); 69.79 (C*C*H$_2$O, gen. 2); 68.32 (O*C*H$_2$CH$_2$, gen. 1); 67.75 (O*C*H$_2$CH$_2$, gen. 2); 60.99 (*C*CH$_2$O, gen. 2); 60.01 (*C*CH$_2$O, gen. 1); 37.86 (CH$_2$*C*H$_2$C(O), gen. 1); 35.25 (CH$_2$*C*H$_2$C(O), gen. 2). IR not acquired. ESI-MS (*m*/*z*): Calc. for $C_{60}H_{91}N_4O_{35}$ 1427.5469; found: 1427.5479 (100%, [M-H]$^-$); 1449.5 (42%, [M-2H+Na]$^-$); 1471.5 (16%, [M-3H+2Na]$^-$); 1493.5 (7%, [M-4H+3Na]$^-$); 1515.5 (3%, [M-5H+4Na]$^-$).

Synthesis of Z-G1-[Arg(Pbf)-Gly-Asp(O^{t}Bu)-O^{t}Bu]$_3$ (2.14)

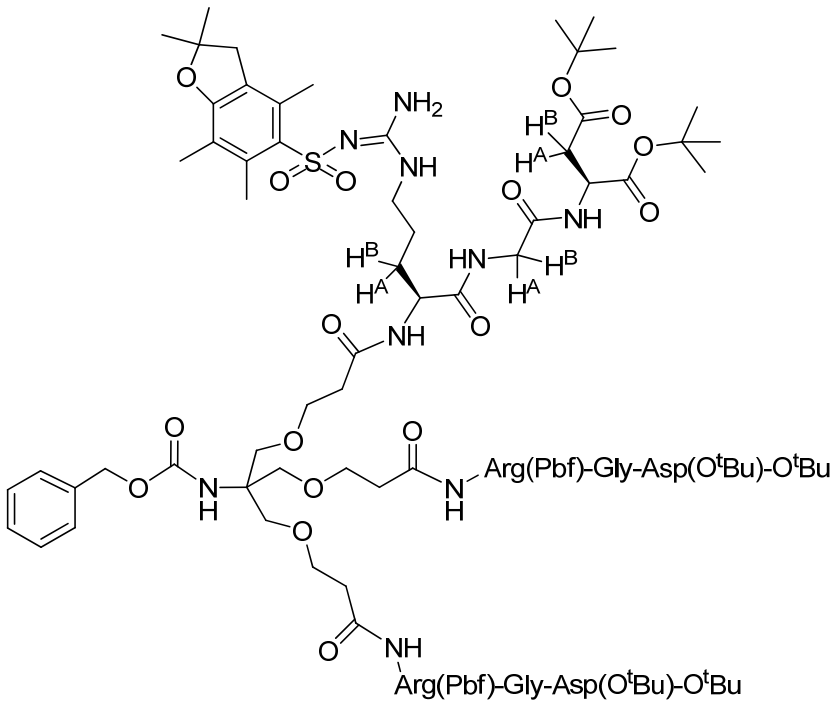

Method A (reaction performed under ambient conditions, using 3.6 eq of **2.8(2.4)** and 3.6 eq of T3P):

Compounds **2.11** (96 mg, 0.2 mmol, 1.0 eq) and **2.8(2.4)** (0.52 g, 0.73 mmol, 3.6 eq) were suspended in dry DCM (10 ml), then DIPEA (0.22 ml, 1.22 mmol, 6 eq) was added and the reaction flask cooled over an ice-water bath. T3P (50 wt. % in EtOAc, 0.44 ml, 0.73 mmol, 3.6 eq) was added dropwise over 20 min. The ice-water bath was removed and the reaction mixture was stirred for 22 h at rt. The reaction mixture was diluted with DCM (100 ml), quenched with water (50 ml), and then the organic layer was washed with saturated $NaHCO_3$ (100 ml), 1.33 M $NaHSO_4$ (100 ml), and finally water (100 ml). The organic layer was dried over $MgSO_4$ and filtered before removing the solvent *in vacuo* to produce the product as a crude white solid/oil (~0.5 g, ~96% crude yield) which was purified by column chromatography (SiO_2, 9:1 DCM/MeOH) to produce the product **2.14** as a white solid (0.4 g, 77%).

Method B (reaction performed under dry conditions, using 6.0 eq of **2.8(2.4)** and 6.0 eq of T3P):

Compound **2.11** (0.2 g, 0.42 mmol, 1.0 eq) was dissolved in dry DCM (10 ml). To this was added **2.8(2.4)** (1.75 g, 2.5 mmol, 6.0 eq) in dry DCM (10 ml), then DIPEA (0.44 ml, 2.5 mmol, 6.0 eq) in dry DCM (5 ml) was added and the reaction flask cooled over an ice-water bath. T3P (50 wt. % in EtOAc, 1.5 ml, 2.5 mmol, 6.0 eq) was added dropwise over 15 min, then a further portion of dry DCM (5 ml) was used to rinse any residual T3P into the reaction flask. The ice-water bath was removed and the reaction mixture was stirred at rt for 18 h under N_2. Following TLC analysis, a

further portion of T3P (50 wt. % in EtOAc, 1.5 ml, 2.5 mmol, 6.0 eq) in dry DCM (5 ml) was added dropwise over 10 min and the reaction was stirred overnight at rt under N_2. The reaction mixture was quenched with water (100 ml), and then the organic layer was washed with saturated $NaHCO_3$ (100 ml), 1.33 M $NaHSO_4$ (100 ml), and finally brine (100 ml). The organic layer was dried over $MgSO_4$ and filtered before removing the solvent *in vacuo* to produce the product as a crude white solid (~2.0 g) which was purified by column chromatography (SiO_2, 100% DCM to 98:2 DCM/MeOH to 95:5 DCM/MeOH to 9:1 DCM/MeOH) to produce the product **2.14** as a white solid (0.7 g, 65%).

R_f 0.36 (9:1 DCM/MeOH, UV and cerium stain). $[\alpha]_D$ = -2.0° (c = 0.25, $CHCl_3$). M.p: 131.7-137.0°C. ^{1}H NMR ($CDCl_3$, 400 MHz) δ 7.70-7.68 (br m, N*H* amide × 3, 3H); 7.33-7.28 (m, N*H* amide × 6 and C*H* aromatic × 5, 11H); 6.35 (br s, N*H*$_2$ guanidine × 3, 6H); 6.22 (br s, N*H* guanidine × 3, 3H); 5.50 (br s, N*H* carbamate, 1H); 5.01 (s, C*H*$_2$ benzylic, 2H); 4.65 (dt, Asp α-*H* × 3, *J* = 8.0 Hz and 5.0 Hz, 3H); 4.54 (m, Arg α-*H* × 3, 3H); 4.00 (dd, Gly C*H*^{A} × 3, *J* = 17.0 Hz and 5.5 Hz, 3H); 3.85 (dd, Gly C*H*^{B} × 3, *J* = 17.0 Hz and 5.5 Hz, 3H); 3.68-3.57 (m, CC*H*$_2$O × 3, OC*H*$_2$CH$_2$ × 3, 12H); 3.30-3.15 (m, Arg C*H*$_2$NH × 3, 6H); 2.93 (s, Pbf C*H*$_2$ × 3, 6H); 2.78 (dd, Asp C*H*^{A} × 3, *J* = 17.0 Hz and 5.0 Hz, 3H); 2.68 (dd, Asp C*H*^{B} × 3, *J* = 17.0 Hz and 5.0 Hz, 3H); 2.56 (s, Pbf C*H*$_3$ × 3, 9H); 2.49 (s, Pbf C*H*$_3$ × 3, 9H); 2.47-2.40 (m, CH$_2$C*H*$_2$C(O) × 3, 6H); 2.07 (s, Pbf C*H*$_3$ × 3, 9H); 1.91-1.83 (m, Arg CHC*H*^{A} × 3, 3H); 1.76-1.67 (m, Arg CHC*H*^{B} × 3, 3H); 1.63-1.56 (m, Arg C*H*$_2$CH$_2$NH × 3, 6H); 1.44 (s, [(Pbf C*H*$_3$ × 2)] × 3, 18H); 1.41, 1.40 (s, [(^{t}Bu C*H*$_3$ × 6)] × 3, 54H). ^{13}C NMR ($CDCl_3$, 100 MHz) δ 173.08, 172.47, 170.16, 169.99, 169.43 (*C*(O)O^{t}Bu × 2, *C*(O)NH amide × 3); 158.72, 156.59 (Pbf aromatic *C*-O, *C*=N guanidine); 138.35 (Pbf aromatic *C*); 136.67 (Benzyl aromatic *C*); 132.96, 132.27 (Pbf aromatic *C*); 128.55, 128.09 (Benzyl aromatic *C*H); 124.63, 117.50 (Pbf aromatic *C*); 86.42 (Pbf CH$_2$*C*(CH$_3$)$_2$O); 82.56, 81.64 (*C*(CH$_3$)$_3$ × 2); 69.38 (C*C*H$_2$O); 67.53 (O*C*H$_2$CH$_2$); 66.28 (*C*H$_2$ benzylic); 59.11 (*C*CH$_2$O); 53.15 (Arg α-*C*H); 49.44 (Asp α-*C*H); 43.28, 42.73, 40.33 (Pbf Ar*C*H$_2$, Gly *C*H$_2$, Arg *C*H$_2$NH); 37.44 (Asp *C*H$_2$); 36.63 (CH$_2$*C*H$_2$C(O)); 29.28 (Arg CH*C*H$_2$); 28.66 (Pbf CH$_2$C(*C*H$_3$)$_2$O); 28.08, 27.92 (C(*C*H$_3$)$_3$ × 2); 25.43 (Arg *C*H$_2$CH$_2$NH); 19.38, 18.03, 12.55 (Pbf Ar*C*H$_3$ × 3). $\tilde{\nu}_{max}$ (cm^{-1}) (solid): 3306*w* (N-H amide stretch); 2975*w* (C-H alkyl and arene stretches); 1727*m* (C=O ester stretch); 1648*m* (C=O amide stretch); 1543*s* (N-H amide bend and C=C arene stretch); 1453*w*, 1367*w* (C-H alkyl bend and S=O stretch); 1243*m*, 1151*s*, 1094*s* (C-O ether, C-O ester and C-N amide stretches, C-H arene bends). ESI-MS (*m*/*z*): Calc. for $C_{120}H_{185}N_{19}Na_2O_{35}S_3$ 1297.1114; found: 1297.1096 (100%, $[M+2Na]^{2+}$), 2572.2 (11%, $[M+Na]^+$).

Synthesis of Z-G2-[Arg(Pbf)-Gly-Asp(O^{t}Bu)-O^{t}Bu]$_9$ (2.15)

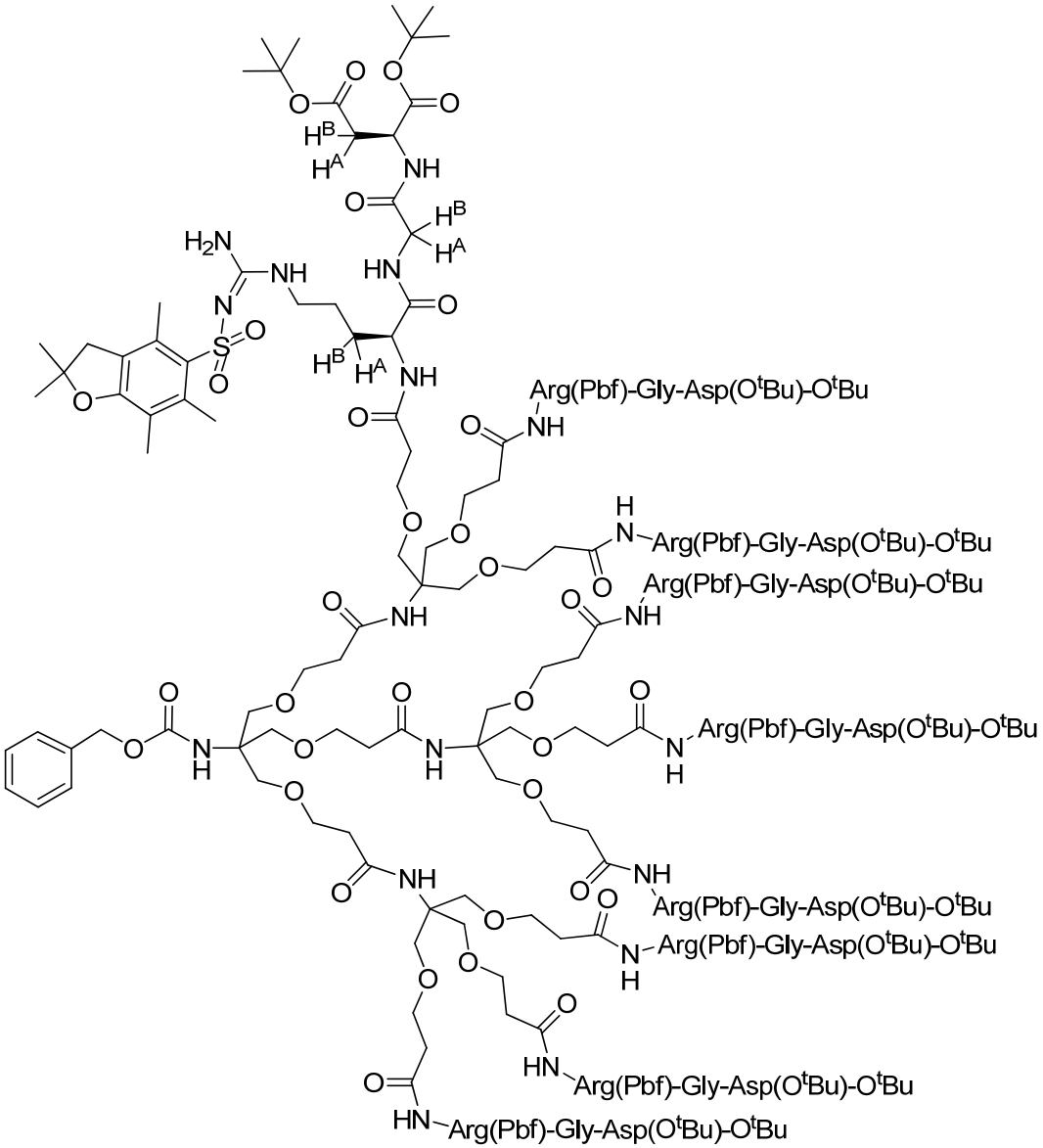

Compounds **2.13** (110 mg, 77 μmol, 1.0 eq) and **2.8(2.4)** (0.98 g, 1.39 mmol, 18.0 eq) were suspended in dry DCM (10 ml), then DIPEA (0.24 ml, 1.39 mmol, 18.0 eq) was added and the reaction flask cooled over an ice-water bath. T3P (50 wt. % in EtOAc, 0.82 ml, 1.39 mmol, 18.0 eq) was added dropwise over 10 min. The ice-water bath was removed and the reaction mixture was stirred for 2 days at rt. The reaction mixture was diluted with DCM (100 ml), quenched with water (100 ml), and then the organic layer was washed with saturated $NaHCO_3$ (100 ml), 1.33 M $NaHSO_4$ (100 ml), saturated $NaHCO_3$ (100 ml), 1.33 M $NaHSO_4$ (100 ml), and finally water (100 ml). The organic layer was dried over $MgSO_4$ and filtered before removing the solvent *in vacuo* to produce a crude white solid (~1.2 g) which was purified by column chromatography (SiO_2, 95:5 DCM/MeOH to 9:1 DCM/MeOH) to produce the product **2.15** as a white solid (0.45 g, 76%).

R_f 0.29 (9:1 DCM/MeOH, UV and cerium stain). $[\alpha]_D$ not acquired. M.p not acquired. ^{1}H NMR ($CDCl_3$, 400 MHz) δ 7.79 (br s, N*H* amide × 9, 9H); 7.54 (br s, N*H* amide × 9, 9H); 7.38 (d, N*H* amide × 9, 9H); 7.30-7.28 (m, C*H* aromatic × 5, 5H); 6.75 (br s, N*H* amide of branching × 3, 3H); 6.38 (br s, NH_2 guanidine × 9, 18H); 6.29 (br s, N*H* guanidine × 9, 9H); 5.81 (br s, N*H* carbamate, 1H); 5.02 (s, CH_2 benzylic, 2H); 4.65 (dt, Asp α-*H* × 9, *J* = 8.0 Hz and 5.0 Hz, 9H); 4.55 (m, Arg α-*H* × 9, 9H); 4.03 (dd, Gly CH^A × 9, *J* = 17.0 Hz and 5.0 Hz, 9H); 3.89 (dd, Gly CH^B × 9, *J* = 17.0 Hz and 5.0 Hz, 9H); 3.71-3.63 (m, CCH_2O × 3 gen. 1, CCH_2O × 9 gen. 2, OCH_2CH_2 × 3 gen. 1, OCH_2CH_2 × 9 gen. 2, 48H); 3.30-3.15 (m, Arg CH_2NH × 9, 18H); 2.93 (s, Pbf CH_2 × 9, 18H); 2.76 (dd, Asp CH^A × 9, *J* = 17.0 Hz and 5.5 Hz, 9H); 2.68 (dd, Asp CH^B × 9, *J* = 17.0 Hz and 5.5 Hz, 9H); 2.56 (s, Pbf CH_3 × 9, 27H); 2.49 (s, Pbf CH_3 × 9, 27H); 2.47-2.40 (m, CH_2CH_2C(O) × 3 gen.1, CH_2CH_2C(O) × 9 gen. 2, 24H); 2.07 (s, Pbf CH_3 × 9, 27H); 1.94-1.84 (m, Arg CHCH^A × 9, 9H); 1.79-1.69 (m, Arg CHCH^B × 9, 9H); 1.66-1.54 (m, Arg CH_2CH_2NH × 9, 18H); 1.44 (s, [(Pbf CH_3 × 2)] × 9, 54H); 1.40 (s, [(^{t}Bu CH_3 × 6)] × 9, 162H). ^{13}C NMR ($CDCl_3$, 100 MHz) δ 173.15, 172.55, 172.43, 170.14, 170.00, 169.45 (*C*(O)O^{t}Bu × 2, *C*(O)NH amide × 4); 158.68, 156.60 (Pbf aromatic *C*-O, *C*=N guanidine); 138.31, 133.01, 132.25 (Pbf aromatic *C*); 128.55, 127.96 (Benzyl aromatic *C*H); 124.60, 117.45 (Pbf aromatic *C*); 86.39 (Pbf CH_2*C*(CH_3)$_2$O); 82.49, 81.57 (*C*(CH_3)$_3$ × 2); 69.38 (C*C*H_2O, gen. 1 and 2, multiple overlapping peaks); 67.56 (O*C*H_2CH_2, gen. 1 and 2, multiple overlapping peaks); 60.21 (*C*CH_2O gen. 1 and 2, multiple overlapping peaks); 53.23 (Arg α-*C*H, multiple overlapping peaks); 49.45 (Asp α-*C*H, multiple overlapping peaks); 43.28, 42.72, 40.45 (Pbf Ar*C*H_2, Gly *C*H_2, Arg *C*H_2NH, multiple overlapping peaks); 37.45 (Asp *C*H_2, multiple overlapping peaks); 36.46 (CH_2*C*H_2C(O), gen. 1 and 2, multiple overlapping peaks); 29.38 (Arg CH*C*H_2, multiple overlapping peaks); 28.66 (Pbf CH_2C(*C*H_3)$_2$O); 28.07, 27.91 (C(*C*H_3)$_3$ × 2); 25.56 (Arg *C*H_2CH_2NH, multiple overlapping peaks); 19.38, 18.04, 12.54 (Pbf Ar*C*H_3 × 3). IR not acquired. ESI-MS (*m*/*z*): Calc. for $C_{357}H_{563}N_{58}O_{107}S_9$ 2555.9; found: 2555.9 (26%, $[M+3H]^{3+}$), 1916.9 (91%, $[M+4H]^{4+}$), 1534.0 (100%, $[M+5H]^{5+}$).

Synthesis of Z-G1-[Arg-Gly-Asp]$_3$ (2.16)

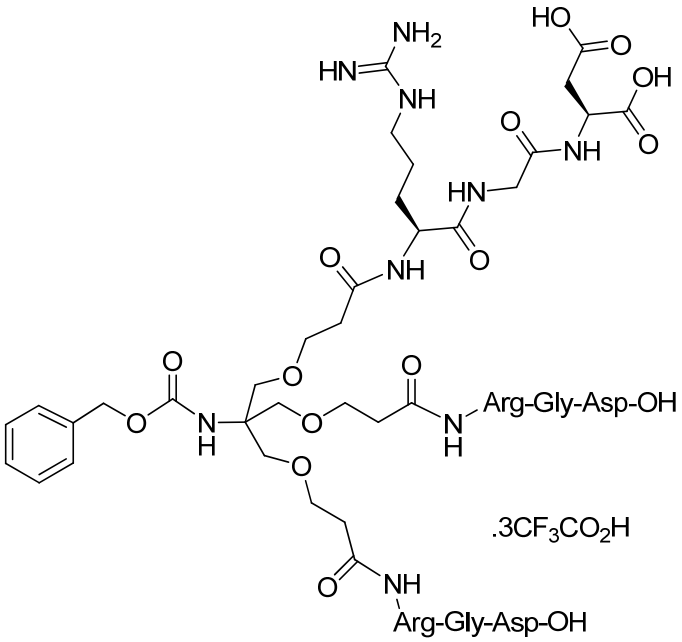

Method A:

Compound **2.14** (100 mg, 39 μmol) was dissolved in a mixture of TFA, water and triisopropylsilane (TIS) (500 μL, 95:2.5:2.5) and shaken for 2.5 h, after which time TLC indicated that the deprotection reaction was complete. The volatile organics were removed *in vacuo,* then the residue was dissolved in 10% aqueous acetic acid (2 ml) and washed three times with a twofold excess of chloroform to extract the non-polar by-products. The volatiles were evaporated *in vacuo* and the residue was redissolved in 10% aqueous acetic acid, shell frozen and lyophilised to yield the product **2.16** as a fluffy white solid (72 mg, quantitative yield as TFA salt).

Method B:

Compound **2.14** (92 mg, 36 μmol) was dissolved in a mixture of TFA, water and triisopropylsilane (TIS) (500 μL, 95:2.5:2.5) and shaken for 4 h, after which time TLC indicated that the deprotection reaction was complete. The volatile organics were removed *in vacuo,* then the residue was dissolved in 10% aqueous acetic acid (2 ml) and washed three times with a twofold excess of chloroform to extract the non-polar by-products. The aqueous acetic acid layer was evaporated *in vacuo* and the residue was redissolved in water (5 ml), shell frozen and lyophilised to yield the product **2.16** as a fluffy white solid (58 mg, 89% as TFA salt).

R_f 0.00 (9:1 DCM/MeOH, cerium stain). $[\alpha]_D$ = -10.8° (c = 0.5, D_2O). M.p: 80.9-88.9°C. ^{1}H NMR (D_2O, 400 MHz) δ 7.26-7.18 (m, C*H* aromatic, 5H); 4.89 (s, CH_2 benzylic, 2H); 4.61 (t, Asp α-*H* × 3, *J* = 6.0 Hz, 3H); 4.14 (dd, Arg α-*H* × 3, *J* = 8.5 Hz and 6.0 Hz, 3H); 3.77 (s, Gly CH_2 × 3, 6H); 3.59-

3.39 (m, CCH_2O × 3, OCH_2CH$_2$ × 3, 12H); 2.99 (t, Arg CH_2NH × 3, J = 7.0 Hz, 6H); 2.78 (d, Asp CH_2 × 3, J = 5.5 Hz, 6H); 2.45-2.31 (m, CH$_2$CH_2C(O) × 3, 6H); 1.75-1.39 (m, Arg CHCH_2 × 3, Arg CH_2CH$_2$NH × 3, 12H). ^{13}C NMR (D_2O, 100 MHz) δ 174.70, 174.64, 174.54, 174.34, 171.16, 157.05 (*C*(O)OH × 2, *C*(O)NH amide × 3, *C*(O)NH carbamate × 1); 137.50 (Benzyl aromatic *C*); 129.13, 128.72, 127.94 (Benzyl aromatic *C*H); 69.20, 67.76 (C*C*H$_2$O, O*C*H$_2$CH$_2$, *C*H$_2$ benzylic, multiple overlapping peaks); 59.44 (*C*CH$_2$O); 53.89 (Arg α-*C*H); 49.44 (Asp α-*C*H); 42.60, 40.87 (Gly *C*H$_2$, Arg *C*H$_2$NH); 36.17, 35.93 (Asp *C*H$_2$, CH$_2$*C*H$_2$C(O)); 28.59 (Arg CH*C*H$_2$); 24.80 (Arg *C*H$_2$CH$_2$NH). $\tilde{\nu}_{max}$ (cm^{-1}) (solid): 3690*w* (O-H acid and N-H amide/guanidino stretches); 3019*w* (C-H alkyl and arene stretches); 1735*w* (C=O acid stretch); 1656*m* (C=O amide stretch); 1543*m* (N-H amide bend and C=C arene stretch); 1475*w*, 1420*w* (C-H alkyl bends); 1181*m*, 1137*m*, 1110*m*, 1048*m* (C-O acid, C-O ether and C-N amide stretches, C-H arene bends). ESI-MS (*m*/*z*): Calc. for $C_{57}H_{91}N_{19}O_{26}$ 728.8186; found: 728.8169 (100%, $[M+2H]^{2+}$), 1456.4682 (2%, $[M+H]^{+}$).

Synthesis of Z-G2-[Arg-Gly-Asp]$_9$ (2.17)

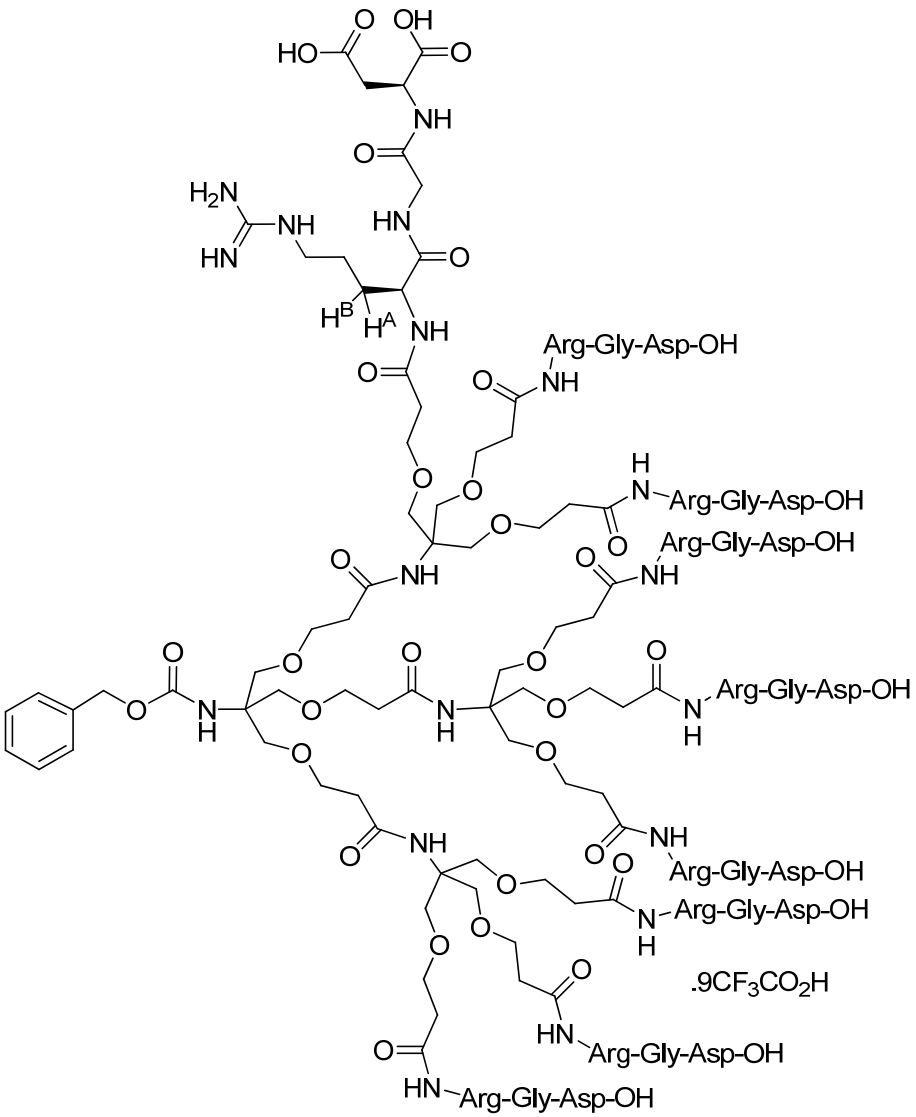

Method A:

Compound **2.15** (110 mg, 14 μmol) was dissolved in a mixture of TFA, water and TIS (500 μL, 95:2.5:2.5) and shaken for 4 h, after which time TLC indicated that the deprotection reaction was complete. The volatile organics were removed *in vacuo,* then the residue was dissolved in 10% aqueous acetic acid (2 ml) and washed three times with a twofold excess of chloroform to extract the non-polar by-products. The volatiles were evaporated *in vacuo* and the residue was redissolved in 10% aqueous acetic acid, shell frozen and lyophilised to yield the product **2.17** as a fluffy white solid (76 mg, 98% as TFA salt).

Method B:

Compound **2.15** (116 mg, 15 μmol) was dissolved in a mixture of TFA, water and TIS (500 μL, 95:2.5:2.5) and shaken for 4 h, after which time TLC indicated that the deprotection reaction was complete. The volatile organics were removed *in vacuo,* then the residue was dissolved in 10% aqueous acetic acid (2 ml) and washed three times with a twofold excess of chloroform to extract the non-polar by-products. The aqueous acetic acid layer was evaporated *in vacuo* and the residue was redissolved in water, shell frozen and lyophilised to yield the product **2.17** as a fluffy white solid (73 mg, 89% as TFA salt).

R_f 0.00 (9:1 DCM/MeOH, cerium stain). $[\alpha]_D$ not acquired. M.p not acquired. ^{1}H NMR (D_2O, 400 MHz) δ 7.17-7.09 (m, C*H* aromatic, 5H); 4.87 (s, CH_2 benzylic, 2H); 4.54 (t, Asp α-*H* × 9, *J* = 6.0 Hz, 9H); 4.08 (dd, Arg α-*H* × 9, *J* = 8.5 Hz and 6.0 Hz, 9H); 3.72 (s, Gly CH_2 × 9, 18H); 3.55-3.35 (m, CCH_2O × 12, OCH_2CH$_2$ × 12, 48H); 2.95 (t, Arg CH_2NH × 9, *J* = 7.0 Hz, 18H); 2.71 (d, Asp CH_2 × 9, *J* = 5.5 Hz, 18H); 2.40-2.20 (m, CH$_2$CH_2C(O) × 12, 24H); 1.66-1.57 (m, Arg CHCH^A × 9, 9H); 1.56-1.48 (m, Arg CHCH^B × 9, 9H); 1.47-1.32 (m, Arg CH_2CH$_2$NH × 9, 18H). ^{13}C NMR not acquired. IR not acquired. ESI-MS (*m/z*): Calc. for $C_{168}H_{278}N_{58}O_{80}$ 731.3239; found: 627.3 (48%, $[M+7H]^{7+}$), 731.4926 (100%, $[M+6H]^{6+}$), 877.8 (48%, $[M+5H]^{5+}$), 1097.0 (36%, $[M+4H]^{4+}$), 1462.3 (7%, $[M+3H]^{3+}$).

Synthesis of PEG-Arg(Pbf)-Gly-Asp(O^{t}Bu)-O^{t}Bu (2.18)

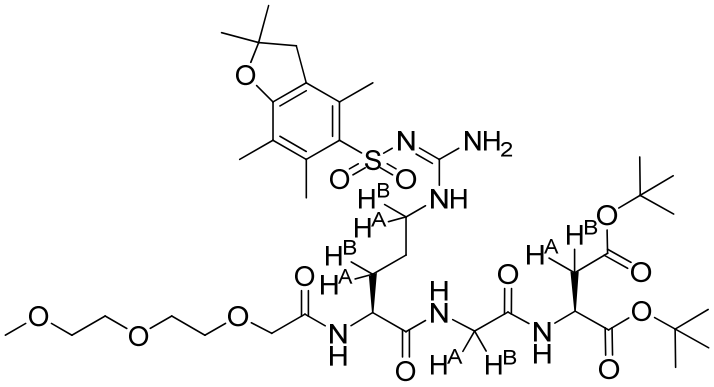

2-[2-(2-methoxyethoxy)-ethoxy)acetic acid (93 mg, 0.52 mmol, 1.0 eq) and **2.8(2.4)** (400 mg, 0.56 mmol, 1.0 eq) were suspended in DCM (10 ml) and DIPEA (200 µL, 1.12 mmol, 2.0 eq) was added with stirring. The solution was cooled in an ice-water bath to 0°C and then T3P (50 wt. % in EtOAc, 400 µL, 0.67 mmol, 1.2 eq) was added dropwise over 10 min. The ice-water bath was removed and the reaction mixture was stirred for 27 h at rt. The solvent was removed *in vacuo* directly, without quenching with water or any prior acid/base workup, to leave a tacky, colourless crude solid (1 g) which was purified by column chromatography (SiO_2, 9:1 DCM/MeOH) to produce the product **2.18** as a fluffy white solid (330 mg, 73%).

R_f 0.40 (9:1 DCM/MeOH, UV and cerium stain). $[\alpha]_D$ = +36.0° (c = 1.0, $CHCl_3$). M.p: 64.0-68.0°C. ^{1}H NMR ($CDCl_3$, 400 MHz) δ 7.69 (br s, N*H* amide (Arg-Gly), 1H); 7.48 (d, N*H* amide (PEG-Arg), *J* = 8.0 Hz, 1H); 7.04 (d, N*H* amide (Gly-Asp), *J* = 8.5 Hz, 1H), 6.28 (br s, N*H*$_2$ guanidine, 2H); 6.12 (br s, N*H* guanidine, 1H); 4.66-4.61 (m, Asp α-*H* and Arg α-*H*, 2H); 4.02 (dd, Gly C*H*^{A}, *J* = 17.0 Hz and 5.5 Hz, 1H); 4.01 (s, OC*H*$_2$C(O)NH, 2H); 3.86 (dd, Gly C*H*^{B}, *J* = 17.0 Hz and 5.5 Hz, 1H); 3.71-3.50 (m, $CH_3OCH_2CH_2OCH_2CH_2$, $CH_3OCH_2CH_2OCH_2CH_2$, $CH_3OCH_2CH_2OCH_2CH_2$, $CH_3OCH_2CH_2OCH_2CH_2$, 8H); 3.34 (s, C*H*$_3$O, 3H); 3.36-3.27 (m, Arg C*H*^{A}NH, 1H); 3.24-3.16 (m, Arg C*H*^{B}NH, 1H); 2.94 (s, Pbf C*H*$_2$, 2H); 2.83 (dd, Asp C*H*^{A}, *J* = 17.0 Hz and 5.0 Hz, 1H); 2.67 (dd, Asp C*H*^{B}, *J* = 17.0 Hz and 4.5 Hz, 1H); 2.58 (s, Pbf C*H*$_3$Ar, 3H); 2.51 (s, Pbf C*H*$_3$Ar, 3H); 2.07 (s, Pbf C*H*$_3$Ar, 3H); 2.01-1.91 (m, Arg CHC*H*^{A}, 1H); 1.75-1.66 (m, Arg CHC*H*^{B}, 1H); 1.61-1.51 (m, Arg C*H*$_2$CH$_2$NH, 2H); 1.44 (s, Pbf C*H*$_3$ × 2, 6H); 1.41, 1.40 (s × 2, C(C*H*$_3$)$_3$ × 2, 18H). ^{13}C NMR ($CDCl_3$, 100 MHz) δ 172.31, 170.54, 170.22, 169.78, 169.17 (*C*(O)O^{t}Bu × 2, *C*(O)NH amide × 3); 158.74, 156.62 (Pbf aromatic *C*-O, *C*=N guanidine); 138.48, 133.04, 132.41, 124.62, 117.51 (Pbf aromatic *C*); 86.41 (Pbf CH$_2$*C*(CH$_3$)$_2$O); 82.60, 81.74 (*C*(CH$_3$)$_3$ × 2); 71.84, 71.11, 70.59, 70.38, 70.32 (*C*H$_2$O's × 5); 59.00 (*C*H$_3$OCH$_2$); 51.99 (Arg α-*C*H); 49.37 (Asp α-*C*H); 43.34, 42.85 (Pbf Ar*C*H$_2$, Gly *C*H$_2$); 40.11 (Arg *C*H$_2$NH); 37.41 (Asp *C*H$_2$); 29.79 (Arg CH*C*H$_2$); 28.70 (Pbf CH$_2$C(*C*H$_3$)$_2$O); 28.12, 27.95 (C(*C*H$_3$)$_3$ × 2); 25.41 (Arg *C*H$_2$CH$_2$NH); 19.41, 18.07, 12.58 (Pbf ArC*H*$_3$ × 3). $\tilde{\nu}_{max}$ (cm^{-1}, solid): 3322*w* (N-H amide stretch); 2976, 2930*w* (C-H alkyl stretches); 1730*m* (C=O ester stretch); 1655*m* (C=O

amide stretch); 1543*s* (N-H amide bend and C=C arene stretch); 1452*w*, 1368*w* (C-H alkyl bend and S=O stretch); 1293*w*, 1278*w*, 1249*m*, 1202*w*, 1150*s*, 1094*s* (C-O ester and C-N amide stretches, C-H arene bends). ESI-MS (*m*/*z*): Calc. for $C_{40}H_{66}N_6NaO_{13}S$ 893.4301; found: 893.4318 (100%, $[M+Na]^+$).

Synthesis of PEG-Arg-Gly-Asp (2.19)

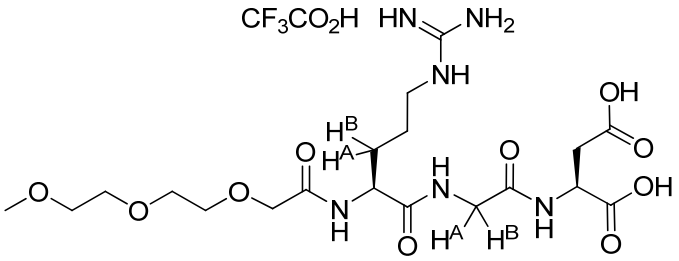

Compound **2.18** (56 mg, 0.064 mmol) was dissolved in a mixture of TFA, water and triisopropylsilane (TIS) (500 μL, 95:2.5:2.5) and shaken for 2 h, after which time TLC indicated that the deprotection reaction was complete. The volatile organics were removed *in vacuo,* then the residue was dissolved in 10% aqueous acetic acid (3 ml) and washed three times with a twofold excess of chloroform to extract the non-polar by-products. The aqueous acetic acid layer was evaporated *in vacuo* and the residue was dissolved in water (5 ml), shell frozen and lyophilised to yield the product **2.19** as a hygroscopic, fluffy white powder which turned to a tacky solid upon standing (22 mg, 55% as TFA salt).

R_f 0.00 (9:1 DCM/MeOH, cerium stain). $[\alpha]_D$ = +10.1° (c = 1.0, CH_3OH). ^{1}H NMR (D_2O, 400 MHz) δ 4.75 (t, Asp α-*H*, *J* = 6.0 Hz, 1H); 4.37 (dd, Arg α-*H*, *J* = 8.5 Hz and 5.5 Hz, 1H); 4.12 (d, Gly C*H*^{A}, *J* = 15.5 Hz, 1H); 4.08 (d, Gly C*H*^{B}, *J* = 15.5 Hz, 1H); 3.92 (s, OC*H*$_2$C(O)NH, 2H); 3.72-3.57 (m, $CH_3OCH_2CH_2OCH_2CH_2$, $CH_3OCH_2CH_2OCH_2CH_2$, $CH_3OCH_2CH_2OCH_2CH_2$, $CH_3OCH_2CH_2OCH_2CH_2$, 8H); 3.33 (s, C*H*$_3$O, 3H); 3.18 (t, Arg C*H*$_2$NH, *J* = 7.0 Hz, 2H); 2.92 (d, Asp C*H*$_2$, *J* = 5.5 Hz, 2H); 1.93-1.84 (m, Arg CHC*H*^{A}, 1H); 1.81-1.71 (m, Arg CHC*H*^{B}, 1H); 1.68-1.56 (m, Arg C*H*$_2$CH$_2$NH, 2H). ^{13}C NMR (D_2O, 100 MHz) δ 175.07, 174.81, 174.75, 173.64, 171.65, 157.43 (*C*(O)OH × 2, *C*(O)NH amide × 3, *C*=N guanidine); 71.16, 70.51, 69.70, 69.68, 69.58 (*C*H$_2$O's × 5, multiple overlapping peaks); 58.20 (*C*H$_3$OCH$_2$); 53.23 (Arg α-*C*H); 49.17 (Asp α-*C*H); 42.38 (Gly *C*H$_2$); 40.53 (Arg *C*H$_2$NH); 35.57 (Asp *C*H$_2$); 28.03 (Arg CH*C*H$_2$); 24.34 (Arg *C*H$_2$CH$_2$NH). $\tilde{\nu}_{max}$ (cm^{-1}) (solid): 3285*m*, 3198*m* (O-H acid and N-H amide/guanidino stretches); 2927*w* (C-H alkyl stretch); 1724*m* (C=O acid stretch); 1651*s* (C=O amide stretch); 1536*s* (N-H amide bend); 1407*w*, 1340*w* (C-H alkyl bends); 1202*m* (C-O acid stretch); 1083*s*, 1049*s* (C-O ether and C-N amide stretches). ESI-MS (*m*/*z*): Calc. for $C_{19}H_{35}N_6O_{10}$ 507.2409; found: 507.2386 (100%, $[M+H]^+$), 529.2197 (95%, $[M+Na]^+$), 551.2022 (16%, $[M+2Na-H]^+$).

Synthesis of PEG-Gly-Gly-Gly (2.20)

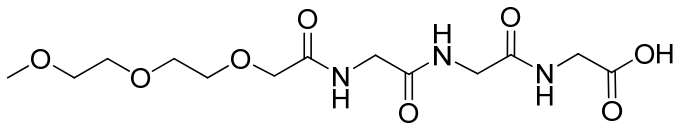

Fmoc-Gly-OH (1.06 g, 3.57 mmol, 2.0 eq) and DIPEA (0.62 ml, 3.57 mmol, 2.0 eq) in dry DCM (25 ml) were added to 2-chlorotrityl chloride resin (1.19 g, 1.00-1.50 mmol/g, 1.19-1.79 mmol) and stirred for 2.25 h. DIPEA (0.4 ml) and MeOH (2 ml) were then added and shaken for 45 minutes to cap the unreacted sites on the resin. The resin was then filtered and washed with DMF (50 ml), DCM (50 ml), MeOH (50 ml), and finally Et_2O (50 ml) before drying *in vacuo*. A loading of 0.91 mmol of Fmoc-Gly was calculated from the resultant mass of the Resin-O-Gly-Fmoc (1.46 g).

To remove the Fmoc-protecting group, a 20% solution of piperidine in DMF was twice added to the resin (50 ml in total) and shaken for 10 minutes each. Filtration of the resin, followed by washing with DMF (100 ml) then DCM (100 ml) until ninhydrin stain of the filtrate showed no visible spot for any residual piperidine or Fmoc-piperidine by-products, yielded Resin-O-Gly-NH_2 (1.22 g) after drying *in vacuo*.

Fmoc-Gly-OH (0.68 g, 2.28 mmol, 2.5 eq with respect to the initial Fmoc-Gly loading), HOBt (0.31 g, 2.28 mmol, 2.5 eq), TBTU (0.73 g, 2.28 mmol, 2.5 eq), and DIPEA (1.1 ml, 6.3 mmol, 7.0 eq) were dissolved in dry DMF (25 ml) and added to a suspension of the resin in dry DMF (50 ml) and shaken overnight. Filtration of the resin, followed by washing with DMF (100 ml) then DCM (100 ml) before drying *in vacuo,* yielded Resin-O-Gly-Gly-Fmoc (1.59 g).

The Fmoc-protecting group was removed as described above to yield Resin-O-Gly-Gly-NH_2.

Fmoc-Gly-OH was coupled to the Fmoc deprotected resin as described above to yield Resin-O-Gly-Gly-Gly-Fmoc (1.58 g).

The Fmoc-protecting group was removed as described above to yield Resin-O-Gly-Gly-Gly-NH_2 (1.32 g).

2-[2-(2-methoxyethoxy)-ethoxy)acetic acid (0.41 g, 2.28 mmol, 2.5 eq with respect to the initial Fmoc-Gly loading), HOBt (0.31 g, 2.28 mmol, 2.5 eq), TBTU (0.73 g, 2.28 mmol, 2.5 eq), and DIPEA (1.1 ml, 6.3 mmol, 7.0 eq) were dissolved in dry DMF (25 ml) and added to a suspension of the resin in dry DMF (50 ml) and shaken overnight. A colorimetric Kaiser Test, performed on a small sample of beads taken from the reaction to monitor the coupling, indicated that some free amines were still present on the beads. 2-[2-(2-methoxyethoxy)-ethoxy)acetic acid (0.41 g, 2.28 mmol, 2.5 eq with respect to the initial Fmoc-Gly loading), HOBt (0.31 g, 2.28 mmol, 2.5 eq), TBTU (0.73 g, 2.28 mmol,

2.5 eq), and DIPEA (1.1 ml, 6.3 mmol, 7.0 eq) were again dissolved in dry DMF (25 ml) and added to the reaction mixture and shaken for 6 days to try and drive the reaction to completion. Subsequently, a Kaiser Test was negative for free amines on the beads. Filtration of the resin, followed by washing with DMF (100 ml) then DCM (100 ml) before drying *in vacuo,* yielded Resin-O-Gly-Gly-Gly-PEG (1.50 g).

The resin (1.50 g) was treated twice with TFA/water (95:5, v/v) (40 ml in total) for 10 minutes each to cleave the peptide from the resin. The resin was further shaken with DCM (3 × 20 ml) for 10 min each, then washed with DCM (100 ml) and all fractions were subsequently collected together and the solvent removed *in vacuo*. The crude peptide was obtained as a brown oil (~400 mg). Purification by column chromatography (SiO_2, 9:1, to 4:1, to 1:1 DCM/MeOH yielded a pale brown hygroscopic foam (320 mg, 0.9 mmol, near quantitative yield based on the initial Fmoc-Gly loading). The product was then dissolved in a ^{t}BuOH/water mixture, filtered over a 0.2 μm PTFE membrane filter, shell-frozen and lyophilised to yield **2.20** as a pale yellow foam.

R_f 0.17 (1:1 DCM/MeOH, $KMnO_4$ stain). M.p not acquired. ^{1}H NMR (CD_3OD, 400 MHz) 4.08, 3.98, 3.93, 3.86 (s × 4, Gly C*H*$_2$ × 3 and OC*H*$_2$C(O), 2H each); 3.75-3.72 (m, PEG C*H*$_2$, 2H); 3.70-3.64 (m, PEG C*H*$_2$ × 2, 4H); 3.57-3.55 (m, PEG C*H*$_2$, 2H); 3.36 (s, C*H*$_3$O, 3H). ^{13}C NMR not acquired. IR not acquired. ESI-MS (*m/z*) (positive ion mode): Calc. for $C_{13}H_{24}N_3O_8$ 350.1558; found: 350.1555 (97%, $[M+H]^+$); 372.1368 (100%, $[M+Na]^+$). ESI-MS (*m/z*) (negative ion mode): Calc. for 348.1412; found: 348.1418 (100%, $[M-H]^-$).

Synthesis of c[R(Pbf)GD(O^{t}Bu)fK(Z)] (2.21)[97, 127, 262]

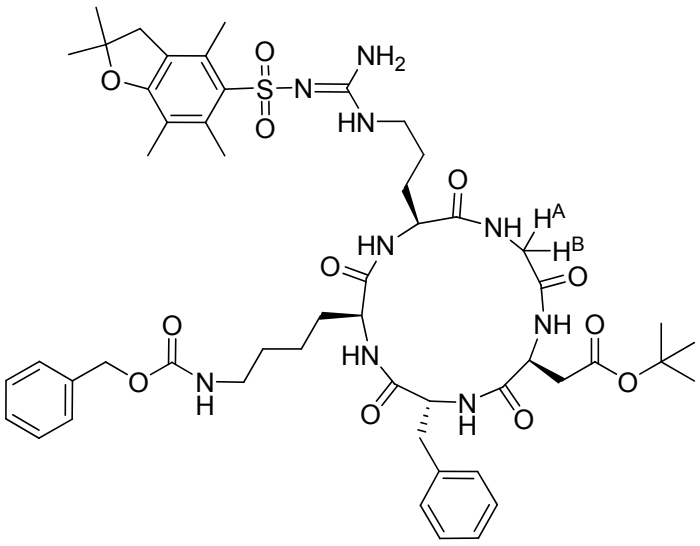

Fmoc-Gly-OH (1.08 g, 3.62 mmol, 2.0 eq) and DIPEA (0.63 ml, 3.62 mmol, 2.0 eq) in dry DCM (20 ml) were added to 2-chlorotrityl chloride resin (1.17 g, ~1.55 mmol/g, 1.81 mmol) and stirred for 2.5

h. DIPEA (2 ml) and MeOH (10 ml) were then added and stirred for 30 minutes to cap any unreacted sites on the resin. The resin was then filtered and washed with DMF (50 ml), DCM (50 ml), MeOH (50 ml), and finally Et_2O (50 ml) before drying *in vacuo*. A loading of 1.75 mmol of Fmoc-Gly was calculated from the resultant mass of the Resin-O-Gly-Fmoc (1.69 g).

To remove the Fmoc-protecting group, a 20 % solution of piperidine in DMF was twice added to the resin (25 ml in total) and stirred for 20 minutes each. Filtration of the resin, followed by washing with DMF (200 ml) then DCM (200 ml) until ninhydrin stain of the filtrate showed no visible spot for any residual piperidine or Fmoc-piperidine by-products, yielded Resin-O-Gly-NH_2 (1.48 g).

Fmoc-Arg(Pbf)-OH (2.27 g, 3.5 mmol, 2.0 eq wrt the initial Fmoc-Gly loading), HOBt (0.47 g, 3.5 mmol, 2.0 eq), TBTU (1.12 g, 3.5 mmol, 2.0 eq), and DIPEA (1.85 ml, 10.5 mmol, 6.0 eq) were added to the resin in dry DMF (25 ml) and stirred for 1.5 h. Filtration of the resin, followed by washing with DMF (200 ml) then DCM (200 ml) before drying *in vacuo*, yielded Resin-O-Gly-Arg(Pbf)-Fmoc (2.19 g).

The Fmoc-protecting group was removed as described above to yield Resin-O-Gly-Arg(Pbf)-NH_2 (2.16 g).

Fmoc-Lys(Z)-OH (1.76 g, 3.5 mmol, 2.0 eq wrt the initial Fmoc-Gly loading), HOBt (0.47 g, 3.5 mmol, 2.0 eq), TBTU (1.12 g, 3.5 mmol, 2.0 eq), and DIPEA (1.85 ml, 10.5 mmol, 6.0 eq) were added to the resin in dry DMF (25 ml) and stirred for 1.5 h. Filtration of the resin, followed by washing with DMF (200 ml) then DCM (200 ml) before drying *in vacuo*, yielded Resin-O-Gly-Arg(Pbf)-Lys(Z)-Fmoc (2.47 g).

The Fmoc-protecting group was removed as described above to yield Resin-O-Gly-Arg(Pbf)-Lys(Z)-NH_2 (2.28 g).

Fmoc-D-Phe-OH (1.36 g, 3.5 mmol, 2.0 eq wrt the initial Fmoc-Gly loading), HOBt (0.47 g, 3.5 mmol, 2.0 eq), TBTU (1.12 g, 3.5 mmol, 2.0 eq), and DIPEA (1.85 ml, 10.5 mmol, 6.0 eq) were added to the resin in dry DMF (25 ml) and stirred for 1.5 h. Filtration of the resin, followed by washing with DMF (200 ml) then DCM (200 ml) before drying *in vacuo*, yielded Resin-O-Gly-Arg(Pbf)-Lys(Z)-D-Phe-Fmoc (2.68 g).

The Fmoc-protecting group was removed as described above to yield Resin-O-Gly-Arg(Pbf)-Lys(Z)-D-Phe-NH_2 (2.45 g).

Fmoc-Asp(O^tBu)-OH (1.44 g, 3.5 mmol, 2.0 eq wrt the initial Fmoc-Gly loading), HOBt (0.47 g, 3.5 mmol, 2.0 eq), TBTU (1.12 g, 3.5 mmol, 2.0 eq), and DIPEA (1.85 ml, 10.5 mmol, 6.0 eq) were added

to the resin in dry DMF (25 ml) and stirred for 1.5 h. Filtration of the resin, followed by washing with DMF (200 ml) then DCM (200 ml) before drying *in vacuo*, yielded Resin-O-Gly-Arg(Pbf)-Lys(Z)-D-Phe-Asp(O^{t}Bu)-Fmoc (2.88 g).

The Fmoc-protecting group was removed as described above to yield Resin-O-Gly-Arg(Pbf)-Lys(Z)-D-Phe-Asp(O^{t}Bu)-NH_2 (2.65 g).

The resin (2.65 g) was treated twice with HFIP/DCM (1:4, v/v) (75 ml in total) for 30 minutes each to cleave the protected peptide from the resin. The resin was further washed with DCM (3 × 20 ml) for 10 min each and all fractions were subsequently collected together and the solvent removed *in vacuo*. The crude protected linear peptide was obtained as a brown solid (1.61 g, 86% crude yield as calculated from the initial Fmoc-Gly loading).

Cyclisation of this compound was carried out without further purification of the protected linear peptide:

The crude linear protected peptide (1.61 g, 1.51 mmol) dissolved in dry DCM (20 ml) was slowly added over 1 h to a solution of T3P (50% w/w in EtOAc, 4.5 ml, 7.55 mmol, 5.0 eq), TEA (4.2 ml, 30.2 mmol, 20.0 eq) and DMAP (20 mg, 0.15 mmol, 0.1 eq) in dry DCM (500 ml), cooled to 0°C in an ice-water bath. The highly diluted solution subsequently turned from pale yellow to bright orange. The reaction was allowed to warm to rt and stirred for 2 days. The solvent was removed *in vacuo* to yield a crude, dark brown oil (6 g).

Purification by column chromatography (SiO_2, 1:10, MeOH/EtOAc) was attempted on the crude material but the compound aggregated/precipitated out at the top of the column. The column was flushed with 100% MeOH and 3 g of the crude material was recovered. ESI-MS showed the molecular ion peaks at m/z 1046.5 ($[M+H]^+$) and m/z 1068.5 ($[M+Na]^+$) but also a peak at m/z 660 which was assigned as a short, linear oligopeptide impurity.

Purification by gel filtration chromatography (Sephadex LH-20, DMF) was carried out to remove the impurity and this was evidenced by the reduced significance, or even disappearance on some attempts, of the peak at m/z 660 in the ESI MS. The product **2.21** was recovered as a pale yellow solid (0.74 g, 40% yield based on the initial Fmoc-Gly loading).

R_f 0.64 (1:10, MeOH/EtOAc, UV and cerium stain). $[\alpha]_D$ = -9.8° (c = 0.5, 1:1 $CHCl_3/CH_3OH$). M.p: decomposes at 198.7°C. ^{1}H NMR (DMSO-d_6, 400 MHz) δ 8.33 (br s, N*H* amide, 1H); 8.04 (d, N*H* amide, *J* = 7.0 Hz, 1H); 7.95 (d, N*H* amide, *J* = 8.5 Hz, 1H); 7.91 (d, N*H* amide, *J* = 9.0 Hz, 1H); 7.50 (d, N*H* amide, *J* = 8.0 Hz, 1H); 7.38-7.28 (m, C*H* aromatic × 5, 5H); 7.26-7.15 (m, C*H* aromatic × 5, 5H); 7.08 (br s, N*H* carbamate, 1H); 6.70 (br s, N*H* guanidine, 1H); 6.46 (br s, NH_2 guanidine, 2H);

5.02 (s, CH_2 benzylic, 2H); 4.66-4.60 (m, α-*H*, 1H); 4.52-4.46 (m, α-*H*, 1H); 4.15-4.10 (m, α-*H*, 1H); 4.08-4.02 (m, Gly CH^A, 1H); 3.96-3.91 (m, α-*H*, 1H); 3.23-3.20 (Gly CH^B, 1H, and Arg CH_2NH, 2H, obscured by the water peak); 3.05-3.01 (m, Lys CH_2NH, 2H); 2.95 (s, Pbf CH_2, 2H); 2.93, 2.82 (dd × 2, Phe CH_2, J = 13.0 Hz and 6.5 Hz, 2H); 2.64, 2.36 (dd × 2, Asp CH_2, J = 15.5 Hz and 8.5 Hz, 2H); 2.48 (s, Pbf CH_3, 3H); 2.42 (s, Pbf CH_3, 3H); 2.01 (s, Pbf CH_3, 3H); 1.74-1.65, 1.60-1.52 (m × 2, Arg CHCH_2, 2H); 1.49-1.26 (m, Lys CHCH_2CH$_2$CH$_2$CH$_2$NH, Lys CHCH$_2$CH$_2$CH_2CH$_2$NH, 4H); 1.41 (s, Pbf CH_3 × 2, 6H); 1.37 (s, ^{t}Bu CH_3 × 3, 9H); 1.09-0.96 (m, Lys CHCH$_2$CH_2CH$_2$CH$_2$NH, 2H). ^{13}C NMR ($CDCl_3$/CD_3OD, 100 MHz) δ 174.03, 173.31, 172.99, 171.93, 171.40, 170.62, 159.35, 158.19, 157.23 (*C*(O)O^{t}Bu, *C*(O)NH amide × 5, *C*(O)NH carbamate, Pbf aromatic *C*-O, *C*=N guanidine); 138.93, 137.46, 137.03, 133.56, 132.91, 125.37, 118.09 (aromatic quaternary *C*'s for: Pbf × 5, Z group, phenylalanine); 129.75, 129.15, 129.02, 128.56, 128.35, 127.53 (aromatic *C*H's for: phenylalanine × 3, Z group × 3); 87.13 (Pbf CH$_2$*C*(CH$_3$)$_2$O); 82.12 (*C*(CH$_3$)$_3$); 67.07 (*C*H$_2$ benzyl Z group); 55.95, 55.68, 53.27, 50.33 (α-*C*H × 4); 44.41, 43.69, 40.84, 37.75, 37.09, (Gly *C*H$_2$, Pbf *C*H$_2$, benzyl *C*H$_2$ (phenylalanine), Arg *C*H$_2$NH, Lys *C*H$_2$NH, Asp *C*H$_2$, multiple overlapping peaks); 31.35, 29.60, 28.58, 26.38, 23.55 (Arg CH*C*H$_2$, Arg *C*H$_2$CH$_2$NH, Lys CH*C*H$_2$, Lys CH$_2$*C*H$_2$CH$_2$NH, Lys *C*H$_2$CH$_2$CH$_2$NH); 28.75 (Pbf CH$_2$C(*C*H$_3$)$_2$O); 28.20 (C(*C*H$_3$)$_3$ × 2); 19.55, 18.29, 12.62 (Pbf Ar*C*H$_3$ × 3). $\tilde{\nu}_{max}$ (cm^{-1}) (solid): 3303*w* (N-H stretch); 2973*w*, 2932*w* (C-H alkyl and arene stretches); 1721*w*, 1678*m*, 1633*s* (C=O ester and C=O amide stretches); 1542*m* (N-H amide bends and C=C arene stretches); 1455*m*, 1368*w* (C-H alkyl bends and S=O stretches); 1244*m*, 1154*m*, 1091*m* (C-O ester and C-N amide stretches, C-H arene bends). ESI-MS (*m*/*z*): Calc. for $C_{52}H_{72}N_9O_{12}S$ 1046.5016; found: 1046.5018 (100%, $[M+H]^+$); 1068.5 (19%, $[M+Na]^+$).

Synthesis of c[R(Pbf)GD(O^{t}Bu)fK] (2.22)

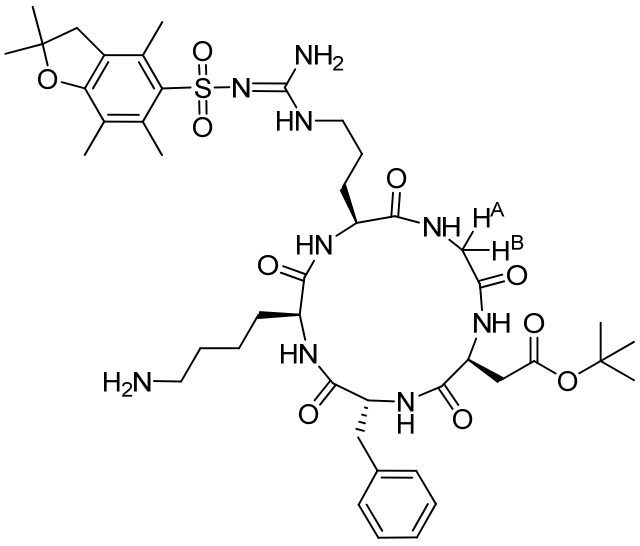

Compound **2.21** (200 mg, 0.19 mmol) was dissolved in DMF followed by the addition of Pd/C catalyst (40 mg, 20%). The flask was subjected to several vacuum/H_2 purges and then stirred for 24 h

under an atmosphere of H_2. The catalyst was filtered off over Celite and carefully washed with DMF. The filtrate, still black in appearance, was passed through a syringe filter (0.45 µm, PTFE membrane) to try and remove the residual catalyst. The solvent was removed *in vacuo* to yield the product **2.22** as a black solid (160 mg, ~92%) as some catalyst still remained due to the fine dispersion of Pd/C in DMF. No further purification was carried out.

R_f 0.00 (9:1 DCM/MeOH or 1:10 MeOH/EtOAc, UV and cerium stain). $[\alpha]_D$ not acquired. M.p not acquired. ^{1}H NMR (DMSO-d_6, 400 MHz) δ 8.42-8.39 (m, N*H* amide, 1H); 8.11-8.03 (m, N*H* amide, 3H); 7.72 (d, N*H* amide, *J* = 7.5 Hz, 1H); 7.27-7.15 (m, C*H* aromatic × 5, 5H); 6.73 (br s, N*H* guanidine, 1H); 6.39 (br s, N*H*$_2$ guanidine, 2H); 4.65-4.59 (m, α-*H*, 1H); 4.50-4.44 (m, α-*H*, 1H); 4.16-4.10 (m, α-*H*, 1H); 4.07-4.01 (m, Gly C*H*^{A}, 1H); 3.98-3.93 (m, α-*H*, 1H); 3.45-3.21 (Gly C*H*^{B}, 1H, and Arg C*H*$_2$NH, 2H, obscured by the water peak); 3.05-3.29 (m, Lys C*H*$_2$NH, 2H); 2.96 (s, Pbf C*H*$_2$, 2H); 2.94, 2.79 (dd × 2, Phe C*H*$_2$, *J* = 13.0 Hz and 6.5 Hz, 2H); 2.63, 2.34 (dd × 2, Asp C*H*$_2$, *J* = 15.5 Hz and 8.5 Hz, 2H); 2.46 (s, Pbf C*H*$_3$, 3H); 2.41 (s, Pbf C*H*$_3$, 3H); 2.00 (s, Pbf C*H*$_3$, 3H); 1.74-1.63, 1.59-1.48 (m × 2, Arg CHC*H*$_2$, 2H); 1.47-1.19 (m, Lys CHC*H*$_2$CH$_2$CH$_2$CH$_2$NH, Lys CHCH$_2$CH$_2$C*H*$_2$CH$_2$NH, 4H); 1.40 (s, Pbf C*H*$_3$ × 2, 6H); 1.35 (s, ^{t}Bu C*H*$_3$ × 3, 9H); 1.09-0.95 (m, Lys CHCH$_2$C*H*$_2$CH$_2$CH$_2$NH, 2H). ^{13}C NMR not acquired. IR not acquired. ESI-MS (*m*/*z*): Calc. for $C_{44}H_{65}N_9NaO_{10}S$ 934.4467; found: 934.4468 (100%, $[M+Na]^+$); 912.46 (68%, $[M+H]^+$).

Synthesis of 5(6)-FL-c[R(Pbf)GD(O^{t}Bu)fK] (2.23)

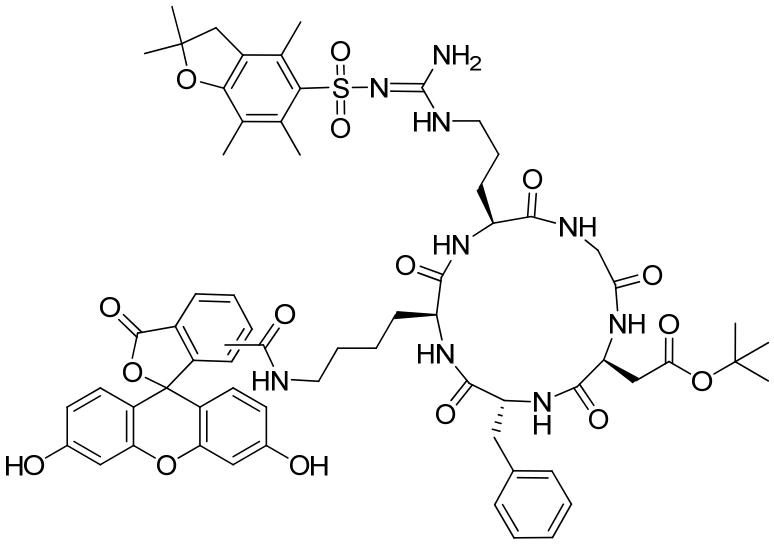

Compound **2.22** (20 mg, 22 µmol, 1.2 eq) was dissolved in dry DMF (400 µl), then TEA (25 µl, 0.18 mmol, 10.0 eq) followed by 5(6)-carboxyfluorescein *N*-hydroxysuccinimide ester (9 mg, 18 µmol, 1.0 eq) were added. Additional dry DMF (600 µl) was used to wash any residual 5(6)-carboxyfluorescein *N*-hydroxysuccinimide ester into the reaction flask. The reaction was stirred at rt for 18 h. Solvent was removed *in vacuo* yielding a crude tacky black oil/solid with a yellow/green pigmentation. This residue

was readily soluble in methanol and seemingly induced the precipitation of a black solid which was deemed to be the residual Pd/C catalyst from the previous hydrogenation step, with possible precipitation of the excess c[R(Pbf)GD(O^{t}Bu)fK] starting material also, which was known to be insoluble in methanol from previous reactions. The solution was filtered over cotton wool and the filtrate evaporated to yield a yellow/orange solid (~28 mg). Purification by gel filtration chromatography (Sephadex LH-20, DMF) yielded the product **2.23** as a yellow solid (20 mg, 83%).

One spot by TLC: R_f 0.67 (4:1 DCM/MeOH, UV and cerium stain). $[\alpha]_D$ not acquired. M.p not acquired. ^{1}H NMR difficult to interpret due to mixture of isomers. ^{13}C NMR not acquired. IR not acquired. ESI-MS (*m/z*) (positive ion mode): Calc. for $C_{65}H_{77}N_9O_{16}S$ 635.7599; found: 635.7643 (100%, $[M+2H]^{2+}$); 1270.3665 (1%, $[M+H]^+$). ESI-MS (*m/z*) (negative ion mode): 1268.5 (82%, $[M-H]^-$), 1314.5 (100%, $[M-H+HCO_2H]^-$).

Synthesis of 5(6)-FL-c[RGDfK] (2.24)

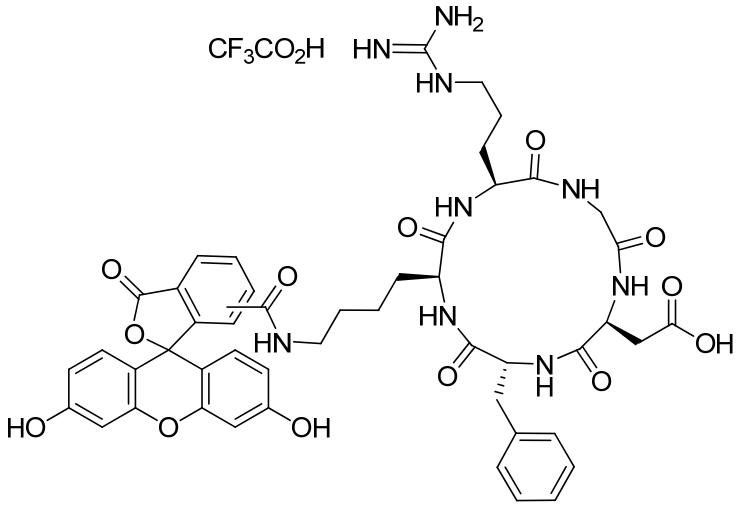

Compound **2.23** (16 mg, 12.6 μmol) was dissolved in a mixture of TFA, water and TIS (500 μl, 95:2.5:2.5) and shaken for 4 h, after which time TLC indicated that the deprotection reaction was complete. The volatiles were removed *in vacuo,* then the residue was dissolved in the minimum amount of methanol and precipitated with cold Et_2O. The yellow solid was filtered over a cotton wool plug, washed with the minimum amount of cold Et_2O then flushed through the cotton wool plug using methanol to re-dissolve. The solvent was removed *in vacuo* to yield **2.24** as a yellow solid (10 mg, 83% as TFA salt).

One spot by TLC: R_f 0.00 (9:1 DCM/MeOH, UV and cerium stain). $[\alpha]_D$ not acquired. M.p not acquired. ^{1}H NMR difficult to interpret due to mixture of isomers. ^{13}C NMR not acquired. IR not acquired. ESI-MS (*m/z*) (positive ion mode): Calc. for $C_{48}H_{52}N_9O_{13}$ 962.3679; found: 962.3663 (100%, $[M+H]^+$). ESI-MS (*m/z*) (negative ion mode): 960.4 (100%, $[M-H]^-$); 982.3 (15%, $[M-2H+Na]^-$).

Synthesis of Z-Gly-Asp(O^{t}Bu)-OMe (2.25)

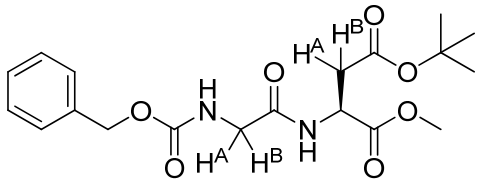

Z-Gly-OH (200 mg, 0.96 mmol, 1.0 eq) and H_2N-Asp(O^{t}Bu)-OMe.HCl (230 mg, 0.96 mmol, 1.0 eq) were dissolved in DCM (~5 ml) and DIPEA (0.34 ml, 1.92 mmol, 2.0 eq) was added. The solution was cooled in an ice-water bath to 0°C and then T3P (50 wt. % in EtOAc, 0.68 ml, 1.14 mmol, 1.2 eq) was added dropwise over 10 min. The ice-water bath was removed and the reaction mixture was stirred overnight at rt. The reaction was quenched with water (20 ml), and then the organic layer was washed with saturated $NaHCO_3$ (20 ml), 1.33 M $NaHSO_4$ (20 ml), water (20 ml), 1.33 M $NaHSO_4$ (60 ml), and finally water (60 ml). The organic phase was dried over $MgSO_4$ and filtered before removing the solvent *in vacuo* to produce the product **2.25** as a clear, colourless oil (0.38 g, quantitative yield). No further purification was required.

R_f 0.65 (9:1 DCM/MeOH, UV and cerium stain). $[\alpha]_D$ = +38.5° (c = 1.0, $CHCl_3$). ^{1}H NMR ($CDCl_3$, 400 MHz) δ 7.34-7.27 (m, C*H* aromatic, 5H); 7.05 (br d, N*H* amide, *J* = 8.0 Hz, 1H); 5.61 (br t, N*H* carbamate, *J* = 5.0 Hz, 1H); 5.10 (app s, CH_2 benzylic, 2H); 4.84-4.80 (m, Asp α-*H*, 1H); 3.94 (br dd, Gly CH^A, *J* = 17.0 Hz and 5.0 Hz, 1H); 3.88 (br dd, Gly CH^B, *J* = 17.0 Hz and 5.0 Hz, 1H); 3.72 (s, C(O)OCH_3, 3H); 2.91 (dd, Asp CH^A, *J* = 17.0 Hz and 4.5 Hz, 1H); 2.71 (dd, Asp CH^B, *J* = 17.0 Hz and 4.5 Hz, 1H); 1.41 (s, C(CH_3)$_3$, 9H). ^{13}C NMR ($CDCl_3$, 100 MHz) δ 171.19, 170.06, 168.91, 156.59 (*C*(O)O^{t}Bu, *C*(O)OCH$_3$, *C*(O)NH amide, *C*(O)NH carbamate); 136.24 (*C* aromatic); 128.61, 128.28, 128.17 (*C*H aromatic); 81.99 (*C*(CH$_3$)$_3$); 67.23 (*C*H$_2$ benzylic); 52.79, 48.67 (C(O)O*C*H$_3$ and Asp α-*C*H); 44.44 (Gly *C*H$_2$); 37.44 (Asp *C*H$_2$); 28.04 (C(*C*H$_3$)$_3$). $\tilde{\nu}_{max}$ (cm^{-1}) (oil): 3310*w* (N-H amide stretch); 2978*m*, 2893*w* (C-H alkyl and arene stretches); 1721*s* (C=O ester stretch); 1674*s* (C=O amide stretch); 1520*s* (N-H amide bend and C=C arene stretch); 1450*m*, 1366*m* (C-H alkyl bends); 1219*s*, 1150*s*, 1049*s* (C-O ester and C-N amide stretches, C-H arene bends); 972*m*, 740*m* (C-H arene bends). ESI-MS (*m*/*z*): Calc. for $C_{19}H_{27}N_2O_7$ 395.1813; found: 395.1803 (72%, $[M+H]^+$). Calc. for $C_{19}H_{30}N_3O_7$ 412.2078; found: 412.2072 (100%, $[M+NH_4]^+$). Calc. for $C_{19}H_{26}N_2NaO_7$ 417.1632; found: 417.1625 (76%, $[M+Na]^+$).

Attempted synthesis of H_2N-Gly-Asp(O^{t}Bu)-OMe (formation of the cyclised product) (2.26)

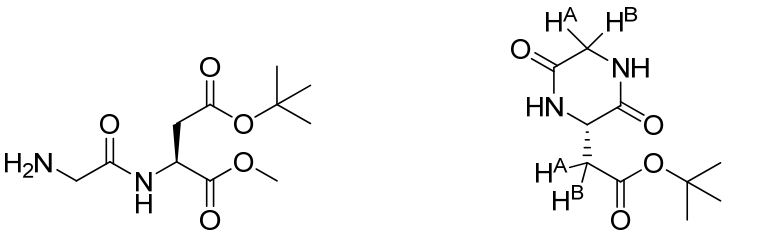

Compound **2.25** (1.61 g, 4.09 mmol) was dissolved in EtOH (25 ml) followed by the addition of Pd/C catalyst (0.16 g, 10%). The flask was subjected to several vacuum/H_2 purges and then stirred for 20 h under an atmosphere of H_2. The catalyst was filtered off over Celite, washed with MeOH, and the filtrate evaporated *in vacuo* to yield **2.26** as a white solid (0.79 g, 75% yield calculated for the linear product). However, NMR and MS analysis showed that the product had intramolecularly cyclised under the hydrogenation conditions to yield **2.26** as the cyclised product (0.79 g, 93% yield calculated for the cyclised product).

R_f not acquired. $[\alpha]_D$ not acquired. M.p not acquired. ^{1}H NMR ($CD_3OD/CDCl_3$, 400 MHz) δ 4.17-4.15 (m, Asp α-*H*, 1H); 4.01 (dd, Gly C*H*^{A}, *J* = 17.5 Hz and 1.2 Hz, 1H); 3.88 (dd, Gly C*H*^{B}, *J* = 17.5 Hz and 1.2 Hz, 1H); 2.85 (dd, Asp C*H*^{A}, *J* = 17.0 Hz and 5.5 Hz, 1H); 2.72 (dd, Asp C*H*^{B}, *J* = 17.0 Hz and 5.5 Hz, 1H); 1.41 (s, C(C*H*$_3$)$_3$, 9H). ^{13}C NMR ($CD_3OD/CDCl_3$, 100 MHz) δ 170.37, 168.73, 167.52 (*C*(O)O^{t}Bu, *C*(O)NH amide × 2); 82.49 (*C*(CH$_3$)$_3$); 52.05 (Asp α-*C*H); 45.12, 38.67 (Gly *C*H$_2$ and Asp *C*H$_2$); 28.20 (C(*C*H$_3$)$_3$). IR not acquired. ESI-MS (*m*/*z*): Calc. for $C_{10}H_{17}N_2O_4$ 229.1; found: 229.1 (8%, [cyclised M+H]$^+$); 251.1 (100%, [cyclised M+Na]$^+$); 173.1 (79%, [cyclised M-C_4H_8+Na]$^+$).

Synthesis of Fmoc-Gly-Asp(O^{t}Bu)-OMe (2.27)

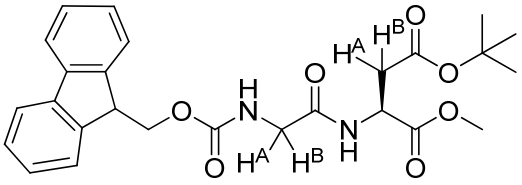

Fmoc-Gly-OH (0.63 g, 2.13 mmol, 1.0 eq) and H_2N-Asp(O^{t}Bu)-OMe.HCl (0.51 g, 2.13 mmol, 1.0 eq) were suspended in DCM (25 ml) then DIPEA (0.74 ml, 4.26 mmol, 2.0 eq) was added and the solids dissolved. The solution was cooled in an ice-water bath to 0°C and then T3P (50 wt. % in EtOAc, 1.5 ml, 2.55 mmol, 1.2 eq) was added dropwise over 30 min. The ice-water bath was removed and the reaction mixture was stirred for 18 h. The reaction was quenched with water (50 ml), and then the organic layer was washed with saturated $NaHCO_3$ (50 ml), 1.33 M $NaHSO_4$ (50 ml), saturated

$NaHCO_3$ (50 ml), then water (50 ml). The organic layer was dried over $MgSO_4$ and filtered before removing the solvent *in vacuo* to produce the product **2.27** as a clear, glassy solid (0.88 g, 85%). No further purification was required.

R_f 0.48 (9:1 DCM/MeOH, UV and cerium stain). $[\alpha]_D$ not acquired. M.p not acquired. ^{1}H NMR ($CDCl_3$, 400 MHz) δ 7.75 (d, C*H* aromatic, *J* = 7.5 Hz, 2H); 7.59 (d, C*H* aromatic, *J* = 7.0 Hz, 2H); 7.39 (app t, C*H* aromatic, *J* = 7.0 Hz, 2H); 7.30 (td, C*H* aromatic, *J* = 7.5 Hz and 1.0 Hz, 2H); 7.07 (d, N*H* amide, *J* = 8.5 Hz, 1H); 5.66 (br t, N*H* carbamate, *J* = 4.5 Hz, 1H); 4.85 (m, Asp α-*H*, 1H); 4.38 (d, Fmoc CH_2, *J* = 7.0 Hz, 2H); 4.21 (t, Fmoc C*H*, *J* = 7.0 Hz, 1H); 3.99 (br dd, Gly CH^A, *J* = 17.0 Hz and 5.5 Hz, 1H); 3.92 (br dd, Gly CH^B, *J* = 17.0 Hz and 5.5 Hz, 1H); 3.72 (s, C(O)OCH_3, 3H); 2.93 (dd, Asp CH^A, *J* = 17.0 Hz and 5.0 Hz, 1H); 2.73 (dd, Asp CH^B, *J* = 17.0 Hz and 5.0 Hz, 1H); 1.39 (s, C(CH_3)$_3$, 9H). ^{13}C NMR ($CDCl_3$, 100 MHz) δ 171.18, 170.09, 168.86, 156.60 (*C*(O)O^{t}Bu, *C*(O)OCH$_3$, *C*(O)NH amide, *C*(O)NH carbamate); 143.88, 143.85, 141.35, 141.35 (Fmoc aromatic *C*); 127.81, 127.17, 125.19, 120.06 (Fmoc aromatic *C*H); 82.02 (*C*(CH$_3$)$_3$); 67.39 (Fmoc *C*H$_2$); 52.82, 48.73, 47.15 (C(O)O*C*H$_3$, Asp α-*C*H, Fmoc *C*H); 44.41 (Gly *C*H$_2$); 37.44 (Asp *C*H$_2$); 28.04 (C(*C*H$_3$)$_3$). IR not acquired. ESI-MS (*m/z*): Calc. for $C_{26}H_{30}N_2NaO_7$ 505.1945; found: 505.1952 (100%, $[M+Na]^+$).

Attempted synthesis of H_2N-Gly-Asp(O^{t}Bu)-OMe (formation of the cyclised product) (2.28)

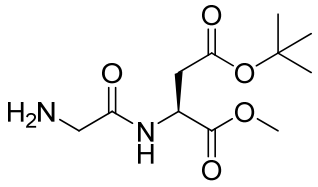

Expected linear product

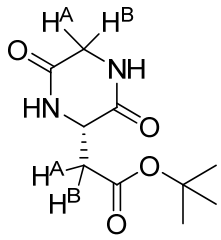

Obtained cyclised product

Compound **2.27** (0.84 g, 1.74 mmol) was dissolved in a 20% piperidine in DCM solution (2.5 ml, 5.1 mmol, 2.9 eq) and stirred overnight. The solvent was then removed *in vacuo* to yield a crude, pale yellow solid. NMR analysis indicates that the product had intramolecularly cyclised under the Fmoc deprotection conditions to form cyclised product **2.28**.

Characterisation data was in agreement with that obtained for **2.26**.

Synthesis of Z-Arg(Pbf)-Gly-OMe (2.29)

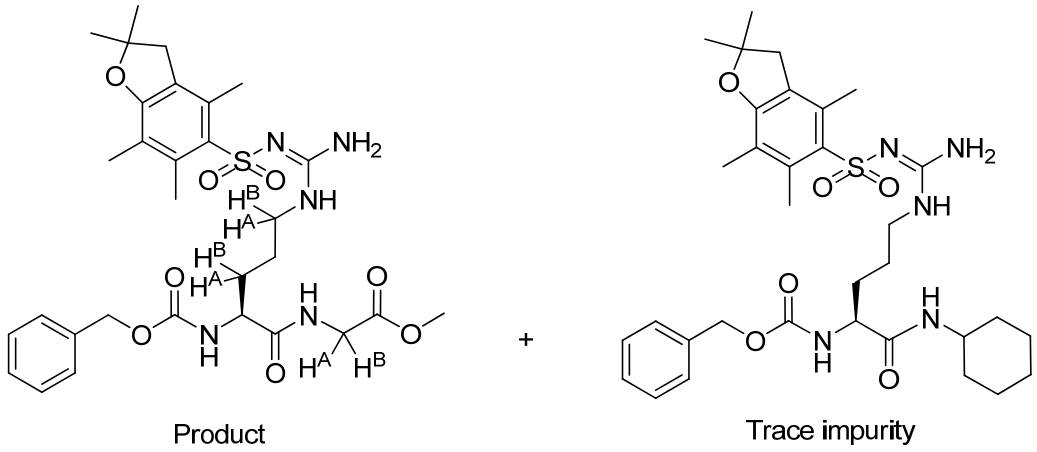

Z-Arg(Pbf)-OH.CHA (0.2 g, 0.3 mmol, 1.0 eq) and H_2N-Gly-OMe.HCl (41 mg, 0.33 mmol, 1.1 eq) were combined as a mixture of solids in DCM (~2 ml). DIPEA (220 μL, 1.2 mmol, 4.0 eq) was added before adding THF (~2 ml) to try and solubilise the solids. T3P (50 wt. % in EtOAc, 220 μL, 0.36 mmol, 1.2 eq) was added rapidly and the solids dissolved with stirring. The reaction was stirred for 2 days before diluting with DCM (20 ml) and quenching with water (20 ml), then the organic layer was washed with saturated $NaHCO_3$ (20 ml), 1.33 M $NaHSO_4$ (20 ml), and water (20 ml). The organic layer was dried over $MgSO_4$, filtered and the filtrate evaporated to produce the product **2.29** as a white solid (200 mg, 86%). No further purification was carried out.

R_f 0.26 (9:1 DCM/MeOH, UV and cerium stain). $[\alpha]_D$ not acquired. M.p not acquired. ^{1}H NMR ($CDCl_3$, 400 MHz) δ 7.69 (app t, N*H* amide, *J* = 5.0 Hz, 1H); 7.32-7.26 (m, C*H* aromatic, 5H); 6.37 (br s, NH_2 guanidine, 2H); 6.20 (br s, N*H* guanidine, 1H); 6.08 (d, N*H* carbamate, *J* = 8.0 Hz, 1H); 5.04 (app s, CH_2 benzylic, 2H); 4.36-4.31 (m, Arg α-*H*, 1H); 4.01 (dd, Gly CH^A, *J* = 18.0 Hz and 6.0 Hz, 1H); 3.87 (dd, Gly CH^B, *J* = 18.0 Hz and 6.0 Hz, 1H); 3.65 (s, C(O)OCH_3, 3H); 3.35-3.22 (m, Arg CH^ANH, 1H); 3.22-3.10 (m, Arg CH^BNH, 1H); 2.92 (s, Pbf CH_2, 2H); 2.54 (s, Pbf CH_3Ar, 3H); 2.46 (s, Pbf CH_3Ar, 3H); 2.06 (s, Pbf CH_3Ar, 3H); 1.94-1.80 (m, Arg CHCH^A, 1H); 1.71-1.62 (m, Arg CHCH^B, 1H); 1.62-1.49 (m, Arg CH_2CH_2NH, 2H); 1.43 (s, Pbf CH_3 × 2, 6H). ^{13}C NMR ($CDCl_3$, 100 MHz) δ 173.60, 171.17, 159.33, 157.03, 156.95 (*C*(O)OCH$_3$, *C*(O)NH amide, *C*(O)NH carbamate, Pbf aromatic *C*-O, *C*=N guanidine); 138.72, 136.60, 132.91, 132.59, 125.02, 117.88 (Pbf aromatic *C* × 5 and benzyl aromatic *C*); 128.82, 128.44, 128.26 (aromatic *C*H × 3); 86.57 (Pbf $CH_2C(CH_3)_2O$); 66.94 (*C*H$_2$ benzylic); 54.13, 52.20 (Arg α-*C*H, C(O)O*C*H$_3$); 43.08 (Pbf Ar*C*H$_2$); 40.91 (Gly *C*H$_2$); 39.96 (Arg *C*H$_2$NH); 29.76 (Arg CH*C*H$_2$); 28.40 (Pbf $CH_2C(CH_3)_2O$); 25.03 (Arg *C*H$_2$CH$_2$NH); 19.04, 17.69, 12.20 (Pbf Ar*C*H$_3$ × 3). IR not acquired. ESI-MS (*m/z*): Calc. for $C_{30}H_{42}N_5O_8S$ 632.2749; found: 632.2763 (100%, $[M+H]^+$); 642.3 (8%, [trace impurity+H]$^+$).

Attempted synthesis of Z-Arg(Pbf)-Gly-OH (2.29)

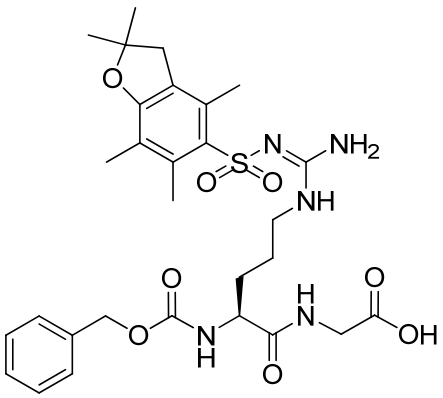

Expected product

Lost to the aqueous phase?

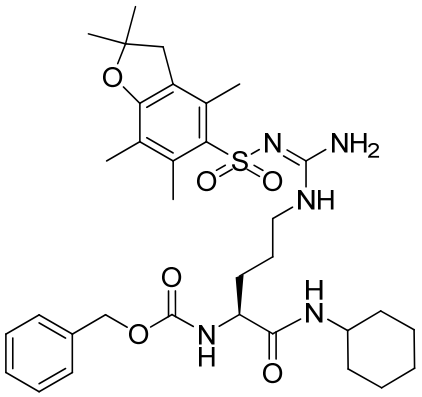

Impurity recovered

Z-Arg(Pbf)-Gly-OMe (0.21 g, 0.33 mmol) was dissolved in MeOH (10 ml), then 1M NaOH (10 ml) was added. The reaction was stirred at 40°C for 1.5 h, and then the solvent was removed *in vacuo*. The residue was dissolved in water (20 ml), acidified to pH 1 with $NaHSO_4$ (1.33 M, ~10ml) and extracted with DCM (4 × 50 ml). The organic fractions were combined, dried over $MgSO_4$, filtered and the filtrate evaporated to yield an oily residue (~10 mg) which corresponded to the trace impurity carried through from the previous step.

Partial characterisation: ESI-MS (*m*/*z*): Calc. for $C_{33}H_{48}N_5O_6S$ 642.82; found: 642.3 (100%, [trace impurity+H]$^+$).

Synthesis of Boc-Gly-Asp(OBn)-NH_2 (2.30)

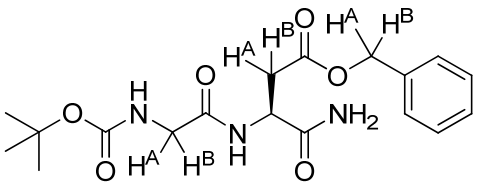

Boc-Gly-OH (0.68 g, 3.88 mmol, 1.0 eq) and DIPEA (1.35 ml, 7.75 mmol, 2.0 eq) were dissolved in dry DCM (15 ml) and cooled over an ice-water bath. TBTU (1.24 g, 3.88 mmol, 1.0 eq) was added as a solid and the reaction was stirred at 0°C for 15 min. H_2N-Asp(OBn)-NH_2.HCl (1.00 g, 3.88 mmol, 1.0 eq) was added as a solid and the reaction was stirred for a further 30 min at 0°C before removing the ice-water bath and stirring the reaction at rt for 12.5 h. TLC indicated possible presence of H_2N-Asp(OBn)-NH_2.HCl starting material and the reaction still appeared cloudy due to residual H_2N-Asp(OBn)-NH_2.HCl, therefore dry DMF (~5 ml) was added and the reaction became clear. The reaction was stirred for a further 5 h and then the organic phase was washed with water (50 ml), separated, and the water layer extracted with DCM (50 ml). The organic fractions were combined and

then washed successively with 1.33 M $NaHSO_4$ (3 × 100 ml), 1 M Na_2CO_3 (3 × 100 ml), water (100 ml), and finally brine (100 ml). The organic phase was dried over $MgSO_4$ and filtered before removing the solvent *in vacuo* to produce the product **2.30** as a clear, colourless oil (1.38 g, 94%). No further purification was carried out.

R_f 0.49 (9:1 DCM/MeOH, UV and cerium stain). $[\alpha]_D$ = -13.0° (c = 0.5, $CHCl_3$). ^{1}H NMR ($CDCl_3$, 400 MHz) δ 7.70 (d, N*H* amide, *J* = 9.0 Hz, 1H); 7.37-7.27 (m, C*H* aromatic, 5H); 7.05 (br s, N*H* amide, 1H); 6.25 (br s, N*H* amide, 1H); 5.89 (br t, N*H* carbamate, *J* = 5.0 Hz, 1H); 5.12 (d, CH^A benzylic, *J* = 12.0 Hz, 1H); 5.08 (d, CH^B benzylic, *J* = 12.5 Hz, 1H); 4.91-4.86 (m, Asp α-*H*, 1H); 3.82 (dd, Gly CH^A, *J* = 17.0 Hz and 6.0 Hz, 1H); 3.72 (dd, Gly CH^B, *J* = 17.0 Hz and 5.0 Hz, 1H); 3.03 (dd, Asp CH^A, *J* = 17.0 Hz and 5.0 Hz, 1H); 2.76 (dd, Asp CH^B, *J* = 17.0 Hz and 5.0 Hz, 1H); 1.42 (s, C(CH_3)$_3$, calc 9H, found 8H). ^{13}C NMR ($CDCl_3$, 100 MHz) δ 173.06, 171.51, 170.13, 156.55 (*C*(O)OBn, *C*(O)NH amide × 2, *C*(O)NH carbamate); 135.34 (*C* aromatic); 128.54, 128.32, 128.20 (*C*H aromatic); 80.28 (*C*(CH_3)$_3$) 66.76 (*C*H_2 benzylic); 48.86 (Asp α-*C*H); 44.38 (Gly *C*H_2); 35.58 (Asp *C*H_2); 28.25 (C(*C*H_3)$_3$). $\tilde{\nu}_{max}$ (cm^{-1}) (oil): 3264*w* (N-H amide stretch); 3055*w* (C-H arene stretch); 2978*w*, 2870*w* (C-H alkyl stretch); 1759*w* (C=O ester stretch); 1697*m*, 1659*s* (C=O amide stretch); 1543*m*, 1504*m* (N-H amide bend and C=C arene stretch); 1450*w*, 1389*m*, 1366*m* (C-H alkyl bends); 1250*s*, 1150*s*, 1088*w*, 1049*w*, 1003*w* (C-O ester and C-N amide stretches, C-H arene bends); 941*w*, 864*w*, 833*w*, 772*w*, 733*m* (C-H arene bends). ESI-MS (*m*/*z*): Calc. for $C_{18}H_{26}N_3O_6$ 380.1816; found: 380.1810 (78%, $[M+H]^+$). Calc. for $C_{18}H_{25}N_3NaO_6$ 402.1636; found: 402.1625 (78%, $[M+Na]^+$).

Synthesis of H_2N-Gly-Asp(OBn)-NH_2 (2.31)

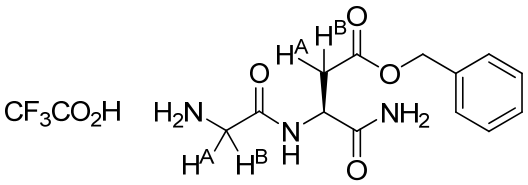

Compound **2.30** (110 mg, 0.29 mmol) was dissolved in DCM (2 ml) and cooled over an ice-water bath. TFA (2 ml) was added dropwise and then the ice-water bath was removed. The reaction was stirred for 20 min and then the solvent was removed *in vacuo* to yield **2.31** as a yellow oil (80 mg, 70%).

R_f 0.00 (9:1 DCM/MeOH, UV and cerium stain). $[\alpha]_D$ = +0.9° (c = 0.1, MeOH). ^{1}H NMR (CD_3OD, 400 MHz) δ 7.36-7.27 (m, C*H* aromatic, 5H); 5.13 (s, CH_2 benzylic, 2H); 4.84 (dd, Asp α-*H*, *J* = 8.0 Hz and 5.0 Hz, 1H); 3.77 (d, Gly CH^A, *J* = 16.0 Hz, 1H); 3.65 (d, Gly CH^B, *J* = 16.0 Hz, 1H); 2.95 (dd, Asp CH^A, *J* = 16.0 Hz and 5.0 Hz, 1H); 2.82 (dd, Asp CH^B, *J* = 16.0 Hz and 5.0 Hz, 1H). ^{13}C NMR (CD_3OD, 100 MHz) δ 175.04, 171.92, 167.64 (*C*(O)OBn, *C*(O)NH amide × 2); 137.26 (*C* aromatic); 129.59, 129.34 (*C*H aromatic, multiple overlapping peaks); 67.79 (*C*H_2 benzylic); 51.07 (Asp

α-*C*H); 41.64 (Gly *C*H$_2$); 37.12 (Asp *C*H$_2$). $\tilde{\nu}_{max}$ (cm^{-1}) (oil): 3186*w* (N-H amide stretch); 3063*w* (C-H arene stretch); 2978*w*, 2870*w*, 2816*w* (C-H alkyl stretch); 1659*s* (C=O amide stretch overlapping C=O ester stretch); 1558*m*, 1520*m* (N-H amide bend and C=C arene stretch); 1427*m*, 1389*m*, 1358*w* (C-H alkyl bends); 1265*w*, 1180*s*, 1126*s* (C-O ester and C-N amide stretches, C-H arene bends); 910*w*, 833*w*, 802*w*, 718*m*, 694*m* (C-H arene bends). ESI-MS (*m*/*z*): Calc. for $C_{13}H_{18}N_3O_4$ 280.1292; found: 280.1294 (100%, $[M+H]^+$).

Synthesis of Fmoc-Arg(Pbf)-Gly-Asp(OBn)-NH$_2$ (2.32)

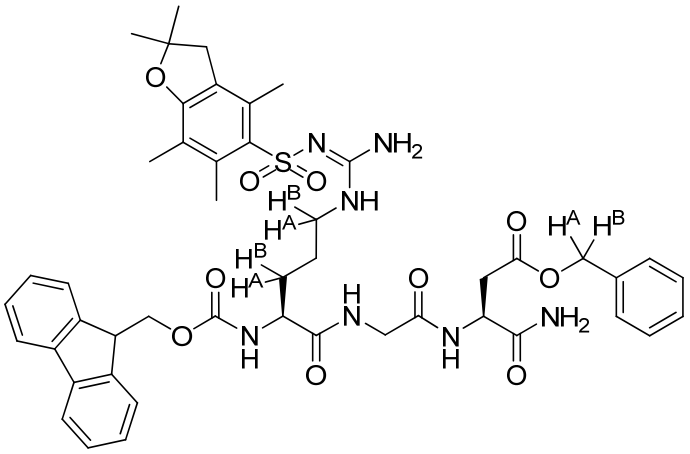

Fmoc-Arg(Pbf)-OH (132 mg, 0.2 mmol, 1.0 eq) was taken up in DCM (2 ml), then DIPEA (75 μL, 0.43 mmol, 2.0 eq) was added and the reaction mixture was cooled over an ice-water bath. TBTU (66 mg, 0.2 mmol, 1.0 eq) was added as a solid and the reaction was stirred at 0°C for 5 min. Compound **2.31** (80 mg, 0.2 mmol, 1.0 eq) was dissolved in DCM/DMF (2:1, 1.5 ml), added dropwise to the reaction flask and a further portion of DCM (1 ml) was used to transfer any residual **2.31** from the vial and into the reaction flask. The reaction was stirred for a further 30 min at 0°C before removing the ice-water bath and stirring the reaction at rt for 2 days and then the organic phase was washed with water (50 ml), separated, and the water layer extracted with DCM (2 × 50 ml). The organic fractions were combined and then washed successively with 1.33 M $NaHSO_4$ (2 × 50 ml), 1 M Na_2CO_3 (50 ml), and finally brine (150 ml). The organic phase was dried over $MgSO_4$ and filtered before removing the solvent *in vacuo* to produce the product **2.32** as a sticky clear oil/foam (150 mg, 81%). No further purification was carried out.

R_f 0.42 (9:1 DCM/MeOH, UV and cerium stain). $[\alpha]_D$ = -6.0° (c = 1.0, $CHCl_3$). ^{1}H NMR ($CDCl_3$, 400 MHz) δ 8.12 (br s, N*H* amide (Arg-Gly), 1H); 7.82 (br s, N*H* amide (Gly-Asp), 1H); 7.67 (d, Fmoc C*H* aromatic × 2, *J* = 7.5 Hz, 2H); 7.53 (t, Fmoc C*H* aromatic × 2, *J* = 8.5 Hz, 2H); 7.34-7.08 (m, Fmoc C*H* aromatic × 4, benzyl C*H* aromatic × 5 and N*H* amide (of C(O)N*H*$_2$), 10H); 6.64 (br s, N*H* amide (of C(O)N*H*$_2$) and N*H* carbamate, 2H); 6.44 (br s, N*H*$_2$ guanidine, 2H); 6.31 (br s, N*H* guanidine, 1H); 4.99 (d, C*H*^{A} benzylic, *J* = 12.0 Hz, 1H); 4.94 (d, C*H*^{B} benzylic, *J* = 12.5 Hz, 1H);

4.84-4.79 (br m, Asp α-*H*, 1H); 4.36-4.18 (br m, Arg α-*H* and Fmoc C*H*$_2$, 3H); 4.08-4.05 (br t, Fmoc C*H*, 1H); 4.00-3.82 (app br m, Gly C*H*$_2$, 2H); 3.41-3.22 (br m, Arg C*H*^{A}NH, 1H); 3.22-3.05 (br m, Arg C*H*^{B}NH, 1H); 2.90 (underlying m obscured by the DMF solvent peaks, Asp C*H*$_2$, 2H); 2.86 (underlying s obscured by the DMF solvent peaks, Pbf C*H*$_2$, 2H); 2.56 (s, Pbf C*H*$_3$Ar, 3H); 2.47 (s, Pbf C*H*$_3$Ar, 3H); 2.02 (s, Pbf C*H*$_3$Ar, 3H); 1.94-1.78 (m, Arg CHC*H*^{A}, 1H); 1.78-1.64 (m, Arg CHC*H*^{B}, 1H); 1.64-1.50 (m, Arg C*H*$_2$CH$_2$NH, 2H); 1.39 (s, Pbf C*H*$_3$ × 2, 6H). ^{13}C NMR ($CDCl_3$, 100 MHz) δ 174.19, 173.59, 171.20, 170.18 (*C*(O)OBn, *C*(O)NH amide × 3); 158.79, 156.86, 156.72 (Pbf aromatic *C*-O, *C*=N guanidine, *C*(O)NH carbamate); 143.82, 143.68, 141.16, 138.30, 135.40, 132.57, 132.21, 128.49, 128.22, 128.09, 127.68, 127.08, 125.23, 124.72, 119.90, 117.60 (Fmoc aromatic *C* and *C*H, benzyl aromatic *C* and *C*H); 86.42 (Pbf CH$_2$*C*(CH$_3$)$_2$O); 67.08 (*C*H$_2$ benzylic); 66.70 (Fmoc *C*H$_2$); 54.82 (Arg α-*C*H); 49.72 (Asp α-*C*H); 46.98 (Fmoc *C*H); 43.42, 43.41, 43.14 (Pbf Ar*C*H$_2$, Gly *C*H$_2$, Arg *C*H$_2$NH); 35.57 (Asp *C*H$_2$); 29.02 (Arg CH*C*H$_2$); 28.55 (Pbf CH$_2$C(*C*H$_3$)$_2$O); 25.47 (Arg *C*H$_2$CH$_2$NH); 19.38, 18.04, 12.49 (Pbf Ar*C*H$_3$ × 3). $\tilde{\nu}_{max}$ (cm^{-1}) (solid): 3441*w*, 3325*w*, 3248*w* (N-H amide stretch); 2978*w*, 2870*w* (C-H alkyl and arene stretches); 1667*m* (C=O amide stretch overlapping C=O ester stretch); 1512*s* (N-H amide bend and C=C arene stretch); 1450*m*, 1381*m* (C-H alkyl bends and S=O stretches); 1242*s*, 1150*m*, 1088*s* (C-O ester and C-N amide stretches, C-H arene bends); 1026*w*, 995*w*, 910*w*, 849*w*, 810*w*, 779*w*, 741*w* (C-H arene bends). ESI-MS (*m*/*z*): Calc. for $C_{47}H_{56}N_7O_{10}S$ 910.3804; found: 910.3818 (100%, $[M+H]^+$).

Attempted Synthesis of H_2N-Arg(Pbf)-Gly-Asp(OBn)-NH_2 (2.33)

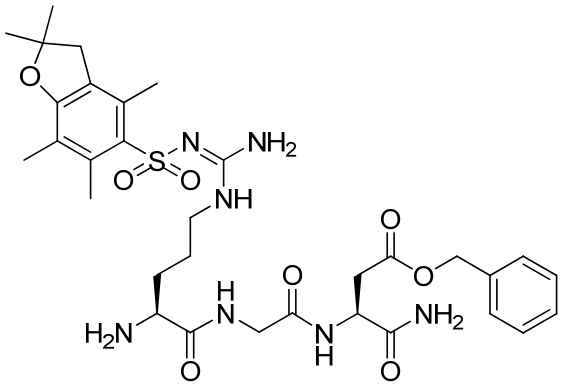

Expected product

Compound **2.32** (2.1 g, 2.31 mmol) was dissolved in a 20% piperidine in DCM solution (10 ml) and stirred for 2 h. The solvent was then removed *in vacuo* to yield a crude, pale yellow solid (3.5 g). Purification by column chromatography (SiO_2, 100% DCM + 1% TEA, to 98:2 DCM/MeOH + 1% TEA, to 95:5 DCM/MeOH + 1% TEA, to 9:1 DCM/MeOH + 1% TEA) yielded a white solid of unknown identity (1.6 g, quantitative yield). ^{1}H NMR showed traces of TEA and so the solid was dissolved in DCM (100 ml), washed with water/brine (100 ml), then brine (100 ml), and then the

organic phase was dried over $MgSO_4$, filtered and the filtrate evaporated to yield an unidentifiable white solid.

See the appendix for ^{1}H NMRs of the material that was obtained after silica column chromatography (spectrum 2.12) and then subsequently after aqueous workup (spectrum 2.13).

Synthesis of Fmoc-Asp(O^{t}Bu)-OBn (2.34)

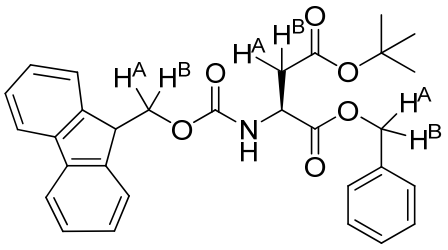

Fmoc-Asp(O^{t}Bu)-OH (1.14 g, 2.77 mmol), TBAB (91 mg, 0.28 mmol, 0.1 eq) and anhydrous K_2CO_3 (0.42 g, 3.05 mmol, 1.1 eq) were combined as a mixture of solids in CH_3CN (20 ml) and the potassium salt allowed to form over a period of 20 min. Benzyl bromide (0.36 ml, 3.05 mmol, 1.1 eq) in CH_3CN (1ml) was added dropwise over 15 min to the vigorously stirred mixture. More CH_3CN (10 ml) was added for good stirring and the reaction stirred for 6 h before more CH_3CN (20 ml) was added. DCM (10 ml) was added after 6.5 h to try and solubilise the SM. The reaction was stirred for another 14 h before the solvent was removed *in vacuo*. The residue was taken up in EtOAc (50 ml) and the white solid dissolved into the aqueous layer upon washing with sat. $NaHCO_3$ (3 × 25 ml), water (3 × 25 ml), then brine. The organic layer was dried over Na_2SO_4, filtered and the filtrate evaporated to yield a clear oil. Recrystallisation from EtOAc/hexane afforded the product, **2.34**, as a white solid (1.39 g, quantitative yield).

R_f 0.83 (9:1 DCM/MeOH, UV and cerium stain). $[\alpha]_D$ = +13.4° (c = 1.0, $CHCl_3$). M.p not acquired. ^{1}H NMR ($CDCl_3$, 400 MHz) δ 7.78 (d, Fmoc C*H* aromatic, *J* = 7.5 Hz, 2H); 7.61 (d, Fmoc C*H* aromatic, *J* = 7.5 Hz, 2H); 7.41 (t, Fmoc C*H* aromatic, *J* = 7.5 Hz, 2H); 7.37-7.30 (multiple overlapping peaks, benzyl C*H* aromatic × 5, Fmoc C*H* aromatic × 2, 7H); 5.90 (d, N*H* carbamate, *J* = 8.5 Hz, 1H); 5.26 (d, C*H*^{A} benzylic, *J* = 12.5 Hz, 1H); 5.19 (d, C*H*^{B} benzylic, *J* = 12.5 Hz, 1H); 4.67 (m, Asp α-*H*, 1H); 4.43 (dd, Fmoc C*H*^{A}, *J* = 10.5 Hz and 7.0 Hz, 1H); 4.35 (dd, Fmoc C*H*^{B}, *J* = 10.5 Hz and 7.0 Hz, 1H); 4.24 (t, Fmoc C*H*, *J* = 7.0 Hz, 1H); 2.99 (dd, Asp C*H*^{A}, *J* = 17.0 Hz and 5.0 Hz, 1H); 2.81 (dd, Asp C*H*^{B}, *J* = 17.0 Hz and 5.0 Hz, 1H); 1.42 (s, C(C*H*$_3$)$_3$, 9H). ^{13}C NMR ($CDCl_3$, 100 MHz) δ 171.39, 170.54, 156.51 (*C*(O)O^{t}Bu, *C*(O)OBn, *C*(O)NH carbamate); 144.33, 144.12, 141.69, 141.66, 135.62 (Fmoc aromatic *C* × 4, benzyl aromatic *C* × 1); 129.37, 129.12, 128.92, 128.76, 128.58, 128.05, 127.41, 125.51, 125.46, 120.27 (Fmoc aromatic *C*H and benzyl aromatic *C*H); 81.97 (*C*(CH$_3$)$_3$); 67.48, 67.31 (Fmoc *C*H$_2$ and *C*H$_2$ benzylic); 50.58, 46.99 (Asp α-*C*H, Fmoc *C*H); 37.59 (Asp *C*H$_2$);

27.80 (C(*C*H$_3$)$_3$). $\tilde{\nu}_{max}$ (cm^{-1}) (solid): 3657*w* (N-H amide stretch); 3040*w* (C-H arene stretch); 2978*m*, 2878*w* (C-H alkyl stretch); 1720*s* (C=O stretch); 1574*m* (N-H carbamate bend and C=C arene stretch); 1489*m*, 1450*m*, 1373*m*, 1342*m* (C-H alkyl bends); 1281*m*, 1250*m*, 1211*m*, 1173*s*, 1134*m*, 1065*m*, 1026*m* (C-O ester and C-N carbamate stretches, C-H arene bends); 988*w*, 941*w*, 895*w*, 849*w*, 733*m*, 694*m* (C-H arene bends). ESI-MS (*m*/*z*): Calc. for $C_{30}H_{31}NNaO_6$ 524.2044; found: 524.2044 (100%, $[M+Na]^+$); 502.2223 (53%, $[M+H]^+$).

Synthesis of H_2N-Asp(O^{t}Bu)-OBn (2.35)

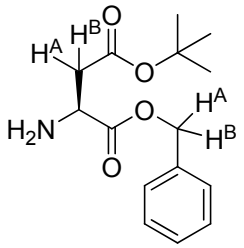

Compound **2.34** (5.7 g, 11.4 mmol) was stirred in a solution of 20% piperidine in DCM (25 ml) for 2 h, after which time water (100 ml) was added and the reaction was stirred vigorously for 30 min. The organic phase was separated, washed with water (2 × 100 ml), dried over $MgSO_4$, filtered and the filtrate evaporated to yield a crude white solid (~5.1 g). Purification by column chromatography (SiO_2, 100% DCM + 1% TEA, to 98:2 DCM/MeOH + 1% TEA, to 95:5 DCM/MeOH + 1% TEA) yielded the product, **2.35**, as a clear, pale yellow oil (1.94 g, 61%).

R_f 0.31 (95:5 DCM/MeOH, cerium stain). $[\alpha]_D$ not acquired. ^{1}H NMR ($CDCl_3$, 400 MHz) δ 7.15-7.03 (m, C*H* aromatic, 5H); 4.95 (d, C*H*^{A} benzylic, *J* = 12.0 Hz, 1H); 4.90 (d, C*H*^{B} benzylic, *J* = 12.0 Hz, 1H); 3.52 (dd, Asp α-*H*, *J* = 6.5 Hz and 5.0 Hz, 1H); 2.70 (dd, Asp C*H*^{A}, *J* = 16.5 Hz and 5.0 Hz, 1H); 2.64 (dd, Asp C*H*^{B}, *J* = 16.5 Hz and 5.0 Hz, 1H); 1.71 (br s, N*H*$_2$, 2H); 1.18 (s, C(C*H*$_3$)$_3$, 9H). 174.27, 170.28 (*C*(O)O^{t}Bu, *C*(O)OBn); 135.57 (Benzyl aromatic *C*); 128.55, 128.33, 128.24 (Benzyl aromatic *C*H × 3); 81.18 (*C*(CH$_3$)$_3$); 66.89 (*C*H$_2$ benzylic); 51.34 (Asp α-*C*H); 39.89 (Asp *C*H$_2$); 28.00 (C(*C*H$_3$)$_3$). $\tilde{\nu}_{max}$ (cm^{-1}) (oil): 3657*w* (N-H amide stretch); 3055*w* (C-H arene stretch); 2978*m*, 2886*w* (C-H alkyl stretch); 1728*s* (C=O stretch); 1674*s*, 1605*m* (N-H bend and C=C arene stretch); 1450*m*, 1366*s*, 1342*m* (C-H alkyl bends); 1273*m*, 1250*m*, 1211*m*, 1150*s* (C-O ester and C-N carbamate stretches, C-H arene bends); 957*w*, 841*s*, 772*w*, 733*m*, 694*m* (C-H arene bends). ESI-MS (*m*/*z*): Calc. for $C_{15}H_{22}NO_4$ 280.1543; found: 280.1537 (12%, $[M+H]^+$); 302.1353 (6%, $[M+Na]^+$); 224.0912 (100%, $[M+H-C_4H_8]^+$).

Synthesis of Alloc-Gly-OH (2.36)

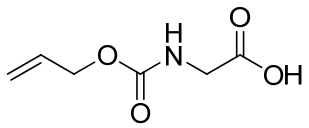

Glycine (4.2 g, 56 mmol, 1.0 eq) was dissolved in a mixture of deionised water/THF (2:1, 90 ml) and then 2 M NaOH (56 ml) and allyl chloroformate (5.9 ml, 56 mmol, 1.0 eq) in THF (30 ml) were added rapidly in succession. The reaction was stirred vigorously for 17 h at rt and then the solvent was removed *in vacuo*. The residue was subsequently dissolved in water (30 ml), acidified to pH ~2 using 1 M HCl and then extracted with EtOAc (2 × 100 ml). The organic fractions were combined and washed with water (100 ml), dried over $MgSO_4$ and filtered before removing the solvent *in vacuo* to produce the product, **2.36**, as a colourless oil/tacky solid (6.7 g, 75%). No further purification was carried out.

R_f 0.00 (9:1 DCM/MeOH, $KMnO_4$ stain). ^{1}H NMR ($CDCl_3$, 400 MHz) δ 10.81 (br s, C(O)O*H*, 1H); 5.86 (ddt, H_2C=C*H*CH_2, *J* = 17.0 Hz, 11.0 Hz and 5.5 Hz, 1H); 5.72 (t, N*H* carbamate, *J* = 5.5 Hz, 1H); 5.29-5.24 (m, *H*-CH=$CHCH_2$, 1H); 5.20-5.16 (m, *H*-CH=$CHCH_2$, 1H); 4.59-4.54 (m, H_2C=CHC*H*$_2$, 2H); 3.96-3.93 (m, Gly C*H*$_2$, 2H). ^{13}C NMR ($CDCl_3$, 100 MHz) δ 174.13, 156.82 (*C*(O)OH and *C*(O)NH carbamate); 132.41 (H_2C=*C*HCH_2); 118.03 (H_2C=CHCH_2); 66.22 (H_2C=CH*C*H_2); 42.44 (Gly *C*H_2). $\tilde{\nu}_{max}$ (cm^{-1}) (solid): 3348*w* (N-H and O-H stretches); 3078*m* (C-H alkene stretch); 2978*m*, 2886*w* (C-H alkyl stretch); 1690*s* (C=O and C=C stretches); 1528*m* (N-H bend); 1404*m*, 1335*w* (C-H alkyl bends); 1196*s*, 1057*m* (C-O carbamate and carboxylic acid, and C-N carbamate stretches); 988*m*, 926*m*, 880*w*, 779*m* (C-H alkene bends). ESI-MS (*m*/*z*): Calc. for $C_6H_9NNaO_4$ 182.0424; found: 182.0426 (100%, $[M+Na]^+$).

Synthesis of Alloc-Gly-Asp(O^{t}Bu)-OBn (2.37)

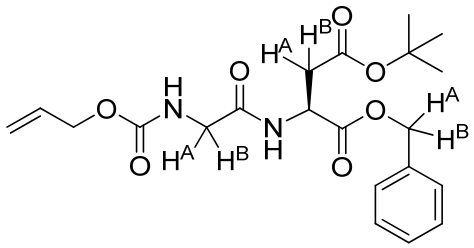

Compound **2.36** (116 mg, 0.73 mmol, 1.0 eq) was taken up in DCM (2 ml), then DIPEA (0.25 ml, 1.43 mmol, 2.0 eq) was added and the reaction mixture was cooled over an ice-water bath. TBTU (234 mg, 0.73 mmol, 1.0 eq) was added as a solid and the reaction was stirred at 0°C for 10 min. Compound **2.35** (206 mg, 0.73 mmol, 1.0 eq) was dissolved in DCM (2 ml), added rapidly to the

reaction flask and a further portion of DCM (6 ml) was used to transfer any residual **2.35** from the vial and into the reaction flask. The reaction was stirred for a further 10 min at 0°C before removing the ice-water bath and stirring the reaction at rt for 4 days. The reaction was then worked up with 1.33 M $NaHSO_4$ (3 × 50 ml), 1 M Na_2CO_3 (2 × 50 ml), water (50 ml) and finally brine (50 ml). The organic phase was dried over $MgSO_4$ and filtered before removing the solvent *in vacuo* to produce the product, **2.37**, as a clear, colourless oil (290 mg, 95%). No further purification was carried out.

R_f 0.66 (9:1 DCM/MeOH, UV and cerium stain). $[\alpha]_D$ = +19.6° (c = 1.0, $CHCl_3$). ^{1}H NMR ($CDCl_3$, 400 MHz) δ 7.36-7.27 (m, C*H* aromatic, 5H); 7.09 (d, N*H* amide, *J* = 8.5 Hz, 1H); 5.89 (ddt, H_2C=C*H*CH_2, *J* = 17.0 Hz, 11.0 Hz and 5.5 Hz, 1H); 5.60 (app br s, N*H* carbamate, 1H); 5.30-5.26 (m, *H*-CH=$CHCH_2$, 1H); 5.20 (d, CH^A benzylic, *J* = 12.5 Hz, 1H); 5.20-5.16 (m, *H*-CH=$CHCH_2$, 1H); 5.12 (d, CH^B benzylic, *J* = 12.5 Hz, 1H); 4.86 (dt, Asp α-*H*, *J* = 8.5 Hz and 4.5 Hz, 1H); 4.56-4.54 (m, H_2C=CHCH_2, 2H); 3.93 (dd, Gly CH^A, *J* = 17.0 Hz and 5.5 Hz, 2H); 3.86 (dd, Gly CH^B, *J* = 17.0 Hz and 5.5 Hz, 2H); 2.94 (dd, Asp CH^A, *J* = 17.0 Hz and 5.0 Hz, 1H); 2.74 (dd, Asp CH^B, *J* = 17.0 Hz and 5.0 Hz, 1H); 1.36 (s, C(CH_3)$_3$, 9H). ^{13}C NMR ($CDCl_3$, 100 MHz) δ 170.56, 169.98, 168.98, 156.44 (*C*(O)O^{t}Bu, *C*(O)OBn, *C*(O)NH amide, *C*(O)NH carbamate); 135.24 (aromatic *C*); 132.62 (H_2C=*C*HCH_2); 128.65, 128.50, 128.29 (aromatic *C*H × 3); 117.94 (H_2C=CHCH_2); 81.98 (*C*(CH_3)$_3$); 67.54 (*C*H_2 benzylic); 66.05 (H_2C=CH*C*H_2); 48.73 (Asp α-*C*H); 44.40 (Gly *C*H_2); 37.34 (Asp *C*H_2); 27.99 (C(*C*H_3)$_3$). $\tilde{\nu}_{max}$ (cm^{-1}) (oil): 3410*w*, 3372*w* (N-H stretch); 2978*m*, 2878*w* (C-H alkyl stretch); 1744*m*, 1713*s* (C=O stretches); 1659*m*, 1512*s* (C=C stretches and N-H bends); 1404*m*, 1366*w*, 1335*w*, 1281*m* (C-H alkyl bends); 1204*s*, 1157*m*, 1057*m* (C-O carbamate and ester, and C-N carbamate and amide stretches); 980*m*, 926*m*, 864*w*, 826*w*, 779*w*, 741*m*, 694*w* (C-H alkene and arene bends). ESI-MS (*m*/*z*): Calc. for $C_{21}H_{29}N_2O_7$ 421.1969; found: 421.1958 (100%, $[M+H]^+$). Calc. for $C_{21}H_{28}N_2NaO_7$ 443.1789; found 443.1778 (82%, $[M+Na]^+$).

Synthesis of Fmoc-Gly-Asp(O^{t}Bu)-OBn (2.38)

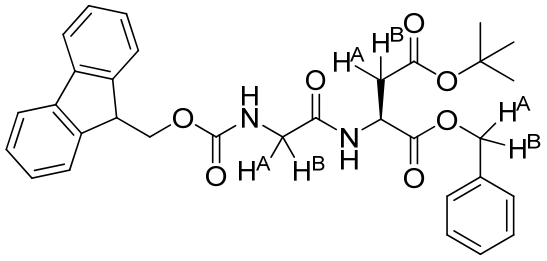

Fmoc-Gly-OH (0.27 g, 0.9 mmol, 1.0 eq) was dissolved in DCM (10 ml) upon the addition of DIPEA (0.32 ml, 1.8 mmol, 2.0 eq) and the reaction mixture was cooled over an ice-water bath. TBTU (0.29 g, 0.9 mmol, 1.0 eq) was added as a solid and the reaction was stirred at 0°C for 10 min. Compound **2.35** (0.25 g, 0.9 mmol, 1.0 eq) was dissolved in DCM (10 ml) and added rapidly to the reaction flask. The reaction was stirred for a further 30 min at 0°C before removing the ice-water bath and stirring the

reaction at rt for 4 days. The reaction was then worked up with 1.33 M $NaHSO_4$ (3 × 50 ml), 1 M Na_2CO_3 (3 × 50 ml), water (50 ml) and finally brine (50 ml). The organic phase was dried over $MgSO_4$ and filtered before removing the solvent *in vacuo* to produce the product, **2.38**, as a pale yellow solid (0.5 g, quantitative yield). No further purification was carried out.

R_f 0.70 (9:1 DCM/MeOH, UV and cerium stain). $[\alpha]_D$ = +33.0° (c = 0.5, $CHCl_3$). M.p not acquired. ^{1}H NMR ($CDCl_3$, 400 MHz) δ 7.75 (d, Fmoc C*H* aromatic, *J* = 7.5 Hz, 2H); 7.60 (br d, Fmoc C*H* aromatic, *J* = 7.0 Hz, 2H); 7.39 (t, Fmoc C*H* aromatic, *J* = 7.0 Hz, 2H); 7.35-7.26 (multiple overlapping peaks, Fmoc C*H* aromatic × 2, benzyl C*H* aromatic × 5, 7H); 7.20 (d, N*H* amide, *J* = 8.0 Hz, 1H); 5.80 (br t, N*H* carbamate, 1H); 5.21 (d, CH^A benzylic, *J* = 12.5 Hz, 1H); 5.21 (d, CH^B benzylic, *J* = 12.5 Hz, 1H); 4.90 (dt, Asp α-*H*, *J* = 8.0 Hz and 5.0 Hz, 1H); 4.37 (d, Fmoc CH_2, *J* = 7.0 Hz, 2H); 4.21 (t, Fmoc C*H*, *J* = 7.0 Hz, 1H); 3.99 (dd, Gly CH^A, *J* = 17.0 Hz and 5.5 Hz, 1H); 3.93 (dd, Gly CH^B, *J* = 17.0 Hz and 5.5 Hz, 1H); 2.96 (dd, Asp CH^A, *J* = 17.0 Hz and 4.5 Hz, 1H); 2.79 (dd, Asp CH^B, *J* = 17.0 Hz and 4.5 Hz, 1H); 1.36 (s, $C(CH_3)_3$, 9H). ^{13}C NMR ($CDCl_3$, 100 MHz) δ 170.52, 169.94, 168.96, 156.57 (*C*(O)O^{t}Bu, *C*(O)OBn, *C*(O)NH amide, *C*(O)NH carbamate); 143.84, 143.81, 141.26 (Fmoc aromatic *C*); 135.18 (benzyl aromatic *C*); 128.59, 128.44, 128.24, 127.72, 127.10, 125.17, 119.98 (Fmoc aromatic *C*H and benzyl aromatic *C*H); 81.89 ($C(CH_3)_3$); 67.48 (CH_2 benzylic); 67.28 (Fmoc CH_2); 48.75 (Asp α-*C*H); 47.06 (Fmoc *C*H); 44.35 (Gly CH_2); 37.29 (Asp CH_2); 27.93 ($C(CH_3)_3$). $\tilde{\nu}_{max}$ (cm^{-1}) (solid): 3426*w*, 3264*w* (N-H stretch); 3040*w* (C-H arene stretch); 2978*m*, 2878*w* (C-H alkyl stretch); 1713*s* (C=O stretch); 1651*m*, 1520*s* (C=C stretches and N-H bends); 1450*m*, 1366*m*, 1335*m*, 1288*m* (C-H alkyl bends); 1234*s*, 1204*s*, 1150*s*, 1042*m* (C-O carbamate and ester, and C-N carbamate and amide stretches); 1003*m*, 957*w*, 895*w*, 856*w*, 733*s*, 694*w* (C-H arene bends). ESI-MS (*m*/*z*): Calc. for $C_{32}H_{35}N_2O_7$ 559.2439; found: 559.2435 (75%, $[M+H]^+$). Calc. for $C_{32}H_{34}N_2NaO_7$ 581.2258; found 581.2248 (100%, $[M+Na]^+$).

Attempted synthesis of H_2N-Gly-Asp(O^{t}Bu)-OBn (2.39)

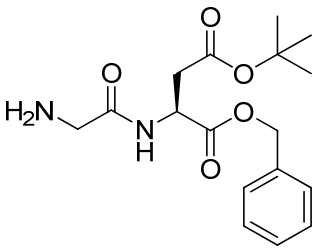

Expected product

Compound **2.38** (0.48 g, 0.86 mmol) was stirred in a solution of 20% piperidine in DCM (2 ml) for 2.5 h, and then the solvent was removed in vacuo to yield a crude, pale yellow solid. It was difficult to deduce by TLC which spot corresponded to the product. It is possible that the product spot overlapped with one of the spots corresponding to the Fmoc/Fmoc-piperidine by-products, therefore

making it a difficult separation of the mixture by silica column chromatography. The synthesis was abandoned as a result.

6.3 Chapter 3 – Self-Assembling Linear RGD Peptides

Synthesis of C12-Arg(Pbf)-Gly-Asp(O^{t}Bu)-O^{t}Bu (3.1)

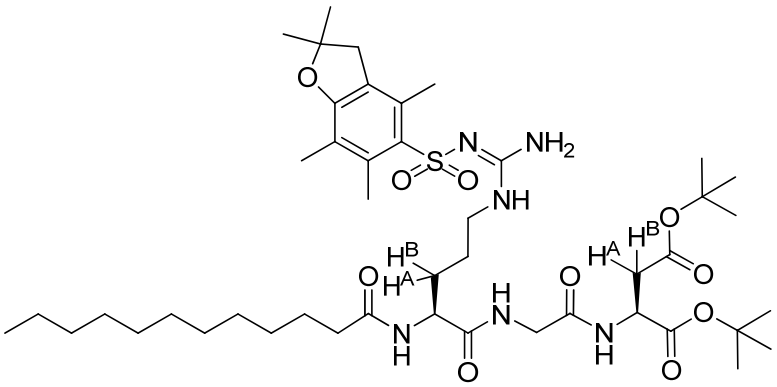

Lauric acid (56 mg, 0.28 mmol, 1.0 eq) and **2.8(2.4)** (200 mg, 0.28 mmol, 1.0 eq) were dissolved in DCM (10 ml), then DIPEA (100 µl, 0.56 mmol, 2.0 eq) was added and the reaction flask cooled over an ice-water bath. TBTU (90 mg, 0.28 mmol, 1.0 eq) was added as a solid and more DCM (2 ml) was used to rinse any residual TBTU into the reaction flask. The reaction was stirred over the ice-water bath overnight then at rt for a further 2 days, then washed with hot 1M HCl (3 × 25 ml), hot 15% Na_2CO_3 (3 × 25 ml), and hot water (25 ml). The organic layer was dried over $MgSO_4$, filtered and the filtrate evaporated to yield **3.1** as a white solid (236 mg, 94%). No further purification was required.

R_f 0.42 (9:1 DCM/MeOH, UV and cerium stain). $[\alpha]_D$ = +5.2° (c = 1.0, $CHCl_3$). M.p: 70.5-78.6°C. ^{1}H NMR ($CDCl_3$, 400 MHz) δ 7.87 (br t, N*H* amide (Arg-Gly), 1H); 7.41 (d, N*H* amide (Gly-Asp), *J* = 8.0 Hz, 1H); 7.06 (br s, N*H* amide (C12-Arg), 1H), 6.38 (br s, NH_2 guanidine, 2H); 6.26 (br s, N*H* guanidine, 1H); 4.63-4.58 (m, Asp α-*H*, 1H); 4.50-4.45 (m, Arg α-*H*, 1H); 4.00-3.80 (br m, Gly CH_2, 2H); 3.28-3.08 (m, Arg CH_2NH, 2H); 2.89 (s, Pbf CH_2, 2H); 2.73 (dd, Asp CH^A, *J* = 17.0 Hz and 5.0 Hz, 1H); 2.64 (dd, Asp CH^B, *J* = 17.0 Hz and 5.0 Hz, 1H); 2.51 (s, Pbf CH_3Ar, 3H); 2.44 (s, Pbf CH_3Ar, 3H); 2.15 (t, C12 CH_2C(O)NH, *J* = 7.5 Hz, 2H); 2.02 (s, Pbf CH_3Ar, 3H); 1.89-1.77 (m, Arg CHCH^A, 1H); 1.70-1.59 (m, Arg CHCH^B, 1H); 1.57-1.45 (m, Arg CH_2CH$_2$NH and C12 CH_2 overlapping, 4H); 1.39 (s, Pbf CH_3 × 2, 6H); 1.35 (s, C(CH_3)$_3$ × 2, 18H); 1.25-1.15 (m, C12 CH_2's, 16H); 0.81 (t, C12 CH_3, *J* = 7.0 Hz, 3H). ^{13}C NMR ($CDCl_3$, 100 MHz) δ 174.04, 172.92, 169.91, 169.74, 169.19 (*C*(O)O^{t}Bu × 2, *C*(O)NH amide × 3); 158.60, 156.54 (Pbf aromatic *C*-O, *C*=N guanidine); 138.23, 132.88, 132.15, 124.47, 117.34 (Pbf aromatic *C*); 86.25 (Pbf CH$_2$*C*(CH$_3$)$_2$O); 82.28, 81.36 (*C*(CH$_3$)$_3$ × 2); 52.71 (Arg α-*C*H); 49.33 (Asp α-*C*H); 43.18 (Pbf ArCH_2); 42.76 (Gly *C*H$_2$); 40.15 (Arg *C*H$_2$NH); 37.30 (Asp *C*H$_2$); 36.22 (C12 *C*H$_2$C(O)NH); 31.84, 29.61, 29.57, 29.51, 29.36, 29.32,

29.29 (C12 *C*H$_2$'s and Arg CH*C*H$_2$, multiple overlapping peaks); 28.54 (Pbf CH$_2$C(*C*H$_3$)$_2$O); 27.96, 27.80 (C(*C*H$_3$)$_3$ × 2); 25.61, 25.33, 22.61 (C12 *C*H$_2$'s and Arg *C*H$_2$CH$_2$NH, multiple overlapping peaks); 19.27, 17.92 (Pbf Ar*C*H$_3$ × 2); 14.07 (C12 *C*H$_3$); 12.42 (Pbf Ar*C*H$_3$ × 1). $\tilde{\nu}_{max}$ (cm^{-1}) (solid): 3317*m* (N-H amide stretch); 2973*w*, 2926*m*, 2853*w* (C-H alkyl stretches); 1733*m* (C=O ester stretch); 1648*s* (C=O amide stretch); 1544*s* (N-H amide bend and C=C arene stretch); 1455*w*, 1408*w*, 1393*w*, 1368*m* (C-H alkyl bends and S=O stretch); 1293*w*, 1276*w*, 1249*m*, 1152*s*, 1106*s*, 1091*s* (C-O ester and C-N amide stretches). ESI-MS (*m*/*z*): Calc. for $C_{45}H_{77}N_6O_{10}S$ 893.5416; found: 893.5424 (100%, $[M+H]^+$).

Synthesis of C12-Arg-Gly-Asp (3.2)

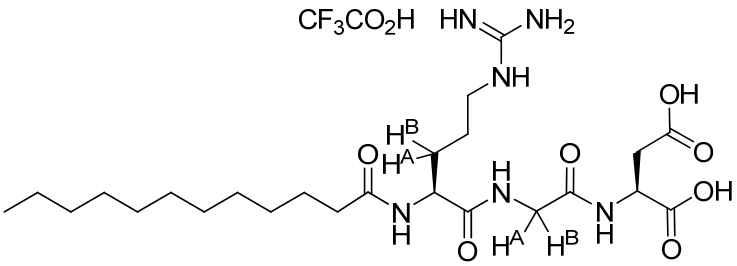

Compound **3.1** (206 mg, 0.23 mmol) was dissolved in a mixture of TFA, water and TIS (2 ml, 95:2.5:2.5) and shaken for 3 h, after which time TLC indicated that the deprotection reaction was complete. The volatiles were removed *in vacuo,* then the residue was dissolved in the minimum amount of MeOH, precipitated with cold Et$_2$O, filtered and washed with the minimum amount of cold Et$_2$O to yield a white solid (116 mg, 78% as TFA salt). The sample was then dissolved in a mixture of water/^{t}BuOH, filtered over a PTFE membrane filter (0.2 μm), shell frozen and lyophilised to yield the product **3.2** as a fluffy white powder.

R_f 0.00 (9:1 DCM/MeOH, cerium stain). $[\alpha]_D$ = +4.8^o (c = 1.0, CH$_3$OH). M.p: decomposed at 187.6°C. ^{1}H NMR (CD$_3$OD, 400 MHz) δ 4.74 (t, Asp α-*H*, *J* = 6.0 Hz, 1H); 4.29 (dd, Arg α-*H*, *J* = 8.0 and 5.5 Hz, 1H); 3.93 (d, Gly C*H*^{A}, *J* = 17.0 Hz, 1H); 3.86 (d, Gly C*H*^{B}, *J* = 17.0 Hz, 1H); 3.19 (t, Arg C*H*$_2$NH, *J* = 6.5 Hz, 2H); 2.90-2.79 (m, Asp C*H*$_2$, 2H); 2.27 (t, C12 C*H*$_2$C(O)NH, *J* = 7.5 Hz, 2H); 1.91-1.83 (m, Arg CHC*H*^{A}, 1H); 1.79-1.57 (m, Arg CHC*H*^{B}, Arg C*H*$_2$CH$_2$NH and C12 C*H*$_2$ overlapping, 5H); 1.35-1.20 (m, C12 C*H*$_2$'s, 16H); 0.88 (t, C12 C*H*$_3$, *J* = 7.0 Hz, 3H). ^{13}C NMR (CD$_3$OD, 100 MHz) δ 176.86, 175.02, 174.06, 173.94, 171.46, 158.49 (*C*(O)OH × 2, *C*(O)NH amide × 3, *C*=N guanidine); 54.79 (Arg α-*C*H); 50.30 (Asp α-*C*H); 43.43 (Gly *C*H$_2$); 41.91 (Arg *C*H$_2$NH); 36.81, 36.73 (Asp *C*H$_2$, C12 *C*H$_2$C(O)NH); 33.06, 30.78, 30.75, 30.67, 30.53, 30.48, 30.43, 29.77, 26.82, 26.19, 23.73 (C12 *C*H$_2$'s, Arg CH*C*H$_2$ and Arg *C*H$_2$CH$_2$NH, multiple overlapping peaks); 14.51 (C12 *C*H$_3$). $\tilde{\nu}_{max}$ (cm^{-1}, solid): 3287*w* (O-H acid and N-H amide/guanidino stretches); 2921*w*, 2853*w* (C-H alkyl stretches); 1728*w* (C=O acid stretch); 1648*m* (C=O amide stretch); 1539*m* (N-H amide

bend); 1170*m*, 1045*m* (C-O acid and C-N amide stretches). ESI-MS (*m/z*) (positive ion mode): Calc. for $C_{24}H_{45}N_6O_7$ 529.3344; found: 529.3331 (100%, $[M+H]^+$). ESI-MS (*m/z*) (negative ion mode): Calc. for $C_{24}H_{43}N_6O_7$ 527.3199; found: 527.3197 (100%, $[M-H]^-$).

Synthesis of Py-Arg(Pbf)-Gly-Asp(O^{t}Bu)-O^{t}Bu (3.3)

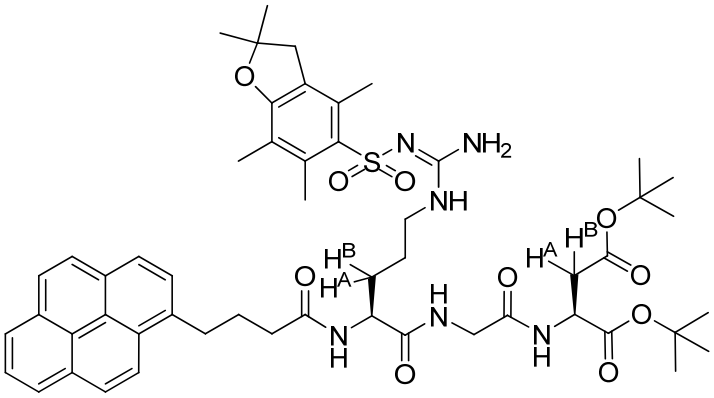

1-pyrenebutyric acid (81 mg, 0.28 mmol, 1.0 eq) was dissolved in DCM (4 ml) upon addition of DIPEA (0.1 ml, 0.57 mmol, 2.0 eq) and the reaction flask was cooled over an ice-water bath. TBTU (90 mg, 0.28 mmol, 1.0 eq) was added as a solid and stirred for 10 min at 0°C before **2.8(2.4)** (200 mg, 0.28 mmol, 1.0 eq) was added as a solid and DCM (6 ml) was used to rinse any residual **2.8(2.4)** into the reaction flask. The reaction was stirred for a further 30 min at 0°C, then the ice-water bath was removed and the reaction stirred at rt for 21 h. The organic phase was washed with 1.33 M $NaHSO_4$ (3 × 50 ml), 1 M Na_2CO_3 (3 × 50 ml), water (50 ml) and finally brine (50 ml). The organic phase was dried over $MgSO_4$ and filtered before removing the solvent *in vacuo* to yield **3.3** as a yellow solid (280 mg, quantitative yield). No further purification was required.

R_f 0.43 (9:1 DCM/MeOH, UV and cerium stain). $[\alpha]_D$ = -0.5° (c = 1.0, $CHCl_3$). M.p not acquired. ^{1}H NMR ($CDCl_3$, 400 MHz) δ 8.18 (d, C*H* aromatic, *J* = 9.5 Hz, 1H); 8.07 (dd, C*H* aromatic, *J* = 7.5 Hz and 5.0 Hz, 2H); 7.98 (d, C*H* aromatic, *J* = 8.5 Hz, 2H); 7.93-7.86 (m, overlapping C*H* aromatic × 3 and N*H* amide (Arg-Gly), 4H); 7.73 (d, C*H* aromatic, *J* = 8.0 Hz, 1H); 7.40 (d, N*H* amide (Gly-Asp), *J* = 7.5 Hz, 1H); 7.13 (app br d, N*H* amide (Py-Arg), 1H), 6.45 (br s, N*H*$_2$ guanidine, 2H); 6.29 (br s, N*H* guanidine, 1H); 4.66 (dt, Asp α-*H*, *J* = 8.0 Hz and 5.0 Hz, 1H); 4.61-4.55 (m, Arg α-*H*, 1H); 3.99 (app br d, Gly C*H*$_2$, 2H); 3.36-3.10 (br m, Arg C*H*$_2$NH, 2H); 3.24 (t, $CH_2CH_2CH_2C(O)NH$, *J* = 7.5 Hz, 2H); 2.79 (s, Pbf C*H*$_2$, 2H); 2.76 (dd, Asp C*H*^{A}, *J* = 17.0 Hz and 5.0 Hz, 1H); 2.68 (dd, Asp C*H*^{B}, *J* = 17.0 Hz and 5.0 Hz, 1H); 2.57 (s, Pbf C*H*$_3$Ar, 3H); 2.45 (s, Pbf C*H*$_3$Ar, 3H); 2.35 (t, $CH_2CH_2CH_2C(O)NH$, *J* = 7.0 Hz, 2H); 2.11 (quintet, $CH_2CH_2CH_2C(O)NH$, *J* = 6.5 Hz, 2H); 2.04 (s, Pbf C*H*$_3$Ar, 3H); 1.96-1.83 (m, Arg CHC*H*^{A}, 1H); 1.77-1.64 (m, Arg CHC*H*^{B}, 1H); 1.64-1.48 (m, Arg C*H*$_2$CH$_2$NH, 2H); 1.36, 1.354, 1.347 (s × 3, Pbf C*H*$_3$ × 2 and C(C*H*$_3$)$_3$ × 2, calc 24H, found 23H). ^{13}C NMR ($CDCl_3$, 100 MHz) δ 173.58, 172.90, 169.98, 169.81, 169.22 (*C*(O)O^{t}Bu × 2, *C*(O)NH amide ×

3); 158.65, 156.58 (Pbf aromatic *C*-O, *C*=N guanidine); 138.28 (Pbf aromatic *C*), 135.87 (pyrene aromatic *C*), 132.90, 132.21 (Pbf aromatic C × 2); 131.30, 130.82, 129.78, 128.60 (pyrene aromatic *C* × 4); 127.44, 127.28, 127.25, 126.54, 125.74 (*C*H aromatic × 5); 124.93, 124.87 (pyrene aromatic *C* × 2); 124.77, 124.69 (*C*H aromatic × 2); 124.58 (Pbf aromatic *C*); 123.32 (*C*H aromatic); 117.42 (Pbf aromatic *C*); 86.30 (Pbf $CH_2C(CH_3)_2O$); 82.39, 81.45 ($C(CH_3)_3$ × 2); 52.85 (Arg α-*C*H); 49.38 (Asp α-*C*H); 43.08 (Pbf ArCH_2); 42.81 (Gly CH_2); 40.33 (Arg CH_2NH); 37.34 (Asp CH_2); 35.73 ($CH_2CH_2CH_2C(O)NH$); 32.75 ($CH_2CH_2CH_2C(O)NH$); 29.48 (Arg $CHCH_2$); 28.50 (Pbf $CH_2C(CH_3)_2O$); 27.97, 27.80 ($C(CH_3)_3$ × 2); 27.36 ($CH_2CH_2CH_2C(O)NH$); 25.37 (Arg CH_2CH_2NH); 19.31, 18.00, 12.48 (Pbf ArCH_3 × 3). $\tilde{\nu}_{max}$ (cm^{-1}) (solid): 3310*w* (N-H amide stretch); 2932*w*, 2870*w* (C-H alkyl and arene stretches); 1728*m* (C=O ester stretch); 1651*m*, 1620*m* (C=O amide stretches); 1543*s* (N-H amide bend and C=C arene stretch); 1450*m*, 1366*m* (C-H alkyl bend and S=O stretch); 1242*s*, 1150*s*, 1096*s* (C-O ester and C-N amide stretches, C-H arene bends); 988*w*, 910*w*, 841*m*, 810*w*, 779*w*, 733*m* (C-H arene bends). ESI-MS (*m*/*z*): Calc. for $C_{53}H_{69}N_6O_{10}S$ 981.4790; found: 981.4797 (100%, $[M+H]^+$); Calc. for $C_{53}H_{68}N_6NaO_{10}S$ 1003.4610; found: 1003.4609 (32%, $[M+Na]^+$).

Synthesis of Py-Arg-Gly-Asp (3.4)

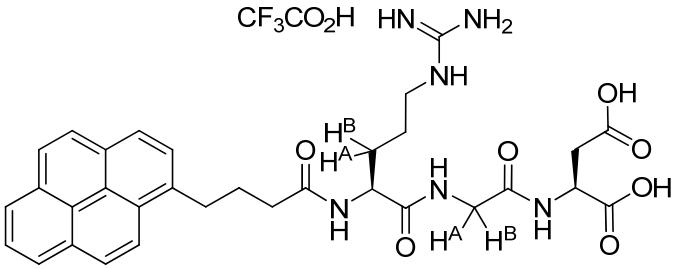

Compound **3.3** (240 mg, 0.24 mmol) was dissolved in a mixture of TFA, water and TIS (5 ml, 95:2.5:2.5) and shaken for 1.5 h, after which time TLC indicated that the deprotection reaction was complete. The volatiles were removed *in vacuo,* then the residue was dissolved in the minimum amount of hot MeOH, precipitated with cold Et_2O, filtered and washed with the minimum amount of cold Et_2O to yield a tanish green solid (137 mg, 77% as TFA salt). The sample was then dissolved in a mixture of water/^{t}BuOH, filtered over a PTFE membrane filter (0.2 μm), shell frozen and lyophilised to yield the product **3.4** as a fluffy, pale green powder.

R_f 0.00 (9:1 DCM/MeOH, UV and cerium stain). $[\alpha]_D$ = +2.6° (c = 0.5, DMSO). M.p not acquired. ^{1}H NMR (3:1:1 $CD_3OD/CDCl_3/D_2O$, 400 MHz) δ 8.23 (d, C*H* aromatic, *J* = 9.0 Hz, 1H); 8.08 (t, C*H* aromatic, *J* = 7.0 Hz, 2H); 8.03 (d, C*H* aromatic, *J* = 9.0 Hz, 2H); 7.95-7.90 (m, C*H* aromatic × 3, 3H); 7.82 (d, C*H* aromatic, *J* = 8.0 Hz, 1H); 4.74 (t, Asp α-*H*, *J* = 5.5 Hz, 1H); 4.33 (app t, Arg α-*H*, *J* = 6.0 Hz, 1H); 3.96 (d, Gly C*H*^{A}, *J* = 17.0 Hz, 1H); 3.91 (d, Gly C*H*^{B}, *J* = 17.0 Hz, 1H); 3.30 (t, $CH_2CH_2CH_2C(O)NH$, *J* = 7.0 Hz, 2H, obscured by the CD_3OD peak); 3.16 (t, Arg CH_2NH, *J* = 6.5

Hz, 2H); 2.94-2.82 (m, Asp C*H*$_2$, 2H); 2.45 (t, C*H*$_2$CH$_2$CH$_2$C(O)NH, *J* = 7.0 Hz, 2H); 2.12 (quintet, CH$_2$C*H*$_2$CH$_2$C(O)NH, *J* = 7.0 Hz, 2H); 1.92-1.79 (m, Arg CHC*H*^{A}, 1H); 1.79-1.56 (m, overlapping Arg CHC*H*^{B} and Arg C*H*$_2$CH$_2$NH, 3H). ^{13}C NMR (3:1:1 CD$_3$OD/CDCl$_3$/D$_2$O, 100 MHz) δ 176.07, 174.62, 174.29, 174.02, 171.11, 157.77 (*C*(O)OH × 2, *C*(O)NH amide × 3, *C*=N guanidine); 136.76, 132.11, 131.63, 130.64, 129.34, 128.13, 127.99, 127.29, 126.55, 125.64, 125.54, 125.43, 124.00 (aromatic *C* and *C*H); 54.22 (Arg α-*C*H); 49.75 (Asp α-*C*H); 43.16 (Gly *C*H$_2$); 41.47 (Arg *C*H$_2$NH); 36.53, 36.18 (*C*H$_2$CH$_2$CH$_2$C(O)NH and Asp *C*H$_2$); 33.44 (CH$_2$CH$_2$*C*H$_2$C(O)NH); 29.51 (Arg CH*C*H$_2$); 28.22 (CH$_2$*C*H$_2$CH$_2$C(O)NH); 25.54 (Arg *C*H$_2$CH$_2$NH). $\tilde{\nu}_{max}$ (cm^{-1}, solid): 3179*w*, 3032*w* (O-H acid and N-H amide/guanidino stretches, broad peaks overlapping C-H alkyl and arene stretches); 1751*w* (C=O acid stretch); 1651*m* (C=O amide stretch); 1520*m* (N-H amide bend and C=C arene stretch); 1420*m*, 1319*m* (C-H alkyl bends); 1188*s*, 1042*s* (C-O acid and C-N amide stretches); 872*s*, 748*m*, 702*m* (C-H arene bends). ESI-MS (*m*/*z*): Calc. for $C_{32}H_{37}N_6O_7$ 617.2718; found: 617.2722 (100%, $[M+H]^+$).

Synthesis of C22-Arg(Pbf)-Gly-Asp(O^{t}Bu)-O^{t}Bu (3.5)

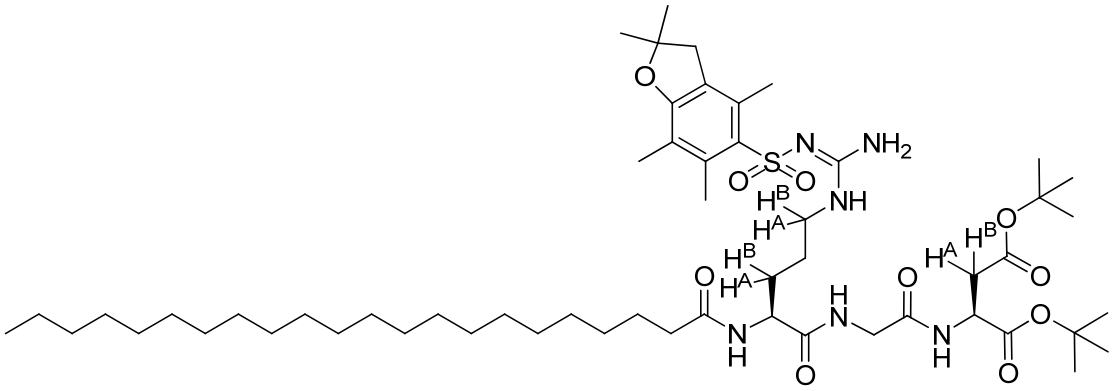

Behenic acid (96 mg, 0.28 mmol, 1.0 eq) was dissolved in DCM (7 ml) upon addition of DIPEA (100 µl, 0.56 mmol, 2.0 eq) and the reaction flask cooled over an ice-water bath. TBTU (90 mg, 0.28 mmol, 1.0 eq) was added as a solid and more DCM (3 ml) was used to rinse any residual TBTU into the reaction flask. The reaction was stirred at 0°C for 10 min, then **2.8(2.4)** (200 mg, 0.28 mmol, 1.0 eq) was added as a solid and more DCM (2 ml) was used to rinse any residual **2.8(2.4)** into the reaction flask. The reaction was stirred for a further 30 min at 0°C, then the ice-water bath was removed and the reaction stirred at rt for 4 days. The organic phase was washed with 1.33 M NaHSO$_4$ (3 × 50 ml), 1 M Na$_2$CO$_3$ (3 × 50 ml), water (50 ml) and finally brine (50 ml). The organic phase was dried over MgSO$_4$ and filtered before removing the solvent *in vacuo* to yield **3.5** as a white solid (280 mg, 96%). No further purification was required.

R_f 0.40 (9:1 DCM/MeOH, UV and cerium stain). $[\alpha]_D$ = -2.6° (c = 1.0, CHCl$_3$). M.p not acquired. ^{1}H NMR (CDCl$_3$, 400 MHz) δ 7.86 (br t, N*H* amide (Arg-Gly), 1H); 7.34 (d, N*H* amide (Gly-Asp), *J* =

8.0 Hz, 1H); 6.97 (br d, N*H* amide (C22-Arg), 1H), 6.39 (br s, NH_2 guanidine, 2H); 6.24 (br s, N*H* guanidine, 1H); 4.64 (dt, Asp α-*H*, *J* = 8.5 Hz and 5.0 Hz, 1H); 4.54 (app q, Arg α-*H*, 1H); 4.03-3.87 (br m, Gly CH_2, 2H); 3.36-3.12 (br m, Arg CH_2NH, 2H); 2.93 (s, Pbf CH_2, 2H); 2.78 (dd, Asp CH^A, *J* = 17.0 Hz and 5.0 Hz, 1H); 2.68 (dd, Asp CH^B, *J* = 17.0 Hz and 5.0 Hz, 1H); 2.55 (s, Pbf CH_3Ar, 3H); 2.48 (s, Pbf CH_3Ar, 3H); 2.19 (t, C22 CH_2C(O)NH, *J* = 7.0 Hz, 2H); 2.06 (s, Pbf CH_3Ar, 3H); 1.95-1.81 (m, Arg CHCH^A, 1H); 1.76-1.62 (m, Arg CHCH^B, 1H); 1.62-1.49 (m, Arg CH_2CH_2NH and C22 CH_2 overlapping, 4H); 1.44 (s, Pbf CH_3 × 2, 6H); 1.40, 1.39 (s × 2, C(CH_3)$_3$ × 2, calc 18H, found 17H); 1.32-1.16 (m, C22 CH_2's, calc 36H, found 37H); 0.86 (t, C22 CH_3, *J* = 7.0 Hz, 3H). ^{13}C NMR ($CDCl_3$, 100 MHz) δ 174.11, 172.99, 170.08, 169.89, 169.28 (*C*(O)O^{t}Bu × 2, *C*(O)NH amide × 3); 158.76, 156.66 (Pbf aromatic *C*-O, *C*=N guanidine); 138.41, 132.95, 132.31, 124.61, 117.52 (Pbf aromatic *C*); 86.39 (Pbf $CH_2C(CH_3)_2O$); 82.53, 81.59 (*C*(CH$_3$)$_3$ × 2); 52.70 (Arg α-*C*H); 49.43 (Asp α-*C*H); 43.32 (Pbf Ar*C*H$_2$); 42.88 (Gly *C*H$_2$); 40.30 (Arg *C*H$_2$NH); 37.43 (Asp *C*H$_2$); 36.46 (C22 *C*H$_2$C(O)NH); 32.00, 29.79, 29.74, 29.68, 29.51, 29.44 (C22 *C*H$_2$'s and Arg CH*C*H$_2$, multiple overlapping peaks); 28.68 (Pbf $CH_2C(CH_3)_2O$); 28.11, 27.94 (C(*C*H$_3$)$_3$ × 2); 25.76, 25.37, 22.77 (C22 *C*H$_2$'s, Arg *C*H$_2$CH$_2$NH); 19.41, 18.05 (Pbf Ar*C*H$_3$ × 2); 14.21 (C22 *C*H$_3$); 12.56 (Pbf Ar*C*H$_3$ × 1). $\tilde{\nu}_{max}$ (cm^{-1}) (solid): 3310*w* (N-H amide stretch); 2924*m*, 2855*w* (C-H alkyl stretches); 1728*m* (C=O ester stretch); 1651*s* (C=O amide stretch); 1543*s* (N-H amide bend and C=C arene stretch); 1450*m*, 1366*m* (C-H alkyl bends and S=O stretch); 1242*s*, 1150*s*, 1103*s* (C-O ester and C-N amide stretches). ESI-MS (*m*/*z*): Calc. for $C_{55}H_{97}N_6O_{10}S$ 1033.6981; found: 1033.6980 (100%, $[M+H]^+$).

Synthesis of C22-Arg-Gly-Asp (3.6)

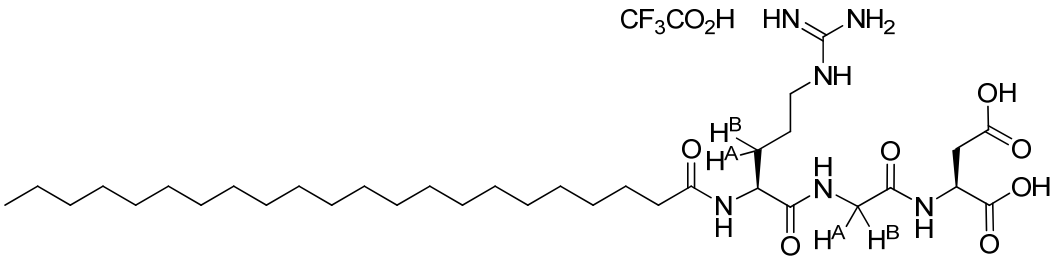

Compound **3.5** (250 mg, 0.24 mmol) was dissolved in a mixture of TFA, water and TIS (10 ml, 95:2.5:2.5) and shaken for 1 h 20 min, after which time TLC indicated that the deprotection reaction was complete. The volatiles were removed *in vacuo,* then the residue was dissolved in the minimum amount of hot MeOH/water/^{t}BuOH and the remaining orange/yellow solid was filtered off. The filtrate was evaporated *in vacuo* to yield a white solid which was redissolved in a mixture of hot water/^{t}BuOH, precipitated with cold Et_2O, filtered and washed with the minimum amount of cold Et_2O to yield a white solid. The sample was then dissolved in a mixture of hot water/^{t}BuOH with sonication, filtered over a PTFE membrane filter (0.2 μm), shell frozen and lyophilised to yield the product **3.6** as a fluffy white powder (120 mg, 63% as TFA salt).

Note: The compound forms a gel in DMSO-d_6 and so NMR analysis was carried out at elevated temperature to induce gel-sol transformation which resulted in better resolved NMR spectra.

R_f 0.00 (9:1 DCM/MeOH, cerium stain). $[\alpha]_D$ = +2.2° (c = 0.5, TFA). M.p not acquired. ^{1}H NMR (DMSO-d_6, 500 MHz, temp = 70°C) δ 8.20-8.00 (br m, N*H* amide (Arg-Gly), Arg CH_2NH, 2H); 7.83 (br d, N*H* amide (Gly-Asp), *J* = 5.5 Hz, 1H); 7.71 (d, N*H* amide (C22-Arg), *J* = 7.5 Hz, 1H), 7.04 (br s, -NH_2 and -NH_2^+ of guanidine, 4H); 4.37 (br m, Asp α-*H*, 1H); 4.28 (app q, Arg α-*H*, *J* = 7.0 Hz, 1H); 3.83 (dd, Gly CH^A, *J* = 16.5 Hz and 6.0 Hz, 1H); 3.62 (dd, Gly CH^B, *J* = 17.0 Hz and 5.0 Hz, 1H); 3.20-3.05 (br m, Arg CH_2NH, 2H); 2.60-2.53 (m, Asp CH_2, 2H); 2.14 (t, C22 CH_2C(O)NH, *J* = 7.5 Hz, 2H); 1.86-1.73 (m, Arg CHCH^A, 1H); 1.66-1.45 (m, overlapping Arg CHCH^B, Arg CH_2CH$_2$NH and C22 CH_2, 5H); 1.34-1.16 (m, C22 CH_2's, 36H); 0.87 (t, C22 CH_3, *J* = 6.5 Hz, 3H). ^{13}C NMR (DMSO-d_6, 125 MHz, temp = 70°C) δ 172.35, 172.05, 171.82, 171.55, 167.86, 156.79 (*C*(O)OH × 2, *C*(O)NH amide × 3, *C*=N guanidine); 51.92 (Arg α-*C*H); 48.65 (Asp α-*C*H); 41.80 (Gly *C*H$_2$); 40.32 (Arg *C*H$_2$NH); 37.37 (Asp *C*H$_2$); 34.89 (C22 *C*H$_2$C(O)NH); 30.83, 29.09, 28.59, 28.58, 28.54, 28.53, 28.37, 28.34, 28.19 (C22 *C*H$_2$'s and Arg CH*C*H$_2$, multiple overlapping peaks); 24.78, 24.49, 21.58 (C22 *C*H$_2$'s, Arg *C*H$_2$CH$_2$NH); 13.36 (C22 *C*H$_3$). $\tilde{\nu}_{max}$ (cm^{-1}, solid): 3287*w*, 3179*w*, 3102*w*, 3032*w* (O-H acid and N-H amide/guanidino stretches); 2916*s*, 2847*m* (C-H alkyl stretches); 1751*w* (C=O acid stretch); 1628*s* (C=O amide stretch); 1535*m* (N-H amide bend); 1466*w*, 1396*w* (C-H alkyl bends); 1327*w*, 1188*m*, 1049*m* (C-O acid and C-N amide stretches). ESI-MS (*m*/*z*): Calc. for $C_{34}H_{65}N_6O_7$ 669.4909; found: 669.4932 (100%, $[M+H]^+$).

Synthesis of Chol-Arg(Pbf)-Gly-Asp(O^{t}Bu)-O^{t}Bu (3.7)

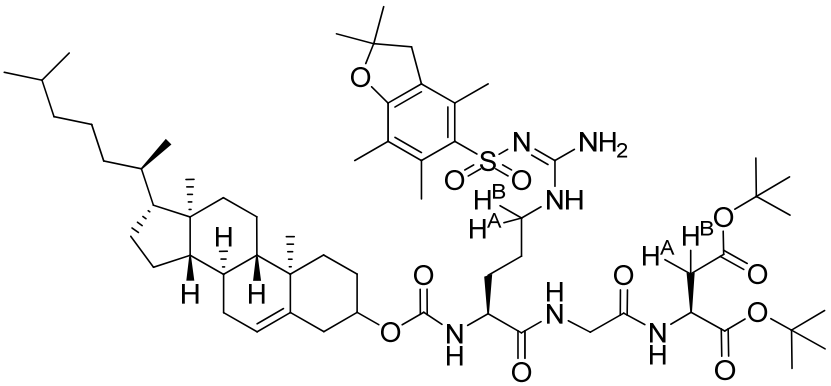

Compound **2.8(2.4)** (100 mg, 0.14 mmol, 1.0 eq) was dissolved in DCM (5 ml), then cholesteryl chloroformate (253 mg, 0.56 mmol, 4.0 eq) dissolved in DCM (2.5 ml) was added dropwise over 1 min to the reaction flask. A further portion of DCM (2.5 ml) was used to rinse any residual cholesteryl chloroformate into the reaction flask. TEA (80 μL, 0.57 mmol, 4.1 eq) was then added rapidly and the reaction stirred at rt for 1.75 days (N.B. TLC analysis after 15 min indicated the reaction was complete), after which time the solvent was removed *in vacuo* to yield a crude white solid (383 mg).

Purification by column chromatography (SiO_2, 100% DCM, to 98:2 DCM/MeOH, to 95:5 DCM/MeOH) yielded **3.7** as a white solid (141 mg, 89%).

R_f 0.50 (9:1, DCM/MeOH, UV and cerium stain). $[\alpha]_D$ = -9.6° (c = 1.0, $CHCl_3$). M.p not acquired. ^{1}H NMR ($CDCl_3$, 400 MHz) δ 7.80 (app br s, N*H* amide (Arg-Gly), 1H); 7.33 (br d, N*H* amide (Gly-Asp), *J* = 7.0 Hz, 1H); 6.37 (br s, NH_2 guanidine, 2H); 6.24 (br s, N*H* guanidine, 1H); 5.94 (app br s, N*H* carbamate, 1H); 5.32 (app br s, C*H*=C, 1H); 4.64 (dt, Asp α-*H*, *J* = 7.5 Hz and 5.0 Hz, 1H); 4.51-4.36 (m, C*H*OC(O)NH, 1H); 4.34-4.23 (m, Arg α-*H*, 1H); 4.03-3.89 (br m, Gly CH_2, 2H); 3.38-3.22 (br m, Arg CH^ANH, 1H); 3.22-3.06 (br m, Arg CH^BNH, 1H); 2.92 (s, Pbf CH_2, 2H); 2.77 (dd, Asp CH^A, *J* = 17.0 Hz and 4.5 Hz, 1H); 2.67 (dd, Asp CH^B, *J* = 17.0 Hz and 4.5 Hz, 1H); 2.55 (s, Pbf CH_3Ar, 3H); 2.48 (s, Pbf CH_3Ar, 3H); 2.35-2.16 (m, chol CH_2CHO, 2H); 2.06 (s, Pbf CH_3Ar, 3H); 2.02-0.77 (m, chol C*H*'s, chol CH_2's, chol CH_3's, Arg CHCH_2, Arg CH_2CH$_2$NH, Pbf CH_3 × 2, C(CH_3)$_3$ × 2, 66H); 0.65 (s, chol CH_3, 3H). ^{13}C NMR ($CDCl_3$, 100 MHz) δ 173.19, 170.06, 169.81, 169.37, 158.73, 156.64, 156.26 (*C*(O)O^{t}Bu × 2, *C*(O)NH amide × 2, *C*(O)NH carbamate, Pbf aromatic *C*-O, *C*=N guanidine); 139.75 (CH=*C*); 138.38, 132.91, 132.31, 124.58 (Pbf aromatic *C* × 4); 122.57 (*C*H=C); 117.47 (Pbf aromatic *C*); 86.36 (Pbf CH$_2$*C*(CH$_3$)$_2$O); 82.50, 81.58 (*C*(CH$_3$)$_3$ × 2); 74.80 (*C*HOC(O)NH); 56.74, 56.21, 54.20, 50.01, 49.46 (chol *C*H/*C*H$_3$'s, Arg α-*C*H, Asp α-*C*H); 43.30 (Pbf Ar*C*H$_2$); 42.89 (Gly *C*H$_2$); 42.34 (chol *C*); 39.79, 39.55, 38.52, 37.40, 36.99 (chol *C*H$_2$'s, Arg *C*H$_2$NH, Asp *C*H$_2$); 36.56 (chol *C*); 36.23 (chol *C*H$_2$); 35.85, 31.89 (chol *C*H/*C*H$_3$'s); 29.85 (Arg CH*C*H$_2$,); 28.65 (Pbf CH$_2$C(*C*H$_3$)$_2$O); 28.28 (chol *C*H$_2$); 28.08, 28.03, 27.91 (chol *C*H/*C*H$_3$, C(*C*H$_3$)$_3$ × 2); 25.35 (Arg *C*H$_2$CH$_2$NH); 24.33, 23.90 (chol *C*H$_2$'s); 22.88, 22.61 (chol *C*H/*C*H$_3$'s); 21.08 (chol *C*H$_2$); 19.38 (Pbf Ar*C*H$_3$); 18.76 (chol *C*H/*C*H$_3$); 18.05 (Pbf Ar*C*H$_3$); 12.54 (Pbf Ar*C*H$_3$); 11.91 (chol *C*H/*C*H$_3$). IR not acquired. ESI-MS (*m*/*z*): Calc. for $C_{61}H_{99}N_6O_{11}S$ 1123.7087; found: 1123.7092 (100%, $[M+H]^+$).

Attempted synthesis of Chol-Arg-Gly-Asp (3.8)

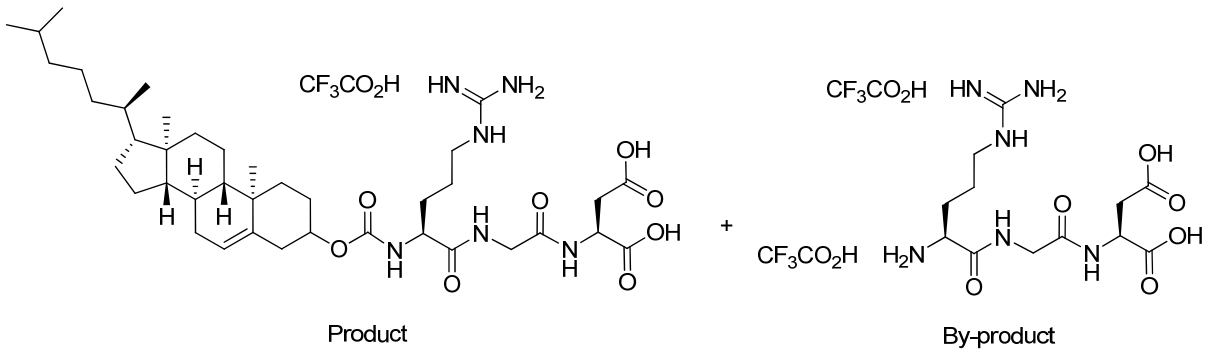

Compound **3.7** (130 mg, 0.12 mmol) was dissolved in a mixture of TFA, water and TIS (1 ml, 95:2.5:2.5) and shaken for 4.5 h, after which time TLC indicated that the deprotection reaction was

complete. The volatiles were removed *in vacuo,* and tried to dissolve the residue in 10% acetic acid but a white solid crashed out. The liquid was evaporated *in vacuo*, and then tried to dissolve the residue in methanol but it was insoluble. The methanol was removed *in vacuo*, and the residue was re-dissolved in TFA, precipitated using diethyl ether, and the white solid filtered off. The white solid was hygroscopic, so the filtrate was evaporated and precipitated from TFA/Et_2O and the two batches of white solid were combined. The solid was lyophilised from water/^{t}BuOH to yield an off-white solid (45 mg, 45%).

Partial characterisation: R_f 0.00 (9:1 DCM/MeOH, cerium stain). ESI-MS (*m/z*) (positive ion mode): Calc. for $C_{40}H_{67}N_6O_8$ 759.5015; found: 759.5003 (20%, $[M+H]^+$); 347.2 (100%, [H_2N-Arg-Gly-Asp-OH by-product + $H]^+$). ESI-MS (*m/z*) (negative ion mode): Found: 757.5 (100%, $[M-H]^-$).

Synthesis of C12-Lys(C12)-OMe (3.9)

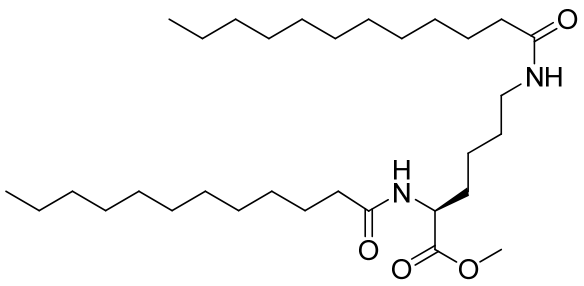

Lauric acid (2.00 g, 10 mmol, 2.0 eq) and L-lysine methyl ester dihydrochloride (1.17 g, 5 mmol, 1.0 eq) were combined in DCM (40 ml) and stirred over an ice-water bath. DIPEA (3.48 ml, 20 mmol, 4.0 eq) and TBTU (3.21 g, 10 mmol, 2.0 eq) were added neat and the reaction was stirred for 64 h. The fine white solid was filtered off and washed with DCM (25 ml). The organic fractions were combined and washed with hot 5% HCl (0.5 M, 3 × 100 ml), hot 1 M Na_2CO_3 (3 × 100 ml), hot 15% Na_2CO_3 (3 × 100 ml), hot 10% HCl (1 M, 3 × 100 ml), and finally hot water (2 × 100 ml). The organic phase was dried over $MgSO_4$, filtered and then the filtrate was evaporated to yield **3.9** as an off-white solid (2.34 g, 89%). No further purification was required.

R_f 0.53 (9:1, DCM/MeOH, cerium stain). $[\alpha]_D$ = +5.6° (c = 1.0, $CHCl_3$). M.p not acquired. ^{1}H NMR ($CDCl_3$, 400 MHz) δ 6.40 (d, α-N*H* amide, *J* = 7.5 Hz, 1H); 6.01 (br t, ε-N*H* amide, *J* = 5.0 Hz, 1H); 4.50 (td, α-H, *J* = 8.0 Hz and 4.5 Hz, 1H); 3.68 (s, C*H*$_3$OC(O), 3H); 3.18 (m, C*H*$_2$NHC(O), 2H); 2.19 (t, C*H*$_2$C(O)NH, *J* = 7.0 Hz, 2H); 2.12 (t, C*H*$_2$C(O)NH, *J* = 7.0 Hz, 2H); 1.85-1.13 (m, C12 and lysine C*H*$_2$'s, calc 42H, found 45 H); 0.83 (t, 2 × C12 C*H*$_3$, *J* = 7.0 Hz, 6H). ^{13}C NMR ($CDCl_3$, 100 MHz) δ 173.67, 173.44, 173.10 (*C*(O)NH amide × 2, *C*(O)OCH$_3$); 52.33 (C(O)O*C*H$_3$); 51.76 (α-*C*H); 38.63 (*C*H$_2$NHC(O)); 36.81, 36.49 (*C*H$_2$C(O)NH × 2); 31.94, 31.82, 29.68, 29.66, 29.58, 29.46, 29.43, 29.38, 29.35, 28.92, 25.91, 25.70, 22.72, 22.35 (C12 and lysine *C*H$_2$'s); 14.14 (C12 *C*H$_3$ × 2). $\tilde{\nu}_{max}$ (cm^{-1})

(solid): 3302*w* (N-H amide stretch); 2916*m*, 2855*w* (C-H alkyl stretches); 1736*m* (C=O ester stretch); 1643*m* (C=O amide stretch); 1543*s* (N-H amide bend); 1458*m*, 1366*m* (C-H alkyl bends); 1242*m*, 1150*s*, 1103*s* (C-O ester and C-N amide stretches). ESI-MS (*m*/*z*): Calc. for $C_{31}H_{61}N_2O_4$ 525.4626; found: 525.4614 (100%, $[M+H]^+$).

Synthesis of C12-Lys(C12)-OH (3.10)

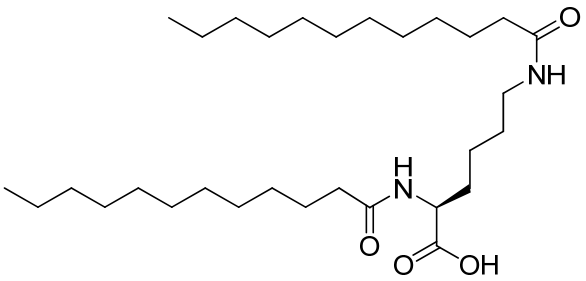

Compound **3.9** (2.24 g, 4.3 mmol, 1.0 eq) was dissolved in MeOH (50 ml) with sonication and then cooled in an ice-water bath, upon which, the starting material precipitated out of solution. 1 M NaOH (13 ml, 13 mmol, 3 eq) was added and the reaction was kept stirring at 0°C for ~2 h, then the ice-water bath was removed and the flask allowed to warm to rt. The mixture was sonicated for 1 h and then more MeOH and 1 M NaOH (8.6 ml, 8.6 mmol, 2 eq, 5 eq in total) were added for smoother stirring and to try to dissolve the starting material. The white suspension was stirred vigorously at rt for 16 h, after which time the white suspension still remained. The reaction was heated at 40°C for 2 h, after which time TLC indicated that the reaction was complete (the white precipitate dissolved after ~30 min of heating) then the solvent was removed *in vacuo*. The white residue was taken up in water (250 ml) and gently heated at 40°C to induce solubilisation, then the solution was acidified to pH 1 using 1.33 M $NaHSO_4$ (~30 ml) upon which a white precipitate formed. This was taken up in DCM (250 ml), separated from the aqueous layer, and then the aqueous layer was washed with more DCM (150 ml) and the organic fractions were combined and washed with hot water (400 ml), then brine (400 ml), and then dried over $MgSO_4$, filtered, and the filtrate evaporated to yield **3.10** as a white solid (~1.8 g, ~83%).

R_f 0.04 (9:1, DCM/MeOH, cerium stain). $[\alpha]_D$ = -72.2° (c = 1.0, $CHCl_3$). M.p not acquired. ^{1}H NMR ($CDCl_3$, 400 MHz) δ 10.17 (br s, CO_2H, 1H); 6.81 (d, α-N*H* amide, *J* = 7.0 Hz, 1H); 6.10 (t, ε-N*H* amide, *J* = 5.5 Hz, 1H); 4.55 (dt, α-*H*, *J* = 7.0 Hz and 5.0 Hz, 1H); 3.35-3.27 (m, CH_2NH, 2H); 3.22-3.14 (m, CH_2NH, 2H); 2.25 (t, CH_2C(O)NH, *J* = 7.0 Hz, 2H); 2.18 (t, CH_2C(O)NH, *J* = 7.0 Hz, 2H); 1.93-1.18 (m, C12 and lysine CH_2's, calc 42H, found 45 H); 0.87 (t, 2 × C12 CH_3, *J* = 7.0 Hz, 6H). ^{13}C NMR ($CDCl_3$, 100 MHz) δ 174.60, 174.47, 174.36 (*C*(O)NH amide × 2, *C*(O)OH); 52.25 (α-*C*H); 39.09 (*C*H_2NHC(O)); 36.86, 36.61 (*C*H_2C(O)NH × 2); 32.04, 31.68, 29.77, 29.67, 29.60, 29.47, 29.07, 25.98, 25.84, 22.78, 22.36 (C12 and lysine *C*H_2's); 14.17 (C12 *C*H_3 × 2). $\tilde{\nu}_{max}$ (cm^{-1}) (solid): 3294*w* (N-

H amide stretch); 2970*m*, 2916*m*, 2855*w* (C-H alkyl stretches); 1736*m* (C=O carboxylic acid stretch); 1643*m* (C=O amide stretch); 1543*s* (N-H amide bend); 1458*m*, 1373*m* (C-H alkyl bends); 1242*m*, 1150*s*, 1103*m* (C-O carboxylic acid and C-N amide stretches). ESI-MS (*m*/*z*): Calc. for $C_{30}H_{59}N_2O_4$ 511.4469; found: 511.4470 (100%, $[M+H]^+$).

Synthesis of C12-Lys(C12)-$(CH_2)_5$-OMe (3.11)

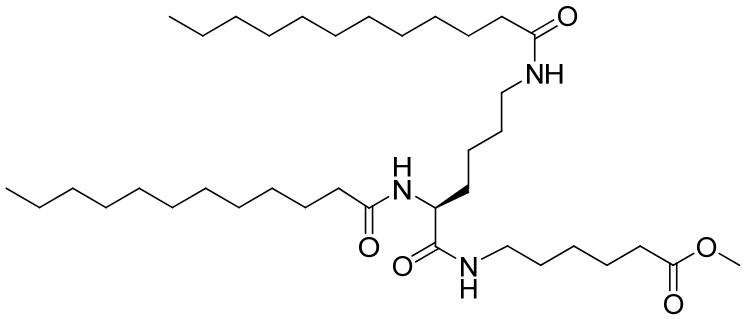

Compound **3.10** (0.5 g, 0.98 mmol, 1.0 eq) dissolved in DCM (20 ml) upon the addition of DIPEA (0.35 ml, 1.96 mmol, 2.0 eq). The reaction flask was cooled over an ice-water bath, then TBTU (315 mg, 0.98 mmol, 1.0 eq) was added as a solid. The reaction mixture was stirred at 0°C for 10 min, then methyl 6-aminohexanoate hydrochloride (179 mg, 0.98 mmol, 1.0 eq) was added as a solid. The reaction was stirred at 0°C for a further 30 min and then the ice-water bath was removed and the reaction allowed to warm to rt. The reaction was refluxed at 40°C for 3 days, then diluted with DCM (50 ml) as material started precipitating out on cooling. The DCM phase was washed with 1 M HCl (150 ml × 3), 1 M Na_2CO_3 (150 ml × 2), water (150 ml), and finally brine (150 ml). The organic phase was dried over $MgSO_4$, filtered and the filtrate evaporated to yield **3.11** as a waxy white solid (0.53 g, 85%). No further purification was required.

R_f 0.44 (9:1, DCM/MeOH, $KMnO_4$ stain). $[\alpha]_D$ = -15.8° (c = 1.0, $CHCl_3$). M.p not acquired. ^{1}H NMR ($CDCl_3$/CD_3OD, 400 MHz) δ 4.27-4.22 (m, α-*H*, 1H); 3.64 (s, C(O)OCH_3, 3H); 3.18-3.12 (m, 2 × CH_2NH, 4H); 2.31 (t, CH_2C(O)OCH$_3$, *J* = 7.5 Hz, 2H); 2.20 (t, CH_2C(O)NH, *J* = 7.0 Hz, 2H); 2.14 (t, CH_2C(O)NH, *J* = 7.0 Hz, 2H); 1.79-1.09 (m, C12 CH_2's, lysine CH_2's and C6 linker CH_2's, 48 H); 0.85 (t, 2 × C12 CH_3, *J* = 7.0 Hz, 6H). ^{13}C NMR ($CDCl_3$/CD_3OD, 100 MHz) δ 174.60, 174.41, 174.35, 172.28 (*C*(O)NH amide × 3, *C*(O)OCH$_3$); 52.67 (α-*C*H); 51.21 (C(O)O*C*H$_3$); 38.89, 38.53 (*C*H$_2$NHC(O) × 2); 36.16, 35.94 (*C*H$_2$C(O)NH × 2); 33.55 (*C*H$_2$C(O)OCH$_3$); 31.61, 31.50, 29.31, 29.23, 29.04, 28.55, 28.44, 26.01, 25.68, 25.49, 24.19, 22.50, 22.36 (C12, lysine and C6 linker *C*H$_2$'s); 13.62 (C12 *C*H$_3$ × 2). $\tilde{\nu}_{max}$ (cm^{-1}) (solid): 3302*w* (N-H amide stretch); 2916*m*, 2847*w* (C-H alkyl stretches); 1736*m* (C=O ester stretch); 1636*m* (C=O amide stretch); 1543*s* (N-H amide bend); 1458*m*, 1373*m* (C-H alkyl bends); 1242*m*, 1150*s*, 1103*m* (C-O ester and C-N amide stretches). ESI-MS (*m*/*z*): Calc. for $C_{37}H_{72}N_3O_5$ 638.5466; found: 638.5465 (78%, $[M+H]^+$).

Synthesis of C12-Lys(C12)-$(CH_2)_5$-OH (3.12)

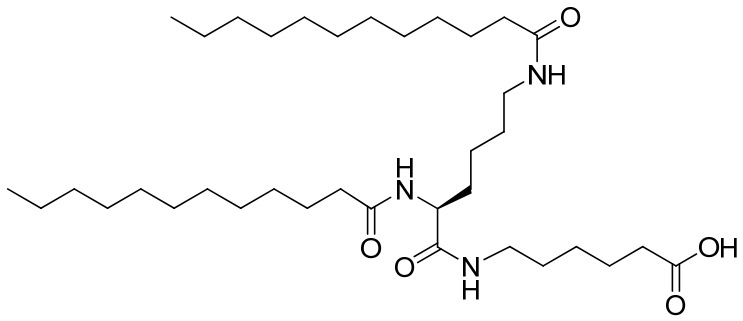

Compound **3.11** (0.5 g, 0.78 mmol, 1.0 eq) was dissolved in MeOH (20 ml) with heating at 40°C. 1 M NaOH (2.35 ml, 2.35 mmol, 3 eq) was added and the reaction was kept stirring at 40°C for 1 h, after which time TLC indicated presence of starting material, so heating was increased to 50°C, after which time TLC still indicated presence of starting material, so heating was increased to 60°C and the reaction refluxed for 3 h after a further addition of 1 M NaOH (2.35 ml, 2.35 mmol, 3 eq, 6 eq in total), after which time TLC did not indicate presence of starting material. The solvent was then removed *in vacuo* and the residue was dissolved in water (50 ml) and heated to 70°C until the sample became cloudy but had dissolved, then 1.33 M $NaHSO_4$ was added until pH ~2 was reached. The white precipitate was taken up in DCM with heating, and the organic layer was separated and washed with hot water (250 ml), then hot brine (250 ml), dried over $MgSO_4$, filtered, and the filtrate evaporated to yield a white solid (~0.5 g). Purification by column chromatography (SiO_2, 9:1 DCM/MeOH) yielded **3.12** as a waxy white solid (0.36 g, 73%).

R_f 0.33 (9:1, DCM/MeOH, $KMnO_4$ stain). $[\alpha]_D$ = -15.5° (c = 1.0, $CHCl_3$). M.p not acquired. ^{1}H NMR ($CDCl_3$, 400 MHz) δ 7.32 (br s, N*H* amide, 1H); 7.12 (br s, N*H* amide, 1H); 6.38 (br s, N*H* amide, 1H); 4.48-4.42 (m, α-*H*, 1H); 3.33-3.08 (m, 2 × C*H*$_2$NH, 4H); 2.29 (t, C*H*$_2$C(O)OH, *J* = 7.0 Hz, 2H); 2.18 (t, C*H*$_2$C(O)NH, *J* = 7.0 Hz, 2H); 2.13 (t, C*H*$_2$C(O)NH, *J* = 7.0 Hz, 2H); 1.81-1.11 (m, C12 C*H*$_2$'s, lysine C*H*$_2$'s and C6 linker C*H*$_2$'s, calc 48 H, found 47 H); 0.83 (t, 2 × C12 C*H*$_3$, *J* = 7.0 Hz, 6H). ^{13}C NMR ($CDCl_3$, 100 MHz) δ 177.27, 174.77, 174.52, 172.80 (*C*(O)NH amide × 3, *C*(O)OH); 52.81 (α-*C*H); 39.03, 38.90 (*C*H$_2$NHC(O) × 2); 36.60, 36.31 (*C*H$_2$C(O)NH × 2); 33.75 (*C*H$_2$C(O)OH); 32.02, 31.76, 29.50, 29.47, 29.40, 29.26, 29.24, 29.19, 28.83, 28.54, 25.94, 25.68, 25.59, 24.09, 22.48, 22.42 (C12, lysine and C6 linker *C*H$_2$'s); 13.87 (C12 *C*H$_3$ × 2). $\tilde{\nu}_{max}$ (cm^{-1}) (solid): 3302*m* (N-H amide stretch); 2970*m*, 2916*s*, 2847*m* (C-H alkyl stretches); 1736*m* (C=O carboxylic acid stretch); 1636*s* (C=O amide stretch); 1543*s* (N-H amide bend); 1458*m*, 1373*m* (C-H alkyl bends); 1242*m*, 1157*s*, 1103*m* (C-O carboxylic acid and C-N amide stretches). ESI-MS (*m*/*z*): Calc. for $C_{36}H_{70}N_3O_5$ 624.5310; found: 624.5293 (100%, $[M+H]^+$); calc. for $C_{36}H_{69}N_3NaO_5$ 646.5129; found: 646.5103 (29%, $[M+Na]^+$).

Synthesis of 2-(2-(2-(2-azidoethoxy)ethoxy)ethoxy)ethanol (3.13)

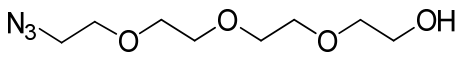

A solution of tetra(ethylene glycol) (27.2 g, 140 mmol) and TEA (15 ml, 108 mmol) in dry THF (100 ml) was cooled to 0°C under nitrogen. To this was added p-toluenesulfonyl chloride solution (9.53 g, 50 mmol) in dry THF (10 ml) dropwise over 45 minutes. The reaction mixture was allowed to warm to rt and stirred for 16 h. The reaction mixture changed from a white to yellow coloured precipitate solution overnight. The solvent was removed *in vacuo* and the yellow residue was dissolved in absolute ethanol (100 ml), then sodium azide (6.5 g, 100 mmol) was added as a solid and the mixture was refluxed for 22.5 h. The solvent was removed *in vacuo* and the residue diluted with Et_2O (250 ml) and washed with brine (50 ml). The organic layer was separated and the aqueous layer extracted with DCM (3 × 100 ml). The organic fractions were combined and dried over $MgSO_4$, filtered and the filtrate evaporated to yield a crude, orange oil (~15 g). Purification by column chromatography (SiO_2, 1:1 cyclohexane/EtOAc to 100% EtOAc) yielded **3.13** as a clear, colourless oil (5.5 g, 50%).

R_f 0.25-0.38 (EtOAc, cerium stain). ^{1}H NMR ($CDCl_3$, 400 MHz) δ 3.73-3.59 (m, C*H*$_2$O, 14H); 3.39 (t, C*H*$_2$N$_3$, *J* = 5.0 Hz, 2H); 2.64 (br s, O*H*, 1H). ^{13}C NMR ($CDCl_3$, 100 MHz) δ 72.47, 70.62, 70.58, 70.51, 70.26, 69.98, 61.59 (7 × *C*H$_2$O); 50.58 (*C*H$_2$N$_3$). $\tilde{\nu}_{max}$ (cm^{-1}) (oil): 3480*w* (O-H alcohol stretch); 2909*m*, 2870*m* (C-H alkyl stretches); 2099*s* (N≡N asymmetric stretch); 1466*w*, 1350*w* (C-H alkyl bends); 1281*m* (N≡N symmetric stretch); 1103*s*, 1065*s* (C-O ether and alcohol stretches). ESI-MS (*m*/*z*): Calc. for $C_8H_{18}N_3O_4$ 220.1292; found: 220.1294 (100%, $[M+H]^+$).

Synthesis of 14-azido-3,6,9,12-tetraoxatetradecan-1-oic acid (3.14)

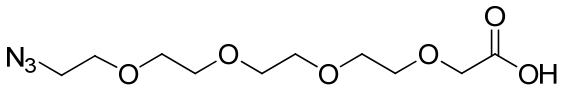

Compound **3.13** (2.4 g, 10.96 mmol) and sodium hydride (0.88 g, 21.92 mmol, 2.0 eq) were solubilised in dry THF (~ 25 ml) and stirred at 0°C for 45 minutes. Bromoacetic acid (1.52 g, 10.96 mmol, 1.0 eq) in dry THF (~ 25 ml) was then added. The reaction was stirred under nitrogen at rt for 26.5 h. The solvent was removed *in vacuo* and the residue taken up in water (100 ml), acidified to pH 2 with 1M HCl (20 ml) and then the aqueous phase was extracted with DCM (3 × 200 ml). The organic fractions were combined, dried over $MgSO_4$, filtered and the solvent removed *in vacuo* to yield a crude, colourless oil (~3.2 g). This was purified by column chromatography (SiO_2, 9:1 DCM/MeOH) to yield **3.14** as a colourless oil (~1.8 g, 59%).

R_f 0.47 (65:25:4 $CHCl_3$/MeOH/H_2O, $KMnO_4$ stain). ^{1}H NMR ($CDCl_3$, 400 MHz) δ 6.08 (br s, C(O)O*H*, 1H); 4.12 (s, OC*H*$_2$C(O)OH, 2H); 3.73-3.59 (m, C*H*$_2$O, 14H); 3.39 (t, C*H*$_2$N$_3$, *J* = 5.0 Hz, 2H). ^{13}C NMR ($CDCl_3$, 100 MHz) δ 172.93 (*C*(O)OH); 72.47, 70.62, 70.58, 70.51, 70.26, 69.98, 63.50, 61.59 (8 × *C*H$_2$O); 50.58 (*C*H$_2$N$_3$). $\tilde{\nu}_{max}$ (cm^{-1}) (oil): 3588*w* (O-H carboxylic acid stretch); 2909*m*, 2870*m* (C-H alkyl stretches); 2099*s* (N≡N asymmetric stretch); 1751*m* (C=O carboxylic acid stretch); 1466*w*, 1435*w*, 1389*w*, 1350*w* (C-H alkyl bends); 1288*m* (N≡N symmetric stretch); 1111*s* (C-O ether and carboxylic acid stretches). ESI-MS (*m*/*z*): Calc. for $C_{10}H_{19}N_3NaO_6$ 300.1166; found: 300.1165 (100%, $[M+Na]^+$).

Synthesis of N$_3$-TEG-Arg(Pbf)-Gly-Asp(O^{t}Bu)-O^{t}Bu (3.15)

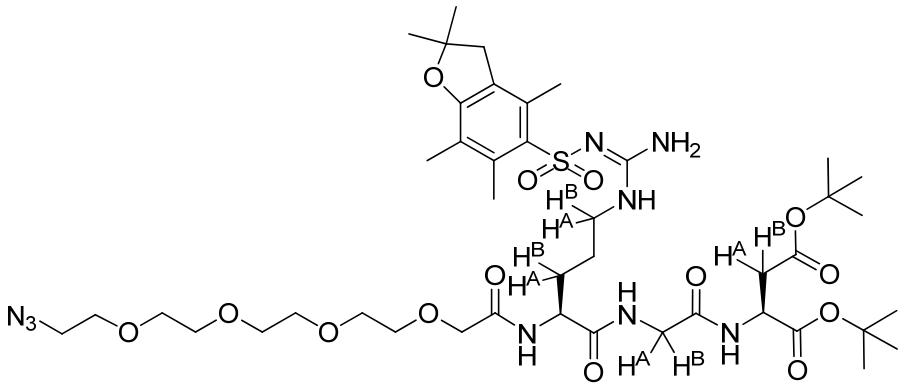

Compound **3.14** (78 mg, 0.28 mmol, 1.0 eq) was suspended in DCM (2 ml) and DIPEA (100 µL, 0.56 mmol, 2.0 eq) was added. The reaction flask was cooled over an ice-water bath, then TBTU (91 mg, 0.28 mmol, 1.0 eq) was added as a solid. The reaction mixture was stirred at 0°C for 10 min, then **2.8(2.4)** (200 mg, 0.28 mmol, 1.0 eq) was added as a solid and more DCM (4 ml) was used to rinse the contents of the vial into the reaction flask. The reaction was stirred at 0°C for a further 20 min, then the ice-water bath was removed and the reaction allowed to warm to rt and stirred for 5 days. The DCM phase was washed with 1.33 M $NaHSO_4$ (50 ml × 3), 1 M Na_2CO_3 (50 ml × 3), 1 M HCl (50 ml), water, and finally brine. The organic phase was dried over $MgSO_4$, filtered and the filtrate evaporated to yield a tacky white foam (0.26 g, 96%). Purification by column chromatography (SiO_2, 100% DCM, to 98:2 DCM/MeOH, to 95:5 DCM/MeOH) yielded **3.15** as a white solid (140 mg, 52%).

R_f 0.53 (9:1 DCM/MeOH, UV and cerium stain). $[\alpha]_D$ = -2.9° (c = 0.4, $CHCl_3$). M.p not acquired. ^{1}H NMR ($CDCl_3$, 400 MHz) δ 7.82 (app br t, N*H* amide (Arg-Gly), 1H); 7.44 (d, N*H* amide, *J* = 7.5 Hz, 1H); 7.16 (d, N*H* amide, *J* = 7.5 Hz, 1H); 6.31 (br s, N*H*$_2$ guanidine, 2H); 6.18 (br s, N*H* guanidine, 1H); 4.61-4.55 (m, Asp α-*H* and Arg α-*H*, 2H); 3.96 (s, OC*H*$_2$C(O)NH, 2H); 3.94 (dd, Gly C*H*^{A}, J = 17.0 Hz and 5.5 Hz, 1H); 3.86 (dd, Gly C*H*^{B}, *J* = 17.0 Hz and 5.5 Hz, 1H); 3.65-3.54 (m, TEG OC*H*$_2$'s, 14H); 3.31 (t, C*H*$_2$N$_3$, *J* = 5.0 Hz, 2H); 3.28-3.20 (br m, Arg C*H*^{A}NH, 1H); 3.18-3.07 (br m,

Arg C*H*^{B}NH, 1H); 2.89 (s, Pbf CH_2, 2H); 2.76 (dd, Asp C*H*^{A}, *J* = 17.0 Hz and 5.0 Hz, 1H); 2.63 (dd, Asp C*H*^{B}, *J* = 17.0 Hz and 5.0 Hz, 1H); 2.53 (s, Pbf CH_3Ar, 3H); 2.45 (s, Pbf CH_3Ar, 3H); 2.02 (s, Pbf CH_3Ar, 3H); 1.95-1.84 (br m, Arg CHC*H*^{A}, 1H); 1.71-1.60 (br m, Arg CHC*H*^{B}, 1H); 1.57-1.46 (br m, Arg CH_2CH$_2$NH, 2H); 1.40 (s, Pbf CH_3 × 2, 6H); 1.359, 1.355 (s × 2, C(CH_3)$_3$ × 2, calc 18H, found 17H). ^{13}C NMR ($CDCl_3$, 100 MHz) δ 172.20, 170.40, 170.01, 169.65, 169.09, 158.56, 156.52 (*C*(O)O^{t}Bu × 2, *C*(O)NH amide × 3, Pbf aromatic *C*-O, *C*=N guanidine); 138.27, 133.00, 132.21, 124.48, 117.34 (Pbf aromatic *C*); 86.27 (Pbf CH$_2$*C*(CH$_3$)$_2$O); 82.37, 81.51 (*C*(CH$_3$)$_3$ × 2); 71.00, 70.52, 70.48, 70.43, 70.21, 69.91 (TEG OCH_2's and OCH_2C(O)NH); 51.89 (Arg α-*C*H); 50.57 (*C*H$_2$N$_3$); 49.26 (Asp α-*C*H); 43.20, 42.71 (Pbf Ar*C*H$_2$, Gly *C*H$_2$); 40.00 (Arg *C*H$_2$NH); 37.29 (Asp *C*H$_2$); 29.66 (Arg CH*C*H$_2$); 28.56 (Pbf CH$_2$C(*C*H$_3$)$_2$O); 27.98, 27.81 (C(*C*H$_3$)$_3$ × 2); 25.30 (Arg *C*H$_2$CH$_2$NH); 19.28, 17.94, 12.45 (Pbf Ar*C*H$_3$ × 3). $\tilde{\nu}_{max}$ (cm^{-1}) (solid): 3325*w* (N-H amide stretch); 2978*w*, 2916*w* (C-H alkyl stretches); 2098*m* (N≡N asymmetric stretch); 1736*w* (C=O ester stretch); 1659*m* (C=O amide stretch); 1543*s*, 1450*w*, 1366*w* (N-H amide bend, C-H alkyl bend, C=C arene stretch and S=O stretch); 1250*m*, 1142*s*, 1096*s* (C-O ester and ether stretches, and C-N amide stretches, overlapping N≡N symmetric stretch at ~1280*m*). ESI-MS (*m*/*z*): Calc. for $C_{43}H_{72}N_9O_{14}S$ 970.4914; found: 970.4893 (100%, $[M+H]^+$).

Synthesis of H$_2$N-TEG-Arg(Pbf)-Gly-Asp(O^{t}Bu)-O^{t}Bu (3.16)

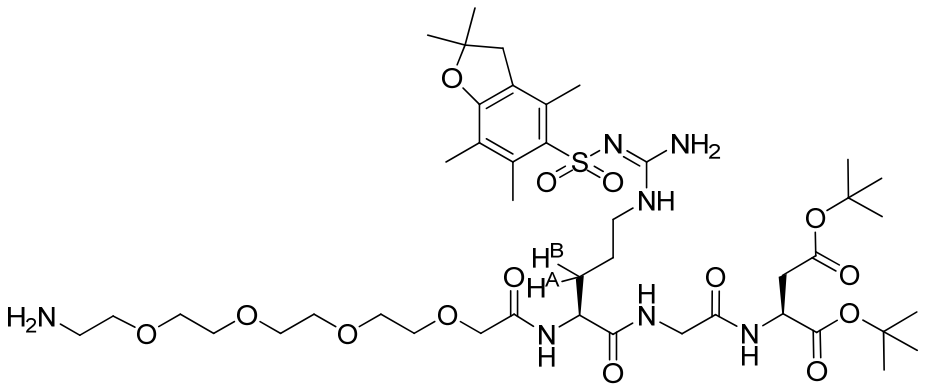

Compound **3.15** (120 mg, 0.12 mmol) was dissolved in EtOH (10 ml) followed by the addition of Pd/C catalyst (24 mg, 20%). The flask was subjected to several vacuum/H_2 purges and then stirred for 3 days under an atmosphere of H_2. The catalyst was filtered off over Celite, washed with MeOH, and the filtrate evaporated *in vacuo* to yield **3.16** as a clear, colourless oil (~120 mg, quantitative yield). No further purification was required.

R_f 0.00 (9:1 DCM/MeOH, cerium stain). $[\alpha]_D$ = -11.6° (c = 0.5, $CHCl_3$). ^{1}H NMR (CD_3OD, 400 MHz) δ 4.66-4.61 (br m, Asp α-*H*, 1H); 4.49-4.40 (br m, Arg α-*H*, 1H); 4.14-4.03 (br m, Gly CH_2, 2H); 3.91 (s, OCH_2C(O)NH, 2H); 3.78-3.60 (m, TEG OCH_2's, 14H); 3.27-3.09 (br m, CH_2NH$_2$ and Arg CH_2NH, 4H); 3.00 (s, Pbf CH_2, 2H); 2.78-2.66 (m, Asp CH_2, 2H); 2.58 (s, Pbf CH_3Ar, 3H); 2.51

(s, Pbf C*H*$_3$Ar, 3H); 2.08 (s, Pbf C*H*$_3$Ar, 3H); 1.95-1.84 (br m, Arg CHC*H*^{A}, 1H); 1.80-1.66 (br m, Arg CHC*H*^{B}, 1H); 1.66-1.52 (br m, Arg C*H*$_2$CH$_2$NH, 2H); 1.45, 1.44 (s × 2, Pbf C*H*$_3$ × 2, C(C*H*$_3$)$_3$ × 2, 24H). ^{13}C NMR (CD_3OD, 100 MHz) δ 172.76, 171.25, 171.23, 171.10, 159.82, 158.08 (*C*(O)O^{t}Bu × 2, *C*(O)NH amide × 3, Pbf aromatic *C*-O, *C*=N guanidine); 139.35, 134.35, 133.48, 126.01, 118.41 (Pbf aromatic *C*); 87.69 (Pbf CH$_2$*C*(CH$_3$)$_2$O); 83.28, 82.47 (*C*(CH$_3$)$_3$ × 2); 71.94, 71.83, 71.38, 71.27, 71.20, 71.10, 70.92, 70.77, 67.79, 66.84 (TEG OC*H*$_2$'s and OC*H*$_2$C(O)NH); 54.00 (Arg α-*C*H); 50.98 (Asp α-*C*H); 43.98, 43.25 (Pbf Ar*C*H$_2$, Gly *C*H$_2$); 41.35 (Arg *C*H$_2$NH); 40.55 (*C*H$_2$NH$_2$); 38.25 (Asp *C*H$_2$); 30.26 (Arg CH*C*H$_2$); 28.79 (Pbf CH$_2$C(*C*H$_3$)$_2$O); 28.41, 28.24 (C(*C*H$_3$)$_3$ × 2); 26.79 (Arg *C*H$_2$CH$_2$NH); 19.68, 18.51, 12.61 (Pbf Ar*C*H$_3$ × 3). $\tilde{\nu}_{max}$ (cm^{-1}) (oil): 3742*w* (N-H amide and amine stretches); 2978*m*, 2886*m* (C-H alkyl stretches); 1736*w* (C=O ester stretch); 1667*m* (C=O amide stretch); 1543*m*, 1458*w*, 1396*w*, 1366*w* (N-H amide bend, C-H alkyl bend, C=C arene stretch and S=O stretch); 1250*m*, 1088*s* (C-O ester and ether stretches, and C-N amide stretches). ESI-MS (*m*/*z*): Calc. for $C_{43}H_{74}N_7O_{14}S$ 944.5009; found: 944.4978 (100%, $[M+H]^+$).

Synthesis of C12-Lys(C12)-(CH$_2$)$_5$-TEG-Arg(Pbf)-Gly-Asp(O^{t}Bu)-O^{t}Bu (3.17)

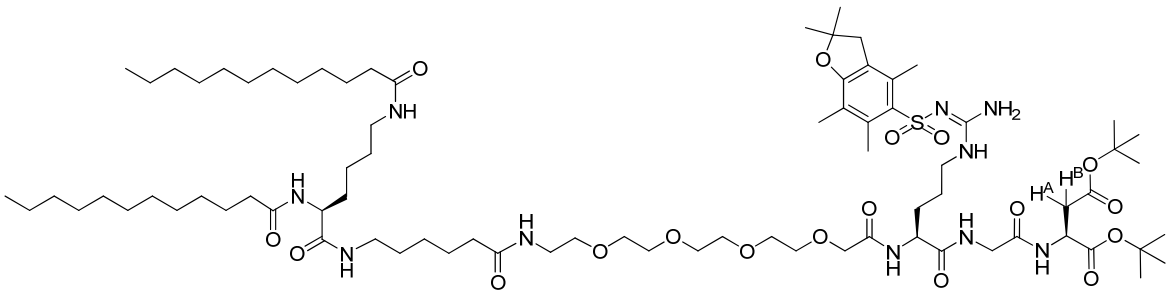

Compound **3.12** (77 mg, 0.12 mmol, 1.0 eq) was suspended in DCM (3 ml) and then DIPEA (50 μL, 0.25 mmol, 2.0 eq) was added. The reaction flask was cooled over an ice-water bath, then TBTU (49 mg, 0.15 mmol, 1.2 eq) was added as a solid. The reaction mixture was stirred at 0°C for 10 min, then **3.16** (120 mg, 0.12 mmol, 1.0 eq) was dissolved in DCM (2 ml) and added rapidly to the reaction flask, then more DCM (5 ml) was used to rinse the contents of the vial into the reaction flask. The ice-water bath was removed; the reaction allowed to warm to rt and then refluxed at 40°C for 13 h. The reaction was diluted with DCM (10 ml), washed with 1.33 M $NaHSO_4$ (50 ml), 1 M Na_2CO_3 (50 ml), and finally brine. The organic phase was dried over $MgSO_4$, filtered and the filtrate evaporated to yield a brown foam/solid (~180 mg, 92%). Purification by column chromatography (SiO_2, 100% DCM, to 98:2 DCM/MeOH, to 95:5 DCM/MeOH, to 9:1 DCM/MeOH) yielded **3.17** as a white solid (50 mg, 26%).

R_f 0.33 (9:1 DCM/MeOH, UV and cerium stain). $[\alpha]_D$ not acquired. M.p not acquired. ^{1}H NMR ($CDCl_3$, 400 MHz) δ 7.99 (br s, N*H* amide, 1H); 7.62 (br s, N*H* amide, 1H); 7.25, 7.23 (br s, N*H*

amide × 2, 2H); 7.02 (br s, N*H* amide, 1H); 6.93 (br s, N*H* amide, 1H); 6.45, 6.38 (br s × 2, NH_2 guanidine, N*H* guanidine, N*H* amide, 4H); 4.65-4.54 (m, Asp α-*H* and Arg α-*H*, 2H); 4.42-4.33 (m, Lys α-*H*, 1H); 4.04 (s, OCH_2C(O)NH, 2H); 4.01-3.86 (m, Gly CH_2, 2H); 3.74-3.48 (m, TEG OCH_2's, 14H); 3.44-3.30, 3.29-3.08 (m × 2, CH_2NHC(O) (Lys), CH_2NHC(O) (C6 linker), C(O)NHCH_2CH$_2$O, Arg CH_2NH, 2H+6H); 2.93 (s, Pbf CH_2, 2H); 2.79 (dd, Asp CH^A, J = 17.0 Hz and 5.0 Hz, 1H); 2.68 (dd, Asp CH^B, J = 17.0 Hz and 5.0 Hz, 1H); 2.56 (s, Pbf CH_3Ar, 3H); 2.49 (s, Pbf CH_3Ar, 3H); 2.21-2.10 (m, CH_2C(O)NH (C6 linker), CH_2C(O)NH × 2 (C12 tails), 6H); 2.06 (s, Pbf CH_3Ar, 3H); 1.98-1.04 (m, C12 CH_2's, lysine CH_2's, C6 linker CH_2's, Arg CH_2 × 2, Pbf CH_3 × 2, C(CH_3)$_3$ × 2, calc 72H, found 75 H); 0.85 (t, 2 × C12 CH_3, J = 7.0 Hz, 6H). ^{13}C NMR ($CDCl_3$, 100 MHz) δ 173.92, 173.88, 172.29, 172.23, 172.17, 170.72, 170.10, 169.73, 168.91, 158.67, 156.63 (*C*(O)O^{t}Bu × 2, *C*(O)NH amide × 7, Pbf aromatic *C*-O, *C*=N guanidine); 138.32, 133.31, 132.23, 124.59, 117.48 (Pbf aromatic *C*); 86.40 (Pbf CH$_2$*C*(CH$_3$)$_2$O); 82.45, 81.64 (*C*(CH$_3$)$_3$ × 2); 77.47, 70.81, 70.35, 70.19, 70.00 (TEG OCH_2's and OCH_2C(O)NH); 53.08, 52.44, 49.38 (Arg α-*C*H, Lys α-*C*H, Asp α-*C*H); 43.35, 42.88 (Pbf Ar*C*H$_2$, Gly *C*H$_2$); 40.22 (Arg *C*H$_2$NH); 39.24, 39.19, 38.95, 37.48, 36.79, 36.56, 36.15 (C(O)NH*C*H$_2$CH$_2$O, Asp *C*H$_2$, *C*H$_2$NHC(O) × 2 (Lys and C6 linker), *C*H$_2$C(O)NH × 2 (C12 tails), *C*H$_2$C(O)NH (C6 linker)); 32.21, 32.12, 31.99, 29.74, 29.71, 29.64, 29.53, 29.49, 29.43, 29.04, 28.90, 28.69, 28.11, 27.96, 26.37, 25.98, 25.86, 25.56, 25.18, 22.76, 22.67 (C12, lysine and C6 linker *C*H$_2$'s, Arg CH*C*H$_2$, Arg *C*H$_2$CH$_2$NH, Pbf CH$_2$C(*C*H$_3$)$_2$O, C(*C*H$_3$)$_3$ × 2); 19.40, 18.08 (Pbf Ar*C*H$_3$ × 2); 14.20 (C12 *C*H$_3$ × 2); 12.57 (Pbf Ar*C*H$_3$). IR not acquired. ESI-MS (*m/z*): Calc. for $C_{79}H_{140}N_{10}NaO_{18}S$ 1571.9960; found: 1571.9976 (12%, $[M+H]^+$). Calc. for $C_{79}H_{142}N_{10}O_{18}S$ 775.5107; found 775.5089 (100%, $[M+2H]^{2+}$).

Synthesis of C12-Lys(C12)-(CH$_2$)$_5$-TEG-Arg-Gly-Asp (3.18)

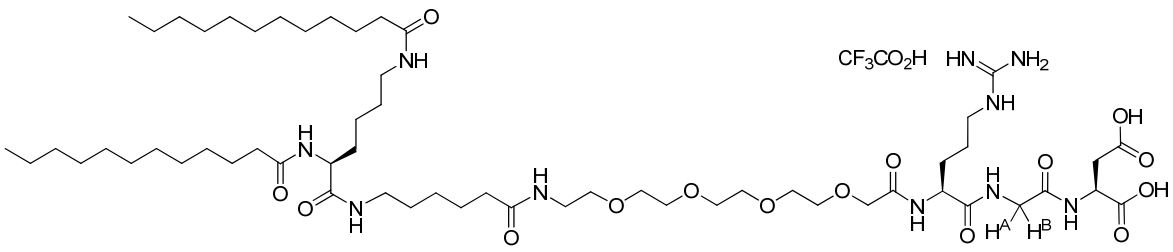

Compound **3.17** (49 mg, 31.6 μmol) was dissolved in a mixture of TFA, water and TIS (2 ml, 95:2.5:2.5) and shaken for 1 h 15 min, after which time TLC indicated that the deprotection reaction was complete. The volatiles were removed *in vacuo,* then the residue was dissolved in the minimum amount of hot MeOH and precipitated with cold Et_2O, filtered and washed with the minimum amount of cold Et_2O to yield a white solid. The sample was then dissolved in a mixture of water/^{t}BuOH, filtered over a PTFE membrane filter (0.2 μm), shell frozen and lyophilised to yield the product **3.18** as a fluffy white powder (17 mg, 41% as TFA salt).

R_f 0.00 (9:1 DCM/MeOH, cerium stain). $[\alpha]_D$ = -2.0° (c = 0.05, MeOH). M.p not acquired. ^{1}H NMR (CD_3OD, 400 MHz) δ 4.72 (t, Asp α-*H*, *J* = 5.5 Hz, 1H); 4.44 (dd, Arg α-*H*, *J* = 7.5 Hz and 6.0 Hz, 1H); 4.22 (dd, Lys α-*H*, *J* = 9.0 Hz and 5.5 Hz, 1H); 4.06 (s, OC*H*$_2$C(O)NH, 2H); 3.97 (d, Gly C*H*^{A}, *J* = 17.0 Hz, 1H); 3.87 (d, Gly C*H*^{B}, *J* = 17.0 Hz, 1H); 3.74-3.56 (m, TEG OC*H*$_2$'s, 14H); 3.52, 3.34, 3.22-3.12 (t (*J* = 5.5 Hz), t (*J* = 5.0 Hz), m, C*H*$_2$NHC(O) (Lys), C*H*$_2$NHC(O) (C6 linker), C(O)NHC*H*$_2$CH$_2$O, Arg C*H*$_2$NH, calc 2H+2H+4H, found 2H+2H+6H); 2.83 (d, Asp C*H*$_2$, *J* = 5.5 Hz, 2H); 2.25-2.13 (m, C*H*$_2$C(O)NH (C6 linker), C*H*$_2$C(O)NH × 2 (C12 tails), 6H); 2.01-1.20 (m, C12 C*H*$_2$'s, lysine C*H*$_2$'s, C6 linker C*H*$_2$'s, Arg C*H*$_2$ × 2, calc 48H, found 52 H); 0.88 (t, 2 × C12 C*H*$_3$, *J* = 7.0 Hz, 6H). $\tilde{\nu}_{max}$ (cm^{-1}) (solid): 3302*m* (O-H acid and N-H amide/guanidino stretches); 2940*m*, 2870*m* (C-H alkyl stretches); 1636*m* (C=O amide stretch); 1551*m*, 1450*m*, 1350*m*, 1273*m* (N-H amide bend, C-H alkyl bend); 1242*m*, 1219*m*, 1096*s* (C-O carboxylic acid and ether stretches, and C-N amide stretches). ESI-MS (*m*/*z*): Calc. for $C_{58}H_{109}N_{10}O_{15}$ 1185.8068; found: 1185.7971 (12%, $[M+H]^+$). Calc. for $C_{58}H_{110}N_{10}O_{15}$ 593.4071; found 593.4052 (100%, $[M+2H]^{2+}$).

6.4 Chapter 4 – Linear RGD Peptide Conjugate Hydrogelators

Synthesis of C12-urea-Arg(Pbf)-Gly-Asp(O^{t}Bu)-O^{t}Bu (4.1)

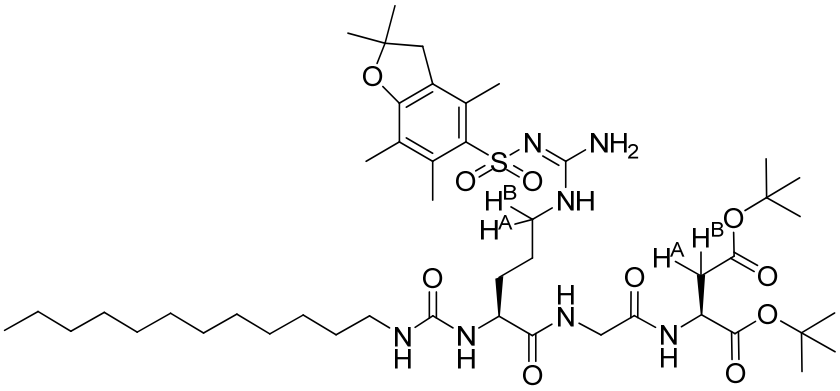

Dodecylisocyanate (68 μL, 0.28 mmol, 1.0 eq) was solubilised in DCM (1.5 ml) and cooled over an ice-water bath. Compound **2.8(2.4)** (200 mg, 0.28 mmol, 1.0 eq) was dissolved in DCM (1.5 ml) and added in one portion to the reaction flask. The ice-water bath was removed and the reaction was stirred at rt for 1.5 h, after which time TLC analysis indicated that the reaction was incomplete (presence of H_2N-Arg(Pbf)-Gly-Asp(O^{t}Bu)$_2$ starting material) so more dodecylisocyanate (68 μL, 0.28 mmol, 1.0 eq, 2.0 eq in total) was added neat and stirring continued overnight. The solvent was removed in vacuo to yield a crude clear oil (290 mg) which was purified by column chromatography (SiO_2, 100% DCM to 98:2 DCM/MeOH, to 95:5 DCM/MeOH) yielding **4.1** as a fluffy, white solid (200 mg, 77%).

R_f 0.18 (9:1 DCM/MeOH, UV and cerium stain). $[\alpha]_D$ = -33.2° (c = 0.1, $CHCl_3$). M.p not acquired. ^{1}H NMR ($CDCl_3$, 400 MHz) δ 7.71 (br t, N*H* amide (Arg-Gly), *J* = 5.0 Hz, 1H); 7.41 (br d, N*H* amide (Gly-Asp), *J* = 6.5 Hz, 1H); 6.38 (br s, N*H* guanidine, N*H*$_2$ guanidine and N*H* urea overlapping, 4H); 5.99 (br s, N*H* urea, 1H); 4.66-4.62 (m, Asp α-*H*, 1H); 4.31-4.22 (br m, Arg α-*H*, 1H); 4.00-3.82 (br m, Gly C*H*$_2$, 2H); 3.46-3.31 (br m, Arg C*H*^{A}NH, 1H); 3.17-3.00 (m, Arg C*H*^{B}NH and C*H*$_2$NHC(O)NH overlapping, 3H); 2.93 (s, Pbf C*H*$_2$, 2H); 2.77 (dd, Asp C*H*^{A}, *J* = 17.0 Hz and 5.0 Hz, 1H); 2.69 (dd, Asp C*H*^{B}, *J* = 17.0 Hz and 5.0 Hz, 1H); 2.55 (s, Pbf C*H*$_3$Ar, 3H); 2.50 (s, Pbf C*H*$_3$Ar, 3H); 2.06 (s, Pbf C*H*$_3$Ar, 3H); 1.85-1.52 (m, Arg CHC*H*$_2$ and Arg C*H*$_2$CH$_2$NH overlapping, 4H); 1.442, 1.437, 1.39 (s × 3, Pbf C*H*$_3$ × 2, C(C*H*$_3$)$_3$ × 2, C12 C*H*$_2$ (underlying multiplet), calc 26H, found 25H); 1.33-1.16 (br m, C12 C*H*$_2$'s, 18H); 0.85 (t, C12 C*H*$_3$, *J* = 7.0 Hz, 3H). ^{13}C NMR ($CDCl_3$, 100 MHz) δ 170.08, 169.95, 169.25, 158.95, 156.90 (*C*(O)O^{t}Bu × 2, *C*(O)NH amide × 2, *C*(O)NH urea, Pbf Ar*C*O, *C*=N guanidine, calc 7 peaks, found 5 peaks, overlapping?); 138.47, 132.61, 132.38, 124.74, 117.68 (Pbf aromatic *C* × 5); 86.50 (Pbf CH$_2$*C*(CH$_3$)$_2$O); 82.50, 81.57 (*C*(CH$_3$)$_3$ × 2); 54.45 (Arg α-*C*H); 49.50 (Asp α-*C*H); 43.38 (Pbf Ar*C*H$_2$); 43.00 (Gly *C*H$_2$); 40.58, 40.34 (*C*H$_2$NHC(O)NH, Arg *C*H$_2$NH); 37.48 (Asp *C*H$_2$); 32.02, 30.29, 29.77, 29.56, 29.47 (C12 *C*H$_2$'s, Arg CH*C*H$_2$ or *C*H$_2$CH$_2$NH, multiple overlapping peaks); 28.71 (Pbf CH$_2$C(*C*H$_3$)$_2$O); 28.14, 27.99 (C(*C*H$_3$)$_3$ × 2); 27.17 (C12 *C*H$_2$); 26.17 (Arg CH*C*H$_2$ or *C*H$_2$CH$_2$NH); 22.79 (C12 *C*H$_2$); 19.47, 18.09 (Pbf Ar*C*H$_3$ × 2); 14.22 (C12 *C*H$_3$); 12.59 (Pbf Ar*C*H$_3$). $\tilde{\nu}_{max}$ (cm^{-1}) (solid): 3341*w* (N-H stretch); 2978*m*, 2932*m*, 2862*w* (C-H alkyl stretches); 1728*m* (C=O ester stretch); 1651*s* (C=O amide/urea stretch); 1551*s* (N-H bend and C=C arene stretch); 1450*m*, 1366*m* (C-H alkyl bends and S=O stretch); 1250*s*, 1150*s*, 1096*s* (C-O ester and C-N stretches). ESI-MS (*m*/*z*): Calc. for $C_{46}H_{80}N_7O_{10}S$ 922.5682; found: 922.5692 (100%, $[M+H]^+$). Calc. for $C_{46}H_{79}N_7NaO_{10}S$ 944.5501; found 944.5507 (44%, $[M+Na]^+$).

Synthesis of C12-urea-Arg-Gly-Asp (4.2)

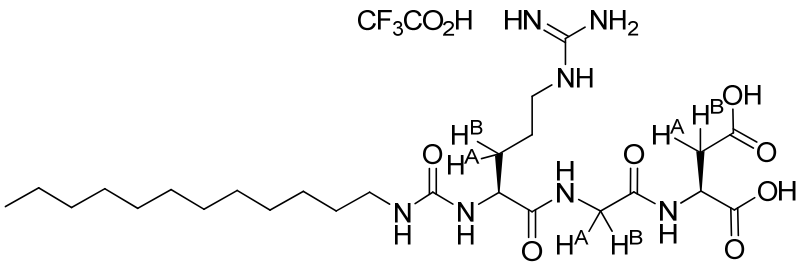

Compound **4.1** (180 mg, 0.2 mmol) was dissolved in a mixture of TFA, water and triisopropylsilane (TIS) (3 ml, 95:2.5:2.5) and shaken for 40 min, after which time TLC indicated that the deprotection reaction was complete. The volatiles were removed *in vacuo,* then the residue was dissolved in the minimum amount of MeOH, precipitated with cold Et_2O, filtered and washed with the minimum amount of cold Et_2O to yield **4.2** as a white solid (105 mg, 80% as TFA salt).

N.B. There was evidence of a small amount of methyl esterification of the carboxylic acids as a consequence of the recovery procedure, but this is not believed to affect gelation behaviour.

R_f 0.00 (9:1, DCM/MeOH, cerium stain). $[\alpha]_D$ = +4.8° (c = 0.25, DMSO). M.p not acquired. ^{1}H NMR (CD_3OD, 400 MHz) δ 4.77 (t, Asp α-*H*, *J* = 6.5 Hz, 1H); 4.17-4.13 (m, Arg α-*H*, 1H); 3.96 (d, Gly C*H*^{A}, *J* = 17.0 Hz, 1H); 3.87 (d, Gly C*H*^{B}, *J* = 17.0 Hz, 1H); 3.24-3.16 (m, Arg C*H*$_2$NH, 2H); 3.15-3.06 (m, C*H*$_2$NHC(O)NH, 2H); 2.90 (dd, Asp C*H*^{A}, *J* = 17.0 Hz and 5.5 Hz, 1H); 2.83 (dd, Asp C*H*^{B}, *J* = 17.0 Hz and 6.5 Hz, 1H); 1.92-1.80 (br m, Arg CHC*H*^{A}, 1H); 1.80-1.63 (br m, Arg CHC*H*^{B} and Arg C*H*$_2$CH$_2$NH overlapping, 3H); 1.54-1.42 (br m, C12 C*H*$_2$, 2H); 1.39-1.22 (br m, C12 C*H*$_2$'s, 18H); 0.90 (t, C12 C*H*$_3$, *J* = 7.0 Hz, 3H). ^{13}C NMR (CD_3OD, 100 MHz) δ 176.20, 174.00, 173.87, 171.55, 160.77, 158.64 (*C*(O)OH × 2, *C*(O)NH amide × 2, *C*(O)NH urea, *C*=N guanidine); 55.34 (Arg α-*C*H); 50.27 (Asp α-*C*H); 43.36 (Gly *C*H$_2$); 42.02, 41.16 (Arg *C*H$_2$NH, *C*H$_2$NHC(O)NH); 36.84 (Asp *C*H$_2$); 33.07, 31.32, 30.80, 30.78, 30.56, 30.52, 30.48, 28.06, 26.06, 23.73 (C12 *C*H$_2$'s, Arg CH*C*H$_2$ and *C*H$_2$CH$_2$NH, multiple overlapping peaks); 14.44 (C12 *C*H$_3$). $\tilde{\nu}_{max}$ (cm^{-1}, solid): 3341*w*, 3202*w* (O-H acid and N-H stretches); 2924*m*, 2862*w* (C-H alkyl stretches); 1705*w* (C=O acid stretch); 1651*s*, 1620*m*, (C=O amide/urea stretch); 1566*m* (N-H bend); 1165*s*, 1034*m* (C-O acid and C-N stretches). ESI-MS (*m*/*z*): Calc. for $C_{25}H_{48}N_7O_7$ 558.3610; found: 558.3621 (100%, $[M+H]^+$).

Synthesis of C12-[urea-Arg(Pbf)-Gly-Asp(O^{t}Bu)-O^{t}Bu]$_2$ (4.3)

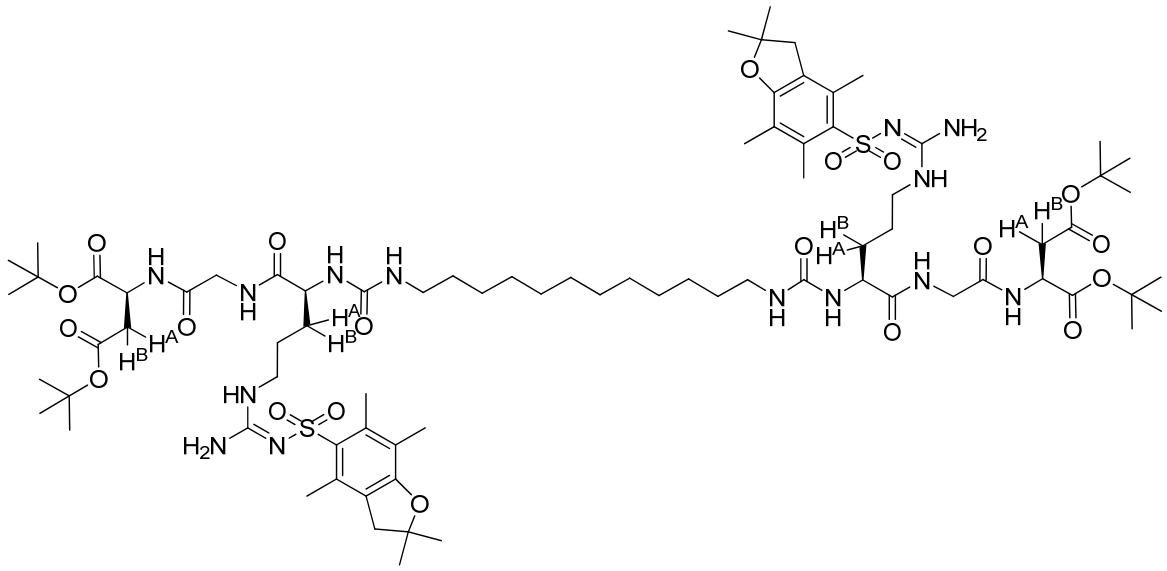

Compound **2.8(2.4)** (0.5 g, 0.70 mmol, 2.4 eq) was dissolved in DCM (5 ml) then 1,12-diisocyanatododecane (74 mg, 0.29 mmol, 1.0 eq), solubilised in DCM (1 ml), was added dropwise over ~1 min and a further portion of DCM (1 ml) was used to wash any residual diisocyanate into the reaction flask. The reaction was stirred vigorously overnight at rt, after which time a white 'jelly-like' solid had precipitated out. Stirring was continued for a total of 19 h then the solvent was removed *in*

vacuo to yield a crude white solid (~600 mg). The crude material was dissolved in the minimum amount of DCM/MeOH (98:2) and purified by column chromatography (SiO_2, 98:2 DCM/MeOH, to 95:5 DCM/MeOH, to 9:1 DCM/MeOH) yielding **4.3** as a fluffy, white solid (480 mg, 98%).

R_f 0.39 (9:1 DCM/MeOH, UV and cerium stain). $[\alpha]_D$ = -1.2° (c = 0.5, MeOH). M.p not acquired. ^{1}H NMR (CD_3OD, 400 MHz) δ 4.65 (t, Asp α-*H* × 2, *J* = 6.0 Hz, 2H); 4.14 (br m, Arg α-*H* × 2, 2H); 3.89 (br m, Gly C*H*$_2$ × 2, 4H); 3.28-3.15 (br m, Arg C*H*$_2$NH × 2, 4H); 3.15-3.04 (m, C*H*$_2$NHC(O)NH × 2, 4H); 2.99 (s, Pbf C*H*$_2$ × 2, 4H); 2.77 (dd, Asp C*H*^{A} × 2, *J* = 17.0 Hz and 6.5 Hz, 2H); 2.68 (dd, Asp C*H*^{B} × 2, *J* = 16.5 Hz and 6.5 Hz, 2H); 2.57 (s, Pbf C*H*$_3$ × 2, 6H); 2.51 (s, Pbf C*H*$_3$ × 2, 6H); 2.07 (s, Pbf C*H*$_3$ × 2, 6H); 1.85-1.72 (m, Arg CHC*H*^{A} × 2, 2H); 1.70-1.52 (m, Arg CHC*H*^{B} × 2, Arg CH$_2$C*H*$_2$CH$_2$ × 2, 6H); 1.44 (s, [(Pbf C*H*$_3$ × 2)] × 2, 12H); 1.44, 1.43 (s, [(^{t}Bu C*H*$_3$ × 6)] × 2, 36H); 1.35-1.28 (br m, C12 C*H*$_2$'s, calc 20H, found 15H). ^{13}C NMR (CD_3OD, 100 MHz) δ 175.96, 171.31, 171.20, 171.08, 160.47, 159.82, 158.06 (*C*(O)O^{t}Bu × 2, *C*(O)NH amide × 2, *C*(O)NH urea, Pbf Ar*C*O, *C*=N guanidine); 139.36, 134.29, 133.48, 125.97, 118.38 (Pbf aromatic *C* × 5); 87.64 (Pbf CH$_2$*C*(CH$_3$)$_2$O); 83.20, 82.36 (*C*(CH$_3$)$_3$ × 2); 55.28 (Arg α-*C*H); 51.01 (Asp α-*C*H); 43.98, 43.31 (Pbf Ar*C*H$_2$, Gly *C*H$_2$); 41.44, 41.06 (Arg *C*H$_2$NH, *C*H$_2$NHC(O)NH); 38.25 (Asp *C*H$_2$); 31.26, 30.69, 30.56, 30.48 (C12 *C*H$_2$'s, Arg CH*C*H$_2$ or *C*H$_2$CH$_2$NH, multiple overlapping peaks); 28.79 (Pbf CH$_2$C(*C*H$_3$)$_2$O); 28.41, 28.25 (C(*C*H$_3$)$_3$ × 2); 27.99, 26.78 (C12 *C*H$_2$, Arg CH*C*H$_2$ or *C*H$_2$CH$_2$NH); 19.69, 18.48, 12.63 (Pbf Ar*C*H$_3$ × 3). $\tilde{\nu}_{max}$ (cm^{-1}) (solid): 3348*w* (N-H stretch); 2978*m*, 2940*m*, 2870*w* (C-H alkyl stretches); 1728*m* (C=O ester stretch); 1651*s* (C=O amide/urea stretch); 1551*s* (N-H bend and C=C arene stretch); 1450*m*, 1366*m* (C-H alkyl bends and S=O stretch); 1250*s*, 1150*s*, 1088*s* (C-O ester and C-N stretches). ESI-MS (*m*/*z*): Calc. for $C_{80}H_{134}N_{14}O_{20}S_2$ 837.4665; found: 837.4638 (100%, $[M+2H]^{2+}$); 848.4538 (28%, $[M+H+Na]^{2+}$); 859.4444 (18%, $[M+2Na]^{2+}$).

Synthesis of C12-[urea-Arg-Gly-Asp]$_2$ (4.4)

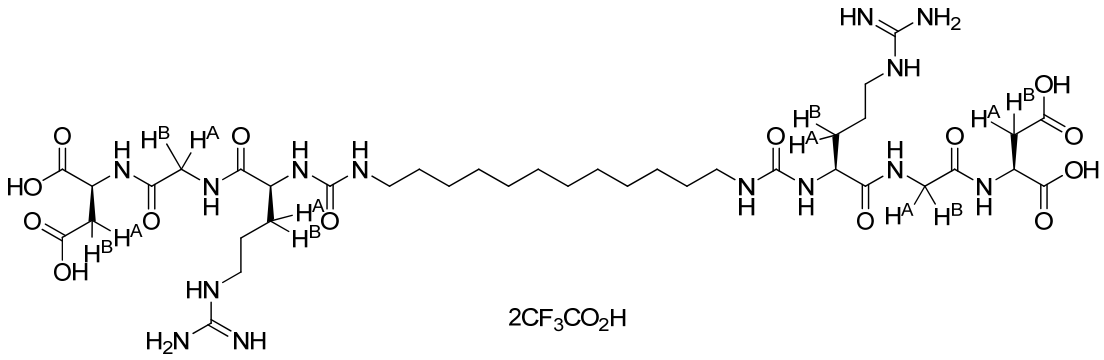

Compound **4.3** (400 mg, 0.24 mmol) was dissolved in a mixture of TFA, water and triisopropylsilane (TIS) (7.5 ml, 95:2.5:2.5) and shaken for 2 h 10 min, after which time TLC indicated that the deprotection reaction was complete. The volatiles were removed *in vacuo,* then the residue was dissolved in the minimum amount of hot MeOH, precipitated with cold Et_2O, filtered and washed

with the minimum amount of cold Et_2O to yield **4.4** as a white solid (280 mg, quantitative yield as TFA salt). The sample was then dissolved in a mixture of water/^{t}BuOH, shell frozen and lyophilised to yield the product **4.4** as a fluffy white powder.

N.B. There was evidence of a small amount of methyl esterification of the carboxylic acids as a consequence of the recovery procedure, but this is not believed to affect gelation behaviour.

R_f 0.00 (9:1, DCM/MeOH, cerium stain). $[\alpha]_D$ = +24.1° (c = 0.5, TFA). M.p not acquired. ^{1}H NMR (CD_3OD, 400 MHz) δ 4.77 (t, Asp α-*H*, *J* = 6.5 Hz, 2H); 4.20-4.17 (m, Arg α-*H*, 2H); 3.97 (d, Gly C*H*^{A}, *J* = 17.0 Hz, 2H); 3.87 (d, Gly C*H*^{B}, *J* = 17.0 Hz, 2H); 3.27-3.18 (m, Arg C*H*$_2$NH, 4H); 3.16-3.06 (m, C*H*$_2$NHC(O)NH, 4H); 2.90 (dd, Asp C*H*^{A}, *J* = 17.0 Hz and 5.5 Hz, 2H); 2.83 (dd, Asp C*H*^{B}, *J* = 17.0 Hz and 6.5 Hz, 2H); 1.92-1.80 (br m, Arg CHC*H*^{A}, 2H); 1.76-1.64 (br m, Arg CHC*H*^{B} and Arg C*H*$_2$CH$_2$NH overlapping, 6H); 1.53-1.43 (br m, C12 C*H*$_2$, 4H); 1.40-1.25 (br m, C12 C*H*$_2$'s, 16H). ^{13}C NMR (CD_3OD, 100 MHz) δ 175.92, 174.00, 173.89, 171.47, 160.69, 158.65 (*C*(O)OH × 2, *C*(O)NH amide × 2, *C*(O)NH urea, *C*=N guanidine); 55.09 (Arg α-*C*H); 50.25 (Asp α-*C*H); 43.29 (Gly *C*H$_2$); 42.08 (Arg *C*H$_2$NH); 41.12 (*C*H$_2$NHC(O)NH); 36.85 (Asp *C*H$_2$); 31.26, 30.71, 30.64, 30.45, 27.97, 26.08 (C12 *C*H$_2$'s, Arg CH*C*H$_2$ and *C*H$_2$CH$_2$NH, multiple overlapping peaks). $\tilde{\nu}_{max}$ (cm^{-1}, solid): 3348*w*, 3210*w* (O-H acid and N-H stretches); 2978*m*, 2878*w* (C-H alkyl stretches); 1705*w* (C=O acid stretch); 1651*s* (C=O amide/urea stretch); 1566*s* (N-H bend); 1165*s*, 1042*m* (C-O acid and C-N stretches). ESI-MS (*m*/*z*): Calc. for $C_{38}H_{69}N_{14}O_{14}$ 945.5112; found: 945.5076 (7%, $[M+H]^+$). Calc. for $C_{38}H_{70}N_{14}O_{14}$ 473.2592; found: 473.2538 (100%, $[M+2H]^{2+}$).

Synthesis of C6-urea-Arg(Pbf)-Gly-Asp(O^{t}Bu)-O^{t}Bu (4.5)

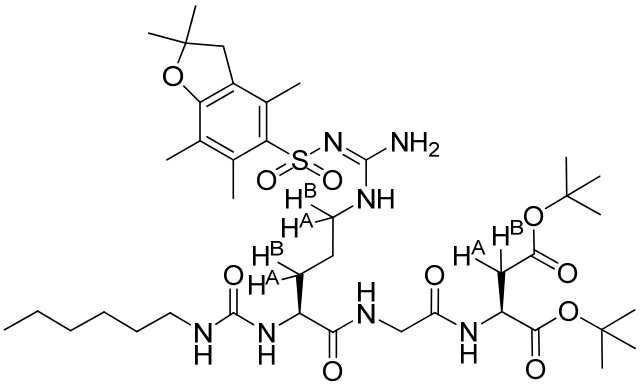

Compound **2.8(2.4)** (0.2 g, 0.28 mmol, 1.0 eq) was dissolved in DCM (2 ml) then hexyl isocyanate (36 mg, 0.28 mmol, 1.0 eq), solubilised in DCM (0.5 ml), was added rapidly to the reaction flask and a further portion of DCM (1.5 ml) was used to wash any residual isocyanate into the reaction flask. The reaction was stirred vigorously for 3 days, then the solvent was removed *in vacuo* to yield a crude clear solid (270 mg). The crude material was purified by column chromatography (SiO_2, 100% DCM, to

98:2 DCM/MeOH, to 95:5 DCM/MeOH, to 9:1 DCM/MeOH) yielding **4.5** as a white solid (210 mg, 89%).

R_f 0.26 (9:1 DCM/MeOH, UV and cerium stain). $[\alpha]_D$ = -12.9° (c = 1.0, $CHCl_3$). M.p not acquired. ^{1}H NMR ($CDCl_3$, 400 MHz) δ 7.76 (br t, N*H* amide (Arg-Gly), 1H); 7.50 (br d, N*H* amide (Gly-Asp), *J* = 7.0 Hz, 1H); 6.39 (br s, N*H* guanidine, N*H*$_2$ guanidine and N*H* urea overlapping, 4H); 5.95 (br s, N*H* urea, 1H); 4.66-4.62 (m, Asp α-*H*, 1H); 4.31-4.19 (br m, Arg α-*H*, 1H); 4.01-3.83 (br m, Gly C*H*$_2$, 2H); 3.42-3.25 (br m, Arg C*H*^{A}NH, 1H); 3.21-2.99 (m, Arg C*H*^{B}NH and C*H*$_2$NHC(O)NH overlapping, 3H); 2.93 (s, Pbf C*H*$_2$, 2H); 2.76 (dd, Asp C*H*^{A}, *J* = 17.0 Hz and 5.5 Hz, 1H); 2.69 (dd, Asp C*H*^{B}, *J* = 17.0 Hz and 5.5 Hz, 1H); 2.54 (s, Pbf C*H*$_3$Ar, 3H); 2.49 (s, Pbf C*H*$_3$Ar, 3H); 2.06 (s, Pbf C*H*$_3$Ar, 3H); 1.83-1.52 (m, Arg CHC*H*$_2$ and Arg C*H*$_2$CH$_2$NH overlapping, 4H); 1.43 (s, Pbf C*H*$_3$ × 2, 6H); 1.38 (s, C(C*H*$_3$)$_3$ × 2, C6 C*H*$_2$ (underlying multiplet), calc 20H, found 19H); 1.27-1.17 (br m, C6 C*H*$_2$'s × 3, 6H); 0.82 (t, C6 C*H*$_3$, *J* = 7.0 Hz, 3H). ^{13}C NMR ($CDCl_3$, 100 MHz) δ 169.99, 169.92, 169.30, 158.90, 158.86, 156.81 (*C*(O)O^{t}Bu × 2, *C*(O)NH amide × 2, *C*(O)NH urea, Pbf Ar*C*O, *C*=N guanidine, calc 7 peaks, found 6 peaks, overlapping?); 138.38, 132.47, 124.68, 117.59 (Pbf aromatic *C* × 5, calc 5 peaks, found 4 peaks, overlapping?); 86.44 (Pbf CH$_2$*C*(CH$_3$)$_2$O); 82.41, 81.47 (*C*(CH$_3$)$_3$ × 2); 54.41 (Arg α-*C*H); 49.49 (Asp α-*C*H); 43.31 (Pbf Ar*C*H$_2$); 42.89 (Gly *C*H$_2$); 40.46 (*C*H$_2$NHC(O)NH, Arg *C*H$_2$NH, calc 2 peaks, found 1 peak, overlapping?); 37.44 (Asp *C*H$_2$); 31.62, 30.17 (C6 *C*H$_2$'s, Arg CH*C*H$_2$ or *C*H$_2$CH$_2$NH, multiple overlapping peaks); 28.66 (Pbf CH$_2$C(*C*H$_3$)$_2$O); 28.08, 27.93 (C(*C*H$_3$)$_3$ × 2); 26.72, 22.64 (C6 CH$_2$, Arg CH*C*H$_2$ or *C*H$_2$CH$_2$NH); 19.41, 18.03 (Pbf Ar*C*H$_3$ × 2); 14.10 (C6 *C*H$_3$); 12.54 (Pbf Ar*C*H$_3$). $\tilde{\nu}_{max}$ (cm^{-1}) (solid): 3341*w* (N-H stretch); 2970*m*, 2870*w* (C-H alkyl stretches); 1728*m* (C=O ester stretch); 1643*m* (C=O amide/urea stretch); 1551*s* (N-H bend and C=C arene stretch); 1450*m*, 1366*m* (C-H alkyl bends and S=O stretch); 1250*s*, 1150*s*, 1096*s* (C-O ester and C-N stretches). ESI-MS (*m*/*z*): Calc. for $C_{40}H_{68}N_7O_{10}S$ 838.4743; found: 838.4734 (100%, $[M+H]^+$). Calc. for $C_{40}H_{67}N_7NaO_{10}S$ 860.4562; found 860.4545 (49%, $[M+Na]^+$).

Synthesis of C6-urea-Arg-Gly-Asp (4.6)

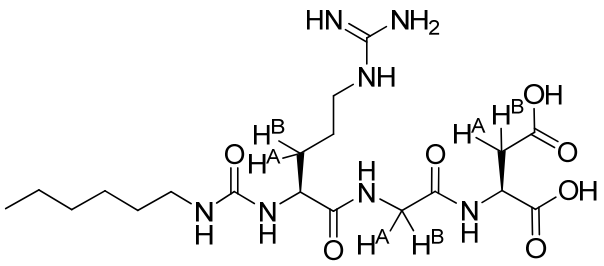

Compound **4.5** (180 mg, 0.22 mmol) was dissolved in a mixture of TFA, water and triisopropylsilane (TIS) (3 ml, 95:2.5:2.5) and shaken for 1 h 20 min, after which time TLC indicated that the deprotection reaction was complete. The volatiles were removed *in vacuo,* then the residue was

dissolved in the minimum amount of hot MeOH, precipitated with cold Et_2O, filtered and washed with the minimum amount of cold Et_2O to yield **4.6** as a white solid (110 mg, 87% as TFA salt).

N.B. There was evidence of a small amount of methyl esterification of the carboxylic acids as a consequence of the recovery procedure.

R_f 0.00 (9:1, DCM/MeOH, cerium stain). $[\alpha]_D$ = +42.0° (c = 0.1, TFA). M.p not acquired. ^{1}H NMR (CD_3OD, 400 MHz) δ 4.77 (t, Asp α-*H*, *J* = 6.5 Hz, 1H); 4.17-4.13 (m, Arg α-*H*, 1H); 3.96 (d, Gly C*H*^{A}, *J* = 17.0 Hz, 1H); 3.87 (d, Gly C*H*^{B}, *J* = 17.0 Hz, 1H); 3.26-3.17 (m, Arg C*H*$_2$NH, 2H); 3.16-3.06 (m, C*H*$_2$NHC(O)NH, 2H); 2.90 (d, Asp C*H*^{A}, *J* = 17.0 Hz and 5.5 Hz, 1H); 2.83 (d, Asp C*H*^{B}, *J* = 17.0 Hz and 6.5 Hz, 1H); 1.92-1.79 (m, Arg CHC*H*^{A}, 1H); 1.79-1.64 (m, Arg CHC*H*^{B} and Arg C*H*$_2$CH$_2$NH overlapping, 3H); 1.53-1.42 (m, C6 C*H*$_2$, 2H); 1.38-1.25 (m, C6 C*H*$_2$'s, 6H); 0.91 (t, C6 C*H*$_3$, *J* = 7.0 Hz, 3H). ^{13}C NMR (CD_3OD, 100 MHz) δ 176.18, 174.03, 173.90, 171.58, 160.80, 158.64 (*C*(O)OH × 2, *C*(O)NH amide × 2, *C*(O)NH urea, *C*=N guanidine); 55.35 (Arg α-*C*H); 50.26 (Asp α-*C*H); 43.35 (Gly *C*H$_2$); 42.05 (Arg *C*H$_2$NH); 41.16 (*C*H$_2$NHC(O)NH); 36.83 (Asp *C*H$_2$); 32.83, 31.31, 30.56, 27.76, 26.10, 23.76 (C6 *C*H$_2$'s × 4, Arg CH*C*H$_2$ and *C*H$_2$CH$_2$NH); 14.48 (C6 *C*H$_3$). $\tilde{\nu}_{max}$ (cm^{-1}, solid): 3341*w*, 3202*w* (O-H acid and N-H stretches); 2956*w*, 2870*w* (C-H alkyl stretches); 1705*w* (C=O acid stretch); 1651*s* (C=O amide/urea stretch); 1574*s* (N-H bend); 1157*s*, 1026*m* (C-O acid and C-N stretches). ESI-MS (*m*/*z*): Calc. for $C_{19}H_{36}N_7O_7$ 474.2671; found: 474.2681 (100%, $[M+H]^+$).

Synthesis of C6-[urea-Arg(Pbf)-Gly-Asp(O^{t}Bu)-O^{t}Bu]$_2$ (4.7)

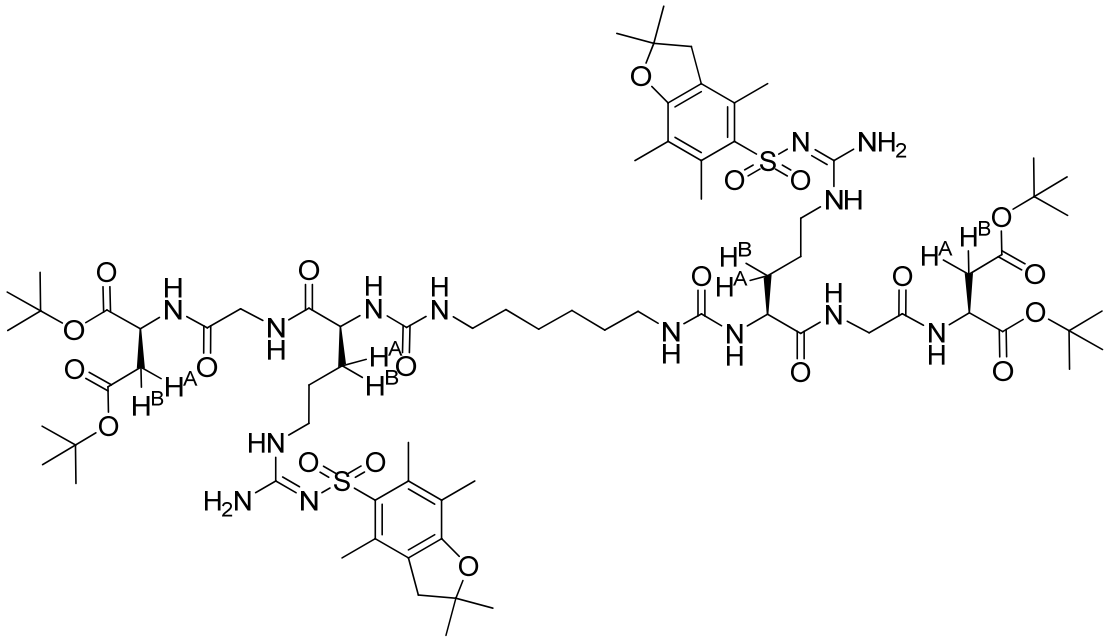

Compound **2.8(2.4)** (0.25 g, 0.35 mmol, 2.0 eq) was dissolved in DCM (2 ml) then 1,6-diisocyanatohexane (30 mg, 0.18 mmol, 1.0 eq), solubilised in DCM (0.5 ml), was added rapidly to the

reaction flask and a further portion of DCM (1.5 ml) was used to wash any residual diisocyanate into the reaction flask. A viscous solution formed upon addition of the diisocyanate, therefore more DCM (~5 ml) was added to try to improve stirring. The reaction was stirred vigorously for 17 h at rt, then the solvent was removed *in vacuo* to yield a crude white solid (280 mg). The crude material was purified by column chromatography (SiO_2, 9:1 DCM/MeOH) yielding **4.7** as a white solid (260 mg, 92%).

R_f 0.17 (9:1 DCM/MeOH, UV and cerium stain). $[\alpha]_D$ = +1.0° (c = 0.1, MeOH). ^{1}H NMR (CD_3OD, 400 MHz) δ 4.64 (t, Asp α-*H* × 2, *J* = 6.0 Hz, 2H); 4.16 (br m, Arg α-*H* × 2, 2H); 3.94-3.85 (br m, Gly C*H*$_2$ × 2, 4H); 3.25-3.16 (br m, Arg C*H*$_2$NH × 2, 4H); 3.14-3.05 (m, C*H*$_2$NHC(O)NH × 2, 4H); 2.98 (s, Pbf C*H*$_2$ × 2, 4H); 2.77 (dd, Asp C*H*^{A} × 2, *J* = 16.5 Hz and 6.0 Hz, 2H); 2.68 (dd, Asp C*H*^{B} × 2, *J* = 17.0 Hz and 6.5 Hz, 2H); 2.57 (s, Pbf C*H*$_3$ × 2, 6H); 2.51 (s, Pbf C*H*$_3$ × 2, 6H); 2.07 (s, Pbf C*H*$_3$ × 2, 6H); 1.86-1.72 (m, Arg CHC*H*^{A} × 2, 2H); 1.69-1.53 (m, Arg CHC*H*^{B} × 2, Arg CH$_2$C*H*$_2$CH$_2$ × 2, 6H); 1.53-1.38 (m, [(Pbf C*H*$_3$ × 2)] × 2, [(^{t}Bu C*H*$_3$ × 6)] × 2, C6 C*H*$_2$'s × 2, calc 52H, found 47H); 1.38-1.29 (m, C6 C*H*$_2$'s × 2, 4H). ^{13}C NMR (CD_3OD, 100 MHz) δ 175.97, 171.28, 171.24, 171.11, 160.48, 159.84, 158.06 (*C*(O)O^{t}Bu × 2, *C*(O)NH amide × 2, *C*(O)NH urea, Pbf Ar*C*O, *C*=N guanidine); 139.39, 134.30, 133.50, 126.00, 118.42 (Pbf aromatic *C* × 5); 87.67 (Pbf CH$_2$*C*(CH$_3$)$_2$O); 83.25, 82.42 (*C*(CH$_3$)$_3$ × 2); 55.26 (Arg α-*C*H); 51.01 (Asp α-*C*H); 44.00, 43.33 (Pbf Ar*C*H$_2$, Gly *C*H$_2$); 41.50, 40.86 (Arg *C*H$_2$NH, *C*H$_2$NHC(O)NH); 38.28 (Asp *C*H$_2$); 31.14, 30.66 (C6 *C*H$_2$, Arg CH*C*H$_2$ or *C*H$_2$CH$_2$NH); 28.83 (Pbf CH$_2$C(*C*H$_3$)$_2$O); 28.44, 28.28 (C(*C*H$_3$)$_3$ × 2); 27.55, 26.83 (C6 *C*H$_2$, Arg CH*C*H$_2$ or *C*H$_2$CH$_2$NH); 19.74, 18.53, 12.67 (Pbf Ar*C*H$_3$ × 3). $\tilde{\nu}_{max}$ (cm^{-1}) (solid): 3341*w* (N-H stretch); 2978*m*, 2878*w* (C-H alkyl stretches); 1728*m* (C=O ester stretch); 1651*m* (C=O amide/urea stretch); 1551*s* (N-H bend and C=C arene stretch); 1450*m*, 1366*s* (C-H alkyl bends and S=O stretch); 1250*s*, 1150*s*, 1088*s* (C-O ester and C-N stretches). ESI-MS (*m*/*z*): Calc. for $C_{74}H_{121}N_{14}O_{20}S_2$ 1589.8318; found: 1589.8104 (12%, $[M+H]^+$). Calc. for $C_{74}H_{122}N_{14}O_{20}S_2$ 795.4195; found: 795.4137 (100%, $[M+2H]^{2+}$).

Synthesis of C6-[urea-Arg-Gly-Asp]$_2$ (4.8)

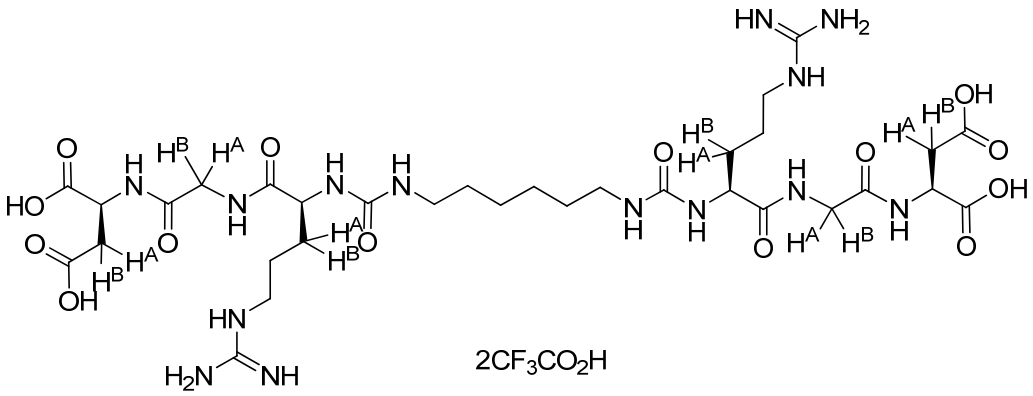

Compound **4.7** (230 mg, 0.14 mmol) was dissolved in a mixture of TFA, water and triisopropylsilane (TIS) (3 ml, 95:2.5:2.5) and shaken for 1 h 20 min, after which time TLC indicated that the deprotection reaction was complete. The volatiles were removed *in vacuo,* then the residue was dissolved in the minimum amount of hot MeOH, precipitated with cold Et_2O, filtered and washed with the minimum amount of cold Et_2O to yield **4.8** as a white solid (160 mg, quantitative yield as TFA salt).

N.B. There was evidence of a small amount of methyl esterification of the carboxylic acids as a consequence of the recovery procedure.

R_f 0.00 (9:1, DCM/MeOH, cerium stain). $[\alpha]_D$ = +51.0° (c = 1.0, TFA). M.p not acquired. ^{1}H NMR (CD_3OD, 400 MHz) δ 4.76 (t, Asp α-*H*, *J* = 6.5 Hz, 2H); 4.19-4.11 (m, Arg α-*H*, 2H); 3.96 (d, Gly C*H*^{A}, *J* = 17.0 Hz, 2H); 3.90 (d, Gly C*H*^{B}, *J* = 17.0 Hz, 2H); 3.27-3.18 (m, Arg C*H*$_2$NH, 4H); 3.18-3.04 (m, C*H*$_2$NHC(O)NH, 4H); 2.92 (dd, Asp C*H*^{A} × 2, *J* = 17.0 Hz and 5.5 Hz, 2H); 2.86 (dd, Asp C*H*^{B} × 2, *J* = 17.0 Hz and 6.5 Hz, 2H); 1.92-1.79 (br m, Arg CHC*H*^{A}, 2H); 1.79-1.64 (br m, Arg CHC*H*^{B} and Arg C*H*$_2$CH$_2$NH overlapping, 6H); 1.53-1.42 (br m, C6 C*H*$_2$, 4H); 1.40-1.27 (br m, C6 C*H*$_2$'s, 4H). ^{13}C NMR (CD_3OD, 100 MHz) δ 176.45, 174.38, 174.16, 171.65, 160.81, 158.35 (*C*(O)OH × 2, *C*(O)NH amide × 2, *C*(O)NH urea, *C*=N guanidine); 55.35 (Arg α-*C*H); 50.15 (Asp α-*C*H); 43.34 (Gly *C*H$_2$); 41.93 (Arg *C*H$_2$NH); 40.77 (*C*H$_2$NHC(O)NH); 36.76 (Asp *C*H$_2$); 30.81, 30.20, 27.24, 26.04 (C6 *C*H$_2$'s, Arg CH*C*H$_2$ and *C*H$_2$CH$_2$NH, multiple overlapping peaks). $\tilde{\nu}_{max}$ (cm^{-1}, solid): 3341*w*, 3186*w* (O-H acid and N-H stretches); 2978*m*, 2870*w* (C-H alkyl stretches); 1643*s*, 1612*s* (C=O amide/urea stretch); 1558*s* (N-H bend); 1389*w* (C-H alkyl bends); 1165*s*, 1034*s* (C-O acid and C-N stretches). ESI-MS (*m*/*z*): Calc. for $C_{32}H_{57}N_{14}O_{14}$ 861.4173; found: 861.4134 (9%, $[M+H]^+$); 431.2016 (100%, $[M+2H]^{2+}$).

Synthesis of CH$_2$-[Ar-urea-Arg(Pbf)-Gly-Asp(O^{t}Bu)-O^{t}Bu]$_2$ (4.9)

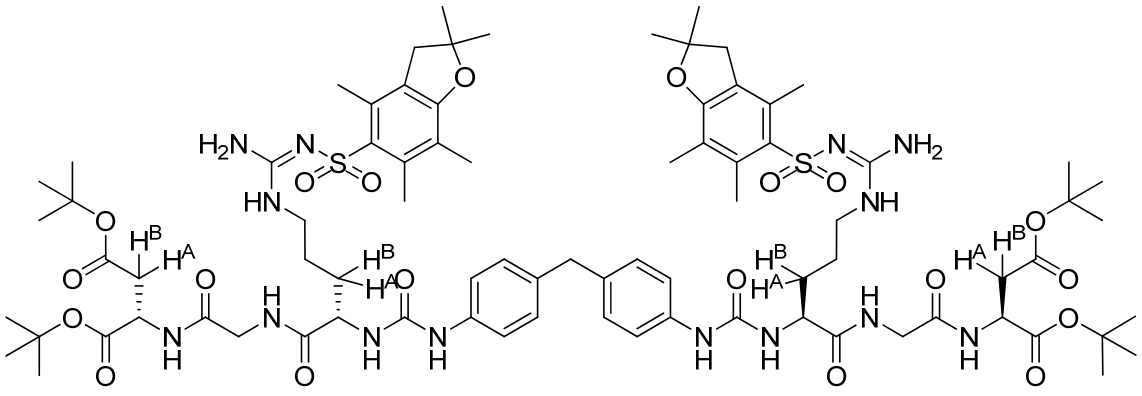

Compound **2.8(2.4)** (0.2 g, 0.28 mmol, 2.4 eq) was dissolved in DCM (2 ml) then 4,4'-methylenbis(phenyl isocyanate) (29 mg, 0.12 mmol, 1.0 eq), solubilised in DCM (0.5 ml), was added

dropwise over ~1 min and a further portion of DCM (3 × 0.5 ml) was used to wash any residual diisocyanate into the reaction flask. The reaction became viscous/ 'jelly-like' and white in appearance a few minutes after the addition of the diisocyanate, therefore more DCM (4 ml) was added to the reaction flask to try to improve stirring. The reaction was stirred vigorously for 3 days at rt, then the solvent was removed *in vacuo* to yield a crude white solid (220 mg). The crude material was purified by column chromatography (SiO_2, 95:5 DCM/MeOH, to 9:1 DCM/MeOH) yielding **4.9** as a white solid (180 mg, 93%).

R_f 0.31 (9:1 DCM/MeOH, UV and cerium stain). $[\alpha]_D$ = -10.1° (c = 0.5, MeOH). M.p not acquired. ^{1}H NMR (CD_3OD, 400 MHz) δ 7.25 (d, C*H* aromatic × 4, *J* = 8.0 Hz, 4H); 7.00 (d, C*H* aromatic × 4, *J* = 9.0 Hz, 4H); 4.63 (t, Asp α-*H* × 2, *J* = 6.0 Hz, 2H); 4.27-4.19 (br m, Arg α-*H* × 2, 2H); 3.95-3.86 (br m, Gly C*H*$_2$ × 2, 4H); 3.81-3.69 (app br s, ArC*H*$_2$Ar, 2H); 3.25-3.07 (br m, Arg C*H*$_2$NH × 2, 4H); 2.91 (s, Pbf C*H*$_2$ × 2, 4H); 2.72 (dd, Asp C*H*^{A} × 2, *J* = 16.5 Hz and 6.0 Hz, 2H); 2.61 (dd, Asp C*H*^{B} × 2, *J* = 16.5 Hz and 6.0 Hz, 2H); 2.55 (s, Pbf C*H*$_3$ × 2, 6H); 2.49 (s, Pbf C*H*$_3$ × 2, 6H); 2.02 (s, Pbf C*H*$_3$ × 2, 6H); 1.88-1.74 (m, Arg CHC*H*^{A} × 2, 2H); 1.74-1.51 (m, Arg CHC*H*^{B} × 2, Arg $CH_2CH_2CH_2$ × 2, 6H); 1.40, 1.38 (s × 2, [(Pbf C*H*$_3$ × 2)] × 2, [(^{t}Bu C*H*$_3$ × 6)] × 2, calc 48H, found 47H). ^{13}C NMR (CD_3OD, 100 MHz) δ 175.68, 171.33, 171.25, 171.09, 159.87, 158.09, 157.67 (*C*(O)O^{t}Bu × 2, *C*(O)NH amide × 2, *C*(O)NH urea, Pbf Ar*C*O, *C*=N guanidine); 139.41, 138.59, 137.05, 134.24, 133.55 (Pbf aromatic *C* × 3, Ar aromatic *C* × 2); 130.24 (Ar aromatic *C*H); 126.06 (Pbf aromatic *C*); 120.39 (Ar aromatic *C*H); 118.45 (Pbf aromatic *C*); 87.68 (Pbf $CH_2C(CH_3)_2O$); 83.28, 82.40 ($C(CH_3)_3$ × 2); 55.21 (Arg α-*C*H); 51.06 (Asp α-*C*H); 43.98, 43.42 (Pbf Ar*C*H$_2$, Gly *C*H$_2$); 41.56, 41.50 (Arg *C*H$_2$NH, Ar*C*H$_2$Ar); 38.30 (Asp *C*H$_2$); 30.58 (Arg CH*C*H$_2$); 28.84 (Pbf $CH_2C(CH_3)_2O$); 28.47, 28.30 ($C(CH_3)_3$ × 2); 26.87 (Arg *C*H$_2$CH$_2$NH); 19.80, 18.56, 12.71 (Pbf Ar*C*H$_3$ × 3). $\tilde{\nu}_{max}$ (cm^{-1}) (solid): 3341*w* (N-H amide stretch); 2978*m*, 2878*w* (C-H alkyl and arene stretches); 1728*m* (C=O ester stretch); 1682*m* (C=O amide/urea stretches); 1543*s*, 1512*s* (N-H bend and C=C arene stretch); 1450*m*, 1366*m* (C-H alkyl bend and S=O stretch); 1242*s*, 1150*s*, 1088*s* (C-O ester and C-N stretches, C-H arene bends); 995*w*, 810*m*, 779*m* (C-H arene bends). ESI-MS (*m*/*z*): Calc. for $C_{81}H_{120}N_{14}O_{20}S_2$ 836.4117; found: 836.4090 (100%, $[M+2H]^{2+}$); 847.3985 (24%, $[M+H+Na]^{2+}$); 858.3903 (14%, $[M+2Na]^{2+}$).

Synthesis of CH_2-[Ar-urea-Arg-Gly-Asp]$_2$ (4.10)

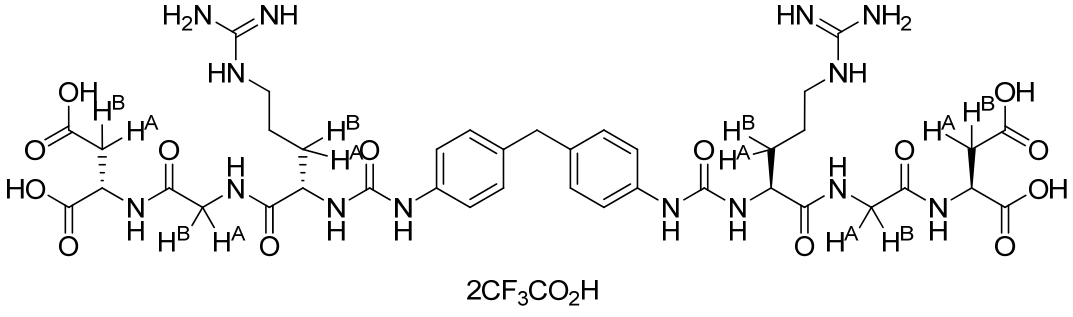

Compound **4.9** (165 mg, 99 μmol) was dissolved in a mixture of TFA, water and triisopropylsilane (TIS) (5 ml, 95:2.5:2.5) and shaken for 45 min, after which time TLC indicated that the deprotection reaction was complete. The volatiles were removed *in vacuo,* then the residue was suspended in the minimum amount of hot MeOH, precipitated with cold Et_2O, filtered and washed with the minimum amount of cold Et_2O to yield **4.10** as a white solid (110 mg, 95% as TFA salt).

N.B. There was evidence of a small amount of methyl esterification of the carboxylic acids as a consequence of the recovery procedure.

R_f 0.00 (9:1, DCM/MeOH, cerium stain). $[\alpha]_D$ = +36.3° (c = 1.0, TFA). M.p not acquired. ^{1}H NMR (CD_3OD/D_2O, 400 MHz) δ 7.25 (d, C*H* aromatic × 4, *J* = 8.5 Hz, 4H); 7.08 (d, C*H* aromatic × 4, *J* = 9.0 Hz, 4H); 4.75 (t, Asp α-*H* × 2, *J* = 6.0 Hz, 2H); 4.24-4.21 (m, Arg α-*H* × 2, 2H); 3.97 (d, Gly CH^A × 2, *J* = 17.0 Hz, 2H); 3.92 (d, Gly CH^B × 2, *J* = 17.0 Hz, 2H); 3.82 (app br s, ArCH_2Ar, 2H); 3.21 (t, Arg CH_2NH × 2, *J* = 7.0 Hz, 4H); 2.85 (dd, Asp CH^A × 2, *J* = 17.0 Hz and 5.5 Hz, 2H); 2.78 (dd, Asp CH^B × 2, *J* = 17.0 Hz and 5.5 Hz, 2H); 1.94-1.82 (m, Arg CHCH^A × 2, 2H); 1.82-1.63 (m, Arg CHCH^B × 2, Arg $CH_2CH_2CH_2$ × 2, 6H). ^{13}C NMR (CD_3OD, 100 MHz) δ 176.07, 174.59, 174.28, 171.64, 158.19, 158.14 (*C*(O)OH × 2, *C*(O)NH amide × 2, *C*(O)NH urea, *C*=N guanidine); 137.85, 137.70 (Ar aromatic *C* × 2); 130.18, 121.03 (Ar aromatic *C*H × 2); 55.11 (Arg α-*C*H); 50.08 (Asp α-*C*H); 43.31 (Gly *C*H_2); 41.85 (Ar*C*H_2Ar); 41.27 (Arg *C*H_2NH); 36.74 (Asp *C*H_2); 30.07 (Arg CH*C*H_2); 25.84 (Arg *C*H_2CH_2NH). $\tilde{\nu}_{max}$ (cm^{-1}, solid): 3341*w*, 3194*w* (O-H acid and N-H stretches); 2978*m*, 2878*w* (C-H alkyl and arene stretches); 1721*w* (C=O acid stretch); 1651*s*, 1605*m* (C=O amide/urea stretch); 1535*s*, 1512*s* (N-H bend and C=C arene stretch); 1404*m*, 1312*m* (C-H alkyl bends); 1157*s*, 1042*s* (C-O acid and C-N stretches); 964*m*, 864*m*, 833*m*, 772*m* (C-H arene bends). ESI-MS (*m*/*z*): Calc. for $C_{39}H_{55}N_{14}O_{14}$ 943.4017; found: 943.3989 (100%, $[M+H]^+$).

Synthesis of Z-Asp(O^{t}Bu)-C12 (4.11)

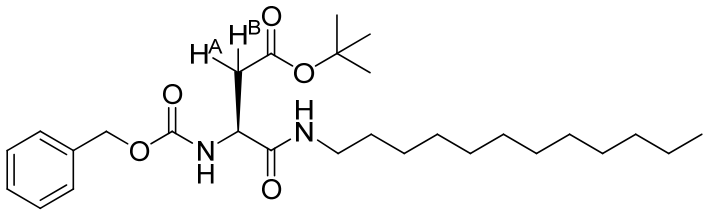

Z-Asp(O^{t}Bu)-OH (1.00 g, 3.09 mmol, 1.0 eq) was dissolved in DCM (25 ml) then DIPEA (1.1 ml, 6.31 mmol, 2.0 eq) was added. The reaction flask was cooled over an ice-water bath then TBTU (1.00 g, 3.1 mmol, 1.0 eq) was added as a solid and the reaction was stirred at 0°C for 10 min before dodecylamine (0.57 g, 3.09 mmol, 1.0 eq) was added as a solid and more DCM was used to rinse any residual dodecylamine into the reaction flask. The reaction was stirred at 0°C for a further 30 min before removing the ice-water bath and stirring the reaction at rt for 22 h. The organic phase was

washed successively with 1.33 M $NaHSO_4$ (3 × 50 ml), 1 M Na_2CO_3 (3 × 50 ml), and finally brine (50 ml). The organic phase was dried over $MgSO_4$ and filtered before removing the solvent *in vacuo* to yield a crude orange oil (1.6 g). Purification by column chromatography (SiO_2, 98:2 DCM/MeOH, to 95:5 DCM/MeOH) yielded **4.11** as an off-white waxy solid (1.03 g, 68%).

R_f 0.59 (95:5, DCM/MeOH, UV and cerium stain). $[\alpha]_D$ = +16.5° (c = 1.0, $CHCl_3$). M.p not acquired. ^{1}H NMR ($CDCl_3$, 400 MHz) δ 7.34-7.27 (m, C*H* aromatic, 5H); 6.54 (app br t, N*H* amide, 1H); 6.05 (d, N*H* carbamate, *J* = 8.0 Hz, 1H); 5.10 (s, CH_2 benzylic, 2H); 4.50-4.45 (br m, Asp α-*H*, 1H); 3.19 (q, C(O)NHCH_2, *J* = 6.5 Hz, 2H); 2.87 (dd, Asp CH^A, *J* = 17.0 Hz and 4.5 Hz, 1H); 2.59 (dd, Asp CH^B, *J* = 17.0 Hz and 6.5 Hz, 1H); 1.49-1.36 (s (+ underlying m), C(CH_3)$_3$ (+ C12 CH_2), 11H); 1.31-1.19 (m, C12 CH_2 × 9, 18H); 0.86 (t, C12 CH_3, *J* = 7.0 Hz, 3H). ^{13}C NMR ($CDCl_3$, 100 MHz) δ 171.25, 170.29, 156.09 (*C*(O)O^{t}Bu, *C*(O)NH amide, *C*(O)NH carbamate); 136.17 (*C* aromatic); 128.60, 128.30, 128.16 (*C*H aromatic); 81.73 (*C*(CH$_3$)$_3$); 67.17 (*C*H$_2$ benzylic); 51.18 (Asp α-*C*H); 39.70 (C(O)NH*C*H$_2$); 37.59 (Asp *C*H$_2$); 31.96, 29.70, 29.67, 29.65, 29.57, 29.47, 29.40, 29.32 (C12 *C*H$_2$'s); 28.05 (C(*C*H$_3$)$_3$); 26.85, 22.73 (C12 *C*H$_2$'s); 14.18 (C12 *C*H$_3$). $\tilde{\nu}_{max}$ (cm^{-1}) (solid): 3302*m* (N-H amide stretch); 2978*m*, 2916*m*, 2855*m* (C-H alkyl and arene stretches); 1728*m* (C=O ester stretch); 1690*m*, 1651*s* (C=O amide stretch); 1535*s* (N-H amide bend and C=C arene stretch); 1458*w*, 1366*m* (C-H alkyl bends); 1288*m*, 1258*s*, 1157*s*, 1049*m*, 1003*w* (C-O ester and C-N amide stretches, C-H arene bends); 949*w*, 903*w*, 849*w*, 694*s* (C-H arene bends). ESI-MS (*m*/*z*): Calc. for $C_{28}H_{47}N_2O_5$ 491.3479; found: 491.3462 (100%, $[M+H]^+$). Calc. for $C_{28}H_{46}N_2NaO_5$ 513.3299; found: 513.3279 (68%, $[M+Na]^+$).

Synthesis of H_2N-Asp(O^{t}Bu)-C12 (4.12)

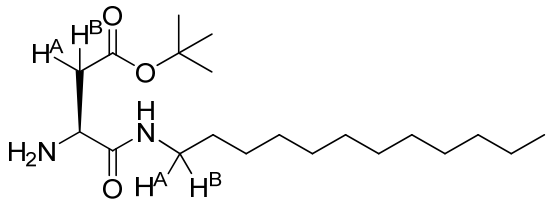

Compound **4.11** (1.00 g, 2.04 mmol) was dissolved in EtOH (20 ml) followed by the addition of Pd/C catalyst (0.20 g, 20%). The flask was subjected to several vacuum/H_2 purges and then stirred for 25 h under an atmosphere of H_2. The catalyst was filtered off over Celite, washed with MeOH, and the filtrate evaporated *in vacuo* to yield **4.12** as a white waxy solid (0.66 g, 90%). No further purification was required.

R_f 0.20 (95:5, DCM/MeOH, cerium stain). $[\alpha]_D$ = -12.5° (c = 0.5, $CHCl_3$). M.p not acquired. ^{1}H NMR ($CDCl_3$, 400 MHz) δ 7.37 (t, N*H* amide, *J* = 4.5 Hz, 1H); 3.63 (dd, Asp α-*H*, *J* = 8.5 Hz and 3.5 Hz, 1H); 3.22 (dd, C(O)NHCH^A, *J* = 7.0 Hz and 3.0 Hz, 1H); 3.19 (dd, C(O)NHCH^B, *J* = 7.0 Hz and 3.0 Hz, 1H); 2.83 (dd, Asp CH^A, *J* = 17.0 Hz and 4.0 Hz, 1H); 2.48 (dd, Asp CH^B, *J* = 17.0 Hz and 8.5

Hz, 1H); 1.93 (br s, N*H*$_2$, 2H); 1.51-1.40 (s (+ underlying m), C(C*H*$_3$)$_3$ (+ C12 C*H*$_2$), 11H); 1.27-1.17 (m, C12 C*H*$_2$ × 9, 18H); 0.85 (t, C12 C*H*$_3$, *J* = 7.0 Hz, 3H). ^{13}C NMR ($CDCl_3$, 100 MHz) δ 173.18, 171.34 (*C*(O)O^{t}Bu, *C*(O)NH amide); 81.08 (*C*(CH$_3$)$_3$); 52.05 (Asp α-*C*H); 40.58 (Asp *C*H$_2$); 39.26 (C(O)NH*C*H$_2$); 31.92, 29.66, 29.63, 29.59, 29.55, 29.35, 29.32 (C12 *C*H$_2$'s); 28.09 (C(*C*H$_3$)$_3$); 26.94, 22.69 (C12 *C*H$_2$'s); 14.13 (C12 *C*H$_3$). $\tilde{\nu}_{max}$ (cm^{-1}) (solid): 3649*m* (N-H stretch); 2978*m*, 2924*m*, 2855*m* (C-H alkyl stretches); 1728*m* (C=O ester stretch); 1659*w* (C=O amide stretch); 1566*w* (N-H amide bend); 1458*w*, 1366*m* (C-H alkyl bends); 1258*w*, 1150*s* (C-O ester and C-N stretches). ESI-MS (*m*/*z*): Calc. for $C_{20}H_{41}N_2O_3$ 357.3112; found: 357.3114 (100%, $[M+H]^+$).

Synthesis of Z-Gly-Asp(O^{t}Bu)-C12 (4.13)

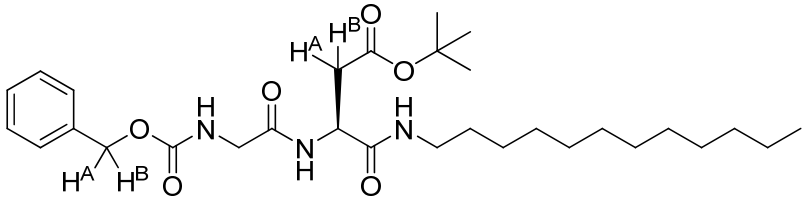

Z-Gly-OH (0.38 g, 1.8 mmol, 1.0 eq) was dissolved in DCM (8 ml) upon the addition of DIPEA (0.63 ml, 3.6 mmol, 2.0 eq). The reaction flask was cooled over an ice-water bath, TBTU (0.58 g, 1.8 mmol, 1.0 eq) was added as a solid and the reaction stirred for 15 min, then compound **4.12** (0.64 g, 1.8 mmol, 1.0 eq) dissolved in DCM (5 ml) was added rapidly to the reaction flask then more DCM (5 ml) was used to rinse any residual **4.12** into the reaction flask. The reaction was stirred at 0°C for a further 30 min before removing the ice-water bath and stirring the reaction at rt for 2 days. The organic phase was washed successively with 1.33 M $NaHSO_4$ (3 × 50 ml), 1 M Na_2CO_3 (3 × 50 ml), water (50 ml) and finally brine (50 ml). The organic phase was dried over $MgSO_4$ and filtered before removing the solvent *in vacuo* to produce the product, **4.13**, as a pale yellow oil (1.05 g, quantitative yield). No further purification was carried out.

R_f 0.53 (95:5, DCM/MeOH, cerium stain). $[\alpha]_D$ = +1.1° (c = 1.0, $CHCl_3$). ^{1}H NMR ($CDCl_3$, 400 MHz) δ 7.55 (d, N*H* amide (Gly-Asp), *J* = 9.0 Hz, 1H); 7.34-7.28 (m, C*H* aromatic, 5H); 6.94 (br t, N*H* amide (Asp-C12), *J* = 5.5 Hz, 1H); 6.12 (br t, N*H* carbamate, *J* = 5.0 Hz, 1H); 5.13 (d, C*H*^{A} benzylic, *J* = 12.0 Hz, 1H); 5.09 (d, C*H*^{B} benzylic, *J* = 12.0 Hz, 1H); 4.79-4.74 (m, Asp α-*H*, 1H); 3.93-3.77 (br m, Gly C*H*$_2$, 2H); 3.26-3.08 (m, C(O)NHC*H*$_2$, 2H); 2.88 (dd, Asp C*H*^{A}, *J* = 17.0 Hz and 5.0 Hz, 1H); 2.59 (dd, Asp C*H*^{B}, *J* = 17.0 Hz and 6.0 Hz, 1H); 1.52-1.39 (s (+ underlying m), C(C*H*$_3$)$_3$ (+ C12 C*H*$_2$), 11H); 1.35-1.17 (m, C12 C*H*$_2$ × 9, 18H); 0.87 (t, C12 C*H*$_3$, *J* = 7.0 Hz, 3H). ^{13}C NMR ($CDCl_3$, 100 MHz) δ 171.12, 170.00, 169.18, 156.99 (*C*(O)O^{t}Bu, *C*(O)NH amide × 2, *C*(O)NH carbamate); 136.13 (*C* aromatic); 128.52, 128.19, 127.99 (*C*H aromatic); 81.65 (*C*(CH$_3$)$_3$); 67.13 (*C*H$_2$ benzylic); 49.31 (Asp α-*C*H); 44.77 (Gly *C*H$_2$); 39.79 (C(O)NH*C*H$_2$); 37.08 (Asp *C*H$_2$); 31.90, 29.63, 29.55, 29.34 (C12 *C*H$_2$'s); 27.98 (C(*C*H$_3$)$_3$); 26.87, 22.68 (C12 *C*H$_2$'s); 14.13 (C12 *C*H$_3$). $\tilde{\nu}_{max}$ (cm^{-1})

(oil): 3279*m* (N-H stretch); 2978*m*, 2924*m*, 2855*m* (C-H alkyl and arene stretches); 1728*m* (C=O ester stretch); 1690*m*, 1643*s* (C=O amide/carbamate stretch); 1551*s*, 1512*m* (N-H bend and C=C arene stretch); 1458*w*, 1366*m* (C-H alkyl bends); 1250*s*, 1219*s*, 1150*s*, 1049*w* (C-O ester and C-N stretches, C-H arene bends); 980*m*, 849*w*, 694*s* (C-H arene bends). ESI-MS (*m*/*z*): Calc. for $C_{30}H_{50}N_3O_6$ 548.3694; found: 548.3690 (82%, $[M+H]^+$). Calc. for $C_{30}H_{49}N_3NaO_6$ 570.3514; found: 570.3511 (100%, $[M+Na]^+$).

Synthesis of H_2N-Gly-Asp(O^tBu)-C12 (4.14)

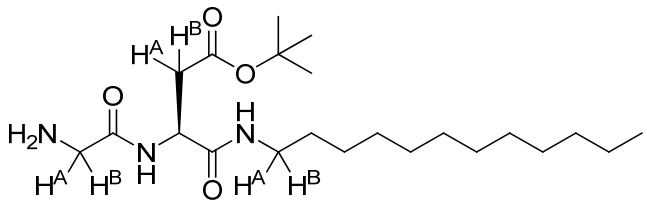

Compound **4.13** (1.00 g, 1.83 mmol) was dissolved in EtOH (25 ml) followed by the addition of Pd/C catalyst (0.20 g, 20%). The flask was subjected to several vacuum/H_2 purges and then stirred for 19 h under an atmosphere of H_2. The catalyst was filtered off over Celite, washed with MeOH, and the filtrate evaporated *in vacuo* to yield **4.14** as a white waxy solid (0.66 g, 87%). No further purification was required.

R_f 0.13 (9:1, DCM/MeOH, cerium stain). $[\alpha]_D$ = -28.0° (c = 0.5, $CHCl_3$). M.p not acquired. ^{1}H NMR ($CDCl_3$, 400 MHz) δ 8.26 (d, N*H* amide (Gly-Asp), *J* = 4.0 Hz, 1H); 7.19 (app br s, N*H* amide (Asp-C12), 1H); 4.77-4.68 (m, Asp α-*H*, 1H); 4.12 (br s, NH_2, 2H); 3.55 (d, Gly CH^A, *J* = 17.0 Hz, 1H); 3.48 (d, Gly CH^B, *J* = 17.0 Hz, 1H); 3.23-3.12 (m, C(O)NHCH^A, 1H); 3.12-3.03 (m, C(O)NHCH^B, 1H); 2.72 (dd, Asp CH^A, *J* = 17.0 Hz and 7.0 Hz, 1H); 2.62 (dd, Asp CH^B, *J* = 17.0 Hz and 7.0 Hz, 1H); 1.46-1.33 (s (+ underlying m), C(CH_3)$_3$ (+ C12 CH_2), 11H); 1.26-1.18 (m, C12 CH_2 × 9, 18H); 0.81 (t, C12 CH_3, *J* = 7.0 Hz, 3H). ^{13}C NMR ($CDCl_3$, 100 MHz) δ 170.75, 170.67, 170.38 (*C*(O)O^{t}Bu, *C*(O)NH amide × 2); 81.52 (*C*(CH$_3$)$_3$); 49.51 (Asp α-*C*H); 43.46 (Gly *C*H$_2$); 39.73 (C(O)NH*C*H$_2$); 37.56 (Asp *C*H$_2$); 31.91, 29.68, 29.64, 29.44, 29.35 (C12 *C*H$_2$'s); 28.02 (C(*C*H$_3$)$_3$); 26.94, 22.67 (C12 *C*H$_2$'s); 14.10 (C12 *C*H$_3$). $\tilde{\nu}_{max}$ (cm^{-1}) (solid): 3294*w* (N-H stretch); 2978*m*, 2924*m*, 2855*m* (C-H alkyl stretches); 1728*m* (C=O ester stretch); 1690*w*, 1643*s* (C=O amide stretches); 1551*m* (N-H amide bend); 1466*w*, 1366*m* (C-H alkyl bends); 1296*w*, 1250*m*, 1150*s* (C-O ester and C-N stretches). ESI-MS (*m*/*z*): Calc. for $C_{22}H_{44}N_3O_4$ 414.3326; found: 414.3324 (100%, $[M+H]^+$).

Synthesis of Z-Arg(Pbf)-Gly-Asp(O^{t}Bu)-C12 (4.15)

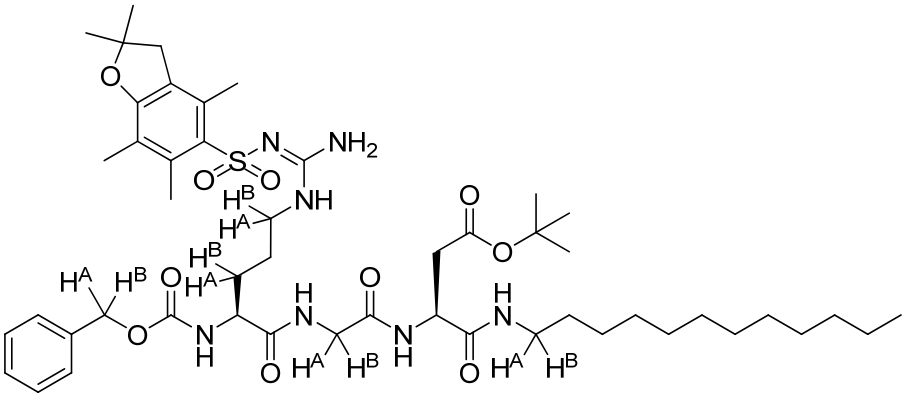

Z-Arg(Pbf)-OH.CHA (5.52 g, 8.37 mmol) was taken up in EtOAc (200 ml) and washed with $NaHSO_4$ (3 × 50 ml). The organic layer was then separated off and evaporated *in vacuo* to yield Z-Arg(Pbf)-OH as a white solid. Z-Arg(Pbf)-OH (0.89 g, 1.6 mmol, 1.0 eq) was dissolved in DCM (5 ml), cooled over an ice-water bath, followed by the addition of DIPEA (0.56 ml, 3.2 mmol, 2.0 eq) and TBTU (513 mg, 1.6 mmol, 1.0 eq). The reaction mixture was stirred at 0°C for 15 min, then **4.14** (0.66 g, 1.6 mmol, 1.0 eq) was dissolved in DCM (7 ml) and added in one portion to the reaction flask, and a further portion of DCM (3 ml) used to rinse any residual **4.14** into the reaction flask. The reaction was stirred at 0°C for a further 30 min before removing the ice-water bath and stirring the reaction at rt for 13 h. The organic phase was washed with 1.33 M $NaHSO_4$ (3 × 50 ml), 1 M Na_2CO_3 (3 × 50 ml), water (50 ml) and finally brine (50 ml). The organic phase was dried over $MgSO_4$ and filtered before removing the solvent *in vacuo* to produce the crude product as a white solid (1.32 g, 86%). Purification by column chromatography (SiO_2, 100% DCM + 1% TEA, to 98:2 DCM/MeOH, to 95:5 DCM/MeOH) yielded **4.15** as a white solid (1.00 g, 65%). Residual TEA was removed by re-dissolving the product in DCM, then washing with water, 1.33 M $NaHSO_4$ and then brine. The organic phase was dried over $MgSO_4$ and filtered before removing the solvent *in vacuo* to produce the product as a white solid (0.87 g, 57%).

R_f 0.50 (9:1, DCM/MeOH, UV and cerium stain). $[\alpha]_D$ = -12.0° (c = 0.1, $CHCl_3$). M.p not acquired. ^{1}H NMR ($CDCl_3$, 400 MHz) δ 8.19 (app br s, N*H* amide (Arg-Gly), 1H); 7.58 (br d, N*H* amide (Gly-Asp), *J* = 7.5 Hz, 1H); 7.32-7.23 (m, C*H* aromatic, 5H); 7.18 (app br s, N*H* amide (Asp-C12), 1H); 6.45 (br s, NH_2 guanidine, 2H); 6.42 (br s, N*H* guanidine, 1H); 6.03 (br s, N*H* carbamate, 1H); 5.12 (d, CH^A benzylic, *J* = 12.5 Hz, 1H); 4.99 (d, CH^B benzylic, *J* = 12.5 Hz, 1H); 4.75-4.70 (m, Asp α-*H*, 1H); 4.42-4.28 (br m, Arg α-*H*, 1H); 4.16-3.99 (br m, Gly CH^A, 1H); 3.86-3.74 (br m, Gly CH^B, 1H); 3.54-3.28 (br m, Arg CH^ANH, 1H); 3.13-2.96 (br m, Arg CH^BNH and C(O)NHCH^A, 2H); 2.92 (s, Pbf CH_2, 2H); 2.88-2.79 (br m, C(O)NHCH^B, 1H); 2.79-2.68 (br m, Asp CH_2, 2H); 2.57 (s, Pbf CH_3Ar, 3H); 2.48 (s, Pbf CH_3Ar, 3H); 2.05 (s, Pbf CH_3Ar, 3H); 1.90-1.75 (br m, Arg CHCH^A, 1H); 1.68-1.48 (br m, Arg CHCH^B and Arg CH_2CH$_2$NH, 3H); 1.43 (s, Pbf CH_3 × 2, 6H); 1.35 (s, C(CH_3)$_3$, 9H); 1.31-1.07 (br m, C12 CH_2 × 10, 20H); 0.86 (t, C12 CH_3, *J* = 7.0 Hz, 3H). ^{13}C NMR ($CDCl_3$, 100 MHz) δ

173.57, 170.69, 170.48, 169.93, 158.93, 157.06, 156.73 (*C*(O)O^{t}Bu, *C*(O)NH amide × 3, *C*(O)NH carbamate, Pbf aromatic *C*-O, *C*=N guanidine); 138.39 (Pbf aromatic *C*); 136.15 (Z group aromatic *C*); 132.43, 132.28 (Pbf aromatic *C*); 128.55, 128.21, 127.99 (Z group aromatic *C*H); 124.73, 117.70 (Pbf aromatic *C*); 86.50 (Pbf $CH_2C(CH_3)_2O$); 81.55 ($C(CH_3)_3$); 67.08 (CH_2 benzylic); 54.43 (Arg α-*C*H); 50.04 (Asp α-*C*H); 43.28 (Pbf ArCH_2, Gly CH_2); 39.83 (C(O)NHCH_2); 39.30 (Arg CH_2NH); 37.24 (Asp CH_2); 31.96, 29.74, 29.69, 29.40, 29.34, 29.26 (C12 CH_2's); 28.65 (Pbf $CH_2C(CH_3)_2O$); 27.97 ($C(CH_3)_3$); 26.93 (C12 CH_2); 25.71 (Arg CH_2CH_2NH); 22.73 (C12 CH_2); 19.47, 18.16 (Pbf ArCH_3 × 2); 14.18 (C12 CH_3); 12.56 (Pbf ArCH_3). $\tilde{\nu}_{max}$ (cm^{-1}) (solid): 3325*w* (N-H amide stretch); 2978*m*, 2939*m*, 2870*w* (C-H alkyl and arene stretches); 1659*s* (C=O amide/carbamate stretch, overlapping C=O ester stretch); 1543*s* (N-H bend and C=C arene stretch); 1450*m*, 1366*m* (C-H alkyl bend and S=O stretch); 1250*s*, 1150*s*, 1088*s* (C-O ester and C-N stretches, C-H arene bends); 1026*w*-733*w* (C-H arene bends). ESI-MS (*m*/*z*): Calc. for $C_{49}H_{78}N_7O_{10}S$ 956.5525; found: 956.5553 (100%, $[M+H]^+$).

Synthesis of H_2N-Arg(Pbf)-Gly-Asp(O^{t}Bu)-C12 (4.16)

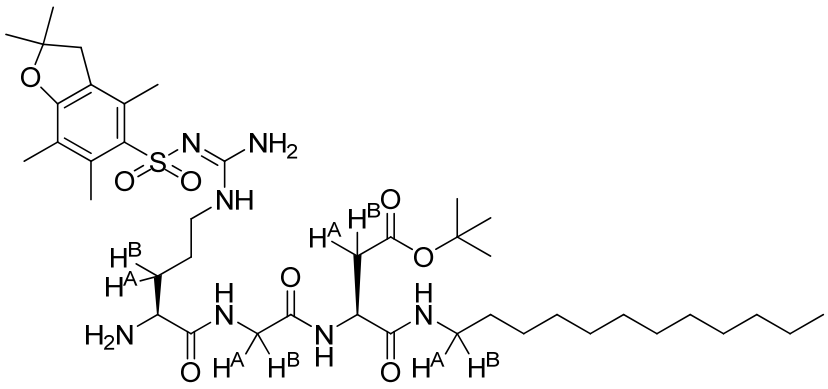

Compound **4.15** (0.84 g, 0.88 mmol) was dissolved in EtOH (10 ml) followed by the addition of Pd/C catalyst (168 mg, 20%). The flask was subjected to several vacuum/H_2 purges and then stirred for 44.5 h under an atmosphere of H_2. The catalyst was filtered off over Celite, washed with MeOH, and the filtrate evaporated *in vacuo* to yield **4.16** as a white solid (0.66 g, 92%). No further purification was required.

R_f 0.11 (9:1, DCM/MeOH, UV and cerium stain). $[\alpha]_D$ = +3.5° (c = 0.5, $CHCl_3$). M.p not acquired. ^{1}H NMR ($CDCl_3$, 400 MHz) δ 8.45 (app br s, N*H* amide (Arg-Gly), 1H); 7.88 (app br s, N*H* amide (Gly-Asp), 1H); 7.31 (app br s, N*H* amide (Asp-C12), 1H); 6.71 (br s, N*H* guanidine, 1H); 6.49 (br s, NH_2 guanidine, 2H); 4.76-4.66 (m, Asp α-*H*, 1H); 4.14-3.99 (br m, Gly CH^A, 1H); 3.99-3.75 (br m, Arg α-*H* and Gly CH^B, 2H); 3.32-3.06 (br m, Arg CH_2NH and C(O)NHCH^A, 3H); 3.06-2.94 (br m, C(O)NHCH^B, 1H); 2.91 (s, Pbf CH_2, 2H); 2.81-2.72 (app br m, Asp CH^A, 1H); 2.71-2.58 (app br m, Asp CH^B, 1H); 2.52 (s, Pbf CH_3Ar, 3H); 2.45 (s, Pbf CH_3Ar, 3H); 2.04 (s, Pbf CH_3Ar, 3H); 1.95-1.82 (br m, Arg CHCH^A, 1H); 1.82-1.70 (br m, Arg CHCH^B, 1H); 1.70-1.52 (br m, Arg CH_2CH_2NH, 2H);

1.42 (s, Pbf C*H*$_3$ × 2, calc 6H, found 5H); 1.36 (s, C(C*H*$_3$)$_3$, calc 9H, found 10H); 1.28-1.00 (br m, C12 C*H*$_2$ × 10, calc 20H, found 21H); 0.84 (t, C12 C*H*$_3$, J = 7.0 Hz, 3H). ^{13}C NMR ($CDCl_3$, 100 MHz) δ 170.89, 170.59, 169.47, 158.84, 156.77 (*C*(O)O^{t}Bu, *C*(O)NH amide × 3, Pbf aromatic *C*-O, *C*=N guanidine); 138.28, 132.57, 132.20, 124.69, 117.60 (Pbf aromatic *C* × 5); 86.46 (Pbf $CH_2C(CH_3)_2O$); 81.67 (*C*(CH$_3$)$_3$); 53.78 (Arg α-*C*H); 49.91 (Asp α-*C*H); 43.27 (Gly *C*H$_2$); 43.03 (Pbf Ar*C*H$_2$); 40.11 (Arg *C*H$_2$NH); 39.86 (C(O)NH*C*H$_2$); 37.51 (Asp *C*H$_2$); 31.96, 29.70, 29.41 (C12 *C*H$_2$'s); 28.64 (Pbf $CH_2C(CH_3)_2O$); 28.03 (C(*C*H$_3$)$_3$); 26.98 (C12 *C*H$_2$); 25.15 (Arg *C*H$_2$CH$_2$NH); 22.72 (C12 *C*H$_2$); 19.39, 18.06 (Pbf Ar*C*H$_3$ × 2); 14.17 (C12 *C*H$_3$); 12.52 (Pbf Ar*C*H$_3$). $\tilde{\nu}_{max}$ (cm^{-1}) (solid): 3649*w* (N-H stretch); 2978*s*, 2886*m* (C-H alkyl stretches); 1659*s* (C=O amide/carbamate stretch, overlapping C=O ester stretch); 1551*s* (N-H bend and C=C arene stretch); 1450*m*, 1366*m* (C-H alkyl bend and S=O stretch); 1250*s*, 1150*s*, 1088*s* (C-O ester and C-N stretches). ESI-MS (*m*/*z*): Calc. for $C_{41}H_{72}N_7O_8S$ 822.5158; found: 822.5171 (100%, $[M+H]^+$).

Synthesis of C12-Arg(Pbf)-Gly-Asp(O^{t}Bu)-C12 (4.17)

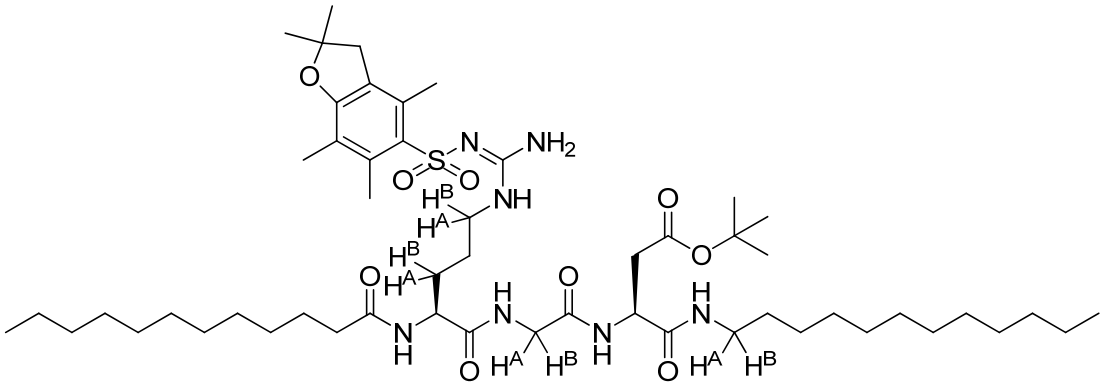

Lauric acid (49 mg, 0.24 mmol, 1.0 eq) was dissolved in DCM (4 ml), cooled over an ice-water bath, followed by the addition of DIPEA (85 μL, 0.49 mmol, 2.0 eq) and TBTU (78 mg, 0.24 mmol, 1.0 eq) and more DCM (2 ml) was used to rinse any residual TBTU into the reaction flask. The reaction mixture was stirred at 0°C for 15 min, then **4.16** (0.2 g, 0.24 mmol, 1.0 eq) was added as a solid, and DCM (2 ml) used to rinse any residual **4.16** into the reaction flask. The reaction was stirred at 0°C for a further 30 min before removing the ice-water bath and stirring the reaction at rt for 19 h. The reaction started to form a gel when cold and then became cloudy and subsequently a clear solution on warming to rt. DCM (20 ml) was added to try to dissolve the fine cloudy precipitate that had formed overnight. The organic phase was washed with cold 1.33 M $NaHSO_4$ which formed an emulsion therefore the layers where gently heated with a heat gun to break down the emulsion. The organic phase was separated and washed again with hot 1.33 M $NaHSO_4$, hot 1 M Na_2CO_3 (2 × 50 ml), hot water (50 ml) and finally brine (50 ml). The organic phase was dried over $MgSO_4$ and filtered before removing the solvent *in vacuo* to produce the crude product as a white solid (0.23 g, 94%). Purification

by column chromatography (SiO_2, 100% DCM, to 98:2 DCM/MeOH, to 95:5 DCM/MeOH) yielded **4.17** as a white solid (180 mg, 74%).

R_f 0.52 (9:1, DCM/MeOH, UV and cerium stain). $[\alpha]_D$ = -2.4° (c = 0.5, $CHCl_3$). M.p not acquired. ^{1}H NMR ($CDCl_3$, 400 MHz) δ 8.14 (app br s, N*H* amide (Arg-Gly), 1H); 7.76 (app br s, N*H* amide (Gly-Asp), 1H); 7.23 (app br s, N*H* amide (Asp-C12), 1H); 6.97 (app br s, N*H* amide (C12-Arg), 1H); 6.45 (br s, NH_2 guanidine, 2H); 6.38 (br s, N*H* guanidine, 1H); 4.79-4.74 (m, Asp α-*H*, 1H); 4.53-4.41 (br m, Arg α-*H*, 1H); 4.08-3.94 (br m, Gly CH^A, 1H); 3.94-3.77 (br m, Gly CH^B, 1H); 3.48-3.29 (br m, Arg CH^ANH, 1H); 3.20-3.01 (br m, Arg CH^BNH and C(O)NHCH^A, 2H); 3.01-2.82 (s (+ underlying m), Pbf CH_2 (+ C(O)NHCH^B), 3H); 2.82-2.67 (app br m, Asp CH_2, 2H); 2.56 (s, Pbf CH_3Ar, 3H); 2.48 (s, Pbf CH_3Ar, 3H); 2.19 (t, C12 CH_2C(O)NH, *J* = 7.5 Hz, 2H); 2.06 (s, Pbf CH_3Ar, 3H); 1.90-1.78 (br m, Arg CHCH^A, 1H); 1.71-1.49 (br m, Arg CHCH^B, Arg CH_2CH$_2$NH, C12 CH_2, 5H); 1.44 (s, Pbf CH_3 × 2, 6H); 1.37 (s, C(CH_3)$_3$, 9H); 1.32-0.99 (br m, C12 CH_2 × 18, calc 36H, found 38H); 0.85 (t, C12 CH_3 × 2, *J* = 7.0 Hz, 6H). ^{13}C NMR ($CDCl_3$, 100 MHz) δ 174.49, 173.50, 170.83, 170.62, 169.95, 158.93, 156.89 (*C*(O)O^{t}Bu, *C*(O)NH amide × 4, Pbf aromatic *C*-O, *C*=N guanidine); 138.36, 132.61, 132.26, 124.74, 117.68 (Pbf aromatic *C* × 5); 86.51 (Pbf CH$_2$*C*(CH$_3$)$_2$O); 81.50 (*C*(CH$_3$)$_3$); 53.53 (Arg α-*C*H); 50.01 (Asp α-*C*H); 43.33 (Gly *C*H$_2$); 43.24 (Pbf Ar*C*H$_2$); 39.89 (C(O)NH*C*H$_2$ and Arg *C*H$_2$NH, overlapping peaks); 37.50 (Asp *C*H$_2$); 36.23 (CH$_2$*C*H$_2$C(O)NH); 31.99, 29.74, 29.69, 29.53, 29.44, 29.36 (C12 *C*H$_2$'s); 28.68 (Pbf CH$_2$C(*C*H$_3$)$_2$O); 28.05 (C(*C*H$_3$)$_3$); 27.00, 25.66, 22.76 (C12 *C*H$_2$'s); 19.47, 18.15 (Pbf Ar*C*H$_3$ × 2); 14.20 (C12 *C*H$_3$ × 2); 12.57 (Pbf Ar*C*H$_3$). $\tilde{\nu}_{max}$ (cm^{-1}) (solid): 3279*w* (N-H stretch); 2978*s*, 2932*s*, 2862*m* (C-H alkyl stretches); 1728*w* (C=O ester stretch); 1628*s* (C=O amide/carbamate stretch); 1543*s* (N-H bend and C=C arene stretch); 1450*m*, 1373*m* (C-H alkyl bend and S=O stretch); 1250*s*, 1150*s*, 1096*s* (C-O ester and C-N stretches). ESI-MS (*m*/*z*): Calc. for $C_{53}H_{94}N_7O_9S$ 1004.6828; found: 1004.6823 (100%, $[M+H]^+$).

Synthesis of C12-Arg-Gly-Asp-C12 (4.18)

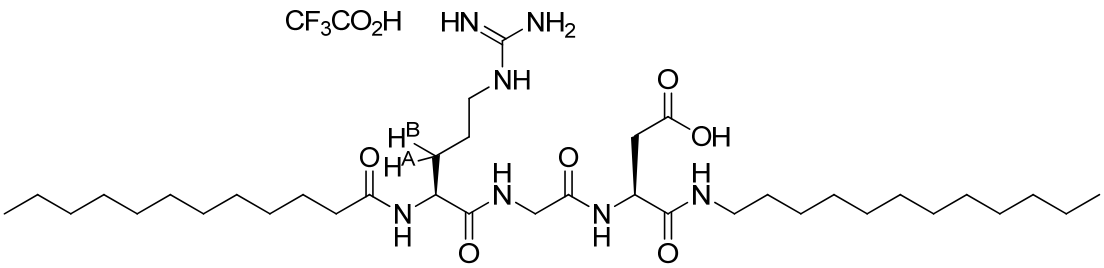

Compound **4.17** (160 mg, 0.16 mmol) was dissolved in a mixture of TFA, water and triisopropylsilane (TIS) (5 ml, 95:2.5:2.5) and shaken for 1 h 30 min, after which time TLC indicated that the deprotection reaction was complete. The volatiles were removed *in vacuo,* then the residue was dissolved in the minimum amount of MeOH, sonicated and then heated until dissolution, then

precipitated with cold Et_2O, filtered and washed with the minimum amount of cold Et_2O to yield **4.18** as a white solid (140 mg, quantitative yield as TFA salt). The sample was then dissolved in a mixture of hot water/^{t}BuOH, filtered over a PTFE membrane filter (0.2 μm), shell frozen and lyophilised to yield the product **4.18** as a fluffy white powder.

N.B. There was evidence of a small amount of methyl esterification of the carboxylic acids as a consequence of the recovery procedure, but this is not believed to affect gelation behaviour.

R_f 0.00 (9:1, DCM/MeOH, cerium stain). $[\alpha]_D$ = -15.6° (c = 0.5, TFA). M.p not acquired. ^{1}H NMR (DMSO-d_6, 400 MHz) δ 8.48 (app br s, N*H* amide (Arg-Gly), 1H); 8.35 (br d, N*H* amide (Gly-Asp), *J* = 7.0 Hz, 1H); 8.05 (d, N*H* amide (C12-Arg), 1H); 7.38 (app br s, N*H* amide (Asp-C12), 1H); 7.17 (br s, NH_2 and N*H* guanidine, 3H); 4.37-4.32 (m, Asp α-*H*, 1H); 4.22-4.17 (br m, Arg α-*H*, 1H); 3.69-3.58 (br m, Gly CH_2, 2H); 3.12-2.90 (br m, Arg CH_2NH and C(O)NHCH_2, 4H); 2.54-2.42 (app m, Asp CH_2, 2H); 2.09 (app t, C12 CH_2C(O)NH, *J* = 7.5 Hz, 2H); 1.84-1.71 (br m, Arg CHCH^A, 1H); 1.58-1.36-1.28-1.10 (br m × 3, Arg CHCH^B, Arg CH_2CH$_2$NH, C12 CH_2's × 19, calc 41H, found 40H); 0.82 (t, C12 CH_3 × 2, *J* = 7.0 Hz, 6H). ^{13}C NMR (DMSO-d_6, 100 MHz) δ 173.14, 172.84, 172.66, 170.24, 168.42, 156.79 (*C*(O)OH, *C*(O)NH amide × 4, *C*=N guanidine); 52.02 (Arg α-*C*H); 49.64 (Asp α-*C*H); 42.50 (Gly *C*H$_2$); 40.17 (Arg *C*H$_2$NH); 38.65 (C(O)NH*C*H$_2$); 36.59 (Asp *C*H$_2$); 34.97 (CH$_2$*C*H$_2$C(O)NH); 31.27, 29.02, 28.94, 28.78, 28.70, 28.65, 26.21, 25.14, 24.73, 22.06 (C12 *C*H$_2$'s); 13.90 (C12 *C*H$_3$ × 2). $\tilde{\nu}_{max}$ (cm^{-1}, solid): 3279*m* (O-H acid and N-H amide/guanidino stretches); 2978*m*, 2924*m*, 2855*m* (C-H alkyl stretches); 1620*s* (C=O amide stretch, overlapping C=O acid stretch); 1543*m* (N-H amide bend); 1466*m*, 1381*m* (C-H alkyl bends); 1250*m*, 1150*m*, 1080*m* (C-O acid and C-N amide stretches). ESI-MS (*m*/*z*): Calc. for $C_{36}H_{70}N_7O_6$ 696.5382; found: 696.5389 (100%, $[M+H]^+$).

Synthesis of 4-iodophenyl-urea-Arg(Pbf)-Gly-Asp(O^{t}Bu)-O^{t}Bu (4.19)

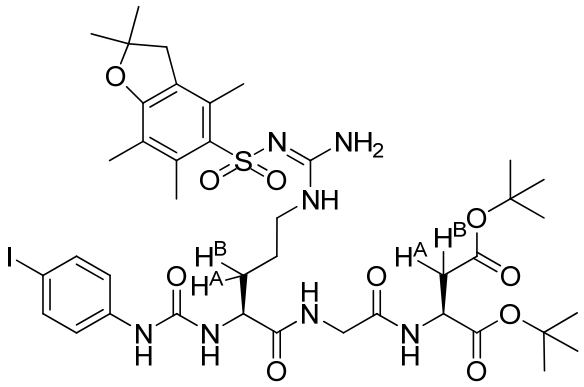

Compound **2.8(2.4)** (0.5 g, 0.7 mmol, 1.2 eq) was dissolved in DCM (10 ml), then 4-iodophenyl isocyanate (144 mg, 0.59 mmol, 1.0 eq) was added as a solid and a further portion of DCM (2 ml) was

used to rinse any residual isocyanate into the reaction flask. Upon adding the isocyanate to the reaction flask, a fibrous-like white precipitate formed. The reaction was stirred vigorously at rt for 16 h, after which time TLC indicated the reaction was complete and MeOH was added to 'quench' any residual isocyanate and dissolve the precipitate. The solvent was removed *in vacuo* to yield a fluffy white solid (0.64 g). Purification of the crude material by column chromatography (SiO_2, 98:2 DCM/MeOH, to 95:5 DCM/MeOH) yielded the product, **4.19**, as a fluffy white solid (0.51 g, 91%).

R_f 0.41 (9:1, DCM/MeOH, UV and cerium stain). $[\alpha]_D$ = -9.8° (c = 0.5, MeOH). M.p not acquired. ^{1}H NMR (CD_3OD, 400 MHz) δ 7.53 (d, CH aromatic, *J* = 9.0 Hz, 2H); 7.21 (d, CH aromatic, *J* = 9.0 Hz, 2H); 4.65 (t, Asp α-*H*, *J* = 6.5 Hz, 1H); 4.22 (dd, Arg α-*H*, *J* = 7.0 Hz and 5.0 Hz, 1H); 3.90 (s, Gly CH_2, 2H); 3.25-3.17 (br m, Arg CH_2NH, 2H); 2.96 (s, Pbf CH_2, 2H); 2.73 (dd, Asp CH^A, *J* = 17.0 Hz and 6.5 Hz, 1H); 2.61 (dd, Asp CH^B, *J* = 17.0 Hz and 6.5 Hz, 1H); 2.57 (s, Pbf CH_3Ar, 3H); 2.50 (s, Pbf CH_3Ar, 3H); 2.06 (s, Pbf CH_3Ar, 3H); 1.91-1.80 (m, Arg CHCH^A, 1H); 1.74-1.57 (m, Arg CHCH^B and Arg CH_2CH_2NH, 3H); 1.50-1.38 (m, Pbf CH_3 × 2, C(CH_3)$_3$ × 2, calc 24H, found 26H). ^{13}C NMR (CD_3OD, 100 MHz) δ 175.55, 171.32, 171.29, 171.14, 159.92, 158.21, 157.35 (*C*(O)O^{t}Bu × 2, *C*(O)NH amide × 2, *C*(O)NH urea, Pbf aromatic *C*-O, *C*=N guanidine); 140.82, 139.43 (aromatic *C*-NHC(O)NH, Pbf aromatic *C*); 138.83 (aromatic *C*H); 134.24, 133.57, 126.08 (Pbf aromatic *C* × 3); 121.92 (aromatic *C*H); 118.49 (Pbf aromatic *C*); 87.71 (Pbf $CH_2C(CH_3)_2O$); 85.43 (aromatic *C*-I); 83.32, 82.46 (*C*(CH_3)$_3$ × 2); 55.21 (Arg α-*C*H); 51.07 (Asp α-*C*H); 43.99, 43.39 (Pbf Ar*C*H$_2$, Gly *C*H$_2$); 41.45 (Arg *C*H$_2$NH); 38.30 (Asp *C*H$_2$); 30.47 (Arg CH*C*H$_2$); 28.77 (Pbf $CH_2C(CH_3)_2O$); 28.42, 28.25 (C(*C*H$_3$)$_3$ × 2); 26.95 (Arg *C*H$_2$CH$_2$NH); 19.66, 18.45, 12.57 (Pbf Ar*C*H$_3$ × 3). $\tilde{\nu}_{max}$ (cm^{-1}) (solid): 3649*w*, 3341*w* (N-H stretch); 2978*s*, 2886*w* (C-H alkyl and arene stretches); 1728*m* (C=O ester stretch); 1690*m* (C=O amide/urea stretches); 1535*s* (N-H bend and C=C arene stretch); 1481*m*, 1450*m*, 1389*m*, 1366*m* (C-H alkyl bend and S=O stretch); 1242*s*, 1150*s*, 1088*s* (C-O ester and C-N stretches, C-H arene bends); 995*w*, 957*w*, 818*m*, 787*w*, 664*m* (C-H arene bends); 563*m* (C-I stretch). ESI-MS (*m*/*z*): Calc. for $C_{40}H_{59}IN_7O_{10}S$ 956.3083; found: 956.3057 (100%, $[M+H]^+$). Calc. for $C_{40}H_{58}IN_7NaO_{10}S$ 978.2903; found: 978.2854 (34%, $[M+Na]^+$).

Synthesis of 1,4-bis((trimethylsilyl)ethynyl)benzene (4.20)

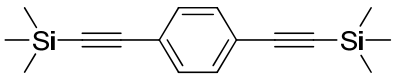

1,4-dibromobenzene (1 g, 4.23 mmol, 1.0 eq), copper iodide (8.7 mg, 45.7 μmol, 1 mol%) and bis(triphenylphosphine)palladium(II) dichloride (60 mg, 84.8 μmol, 2 mol%) were dissolved in diethylamine (25 ml) and the reaction flask was subjected to several vacuum/argon purges. Trimethylsilylethyne (2.4 ml, 17 mmol, 4 eq) was injected dropwise over ~2 min and the reaction was refluxed at 70°C under argon for 14.5 h. The diethylammonium bromide salt, which had formed

overnight, was filtered off, washed with Et_2O and the filtrate evaporated *in vacuo* to yield a black solid (1.3 g). The crude material was then dissolved in hexane (10 ml) and filtered to remove most of the palladium catalyst, before evaporating the filtrate *in vacuo* to yield a brown solid (1.2 g). Purification of the crude material by column chromatography (SiO_2, hexane) yielded the product, **4.20**, as a brown solid (0.95 g, 83%).

R_f 0.22 (hexane, UV and $KMnO_4$ stain). M.p not acquired. ^{1}H NMR ($CDCl_3$, 400 MHz) δ 7.39 (s, C*H* aromatic, 4H); 0.25 (s, Si(C*H*$_3$)$_3$, calc 18H, found 16H). ^{13}C NMR ($CDCl_3$, 100 MHz) δ 131.88 (*C*H aromatic); 123.27 (*C* aromatic); 104.69 (-*C*≡C-Si(CH$_3$)$_3$); 96.41 (-C≡*C*-Si(CH$_3$)$_3$); 0.05 (Si(*C*H$_3$)$_3$). $\tilde{\nu}_{max}$ (cm^{-1}) (solid): 2963*m*, 2893*w* (C-H alkyl and arene stretches); 2153*m* (C≡C stretch); 1574*w* (C=C arene stretch); 1489*m*, 1389*m* (C-H alkyl bend); 1242*s* (Si-C stretch); 826*s*, 748*s*, 694*m*, 625*m* (C-H arene bends). No MS data.

Synthesis of 1,4-diethynylbenzene (4.21)

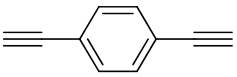

Compound **4.20** (0.88 g, 3.26 mmol, 1.0 eq) was dissolved in THF (15 ml) and 1 M NaOH (6.5 ml, 6.5 mmol, 2.0 eq) was added. The reaction was stirred vigorously at rt for 3 h, after which time TLC indicated that the reaction was complete, and then the THF was removed *in vacuo* yielding a white precipitate. The white precipitate was taken up in DCM (40 ml), the organic layer was separated, and the aqueous layer was extracted with DCM (2 × 40 ml). The organic fractions were combined, dried over Na_2SO_4, filtered and the filtrate was evaporated to yield **4.21** as a white solid (0.33 g, 80%). No further purification was required.

N.B. the compound was found to be quite volatile and leaving the material to dry on the high-vacuum line overnight resulted in the majority of it subliming off under vacuum.

R_f 0.22 (hexane, UV and $KMnO_4$ stain). M.p not acquired. ^{1}H NMR ($CDCl_3$, 500 MHz) δ 7.42 (s, C*H* aromatic, 4H); 3.15 (s, C*H* alkyne, 2H). ^{13}C NMR ($CDCl_3$, 125 MHz) δ 132.10 (*C*H aromatic); 122.66 (*C* aromatic); 83.12 (-C≡*C*-H); 79.15 (-*C*≡C-H). $\tilde{\nu}_{max}$ (cm^{-1}) (solid): 2970*m*, 2916*s*, 2855*m* (C-H alkyne and arene stretches); 2106*w* (C≡C stretch); 1597*w* (C=C arene stretch); 833*s* (C-H arene bends); 648*m* (C-H alkyne bend). No MS data.

Synthesis of linear OPE-[Arg(Pbf)-Gly-Asp(O^{t}Bu)-O^{t}Bu]$_2$ (4.22)

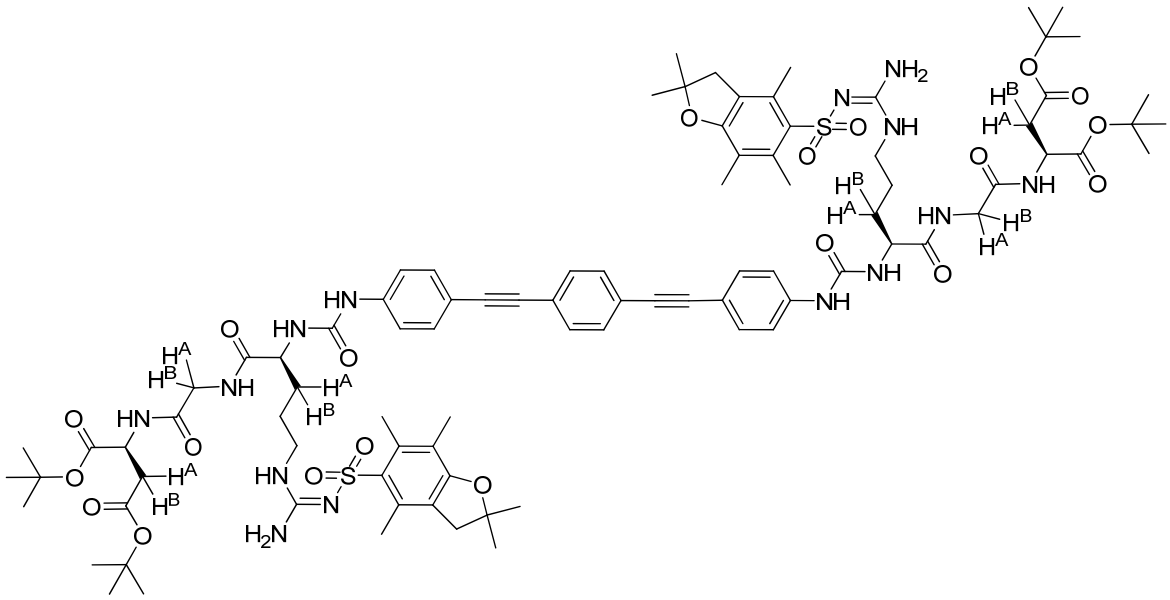

Compound **4.19** (200 mg, 0.21 mmol, 4.0 eq) copper iodide (0.24 mg, 1.05 μmol, 2 mol%) and bis(triphenylphosphine)palladium(II) dichloride (0.74 mg, 1.05 μmol, 2 mol%) were dissolved in diethylamine (6 ml) and the reaction flask was subjected to several vacuum/argon purges. Compound **4.21** (6.6 mg, 52.4 μmol, 1.0 eq), dissolved in diethylamine (1 ml), was injected dropwise over ~1 min and more diethylamine (3 ml) was used to rinse any residual **4.21** into the reaction flask. The reaction was refluxed at 60°C under argon for 20 h and then a further portion of both copper iodide (0.24 mg, 1.05 μmol, 2 mol%, 4 mol% in total) and bis(triphenylphosphine)palladium(II) dichloride (0.74 mg, 1.05 μmol, 2 mol%, 4 mol% in total) were added to ensure the reaction was driven to completion. The reaction was refluxed at 60°C under argon for a further 3 h before removing the solvent *in vacuo* to yield a crude orange/brown solid. Purification of the crude material by column chromatography (SiO_2, 98:2 DCM/MeOH, to 95:5 DCM/MeOH, to 9:1 DCM/MeOH) yielded the product, **4.22**, as an orange/brown solid (90 mg, 97% yield, 97% pure (contains some residual diethylamine)).

R_f 0.26 (9:1, DCM/MeOH, UV and cerium stain). $[\alpha]_D$ = +12.0° (c = 0.1, DMSO). M.p not acquired. ^{1}H NMR ($CD_3OD/CDCl_3$, 400 MHz) δ 7.43-7.29 (m, C*H* aromatic, 12H); 4.65 (obscured by the water peak, Asp α-*H*, calc 2H); 4.23 (dd, Arg α-*H*, *J* = 6.5 Hz and 5.0 Hz, 2H); 3.96 (d, Gly C*H*^{A}, *J* = 17.0 Hz, 2H); 3.90 (d, Gly C*H*^{B}, *J* = 17.0 Hz, 2H); 3.29-3.16 (br m, Arg C*H*$_2$NH, 4H); 2.93 (s, Pbf C*H*$_2$, 4H); 2.73 (dd, Asp C*H*^{A}, *J* = 17.0 Hz and 6.5 Hz, 2H); 2.64 (dd, Asp C*H*^{B}, *J* = 17.0 Hz and 6.0 Hz, 2H); 2.56 (s, Pbf C*H*$_3$Ar, 6H); 2.49 (s, Pbf C*H*$_3$Ar, 6H); 2.05 (s, Pbf C*H*$_3$Ar, 6H); 1.90-1.79 (m, Arg CHC*H*^{A}, 2H); 1.77-1.56 (m, Arg CHC*H*^{B} and Arg C*H*$_2$CH$_2$NH, 6H); 1.49-1.35 (m, Pbf C*H*$_3$ × 2, C(C*H*$_3$)$_3$ × 2, calc 48H, found 46H). ^{13}C NMR ($CD_3OD/CDCl_3$, 100 MHz) δ 175.02, 170.75, 170.54, 159.43, 157.39, 156.62 (*C*(O)O^{t}Bu × 2, *C*(O)NH amide × 2, *C*(O)NH urea, Pbf aromatic *C*-O, *C*=N

guanidine, calc 7 peaks, found 6 peaks); 140.33, 138.93, 133.24, 132.96 (aromatic *C* × 4); 132.84, 131.86 (aromatic *C*H × 2); 125.45, 123.74 (aromatic *C* × 2); 119.06 (aromatic *C*H); 118.17, 117.19 (aromatic *C* × 2); 91.96, 88.72 (alkyne *C* × 2); 87.19 (Pbf $CH_2C(CH_3)_2O$); 83.16, 82.24 ($C(CH_3)_3$ × 2); 54.87 (Arg α-*C*H); 50.33 (Asp α-*C*H); 43.69, 43.16 (Pbf ArCH_2, Gly CH_2); 40.79 (Arg CH_2NH); 37.90 (Asp CH_2); 29.52 (Arg $CHCH_2$); 28.80 (Pbf $CH_2C(CH_3)_2O$); 28.31, 28.16 ($C(CH_3)_3$ × 2); 26.37 (Arg CH_2CH_2NH); 19.62, 18.34, 12.69 (Pbf ArCH_3 × 3). $\tilde{\nu}_{max}$ (cm^{-1}) (solid): 3649*w*, 3325*w*, 3248*w* (N-H stretch); 2978*s*, 2886*w* (C-H alkyl and arene stretches); 2214*w* (C≡C stretch); 1721*m* (C=O ester stretch); 1690*m* (C=O amide/urea stretches); 1520*s* (N-H bend and C=C arene stretch); 1450*m*, 1366*s* (C-H alkyl bend and S=O stretch); 1242*s*, 1150*s*, 1088*s* (C-O ester and C-N stretches, C-H arene bends); 957*m*, 833*m*, 787*w*, 664*m* (C-H arene bends). ESI-MS (*m*/*z*): Calc. for $C_{90}H_{122}N_{14}O_{20}S_2$ 891.9234; found: 891.9160 (100%, $[M\{^{13}C\}+2H]^{2+}$). Calc. for $C_{90}H_{121}N_{14}O_{20}S_2$ 1782.8396; found: 1782.8112 (14%, $[M\{^{13}C\}+H]^{+}$).

Attempted synthesis of linear OPE-[Arg-Gly-Asp]$_2$ (4.23)

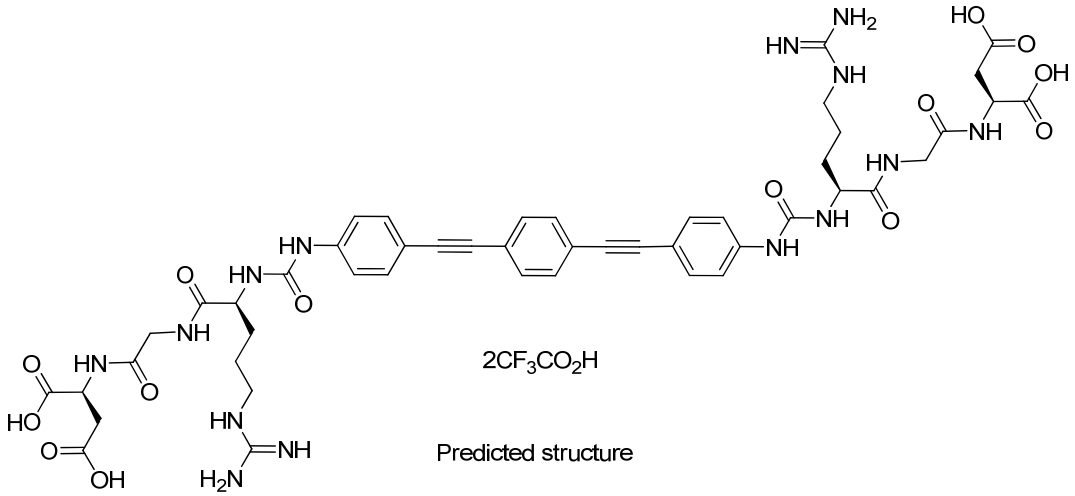

Compound **4.22** (80 mg, 45 μmol) was dissolved in a mixture of TFA, water and TIS (5 ml, 95:2.5:2.5) and shaken for ~2 h, after which time TLC indicated that the deprotection reaction was complete. The reaction mixture was cooled over an ice-water bath, precipitated with cold Et_2O, filtered and washed with the minimum amount of cold Et_2O and dried *in vacuo*. The sample was then dissolved in a mixture of water/^{t}BuOH, filtered over a PTFE membrane filter (0.2 μm), shell frozen and lyophilised to yield predicted structure, **4.23**, as a fluffy, yellow powder (61 mg, near quantitative yield as TFA salt).

R_f 0.00 (9:1, DCM/MeOH, UV and cerium stain). $[\alpha]_D$ = +14.0° (c = 0.1, DMSO). M.p not acquired. No discernible ^{1}H NMR data (see appendix – spectrum 4.8). No discernible ^{13}C NMR data. IR not acquired. No MS data.

Synthesis of 1,3,5-tris((trimethylsilyl)ethynyl)benzene (4.24)[276]

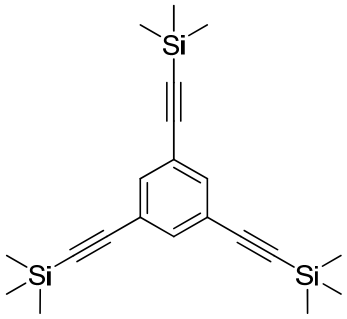

1,3,5-tribromobenzene (1 g, 3.18 mmol, 1.0 eq), copper iodide (6 mg, 31.8 μmol, 1 mol%) and bis(triphenylphosphine)palladium(II) dichloride (45 mg, 63.5 μmol, 2 mol%) were dissolved in diethylamine (25 ml) and the reaction flask was subjected to several vacuum/argon purges. Trimethylsilylethyne (2.69 ml, 19.1 mmol, 6 eq) was injected dropwise over ~2 min and the reaction was refluxed at 70°C under argon for 21 h. The diethylammonium bromide salt, which had formed overnight, was filtered off, washed with Et_2O and the filtrate evaporated *in vacuo* to yield a brown residue (1.4 g). Purification of the crude material by column chromatography (SiO_2, hexane) yielded the product, **4.24**, as a pale yellow solid (0.89 g, 77%).

R_f 0.30 (hexane, UV and $KMnO_4$ stain). M.p not acquired. ^{1}H NMR ($CDCl_3$, 400 MHz) δ 7.49 (s, C*H* aromatic, 3H); 0.23 (s, Si(CH_3)$_3$, 27H). ^{13}C NMR ($CDCl_3$, 100 MHz) δ 135.06 (*C*H aromatic); 123.79 (*C* aromatic); 103.29 (-*C*≡C-Si(CH$_3$)$_3$); 95.73 (-C≡*C*-Si(CH$_3$)$_3$); -0.01 (Si(*C*H$_3$)$_3$). $\tilde{\nu}_{max}$ (cm^{-1}) (solid): 2970*m*, 2893*w* (C-H alkyl and arene stretches); 2160*m* (C≡C stretch); 1574*w* (C=C arene stretch); 1412*m* (C-H alkyl bend); 1250*s* (Si-C stretch); 980*s*, 833*s*, 756*m*, 702*m*, 648*m* (C-H arene bends). EI-MS (*m*/*z*): Found: 366.1668 (18%, M$^{+\bullet}$); 351.1449 (42%, [M$^{+\bullet}$-$^{\bullet}$CH$_3$]$^+$); 41.0195 (100%, Si≡C-H$^+$).

Synthesis of 1,3,5-triethynylbenzene (4.25)[277]

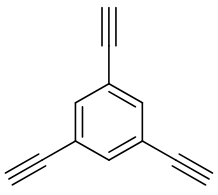

Compound **4.24** (0.6 g, 1.64 mmol, 1.0 eq) was dissolved in THF (8 ml) and 1 M NaOH (4 ml, 4 mmol, 2.4 eq) was added. The reaction was stirred vigorously at rt for 3 h, after which time TLC indicated that the reaction was complete, and then the THF was removed *in vacuo* yielding a white precipitate. The white precipitate was taken up in DCM (20 ml), the organic layer was separated, and the aqueous layer was extracted with DCM (2 × 25 ml). The organic fractions were combined, dried

over Na_2SO_4, filtered and the filtrate was evaporated to yield **4.25** as a yellow solid (140 mg, 56%). No further purification was required.

R_f 0.21 (hexane, UV and $KMnO_4$ stain). M.p not acquired. ^{1}H NMR ($CDCl_3$, 500 MHz) δ 7.57 (s, C*H* aromatic, 3H); 3.11 (s, C*H* alkyne, 3H). ^{13}C NMR ($CDCl_3$, 125 MHz) δ 135.72 (*C*H aromatic); 123.00 (*C* aromatic); 81.71 (-C≡*C*-H); 78.78 (-*C*≡C-H). $\tilde{\nu}_{max}$ (cm^{-1}) (solid): 2978*s*, 2886*m* (C-H alkyne and arene stretches); 1582*w* (C=C arene stretch); 957*m*, 841*m* (C-H arene bends); 648*m* (C-H alkyne bend). EI-MS (*m*/*z*): Calc for $C_{12}H_6$ 150.0470; found: 150.0461 (29%, $M^{+\bullet}$).

Synthesis of triangular-shaped OPE-[Arg(Pbf)-Gly-Asp(O^{t}Bu)-O^{t}Bu]$_3$ (4.26)

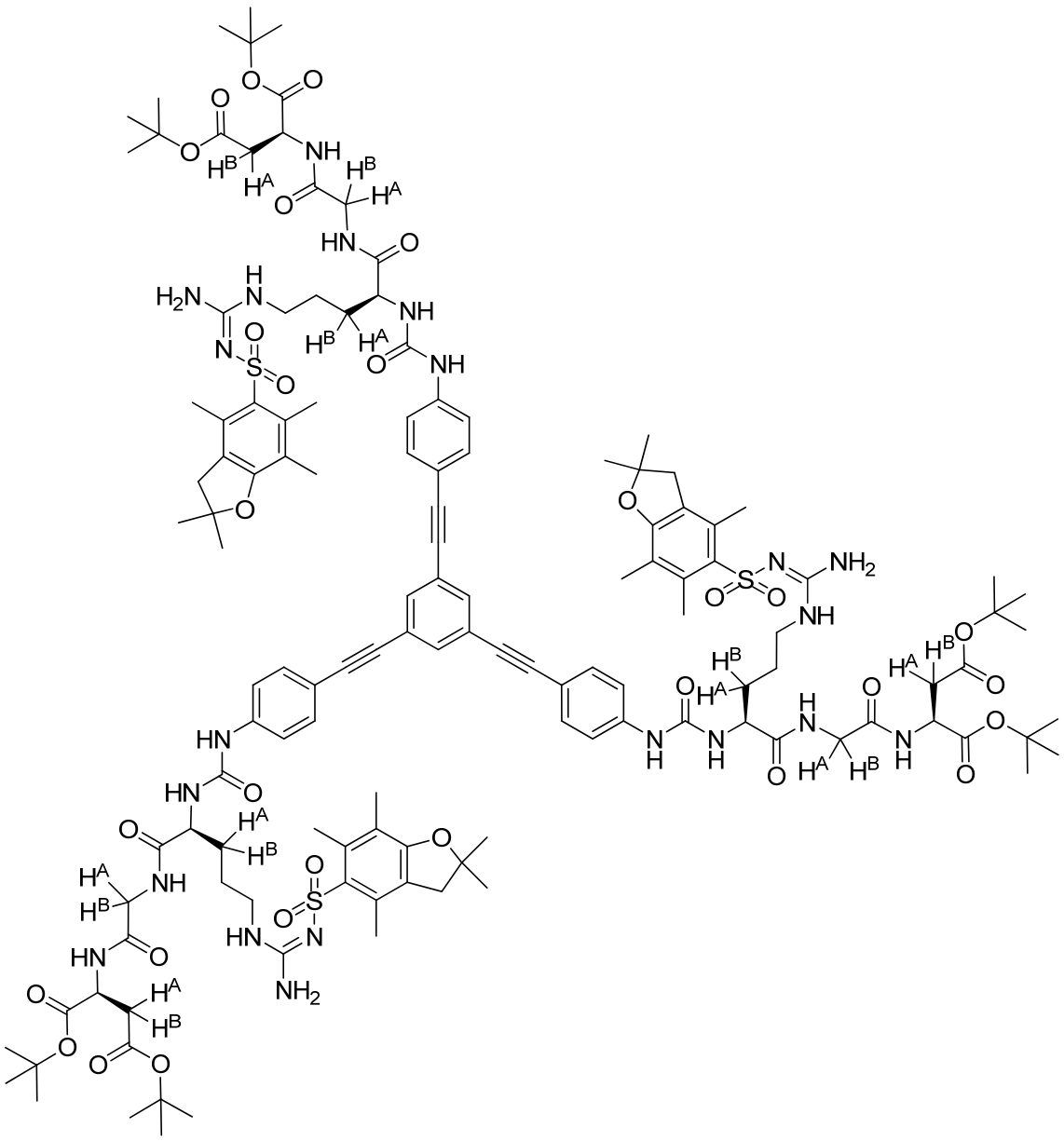

Compound **4.19** (200 mg, 0.21 mmol, 6.0 eq) copper iodide (0.2 mg, 1.05 μmol, 2 mol%) and bis(triphenylphosphine)palladium(II) dichloride (0.5 mg, 0.71 μmol, 2 mol%) were dissolved in diethylamine (6 ml) and the reaction flask was subjected to several vacuum/argon purges. Compound **4.25** (5.2 mg, 34.9 μmol, 1.0 eq), dissolved in diethylamine (1 ml), was injected dropwise over ~1 min and more diethylamine (1 ml) was used to rinse any residual **4.25** into the reaction flask. The reaction was refluxed at 60°C under argon for 20 h and then a further portion of both copper iodide (0.2 mg, 1.05 μmol, 2 mol%, 4 mol% in total) and bis(triphenylphosphine)palladium(II) dichloride (0.5 mg, 0.71 μmol, 2 mol%, 4 mol% in total) were added to ensure the reaction was driven to completion. The reaction was refluxed at 60°C under argon for a further 2 h before removing the solvent *in vacuo* to yield a crude brown residue. Purification of the crude material by column chromatography (SiO_2, 98:2 DCM/MeOH, to 95:5 DCM/MeOH, to 9:1 DCM/MeOH) yielded the product, **4.26**, as a brown solid (75 mg, 82% yield, 97% pure (contains some residual diethylamine)).

N.B. Advantageously, the excess starting material, **4.19**, could be recovered from the silica column purification procedure, in near quantitative yield, and could potentially be re-used.

R_f 0.28 (9:1, DCM/MeOH, UV and cerium stain). $[\alpha]_D$ = +8.0° (c = 0.1, DMSO). M.p not acquired. ^{1}H NMR ($CD_3OD/CDCl_3$, 400 MHz) δ 7.39 (s, C*H* aromatic, 3H); 7.25 (s, C*H* aromatic, 12H); 4.65 (obscured by the water peak, Asp α-*H*, calc 3H); 4.25 (app br t, Arg α-*H*, 3H); 4.01 (d, Gly CH^A, *J* = 17.0 Hz, 3H); 3.91 (d, Gly CH^B, *J* = 17.0 Hz, 3H); 3.29-3.17 (br m, Arg CH_2NH, 6H); 2.94 (s, Pbf CH_2, 6H); 2.77 (dd, Asp CH^A, *J* = 17.0 Hz and 6.5 Hz, 3H); 2.68 (dd, Asp CH^B, *J* = 17.0 Hz and 6.5 Hz, 3H); 2.56 (s, Pbf CH_3Ar, 9H); 2.49 (s, Pbf CH_3Ar, 9H); 2.06 (s, Pbf CH_3Ar, 9H); 1.94-1.81 (m, Arg CHCH^A, 3H); 1.78-1.56 (m, Arg CHCH^B and Arg CH_2CH$_2$NH, 9H); 1.52-1.36 (m, Pbf CH_3 × 2, C(CH_3)$_3$ × 2, calc 72H, found 69H). ^{13}C NMR ($CD_3OD/CDCl_3$, 100 MHz) δ 175.35, 170.74, 170.57, 159.44, 157.42, 156.66 (*C*(O)O^{t}Bu × 2, *C*(O)NH amide × 2, *C*(O)NH urea, Pbf aromatic *C*-O, *C*=N guanidine, calc 7 peaks, found 6 peaks); 140.26, 138.96, 133.63 (aromatic *C* × 3); 133.29, 132.98 (aromatic *C*H × 2); 132.87, 125.46, 124.85 (aromatic *C* × 3); 119.00 (aromatic *C*H); 118.18, 117.02 (aromatic *C* × 2); 91.24, 87.62 (alkyne *C* × 2); 87.20 (Pbf CH$_2$*C*(CH$_3$)$_2$O); 83.19, 82.28 (*C*(CH$_3$)$_3$ × 2); 54.86 (Arg α-*C*H); 50.40 (Asp α-*C*H); 43.72, 43.06 (Pbf Ar*C*H$_2$, Gly *C*H$_2$); 40.78 (Arg *C*H$_2$NH); 37.95 (Asp *C*H$_2$); 29.50 (Arg CH*C*H$_2$); 28.81 (Pbf CH$_2$C(*C*H$_3$)$_2$O); 28.38, 28.18 (C(*C*H$_3$)$_3$ × 2); 26.55 (Arg *C*H$_2$CH$_2$NH); 19.64, 18.36, 12.70 (Pbf Ar*C*H$_3$ × 3). $\tilde{\nu}_{max}$ (cm^{-1}) (solid): 3649*w* (N-H stretch); 2978*s*, 2886*w* (C-H alkyl and arene stretches); 2207*w* (C≡C stretch); 1728*w* (C=O ester stretch); 1512*m* (N-H bend and C=C arene stretch, overlapping C=O amide/urea stretches); 1450*s*, 1373*s* (C-H alkyl bend and S=O stretch); 1250*s*, 1150*s*, 1088*s* (C-O ester and C-N stretches, C-H arene bends); 957*m*, 833*m*, 787*w*, 664*m* (C-H arene bends). ESI-MS (*m*/*z*): Calc. for $C_{132}H_{180}N_{21}O_{30}S_3$ 878.7476; found: 878.7668 (100%, [M+^{13}C+3H]$^{3+}$). Calc. for $C_{132}H_{179}N_{21}O_{30}S_3$ 1317.6178; found: 1317.6704 (100%, [M+^{13}C+2H]$^{2+}$).

Attempted synthesis of triangular-shaped OPE-[Arg-Gly-Asp]$_3$ (4.27)

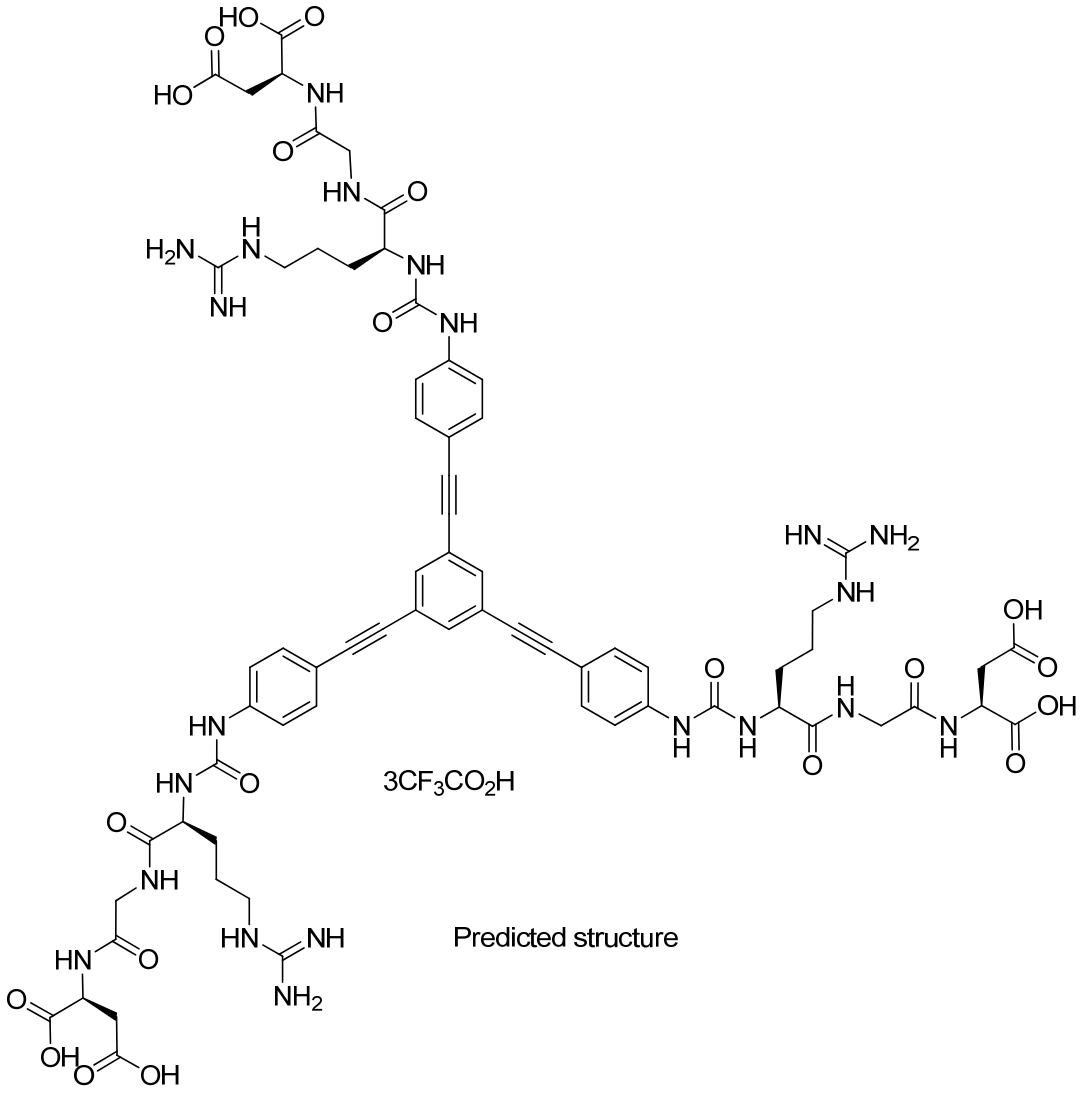

Compound **4.26** (70 mg, 26.6 μmol) was dissolved in a mixture of TFA, water and TIS (5 ml, 95:2.5:2.5) and shaken for 1 h, after which time TLC indicated that the deprotection reaction was complete. A small amount of solid had precipitated which was filtered off. The filtrate was cooled over an ice-water bath, precipitated with cold Et_2O, filtered and washed with the minimum amount of cold Et_2O and dried *in vacuo*. The sample was then dissolved in a mixture of water/^{t}BuOH, shell frozen and lyophilised to yield predicted structure, **4.27**, as a fluffy, beige powder (45 mg, 90% as TFA salt).

R_f 0.00 (9:1, DCM/MeOH, UV and cerium stain). $[\alpha]_D$ = +60.0° (c = 0.1, DMSO). M.p not acquired. No discernible ^{1}H NMR data (see appendix – spectrum 4.10). No discernible ^{13}C NMR data. IR not acquired. No MS data.

Synthesis of Z-Asp(O^{t}Bu)-Lys(Boc)-O^{t}Bu (4.28)

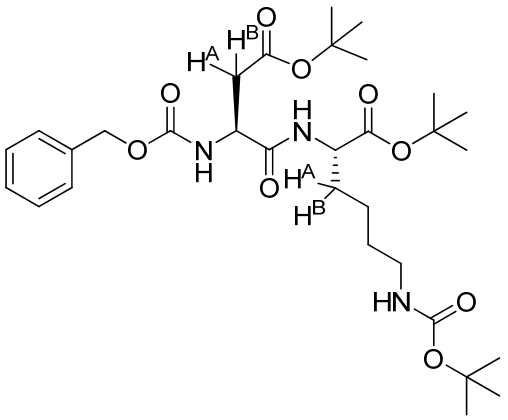

Z-Asp(O^{t}Bu)-OH (1.01 g, 2.95 mmol, 1.0 eq) was solubilised in DCM (25 ml) upon addition of DIPEA (1.05 ml, 5.9 mmol, 2.0 eq). The reaction flask was cooled over an ice-water bath then TBTU (0.96 g, 2.95 mmol, 1.0 eq) was added as a solid and the reaction was stirred at 0°C for 10 min before H_2N-Lys(Boc)-O^{t}Bu.HCl (1.00 g, 2.95 mmol, 1.0 eq) was added as a solid and more DCM (25 ml) was used to rinse any residual H_2N-Lys(Boc)-O^{t}Bu.HCl into the reaction flask. The reaction was stirred at 0°C for a further 20 min before removing the ice-water bath and stirring the reaction at rt for 3 days. The organic phase was washed successively with 1.33 M $NaHSO_4$ (3 × 100 ml), sat. $NaHCO_3$ (100 ml), water (100 ml) and finally brine (100 ml). The organic phase was dried over $MgSO_4$ and filtered before removing the solvent *in vacuo* to yield the product, **4.28**, as a clear, tacky solid/oil (1.76 g, 98%). No further purification was required.

R_f 0.76 (9:1, DCM/MeOH, UV and cerium stain). $[\alpha]_D$ = +24.3° (c = 1.0, $CHCl_3$). M.p not acquired. ^{1}H NMR ($CDCl_3$, 400 MHz) δ 7.39-7.29 (m, C*H* aromatic, 5H); 7.04 (br d, N*H* amide, *J* = 8.0 Hz, 1H); 6.05 (br d, Z group N*H* carbamate, *J* = 7.0 Hz, 1H); 5.13 (s, CH_2 benzylic, 2H); 4.80 (app br s, Boc group N*H* carbamate, 1H); 4.60-4.51 (br m, Asp α-*H*, 1H); 4.45-4.40 (m, Lys α-*H*, 1H); 3.12-2.99 (br m, Lys CH_2NH, 2H); 2.92 (dd, Asp CH^A, *J* = 17.0 Hz and 5.0 Hz, 1H); 2.64 (dd, Asp CH^B, *J* = 17.0 Hz and 6.0 Hz, 1H); 1.85-1.77 (m, Lys CHCH^A, 1H); 1.67-1.57 (m, Lys CHCH^B, 1H); 1.49-1.37 (m, C(CH_3)$_3$ × 3 (+ Lys CH_2), calc 29H, found 31H); 1.35-1.24 (m, Lys CH_2, 2H). ^{13}C NMR ($CDCl_3$, 100 MHz) δ 171.57, 171.40, 170.72, 156.48, 156.42 (*C*(O)O^{t}Bu × 2, *C*(O)NH amide, *C*(O)NH carbamate × 2); 136.46 (*C* aromatic); 128.82, 128.49, 128.44 (*C*H aromatic); 82.06, 81.75, 78.94 (*C*(CH$_3$)$_3$ × 3); 67.13 (*C*H$_2$ benzylic); 52.53 (Lys α-*C*H); 51.06 (Asp α-*C*H); 39.97, 37.22 (Asp *C*H$_2$, Lys *C*H$_2$NH); 31.76, 29.01 (Lys *C*H$_2$ × 2); 28.17, 27.76, 27.73 (C(*C*H$_3$)$_3$ × 3); 21.76 (Lys *C*H$_2$). $\tilde{\nu}_{max}$ (cm^{-1}) (solid): 3657*w*, 3356*w* (N-H stretch); 2978*s*, 2886*m* (C-H alkyl and arene stretches); 1705*s* (C=O ester stretch, overlapping C=O amide/carbamate stretch); 1504*s* (N-H bend and C=C arene stretch); 1458*w*, 1366*s* (C-H alkyl bends); 1250*s*, 1150*s*, 1049*m* (C-O ester and C-N stretches, C-H arene bends);

957*m*, 849*m*, 741*m* (C-H arene bends). ESI-MS (*m/z*): Calc. for $C_{31}H_{50}N_3O_9$ 608.3542; found: 608.3555 (100%, $[M+H]^+$). Calc. for $C_{31}H_{49}N_3NaO_9$ 630.3361; found: 630.3371 (75%, $[M+Na]^+$).

Synthesis of H_2N-Asp(O^{t}Bu)-Lys(Boc)-O^{t}Bu (4.29)

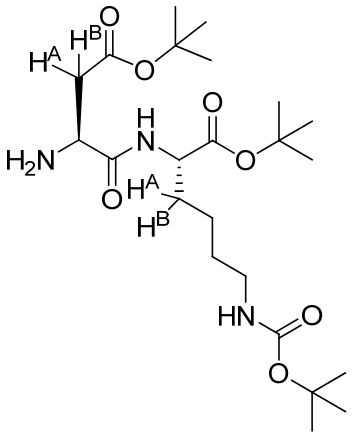

Compound **4.28** (1.66 g, 2.73 mmol) was dissolved in EtOH (50 ml) followed by the addition of Pd/C catalyst (0.33 g, 20%). The flask was subjected to several vacuum/H_2 purges and then stirred for 17.5 h under an atmosphere of H_2. The catalyst was filtered off over Celite, washed with MeOH, and the filtrate evaporated *in vacuo* to yield **4.29** as a clear colourless oil (1.26 g, 98%). No further purification was required.

R_f 0.49 (9:1, DCM/MeOH, cerium stain). $[\alpha]_D$ = +6.3° (c = 1.0, $CHCl_3$). ^{1}H NMR ($CDCl_3$, 400 MHz) δ 7.85 (br d, N*H* amide, *J* = 8.0 Hz, 1H); 4.84 (app br s, Boc group N*H* carbamate, 1H); 4.40-4.34 (br m, Lys α-*H*, 1H); 3.75-3.66 (br m, Asp α-*H*, 1H); 3.12-2.88 (br m, Lys CH_2NH and NH_2, 4H); 2.77 (dd, Asp CH^A, *J* = 17.0 Hz and 5.0 Hz, 1H); 2.59 (dd, Asp CH^B, *J* = 17.0 Hz and 6.0 Hz, 1H); 1.81-1.72 (m, Lys CHCH^A, 1H); 1.65-1.52 (m, Lys CHCH^B, 1H); 1.50-1.22 (m, C(CH_3)$_3$ × 3 (+ Lys CH_2 × 2), calc 31H, found 30H). ^{13}C NMR ($CDCl_3$, 100 MHz) δ 172.70, 171.39, 171.08, 156.10 (*C*(O)O^{t}Bu × 2, *C*(O)NH amide, *C*(O)NH carbamate); 81.92, 81.37, 78.92 (*C*(CH$_3$)$_3$ × 3); 52.34 (Lys α-*C*H); 51.73 (Asp α-*C*H); 40.21 (Lys *C*H$_2$NH); 39.88 (Asp *C*H$_2$); 32.17, 29.26 (Lys *C*H$_2$ × 2); 28.45, 28.09, 28.00 (C(*C*H$_3$)$_3$ × 3); 22.29 (Lys *C*H$_2$). $\tilde{\nu}_{max}$ (cm^{-1}) (oil): 3657*w*, 3372*w* (N-H stretch); 2978*s*, 2886*m* (C-H alkyl stretch); 1713*s* (C=O ester stretch, overlapping C=O amide/carbamate stretch); 1512*s* (N-H bend); 1458*w*, 1366*s* (C-H alkyl bends); 1250*s*, 1150*s* (C-O ester and C-N stretches). ESI-MS (*m/z*): Calc. for $C_{23}H_{44}N_3O_7$ 474.3174; found: 474.3182 (100%, $[M+H]^+$). Calc. for $C_{23}H_{43}N_3NaO_7$ 496.2993; found: 496.3000 (20%, $[M+Na]^+$).

Synthesis of Z-Gly-Asp(O^{t}Bu)-Lys(Boc)-O^{t}Bu (4.30)

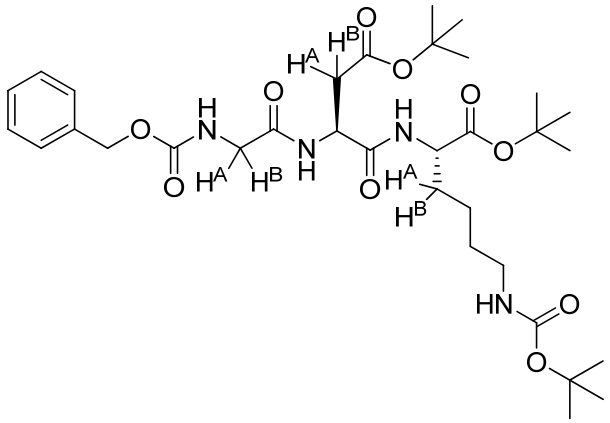

Z-Gly-OH (0.51 g, 2.45 mmol, 1.0 eq) was solubilised in DCM (20 ml) upon addition of DIPEA (0.85 ml, 4.9 mmol, 2.0 eq). The reaction flask was cooled over an ice-water bath then TBTU (0.79 g, 2.45 mmol, 1.0 eq) was added as a solid and the reaction was stirred at 0°C for 20 min before compound **4.29** (1.16 g, 2.45 mmol, 1.0 eq), dissolved in DCM (15 ml), was added in one portion and more DCM (10 ml) was used to rinse any residual **4.29** into the reaction flask. The reaction was stirred at 0°C for a further 15 min before removing the ice-water bath and stirring the reaction at rt for 3 days. The organic phase was washed successively with 1.33 M $NaHSO_4$ (150 ml), sat. $NaHCO_3$ (150 ml), 1.33 M $NaHSO_4$ (150 ml), and finally water (150 ml). The organic phase was dried over $MgSO_4$ and filtered before removing the solvent *in vacuo* to yield the product, **4.30**, as a white solid (1.44 g, 88%). No further purification was required.

R_f 0.56 (9:1, DCM/MeOH, UV and cerium stain). $[\alpha]_D$ = +1.3° (c = 1.0, $CHCl_3$). M.p not acquired. ^{1}H NMR ($CDCl_3$, 400 MHz) δ 7.42 (br d, N*H* amide, *J* = 7.5 Hz, 1H); 7.33-7.25 (m, C*H* aromatic, 5H); 7.10 (d, N*H* amide, *J* = 8.0 Hz, 1H); 5.96 (app br s, Z group N*H* carbamate, 1H); 5.09 (s, CH_2 benzylic, 2H); 4.83 (app br s, Boc group N*H* carbamate, 1H); 4.80-4.75 (m, Asp α-*H*, 1H); 4.44-4.32 (br m, Lys α-*H*, 1H); 3.92 (dd, Gly CH^A, *J* = 17.0 Hz and 5.0 Hz, 1H); 3.84 (dd, Gly CH^B, *J* = 17.0 Hz and 5.0 Hz, 1H); 3.10-2.95 (br m, Lys CH_2NH, 2H); 2.88-2.80 (app m, Asp CH^A, 1H); 2.60 (dd, Asp CH^B, *J* = 17.0 Hz and 6.0 Hz, 1H); 1.82-1.73 (m, Lys CHCH^A, 1H); 1.68-1.53 (m, Lys CHCH^B, 1H); 1.50-1.34 (m, C(CH_3)$_3$ × 3 (+ Lys CH_2), calc 29H, found 27H); 1.32-1.19 (m, Lys CH_2, 2H). ^{13}C NMR ($CDCl_3$, 100 MHz) δ 171.13, 170.91, 170.01, 169.34, 156.96, 156.15 (*C*(O)O^{t}Bu × 2, *C*(O)NH amide × 2, *C*(O)NH carbamate × 2); 136.24 (*C* aromatic); 128.58, 128.24, 128.12 (*C*H aromatic); 81.98, 81.85, 79.16 (*C*(CH$_3$)$_3$ × 3); 67.23 (*C*H$_2$ benzylic); 52.84 (Lys α-*C*H); 49.33 (Asp α-*C*H); 44.73 (Gly *C*H$_2$); 40.35 (Lys *C*H$_2$NH); 36.81 (Asp *C*H$_2$); 31.70, 29.46 (Lys *C*H$_2$ × 2); 28.49, 28.07, 28.03 (C(*C*H$_3$)$_3$ × 3); 22.39 (Lys *C*H$_2$). $\tilde{\nu}_{max}$ (cm^{-1}) (solid): 3657*w*, 3294*w* (N-H stretch); 2978*s*, 2886*w* (C-H alkyl and arene stretches); 1705*s* (C=O ester stretch); 1674*m* (C=O amide/carbamate stretch); 1512*s* (N-H bend and C=C arene stretch); 1458*w*, 1366*m* (C-H alkyl bends); 1242*s*, 1150*s*, 1049*w* (C-O ester and C-N

stretches, C-H arene bends); 972*m*, 841*w*, 756*w* (C-H arene bends). ESI-MS (*m*/*z*): Calc. for $C_{33}H_{53}N_4O_{10}$ 665.3756; found: 665.3739 (37%, $[M+H]^+$). Calc. for $C_{33}H_{52}N_4NaO_{10}$ 687.3576; found: 687.3569 (100%, $[M+Na]^+$).

Synthesis of H_2N-Gly-Asp(O^{t}Bu)-Lys(Boc)-O^{t}Bu (4.31)

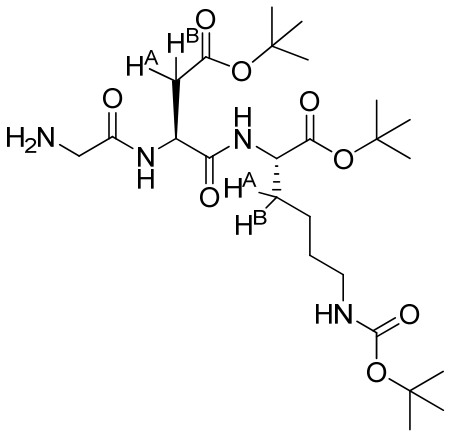

Compound **4.30** (1.3 g, 1.96 mmol) was dissolved in EtOH (25 ml) followed by the addition of Pd/C catalyst (0.26 g, 20%). The flask was subjected to several vacuum/H_2 purges and then stirred for 23 h under an atmosphere of H_2. The catalyst was filtered off over Celite, washed with MeOH, and the filtrate evaporated *in vacuo* to yield **4.31** as a white solid (0.84 g, 81%). No further purification was required.

R_f 0.28 (9:1, DCM/MeOH, cerium stain). $[\alpha]_D$ = -1.5° (c = 0.5, $CHCl_3$). M.p not acquired. ^{1}H NMR ($CDCl_3$, 400 MHz) δ 8.17 (d, N*H* amide, *J* = 8.0 Hz, 1H); 7.06 (d, N*H* amide, *J* = 7.5 Hz, 1H); 4.84 (br t, Boc group N*H* carbamate, *J* = 5.0 Hz, 1H); 4.77-4.72 (m, Asp α-*H*, 1H); 4.37-4.32 (br m, Lys α-*H*, 1H); 3.39 (app s, Gly CH_2, 2H); 3.07-2.95 (br m, Lys CH_2NH, 2H); 2.81 (dd, Asp CH^A, *J* = 17.0 Hz and 5.0 Hz, 1H); 2.60 (dd, Asp CH^B, *J* = 17.0 Hz and 7.0 Hz, 1H); 1.99 (br s, NH_2, 2H); 1.81-1.73 (m, Lys CHCH^A, 1H); 1.64-1.53 (m, Lys CHCH^B, 1H); 1.48-1.34 (m, C(CH_3)$_3$ × 3 (+ Lys CH_2), calc 29H, found 27H); 1.32-1.21 (m, Lys CH_2, 2H). ^{13}C NMR ($CDCl_3$, 100 MHz) δ 173.15, 170.98, 170.85, 170.24, 156.07 (*C*(O)O^{t}Bu × 2, *C*(O)NH amide × 2, *C*(O)NH carbamate); 82.03, 81.65, 78.99 (*C*(CH$_3$)$_3$ × 3); 52.75 (Lys α-*C*H); 49.09 (Asp α-*C*H); 44.69 (Gly *C*H$_2$); 40.26 (Lys *C*H$_2$NH); 37.10 (Asp *C*H$_2$); 31.91, 29.37 (Lys *C*H$_2$ × 2); 28.47, 28.04, 28.00 (C(*C*H$_3$)$_3$ × 3); 22.25 (Lys *C*H$_2$). $\tilde{\nu}_{max}$ (cm^{-1}) (solid): 3649*w*, 3333*w* (N-H stretch); 2978*s*, 2886*m* (C-H alkyl stretch); 1690*s* (C=O amide/carbamate stretch, overlapping C=O ester stretch); 1512*s* (N-H bend); 1458*w*, 1366*s* (C-H alkyl bends); 1250*s*, 1150*s* (C-O ester and C-N stretches). ESI-MS (*m*/*z*): Calc. for $C_{25}H_{47}N_4O_8$ 531.3388; found: 531.3402 (100%, $[M+H]^+$).

Synthesis of Z-Arg(Pbf)-Gly-Asp(O^{t}Bu)-Lys(Boc)-O^{t}Bu (4.32)

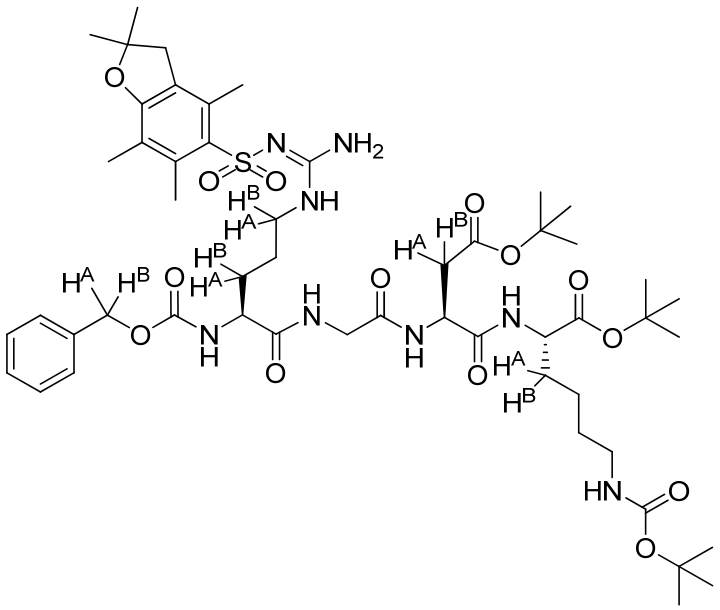

Z-Arg(Pbf)-OH.CHA (5.52 g, 8.37 mmol) was taken up in EtOAc (200 ml) and washed with $NaHSO_4$ (3 × 50 ml). The organic layer was then separated off and evaporated *in vacuo* to yield Z-Arg(Pbf)-OH as a white solid. Z-Arg(Pbf)-OH (0.85 g, 1.51 mmol, 1.0 eq) was dissolved in DCM (10 ml), cooled over an ice-water bath, followed by the addition of DIPEA (0.53 ml, 3.02 mmol, 2.0 eq) and TBTU (0.49 g, 1.51 mmol, 1.0 eq). The reaction mixture was stirred at 0°C for 10 min, then compound **4.31** (0.8 g, 1.51 mmol, 1.0 eq) was taken up in DCM (5 ml) and added in one portion to the reaction flask, and a further portion of DCM (5 ml) used to rinse any residual **4.31** into the reaction flask. The reaction was stirred at 0°C for a further 45 min before removing the ice-water bath and stirring the reaction at rt for 7 days. The organic phase was washed with 1.33 M $NaHSO_4$ (50 ml), saturated $NaHCO_3$ (50 ml), 1.33 M $NaHSO_4$ (50 ml), saturated $NaHCO_3$ (50 ml), water and finally brine. The organic phase was dried over $MgSO_4$ and filtered before removing the solvent *in vacuo* to produce the crude product as an off-white solid (~1.3 g, 80% crude yield). Purification by column chromatography (SiO_2, 100% DCM, to 98:2 DCM/MeOH, to 95:5 DCM/MeOH, to 9:1 DCM/MeOH) yielded **4.32** as a white solid (0.92 g, 57%).

R_f 0.35 (9:1, DCM/MeOH, UV and cerium stain). $[\alpha]_D$ = -11.6° (c = 0.5, $CHCl_3$). M.p not acquired. ^{1}H NMR ($CDCl_3$, 400 MHz) δ 8.00 (app br s, N*H* amide (Arg-Gly), 1H); 7.56 (br d, N*H* amide (Gly-Asp), *J* = 7.0 Hz, 1H); 7.29-7.23 (m, C*H* aromatic and N*H* amide (Asp-Lys), 6H); 6.36 (br s, N*H*$_2$ guanidine, 2H); 6.24 (br s, N*H* guanidine and Z group N*H* carbamate, 2H); 5.09 (d, C*H*^{A} benzylic, *J* = 12.5 Hz, 1H); 5.01 (d, C*H*^{B} benzylic and underlying Boc group N*H* carbamate, *J* = 12.5 Hz, 2H); 4.80-4.75 (m, Asp α-*H*, 1H); 4.37-4.21 (br m, Lys α-*H* and Arg α-*H*, 2H); 4.01-3.78 (br m, Gly C*H*$_2$, 2H); 3.39-3.22 (br m, Arg C*H*^{A}NH, 1H); 3.17-3.06 (br m, Arg C*H*^{B}NH, 1H); 3.06-2.94 (br m, Lys C*H*$_2$NH,

2H); 2.91 (s, Pbf CH_2, 2H); 2.83-2.67 (br m, Asp CH_2, 2H); 2.54 (s, Pbf CH_3Ar, 3H); 2.47 (s, Pbf CH_3Ar, 3H); 2.05 (s, Pbf CH_3Ar, 3H); 1.89-1.76 (br m, Arg CHCH^A, 1H); 1.76-1.49 (br m, Lys CH_2, Arg CHCH^B and Arg CH_2CH$_2$NH, 5H); 1.49-1.16 (m, Pbf CH_3 × 2, C(CH_3)$_3$ × 3 and Lys CH_2 × 2, calc 37H, found 36H). ^{13}C NMR ($CDCl_3$, 100 MHz) δ 173.62, 171.24, 170.80, 170.52, 169.76, 158.81, 156.69, 156.28 (*C*(O)O^{t}Bu × 2, *C*(O)NH amide × 3, *C*(O)NH carbamate × 2, Pbf aromatic *C*-O, *C*=N guanidine, calc 9 peaks, found 8 peaks); 138.40, 136.29, 132.85, 132.31 (Pbf aromatic *C* × 3 and Z group aromatic *C*); 128.53, 128.16, 128.06 (Z group aromatic *C*H × 3); 124.67, 117.56 (Pbf aromatic *C* × 2); 86.46 (Pbf CH$_2$*C*(CH$_3$)$_2$O); 81.91, 81.62, 79.10 (*C*(CH$_3$)$_3$ × 3); 67.06 (*C*H$_2$ benzylic); 54.62 (Arg α-*C*H); 53.11 (Lys α-*C*H); 49.68 (Asp α-*C*H); 43.41, 43.29 (Pbf Ar*C*H$_2$, Gly *C*H$_2$); 40.33 (Lys *C*H$_2$NH and Arg *C*H$_2$NH, multiple overlapping peaks); 36.82 (Asp *C*H$_2$); 31.37, 29.32 (Lys *C*H$_2$ × 2, Arg CH*C*H$_2$, calc 3 peaks, found 2 peaks); 28.66 (Pbf CH$_2$C(*C*H$_3$)$_2$O); 28.51, 28.03, 28.00 (C(*C*H$_3$)$_3$ × 3); 25.44 (Arg *C*H$_2$CH$_2$NH); 22.64 (Lys *C*H$_2$); 19.39, 18.05, 12.54 (Pbf Ar*C*H$_3$ × 3). $\tilde{\nu}_{max}$ (cm^{-1}) (solid): 3657*w*, 3333*w* (N-H stretches); 2978*s*, 2886*m* (C-H alkyl and arene stretches); 1690*s* (C=O amide/carbamate stretch, overlapping C=O ester stretch); 1512*s* (N-H bend and C=C arene stretch); 1450*m*, 1366*m* (C-H alkyl bend and S=O stretch); 1250*s*, 1150*s*, 1088*s* (C-O ester and C-N stretches, C-H arene bends); 957*m*; 849*w*, 779*w* (C-H arene bends). ESI-MS (*m*/*z*): Calc. for $C_{52}H_{81}N_8O_{14}S$ 1073.5587; found: 1073.5533 (100%, $[M+H]^+$).

Synthesis of H$_2$N-Arg(Pbf)-Gly-Asp(O^{t}Bu)-Lys(Boc)-O^{t}Bu (4.33)

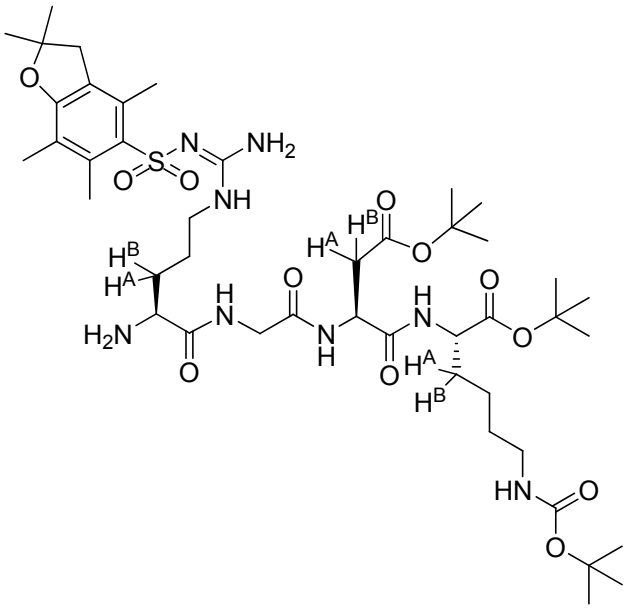

Compound **4.32** (0.9 g, 0.84 mmol) was dissolved in EtOH (10 ml) followed by the addition of Pd/C catalyst (0.18 g, 20%). The flask was subjected to several vacuum/H_2 purges and then stirred for 2 days under an atmosphere of H_2. TLC indicated presence of starting material so more Pd/C catalyst (0.18 g, 20%, 40% in total) was added and the reaction stirred for a further 4 days. The catalyst was

filtered off over Celite, washed with MeOH, and the filtrate evaporated *in vacuo* to yield **4.33** as a white solid (0.74 g, 94%). No further purification was required.

R_f 0.26 (9:1, DCM/MeOH, UV and cerium stain). $[\alpha]_D$ = -3.2° (c = 1.0, MeOH). M.p not acquired. ^{1}H NMR (CD_3OD, 400 MHz) δ 4.83-4.73 (m, Asp α-*H*, 1H); 4.28-4.18 (br m, Lys α-*H*, 1H); 4.02-3.94 (br m, Gly CH_2 and Arg α-*H*, 3H); 3.29-3.19 (m, Arg CH_2NH, 2H); 3.05-2.97 (br m, Lys CH_2NH and Pbf CH_2, 4H); 2.81 (dd, Asp CH^A, *J* = 16.5 Hz and 5.5 Hz, 1H); 2.63 (dd, Asp CH^B, *J* = 16.5 Hz and 7.5 Hz, 1H); 2.56 (s, Pbf CH_3Ar, 3H); 2.51 (s, Pbf CH_3Ar, 3H); 2.08 (s, Pbf CH_3Ar, 3H); 1.97-1.87 (br m, Arg CHCH^A and Lys CHCH^A, 2H); 1.84-1.76 (br m, Arg CHCH^B or Lys CHCH^B, 1H); 1.73-1.60 (br m, Arg CHCH^B or Lys CHCH^B, and Arg CH_2CH$_2$NH, 3H); 1.53-1.26 (m, Pbf CH_3 × 2, C(CH_3)$_3$ × 3 and Lys CH_2 × 2, calc 37H, found 35H). ^{13}C NMR (CD_3OD, 100 MHz) δ 172.65, 171.29, 170.90, 170.74, 159.99, 158.50, 158.10 (*C*(O)O^{t}Bu × 2, *C*(O)NH amide × 3, *C*(O)NH carbamate, Pbf aromatic *C*-O, *C*=N guanidine, calc 8 peaks, found 7 peaks); 139.44, 134.01, 133.60, 126.10, 118.52 (Pbf aromatic *C* × 5); 87.76 (Pbf CH$_2$*C*(CH$_3$)$_2$O); 82.94, 82.55, 79.89 (*C*(CH$_3$)$_3$ × 3); 54.61 (Lys α-*C*H); 54.07 (Arg α-*C*H); 51.21 (Asp α-*C*H); 43.98, 43.25 (Pbf Ar*C*H$_2$, Gly *C*H$_2$); 41.15 (Lys *C*H$_2$NH and Arg *C*H$_2$NH, multiple overlapping peaks); 38.32 (Asp *C*H$_2$); 32.22, 30.44, 29.55 (Lys *C*H$_2$ × 2 and Arg CH*C*H$_2$); 28.87, 28.77, 28.37, 28.31 (Pbf CH$_2$C(*C*H$_3$)$_2$O and C(*C*H$_3$)$_3$ × 3); 25.83 (Arg *C*H$_2$CH$_2$NH); 24.06 (Lys *C*H$_2$); 19.66, 18.46, 12.57 (Pbf Ar*C*H$_3$ × 3). $\tilde{\nu}_{max}$ (cm^{-1}) (solid): 3649*w* (N-H stretch); 2978*s*, 2886*m* (C-H alkyl stretch); 1690*m* (C=O amide/carbamate stretch, overlapping C=O ester stretch); 1551*m* (N-H bend and C=C arene stretch); 1450*m*, 1366*s* (C-H alkyl bend and S=O stretch); 1250*s*, 1150*s*, 1088*s* (C-O ester and C-N stretches). ESI-MS (*m*/*z*): Calc. for $C_{44}H_{75}N_8O_{12}S$ 939.5220; found: 939.5189 (100%, $[M+H]^+$).

Synthesis of C12-urea-Arg(Pbf)-Gly-Asp(O^{t}Bu)-Lys(Boc)-O^{t}Bu (4.34)

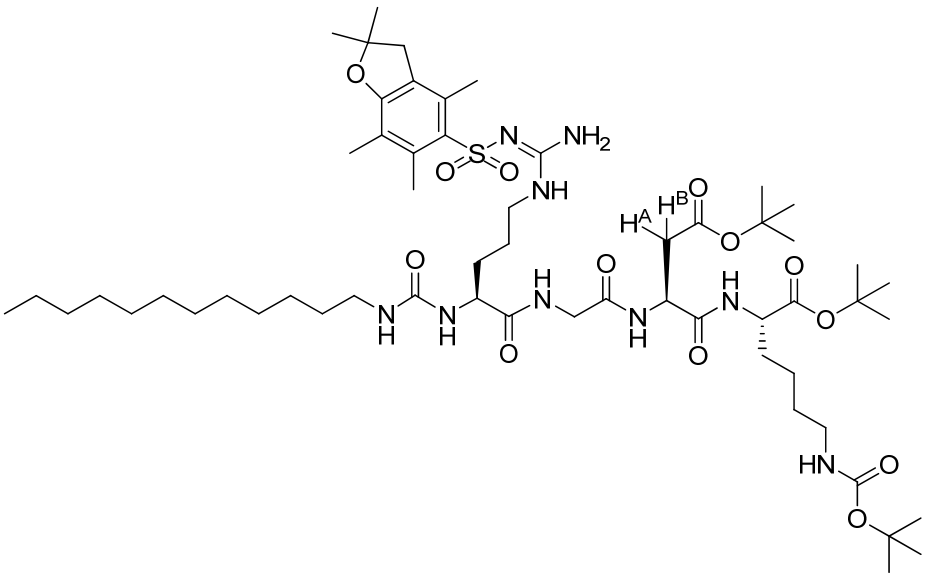

Compound **4.33** (200 mg, 0.21 mmol, 1.0 eq) was dissolved in DCM (2.5 ml) then dodecyl isocyanate (90 mg, 0.43 mmol, 2.0 eq), solubilised in DCM (1 ml), was added rapidly and a further portion of DCM (1.5 ml) was used to wash any residual isocyanate into the reaction flask. The reaction was stirred for 15 h at rt, then the solvent was removed *in vacuo* to yield a crude oil/white solid. The crude material was dissolved in the minimum amount of DCM/MeOH (95:5) and purified by column chromatography (SiO_2, 95:5 DCM/MeOH) yielding **4.34** as a fluffy, white solid (110 mg, 45%).

R_f 0.43 (9:1, DCM/MeOH, UV and cerium stain). $[\alpha]_D$ = -9.2° (c = 0.5, MeOH). M.p not acquired. ^{1}H NMR (CD_3OD, 400 MHz) δ 4.80 (dd, Asp α-*H*, *J* = 8.0 Hz and 5.0 Hz, 1H); 4.22-4.19, 4.09-4.06 (m, Lys α-*H* and Arg α-*H*, 2H); 3.87 (app s, Gly C*H*$_2$, 2H); 3.28-2.96 (br m, Arg C*H*$_2$NH, C12 C*H*$_2$NHC(O)NH, Lys C*H*$_2$NH, and Pbf C*H*$_2$, 8H); 2.88 (dd, Asp C*H*^{A}, *J* = 16.5 Hz and 5.5 Hz, 1H); 2.68 (dd, Asp C*H*^{B}, *J* = 17.0 Hz and 8.5 Hz, 1H); 2.58 (s, Pbf C*H*$_3$Ar, 3H); 2.52 (s, Pbf C*H*$_3$Ar, 3H); 2.08 (s, Pbf C*H*$_3$Ar, 3H); 1.85-1.22 (br m, Arg CHC*H*$_2$, Arg C*H*$_2$CH$_2$NH, Lys C*H*$_2$ × 3, Pbf C*H*$_3$ × 2, C(C*H*$_3$)$_3$ × 3, C12 C*H*$_2$ × 10, calc 63H, found 64H). ^{13}C NMR (CD_3OD, 100 MHz) δ 176.59, 172.72, 172.53, 171.69, 171.36, 160.68, 159.90, 158.43, 158.16 (*C*(O)O^{t}Bu × 2, *C*(O)NH amide × 3, *C*(O)NH urea, *C*(O)NH carbamate, Pbf aromatic *C*-O, *C*=N guanidine); 139.43, 134.32, 133.54, 126.02, 118.45 (Pbf aromatic *C* × 5); 87.69 (Pbf CH$_2$*C*(CH$_3$)$_2$O); 82.80, 82.34, 79.83 (*C*(CH$_3$)$_3$ × 3); 55.91, 54.69 (Lys α-*C*H and Arg α-*C*H); 51.28 (Asp α-*C*H); 44.04, 43.82 (Pbf Ar*C*H$_2$, Gly *C*H$_2$); 41.32, 41.21, 41.17 (Lys *C*H$_2$NH, Arg *C*H$_2$NH and C12 *C*H$_2$NHC(O)NH); 38.19 (Asp *C*H$_2$); 33.10, 32.16, 31.30, 30.79, 30.56, 30.51, 30.43, 30.23 (C12 *C*H$_2$'s and Arg CH*C*H$_2$, multiple overlapping peaks); 28.92, 28.82, 28.42, 28.35 (Pbf CH$_2$C(*C*H$_3$)$_2$O and C(*C*H$_3$)$_3$ × 3); 28.08, 26.97, 24.07, 23.77 (C12 *C*H$_2$'s and Arg *C*H$_2$CH$_2$NH, multiple overlapping peaks); 19.72, 18.54 (Pbf Ar*C*H$_3$ × 2); 14.54 (C12 *C*H$_3$); 12.65 (Pbf Ar*C*H$_3$ × 1). $\tilde{\nu}_{max}$ (cm^{-1}) (solid): 3649*w*, 3341*w* (N-H stretches); 2978*s*, 2886*m* (C-H alkyl stretch); 1690*m* (C=O amide/carbamate/urea stretch, overlapping C=O ester stretch); 1551*m* (N-H bend and C=C arene stretch); 1450*m*, 1366*s* (C-H alkyl bend and S=O stretch); 1250*s*, 1150*s*, 1088*s* (C-O ester and C-N stretches). ESI-MS (*m*/*z*): Calc. for $C_{57}H_{100}N_9O_{13}S$ 1150.7156; found: 1150.7165 (100%, $[M+H]^+$).

Synthesis of C12-urea-Arg-Gly-Asp-Lys (4.35)

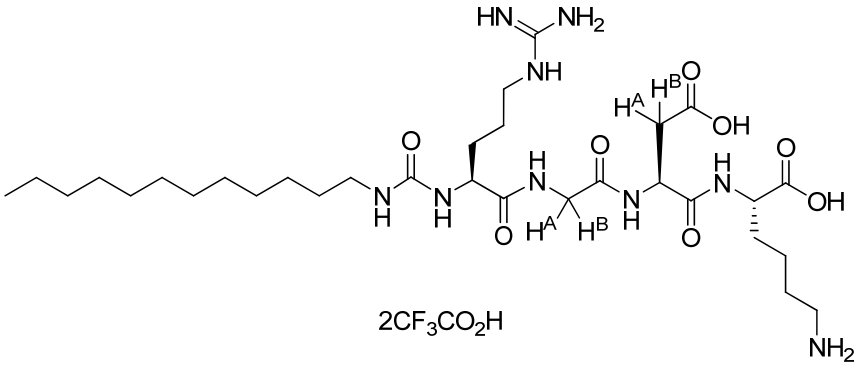

Compound **4.34** (90 mg, 78 μmol) was dissolved in a mixture of TFA, water and TIS (2 ml, 95:2.5:2.5) and shaken for 2 h, after which time TLC indicated that the deprotection reaction was complete. The reaction mixture was cooled over an ice-water bath, precipitated with cold Et_2O, filtered and washed with the minimum amount of cold Et_2O and dried *in vacuo*. The sample was then dissolved in a mixture of water/^{t}BuOH, filtered over a PTFE membrane filter (0.2 μm), shell frozen and lyophilised to yield the product, **4.35**, as a fluffy, white powder (40 mg, 56% as TFA salt).

R_f 0.00 (9:1, DCM/MeOH, cerium stain). $[\alpha]_D$ = -9.0° (c = 0.1, DMSO). M.p not acquired. ^{1}H NMR (CD_3OD, 400 MHz) δ 4.74 (dd, Asp α-*H*, *J* = 8.0 Hz and 5.5 Hz, 1H); 4.41 (dd, Lys α-*H*, *J* = 10.0 and 4.0 Hz, 1H); 4.08 (app m, Arg α-*H*, 1H); 3.91 (d, Gly C*H*^{A}, *J* = 17.0 Hz, 1H); 3.85 (d, Gly C*H*^{B}, *J* = 17.0 Hz, 1H); 3.28-3.05 (m, Arg C*H*$_2$NH, C12 C*H*$_2$NHC(O)NH, 4H); 2.96 (t, Lys C*H*$_2$NH, *J* = 7.0 Hz, 2H); 2.92 (dd, Asp C*H*^{A}, *J* = 17.0 Hz and 5.0 Hz, 1H); 2.81 (dd, Asp C*H*^{B}, *J* = 17.0 Hz and 8.0 Hz, 1H); 2.02-1.23 (br m, Arg CHC*H*$_2$, Arg C*H*$_2$CH$_2$NH, Lys C*H*$_2$ × 3, C12 C*H*$_2$ × 10, calc 30H, found 28H); 0.90 (t, C12 C*H*$_3$, *J* = 7.0 Hz, 3H). ^{13}C NMR (CD_3OD, 100 MHz) δ 176.98, 174.98, 174.15, 173.04, 172.13, 160.97, 158.71 (*C*OOH × 2, *C*ONH amide × 3, *C*(O)NH urea, *C*=N guanidine); 55.90, 53.35 (Lys α-*C*H and Arg α-*C*H); 51.58 (Asp α-*C*H); 43.91 (Gly *C*H$_2$); 41.99, 41.25, 40.66 (Lys *C*H$_2$NH, C12 *C*H$_2$NHC(O)NH and Arg *C*H$_2$NH); 36.45 (Asp *C*H$_2$); 33.13, 31.81, 31.40, 31.16, 30.85, 30.64, 30.54, 30.25, 28.14, 27.86, 26.14, 23.79, 23.63 (C12 *C*H$_2$ × 10, Arg CH*C*H$_2$, Arg *C*H$_2$CH$_2$NH and Lys *C*H$_2$ × 3, multiple overlapping peaks); 14.50 (C12 *C*H$_3$). $\tilde{\nu}_{max}$ (cm^{-1}, solid): 3649*w*, 3364*w* (O-H acid and N-H stretches); 2978*s*, 2886*m* (C-H alkyl stretches); 1651*m* (C=O amide/urea stretch, overlapping C=O acid stretch); 1574*s* (N-H bend); 1381*m* (C-H alkyl bend); 1250*m*, 1142*s*, 1080*s* (C-O acid and C-N stretches). ESI-MS (*m*/*z*): Calc. for $C_{31}H_{60}N_9O_8$ 686.4559; found: 686.4568 (12%, $[M+H]^+$); 343.7310 (100%, $[M+2H]^{2+}$).

Synthesis of C12-amide-Arg(Pbf)-Gly-Asp(O^{t}Bu)-Lys(Boc)-O^{t}Bu (4.36)

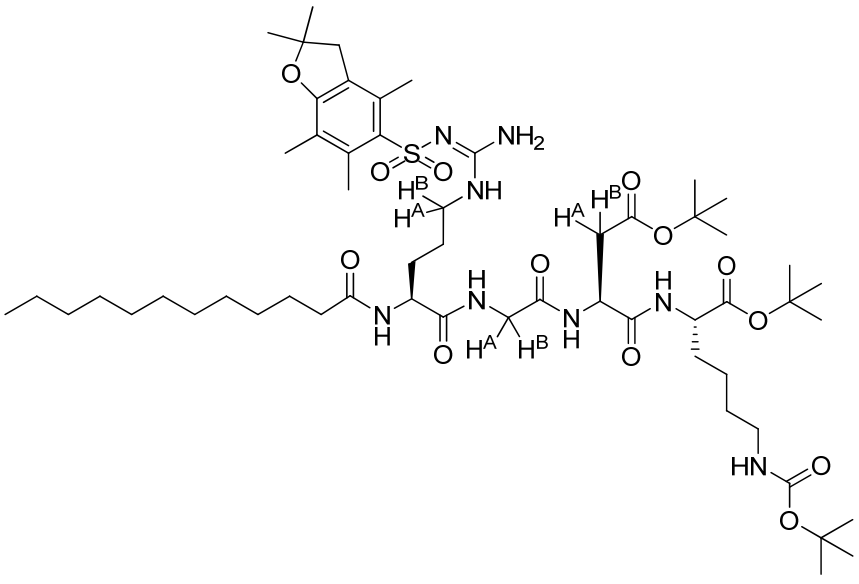

Compound **4.33** (200 mg, 0.21 mmol, 1.0 eq) was dissolved in DCM (4 ml), then lauric acid (43 mg, 0.21 mmol, 1.0 eq) and DIPEA (74 μL, 0.42 mmol, 2.0 eq) were solubilised in DCM (3 ml) and added to the reaction flask. The flask was cooled over an ice-water bath and then TBTU (70 mg, 0.21 mmol, 1.0 eq) was added as a solid and more DCM (3 ml) was used to transfer any residual TBTU to the reaction flask. The reaction was stirred at 0°C for 20 min before removing the ice-water bath and stirring at rt for 3 days. The reaction was worked up with 1.33 M $NaHSO_4$ (30 ml), saturated $NaHCO_3$ (30 ml), 1.33 M $NaHSO_4$ (30 ml), and finally brine (30 ml). The organic phase was dried over $MgSO_4$ and filtered before removing the solvent *in vacuo* to produce the crude product as a white solid (230 mg, 96% crude yield). Purification by column chromatography (SiO_2, 100% DCM, to 98:2 DCM/MeOH, to 95:5 DCM/MeOH) yielded **4.36** as a white solid (180 mg, 75%).

R_f 0.33 (9:1, DCM/MeOH, UV and cerium stain). $[\alpha]_D$ = -7.3° (c = 0.5, MeOH). M.p not acquired. ^{1}H NMR (CD_3OD, 400 MHz) δ 4.78 (dd, Asp α-*H*, *J* = 8.0 Hz and 5.5 Hz, 1H); 4.28-4.19 (m, Lys α-*H* and Arg α-*H*, 2H); 3.93 (d, Gly C*H*^{A}, *J* = 17.0 Hz, 1H); 3.84 (d, Gly C*H*^{B}, *J* = 17.0 Hz, 1H); 3.29-3.20 (br m, Arg C*H*^{A}NH, 1H); 3.19-3.12 (m, Arg C*H*^{B}NH, 1H); 3.07-2.94 (br m, Lys C*H*$_2$NH and Pbf C*H*$_2$, 4H); 2.86 (dd, Asp C*H*^{A}, *J* = 16.5 Hz and 5.5 Hz, 1H); 2.69 (dd, Asp C*H*^{B}, *J* = 17.0 Hz and 8.0 Hz, 1H); 2.58 (s, Pbf C*H*$_3$Ar, 3H); 2.52 (s, Pbf C*H*$_3$Ar, 3H); 2.26 (t, C12 C*H*$_2$C(O)NH, *J* = 7.0 Hz, 2H); 2.08 (s, Pbf C*H*$_3$Ar, 3H); 1.88-1.21 (br m, Arg CHC*H*$_2$, Arg C*H*$_2$CH$_2$NH, Lys C*H*$_2$ × 3, Pbf C*H*$_3$ × 2, C(C*H*$_3$)$_3$ × 3, C12 C*H*$_2$ × 9, calc 61H, found 60H). ^{13}C NMR (CD_3OD, 100 MHz) δ 176.62, 175.21, 172.68, 172.51, 171.49, 171.31, 159.88, 158.42, 158.12 (*C*(O)O^{t}Bu × 2, *C*(O)NH amide × 4, *C*(O)NH carbamate, Pbf aromatic *C*-O, *C*=N guanidine); 139.42, 134.37, 133.52, 125.99, 118.42 (Pbf aromatic *C* × 5); 87.67 (Pbf CH$_2$*C*(CH$_3$)$_2$O); 82.78, 82.35, 79.81 (*C*(CH$_3$)$_3$ × 3); 55.04, 54.62 (Lys α-*C*H and Arg α-*C*H); 51.25 (Asp α-*C*H); 44.03, 43.74 (Pbf Ar*C*H$_2$, Gly *C*H$_2$); 41.30, 41.18 (Lys *C*H$_2$NH and Arg *C*H$_2$NH); 38.14 (Asp *C*H$_2$); 36.68 (C12 *C*H$_2$C(O)NH); 33.10, 32.16, 30.80, 30.77, 30.70, 30.52, 30.44, 29.63 (C12 *C*H$_2$'s, Arg CH*C*H$_2$, and Lys *C*H$_2$ × 2, multiple overlapping peaks); 28.91, 28.83, 28.41, 28.34 (Pbf CH$_2$C(*C*H$_3$)$_2$O and C(*C*H$_3$)$_3$ × 3); 26.77, 24.06, 23.77 (C12 *C*H$_2$'s, Arg *C*H$_2$CH$_2$NH and Lys *C*H$_2$, multiple overlapping peaks); 19.74, 18.56 (Pbf Ar*C*H$_3$ × 2); 14.55 (C12 *C*H$_3$); 12.67 (Pbf Ar*C*H$_3$ × 1). $\tilde{\nu}_{max}$ (cm^{-1}) (solid): 3657*w* (N-H stretches); 2978*s*, 2886*m* (C-H alkyl stretch); 1697*m* (C=O amide/carbamate stretch, overlapping C=O ester stretch); 1505*w* (N-H bend and C=C arene stretch); 1458*w*, 1373*s* (C-H alkyl bend and S=O stretch); 1250*s*, 1150*s*, 1088*s* (C-O ester and C-N stretches). ESI-MS (*m*/*z*): Calc. for $C_{56}H_{97}N_8O_{13}S$ 1121.6890; found: 1121.6819 (100%, $[M+H]^+$).

Synthesis of C12-amide-Arg-Gly-Asp-Lys (4.37)

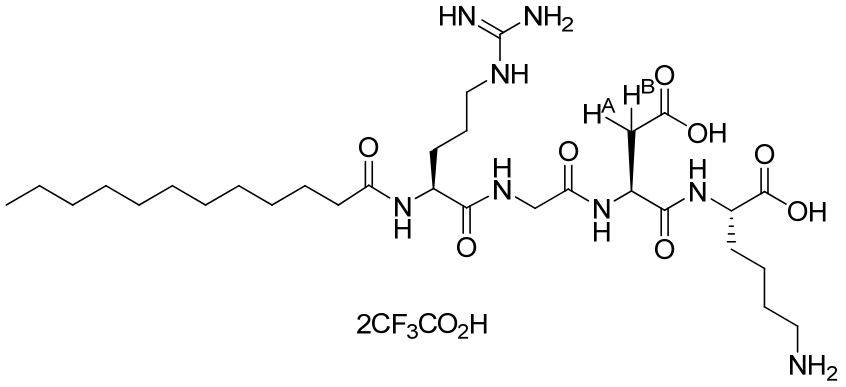

Compound **4.36** (200 mg, 0.18 mmol) was dissolved in a mixture of TFA, water and TIS (2 ml, 95:2.5:2.5) and shaken for 2 h, after which time TLC indicated that the deprotection reaction was complete. The reaction mixture was cooled over an ice-water bath, precipitated with cold Et_2O, filtered and washed with the minimum amount of cold Et_2O and dried *in vacuo*. The sample was then dissolved in a mixture of water/^{t}BuOH, filtered over a PTFE membrane filter (0.2 μm), shell frozen and lyophilised to yield the product, **4.37**, as a fluffy, white powder (102 mg, 65% as TFA salt).

R_f 0.00 (9:1, DCM/MeOH, cerium stain). $[\alpha]_D$ = +16.0° (c = 0.1, DMSO). M.p not acquired. ^{1}H NMR (CD_3OD, 400 MHz) δ 4.73 (dd, Asp α-*H*, *J* = 7.5 Hz and 5.5 Hz, 1H); 4.41 (dd, Lys α-*H*, *J* = 9.5 and 4.5 Hz, 1H); 4.28 (dd, Arg α-*H*, *J* = 8.5 and 5.0 Hz, 1H); 3.90 (app s, Gly CH_2, 2H); 3.22 (t, Arg CH_2NH, *J* = 6.0 Hz, 2H); 2.97 (t, Lys CH_2NH, *J* = 7.0 Hz, 2H); 2.90 (dd, Asp CH^A, *J* = 17.0 Hz and 5.0 Hz, 1H); 2.82 (dd, Asp CH^B, *J* = 17.0 Hz and 8.0 Hz, 1H); 2.31 (t, C12 CH_2C(O)NH, *J* = 7.0 Hz, 2H); 2.00-1.24 (br m, Arg CHCH_2, Arg CH_2CH$_2$NH, Lys CH_2 × 3, C12 CH_2 × 9, calc 28H, found 25H); 0.90 (t, C12 CH_3, *J* = 7.0 Hz, 3H). ^{13}C NMR (CD_3OD, 100 MHz) δ 177.07, 175.48, 175.01, 174.17, 173.07, 172.03, 158.67 (*C*OOH × 2, *C*ONH amide × 4, *C*=N guanidine); 55.04, 53.36 (Lys α-*C*H and Arg α-*C*H); 51.57 (Asp α-*C*H); 43.88 (Gly *C*H$_2$); 41.83, 40.66 (Lys *C*H$_2$NH and Arg *C*H$_2$NH); 36.77 (Asp *C*H$_2$); 36.49 (C12 *C*H$_2$C(O)NH); 33.13, 31.75, 31.16, 30.82, 30.75, 30.60, 30.55, 30.51, 29.68, 27.83, 26.87, 26.14, 23.79, 23.65 (C12 *C*H$_2$ × 9, Arg CH*C*H$_2$, Arg *C*H$_2$CH$_2$NH and Lys *C*H$_2$ × 3, multiple overlapping peaks); 14.51 (C12 *C*H$_3$). $\tilde{\nu}_{max}$ (cm^{-1}, solid): 3657*w*, 3341*w* (O-H acid and N-H stretches); 2978*s*, 2886*m* (C-H alkyl stretches); 1643*s* (C=O amide stretch, overlapping C=O acid stretch); 1512*m* (N-H bend); 1389*m* (C-H alkyl bend); 1250*m*, 1142*s*, 1080*s* (C-O acid and C-N stretches). ESI-MS (*m*/*z*): Calc. for $C_{30}H_{57}N_8O_8$ 657.4294; found: 657.4292 (23%, $[M+H]^+$); 329.2185 (100%, $[M+2H]^{2+}$).

6.5 Procedures

Fluorescence Polarisation Assays

The FP competition experiment was adapted from a literature method.[75] To demonstrate that the probe **2.24** could bind integrin and produce a FP response, 10 nM of the probe was assayed as a function of increasing concentration of integrin (Chapter 2 - Fig. 2.3). When no integrin was present the FP signal was around 35 mP (milli polarisation units). This is the background signal from intrinsic polarisation of the probe. This increased to over 100 mP when the concentration of integrin was more than 400 nM. This was envisaged as more integrin is available for binding to the probe and hence more [probe:protein] complex is formed. The calibration curve provides evidence that **2.24** binds to integrin $\alpha_v\beta_3$. The binding was found to be fast; incubating the mixed samples for longer than 5 min did not have any significant effect on the FP signal (data not shown).

A solution of 187 μM **2.24** in PBS buffer (0.01 M phosphate, pH 7.4, 0.138 M NaCl, 0.0027 M KCl) was diluted with Tris buffer (50 mM TRIS, pH 7.4, 1 mM $CaCl_2$, 10 μM $MnCl_2$, 1 mM $MgCl_2$, 100 mM NaCl) to give a 100 nM stock. The assay mixture (200 μl in a 100 μl volume fluorescence microcuvette) was composed of 280 nM integrin $\alpha_v\beta_3$ (13.25 μg) and 10 nM **2.24** in TRIS buffer.

Competition experiments were performed with the synthetic ligands, with **PEG-GGG** (**2.20**) and SDS serving as negative controls. Stocks of these compounds were made in PBS and diluted in the TRIS assay buffer to the desired concentration in the final stock titre (100 μl), which also contained 280 nM integrin $\alpha_v\beta_3$ (6.625 μg) and 10 nM **2.24**. The titre was incubated at 29°C in a water bath for at least 5 min before carrying out the titration experiment. The titre was added to the assay mixture in microlitre aliquots, the cuvette gently shaken and incubated at 29°C for at least 5 min, and then the single-point FP value recorded using λ_{ex} = 485 nm, λ_{em} = 510 nm, while incubation of the stock titre was resumed at 29°C in between titrations. **2.24** alone (10 nM) served as control and all subsequent data with the protein present was normalised to 100 mP units using this value. All data points are presented as mean values ± standard deviations from at least 5 independent scans. The mP values were plotted against synthetic ligand concentration in Microsoft Excel and the concentration at which 50% inhibition of probe **2.24**'s binding to integrin $\alpha_v\beta_3$ was achieved (IC_{50}) was extrapolated at 50 mP units from the normalised data.

Nile Red Assays

The Nile Red encapsulation experiment was adapted from previously published methods.[270, 312] To monitor the aggregation behaviour of the self-assembling surfactants in aqueous solution, encapsulation experiments with the hydrophobic dye Nile Red were carried out. The Nile Red

concentration was kept constant while a range of surfactant concentrations were examined, and the fluorescence emission of the dye was monitored.

A stock solution of the surfactant was made in PBS buffer. Aliquots of the stock were taken and diluted to the desired concentration to make 1 ml assay samples in PBS buffer. A 2.5 mM Nile Red (technical grade, Sigma) stock solution was made in EtOH and diluted ~1000-fold in the surfactant assay samples (i.e. 1 μL was added to a 1 ml surfactant assay sample), swirled, and the fluorescence emission measured immediately after mixing. Nile Red fluorescence was measured at room temperature using an excitation wavelength of 550 nm. Fluorescence emission was monitored from 550 to 700 nm at 1 nm intervals. Data are presented as mean values from 3 independent experiments.

The critical aggregation concentration (CAC) was calculated by plotting the absorption of Nile Red at λ_{max} against the log of the surfactant concentration (e.g. Chapter 3 – Fig. 3.5), setting the equation from each of the two trendlines as equal to one another and solving for x at the turning point. As x is log concentration, 10^x yields the CAC in mol dm^{-3}.

TEM

Samples were 'drop-cast' onto a standard heat-treated (HT) copper TEM grid using either a Gilson pipette or a spatula, and allowed to equilibrate for several minutes before excess liquid was wicked off with filter paper and left to dry for 15-30 min prior to imaging. If the sample was deposited from buffered solution, the grids were washed with a few drops of deionised water to wash off crystallised salt from the buffer, and excess liquid was wicked off with filter paper and left to dry for 15-30 min prior to imaging. Depending on the sample, a few drops of a uranyl acetate stain (1% in water, pH 4.5) was sometimes used for contrast, as denoted in each figure. Excess stain was wicked off with filter paper and then allowed to dry for 10-15 minutes. Imaging was performed immediately afterwards.

SEM

A small portion of the gel was removed with a spatula and placed on a copper support, then freeze-dried by immersing in liquid nitrogen and then placing under high vacuum overnight. Excess solid material was broken off with a spatula and then the sample was sputter coated with a thin layer (about 12 nm) of gold/palladium to prevent sample charging, before placing the sample on a metal SEM stub and imaging.

ASEM

A small portion of the gel was removed with a spatula and placed on an ASEM thin film dish. The sample was negatively stained with uranyl acetate (1% in water, pH 4.5) and glucose (10 mg/ml in

water) was deposited on the sample to act as a free radical scavenger. Imaging was performed immediately afterwards.

T_{gel}'s

Eppendorf tubes containing different concentrations of freshly prepared gel samples were placed in a high precision thermoregulated oil bath and heated from 20°C at a rate of 1°C min^{-1}. The temperature at which the gel collapsed was deemed the gel-sol transition end-point.

Circular Dichroism

CD samples were prepared by heating the hydrogel to a homogenous suspension and then quickly transferring this hot sample (~400 μL using a Gilson pipette) into the quartz CD cuvette (1 mm pathlength) and allowing the sample to cool to rt for several minutes until gelation was complete. CD spectra were then ascertained for the different concentrations of hydrogel using the following parameters:

Temperature: 20°C
Sensitivity: Standard (100mdeg)
Start: 300nm
End: 200nm
Data Pitch: 1 nm
Scanning Mode: Continuous
Scan Speed: 100nm/min
Response: 1 sec
Band Width: 2nm
Accumulation: 5

A CD spectrum of Millipore pure water at 20°C was subtracted from the CD spectrum of each sample.

VT-CD was carried out on a 1 mg/ml **C12-[urea-RGD]$_2$** hydrogel sample, and the parameters were as follows:

Start: 30 °C
End: 90 °C
Data Pitch: 10 °C
Delay Time: 120 sec
Temperature Slope: 5 °C/min

Sensitivity: Standard (100mdeg)
Response: 1 sec
Band Width: 2nm
Wavelength Settings: Same settings as for the 20°C scan.
Delay (Equilibration) Time: 300 sec

A CD spectrum of Millipore pure water at 20°C was subtracted from the CD spectrum of the sample at each temperature.

VT-NMR

Solid gelator was deposited in an NMR tube, then 0.5 ml of D_2O (+0.05 wt% TSP-d_4 as internal standard) was added, the sample was heated vigorously until a homogenous suspension formed and allowed to cool to rt to initiate gelation. Analysis was performed overnight on a JEOL ECX400 NMR spectrometer, at temperatures ranging from 25 to 90°C with 5°C increments.

Small Molecule Encapsulation-Release

Fluorescent molecule encapsulation was studied by using aqueous solutions of two different fluorescent molecules: fluorescein (Sigma) and FITC-dextran with an average MW of 70,000 g mol^{-1} (Sigma). Fluorescein was pre-dissolved in DMSO (0.25 M) before diluting with Millipore pure water to 50 μM. FITC-dextran was dissolved directly in Millpore pure water to 50 μM. These solutions were used to prepare the two gel samples. A 1 ml gel (5 mg/ml) was prepared in an eppendorf tube by using 5 mg of gelator, dissolving it in 200 μL of DMSO and then gently adding 800 μL of one of the fluorescent solutions, capturing all of the aqueous solution in the gel. Next, 1 ml of Millipore pure water was pipetted on top of the gel which was replaced with fresh water every 5 min and the fluorescence emission of the water removed was measured (excitation at 495 nm, 1 nm slit, emission at 512 nm for fluorescein and 521 nm for FITC-dextran, 2 nm slit).

Appendix

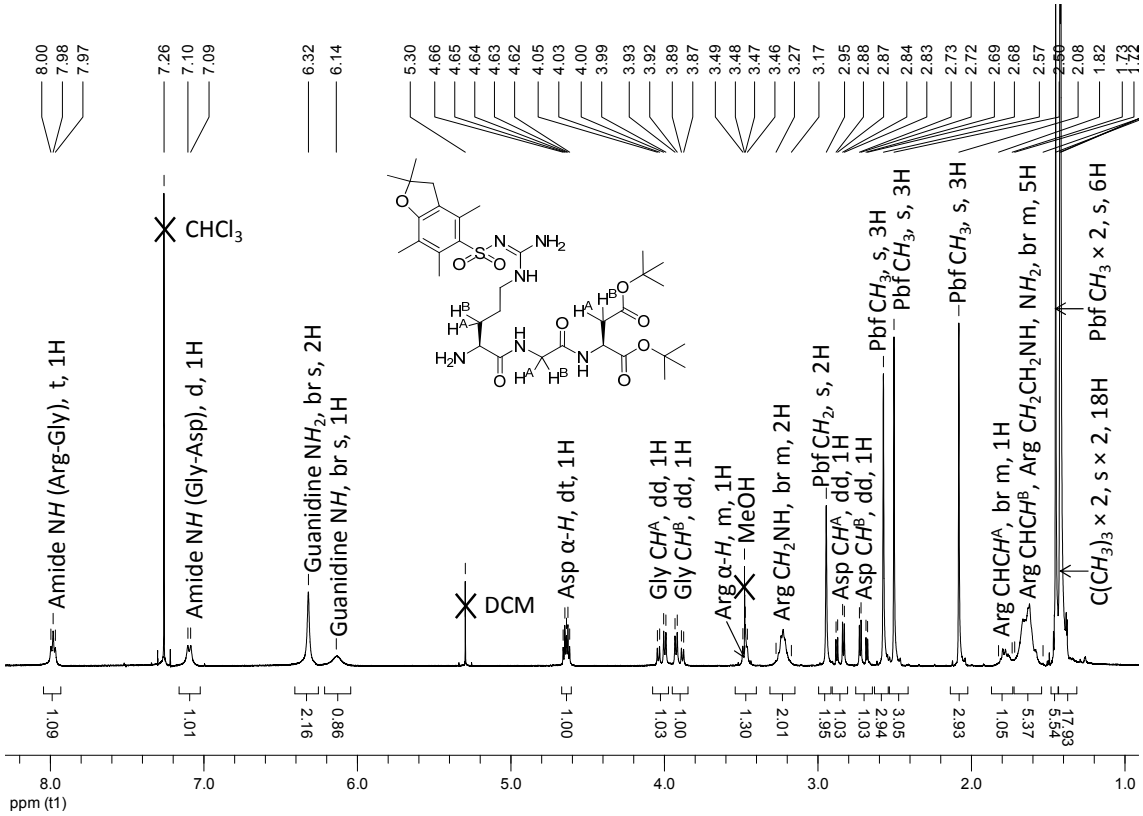

Spectrum 2.1 – ^{1}H NMR spectrum of H_2N-Arg(Pbf)-Gly-Asp(O^{t}Bu)-O^{t}Bu (**2.4**), in $CDCl_3$.

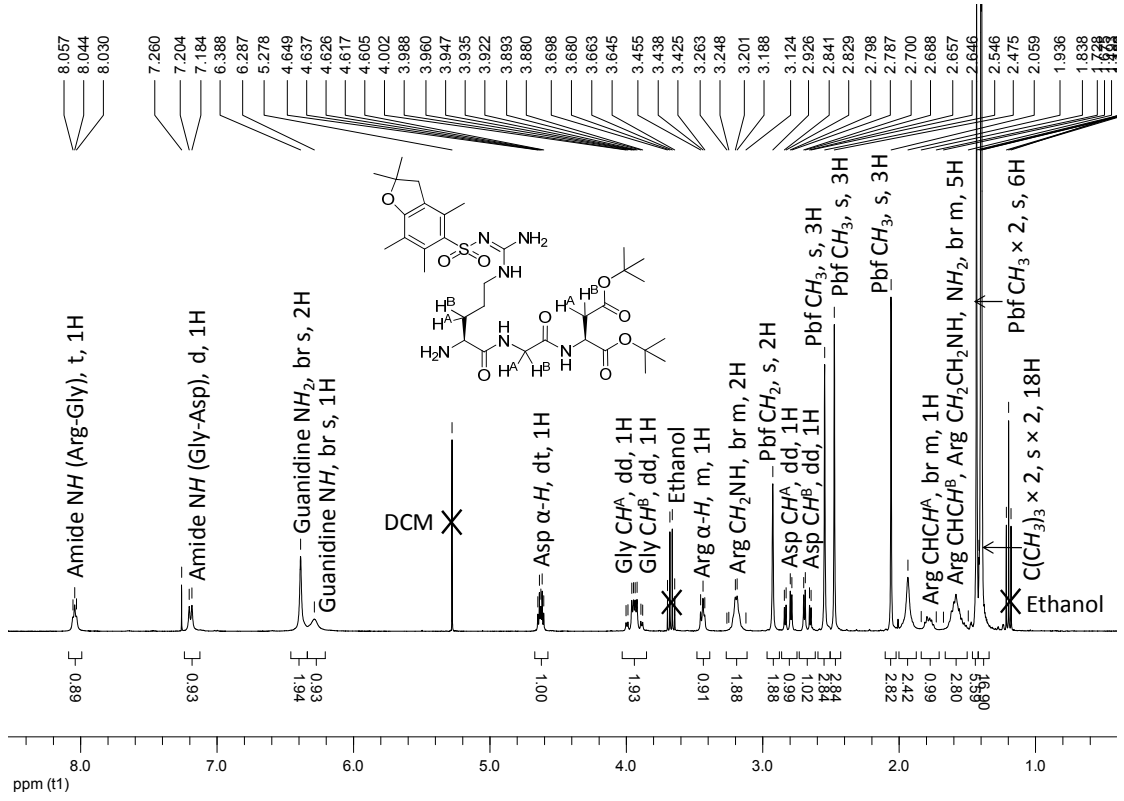

Spectrum 2.2 – ^{1}H NMR spectrum of H_2N-Arg(Pbf)-Gly-Asp(O^{t}Bu)-O^{t}Bu (**2.8**), in $CDCl_3$.

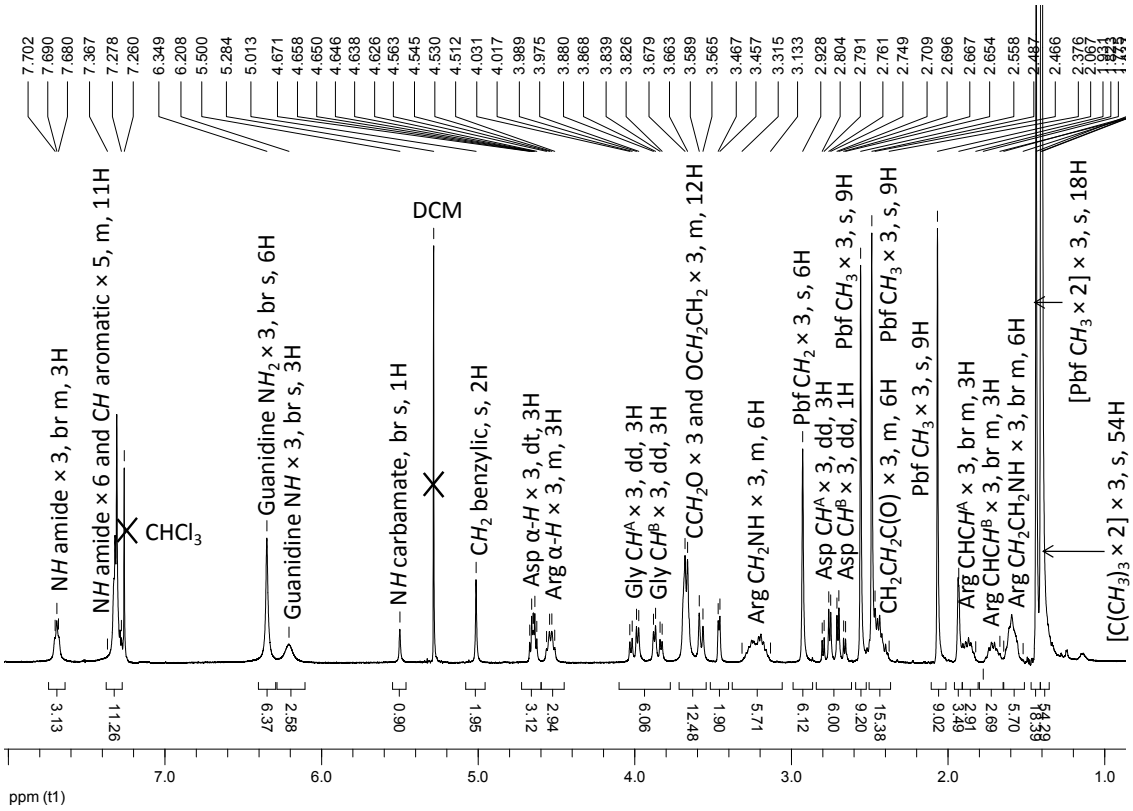

Spectrum 2.3 – ^{1}H NMR spectrum of **2.14**, in $CDCl_3$.

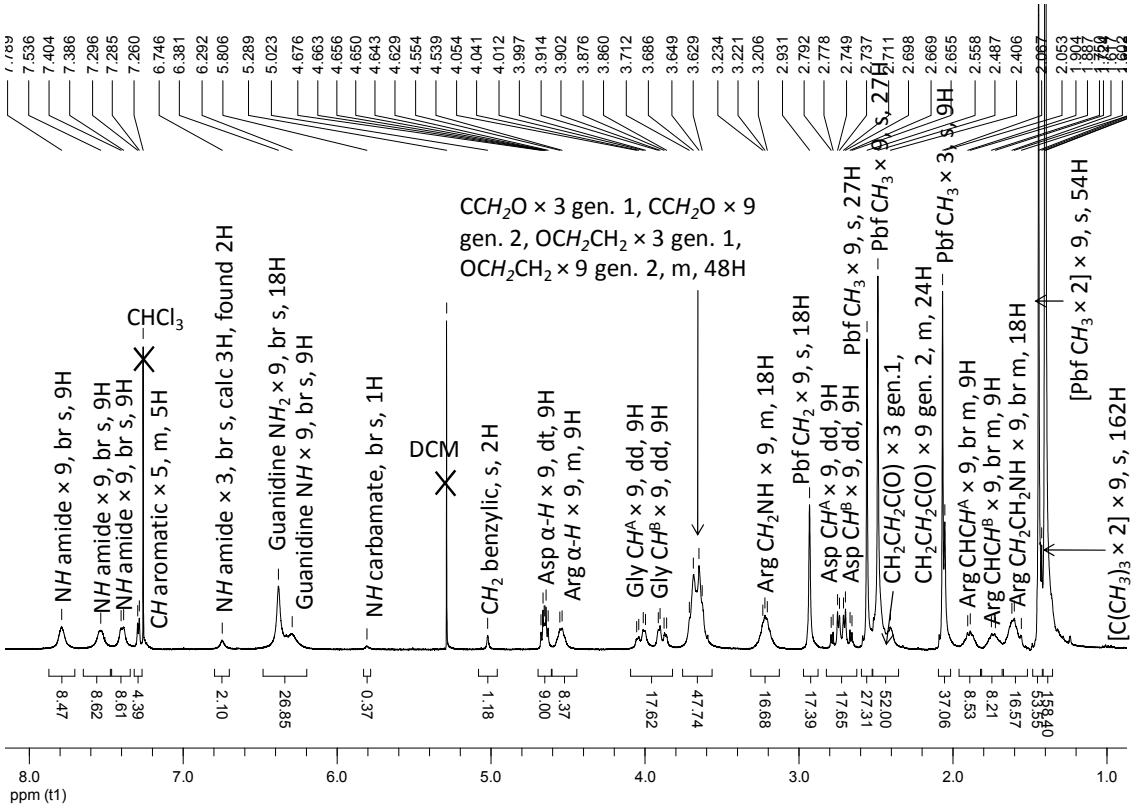

Spectrum 2.4 – ^{1}H NMR spectrum of **2.15**, in $CDCl_3$.

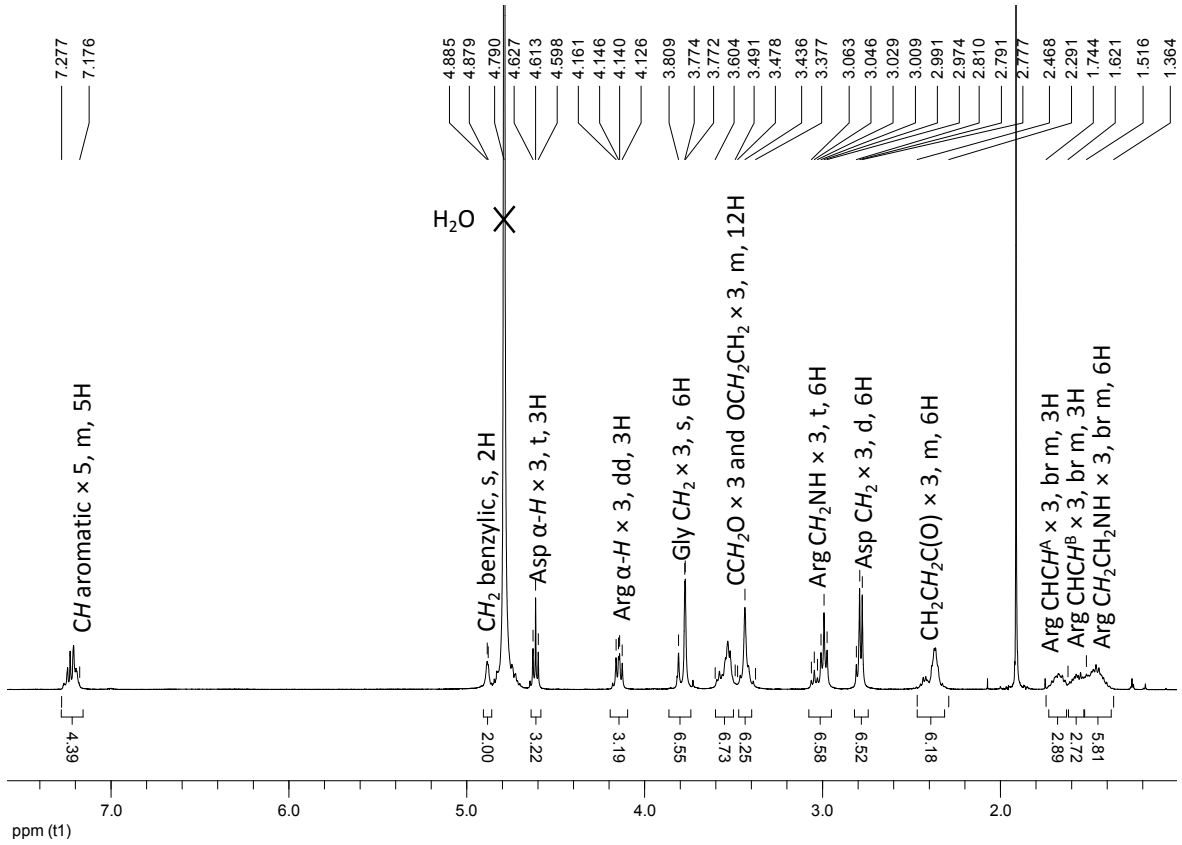

Spectrum 2.5 – ^{1}H NMR spectrum of **2.16**, in D_2O.

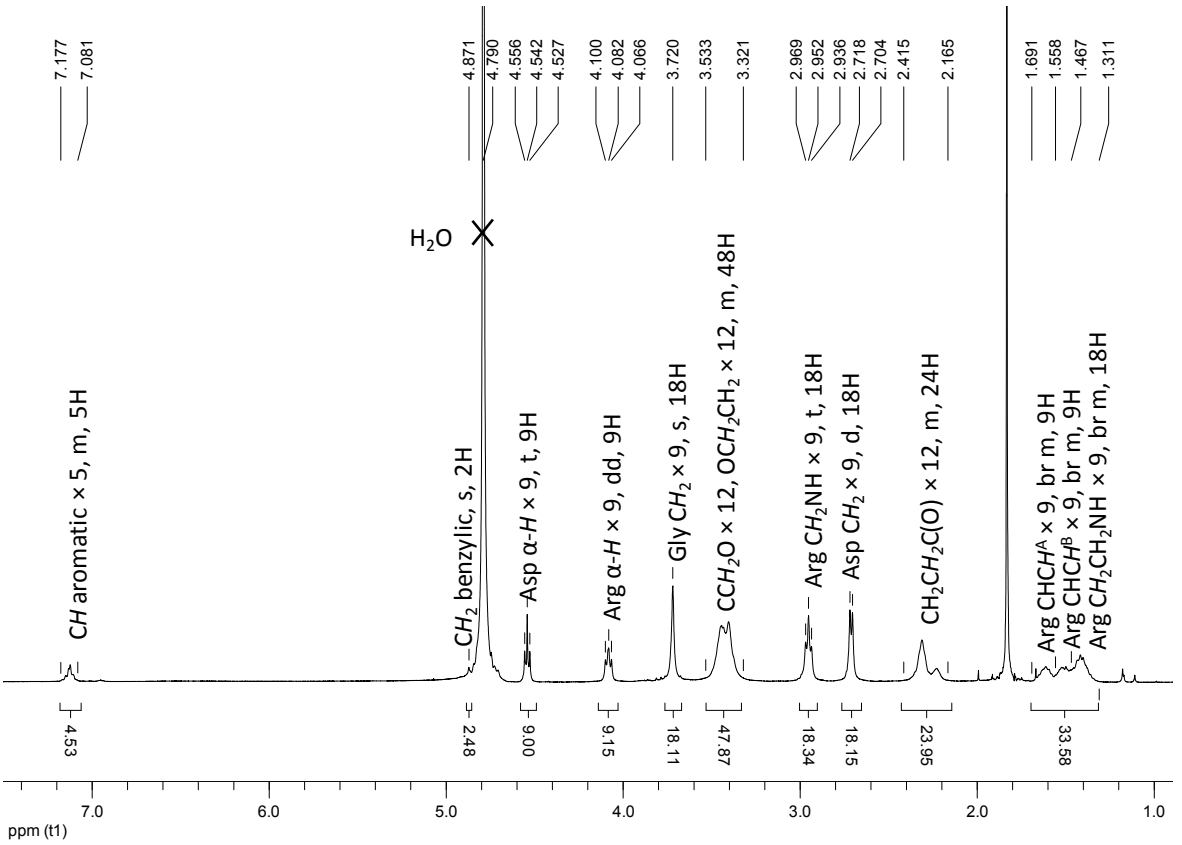

Spectrum 2.6 – ^{1}H NMR spectrum of **2.17**, in D_2O.

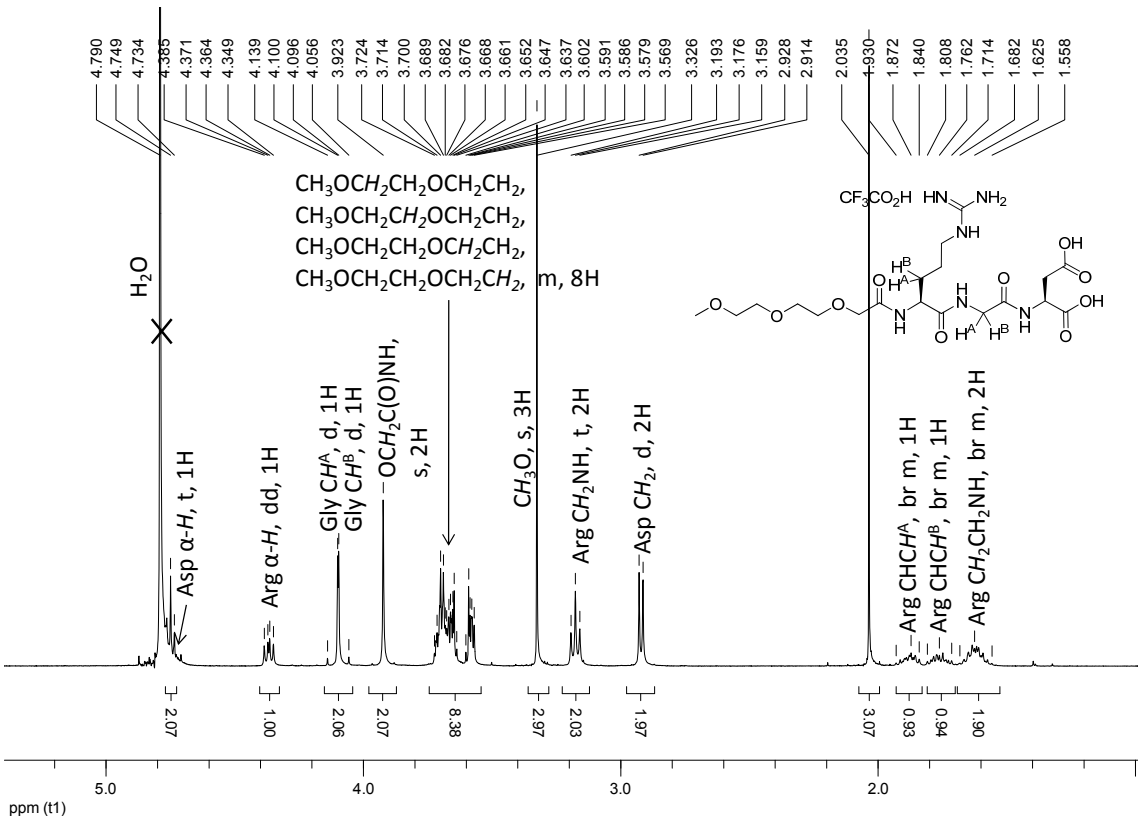

Spectrum 2.7 – ^{1}H NMR spectrum of **PEG-RGD** (**2.19**), in D_2O.

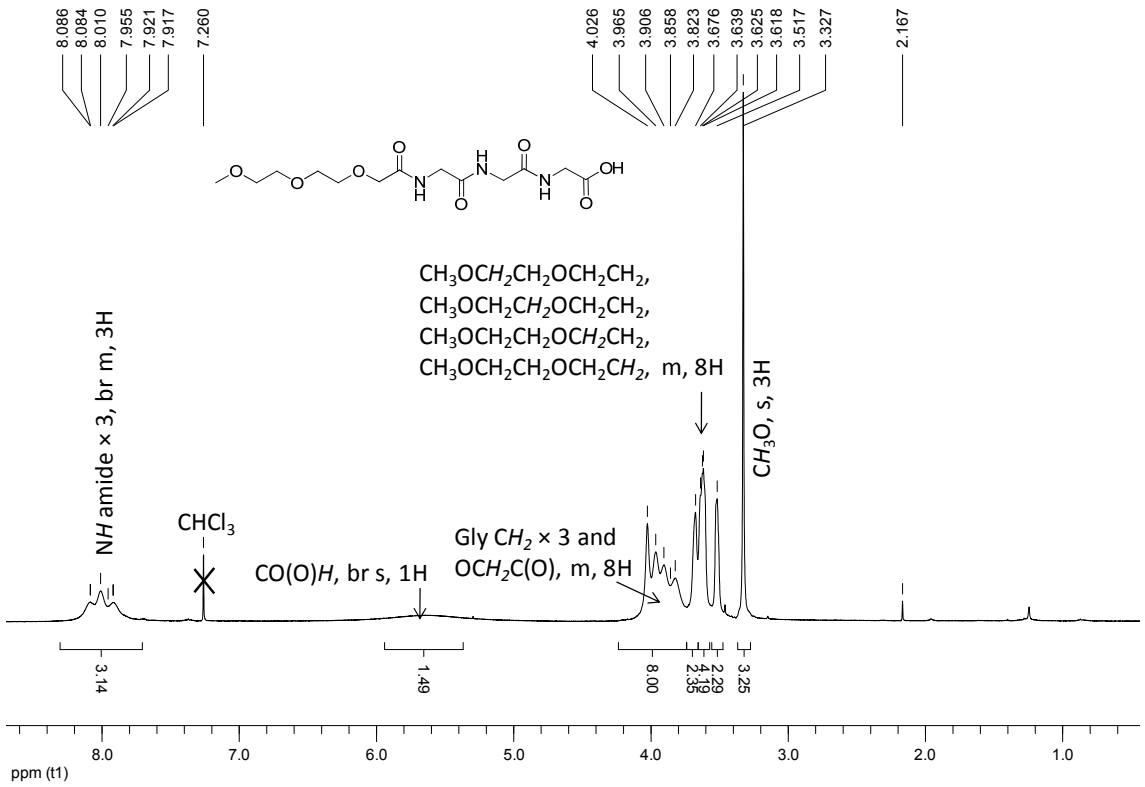

Spectrum 2.8 – ^{1}H NMR spectrum of **PEG-GGG** (**2.20**), in $CDCl_3$.

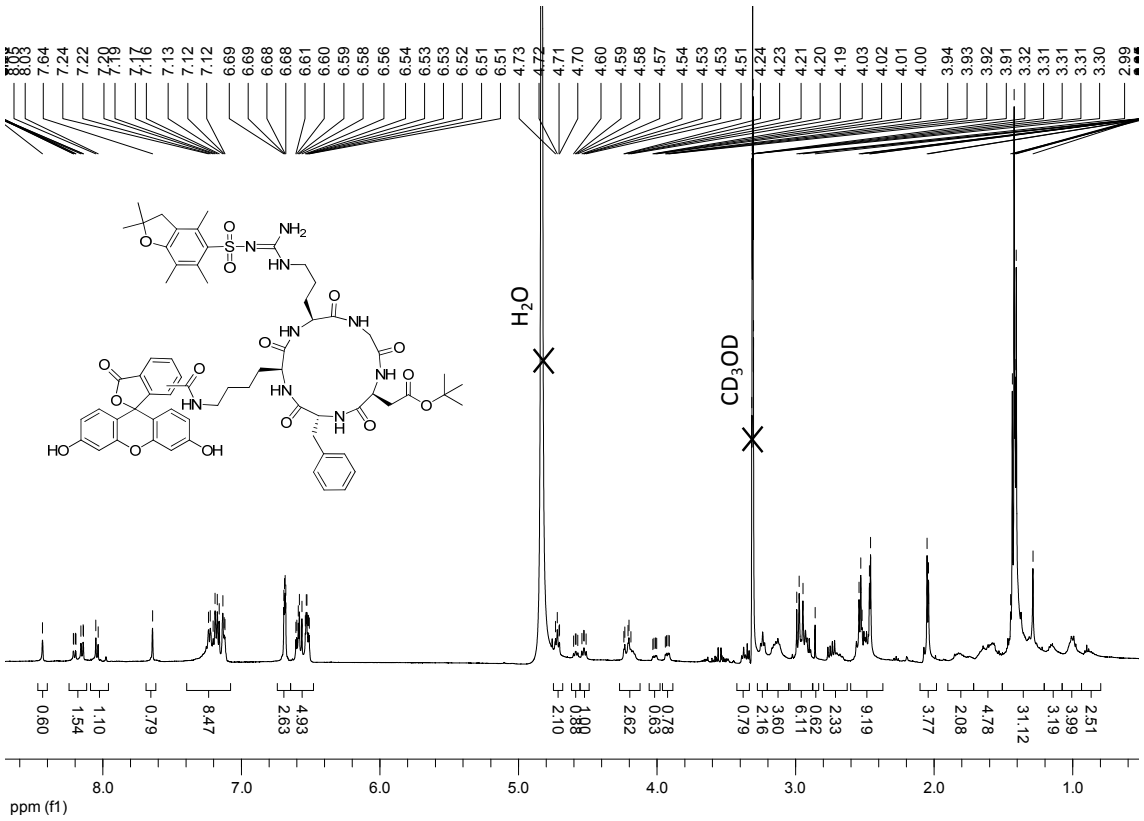

Spectrum 2.9 – ^{1}H NMR spectrum of **2.23**, in CD_3OD.

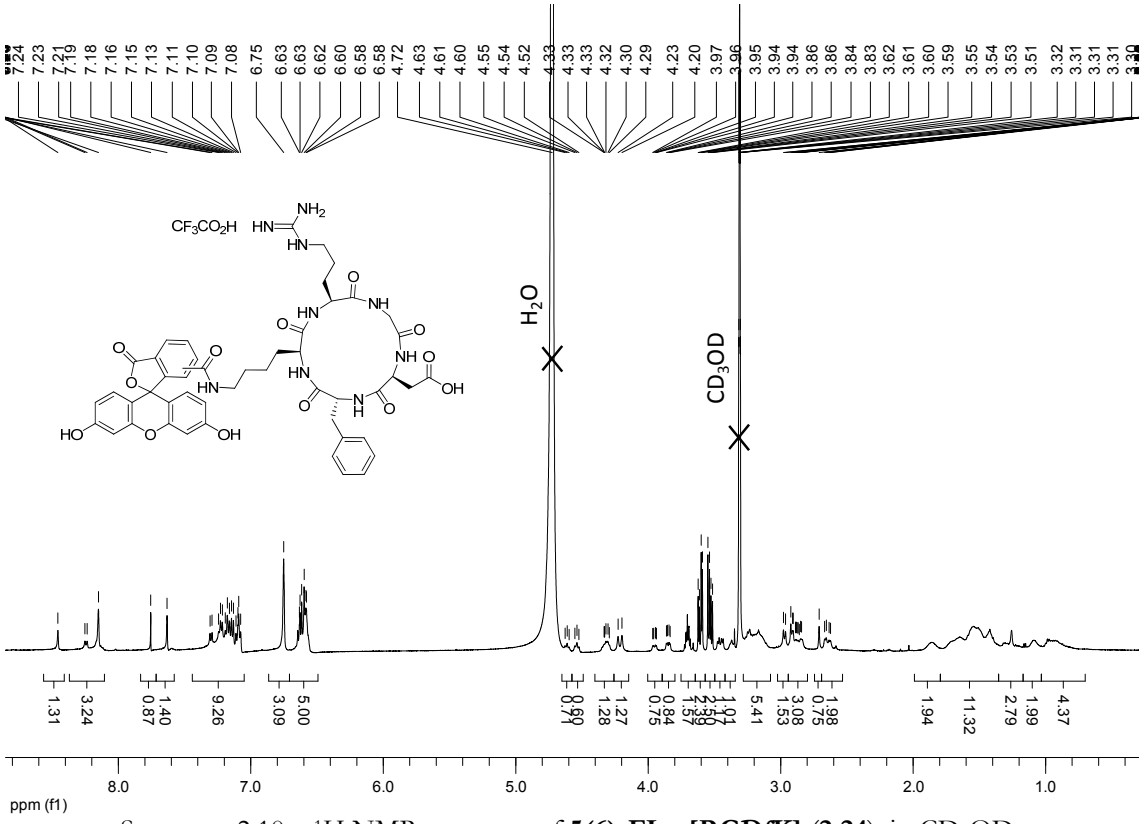

Spectrum 2.10 – ^{1}H NMR spectrum of **5(6)-FL-c[RGDfK]** (**2.24**), in CD_3OD.

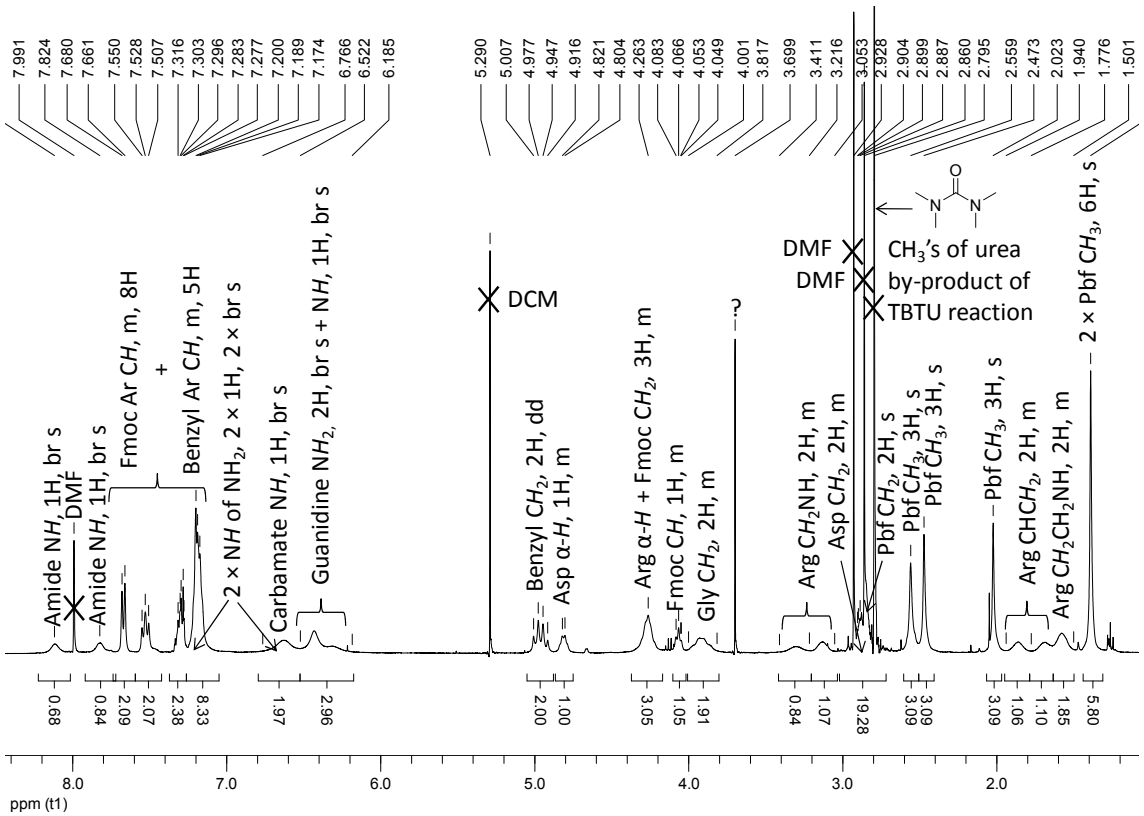

Spectrum 2.11 – ^{1}H NMR spectrum of **2.32**, in $CDCl_3$.

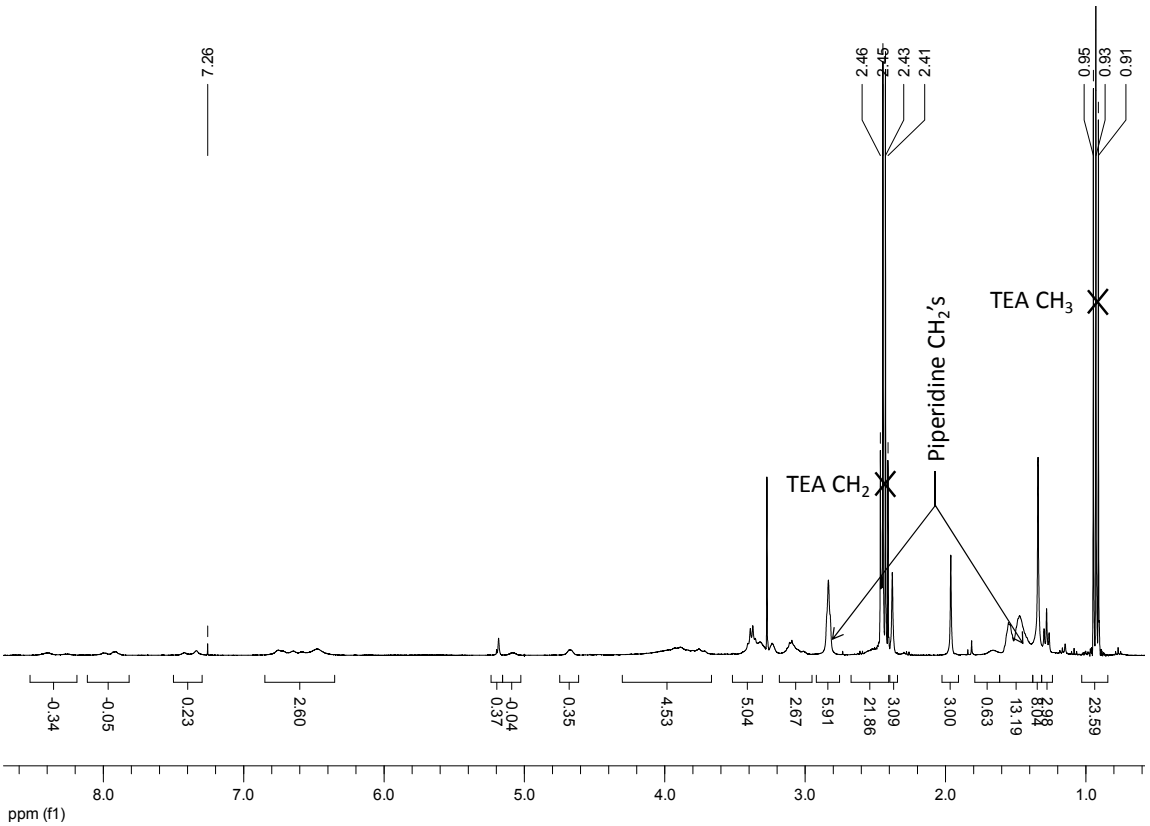

Spectrum 2.12 – ^{1}H NMR spectrum of the material isolated from the deprotection of **2.32** following silica column purification, in $CDCl_3$.

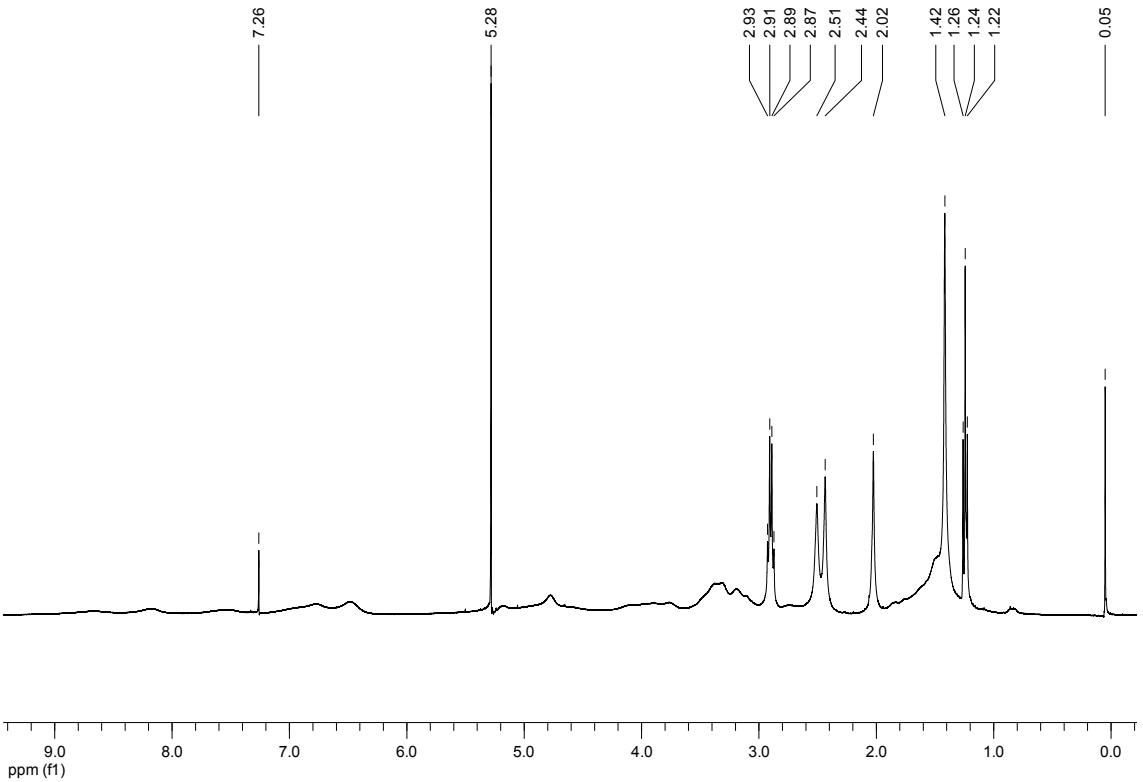

Spectrum 2.13 – ^{1}H NMR spectrum of the material shown in spectrum 2.12 following an aqueous workup, in $CDCl_3$.

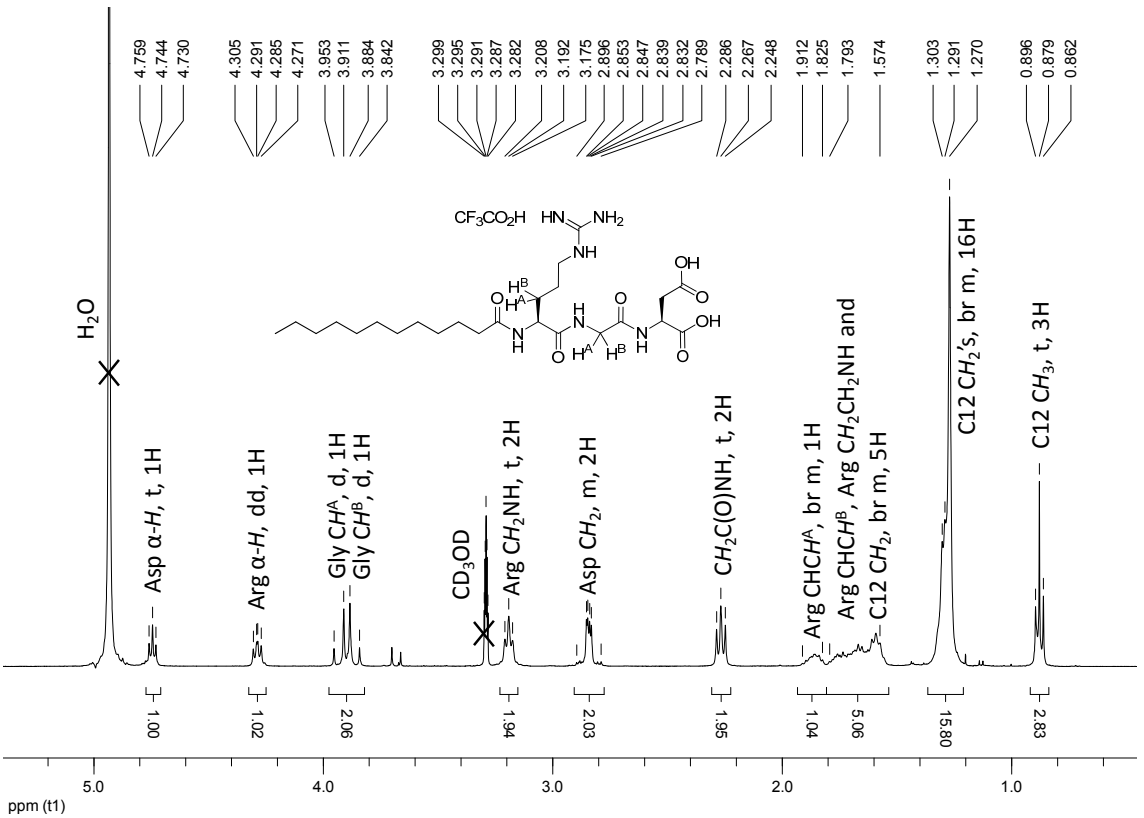

Spectrum 3.1 – ^{1}H NMR spectrum of **C12-RGD** (**3.2**), in CD_3OD.

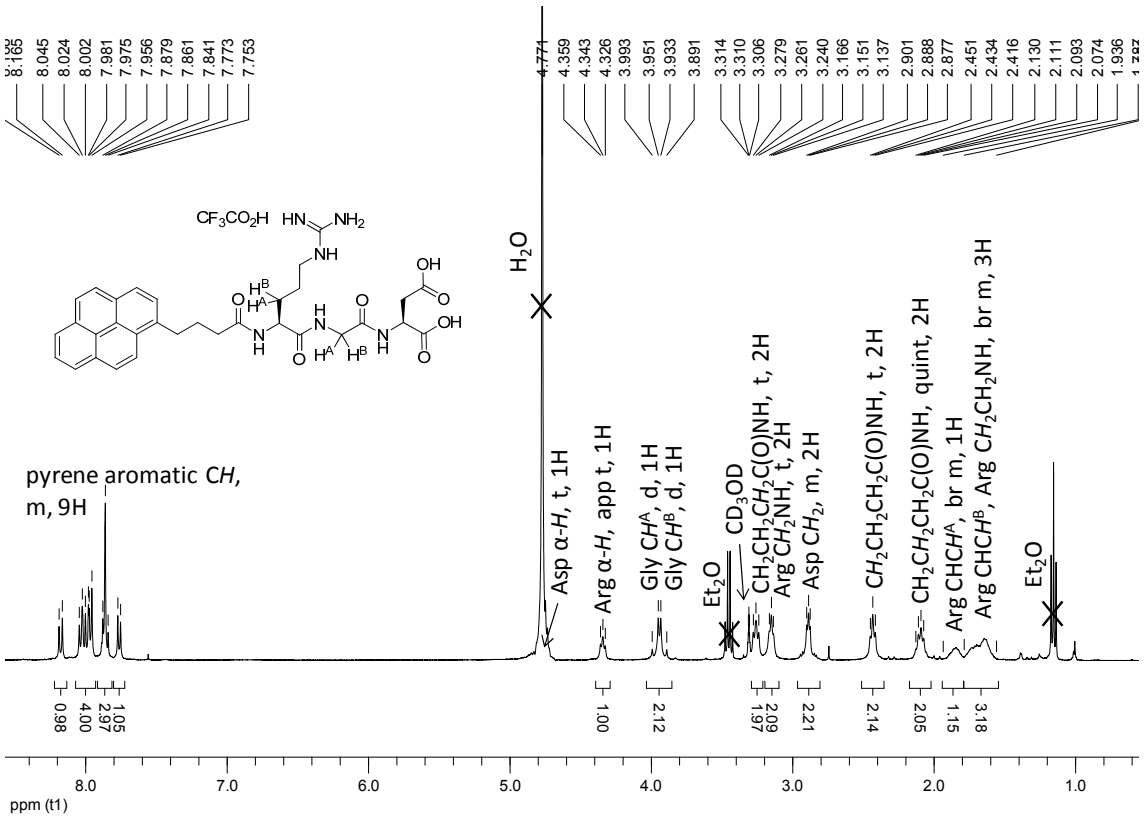

Spectrum 3.2 – ^{1}H NMR spectrum of **Py-RGD** (**3.4**), in a mixture of $CDCl_3$, CD_3OD and D_2O.

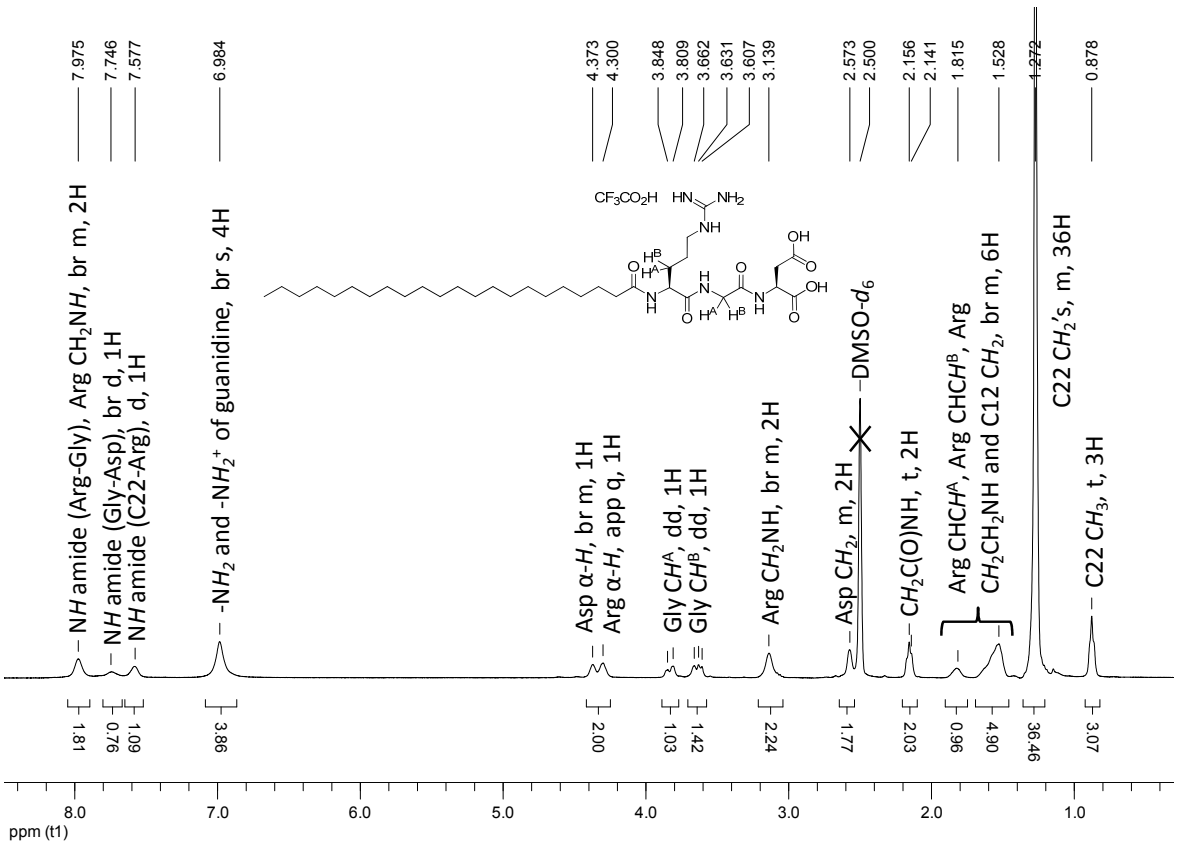

Spectrum 3.3 – ^{1}H NMR spectrum of **C22-RGD** (**3.6**), in DMSO-d_6.

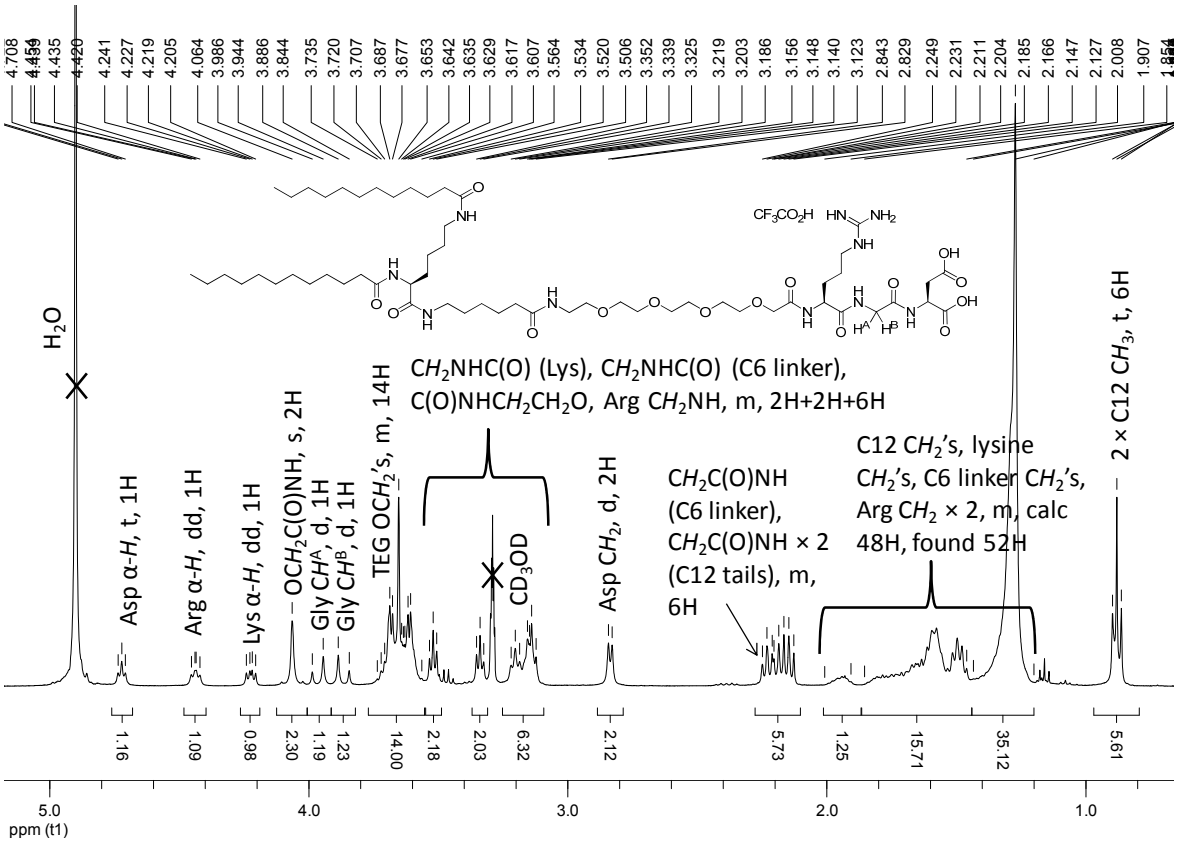

Spectrum 3.4 – ^{1}H NMR spectrum of **C12-Lys(C12)-(CH$_2$)$_5$-TEG-RGD** (**3.18**), in CD$_3$OD.

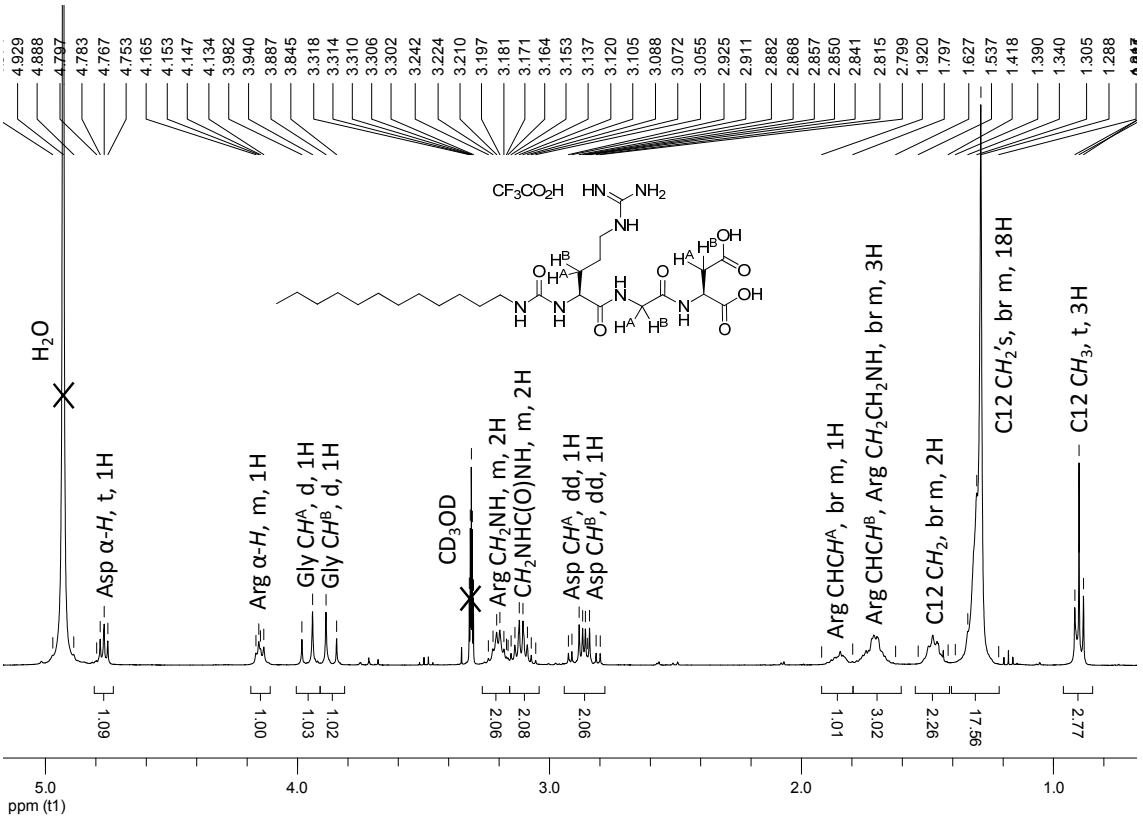

Spectrum 4.1 – ^{1}H NMR spectrum of **C12-urea-RGD** (**4.2**), in CD$_3$OD.

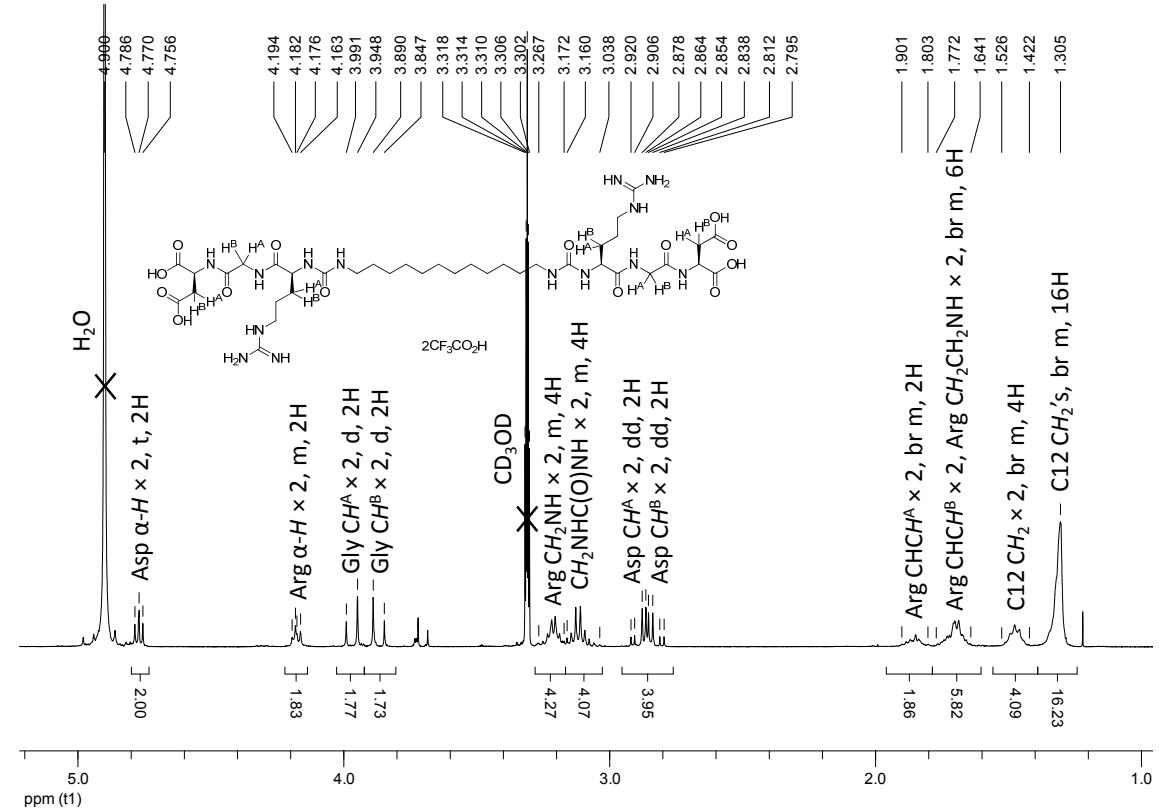

Spectrum 4.2 – ^{1}H NMR spectrum of **C12-[urea-RGD]$_2$** (**4.4**), in CD_3OD.

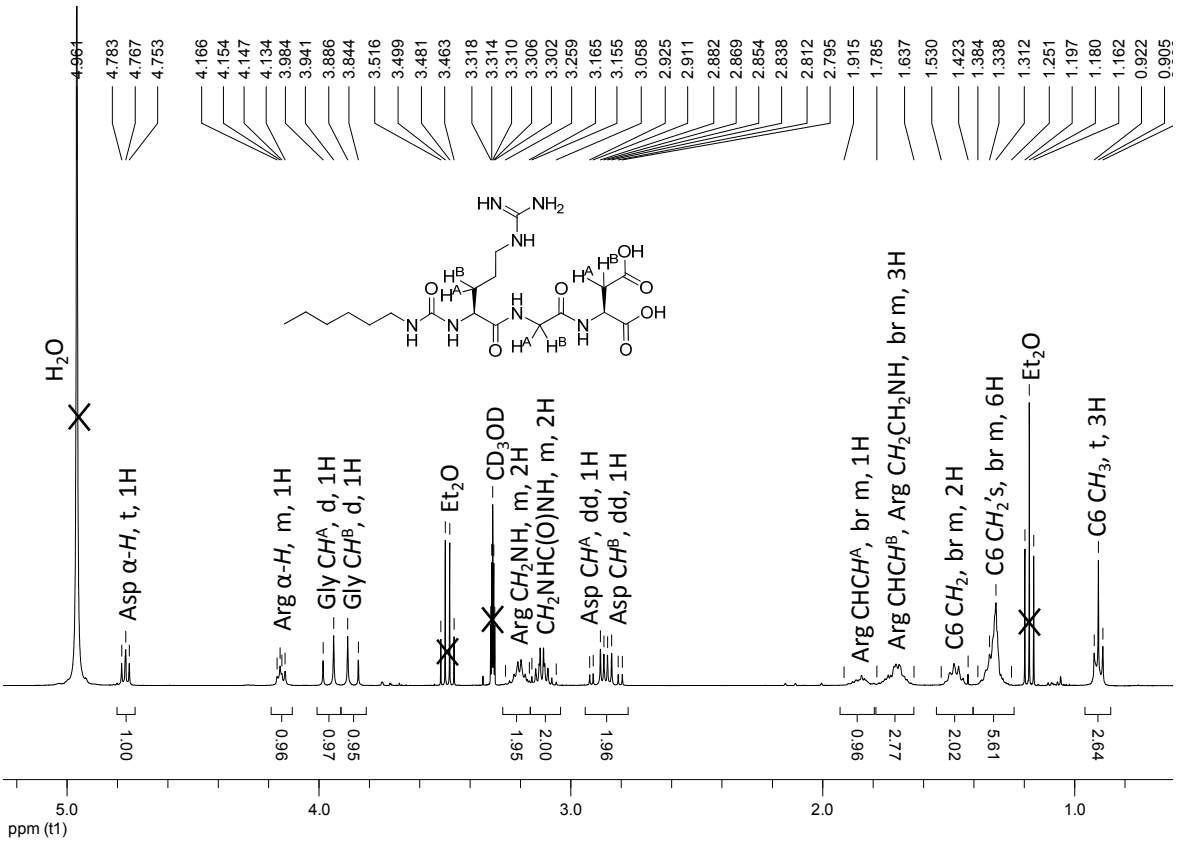

Spectrum 4.3 – ^{1}H NMR spectrum of **C6-urea-RGD** (**4.6**), in CD_3OD.

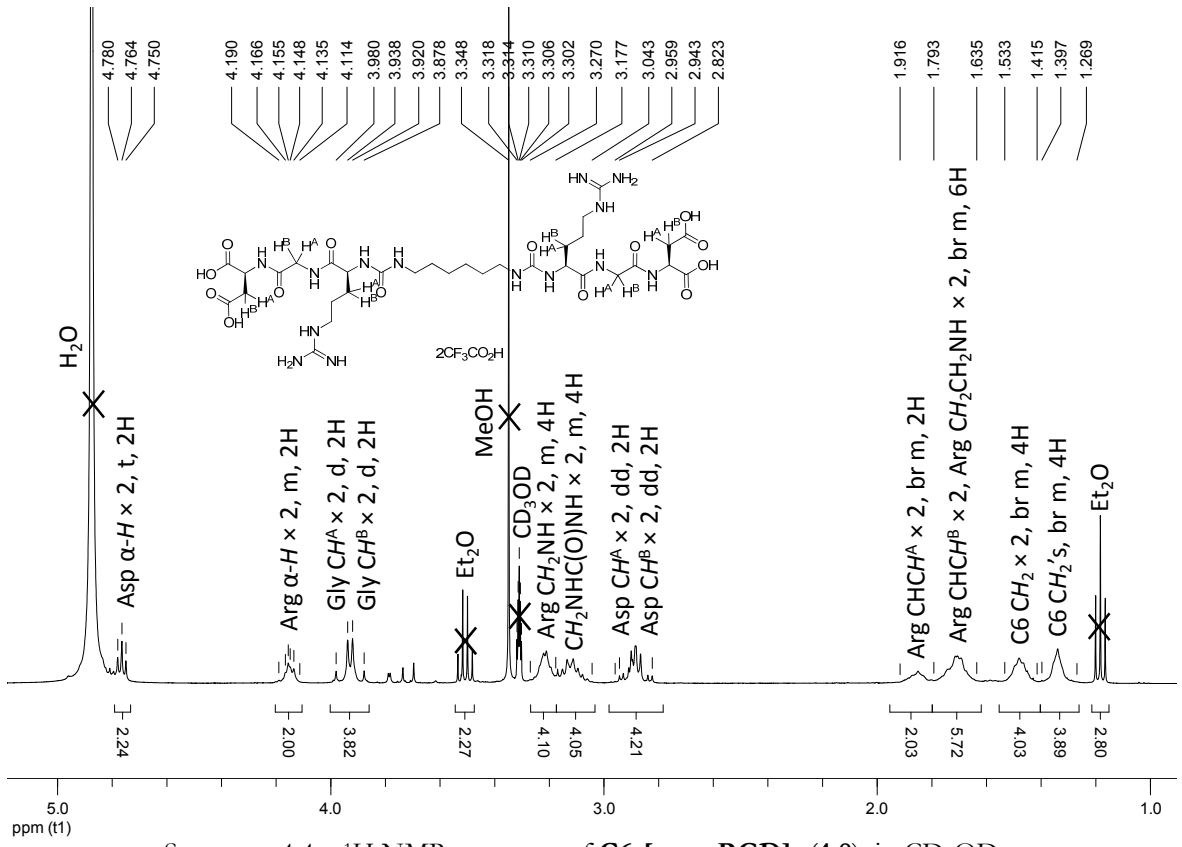

Spectrum 4.4 – ^{1}H NMR spectrum of **C6-[urea-RGD]$_2$** (**4.8**), in CD_3OD.

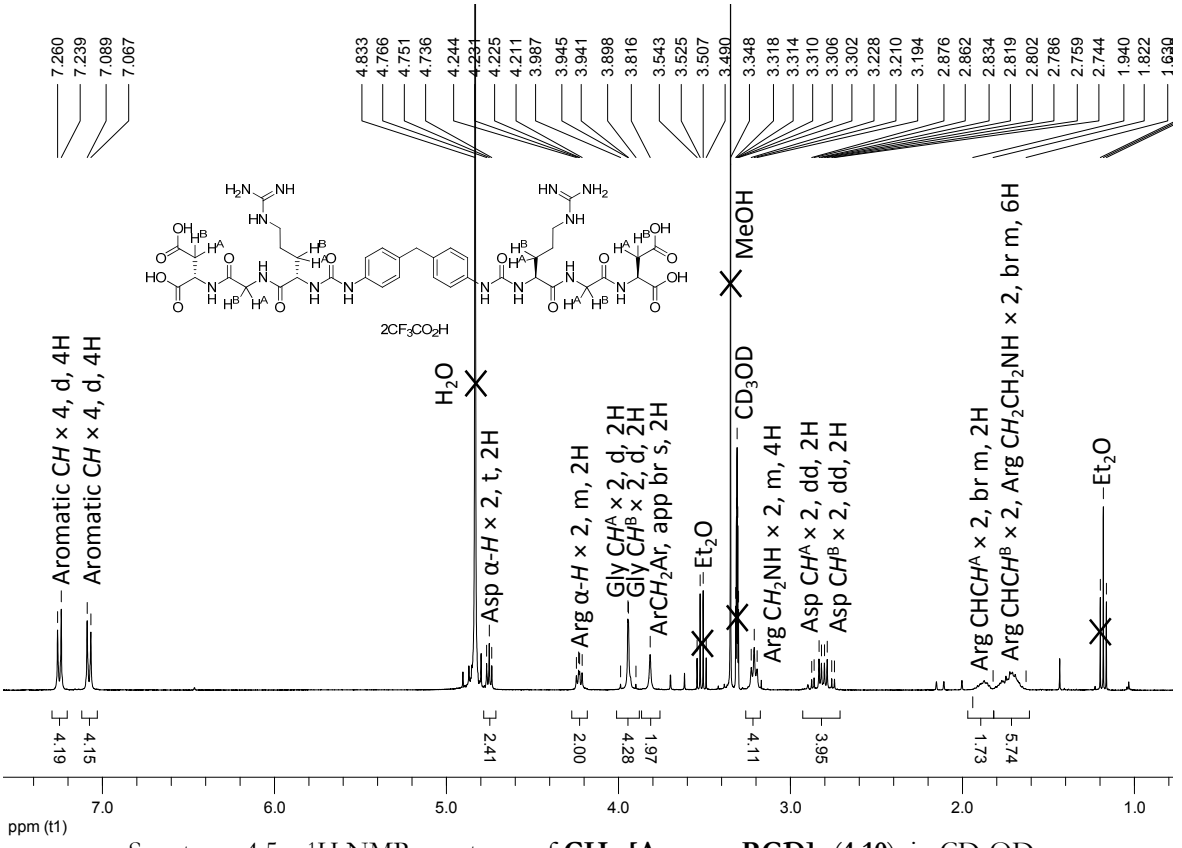

Spectrum 4.5 – ^{1}H NMR spectrum of **CH$_2$-[Ar-urea-RGD]$_2$** (**4.10**), in CD_3OD.

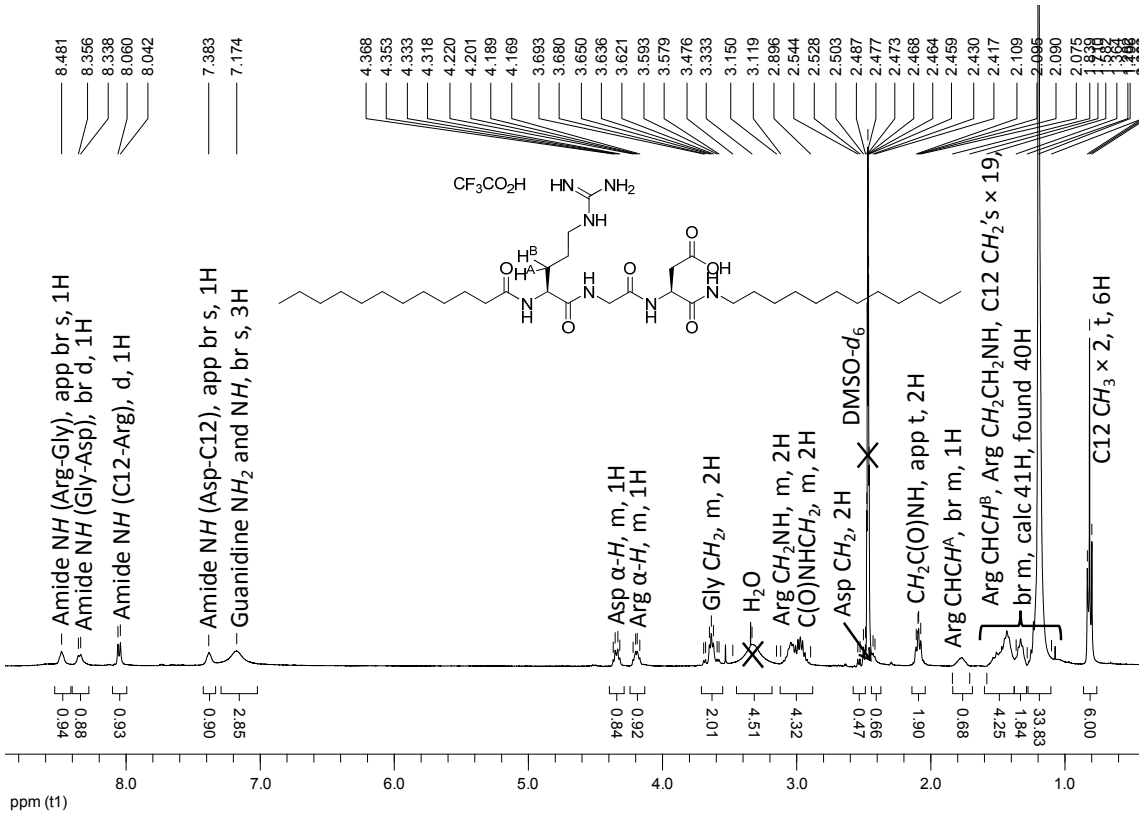

Spectrum 4.6 – ^{1}H NMR spectrum of **C12-RGD-C12** (**4.18**), in DMSO-d_6.

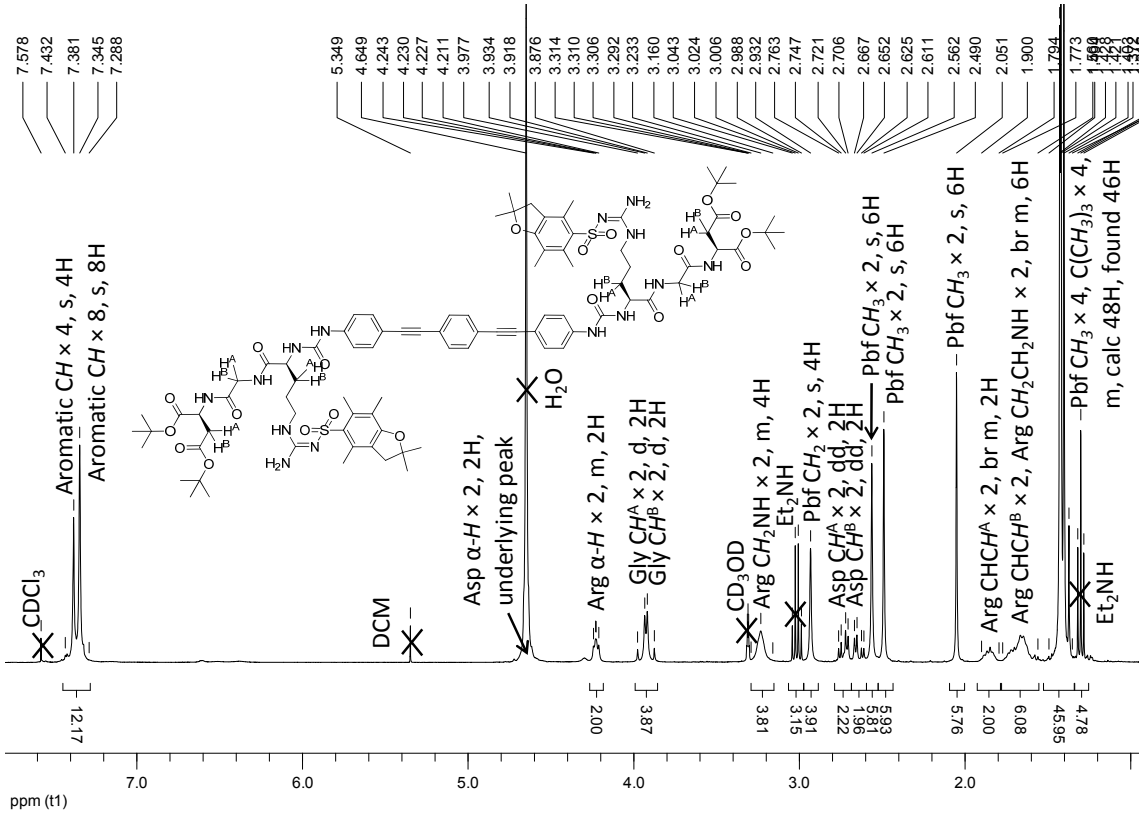

Spectrum 4.7 – ^{1}H NMR spectrum of **linear OPE-[R(Pbf)GD(O^{t}Bu)O^{t}Bu]$_2$** (**4.22**), in $CD_3OD/CDCl_3$.

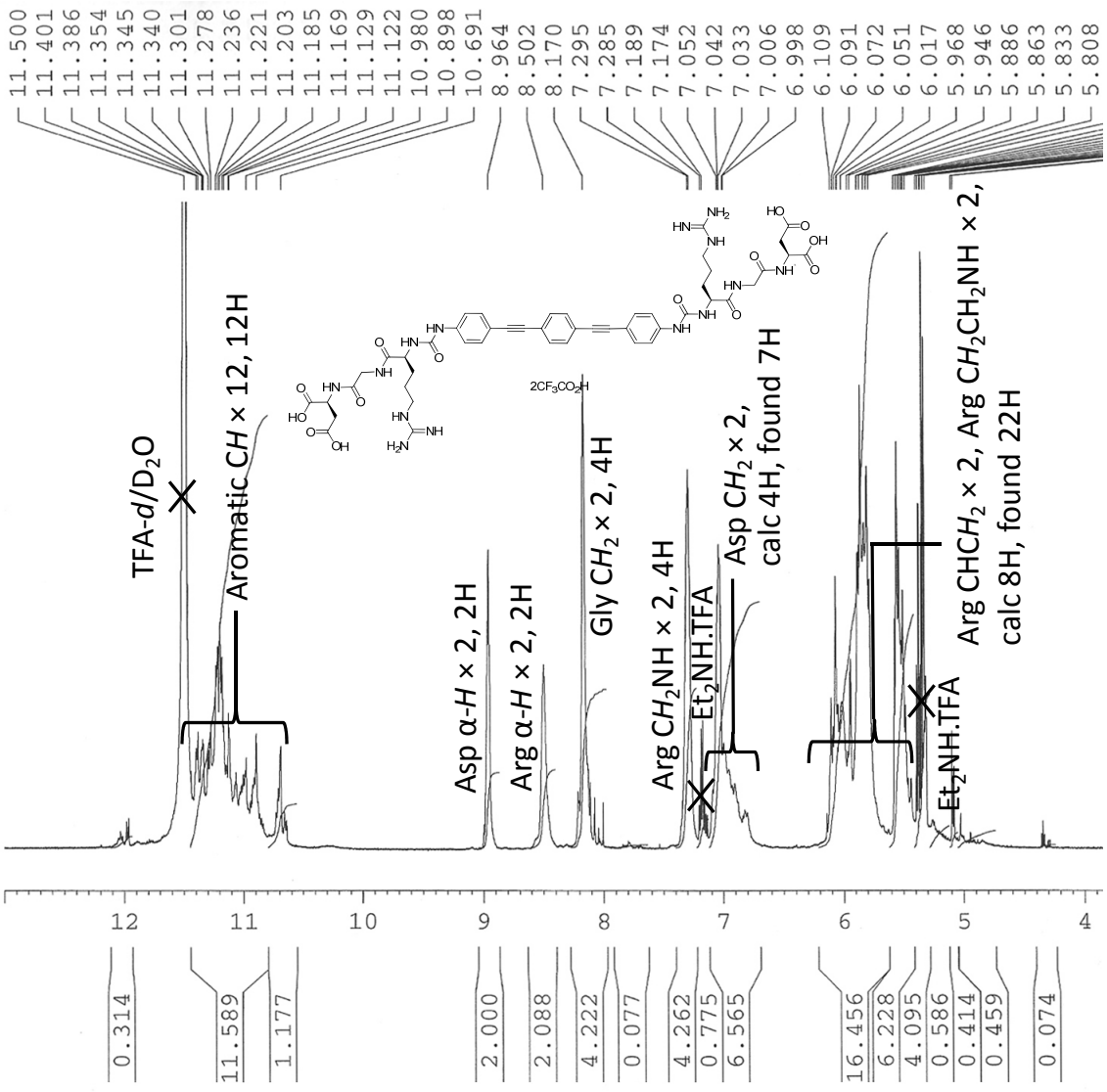

Spectrum 4.8 – 500 MHz ^{1}H NMR spectrum of the material obtained following the deprotection reaction on **linear OPE-[R(Pbf)GD(O^{t}Bu)O^{t}Bu]$_2$** (**4.22**), in an attempt to form **linear OPE-[RGD]$_2$** (**4.23**), in TFA-*d*/D_2O (referenced to TFA-*d*).

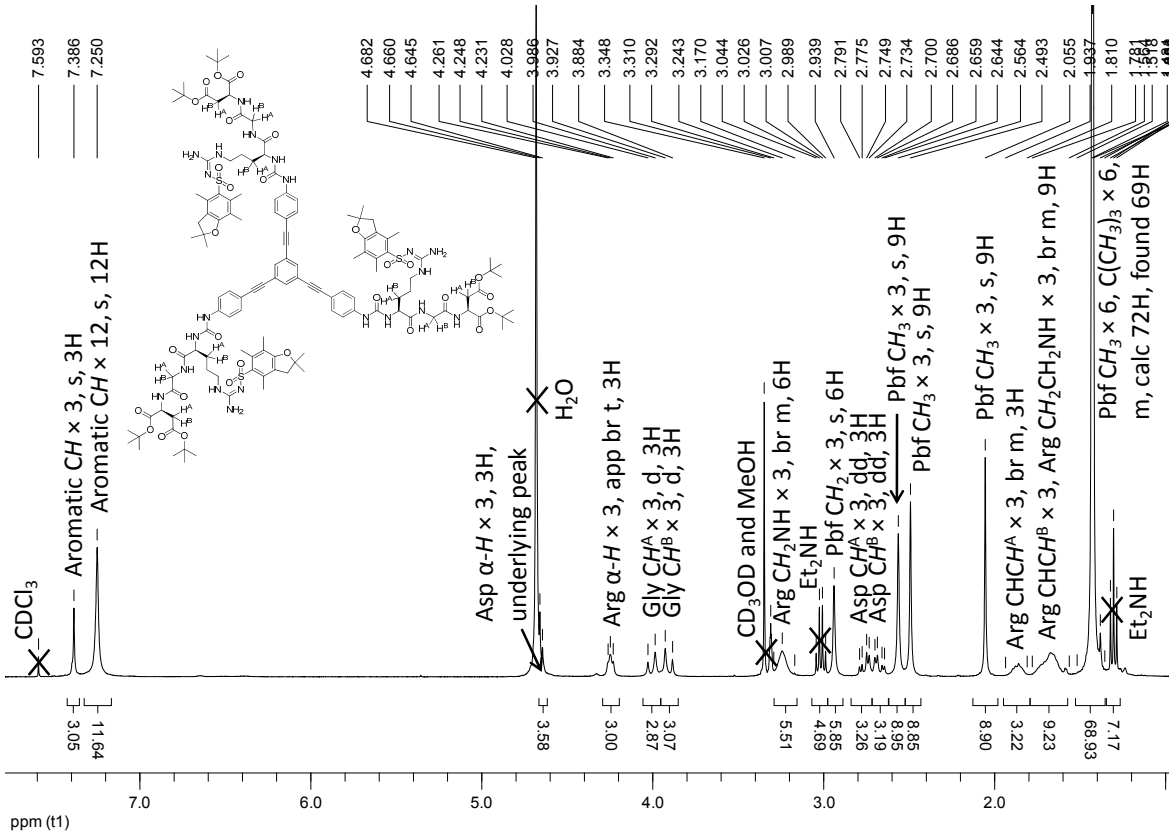

Spectrum 4.9 – ^{1}H NMR spectrum of **triangular-shaped OPE-[R(Pbf)GD(O^{t}Bu)O^{t}Bu]$_3$** (**4.26**), in $CD_3OD/CDCl_3$.

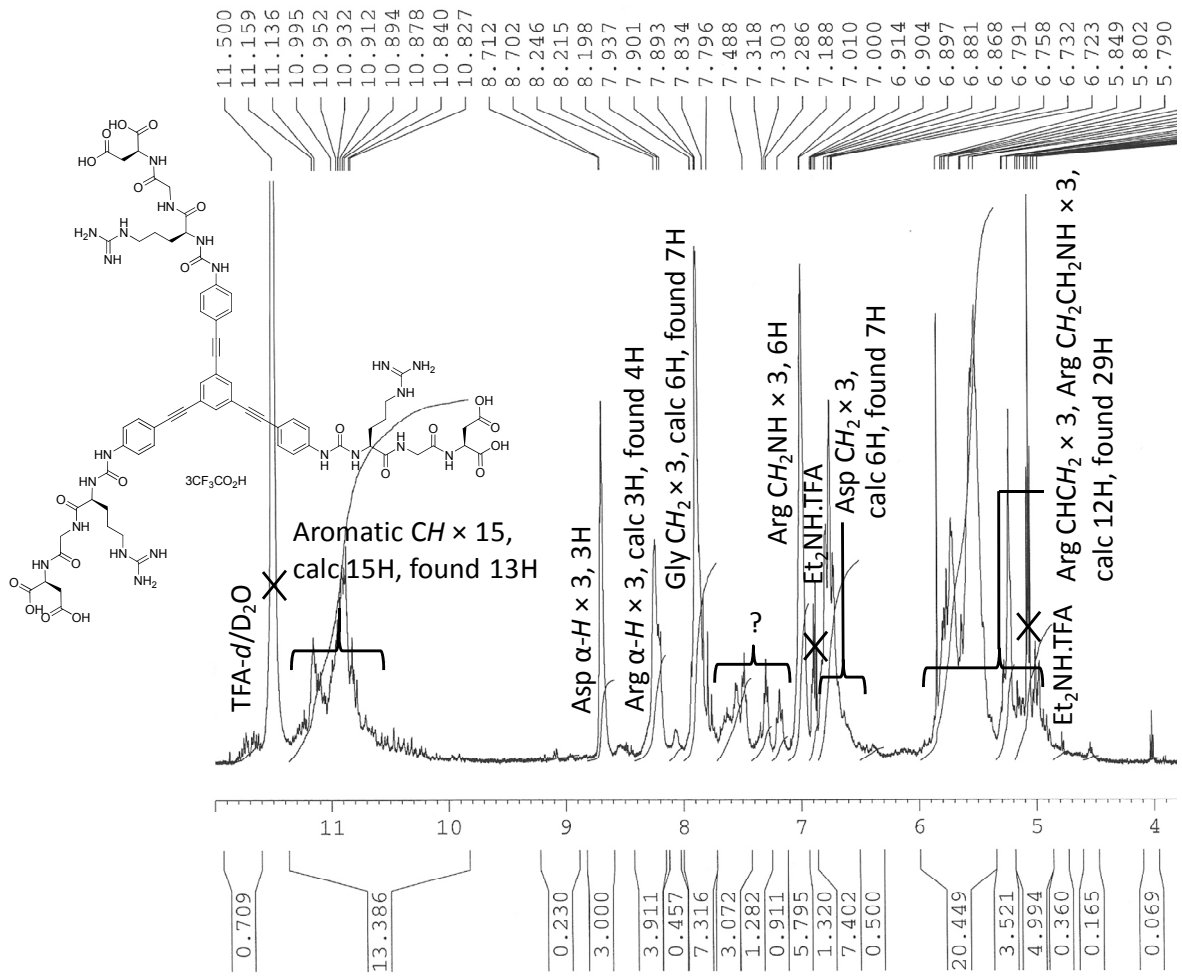

Spectrum 4.10 – 500 MHz ^{1}H NMR spectrum of the material obtained following the deprotection reaction on **triangular-shaped OPE-[R(Pbf)GD(O^{t}Bu)O^{t}Bu]$_3$** (**4.26**), in an attempt to form **triangular-shaped OPE-[RGD]$_3$** (**4.27**), in TFA-*d*/D_2O (referenced to TFA-*d*).

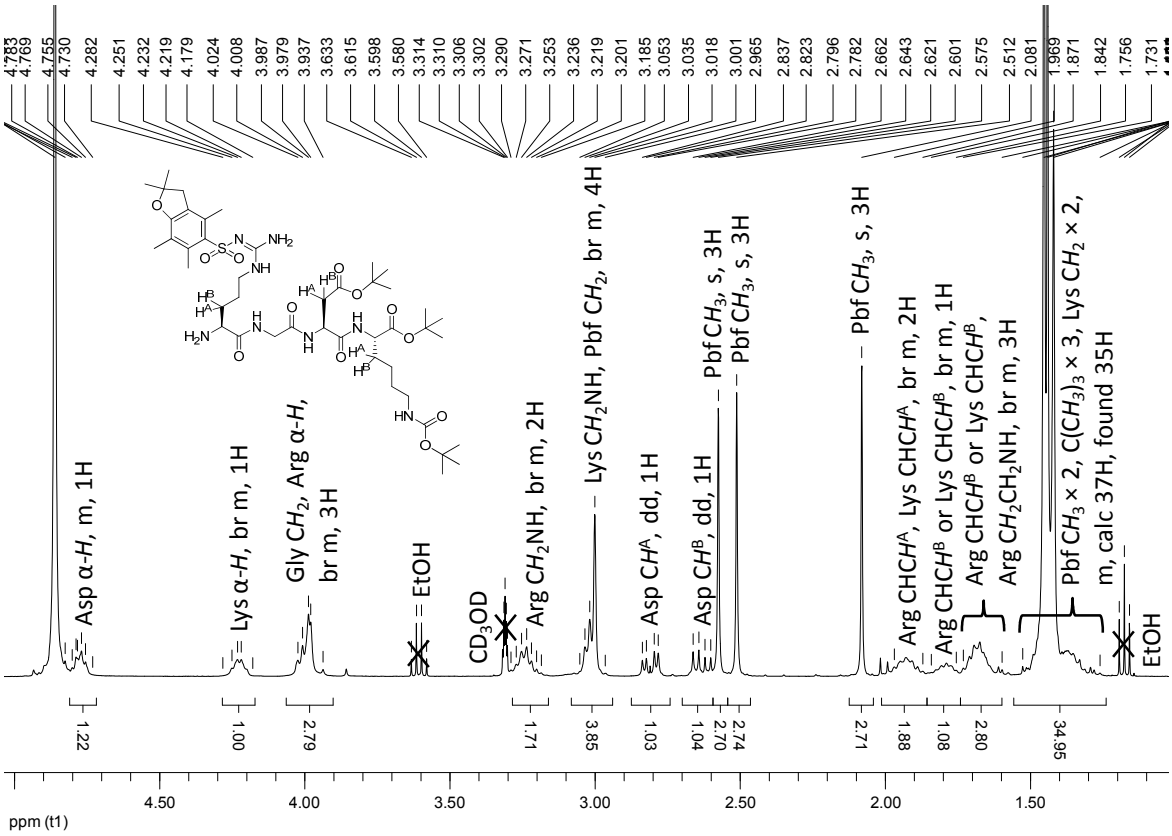

Spectrum 4.11 – ^{1}H NMR spectrum of **4.33**, in CD_3OD.

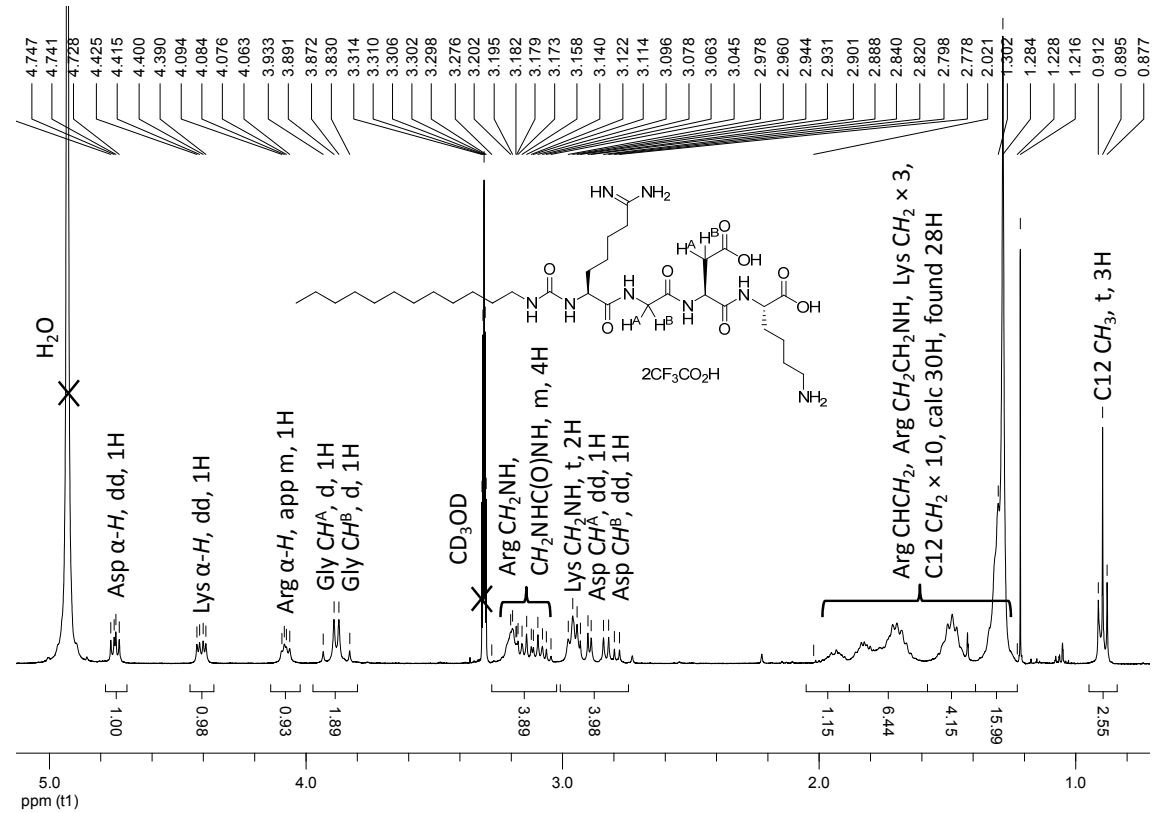

Spectrum 4.12 – ^{1}H NMR spectrum of **C12-urea-RGDK** (**4.35**), in CD_3OD.

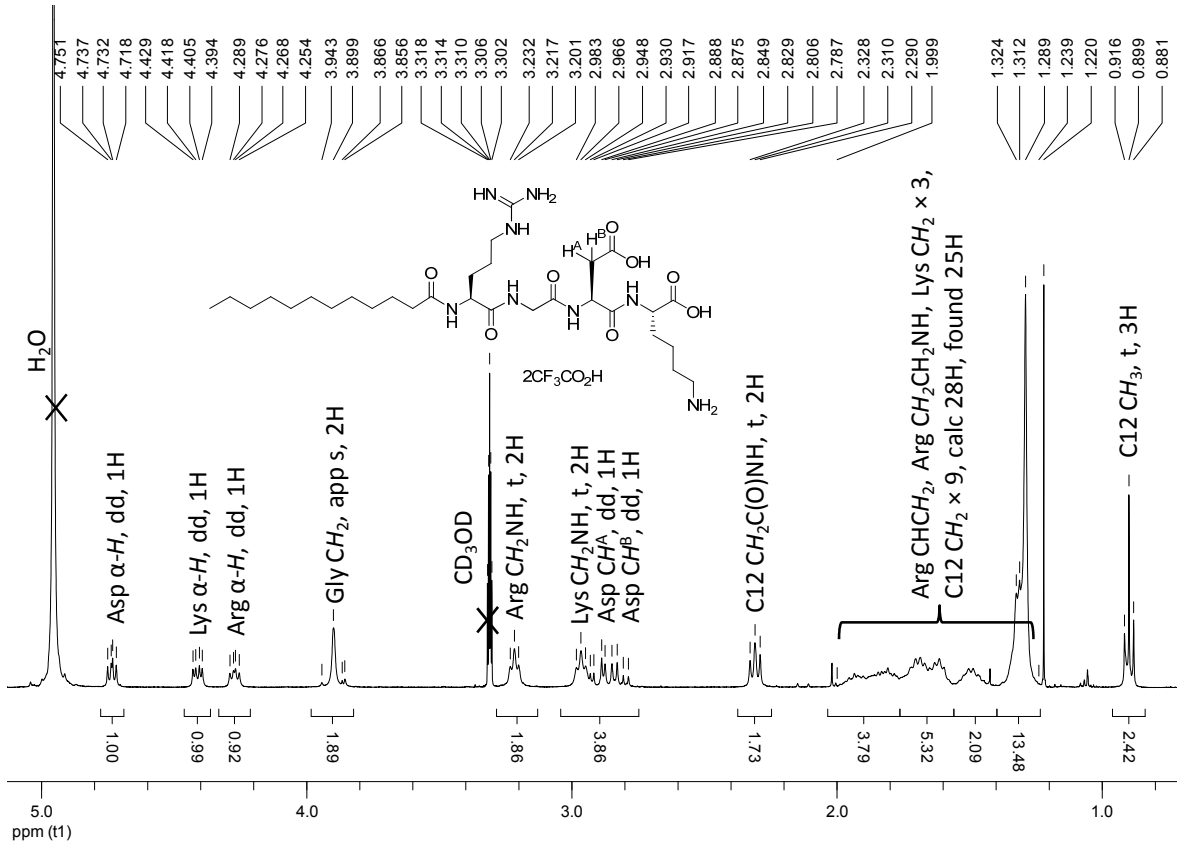

Spectrum 4.13 – ^{1}H NMR spectrum of **C12-amide-RGDK** (**4.37**), in CD_3OD.

Abbreviations

$[\alpha]_D$	specific rotation
$\tilde{\nu}_{max}$ (cm^{-1})	wavenumber at maximum peak intensity (IR)
5(6)-FL-c[RGDfK]	5(6)-carboxyfluorescein, as a mixture of isomers in either the 5 or 6 positions, conjugated to the cyclic peptide Arg-Gly-Asp-D-Phe-Lys through the lysine side-chain
5(6)-FLSE	5(6)-carboxyfluorescein *N*-hydroxysuccinimide ester, a fluorescent dye purchased as a mixture of isomers, functionalised with an *N*-hydroxysuccinimide activated ester in either the 5 or 6 positions
Alloc	allyloxycarbonyl
app	apparent
B.p.	boiling point
Boc	*tert*-butyloxycarbonyl
Boc-Gly-OH	Boc-glycine
br	broad (NMR)
CD	circular dichroism spectroscopy
$CD_3C(O)CD_3$	deuterated acetone
CD_3OD	deuterated methanol
$CDCl_3$	deuterated chloroform
CHA	cyclohexylammonia
Chol	cholesterol
cont	continued
D	L-aspartic acid
d	doublet (NMR)
DCM	dichloromethane
dd	doublet of doublets (NMR)
DIPEA	diisopropylethylamine
DMAP	*N,N*-dimethyl-4-aminopyridine
DMF	dimethylformamide
DMSO	dimethylsulfoxide
DMSO-d_6	deuterated dimethylsulfoxide
dt	doublet of triplets (NMR)
EC_{50}	effective concentration at 50% binding
ECM	extracellular matrix
EDTA	ethylenediaminetetraacetic acid

EI-MS	electron ionisation mass spectrometry
eq	equivalent/s
ESI-MS	electrospray ionisation mass spectrometry
Et_2O	diethyl ether
EtOAc	ethyl acetate
f	D-phenylalanine
Fmoc	9*H*-fluoren-9-ylmethoxycarbonyl, protecting group for the N-terminus of a peptide
Fmoc-Arg(Pbf)-OH	N_a-Fmoc-N_ω-Pbf-L-arginine
Fmoc-Gly-OH	Fmoc-glycine
FP	fluorescence polarisation
FT-IR	Fourier transform infra-red spectroscopy
FW	formula weight
G	Glycine
G1	generation 1
G2	generation 2
GPC	gel permeation chromatography
h	hours
H_2N-Asp(OBn)-NH_2.HCl	L-aspartamide β-benzyl ester hydrochloride
H_2N-Asp(O^tBu)-O^tBu.HCl	L-aspartic acid di-*tert*-butyl ester hydrochloride
HBTU	*O*-(Benzotriazol-1-yl)-*N,N,N′,N′*-tetramethyluronium hexafluorophosphate
HEPES	4-(2-hydroxyethyl)-1-piperazineethanesulfonic acid buffer solution
HFIP	1,1,1,3,3,3-hexafluoro-2-propanol
HOBt	1-hydroxybenzotriazole
HRMS	high resolution mass spectrometry
Hz	hertz
in vacuo	under vacuum
IR	infrared
J	coupling constant (in Hz)
m	multiplet (NMR)
m	medium (IR)
M.p.	melting point
m/z	mass to charge ratio
mdeg	millidegrees
MeOH	methanol

mg	milligrams
MGC	minimum gel concentration
min	minutes
ml	millilitres
MS	mass spectrometry
MW	molecular weight
Na_2CO_3	sodium carbonate
$NaHCO_3$	sodium hydrogen carbonate
$NaHSO_4$	sodium hydrogen sulfate
nm	nanometre
NMR	nuclear magnetic resonance
OBn	benzyl ester (wrt abbreviated amino acid nomenclature)
OPE	oligo(phenylene ethynylene)
O^{t}Bu	*tert*-butyl ester (wrt abbreviated amino acid nomenclature)
PA	peptide amphiphile
PB	poly(butadiene)
Pbf	N_ω-(2,2,4,6,7-pentamethyldihydrobenzofuran-5-sulfonyl), an L-arginine side chain protecting group
PBS	phosphate buffered saline solution
PEG	poly(ethylene glycol) (N.B. in this work the term 'PEG' is sometimes used to refer to a short ethylene oxide chain)
PEO	poly(ethylene oxide)
pH	negative logarithm of the concentration of hydrogen ions
pKa	negative logarithm of the acid dissociation constant
ppm	parts per million
Py	pyrene
q	quartet (NMR)
R	L-arginine
R_f	retention factor
RGD	the tripeptide Arg-Gly-Asp
RSA	retrosynthetic analysis
R_t	retention time
rt	room temperature
s	singlet (NMR)
s	strong (IR)
SEM	scanning electron microscopy
SHE	buffer solution containing sodium chloride, HEPES and EDTA

SiO_2	silica
SM	starting material
Sol	a dispersion of discrete particles within a liquid
t	triplet (NMR)
T3P (50 wt % in EtOAc or DMF)	propylphosphonic anhydride (supplied as a 50 wt% solution in ethyl acetate or DMF)
TBTU	*O*-(Benzotriazol-1-yl)-*N,N,N′,N*'-tetramethyluronium tetrafluoroborate
TEA	triethylamine
TEG	tetraethyleneglycol
TEM	transmission electron microscopy
TFA	trifluoroacetic acid
T_{gel}	gel-sol transition temperature
THF	tetrahydrofuran
TIS	triisopropylsilane, used as a scavenger of the pbf protecting group during the deprotection reaction
TLC	thin layer chromatography
TOF	time of flight
TRIS	tris(hydroxymethyl)aminomethane
TSP-d_4	deuterated trimethyl silyl propionate, an NMR internal standard
UV	ultraviolet
UV/Vis	ultraviolet/visible
V	L-valine
VT-CD	variable temperature circular dichroism spectroscopy
VT-NMR	variable temperature nuclear magnetic resonance
w	weak (IR)
w/v	weight for volume ratio
wrt	with respect to
wt %	weight percent
Z or Cbz	benzyloxy carbonyl (or benzyl carbamate) protecting group
Z-Arg(Pbf)-OH.CHA	N_a-Z-N_ω-Pbf-L-arginine cyclohexylammonium salt
δ	NMR chemical shift (in ppm)
μL	microlitres
μm	micrometre
μM	micromolar

References

1. J.-P. Xiong, T. Stehle, R. Zhang, A. Joachimiak, M. Frech, S. L. Goodman, M. A. Arnaout, *Science*, **2002**, *296*, 151-155.
2. C. Mas-Moruno, F. Rechenmacher, H. Kessler, *Anti-Cancer Agents Med. Chem.*, **2010**, *10*, 753-768.
3. M. Mammen, S.-K. Choi, G. M. Whitesides, *Angew. Chem. Int. Ed.*, **1998**, *37*, 2754-2794.
4. L. L. Kiessling, J. E. Gestwicki, L. E. Strong, *Angew. Chem. Int. Ed.*, **2006**, *45*, 2348-2368.
5. J. Huskens, *Curr. Opin. Chem. Biol.*, **2006**, *10*, 537-543.
6. V. Martos, P. Castreño, J. Valero, J. de Mendoza, *Curr. Opin. Chem. Biol.*, **2008**, *12*, 698-706.
7. W. P. Jencks, *Proc. Natl. Acad. Sci. U.S.A.*, **1981**, *78*, 4046-4050.
8. Y. M. Chabre, R. Roy, *Curr. Top. Med. Chem.*, **2008**, *8*, 1237-1285.
9. N. Jayaraman, *Chem. Soc. Rev.*, **2009**, *38*, 3463-3483.
10. M. A. Kostiainen, J. G. Hardy, D. K. Smith, *Angew. Chem. Int. Ed.*, **2005**, *44*, 2556-2559.
11. D. J. Welsh, S. P. Jones, D. K. Smith, *Angew. Chem. Int. Ed.*, **2009**, *48*, 4047-4051.
12. G. M. Pavan, A. Danani, S. Pricl, D. K. Smith, *J. Am. Chem. Soc.*, **2009**, *131*, 9686-9694.
13. S. P. Jones, G. M. Pavan, A. Danani, S. Pricl, D. K. Smith, *Chem. Eur. J.*, **2010**, *16*, 4519-4532.
14. http://mattison0922.wordpress.com/2010/07/21/a-universal-flu-vaccine/
15. C. C. Lee, J. A. MacKay, J. M. J. Fréchet, F. C. Szoka, *Nat. Biotech.*, **2005**, *23*, 1517-1526.
16. E. W. Meijer, A. W. Bosman, H. M. Janssen, *Chem. Rev.*, **1999**, *99*, 1665-1688.
17. J. M. J. Fréchet, *Proc. Nat. Acad. Sci.*, **2002**, *99*, 4782-4787.
18. P. J. Gittins, L. J. Twyman, *Supramol. Chem.*, **2003**, *15*, 5 - 23.
19. A. Mulder, J. Huskens, D. N. Reinhoudt, *Org. Biomol. Chem.*, **2004**, *2*, 3409-3424.
20. J. D. Badjic, A. Nelson, S. J. Cantrill, W. B. Turnbull, J. F. Stoddart, *Acc. Chem. Res.*, **2005**, *38*, 723-732.
21. D. K. Smith, A. R. Hirst, C. S. Love, J. G. Hardy, S. V. Brignell, B. Huang, *Prog. Polym. Sci.*, **2005**, *30*, 220-293.
22. M. J. Cloninger, *Curr. Opin. Chem. Biol.*, **2002**, *6*, 742-748.
23. U. Boas, P. M. H. Heegaard, *Chem. Soc. Rev.*, **2004**, *33*, 43-63.
24. S. Borman, *Chem. Eng. News*, **2000**, *78*, 48-53.
25. P. I. Kitov, D. R. Bundle, *J. Am. Chem. Soc.*, **2003**, *125*, 16271-16284.
26. R. J. Pieters, *Trends Glycosci. Glycotechnol.*, **2004**, *16*, 243-254.
27. J. D. Reuter, A. Myc, M. M. Hayes, Z. Gan, R. Roy, D. Qin, R. Yin, L. T. Piehler, R. Esfand, D. A. Tomalia, J. R. Baker, *Bioconjugate Chem.*, **1999**, *10*, 271-278.
28. P. I. Kitov, J. M. Sadowska, G. Mulvey, G. D. Armstrong, H. Ling, N. S. Pannu, R. J. Read, D. R. Bundle, *Nature*, **2000**, *403*, 669-672.
29. J. A. F. Joosten, N. T. H. Tholen, F. A. E. Maate, A. J. Brouwer, G. W. v. Esse, D. T. S. Rijkers, R. M. J. Liskamp, R. J. Pieters, *Eur. J. Org. Chem.*, **2005**, *2005*, 3182-3185.

30. Y. M. Chabre, P. Contino, C. Pin, V. Placide, T. C. Shiao, R. Roy, *J. Org. Chem.*, **2008**, *73*, 5602-5605.
31. P. Wu, X. Chen, N. Hu, U. C. Tam, O. Blixt, A. Zettl, C. R. Bertozzi, *Angew. Chem. Int. Ed.*, **2008**, *47*, 5022-5025.
32. P. R. Cullis, B. De Kruijff, *Biochim. Biophys. Acta*, **1979**, *559*, 399-420.
33. J. N. Israelachvili, S. Marčelja, R. G. Horn, *Quart. Rev. Biophys.*, **1980**, *13*, 121-200.
34. X.-L. Sun, Y. Kanie, C.-T. Guo, O. Kanie, Y. Suzuki, C.-H. Wong, *Eur. J. Org. Chem.*, **2000**, *2000*, 2643-2653.
35. R. O. Hynes, *Cell*, **1992**, *69*, 11-25.
36. E. F. Plow, T. A. Haas, L. Zhang, J. Loftus, J. W. Smith, *J. Biol. Chem.*, **2000**, *275*, 21785-21788.
37. R. O. Hynes, *Nat. Med.*, **2002**, *8*, 918-921.
38. R. O. Hynes, *Cell*, **2002**, *110*, 673-687.
39. O. Cleaver, D. A. Melton, *Nat. Med.*, **2003**, *9*, 661-668.
40. J. D. Humphries, A. Byron, M. J. Humphries, *J. Cell Sci.*, **2006**, *119*, 3901-3903.
41. D. Valdembri, C. Sandri, M. Santambrogio, G. Serini, *Mol. BioSyst.*, **2011**, *7*, 2539-2546.
42. U. Hersel, C. Dahmen, H. Kessler, *Biomaterials*, **2003**, *24*, 4385-4415.
43. L. Perlin, S. MacNeil, S. Rimmer, *Soft Matter*, **2008**, *4*, 2331-2349.
44. D. Cox, M. Brennan, N. Moran, *Nat. Rev. Drug Discov.*, **2010**, *9*, 804-820.
45. P. C. Brooks, R. A. F. Clark, D. A. Cheresh, *Science*, **1994**, *264*, 569-571.
46. S. Strömblad, D. A. Cheresh, *Chem. Biol.*, **1996**, *3*, 881-885.
47. H. Jin, J. A. Varner, *Br. J. Cancer*, **2004**, *90*, 561-565.
48. C. J. Avraamides, B. Garmy-Susini, J. A. Varner, *Nat. Rev. Cancer*, **2008**, *8*, 604-617.
49. J. S. Desgrosellier, D. A. Cheresh, *Nat. Rev. Cancer*, **2010**, *10*, 9-22.
50. P. C. Brooks, A. M. P. Montgomery, M. Rosenfeld, R. A. Reisfeld, T. Hu, G. Klier, D. A. Cheresh, *Cell*, **1994**, *79*, 1157-1164.
51. C. S. Chen, M. Mrksich, S. Huang, G. M. Whitesides, D. E. Ingber, *Science*, **1997**, *276*, 1425-1428.
52. W. Arap, R. Pasqualini, E. Ruoslahti, *Science*, **1998**, *279*, 377-380.
53. C. P. Carron, D. M. Meyer, J. A. Pegg, V. W. Engleman, M. A. Nickols, S. L. Settle, W. F. Westlin, P. G. Ruminski, G. A. Nickols, *Cancer Res.*, **1998**, *58*, 1930-1935.
54. K.-E. Gottschalk, H. Kessler, *Angew. Chem. Int. Ed.*, **2002**, *41*, 3767-3774.
55. K. N. Sugahara, T. Teesalu, P. P. Karmali, V. R. Kotamraju, L. Agemy, D. R. Greenwald, E. Ruoslahti, *Science*, **2010**, *328*, 1031-1035.
56. N. Kieffer, D. R. Phillips, *Annu. Rev. Cell Biol.*, **1990**, *6*, 329-357.
57. S. Cheng, W. S. Craig, D. Mullen, J. F. Tschopp, D. Dixon, M. D. Pierschbacher, *J. Med. Chem.*, **1994**, *37*, 1-8.

58. A. P. Mould, M. J. Humphries, *Nature*, **2004**, *432*, 27-28.
59. S. J. Shattil, C. Kim, M. H. Ginsberg, *Nat. Rev. Mol. Cell Biol.*, **2010**, *11*, 288-300.
60. D. A. Cheresh, D. G. Stupack, *Nat. Med.*, **2002**, *8*, 193-194.
61. D. G. Stupack, D. A. Cheresh, *Nat. Cell Biol.*, **2004**, *6*, 388-389.
62. M. D. Pierschbacher, E. G. Hayman, E. Ruoslahti, *Cell*, **1981**, *26*, 259-267.
63. M. D. Pierschbacher, E. Ruoslahti, J. Sundelin, P. Lind, P. A. Peterson, *J. Biol. Chem.*, **1982**, *257*, 9593-9597.
64. M. D. Pierschbacher, E. Ruoslahti, *Nature*, **1984**, *309*, 30-33.
65. M. D. Pierschbacher, E. Ruoslahti, *Proc. Natl. Acad. Sci. U.S.A.*, **1984**, *81*, 5985-5988.
66. R. Pytela, M. D. Pierschbacher, E. Ruoslahti, *Cell*, **1985**, *40*, 191-198.
67. J. W. Tamkun, D. W. DeSimone, D. Fonda, R. S. Patel, C. Buck, A. F. Horwitz, R. O. Hynes, *Cell*, **1986**, *46*, 271-282.
68. E. Ruoslahti, M. D. Pierschbacher, *Science*, **1987**, *238*, 491-497.
69. M. J. Humphries, *J. Cell Sci.*, **1990**, *97*, 585-592.
70. S. E. D'Souza, M. H. Ginsberg, E. F. Plow, *Trends Biochem. Sci.*, **1991**, *16*, 246-250.
71. E. Ruoslahti, *J. Clin. Invest.*, **1991**, *87*, 1-5.
72. J. H. Beer, K. T. Springer, B. S. Coller, *Blood*, **1992**, *79*, 117-128.
73. R. Meinecke, B. Meyer, *J. Med. Chem.*, **2001**, *44*, 3059-3065.
74. A. J. Garcia, J. E. Schwarzbauer, D. Boettiger, *Biochemistry*, **2002**, *41*, 9063-9069.
75. W. Wang, Q. Wu, M. Pasuelo, J. S. McMurray, C. Li, *Bioconjugate Chem.*, **2005**, *16*, 729-734.
76. E. Ruoslahti, *Annu. Rev. Cell Dev. Biol.*, **1996**, *12*, 697-715.
77. R. Haubner, D. Finsinger, H. Kessler, *Angew. Chem. Int. Ed.*, **1997**, *36*, 1374-1389.
78. D. Heckmann, H. Kessler, D. A. Cheresh, *Method. Enzymol.*, **2007**, *426*, 463-503.
79. E. Ruoslahti, M. D. Pierschbacher, *Cell*, **1986**, *44*, 517-518.
80. I. A. Wilson, D. H. Haft, E. D. Getzoff, J. A. Tainer, R. A. Lerner, S. Brenner, *Proc. Natl. Acad. Sci. U.S.A.*, **1985**, *82*, 5255-5259.
81. H. Kessler, *Angew. Chem. Int. Ed.*, **1982**, *21*, 512-523.
82. J.-P. Xiong, T. Stehle, B. Diefenbach, R. Zhang, R. Dunker, D. L. Scott, A. Joachimiak, S. L. Goodman, M. A. Arnaout, *Science*, **2001**, *294*, 339-345.
83. T. Xiao, J. Takagi, B. S. Coller, J.-H. Wang, T. A. Springer, *Nature*, **2004**, *432*, 59-67.
84. H. Kessler, R. Gratias, G. Hessler, M. Gurrath, G. Müller, *Pure Appl. Chem*, **1996**, *68*, 1201-1205.
85. T. Weide, A. Modlinger, H. Kessler, *Top. Curr. Chem.*, **2007**, *272*, 1-50.
86. J. Chatterjee, C. Gilon, A. Hoffman, H. Kessler, *Acc. Chem. Res.*, **2008**, *41*, 1331-1342.
87. M. Aumailley, M. Gurrath, G. Müller, J. Calvete, R. Timpl, H. Kessler, *FEBS Lett.*, **1991**, *291*, 50-54.

88. M. Gurrath, G. Müller, H. Kessler, M. Aumailley, R. Timpl, *Eur. J. Biochem.*, **1992**, *210*, 911-921.

89. R. Haubner, R. Gratias, B. Diefenbach, S. L. Goodman, A. Jonczyk, H. Kessler, *J. Am. Chem. Soc.*, **1996**, *118*, 7461-7472.

90. R. Haubner, H.-J. Wester, F. Burkhart, R. Senekowitsch-Schmidtke, W. Weber, S. L. Goodman, H. Kessler, M. Schwaiger, *J. Nucl. Med.*, **2001**, *42*, 326-336.

91. C. Frochot, B. D. Stasio, R. Vanderesse, M.-J. Belgy, M. Dodeller, F. Guillemin, M.-L. Viriot, M. Barberi-Heyob, *Bioorg. Chem.*, **2007**, *35*, 205-220.

92. C. L. Conway, I. Walker, A. Bell, D. J. H. Roberts, S. B. Brown, D. I. Vernon, *Photochem. Photobiol. Sci.*, **2008**, *7*, 290-298.

93. X. Chen, R. Park, M. Tohme, A. H. Shahinian, J. R. Bading, P. S. Conti, *Bioconjugate Chem.*, **2004**, *15*, 41-49.

94. I. Dijkgraaf, J. A. W. Kruijtzer, C. Frielink, A. C. Soede, H. W. Hilbers, W. J. G. Oyen, F. H. M. Corstens, R. M. J. Liskamp, O. C. Boerman, *Nucl. Med. Biol.*, **2006**, *33*, 953-961.

95. L. Xiong, M. Yu, M. Cheng, M. Zhang, X. Zhang, C. Xu, F. Li, *Mol. BioSyst.*, **2009**, *5*, 241-243.

96. H. Cai, Z. Li, C.-W. Huang, A. H. Shahinian, H. Wang, R. Park, P. S. Conti, *Bioconjugate Chem.*, **2010**, *21*, 1417-1424.

97. X. Dai, Z. Su, J. O. Liu, *Tetrahedron Lett.*, **2000**, *41*, 6295-6298.

98. C. F. McCusker, P. J. Kocienski, F. T. Boyle, A. G. Schätzlein, *Bioorg. Med. Chem. Lett.*, **2002**, *12*, 547-549.

99. A. Jonczyk, S. L. Goodman, B. Diefenbach, A. Sutter, G. Hölzemann, H. Kessler, M. A. Dechantsreiter. Preparation of cyclic peptides as integrin inhibitors. DE 19534177; EP 0770622; JP 1997132593; US 6001961.

100. M. A. Dechantsreiter, E. Planker, B. Matha, E. Lohof, G. Hölzemann, A. Jonczyk, S. L. Goodman, H. Kessler, *J. Med. Chem.*, **1999**, *42*, 3033-3040.

101. G. Tabatabai, M. Weller, B. Nabors, M. Picard, D. Reardon, T. Mikkelsen, C. Ruegg, R. Stupp, *Targeted Oncol.*, **2010**, *5*, 175-181.

102. K. C. Nicolaou, J. I. Trujillo, B. Jandeleit, K. Chibale, M. Rosenfeld, B. Diefenbach, D. A. Cheresh, S. L. Goodman, *Bioorg. Med. Chem.*, **1998**, *6*, 1185-1208.

103. M. Paolillo, M. A. Russo, M. Serra, L. Colombo, S. Schinelli, *Mini-Rev. Med. Chem.*, **2009**, *9*, 1439-1446.

104. L. J. Kornberg, H. S. Earp, C. E. Turner, C. Prockop, R. L. Juliano, *Proc. Natl. Acad. Sci. U.S.A.*, **1991**, *88*, 8392-8396.

105. S. Miyamoto, S. K. Akiyama, K. M. Yamada, *Science*, **1995**, *267*, 883-885.

106. M. S. Bretscher, *Cell*, **1996**, *85*, 465-467.

107. D. G. Stupack, E. Li, S. A. Silletti, J. A. Kehler, R. L. Geahlen, K. Hahn, G. R. Nemerow, D. A. Cheresh, *J. Cell Biol.*, **1999**, *144*, 777-788.

108. G. Maheshwari, G. Brown, D. A. Lauffenburger, A. Wells, L. G. Griffith, *J. Cell Sci.*, **2000**, *113*, 1677-1686.
109. M. Roberts, S. Barry, A. Woods, P. van der Sluijs, J. Norman, *Curr. Biol.*, **2001**, *11*, 1392-1402.
110. D. C. Worth, M. Parsons, *Int. J. Biochem. Cell Biol.*, **2008**, *40*, 2397-2409.
111. L. Auzzas, F. Zanardi, L. Battistini, P. Burreddu, P. Carta, G. Rassu, C. Curti, G. Casiraghi, *Curr. Med. Chem.*, **2010**, *17*, 1255-1299.
112. J. Murata, I. Saiki, R. Ogawa, N. Nishi, S. Tokura, I. Azuma, *Int. J. Pept. Prot. Res.*, **1991**, *38*, 212-217.
113. H. D. Maynard, S. Y. Okada, R. H. Grubbs, *J. Am. Chem. Soc.*, **2001**, *123*, 1275-1279.
114. B. R. Line, A. Mitra, A. Nan, H. Ghandehari, *J. Nucl. Med.*, **2005**, *46*, 1552-1560.
115. H.-J. Wester, H. Kessler, *J. Nucl. Med.*, **2005**, *46*, 1940-1945.
116. J. G. Zhang, O. B. Krajden, R. K. Kainthan, J. N. Kizhakkedathu, I. Constantinescu, D. E. Brooks, M. I. C. Gyongyossy-Issa, *Bioconjugate Chem.*, **2008**, *19*, 1241-1247.
117. S. J. Todd, D. J. Scurr, J. E. Gough, M. R. Alexander, R. V. Ulijn, *Langmuir*, **2009**, *25*, 7533-7539.
118. R. J. Kok, A. J. Schraa, E. J. Bos, H. E. Moorlag, S. A. Asgeirsdottir, M. Everts, D. K. F. Meijer, G. Molema, *Bioconjugate Chem.*, **2002**, *13*, 128-135.
119. X. Montet, M. Funovics, K. Montet-Abou, R. Weissleder, L. Josephson, *J. Med. Chem.*, **2006**, *49*, 6087-6093.
120. J. Xie, K. Chen, H.-Y. Lee, C. Xu, A. R. Hsu, S. Peng, X. Chen, S. Sun, *J. Am. Chem. Soc.*, **2008**, *130*, 7542-7543.
121. S. Monaghan, D. Griffith-Johnson, I. Matthews, M. Bradley, *Arkivoc*, **2001**, *2*, 46-53.
122. C. A. Boswell, P. K. Eck, C. A. S. Regino, M. Bernardo, K. J. Wong, D. E. Milenic, P. L. Choyke, M. W. Brechbiel, *Mol. Pharm.*, **2008**, *5*, 527-539.
123. T. L. Kaneshiro, Z.-R. Lu, *Biomaterials*, **2009**, *30*, 5660-5666.
124. C. L. Waite, C. M. Roth, *Bioconjugate Chem.*, **2009**, *20*, 1908-1916.
125. Z. Li, P. Huang, X. Zhang, J. Lin, S. Yang, B. Liu, F. Gao, P. Xi, Q. Ren, D. Cui, *Mol. Pharm.*, **2009**, *7*, 94-104.
126. D. T. S. Rijkers, G. W. v. Esse, R. Merkx, A. J. Brouwer, H. J. F. Jacobs, R. J. Pieters, R. M. J. Liskamp, *Chem. Commun.*, **2005**, 4581-4583.
127. I. Dijkgraaf, A. Y. Rijnders, A. Soede, A. C. Dechesne, G. W. van Esse, A. J. Brouwer, F. H. M. Corstens, O. C. Boerman, D. T. S. Rijkers, R. M. J. Liskamp, *Org. Biomol. Chem.*, **2007**, *5*, 935-944.
128. D. Boturyn, J.-L. Coll, E. Garanger, M.-C. Favrot, P. Dumy, *J. Am. Chem. Soc.*, **2004**, *126*, 5730-5739.
129. P. Dumy, I. M. Eggleston, S. Cervigni, U. Sila, X. Sun, M. Mutter, *Tetrahedron Lett.*, **1995**, *36*, 1255-1258.

130. E. Garanger, D. Boturyn, O. Renaudet, E. Defrancq, P. Dumy, *J. Org. Chem.*, **2006**, *71*, 2402-2410.

131. Z. H. Jin, V. Josserand, J. Razkin, E. Garanger, D. Boturyn, M.-C. Favrot, P. Dumy, J.-L. Coll, *Mol. Imaging*, **2006**, *5*, 188-197.

132. J. Razkin, V. Josserand, D. Boturyn, Z.-H. Jin, P. Dumy, M.-C. Favrot, J.-L. Coll, I. Texier, *ChemMedChem*, **2006**, *1*, 1069-1072.

133. Z.-H. Jin, V. Josserand, S. Foillard, D. Boturyn, P. Dumy, M.-C. Favrot, J.-L. Coll, *Mol. Cancer*, **2007**, *6*, 41-49.

134. L. Sancey, E. Garanger, S. Foillard, G. Schoehn, A. Hurbin, C. Albiges-Rizo, D. Boturyn, C. Souchier, A. Grichine, P. Dumy, J.-L. Coll, *Mol. Ther.*, **2009**, *17*, 837-843.

135. S. Foillard, Z.-H. Jin, E. Garanger, D. Boturyn, M.-C. Favrot, J.-L. Coll, P. Dumy, *ChemBioChem*, **2008**, *9*, 2326-2332.

136. S. Foillard, L. Sancey, J.-L. Coll, D. Boturyn, P. Dumy, *Org. Biomol. Chem.*, **2009**, *7*, 221-224.

137. E. Garanger, D. Boturyn, Z. H. Jin, P. Dumy, M.-C. Favrot, J.-L. Coll, *Mol. Ther.*, **2005**, *12*, 1168-1175.

138. E. Garanger, D. Boturyn, J.-L. Coll, M.-C. Favrot, P. Dumy, *Org. Biomol. Chem.*, **2006**, *4*, 1958-1965.

139. B. Hu, D. Finsinger, K. Peter, Z. Guttenberg, M. Bärmann, H. Kessler, A. Escherich, L. Moroder, J. Böhm, W. Baumeister, S. Sui, E. Sackmann, *Biochemistry*, **2000**, *39*, 12284-12294.

140. V. Marchi-Artzner, B. Lorz, U. Hellerer, M. Kantlehner, H. Kessler, E. Sackmann, *Chem. Eur. J.*, **2001**, *7*, 1095-1101.

141. V. Marchi-Artzner, B. Lorz, C. Gosse, L. Jullien, R. Merkel, H. Kessler, E. Sackmann, *Langmuir*, **2003**, *19*, 835-841.

142. S. Cressman, I. Dobson, J. B. Lee, Y. Y. C. Tam, P. R. Cullis, *Bioconjugate Chem.*, **2009**, *20*, 1404-1411.

143. J. A. Zupancich, F. S. Bates, M. A. Hillmyer, *Biomacromolecules*, **2009**, *10*, 1554-1563.

144. Y.-b. Lim, O.-J. Kwon, E. Lee, P.-H. Kim, C.-O. Yun, M. Lee, *Org. Biomol. Chem.*, **2008**, *6*, 1944-1948.

145. B.-S. Kim, D.-J. Hong, J. Bae, M. Lee, *J. Am. Chem. Soc*, **2005**, *127*, 16333-16337.

146. Y.-b. Lim, M. Lee, *Org. Biomol. Chem.*, **2007**, *5*, 401-405.

147. M. K. Müller, L. Brunsveld, *Angew. Chem. Int. Ed.*, **2009**, *48*, 2921-2924.

148. S. W. A. Reulen, P. Y. W. Dankers, P. H. H. Bomans, E. W. Meijer, M. Merkx, *J. Am. Chem. Soc.*, **2009**, *131*, 7304-7312.

149. P. P. Karmali, A. Chaudhuri, *Med. Res. Rev.*, **2007**, *27*, 696-722.

150. S. Bhattacharya, A. Bajaj, *Chem. Commun.*, **2009**, 4632-4656.

151. N. M. Rao, *Chem. Phys. Lipids*, **2010**, *163*, 245-252.

152. P. Posocco, S. Pricl, S. Jones, A. Barnard, D. K. Smith, *Chem. Sci.*, **2010**, *1*, 393-404.

153. S. P. Jones, N. P. Gabrielson, C.-H. Wong, H.-F. Chow, D. W. Pack, P. Posocco, M. Fermeglia, S. Pricl, D. K. Smith, *Mol. Pharm.*, **2011**, *8*, 416-429.
154. I. W. Hamley, *Angew. Chem. Int. Ed.*, **2003**, *42*, 1692-1712.
155. A. R. Hirst, B. Escuder, J. F. Miravet, D. K. Smith, *Angew. Chem. Int. Ed.*, **2008**, *47*, 8002-8018.
156. M. O. Guler, L. Hsu, S. Soukasene, D. A. Harrington, J. F. Hulvat, S. I. Stupp, *Biomacromolecules*, **2006**, *7*, 1855-1863.
157. D. A. Harrington, E. Y. Cheng, M. O. Guler, L. K. Lee, J. L. Donovan, R. C. Claussen, S. I. Stupp, *J. Biomed. Mater. Res. Part A*, **2006**, *78A*, 157-167.
158. M. Zhou, A. M. Smith, A. K. Das, N. W. Hodson, R. F. Collins, R. V. Ulijn, J. E. Gough, *Biomaterials*, **2009**, *30*, 2523-2530.
159. A. R. Hirst, D. K. Smith, *Top. Curr. Chem.*, **2005**, *256*, 237-273.
160. M. George, R. G. Weiss, *Acc. Chem. Res.*, **2006**, *39*, 489-497.
161. D. K. Smith, *Molecular Gels - Nanostructured Soft Materials*, in *Organic Nanostructures* (Eds. J. W. Steed, J. L. Atwood), Wiley-VCH, Weinheim, **2008**.
162. A. Vintiloiu, J. C. Leroux, *J. Controlled Release*, **2008**, *125*, 179-192.
163. J. L. Drury, D. J. Mooney, *Biomaterials*, **2003**, *24*, 4337-4351.
164. N. A. Peppas, P. Bures, W. Leobandung, H. Ichikawa, *Eur. J. Pharm. Biopharm.*, **2000**, *50*, 27-46.
165. M. Zinic, F. Vogtle, F. Fages, *Top. Curr. Chem.*, **2005**, *256*, 39-76.
166. R. G. Weiss, P. Terech, *Molecular Gels: Materials with Self-Assembled Fibrillar Networks*, Springer, Dordrecht, **2006**.
167. M. Suzuki, K. Hanabusa, *Chem. Soc. Rev.*, **2009**, *38*, 967-975.
168. L. A. Estroff, A. D. Hamilton, *Chem. Rev.*, **2004**, *104*, 1201-1218.
169. D. J. Adams, P. D. Topham, *Soft Matter*, **2010**, *6*, 3707-3721.
170. R. V. Ulijn, A. M. Smith, *Chem. Soc. Rev.*, **2008**, *37*, 664-675.
171. Y. Nagai, L. D. Unsworth, S. Koutsopoulos, S. Zhang, *J. Controlled Release*, **2006**, *115*, 18-25.
172. S. R. Veith, E. Hughes, S. E. Pratsinis, *J. Controlled Release*, **2004**, *99*, 315-327.
173. J. Naskar, G. Palui, A. Banerjee, *J. Phys. Chem. B*, **2009**, *113*, 11787-11792.
174. S. Zhang, *Nat. Biotechnol.*, **2003**, *21*, 1171-1178.
175. G. A. Silva, C. Czeisler, K. L. Niece, E. Beniash, D. A. Harrington, J. A. Kessler, S. I. Stupp, *Science*, **2004**, *303*, 1352-1355.
176. J. H. Collier, J. S. Rudra, J. Z. Gasiorowski, J. P. Jung, *Chem. Soc. Rev.*, **2010**, *39*, 3413-3424.
177. S. Verma, A. J. Domb, N. Kumar, *Nanomedicine*, **2011**, *6*, 157-181.
178. Z. Yang, G. Liang, M. Ma, Y. Gao, B. Xu, *J. Mater. Chem.*, **2007**, *17*, 850-854.
179. R. J. Mart, R. D. Osborne, M. M. Stevens, R. V. Ulijn, *Soft Matter*, **2006**, *2*, 822-835.
180. M. de Loos, B. L. Feringa, J. H. van Esch, *Eur. J. Org. Chem.*, **2005**, *2005*, 3615-3631.
181. W. T. Truong, Y. Su, J. T. Meijer, P. Thordarson, F. Braet, *Chem. Asian. J.*, **2011**, *6*, 30-42.

182. T. R. Hoare, D. S. Kohane, *Polymer*, **2008**, *49*, 1993-2007.
183. A. Friggeri, B. L. Feringa, J. van Esch, *J. Controlled Release*, **2004**, *97*, 241-248.
184. R. O. Hynes, *Science*, **2009**, *326*, 1216-1219.
185. S. Zhang, T. C. Holmes, C. M. DiPersio, R. O. Hynes, X. Su, A. Rich, *Biomaterials*, **1995**, *16*, 1385-1393.
186. J. Kisiday, M. Jin, B. Kurz, H. Hung, C. Semino, S. Zhang, A. J. Grodzinsky, *Proc. Natl. Acad. Sci. U.S.A.*, **2002**, *99*, 9996-10001.
187. J. D. Hartgerink, E. Beniash, S. I. Stupp, *Proc. Natl. Acad. Sci. U.S.A.*, **2002**, *99*, 5133-5138.
188. E. Beniash, J. D. Hartgerink, H. Storrie, J. C. Stendahl, S. I. Stupp, *Acta Biomater.*, **2005**, *1*, 387-397.
189. J. K. Kretsinger, L. A. Haines, B. Ozbas, D. J. Pochan, J. P. Schneider, *Biomaterials*, **2005**, *26*, 5177-5186.
190. V. Jayawarna, M. Ali, T. A. Jowitt, A. F. Miller, A. Saiani, J. E. Gough, R. V. Ulijn, *Adv. Mater.*, **2006**, *18*, 611-614.
191. L. Haines-Butterick, K. Rajagopal, M. Branco, D. Salick, R. Rughani, M. Pilarz, M. S. Lamm, D. J. Pochan, J. P. Schneider, *Proc. Natl. Acad. Sci. U.S.A.*, **2007**, *104*, 7791-7796.
192. K. Rajangam, H. A. Behanna, M. J. Hui, X. Han, J. F. Hulvat, J. W. Lomasney, S. I. Stupp, *Nano Lett.*, **2006**, *6*, 2086-2090.
193. H. Storrie, M. O. Guler, S. N. Abu-Amara, T. Volberg, M. Rao, B. Geiger, S. I. Stupp, *Biomaterials*, **2007**, *28*, 4608-4618.
194. M. P. Lutolf, J. A. Hubbell, *Nat. Biotechnol.*, **2005**, *23*, 47-55.
195. D. L. Hern, J. A. Hubbell, *J. Biomed. Mater. Res. Part A*, **1998**, *39*, 266-276.
196. S. L. Gras, A. K. Tickler, A. M. Squires, G. L. Devlin, M. A. Horton, C. M. Dobson, C. E. MacPhee, *Biomaterials*, **2008**, *29*, 1553-1562.
197. S. P. Massia, J. A. Hubbell, *J. Cell Biol.*, **1991**, *114*, 1089-1100.
198. E. A. Cavalcanti-Adam, A. Micoulet, J. Blümmel, J. Auernheimer, H. Kessler, J. P. Spatz, *Eur. J. Cell Biol.*, **2006**, *85*, 219-224.
199. S. Woerly, E. Pinet, L. de Robertis, D. Van Diep, M. Bousmina, *Biomaterials*, **2001**, *22*, 1095-1111.
200. K.-H. Park, *Biotechnol. Lett.*, **2002**, *24*, 1131-1135.
201. Y. Mei, K. L. Beers, H. C. M. Byrd, D. L. VanderHart, N. R. Washburn, *J. Am. Chem. Soc.*, **2004**, *126*, 3472-3476.
202. S. J. Todd, D. Farrar, J. E. Gough, R. V. Ulijn, *Soft Matter*, **2007**, *3*, 547-550.
203. C. Chun, H. J. Lim, K.-Y. Hong, K.-H. Park, S.-C. Song, *Biomaterials*, **2009**, *30*, 6295-6308.
204. J. Zhu, C. Tang, K. Kottke-Marchant, R. E. Marchant, *Bioconjugate Chem.*, **2009**, *20*, 333-339.
205. S. Garty, N. Kimelman-Bleich, Z. Hayouka, D. Cohn, A. Friedler, G. Pelled, D. Gazit, *Biomacromolecules*, **2010**, *11*, 1516-1526.

206. Y. Shibasaki, S. Hirohara, K. Terada, T. Ando, M. Tanihara, *Pept. Sci.*, **2011**, *96*, 302-315.
207. Y. Zhang, H. Gu, Z. Yang, B. Xu, *J. Am. Chem. Soc.*, **2003**, *125*, 13680-13681.
208. Y. Zhang, Z. Yang, F. Yuan, H. Gu, P. Gao, B. Xu, *J. Am. Chem. Soc.*, **2004**, *126*, 15028-15029.
209. A. Mahler, M. Reches, M. Rechter, S. Cohen, E. Gazit, *Adv. Mater.*, **2006**, *18*, 1365-1370.
210. R. Orbach, L. Adler-Abramovich, S. Zigerson, I. Mironi-Harpaz, D. Seliktar, E. Gazit, *Biomacromolecules*, **2009**, *10*, 2646-2651.
211. J. D. Hartgerink, E. Beniash, S. I. Stupp, *Science*, **2001**, *294*, 1684-1688.
212. S. Roy, A. Dasgupta, P. K. Das, *Langmuir*, **2007**, *23*, 11769-11776.
213. J. H. Collier, B.-H. Hu, J. W. Ruberti, J. Zhang, P. Shum, D. H. Thompson, P. B. Messersmith, *J. Am. Chem. Soc.*, **2001**, *123*, 9463-9464.
214. H. Rapaport, H. Grisaru, T. Silberstein, *Adv. Funct. Mater.*, **2008**, *18*, 2889-2896.
215. C. J. Bowerman, B. L. Nilsson, *J. Am. Chem. Soc.*, **2010**, *132*, 9526-9527.
216. A. P. Nowak, V. Breedveld, L. Pakstis, B. Ozbas, D. J. Pine, D. Pochan, T. J. Deming, *Nature*, **2002**, *417*, 424-428.
217. T. J. Deming, *Polypeptide and Polypeptide Hybrid Copolymer Synthesis via NCA Polymerization*, in *Peptide Hybrid Polymers* (Eds. H.-A. Klok, H. Schlaad), Springer, **2006**, *202*, 1-18.
218. W. A. Petka, J. L. Harden, K. P. McGrath, D. Wirtz, D. A. Tirrell, *Science*, **1998**, *281*, 389-392.
219. C. Xu, V. Breedveld, J. Kopeček, *Biomacromolecules*, **2005**, *6*, 1739-1749.
220. C. Xu, J. Kopeček, *Pharm. Res.*, **2008**, *25*, 674-682.
221. L. Mi, S. Fischer, B. Chung, S. Sundelacruz, J. L. Harden, *Biomacromolecules*, **2005**, *7*, 38-47.
222. D. W. P. M. Lowik, J. C. M. van Hest, *Chem. Soc. Rev.*, **2004**, *33*, 234-245.
223. S. E. Paramonov, H.-W. Jun, J. D. Hartgerink, *J. Am. Chem. Soc.*, **2006**, *128*, 7291-7298.
224. R. G. Ellis-Behnke, Y.-X. Liang, S.-W. You, D. K. C. Tay, S. Zhang, K.-F. So, G. E. Schneider, *Proc. Natl. Acad. Sci. U.S.A.*, **2006**, *103*, 5054-5059.
225. S. Ray, A. K. Das, A. Banerjee, *Chem. Mater.*, **2007**, *19*, 1633-1639.
226. I. Yoshimura, Y. Miyahara, N. Kasagi, H. Yamane, A. Ojida, I. Hamachi, *J. Am. Chem. Soc.*, **2004**, *126*, 12204-12205.
227. H. Komatsu, S. Matsumoto, S.-i. Tamaru, K. Kaneko, M. Ikeda, I. Hamachi, *J. Am. Chem. Soc.*, **2009**, *131*, 5580-5585.
228. D. J. Beebe, J. S. Moore, J. M. Bauer, Q. Yu, R. H. Liu, C. Devadoss, B.-H. Jo, *Nature*, **2000**, *404*, 588-590.
229. D. Diaz Diaz, D. Kuhbeck, R. J. Koopmans, *Chem. Soc. Rev.*, **2011**, *40*, 427-448.
230. Z. Yang, G. Liang, B. Xu, *Soft Matter*, **2007**, *3*, 515-520.
231. Z. Yang, G. Liang, B. Xu, *Acc. Chem. Res.*, **2008**, *41*, 315-326.
232. R. V. Ulijn, *J. Mater. Chem.*, **2006**, *16*, 2217-2225.

233. A. R. Hirst, S. Roy, M. Arora, A. K. Das, N. Hodson, P. Murray, S. Marshall, N. Javid, J. Sefcik, J. Boekhoven, J. H. van Esch, S. Santabarbara, N. T. Hunt, R. V. Ulijn, *Nat. Chem.*, **2010**, *2*, 1089-1094.
234. Z. Yang, B. Xu, *Chem. Commun.*, **2004**, 2424-2425.
235. Z. Yang, P.-L. Ho, G. Liang, K. H. Chow, Q. Wang, Y. Cao, Z. Guo, B. Xu, *J. Am. Chem. Soc.*, **2006**, *129*, 266-267.
236. M.-O. M. Piepenbrock, G. O. Lloyd, N. Clarke, J. W. Steed, *Chem. Rev.*, **2010**, *110*, 1960-2004.
237. A. A. Sobczuk, S.-i. Tamaru, S. Shinkai, *Chem. Commun.*, **2011**, *47*, 3093-3095.
238. S. V. Brignell, D. K. Smith, *New J. Chem.*, **2007**, *31*, 1243-1249.
239. Y. Qiao, Y. Lin, Z. Yang, H. Chen, S. Zhang, Y. Yan, J. Huang, *J. Phys. Chem. B*, **2010**, *114*, 11725-11730.
240. Y. Qiao, Y. Lin, Y. Wang, Z. Yang, J. Liu, J. Zhou, Y. Yan, J. Huang, *Nano Lett.*, **2009**, *9*, 4500-4504.
241. C. E. Stanley, N. Clarke, K. M. Anderson, J. A. Elder, J. T. Lenthall, J. W. Steed, *Chem. Commun.*, **2006**, 3199-3201.
242. G. O. Lloyd, J. W. Steed, *Nat. Chem.*, **2009**, *1*, 437-442.
243. J. W. Steed, *Chem. Soc. Rev.*, **2010**, *39*, 3686-3699.
244. J. A. Foster, M. PiepenbrockMarc-Oliver, G. O. Lloyd, N. Clarke, A. K. HowardJudith, J. W. Steed, *Nat. Chem.*, **2010**, *2*, 1037-1043.
245. J. E. A. Webb, M. J. Crossley, P. Turner, P. Thordarson, *J. Am. Chem. Soc.*, **2007**, *129*, 7155-7162.
246. K. W. K. Tong, S. Dehn, J. E. A. Webb, K. Nakamura, F. Braet, P. Thordarson, *Langmuir*, **2009**, *25*, 8586-8592.
247. M.-O. M. Piepenbrock, G. O. Lloyd, N. Clarke, J. W. Steed, *Chem. Commun.*, **2008**, 2644-2646.
248. M. Yamanaka, N. Haraya, S. Yamamichi, *Chem. Asian J.*, **2011**, *6*, 1022-1025.
249. P. Bairi, B. Roy, A. K. Nandi, *J. Mater. Chem.*, **2011**, *21*, 11747-11749.
250. J.-S. Shen, D.-H. Li, Q.-G. Cai, Y.-B. Jiang, *J. Mater. Chem.*, **2009**, *19*, 6219-6224.
251. L. A. Estroff, A. D. Hamilton, *Angew. Chem. Int. Ed.*, **2000**, *39*, 3447-3450.
252. F. Fages, F. Vogtle, M. Zinic, *Top. Curr. Chem.*, **2005**, *256*, 77-131.
253. H. Wissmann, H.-J. Kleiner, *Angew. Chem. Int. Ed.*, **1980**, *19*, 133-134.
254. J. Klose, M. Bienert, C. Mollenkopf, D. Wehle, C.-w. Zhang, L. A. Carpino, P. Henklein, *Chem. Commun.*, **1999**, 1847-1848.
255. R. Knorr, A. Trzeciak, W. Bannwarth, D. Gillessen, *Tetrahedron Lett.*, **1989**, *30*, 1927-1930.
256. I. Abdelmoty, F. Albericio, L. A. Carpino, B. M. Foxman, S. A. Kates, *Lett. Pept. Sci.*, **1994**, *1*, 57-67.
257. G. R. Newkome, X. F. Lin, *Macromolecules*, **1991**, *24*, 1443-1444.

258. J. K. Young, G. R. Baker, G. R. Newkome, K. F. Morris, C. S. Johnson, *Macromolecules*, **1994**, *27*, 3464-3471.
259. C. M. Cardona, R. E. Gawley, *J. Org. Chem.*, **2002**, *67*, 1411-1413.
260. C. A. G. N. Montalbetti, V. Falque, *Tetrahedron*, **2005**, *61*, 10827-10852.
261. A. Isidro-Llobet, M. Álvarez, F. Albericio, *Chem. Rev.*, **2009**, *109*, 2455-2504.
262. R. Bollhagen, M. Schmiedberger, K. Barlos, E. Grell, *J. Chem. Soc., Chem. Commun.*, **1994**, 2559-2560.
263. D. M. Jameson, J. A. Ross, *Chem. Rev.*, **2010**, *110*, 2685-2708.
264. C. Yung-Chi, W. H. Prusoff, *Biochem. Pharmacol.*, **1973**, *22*, 3099-3108.
265. P. Zajdel, G. Subra, A. J. Bojarski, B. Duszynska, E. Tatarczynska, A. Nikiforuk, E. Chojnacka-Wójcik, M. Pawlowski, J. Martinez, *Bioorg. Med. Chem.*, **2007**, *15*, 2907-2919.
266. M. Mori, A. Somada, S. Oida, *Chem. Pharm. Bull.*, **2000**, *48*, 716-728.
267. S. I. Shen, P. Kotamraj, S. Bhattacharya, X. Li, B. R. Jasti, *J. Drug Target.*, **2007**, *15*, 51-58.
268. P. Gomes, M. J. Araujo, E. F. Marques, S. Falcao, R. O. Brito, *Synth. Comm.*, **2008**, *38*, 2025-2036.
269. R. Dhawan, M. G. A. Kadijk, T. J. Joikinen, M. Feng, S. M. Ansell, *Bioconjugate Chem.*, **2000**, *11*, 14-21.
270. M. C. A. Stuart, J. C. van de Pas, J. B. F. N. Engberts, *J. Phys. Org. Chem.*, **2005**, *18*, 929-934.
271. K. Kalyanasundaram, J. K. Thomas, *J. Am. Chem. Soc.*, **1977**, *99*, 2039-2044.
272. S. Gouin, X. X. Zhu, *Langmuir*, **1998**, *14*, 4025-4029.
273. R. O. Brito, E. F. Marques, P. Gomes, S. Falcão, O. Söderman, *J. Phys. Chem. B.*, **2006**, *110*, 18158-18165.
274. D. J. Welsh, D. K. Smith, *Org. Biomol. Chem.*, **2011**, *9*, 4795-4801.
275. L. A. Estroff, L. Leiserowitz, L. Addadi, S. Weiner, A. D. Hamilton, *Adv. Mater.*, **2003**, *15*, 38-42.
276. W. Uhl, H. R. Bock, F. Breher, M. Claesener, S. Haddadpour, B. Jasper, A. Hepp, *Organometallics*, **2007**, *26*, 2363-2369.
277. O. Mongin, C. Papamicael, N. Hoyler, A. Gossauer, *J. Org. Chem.*, **1998**, *63*, 5568-5580.
278. A. de Meijere, F. Diederich, *Metal-Catalyzed Cross-Coupling Reactions*, Wiley-VCH, Weinheim, **2004**.
279. M. Levitt, *Biochemistry*, **1978**, *17*, 4277-4285.
280. E. L. Rexeisen, W. Fan, T. O. Pangburn, R. R. Taribagil, F. S. Bates, T. P. Lodge, M. Tsapatsis, E. Kokkoli, *Langmuir*, **2009**, *26*, 1953-1959.
281. J. Nagasawa, M. Kudo, S. Hayashi, N. Tamaoki, *Langmuir*, **2004**, *20*, 7907-7916.
282. T. Tu, W. Assenmacher, H. Peterlik, R. Weisbarth, M. Nieger, K. H. Dötz, *Angew. Chem. Int. Ed.*, **2007**, *46*, 6368-6371.
283. J. Liu, P. He, J. Yan, X. Fang, J. Peng, K. Liu, Y. Fang, *Adv. Mater.*, **2008**, *20*, 2508-2511.

284. H. Kobayashi, A. Friggeri, K. Koumoto, M. Amaike, S. Shinkai, D. N. Reinhoudt, *Org. Lett.*, **2002**, *4*, 1423-1426.

285. K. J. C. van Bommel, C. van der Pol, I. Muizebelt, A. Friggeri, A. Heeres, A. Meetsma, B. L. Feringa, J. van Esch, *Angew. Chem. Int. Ed.*, **2004**, *43*, 1663-1667.

286. H. Wang, C. Yang, M. Tan, L. Wang, D. Kong, Z. Yang, *Soft Matter*, **2011**, *7*, 3897-3905.

287. G. Cravotto, P. Cintas, *Chem. Soc. Rev.*, **2009**, *38*, 2684-2697.

288. S. R. Raghavan, B. H. Cipriano, *Gel formation: phase diagrams using tabletop rheology*, in *Molecular Gels: Materials with Self-Assembled Fibrillar Networks* (Eds. R. G. Weiss, P. Terech), Springer, Dordrecht, **2006**.

289. T. Liebmann, S. Rydholm, V. Akpe, H. Brismar, *BMC Biotechnol.*, **2007**, *7*, 88-98.

290. W. C. Griffin, *J. Soc. Cosmetic Chem.*, **1949**, *1*, 311-326.

291. J. T. Davies, *Interfacial Phenomena*, Academic Press, **1963**.

292. D. J. Hill, M. J. Mio, R. B. Prince, T. S. Hughes, J. S. Moore, *Chem. Rev.*, **2001**, *101*, 3893-4012.

293. F. García, L. Sánchez, *Chem. Eur. J.*, **2010**, *16*, 3138-3146.

294. N. Berova, K. Nakanishi, R. W. Woody, *Circular Dichroism: Principles and Applications*, Wiley-VCH, New York, **2000**.

295. S. M. Kelly, N. C. Price, *Curr. Protein Pept. Sci.*, **2000**, *1*, 349-384.

296. B. Ranjbar, P. Gill, *Chem. Biol. Drug Des.*, **2009**, *74*, 101-120.

297. B. Escuder, M. Llusar, J. F. Miravet, *J. Org. Chem.*, **2006**, *71*, 7747-7752.

298. A. R. Hirst, J. F. Miravet, B. Escuder, L. Noirez, V. Castelletto, I. W. Hamley, D. K. Smith, *Chem. Eur. J.*, **2009**, *15*, 372-379.

299. F. Rodríguez-Llansola, B. Escuder, J. F. Miravet, *J. Am. Chem. Soc.*, **2009**, *131*, 11478-11484.

300. A. Aggeli, M. Bell, L. M. Carrick, C. W. G. Fishwick, R. Harding, P. J. Mawer, S. E. Radford, A. E. Strong, N. Boden, *J. Am. Chem. Soc.*, **2003**, *125*, 9619-9628.

301. S. Nishizawa, P. Bühlmann, M. Iwao, Y. Umezawa, *Tetrahedron Lett.*, **1995**, *36*, 6483-6486.

302. P. Bühlmann, S. Nishizawa, K. P. Xiao, Y. Umezawa, *Tetrahedron*, **1997**, *53*, 1647-1654.

303. Y. Zhang, P. S. Cremer, *Curr. Opin. Chem. Biol.*, **2006**, *10*, 658-663.

304. T. Becker, C. Yong Goh, F. Jones, M. J. McIldowie, M. Mocerino, M. I. Ogden, *Chem. Commun.*, **2008**, 3900-3902.

305. L. A. Estroff, L. Addadi, S. Weiner, A. D. Hamilton, *Org. Biomol. Chem.*, **2004**, *2*, 137-141.

306. N. Shi, G. Yin, M. Han, Z. Xu, *Colloids Surf., B*, **2008**, *66*, 84-89.

307. J. A. Foster, M.-O. M. Piepenbrock, G. O. Lloyd, N. Clarke, J. A. K. Howard, J. W. Steed, *Nat. Chem.*, **2010**, *2*, 1037-1043.

308. G. P. Stahly, *Cryst. Growth Des.*, **2007**, *7*, 1007-1026.

309. Y. Zhao, T. Tan, H. Yokoi, M. Tanaka, T. Kinoshita, *J. Polym. Sci. A*, **2008**, *46*, 4927-4933.

310. A. Mata, L. Hsu, R. Capito, C. Aparicio, K. Henrikson, S. I. Stupp, *Soft Matter*, **2009**, *5*, 1228-1236.

311. G. Han, M. Tamaki, V. J. Hruby, *J. Pept. Res.*, **2001**, *58*, 338-341.

312. Y.-b. Lim, E. Lee, M. Lee, *Angew. Chem. Int. Ed.*, **2007**, *46*, 9011-9014.